PORE STRUCTURAL ASPECTS OF COKE LAYDOWN IN FCC CATALYST

by

Omran H. J. Muhammad

A Thesis submitted to the
University of Manchester
for the degree of

DOCTOR OF PHILOSOPHY

Department of Chemical Engineering
University of Manchester Institute of Science and Technology

1992

DECLARATION

No portion of the work referred to in this thesis has been submitted in support of an application for another degree or qualification of this or any other university or institution of learning.

Omran H. J. Muhammad

DEDICATION

To:

My Parents,

My Wife and Children

and My Family

AKNOWLEDGEMENTS

Praise be to God, The Cherisher and Sustainer of the Worlds

The author would like to take this opportunity to express his gratitute to:

Dr. R. Mann: for all his invaluable advice, encouragement and understanding,

Kuwait Institute For Scientific Research: for their financial support and for the help in catalyst characterisation,

Prof. J. Garside, Prof. E. Woodburn, Prof. G. Davies and the Department of Chemical Engineering: for laboratory and computer facilities,

The Computation Staff: for helping with computational problems,

Technicians and the Secretarial Staff: for advice and help in making the most of the available facilities,

Colleaques and Friends at UMIST: for their help and friendship,

Dr. M. Al–Mudafer and Mr. A. Singace: for their unique support and help,

Friends and Relatives: for their prayers and help in different ways,

My Brothers, Sisters and their Families: for all the understanding, support and help when needed most, especially my sister Nasreen,

My Wife Zakieh Ashkanani: for her care, patience, wisdom and support always,

My Children Mohammad, Fatimah, Zainab and Hassan: for sharing the difficulties of my long study period with a wonderful understanding.

THE AUTHOR

The author was educated at Yousuf Bin Essa secondary school, Kuwait. In 1979 he graduated from Iowa State University, Ames, Iowa, USA with the degree of B.Sc. in Chemical Engineering. In 1981 he was awarded the Masters degree in Chemical Engineering from University of South Carolina, Columbia, South Carolina, USA.

Since 1979, the author has been a member of the research staff in the Petroleum Technology Department at Kuwait Institute for Scientific Research (KISR), Kuwait.

ABSTRACT

The theoretical and practical aspects of the deactivation by coking of a commercial supported zeolitic catalyst, Super D, has been investigated. Deactivation studies have been carried out in a laboratory scale fluidised bed reactor and the disproportionation of cumene at 500°C was used as the model reaction. The catalyst:feed ratio was varied from 1:1 to 100:1 g/g/min with run times up to two hours. A blank experimental run with no catalyst in the reactor was also carried out which deduced that at the reactor conditions there was no significant thermal cracking of the cumene to products, and that the material balance over the reactor system for the cumene was within four percent. The benzene selectivity was determined and found to increase with time on stream.

Since the deactivation of the catalyst was due to coke laydown on the support macropores and in the zeolite micropores, the coke content was measured using a Leco carbon/sulphur analyser. The changes in the catalyst's structure as a result of this deactivation was monitored by measuring the catalyst surface area using a Quantasorb adsorption unit. The results of these experiments have shown an initial period of rapid drop in the conversion of the feed, rapid coke build–up within the catalyst and a sharp drop in the surface area, followed by a period of much slower rate of deactivation.

A theoretical model has been proposed to account for the catalyst deactivation by coke deposition based upon the interaction of the geometries of the coke deposit and the pore structure. Coke is assumed to deposit randomly on the support macropores and in the zeolite micropores allowing for deactivation by both active site coverage and pore blockage. The support pore structure was represented by two different models, namely, the corrugated parallel bundle pore model, and the stochastic network pore model. The diffusion–reaction equations are solved rigorously in these pores to produce

predictions of conversion, coke content and surface area as a function of time on stream. Computer simulations have been carried out in both of these structures to study the influence of the various parameters on the model. In these simulations, three different deactivation types were investigated, namely, the series, parallel and the triangular. Using the information gathered from these simulations as a guide, an attempt was made to see if the model could successfully describe the observed deactivation behaviour of the commercial catalyst Super D.

Application of the theory to the experimental results has shown that the timewise deactivation could be represented by either a support active site poisoning coking mechanism or a heavy support coking mechanism, though from investigations on the coke accumulation within the catalyst, the latter appeared to be more representative of the total deactivation behaviour. The series type of coking with the product being the coke precursor best fitted the experiments. From the two pore structural models under consideration, the network model provided the better fit. However the corrugated parallel bundle model could not accurately reproduce either the coke content or the surface area profiles. On the other hand not only did the network pore model reproduced the observed deactivation but it also simulated the coke content and surface area profiles for the entire duration of the catalytic cracking runs and over the range of catalyst:feed ratios that were used.

CONTENTS

CHAPTER ONE

A REVIEW OF THE LITERATURE

CHAPTER ONE

A REVIEW OF THE LITERATURE

1.1 INTRODUCTION:

Catalysis is one of the most important chemical processes carried out on an industrial scale in the world today. Nearly 95% of all chemical products have been in contact with a catalyst of one kind or another during their synthesis, and particularly in the context of the petroleum and petrochemical industry (Trimm, 1985).

Catalysis of a specific reaction provides a route which proceeds in parallel with any existing thermal, or even other catalytic (possibly unrecognised), modes of reaction within the particular mixture (Heaton, 1991).

Catalysis is defined as "The acceleration or retardation of a chemical reaction by a substance which itself undergoes no permanent chemical change, or which can be recovered when the chemical reaction is completed. It lowers the energy of activation. A catalyst is a substance which catalyses a reaction" (Chambers Science And Technology Dictionary, 1991). Hidden within this definition, however, are several important facts. A catalyst will not alter the position of the thermodynamic equilibrium, and the end result is the same whether or not a catalyst is present. The time to reach equilibrium should be drastically reduced by a catalyst . Although the catalyst should not undergo a permanent change, it will when involved in chemical reactions, but, it should return to its original state. The three most important aspects of the application of any heterogeneous catalyst are activity, selectivity and life.

Catalyst life defined as "the time required for the activity of a catalyst to fall by a considerable level " has received least attention despite the fact that deactivation

can often dictate the viability of a process. Unfortunately, most catalysts used in heterogeneous catalytic processes are subject to a decrease in the initial activity over a period of time. Catalyst life varies with the type of a catalyst, the severity of the process conditions and with the type of reaction being catalysed (Hughes, 1984). In the cracking of high molecular weight hydrocarbons into higher and more valuable products, Blanding (1953) noted long ago the activity of the catalyst after only one minute of use could be as little as 1% of its initial value. Pearce and Patterson (1981) report on the other hand, that the active life of the granular catalysts used in the synthesis of ammonia is in the range of 5 to 10 years (Table 1.1). Deactivation can result from a variety of physical, mechanical, chemical and thermal causes.

1.2 TYPES OF DEACTIVATION:

1.2.1 Physical Deactivation (Fouling):

Physical deactivation is caused by fouling processes resulting in the formation of coke, or the deposition of inorganic materials on a catalyst.

1.2.1.1 Catalytic Coking:

Coking is the most common form of catalyst deactivation involving the deposition of carbonaceous materials on most catalysts used in the processing of petroleum fractions or other organic feedstocks. The cracking of hydrocarbons over zeolite catalysts is a challenging example of coke forming reactions where the activity of the catalyst decreases by orders of magnitude in very short times (Reyes and Scriven, 1991). They reported that for a typical riser–reactor operation the deactivation time is of the order of seconds. Corella and Monzon (1988) investigated processes in which catalyst deactivation was due to two or more simultaneous causes but coking was the common cause (Table 1.2). They reported experimental data on a

Process	Catalyst	Physical form	Typical life (years)
Ammonia synthesis $N_2+3H_2 \rightarrow 2NH_3$	$Fe/Al_2O_3/CaO/K_2O$	Granules	5–10
Methanation (ammonia and hydrogen plants) $CO+3H_2 \rightarrow CH_4 + H_2O$	$Ni/Al_2O_3/CaO$	Pellets	5–10
Low temperature carbon monoxide shift $CO+H_2O \leftrightharpoons CO_2+H_2$	$Cu/Al_2O_3/ZnO$	Pellets	2–6
Hydrodesulphurisation $R_2S+2H_2 \rightarrow 2RH+H_2S$	Co+Mo sulphides on Al_2O_3	Extrudate	2–4
Natural gas steam reforming $CH_4+H_2O \rightarrow 3H_2+CO$	Ni on ceramic support	Rings	2–4
Ethylene selective oxidation $C_2H_4+\frac{1}{2}O_2 \rightarrow C_2H_4O$	$AgAl_2O_3$	Rings	1–4
Partial oxidation of methanol to formaldehyde $CH_3OH+\frac{1}{2}O_2 \rightarrow CH_2O+H_2O$ $CH_3OH \rightarrow CH_2O+H_2$	Unsupported Ag	Granules/ crystals	0.3–1
Ammonia oxidation $2NH_3+\frac{5}{2}O_2 \rightarrow 2NO+3H_2O$	Platinum alloy	Gauze	0.1–0.5
Catalytic hydrocarbon reforming	$Pt/Al_2O_3/Cl^-$	Spheres	0.01–0.5
Catalytic cracking	Synthetic zeolites	Fine particles (fluidised bed)	Very short ("continuous") regeneration requires catalyst removal from main reactor to burn off coke

Table 1.1 Typical lives of some industrial heterogeneous catalysts (Reproduced from Pearce and Patterson (1981)).

Authors	Causes
Mirodatos et al. (1984), Jodra et al. (1981) & Carberry (1976)	coking + sintering
Coughlin et al. (1984) & Namba et al. (1984)	coking + N compounds
Apesteguia et al. (1983)	coking + S
Masai et al.(1984)	coking + metals
Levy & De Groot (1982)	$H_2O + O_2$
Gavalas et al. (1984)	sintering+loss of active phase
Corella & Asua (1982) & Corella et al.(1984)	coking+ loss of active phase
Kelley et al. (1983)	coking + transformation of active phase
Baiker et al. (1984)	metallic nitrides + metallic carbides + coke
Tsakalis et al. (1984) & Stiegel et al. (1985)	coke + metal deposition + poison + sintering
Bartholomew (1982), Hayes et al.(1985) Duncan et al. (1985) & Tan & Bennett (1985)	several types of cokes, carbons, or carbides
Soong et al.(1986)	several types of coke + transformation of active phase

Table 1.2 Situations of deactivation by two or more simultaneous causes (Reproduced from Corella and Monzon(1988)).

bifunctional reforming catalyst deactivated by coke and sulphur and on a zinc oxide catalyst deactivated by coke and sintering. Coke deposits contain, in addition to carbon , significant amounts of hydrogen plus traces of oxygen , sulphur and nitrogen. It is important to recognize that the coke deposits originate from the reactions occurring and is not an impurity, so, it can not usually be eliminated by purification of the feed. Bartholemew (1984) proposed a catalyst deactivation model which included the combined effect of pore plugging and active site coverage. He confirmed his model by experimental coal liquefaction catalyst development work by researchers at Amoco Oil Company. The main cause of deactivation was coke deposition which resulted in substantial reduction in surface area and micropore volume.

1.2.1.2 Inorganic Foulants:

This class of fouling reactions include that of metal sulphide deposition arising from the organometallic constituents of petroleum which react with sulphur–containing molecules and deposit within the pores of the catalyst during hydrotreating operations (Newson, 1975). Another example is the deposition of iron, titanium, nickel or vanadium metals or compounds on catalysts used for hydrotreating heavy oils (Rautiainen and Wei, 1990 and Holloway and Kramer, 1977). Other examples include the dusting of platinum–rhodium gauzes by iron during the oxidation on ammonia (Bond, 1962), the deposition of nickel on cracking catalysts (Cadet et al., 1991 and Venuto and Habib, 1979), and the deposition of inorganic salts in hydrotreating catalysts (Kovach et al., 1978). Most investigators have found that catalysts in a hydrodesulfurization (HDS) reactor deactivate in two steps. The first being a rapid decline in activity due to coke formation. The second being a slow decline in activity due to metals deposition (Agrawal and Wei, 1984). Beuther and Schmid (1963) observed that of the total carbon deposited on the HDS catalyst in 16 days of operation, one half deposited in the first 12 hours. Unlike coke deposition, they reported that the metals deposition rate was nearly constant in time. Fouling is

associated with relatively large amounts of deposits which will cover the active sites of the catalyst and may, by interfering with the pore volume, affect the diffusional properties of the porous catalyst pellet. Pore–plugging may occur for both coke and metals deposition, and if allowed to continue the deposits might eventually plug the void spaces between the catalyst pellets, necessitating a complete shut–down of the reactor (Hughes, 1984).

1.2.2 Mechanical Deactivation:

An important characteristic of any commercial catalyst is that of mechanical strength. This must be retained throughout the life of the catalyst, otherwise, pellet disintegration will occur and any associated severe pressure drop resulting from the catalyst breakdown may make it necessary for the reactor to be shut down. Murphy (1970) stressed the importance for fluid cracking catalysts to be resistant to mechanical attrition (i.e. the formation of particles less than 20 micrometers). Catalyst break–up can occur with severe catalyst fouling alone, but more often it is associated with a combination of severe catalyst fouling and extreme operating conditions of the catalyst. These conditions may be physical such as extreme and frequent temperature cycling. Also, maloperation of the process may be a cause which may include extreme feed variations and wrong sequencing of the feed stream. A study by Weisz (1969) showed that with bead catalysts the rate of attrition was indirectly dependent upon both regeneration kinetics and diffusion/mass transport inside the bead.

1.2.3 Chemical Deactivation:

Chemical deactivation is caused by either poisoning the catalyst active sites (i.e. locations where catalysis proceeds) or by loss of catalyst through vapour transport.

1.2.3.1 Poisoning:

Heterogeneous catalysts are often composed of small crystals of metal, metal oxides or metal sulphide attached to inert carriers. Poisoning is the strong chemisorption of impurities, products or reactants onto the active metal sites. Hegedus and McCabe (1980) suggested that besides blockage of active sites by poisons, they may induce changes in the surface or result in the formation of compounds. Some of the most common poisons for metals are S, N, P, O compounds, carbon monoxide and mercury.

In evaluations of pilot plant and commercial operations by Englehard Corp., high rhenium content reforming catalysts have been used with low–sulfur naphtha feeds which have been shown to dramatically affect catalyst cycle length and gasoline yield (McClung, 1990). He concluded that insufficient removal of sulfur caused more rapid catalyst deactivation by poisoning. Ilavsky and co–workers (1986) proposed a model for thiophene poisoning of Ni/Al_2O_3 catalyst used for benzene hydrogenation.

Most reported work on the poisoning of non–metallic catalysts refers to cracking catalysts, which are usually acidic oxides. It is now well established that basic nitrogen compounds are poisons for these catalysts. Early works by Mills et al. (1950) on silica alumina catalysts used for cumene cracking, established the poisoning effectiveness of some basic organic nitrogen compounds.

Bifunctional catalysts are composed of a metal dispersed as very small crystallites on a large area support which also has some catalytic function. A useful study on the deactivation of a bifunctional reforming catalyst by sulphur poisoning and coking has been given by Corella and Monzon (1988).

1.2.3.2 Vapour Transport:

The direct volatilization of catalytic metals is generally not a factor in catalytic processes (except catalytic combustion), since temperatures for metal vaporization will usually need to exceed 1000°C (except for Hg). Often a more important factor is the loss of catalytic metal through the formation of compounds such as metal carbonyls, oxides, sulphides and halides in environments containing CO, NO, O_2, H_2S and halogens (Bartholomew, 1984). There have been only a few studies that have attempted to define the effects of metal loss on catalytic activity. Qamar and Goodwin (1983) reported the loss of significant amount of Ru in the case of Ru/Al_2O_3 catalysts, due to carbonyl formation after an extended period of CO hydrogenation (H_2/CO= 1, 200– 250°C, 1 atm). Delmon (1980) has classified the solid state transformations in which activity loss is due to changes in the nature of the catalyst (Table 1.3).

1.2.4 Thermal Deactivation:

Thermal deactivation is variously referred to in the literature as sintering, aging or thermal degradation.

1.2.4.1 Sintering:

Sintering is associated with the loss of active catalytic surface area when the catalyst is operated above the normal range of temperature. Lee and Luss (1969) noted that temperature rises may occur throughout the catalyst or may be localized at the individual areas where reaction occurs. Sintering processes generally take place at high temperatures (>500°C) and are generally accelerated by the presence of water vapour (Eastwood, 1971). In the case of silica–alumina cracking catalysts, operation at high temperatures in a steam atmosphere will cause a loss of activity due to reduction of specific surface with associated changes in the pore structure and acidic properties

Classification	Definition	Examples of Catalysts Affected
Absence of change of composition of catalyst	Phase transformation	Ni/Al_2O_3, Cu/Al_2O_3
	Phase segregation	V_2O_5–TiO_2, Multicomponent Oxidation Catalysts
	Reactions between solid phases	CoO/Al_2O_3, Ni/Al_2O_3, $CoMo/Al_2O_3$
Change of catalyst composition	Reaction with liquid and gaseous phases	V_2O_5–P_2O_5, $MgFe_2O_4$, TeO_2–MoO_3
	Loss of one or more compounds from the catalyst	$Fe_2(MoO_4)_3$–MoO_3, V_2O_5–P_2O_5
	Formation of compounds with deposits of impurities	$CoMo/Al_2O_3$
Complex Processes	Simultaneous combinations of the preceding effects	

Table 1.3 Classification of the solid state reactions that cause loss of activity [Reproduced from Delmon (1980)].

(Hashimoto et al., 1988).

Sintering can take the form of agglomeration or loss of dispersion of the metal crystallites, e.g. nickel and platinum supported on alumina or silica, causing a sharp drop in activity (Hughes, 1984). A useful visualization of deactivation types has been given by Bartholomew (1984) (Fig. 1.1).

1.3 MECHANISMS OF CATALYST DEACTIVATION:

The deactivation of a porous catalyst is dependent on many factors which include the diffusional resistances inside the catalyst pores for the reacting species and poisons present, also on the way these poisons behave on the catalytic surface. An important engineering factor is the actual rate of decay of activity regardless of the type of deactivation, whether it be by fouling, poisoning, sintering or vapour transport. Levenspiel (1972) has proposed a catalogue of the following kinetic schemes responsible for catalyst deactivation (Table 1.4).

Deactivation Type	Mechanism
Side–by–side	$A \rightarrow B$ $P \rightarrow P\downarrow$
Parallel (simultaneous)	$A \rightarrow B\cdot$ $A \rightarrow P$
Series (consecutive)	$A \rightarrow B \rightarrow P\downarrow$
Simultaneous–Consecutive (Triangular)	$A \rightarrow B$ $\searrow P \swarrow$
Independent	$A \rightarrow B$ $S_{sites} \rightarrow (S\text{–}s)_{sites}$

NB A, B & P denote the reactant, product and poison.
S_{sites} denotes the active sites.

Table 1.4 Deactivation Mechanisms(Reproduced from Levenspiel(1972)).

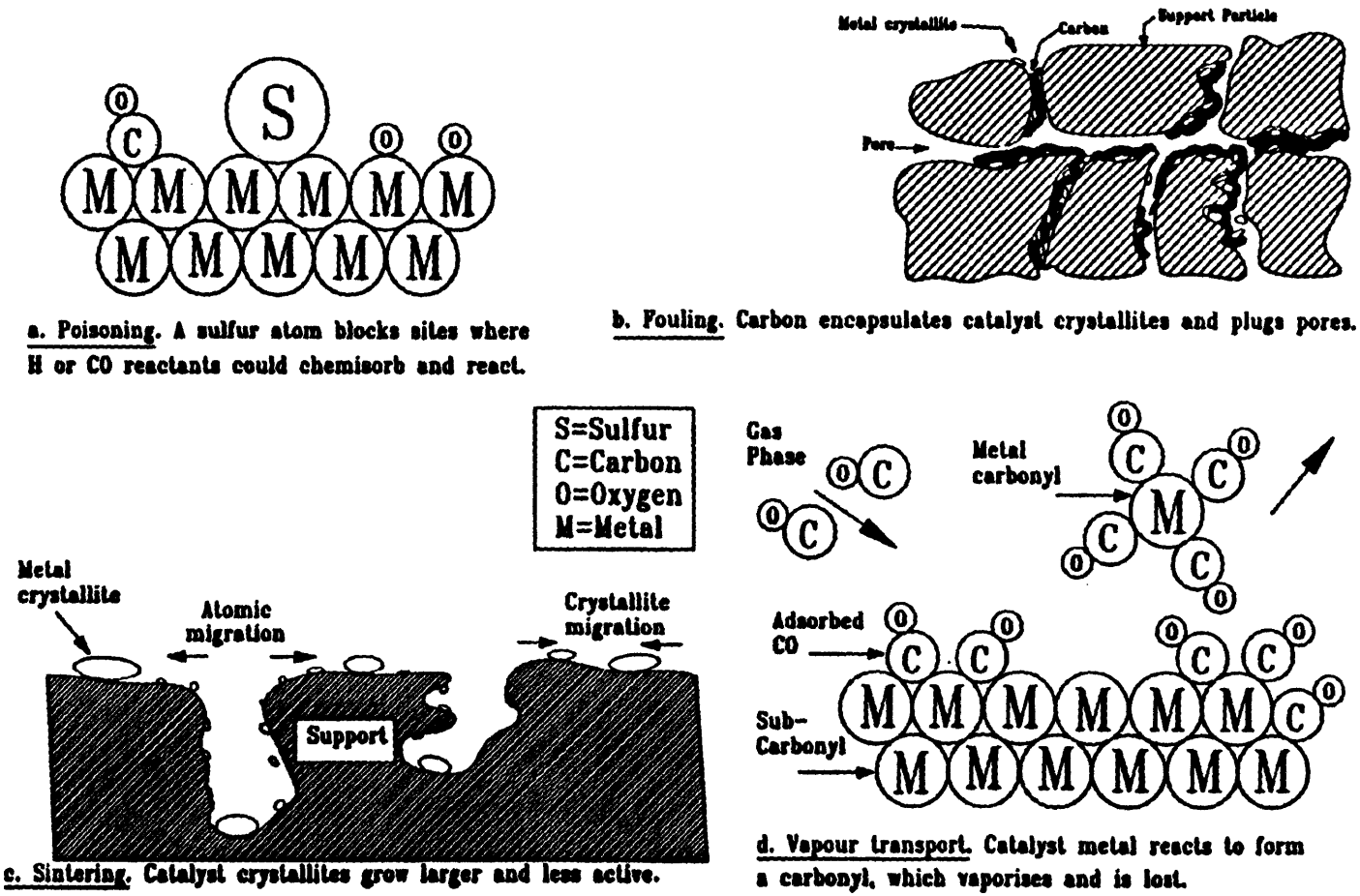

a. Poisoning. A sulfur atom blocks sites where H or CO reactants could chemisorb and react.

b. Fouling. Carbon encapsulates catalyst crystallites and plugs pores.

c. Sintering. Catalyst crystallites grow larger and less active.

d. Vapour transport. Catalyst metal reacts to form a carbonyl, which vaporises and is lost.

Figure 1.1 An illustration of the different types of catalyst deactivation (Redrawn from Bartholomew (1984)).

1.3.1 Parallel Deactivation (Simultaneous):

The reactant produces a side product which deposits on and deactivates the surface. Bharati and Bhatia (1987) studied the kinetics and mechanisms of deactivation by coking of H mordenite catalyst for the disproportionation of PhMe along with the kinetics of the main reaction. The results of their studies showed that deactivation occurs in parallel with the main reaction where PhMe was adsorbed in different ways in the main and deactivation reactions. Chang and Crynes (1986) have observed parallel mechanism of deactivation of Ni/Mo alumina catalyst used in the coal oil hydrotreatment process. Murakami et al. (1968) have shown that parallel deactivation can be the mechanism of the alumina–boria catalyst used in disproportionation of toluene. Froment and Bischoff (1961) in their study of coking in catalysts, noticed greater deposition of coke at the inlet of the reactor where reactant concentration is highest. They concluded that a parallel mechanism of deactivation was in this case responsible for coking.

1.3.2 Series Deactivation (Consecutive):

The reaction product decomposes or reacts further to produce a material which then deposits and deactivates the surface. A study of zeolite catalyst coking in cumene cracking was performed by Viner and Wojciechowski (1984). They observed that out of five possible reaction schemes for poisoning of the catalyst sites, only the series mechanism of deactivation involving the intermediate propylene can explain the experimental data. Acharya et al. (1989) found, in their study of cumene cracking over a silica–alumina catalyst, that the best fit to the experimental data for the coking reaction was obtained using a series mechanism. Noda et al. (1974) observed a distribution of coke deposits along the reactor in a study of isopentane isomerization. In this case, the coke deposited increased with axial distance from the reactor inlet, suggesting that coking was occurring by a series mechanism.

Beyne and Froment (1990) modelled the deactivation of a zeolite catalyst by instantaneous coke formation leading to site coverage and pore blockage. In the presence of diffusional limitations, they considered both the parallel and series mechanisms of coking.

1.3.3 Triangular Deactivation (Simultaneous– Consecutive):

Both the reactants and products produce a side product which deposits and deactivates the surface. Lin et al. (1983) studied the deactivation of a lanthanum exchanged zeolite Y catalyst for cumene cracking using a thermobalance. They found that the kinetic mechanism that gave the best fit for experimental data was one in which parallel and series coking reactions occurred simultaneously (triangular), but with more coke forming from products than from reactants. Angelli et al. (1982) investigated the hydrogenolysis of cyclopropane over a platinum catalyst. They concluded that the experimental data corresponded to a triangular mechanism of deactivation. Parasad and Valdyeswaran (1986) modelled the transient deactivation process taking into account for the first time pore size reduction due to coking and consequent changes in voidage and Knudsen diffusivity. They also assumed a triangular reaction network.

1.3.4 Side–by–Side Deactivation:

An impurity in the feed deposits on and deactivates the surface of the catalyst. Some of these impurities are typically S, N and P compounds and metals such as Ni and V. Markos and Brunovska (1988) studied the deactivation of a nickel catalyst used in the hydrogenation of benzene in a fixed bed reactor. They observed that irreversible deactivation of the catalyst was due to the presence of thiophene acting as a poison side by side with the main reaction. Adkins et al. (1988) developed a model to predict the diffusion–limited accumulation of Fe and Ti in coal liquefaction catalysts used in a

2–stage liquefaction pilot plant. Metals poisoning of HDS catalysts is categorised by this mechanism. Oxenreiter et al. (1972) reported the amount of deposited vanadium to be as high as 56 wt% and nickel 17 wt%.

1.3.5 Kinetic Lumping:

For pure compounds and systems containing few components, the previous reaction schemes are sufficient to describe the main and decay reactions. In catalytic cracking where the feed is complex, Jacob et al. (1976) have described a complex reaction scheme which included deactivation by poisoning and coking. In their model, different kinetic groups of components with similar behaviour were lumped together (Fig. 1.2). This was an improvement to an earlier model proposed by Weekman and Nace (1970). John and Wojciechowski (1975) proposed a kinetic model for the cracking of gas oil which had been pretreated on La–Y zeolite catalyst (Fig. 1.3).

Larocca et al. (1990) applied kinetic lumping in the study of the deactivation of different commercial catalysts used in the cracking of gas oils. In their study, the poisoning effects of nickel and vanadium have been demonstrated through the changes obtained in overall conversions and product selectivities.

1.3.6 Independent Deactivation:

This involves the structural modification or sintering of the catalyst surface caused by exposure to extreme conditions. This type of decay may be independent of any materials in the gas phase. It may only be dependent on the time that the catalyst is exposed to a high temperature environment. Stohl and Stephens (1987) observed sintering of the active sites in their study of catalyst deactivation in an integrated 2–stage direct coal liquefaction processes. In the aged catalyst, Mo sintering was due to the combined effects of time and temperature, whereas Nickel sintering required high

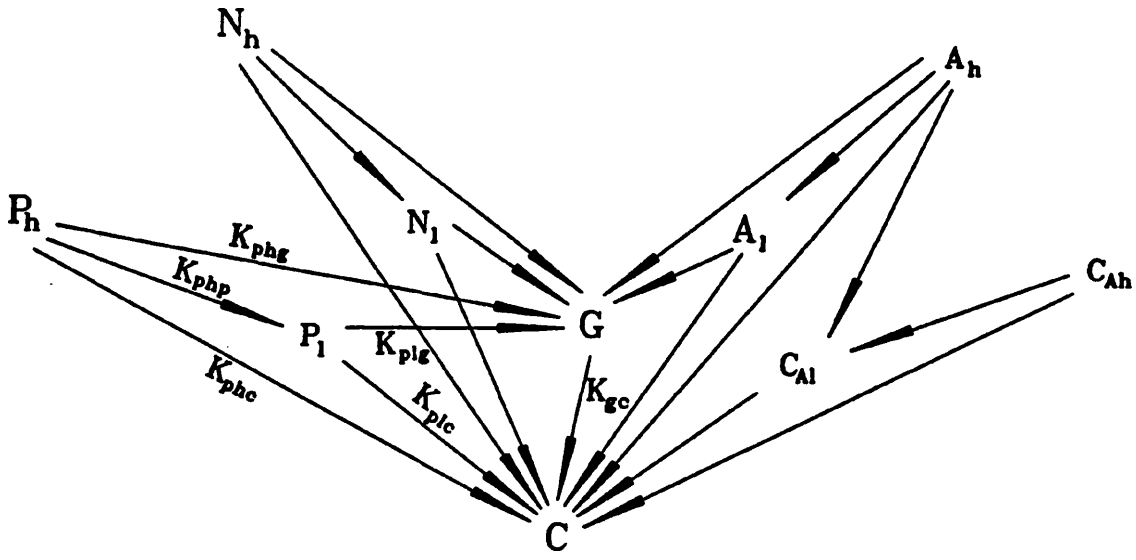

Figure 1.2 Lumped kinetic model for fluid catalyst cracking (Redrawn from Jacob et al. (1976)).

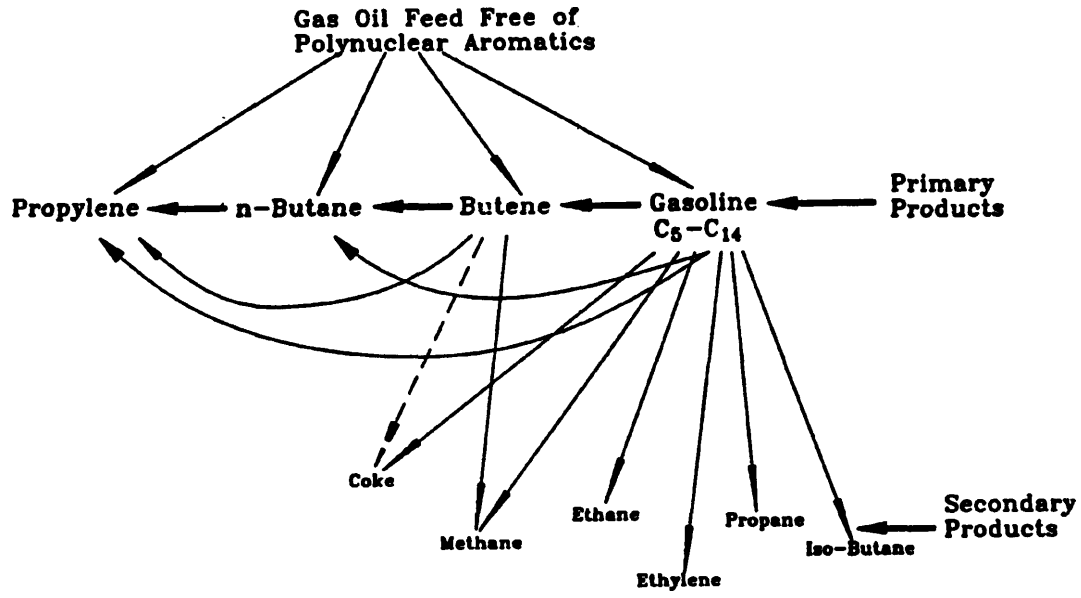

Figure 1.3 Lumped kinetic model for the cracking of gas oil (Redrawn from John and Wojciechowski (1975)).

temperatures . Anthony and Liu (1981) reported a loss of active species through leaching or vaporization in the use of a supported phosphoric acid catalyst. Maclver et al. (1963) explained the loss of the surface area by a growth in crystallite size caused by temperature effects.

1.4 PORE STRUCTURE:

For porous catalysts, adsorbents, coal, as well as all porous solids, an adequate representation of the internal structure is an essential prerequisite to the realistic description of reaction and transport processes in the solid. The practical consequences of the pore structure are of importance. They include the kinetics of adsorption and desorption, permeability and fluid flow, wetting and dewetting, fluid–fluid displacement, catalytic properties, mechanical strength and resistance to freezing (Everett, 1988). In the case of coupled diffusion and reaction in porous catalysts, one of the difficulties encountered is the proper choice of the pore structure model that best represents the catalyst under investigation. Hammon and Kotter (1986) have reported on making mechanically stable aluminum oxide pellets with a well–defined pore structure by wet pelletization and extrusion.

1.4.1 Pore Structure Models:

A number of pore structural models have been formulated in the literature to facilitate the analysis of reactions in porous solids. These models range from some very simple unrealistic pore structures to highly complicated models involving the use of complex mathematics and extensive computation. The following are some of the models proposed which can be classified as one, two and three–dimensional pore models.

1.4.1.1 One–Dimensional Pore Structure Models:

1.4.1.1.1 Pores of Uniform Cross–Section:

These models consist of pores having uniform diffusional resistance along their length. It is the simplest model of pore structure, with most of the authors considering the pores to be cylindrical. A straight parallel bundle model is a special case consisting of parallel, cylindrical tubes of various radii but equal length for which it is relatively easy to derive equations describing some equilibrium and flow phenomena (Fig. 1.4). The diffusional resistance was related to the activity of porous catalysts by many authors, among the earliest was Thiele (1939). The dimensionless group known as "Thiele modulus" was derived by him as a measure of the diffusional effect. Levenspiel (1972) in his study of pore diffusion resistance inside a single cylindrical pore (Fig. 1.5) with first order reaction expressed the Thiele modulus as:

$$mL = L\left(\frac{2ks}{Dr}\right)^{0.5} \qquad (1.1)$$

where

mL :Thiele modulus (dimensionless)

L :pore length (m)

ks :rate constant (m/hr)

D :diffusion coefficient (m^2/hr)

r :pore radius (m)

Levenspiel(1972) also defined the "effectiveness factor" ξ to measure how much the reaction rate is lowered because of the resistance to pore diffusion. Effectiveness factor is defined as:

$$\xi = \frac{\text{actual reaction rate within pore}}{\text{rate if not slowed by pore diffusion}} \qquad (1.2)$$

The concentration gradient across the length of a single cylindrical pore and the effectiveness factor as a function of Thiele modulus are illustrated in Figure 1.6 and

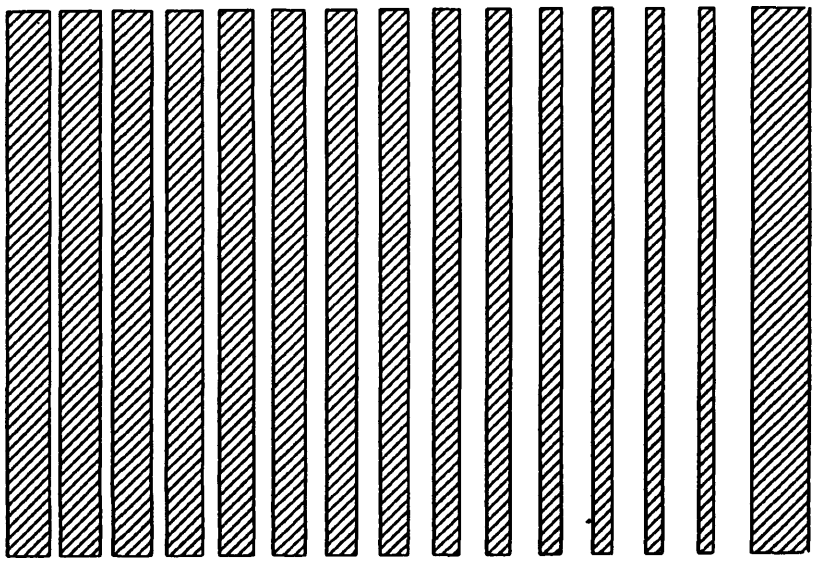

Figure 1.4 Cross–section through a straight parallel bundle of pores.

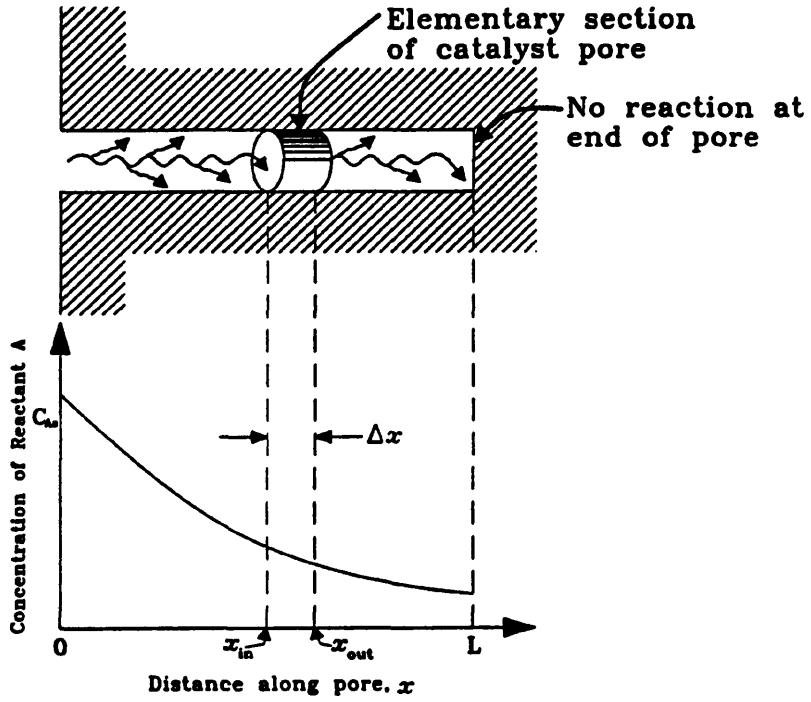

Figure 1.5 Single cylindrical pore with reactant concentration across the pore length (Redrawn from Levenspiel (1972)).

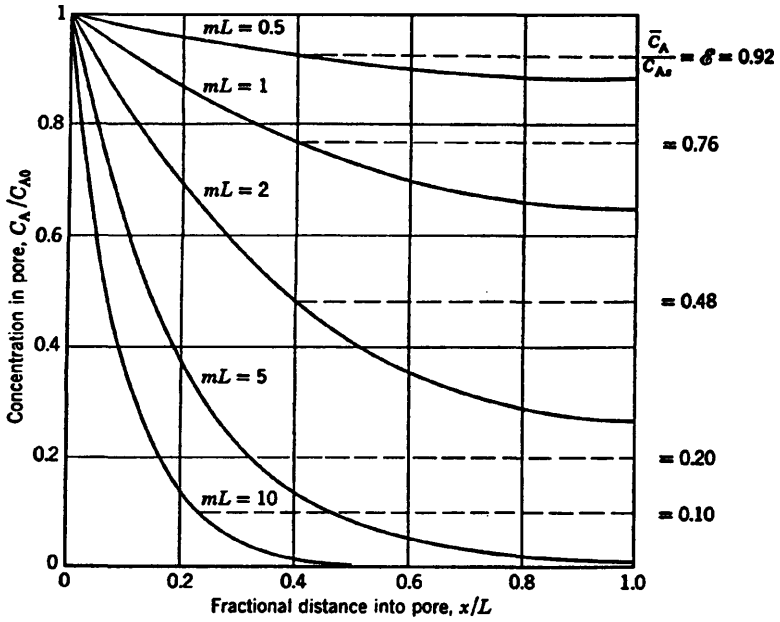

Figure 1.6 Distribution and average value of reactant concentration within a catalyst pore as a function of the parameter mL (Reproduced from Levenspiel (1972)).

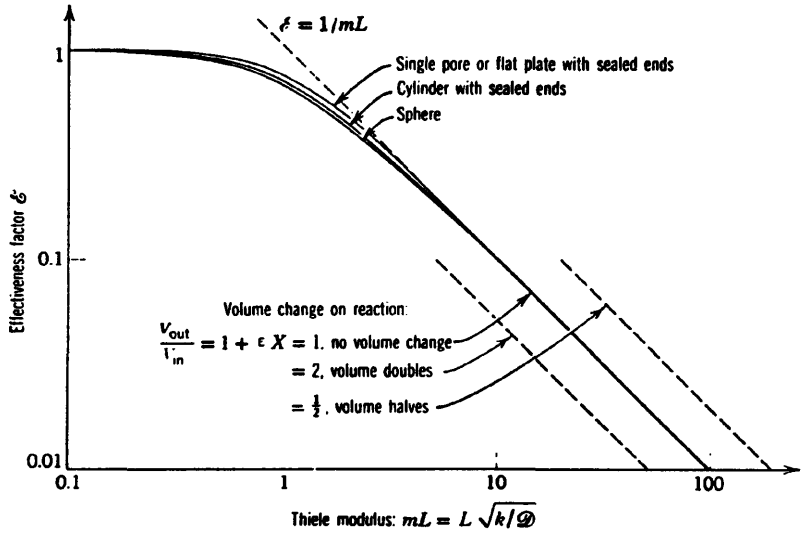

Figure 1.7 The effectiveness factor as a function of the parameter mL for various catalyst shapes and for volume change during reaction (Reproduced from Levenspiel (1972)).

Figure 1.7 respectively. Wheeler (1951) accounted for the fact that pores are not straight by introducing a geometrical "deviousness factor" and extended Thiele's studies to include selectivity. Johnson and Stewart (1965) allowed pores to lie in random directions and introduced the mean diffusivity by integrating the diffusivity over the pore size distribution. Although the model of pores of uniform cross section has been applied successfully in reproducing the observed activity behaviour of a zeolitic catalyst (Thomson, 1986), it is incapable of accounting for entrapment of mercury in porosimetry following depressurization (Androutsopoulos and Mann, 1979).

1.4.1.1.2 Pores of Non–Uniform Cross–Section:

It is a fact that catalyst pores are not of uniform cross–section, on the contrary, they can be expected to contain inter–connected pore spaces which are chaotically conFigured with respect to size, shape, and orientation (Mann and Sharrat, 1988). Many authors proposed models consisting of a series of different diffusion resistances. Petersen (1958) investigated bulk diffusion in pores with periodic constrictions to study the effect of a non–uniform pore cross–section on the diffusion process (Fig. 1.8). Nicholson and Petropoulos (1968) proposed a pore structural model constructed from a series of cylindrical segments with a specific statistical distribution function assigning the sizes of these segments.

Wakao and Smith (1962) suggested a more realistic pore model which accounts for the existence of micropores beside the macropores and thereby assigned a bimodal pore size distribution for the catalyst. They explained the possible diffusion paths through having a bi–disperse porous material (Fig. 1.9). Androutsopoulos (1976) developed a one–dimensional series of pores model with the diameters randomly changing along the axis of tubes in a regular and discrete manner. The author presented mathematical expressions for a series of pores model with one or different pore size distribution functions. This model is superior to the model of pores of uniform

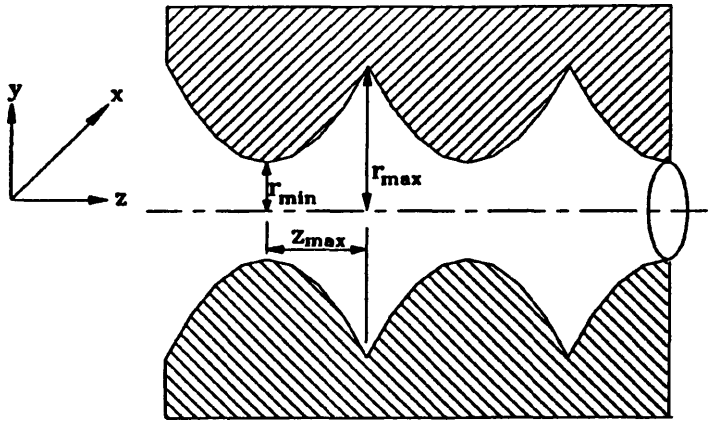

Figure 1.8 The pore model with periodic constrictions (Redrawn from Petersen (1958)).

cross–section for its ability to account for hysteresis but it is still incapable of predicting entrapment of mercury following depressurization.

Thomson (1986) in his study of a zeolite cracking catalyst deactivation used a corrugated parallel bundle model to describe the pore structure (Fig. 1.10). Pore size distribution was determined from mercury porosimetry data which was then used to assign values randomly from the distribution for the radii of each segment of pores. Smith (1986) investigated restricted diffusion through pores with periodic constrictions. A single pore comprised of unit cells containing large and small capillaries in series was used. The author demonstrated the effect of changes in the ratio of molecule size of diffusing particle to pore size on the convergence factor and hence on tortuosity.

1.4.1.1.3 Convergent–Divergent Pore Model:

This model considers the void volume within the porous solid composed of two major arrays of pores centrally convergent, and centrally divergent, respectively (Fig. 1.11). These two parallel pores are assumed to be cross mixed at specific intervals

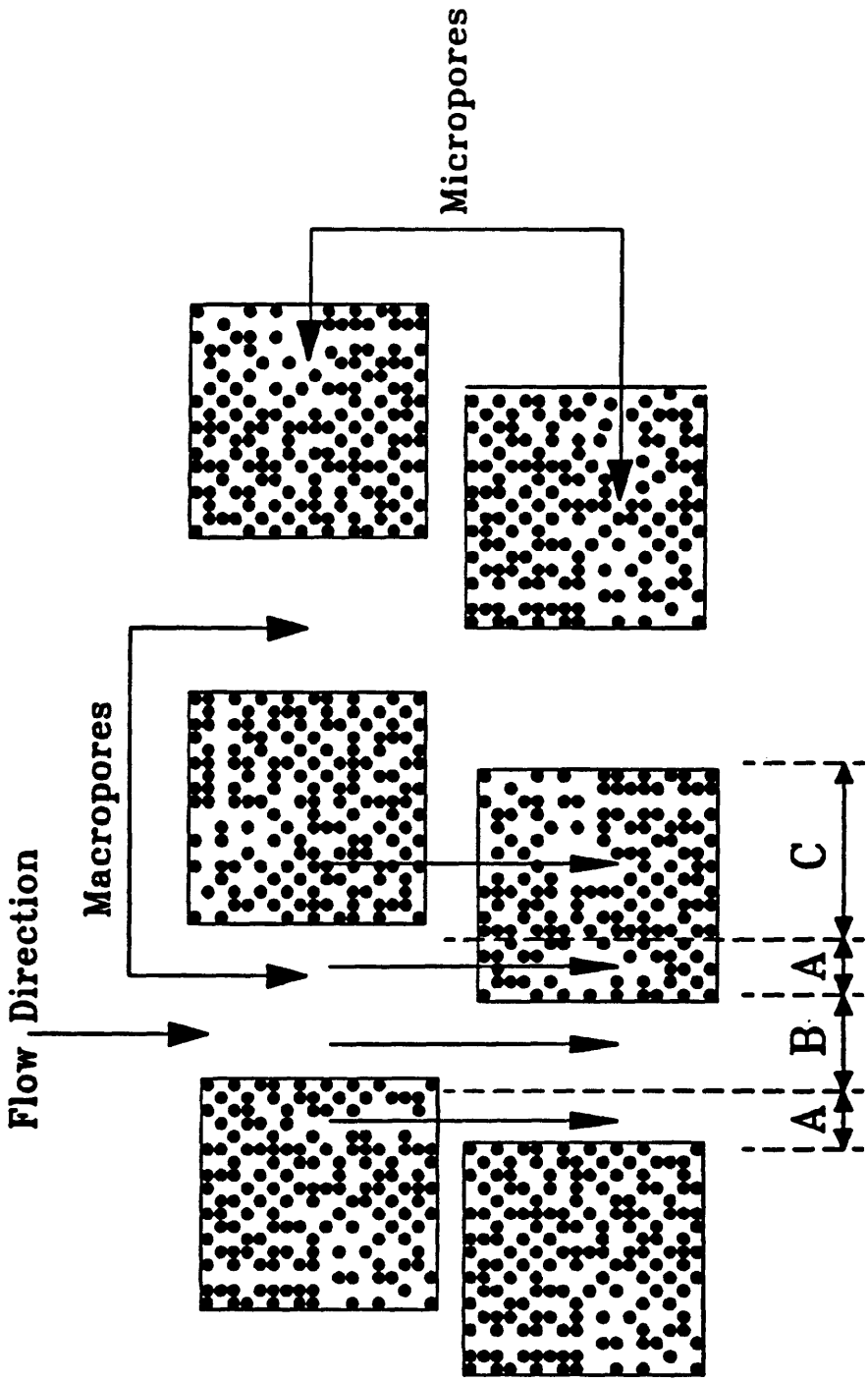

Figure 1.9: The pore model with bimodal pore size distribution [Redrawn from Wakao and Smith, 1962].

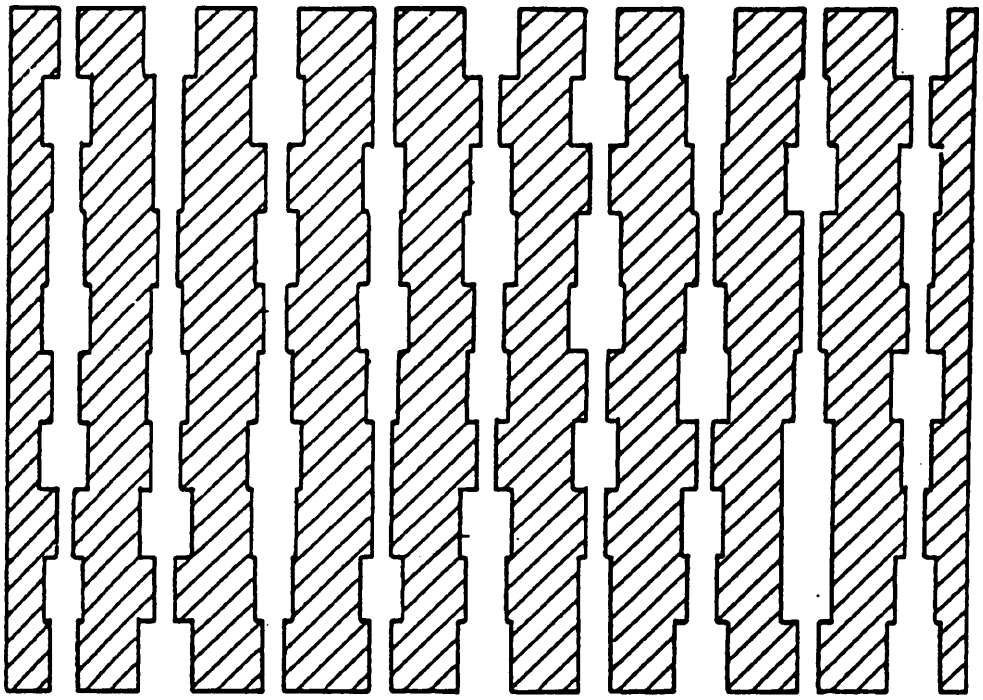

Figure 1.10 The corrugated parallel bundle pore model.

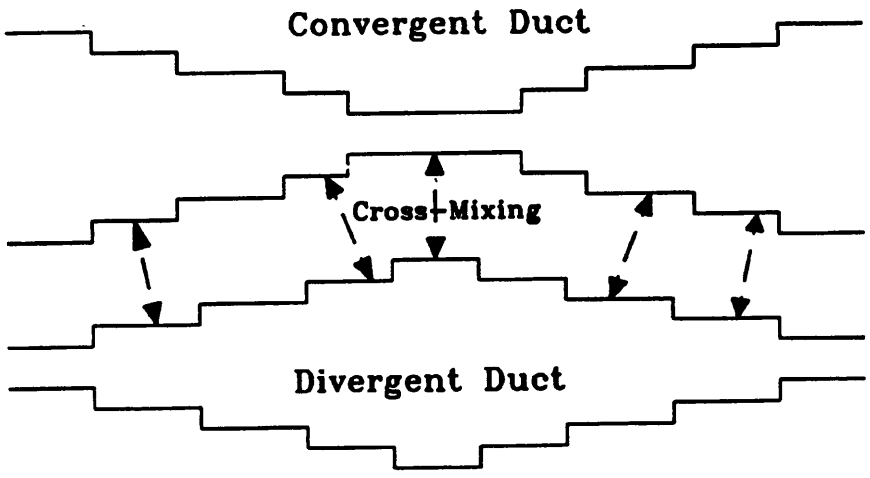

Figure 1.11 The Convergent–Divergent duct model (Redrawn from Foster & Butt (1966)).

within the array. The exact shape of these arrays is determined uniquely from volume–area distribution of the porous structure. Foster and Butt (1966) developed the convergent–divergent pore model for the evaluation of the pore structure of porous material. The cross–mixing in the model expresses the possibility of an alternative path being taken by the diffusing material around a segment of a pore having very high resistance. This model may be considered as a very simple network of pores with a virtual interconnectivity which does not have any real structural basis.

1.4.1.1.4 Dusty Gas Model:

This model considers the solid medium distributed along the surface of the pores as a set of massive molecules, among which much smaller gaseous molecules have to diffuse. This model arises from concepts closely related to the kinetic theory of gases. This model has been developed by many authors, among them are Evans et al. (1961), Mason et al. (1967), Chen and Rinker (1979), Liapis (1979) and Klavetter et al. (1982, 1984). Most recently, Horng and Liapis (1987) studied the influence of dusty–gas permeabilities on the behaviour of a parallel reaction occurring in a porous catalyst pellet. They have shown that the overall selectivity is almost independent of the viscous permeability, but selectivity decreases as the Knudsen diffusion permeability and/or the molecular permeability increases.

The dusty–gas model is popular because it contains only three adjustable parameters which can be determined from rather easy to perform experiments (Mason and Malinauskas, 1983), and though in some ways undesirably, does not make any assumptions about the geometry of the pores. The dusty–gas model predictions are claimed to provide good agreement with experimental data especially for materials with narrow pore size distribution. Chin and Rinker (1979) and Klavetter et al. (1982) have suggested certain modifications of the dusty–gas equations so that the model becomes applicable to systems with wider pore size distributions. The modified

dusty–gas model contains correction factors which account for the effects the pore size and tortuosity distributions have on the mass fluxes in heteroporous media (like corrugated parallel pores). Klavetter et al. (1984) showed that the effectiveness factors predicted by the dusty–gas model were up to 30% larger than those estimated by the modified dusty–gas model. Their results were for the special case of a diffusional transition regime of second order irreversible reactions accompanied by mole changes in a heteroporous catalyst.

1.4.1.2 Two–Dimensional Pore Structure Models:

1.4.1.2.1 Network Models:

Network models consist basically of pores which are more or less thoroughly interconnected. Fatt (1956) was the first to propose a pore system consisting of short, cylindrical tubes of differing radii distributed randomly with respect to position over a regular two–dimensional network. He characterized each network by the connectivity ie. the number of tubes to which each tube is itself connected. He concluded from his study of four different kinds of networks that the capillary pressure curve is more sensitive to changes in the tube radius distribution than to changes in the type of network. Dodd and Kiel (1959) modified Fatt's network model to allow for the entrapment of wetting fluid during the penetration capillary process. Wakao et al. (1969) used a two–dimensional model of macro and micropores and found that values of effective diffusivity for reacting systems were predicted to be smaller than those for inert systems, and they also showed that the presence of dead end pores could reduce the difference. Simson and Kelsey (1971) used network models for calculating displacement behaviour in porous media, such as petroleum reservoirs.

Wakao and Narusa (1974) studied a network of mixed micropores and macropores and calculated the concentrations at the nodes of the network. Equations

describing diffusion through the network were set using an analogy to Kirchoff's analysis of electrical networks. The node concentrations were calculated using a relaxation method. Kown and Picket (1975) visually examined photo micrographs of porous petroleum reservoir rocks, and developed their own network model. Chatzis and Dullien (1977) have also studied the properties of two– and three–dimensional network models of capillary tubes. They concluded that the properties of them are significantly different, due to the fact that bi–continua can not exist in a two dimensional network, so that they must be unsuitable for the simulation of two–phase flow phenomena.

1.4.1.2.2 Stochastic Pore Network Models:

A stochastic pore network is an interconnecting network of pores, for which each segment of the network has a radius assigned to it randomly using a suitable probability distribution (Fig. 1.12). The stochastic pore network model has been used by Mann and his co–workers to describe a number of processes in porous solids. Some of these processes were mercury porosimetry (Androutsopoulos and Mann, 1979) and (Khalaf, 1988), displacement of oil from sandstone (Ghabaee, 1986), catalyst deactivation by coking (Mann, Sharrat and Thomson, 1986), and coupled diffusion and reaction in porous catalysts (Sharrat, 1985) and (Mann and Sharrat, 1987). Androutsopoulos and Mann (1979) proposed a square network model to interpret penetration and retraction capillary pressure curves derived using the mercury porosimetry technique for pore structure and pore size distribution. The network which consisted of equal length cylindrical pore segments of differing diameters was used with a pseudo–random number generator and the Washburn equation to make predictions of mercury penetration and retraction behaviour.

1.4.1.3 Three–Dimensional Pore Structure Models:

1.4.1.3.1 Sphere Pack Models:

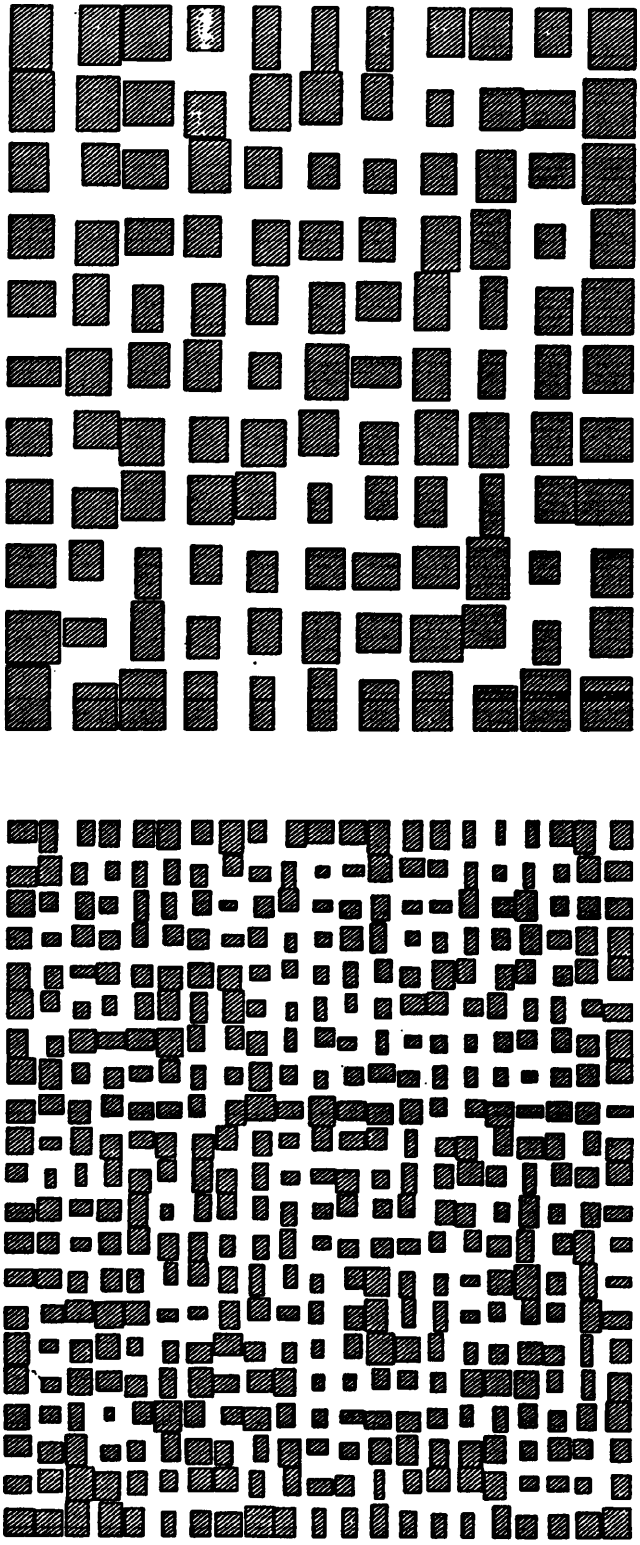

Figure 1.12 Two–dimensional stochastic pore networks with uniform pore size distribution in the range 60–3200 Angstroms.
10x10 network (top), 20x20 network (bottom).

The "random sphere pack models" consider the porous solid to be composed of large numbers of solid microspheres which are randomly overlapping. The remaining spaces between the microspheres represent the voids. The cavity centred between eight spheres forms the pore space. Each pore is connected to other pores through six throats (openings) located in the plane of four adjacent spheres. In an investigation of the subatmospheric intrusion into 0.5–1.0 mm particles, Kruyer (1958) reported the results of his studies, concluding that intrusion is determined by the size of the throats, whereas, extrusion is determined by the size of the pores. Other authors modified the analysis by relating the throat geometry to breakthrough pressure, among them are Frevel and Kressley (1963) and Mayer and Showe (1966). An investigation into the effect of different factors such as sample size, non–random heterogeneities, coordination number and pore to throat ratio of the random sphere pack models have been performed by Wardlaw and McKeller (1981) and Wardlaw (1980, 1982).

1.4.1.3.2 Three–Dimensional Network Models:

These models consist of fully interconnected cylindrical tubes. Ksenzhek (1963) used equal length pores with radii distributed randomly over the three–dimensional network. He used the model to determine the accessibility effect on the distribution of the non–wetting phase entering a porous medium. Nicholson and Petropolous (1971) have generalized the model to a variable number of tubes per junction to study gas phase processes. Dullien (1975) presented a mathematical model consisting of a set of cubic networks of arbitrary orientation with respect to the macroscopic flow direction, for predicting permeabilities of porous media. The networks consisted of capillary tubes composed of different size segments. The porosity of the sample and two pore size distributions were required by the network model for calculations of permeabilities.

Golshan (1979) developed a three–dimensional model for pressurizing and depressurizing processes. He increased the interconnectivity factor, and found that as

the interconnectivity factor increases, the network capillary pressure curve evidently approaches the bundle of tubes model which has infinite connectivity factor. Golshan also concluded that the curves for penetration and retraction for all pore structure models lie between the respective curves of the bundle of tubes model and the series pore model which has a minimum connectivity factor of two. Wall and Brown (1981) discussed the determination of pore size distribution from gas sorption and mercury penetration in three–dimensional networks. They illustrated the effect of neck shape, size and distribution on the shapes of desorption isotherms and mercury penetration. Lin and Slattery (1982) studied two phase flow through porous media using a three–dimensional cubic face–centered network. They used pore radii which were allowed to be sinusoidal functions of axial positions. Conner and Lane (1984) performed computer simulation of mercury porosimetric processes using a three–dimensional simple cubic pore/throat network model. They investigated lattice size, connectivity and pore/throat sizes and proposed helpful rules for simplifying the interpretation of capillary pressure curves.

Lapidus et al. (1985) in their study of mercury intrusion and extrusion proposed a three–dimensional cubic network consisting of pores and throats with a connectivity of six (Fig. 1.13). Each pore was randomly assigned a size according to a pore size distribution (PSD), whereas, each throat was randomly assigned a size according to a throat size distribution (TSD). They concluded that PSD, TSD and interconnectivity influenced the intrusion and extrusion curves. Reyes and Jensen (1985) used a network model with a special pore topology, a Bethe lattice, to estimate the pore space related properties in porous solids. The Bethe network representation (Fig. 1.14) of the pore space allowed an exact evaluation of effective transport coefficients for binary mixtures, and no resort has to be made to tortuosity factors. They provided a tree like branching network model for exact evaluation of the effective diffusion coefficient in porous solids. They reported that porous materials can exhibit significantly different effective diffusion coefficients, even with similar properties and pore size distribution

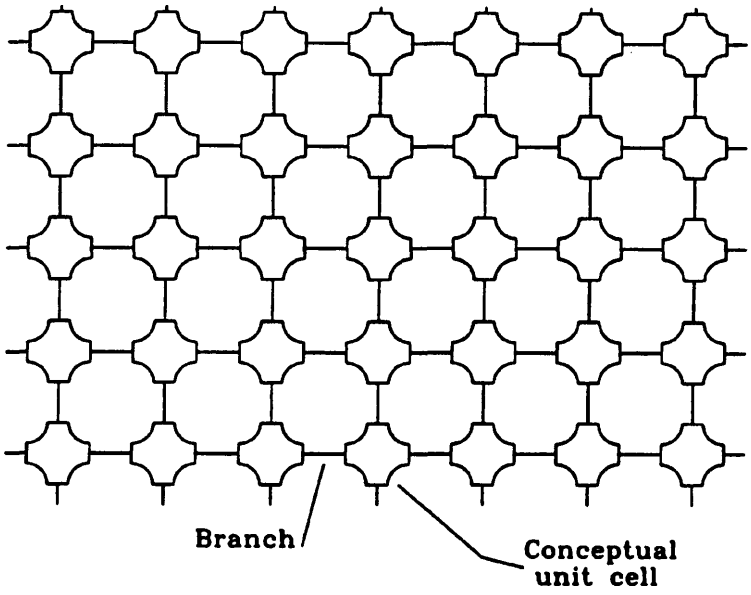

Figure 1.13 A 2–D depiction of a 3–D cubic network consisting of pores and throats (Redrawn from Lapidus et al. (1985)).

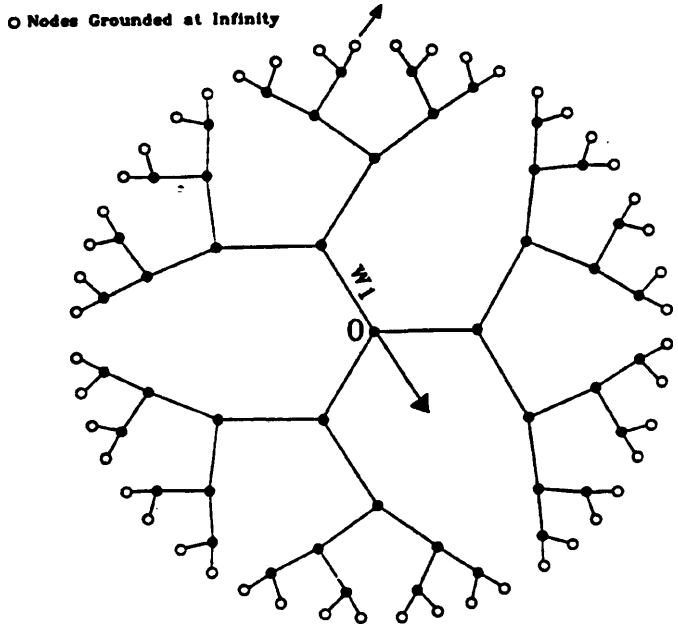

Figure 1.14 A Bethe lattice of connectivity three (Redrawn from Reyes and Jensen(1985)).

depending on the connectivity of their pore models.

Khalaf (1988) used a three–dimensional stochastic pore network to interpret porosimeter tests on fluid catalytic cracking (FCC) catalyst powder and pellets of different sizes to elucidate an improved measure of the powders internal pore structure. The elucidated pore structure was evaluated against image analysis of low melting point alloy penetration sections examined on a scanning electron microscope (SEM) (Fig. 1.15). The more realistic pore structure provided by three–dimensional stochastic network was judged to be better suited to the analysis of diffusion, reaction and coking in catalytic cracking operation.

1.4.1.4 Some Other Pore Structure Models:

1.4.1.4.1 Percolation Theory:

Percolation theory expresses the transport properties of a porous solid in terms of some simple easily measured quantities. Monhanty et al. (1982) used the accessible active surface area and the transporting porosity to modify the continuum diffusion–reaction equation. They proposed the possibility of extrapolating the activity data as a function of porosity, by selecting a proper model among those used in percolation theory. Reyes and Jensen (1985) chose the Bethe lattice as a pore structure model and justified their choice using the percolation theory. The Bethe lattice can mimic the percolation properties of many complex and realistic structures by changing its pore connectivity.

Beyne and Froment (1990) applied percolation theory to the modelling of the deactivation of zeolite catalysts by coking leading to site coverage and pore blockage.

1.4.1.4.2 Fractals:

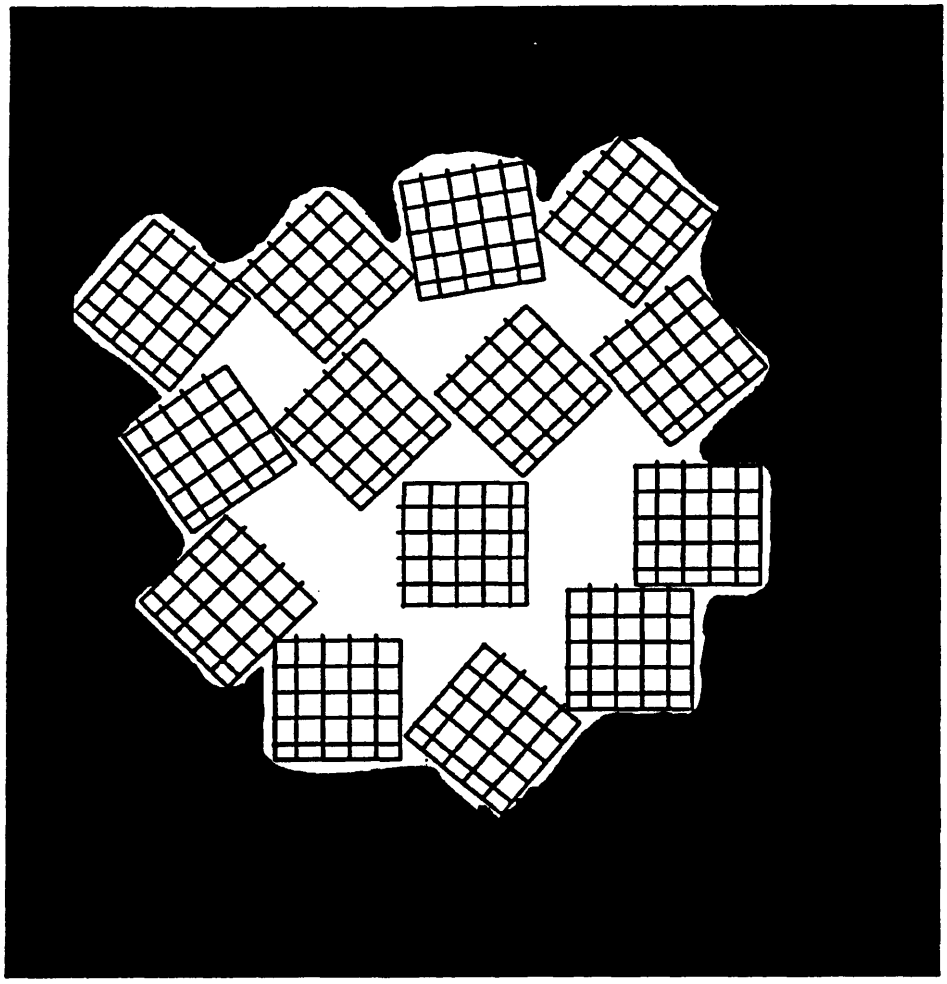

Figure 1.15 A schematic diagram of intra– and inter–particle void volume in FCC catalyst powder (Redrawn from (Khalaf, 1988)).

Mandelbrot (1977) used the term "Fractals" to describe certain special geometric structures. A typical fractal presented by Pteigen and Richter (1985) is shown in (Fig. 1.16). Fractals can be described by simple mathematics while having highly complex and irregular shapes. This property makes fractals suitable candidates for the representation of pore structures, though a predictive theory for diffusion and reaction within a fractal geometry does not yet exist (Wasilewski, 1986).

Mann and Wasilewski (1990) presented attempts to use fractally based computer graphic images to generate theoretical constructions for comparison with real scanning electron microscope (SEM) images. Their image–based approach is intended to displace those difficult and expensive laboratory tests such as porosimetry and adsorption which are conventionally applied to deduce pore structure information.

1.4.1.4.3 Volume–Averaging Techniques:

Whitaker (1967) presented a volume–averaging technique for modelling diffusion through porous solids. This technique was later developed by Ryan et al. (1980, 1981), Ochao et al. (1986) and Whitaker (1986) to model diffusion and diffusion coupled with reaction in porous solids (Fig. 1.17). The local concentration is expressed as the sum of a volume–averaged mean concentration term and a perturbation term arising from the pore structure within the averaging–volume. It is possible to simplify local perturbation terms since the length scales of pellet and individual pore spaces are so different.

1.4.1.4.4 Monte–Carlo Models:

The motion of a particle is traced as it moves through the pore structure model. The bulk transport properties can be estimated by averaging over a large number of such trajectories. Abbasi et al. (1983) simulated the motion of particles in the spaces

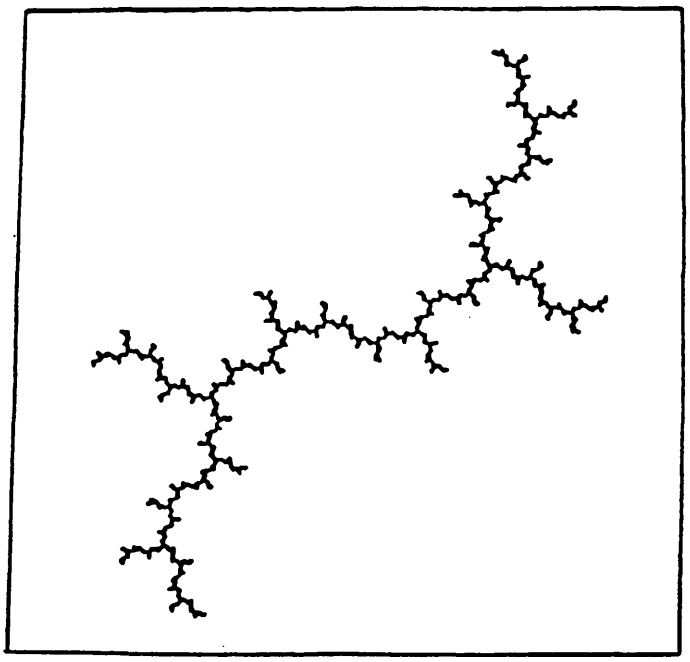

Figure 1.16 A dendritic fractal [Pteigen and Richter (1985)]

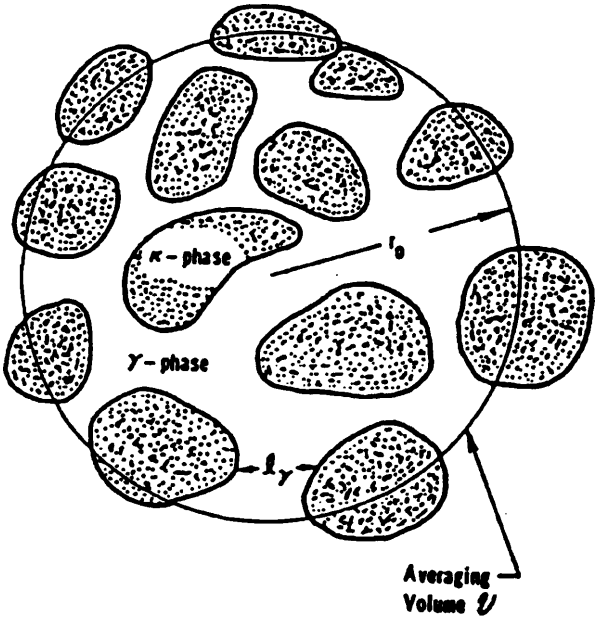

Figure 1.17 Volume–Averaging method of pore structure representation (Whitaker (1986)).

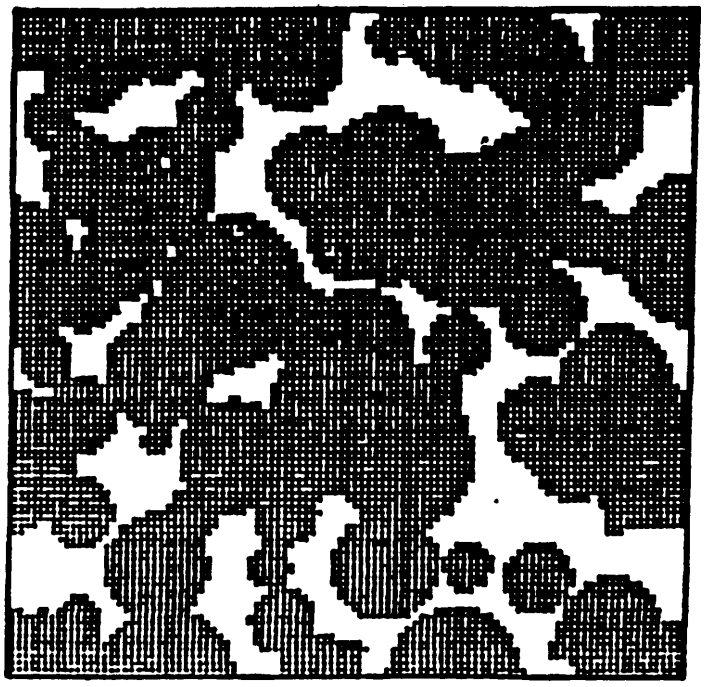

Figure 1.18 An intersection sphere model used by Abbasi et al. (1984) for Monte–Carlo modelling of diffusion.

between randomly–packed and intersecting spheres of variable size (Fig. 1.18). They considered both the Knudsen and bulk regimes. The results were correlated to express the diffusivities as functions of the mean pore diameter, the standard deviation of the pore diameter and the porosity. Smith (1986) applied the method to investigate the influence of variable pore cross–section on diffusivity in the Knudsen regime.

Beekman (1990) outlined an approach for the mathematical description of the strongly interconnected nature of the pores in heterogeneous catalysts. He presented Monte Carlo simulations in 2–D space which showed the chaotic arrangement of the pore segments, and the computed global properties were in good agreement with theoretical predictions.

1.4.2 Selecting the Proper Pore Model:

The choice of a particular pore model for a specific application can be influenced by the following factors.

(1) The usefulness of a model is proportional to the extent to which it is able to rationalize a range of experimental observations.

(2) It is important that the pore model has a significant degree of physical reality and applicability to the actual phenomenon being modelled. A parallel bundle might be suitable to represent a catalyst having pores of nearly uniform size. On the other hand, for studying the deactivation phenomenon for a catalyst that undergoes pore plugging, the parallel bundle is a poor choice and a network model might well be more appropriate.

(3) The level of information about diffusion and reaction processes which different pore models can incorporate. They do vary significantly. It is true to some extent that more detailed models for diffusion and intrinsic kinetics can often be included only by sacrificing some structural detail.

(4) The level of complexity of the model and the knowledge required for using it. A highly complex model can make the use of it very restricted and beyond the usual skills of an average engineer.

(5) The economic factor that determines whether the choice of a particular model is cost–effective or not. The data required for one model may not be required for another model. For example the dusty gas model includes three adjustable structural parameters (i.e. the voidage, the permeability and the tortuosity) which in some cases are unavailable. Also, computational requirements can be costly for some models. Percolation theory attempts to relate transport properties of a porous medium to a few simple easily measured quantities without the use of excessive computation. These qualities can make it a good candidate from an economic point of view.

1.5 MODELLING OF THE CATALYST DEACTIVATION PROCESS:

Catalyst deactivation models can be classified into three categories:

(1) Empirical models.

(2) Kinetic models which are structure–independent.

(3) Kinetic models which are structure–dependent.

1.5.1 Empirical Models:

The first significant quantitative work on coke deposition on acid catalysts was due to Voorhies (1945). He proposed from his cracking experiments on gas–oils over natural and synthetic catalysts a relationship between time on stream (t) and coke content of the catalyst (Cc). His "coke clock" expression was of the form

$$C_c = A\, t^n \qquad 0<n<1 \qquad (1.3)$$

A was a constant which is a function of the operating conditions, and n was a constant describing the coking method. Typical Voorhies plots are shown in Figure 1.19. He observed no significant effect of space velocity on coking rate. From the low temperature dependence of the rate of coking he deduced that the process was diffusion controlled. This, together with the decreasing rate of coking with time on stream led to the suggestion that it was the coke itself which caused the increasing diffusion limitation. Ruderhausen and Watson (1954), in studies on the aromatization of hexane, found similar trends to Voorhies with the contrast however that the coking had a strong temperature dependence. Eberley et al. (1966) showed that the coke laydown rate was a discernible function of space velocity, and that Voorhies correlations could then be applied over limited ranges of space velocities. Their results of the coking process of an amorphous cracking catalyst, shown in Figure 1.20, were fitted by an

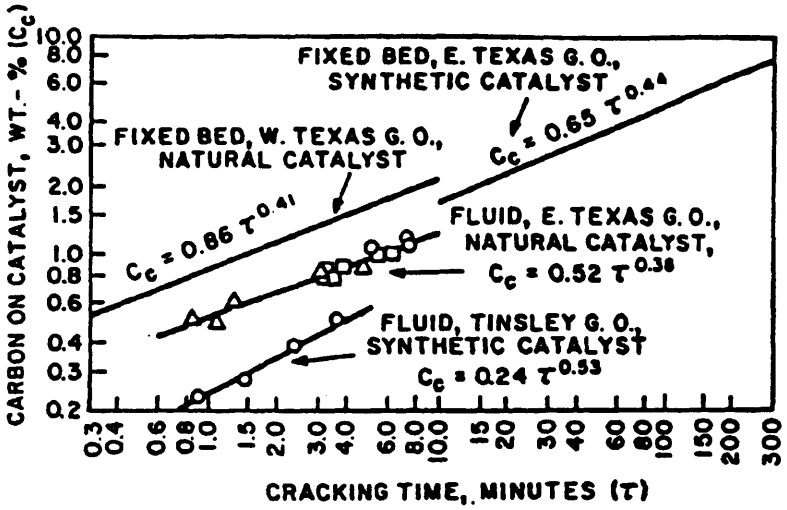

. Adaptation of original data of Voorhies for the formation of carbon on catalyst vs catalyst residence time for fixed and fluidized bed cracking catalysts. τ in the equation $C_c = A\tau^n$ averages about 0.44 for these amorphous catalysts; A ranges from about 0.2 to 0.9 for the various feedstocks. All catalysts were very well stripped, so that carbon formation represents substantially catalytic carbon alone.

Figure 1.19 Voorhies plots (Venuto and Habib (1979)).

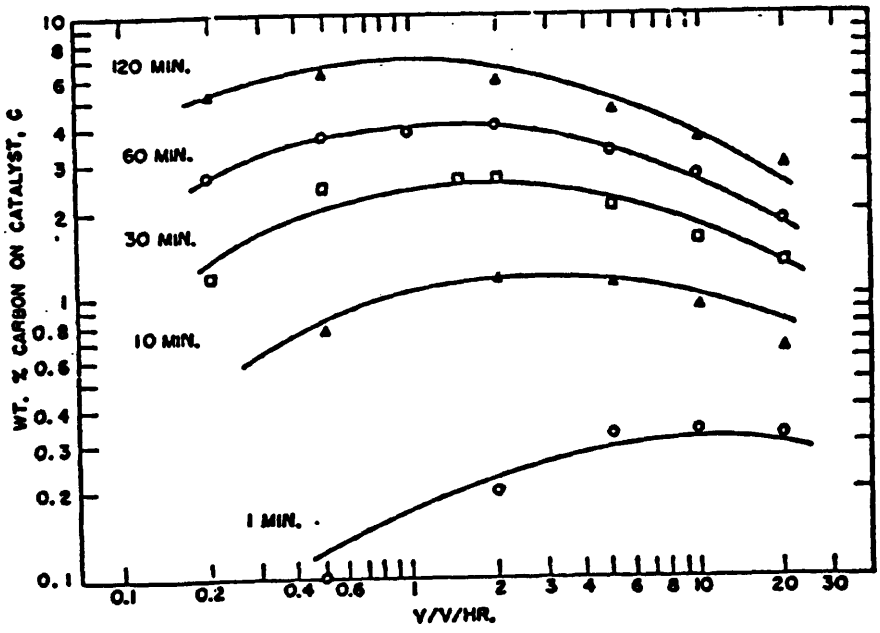

Figure 1.20 Carbon formation from the cracking of n–hexadecane at 500°C (Eberly et al. (1966)).

equation of the form:

$$\text{Log}_{10} C = -0.2666\ \text{Log}_{10}^2(V/V/hr) + (0.5485 - 0.2666\ \text{Log}_{10} t)\ \text{Log}_{10}(V/V/hr) + 0.7838\ \text{Log}_{10} t - 0.7958 \quad (1.4)$$

where

C :is the weight percent carbon on catalyst

(V/V/hr) :is the space velocity, and

t :is the catalyst residence time (minutes).

Ozawa and Bischoff (1968), studying the fouling of a silica–alumina catalyst during ethylene cracking, investigated the relationship between conversion and time on stream, (Fig. 1.21). They noted two distinct regions, an initial rapid coking ($t<10$ minutes) followed by a slower, long term deactivation. Ruderhausen (1954) had earlier observed similar conversion–time behaviour. Nace et al. (1971) studied the deactivation of zeolite catalysts, and produced Voorhies correlations with average values of n much lower than those previously found by Voorhies (0.21 opposed to 0.41). They concluded that the coking method in the zeolite was different from that in the amorphous catalyst used earlier by Voorhies. Modelling cumene disproportionation over a commercial hydro–cracking catalyst, Absil et al. (1984) used a modified Voorhies type correlation to relate conversion (X) and time on stream (t):

$$X = A \exp(-k\ t^{0.5}) \quad (1.5)$$

where

A :is equal to the initial conversion.

Paloumbis and Petersen (1982) proposed an expression for coke content (C_c) in the steam reforming catalyst of the form:

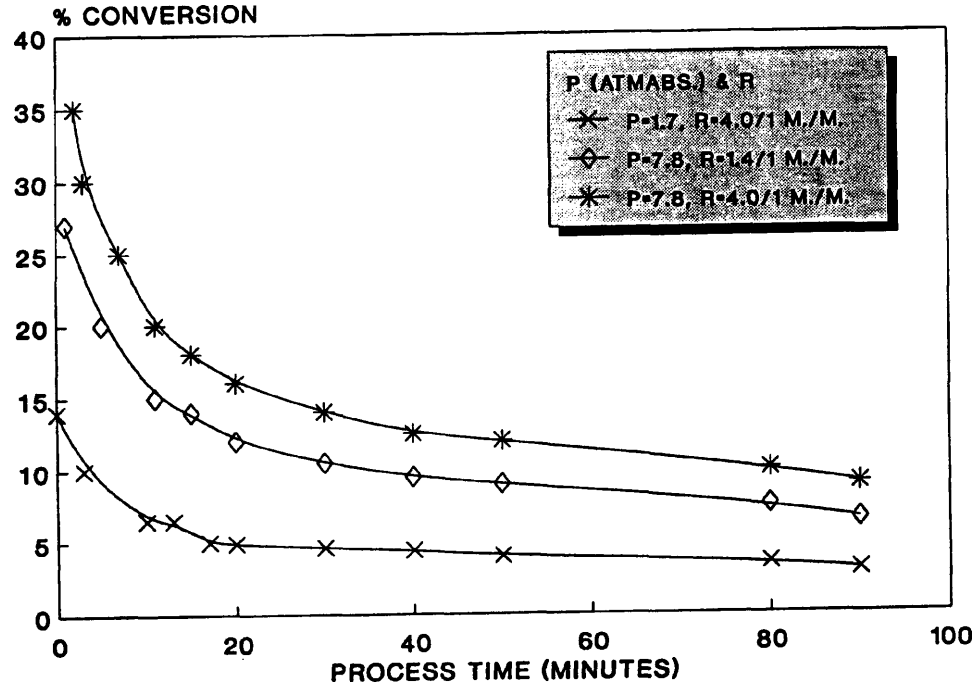

Figure 1.21 The conversion of ethylene as a function of time on stream (Reproduced from Ozawa and Bischoff (1968)).

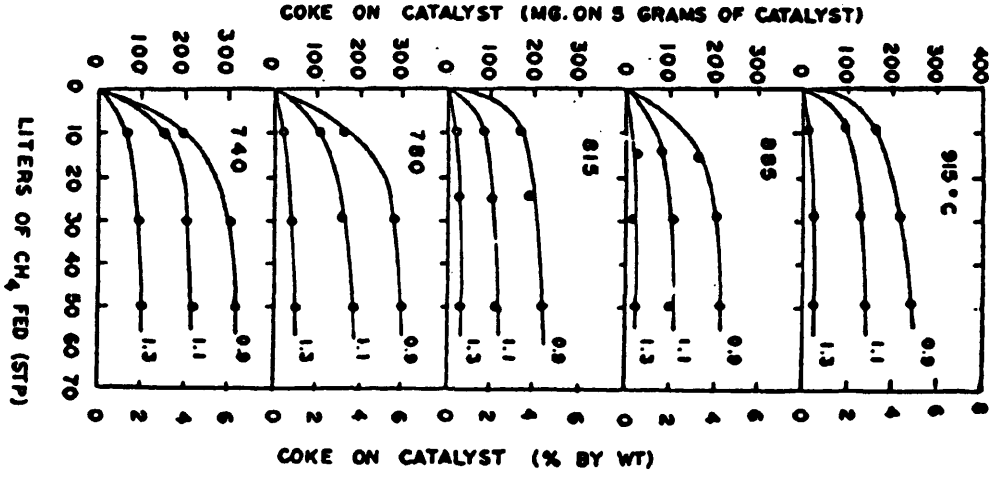

Figure 1.22 Coke content of steam reforming catalyst. The parameter is steam/methane ratio (Paloumbis & Petersen (1982)).

$$C_c = A\, F^{1/3} \qquad (1.6)$$

where

F :is the feed flow rate, and

A :is a temperature–dependent coefficient.

Their experimental results are presented in Figure 1.22. Pozzi and Rase (1958) described a declining catalyst activity by an equation of the from:

$$\frac{X_\tau}{X_0} = \frac{X_a}{X_0} + \frac{1 - (X_a/X_0)}{1 + M\tau} \qquad (1.7)$$

where

τ :is reaction time,

X_τ :is fractional conversion at the reaction time τ,

X_0 :is initial fractional conversion,

X_a :is fractional conversion after infinite time on stream, and

M :is a function of catalyst surface properties and the partial pressure of a given component.

Due to the quantity of data required to obtain the best fit parameters, their model has little research value but its use is seen in reactor design and operation. In the case of coking of a Ni catalyst, Rostrup–Nielsen (1974) found that there was an "induction period" where very little coke was deposited on the catalyst. After this induction period, the rate of coking increased until it reached some constant value. It was quite reasonably concluded from this work that there are fundamental differences between coking behaviour on Ni and cracking catalyst. Some empirical correlations have been presented in the form of monographs. The American oil industry makes extensive use of these monographs to predict deactivation characteristics. Castiglioni (1983) presented a monograph dealing with yields and amount of coke obtained from riser cracker units based on process conditions.

The primary limitations of these empirical correlations is that they can not be generalized. Their application is limited to the particular reaction condition that existed during their experimentation. Another disadvantage of the use of empirical models is that they do not provide any information whatsoever on the basic mechanisms of deactivation.

1.5.2 Kinetic Models Which are Structure–Independent:

Many authors have used a kinetic approach in their work and they have found that the derived models can be made to closely fit the reaction and deactivation mechanisms under investigation. In all cases, the definition of an activity factor is of prime importance and there is some disagreement as to the basis upon which this should be defined. Most workers used time as the independent variable as it is most easily measured and directly useful for design purposes. Other workers have presented activity decline as a function of coke on catalyst or as a function of availability of reaction sites.

1.5.2.1 Time–on–Stream Theory:

Khang and Levenspiel (1973) put forward a number of n^{th} order rate forms to present deactivating catalyst pellets based on the different possible mechanisms of deactivation. They investigated the effect of diffusional resistances on the deactivating catalyst and showed two distinct limiting cases of activity decay, namely, shell model and core model deactivation. In the case of strong diffusional resistances, reaction and deactivation by a parallel or side–by–side mechanism occurs only on the outer layers of the catalyst pellet. As time on stream increases, the poison moves inside the pellet producing a shell progressive type of deactivation. In the case of strong pore resistances with a series deactivation reaction, the poison concentrates in the centre of the pellet. As time on stream increases, the poison moves outwards producing a core type of

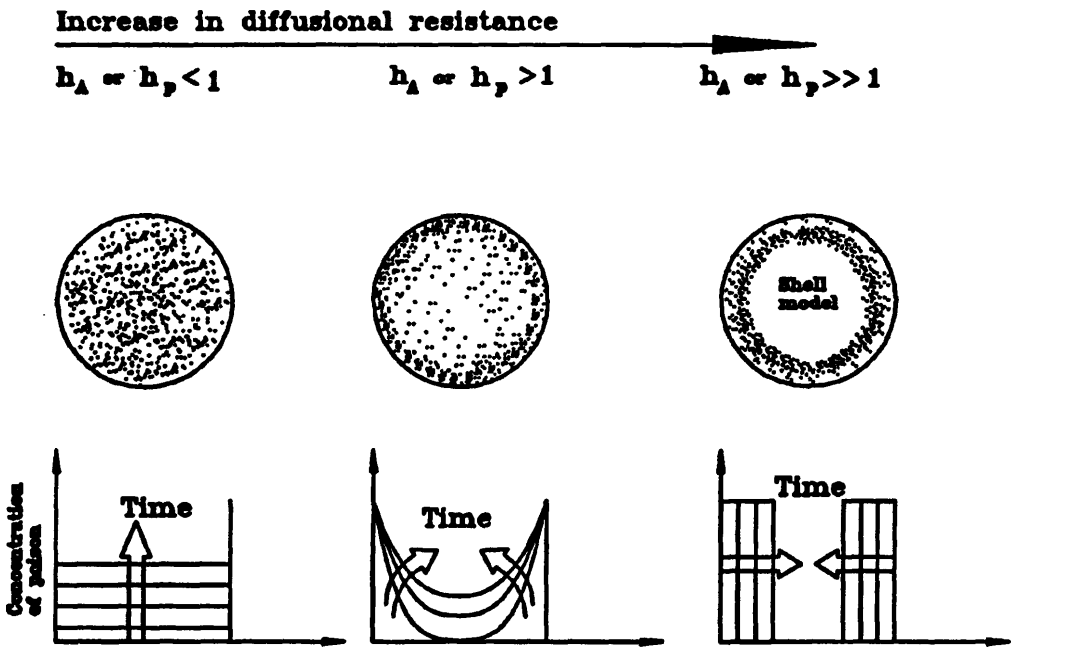

Resistance to pore diffusion determines where the poison deposits; for parallel or side-by-side deactivation

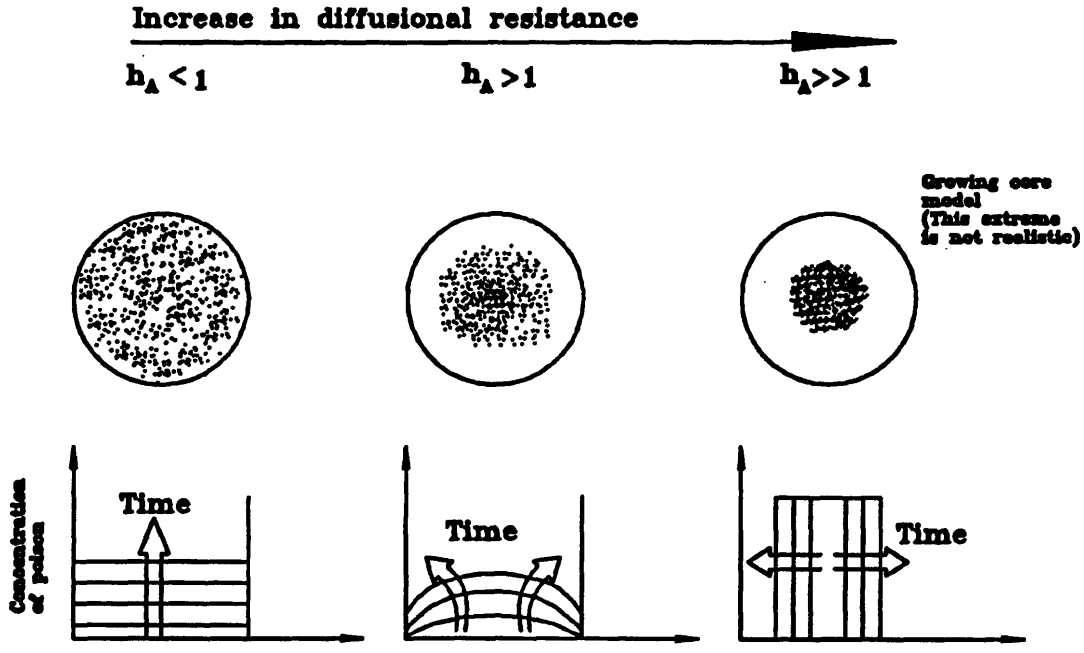

Resistance to pore diffusion determines where the poison deposits; for series deactivation

Figure 1.23 Location of poison deposits is influenced by the diffusional effects and by the type of decay reaction (Redrawn from Khang & Levenspiel (1973)).

deactivation (Fig. 1.23). The power law expression for the activity coefficient (a) which has been reported in many models takes the form:

$$\frac{da}{dt} = -k\, a^{d} \qquad (1.8)$$

where

a :is activity coefficient, which is a method of describing the changes caused by deactivation,

t :is time on stream,

k :is a function dependent on process and surface conditions, and

d :is a constant.

Khang and Levenspiel (1973) reported that the value of d was dependent on the level of the Thiele modulus, and that most of the deactivation data can be modelled using values in the range 3>d>0. Corella and Asua (1981) produced a comprehensive review of the power law expressions used by various authors in the modelling of the deactivation process. Viner and Wojciechowski (1982) used a more complicated expression in their time–on–stream theory of deactivation which took the form:

$$\Theta = \{1 + (m-1)\, kt\}^{-1/(m-1)} \qquad (1.9)$$

where

Θ :is fraction of active sites remaining

m :is the number of active sites removed per deactivation step ($m \neq 1$)

t :is the time on stream of the catalyst, and

k :is a constant.

The dehydrogenation of methyl cyclohexane was modelled by Pacheco and Petersen (1984) using the expression

$$a(t) = (1 + kt)^{n/(m-1)} \qquad (1.10)$$

where

n :is the order of the main reaction, and

m :is the order of the fouling reaction.

They found values of 0.2 to 0.5 required for the group (n/(m–1)) to model the observed deactivation behaviour. They proposed that in the case of variable reaction order, several competing parallel coking reactions are taking place simultaneously. Each coking reaction required different numbers of active sites.

Gendy and Pratt (1982) in their model of the deactivation of H–Y zeolite used in xylene isomerisation, investigated the following four expressions:

$$B_i = Bo_i(1-\alpha_i t) \qquad \text{Linear} \qquad (1.11)$$

$$B_i = Bo_i\, e^{-\alpha_i t} \qquad \text{Exponential} \qquad (1.12)$$

$$B_i = \bar{B}o_i\, t^{-\alpha_i} \qquad \text{Powerlaw} \qquad (1.13)$$

$$B_i = Bo_i\, t^{-\alpha_i(t/\tau)} \qquad (1.14)$$

where

B_i :reaction rate constant at time t (kmol/kg cat/s),

Bo_i :reaction rate constant at t=0,

$\bar{B}o_i$:reaction rate constant at t=1 hr,

α :decay velocity constant, hr^{-1}

t :time on stream, hr, and

τ :space time kg. hr/kmol.

They found that the power law decay function best fitted the vapour phase deactivation behaviour of the rate constant, whereas the exponential equation (1.11) best fitted the liquid phase deactivation behaviour.

Correla and Asua (1980) proposed a kinetic model with a parallel deactivation mechanism, with an activity factor defined as follow:

$$a = \exp \int_0^t -\frac{k_d \; k_A^* \; P_A^{n+1}}{1 + (k_A + k_A^*) \; P_A + k_R \; D_R} \qquad (1.15)$$

where

t	:is time in minutes
k_d	:is deactivation rate constant
k_A, k_A^*, k_R	:are equilibrium adsorption constants, and,
P_A, P_R	:is partial pressure, atm.

They found that a value n=1 in the activity equation gave a model fit for the experimental data of the catalytic hydrogenation of benzyl alcohol.

We see from these previous examples, that a "time–on–stream theory" can represent the catalyst deactivation, but some authors have very reasonably expressed reservations. Hatcher (1985) discounted the theory as an accurate method of modelling deactivation during the disproportionation of cumene. It was noted that in a tubular reactor, coke profiles were produced along the axial coordinate of the reactor; a phenomenon that the "time–on–stream theory" could never predict.

Abbot and Wojciechowski (1988) investigated the chain length effect on the kinetics and selectivity of reactions of 1–alkenes on H–Y zeolite. The kinetics of these processes have been fitted by a Langmuir model for adsorption, and time–on–stream theory to account for the associated catalyst decay. It was found that rate constants for both skeletal isomerisation and cracking increased with chain length of the feed alkene (Fig. 1.24).

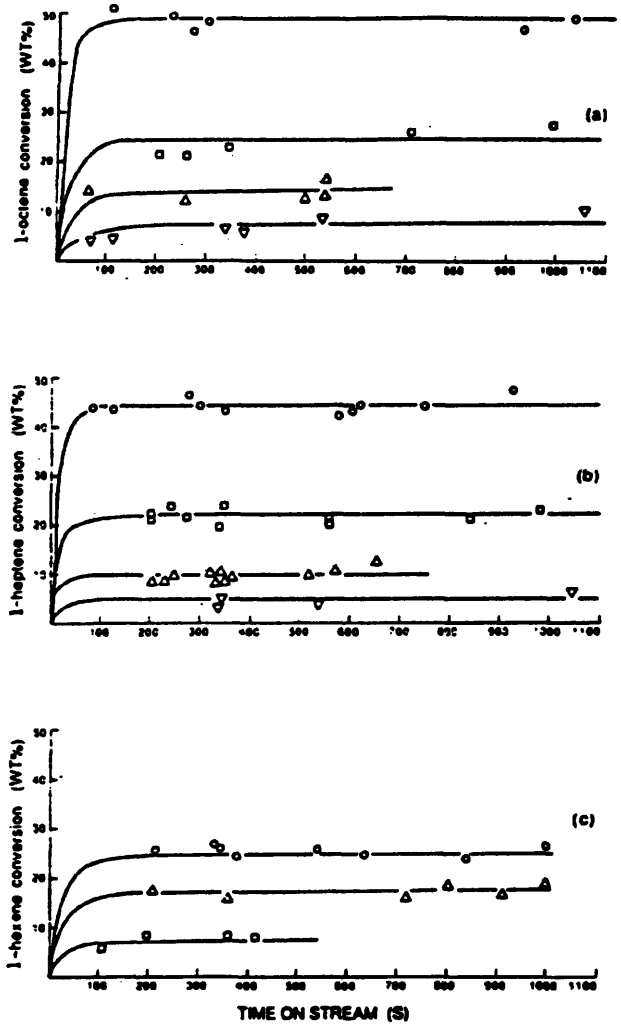

— Theoretical curves and experimental points for cumulative conversion of 1-alkenes on HY zeolite at 400°C. A) 1-octene, catalyst-to-reactant ratios: o : 0.0402, □ : 0.0134, Δ: 0.0068; ▽ : 0.0034. B) 1-heptene, catalyst-to-reactant ratios: o : 0.1077, □ : 0.0370, Δ: 0.0142, ▽ : 0.0072. C) 1-hexene, catalyst-to-reactant ratios: o : 0.0522, Δ: 0.0344; □ : 0.0140.

Figure 1.24 The chain length effect on the conversion of 1–alkenes on H–Y zeolite as a function of catalyst/reactant ratio (Abbot & Wojciechowski (1988)).

1.5.2.2 Activity Based on Coke Content:

In a study of the non–steady state behaviour of a fixed bed catalytic reactor with catalyst deactivation due to coking, Froment and Bischoff (1961, 1962) suggested that the activity function ϕ should be expressed as a function of the carbon content of the catalyst instead of time–on–stream. In these papers and in further investigations by Dumez and Froment (1976) they used activity coefficients, ϕ, relating the variable rate coefficients to the carbon content of the catalyst,

$$k = k^{\circ}\,\phi \qquad (1.16)$$

where k° is rate coefficient at zero coke content. The activity function (ϕ) has taken the following forms:

$\phi = \exp(-\alpha C_c)$	exponential	(1.17)
$\phi = (1 - \alpha C_c)$	linear	(1.18)
$\phi = (1 - \alpha C_c)^2$	power law	(1.19)
$\phi = 1/(1 + \alpha C_c)$	hyperbolic	(1.20)
$\phi = 1/(1 + \alpha C_c)^2$	hyperbolic	(1.21)

where C_c is the carbon content of the catalyst.

The case of cumene cracking over a lanthanum exchanged Y–zeolite catalyst has been investigated by Lin and Hatcher (1982). They applied the Froment–Bischoff approach to model the deactivation behaviour of the cracking catalyst. Using similar activity functions for the main and fouling reactions, they demonstrated that a combined kinetic mechanism of deactivation could be the cause of catalyst decay (Fig. 1.25). Nam and Kittrell (1984) joined the "time–on–stream" model and "coke content" model using an active site balance to produce the following equation relating activity to time–on–stream:

$$\ln a(t) = -\lambda t \qquad (1.22)$$

where λ is a function of reactant and products partial pressures. They used this activity function, a, to produce an expression for coke content of the catalyst (q):

$$q = \alpha_1 (1 - a) + \alpha_2 \ln (a) \qquad (1.23)$$

where α_1 and α_2 are functions of initial active site concentration and reactant and products partial pressures. They used the above expressions to simulate experimental deactivation data of systems modelled by Froment's activity functions (Fig. 1.26).

1.5.2.3 Activity Based on Active Sites Loss:

Polinski et al. (1981) have used an expression defining a catalyst activity factor based on the fraction of active sites available for a reaction. They expressed the reaction rate constant for the catalyst undergoing deactivation, k_d, as follows:

$$k_d = k_o (1 - \alpha) \qquad (1.24)$$

where

k_o :is reaction rate constant of the fresh catalyst, and

α :is the fraction of active sites poisoned.

Using this model, they concluded from their studies that larger diameter pellets may have longer life. Angelli et al. (1982) used a similar activity function, Θ, defined as:

$$\Theta = \frac{\alpha_0 - \alpha_p}{\alpha_0} \qquad (1.25)$$

where

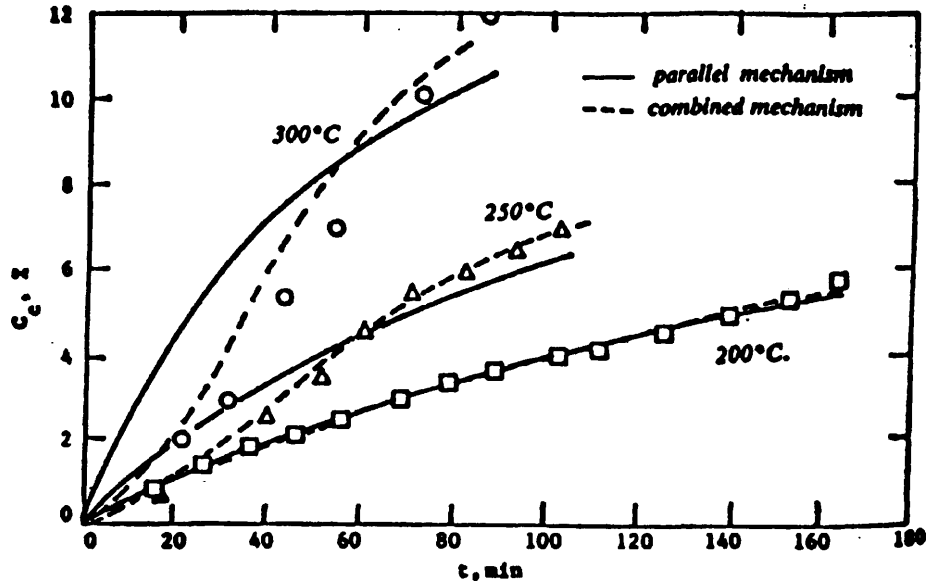

Figure 1.25 Carbon content vs. time on stream for coking reaction (Lin & Hatcher (1982)).

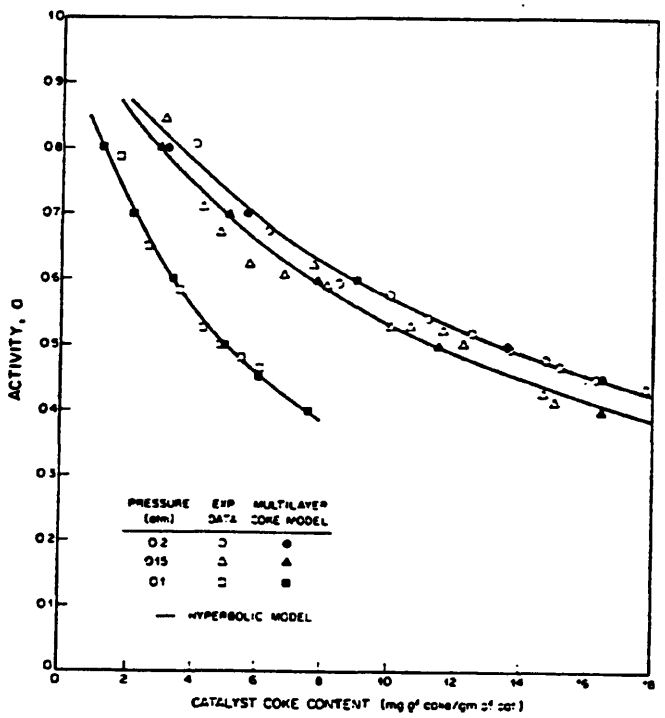

Figure 1.26 Hyperbolic relationship of catalyst activity to coke content (Nam & Kittrell (1984)).

α_0 :is the initial active surface, and

α_p :is the poisoned surface.

This model was successful in describing a flow reactor which was to distinguish the poisoning mechanism and its kinetics.

Bharati and Bhatia (1987) studied the kinetics and mechanism of deactivation by coking of a hydrogen mordenite catalyst for the disproportionation of toluene along with the kinetics of the main reaction. They used an activity function given by:

$$\alpha = \left[\frac{L - C_{\rho 1}}{L} \right]^m \qquad (1.26)$$

where

L :is the total concentration of active sites,

$C_{\rho 1}$:is the concentration of active sites covered by coke, and

m :is number of active sites involved in the controlling step of the main reaction.

The deactivation kinetic equation was represented by a heterogeneous model incorporating coke formation by a parallel reaction scheme.

Corella et al. (1988) studied some intrinsic kinetic equations and deactivation mechanisms, leading to deactivation curves with residual activity. They used equations which account for the number of active sites involved in the controlling step of the main and deactivation reactions.

A common weakness among all the kinetic and empirical models discussed so far is that they have not taken into account the important role of interaction of the catalyst pore structure and the deactivation process.

1.5.3 Kinetic Models Which are Structure–Dependent:

A number of models have been proposed which incorporate a representation of the pore structure. Wheeler (1951) studied a reaction inside a cylindrical pore undergoing poisoning at the mouth. Newson (1975) used a parallel bundle representation of the desulphurization catalyst pore structure undergoing deactivation by metals and coke deposition.

The foulants being deposited in small increments, gradually reduce both the pore mouth radii and catalytic activity. Beekman and Froment (1980, 1982) and Froment (1980) studied deactivation by both site coverage and pore plugging. Probability theory was used to predict deactivation functions for the main and coking reactions. They predicted coke profiles and concentration profiles within catalyst particles. Figure 1.27 illustrates how the coke profiles, represented by degree of site coverage, build up within a catalyst pore with increased time–on–stream for both parallel and series (consecutive) coking. A more fundamental approach to the problem of pore plugging was offered by Mann and his co–workers (Hughes and Mann (1978); El–Kady and Mann (1981, 1982); Moore (1983); Mann, El–Kady and Moore (1984) and Thomson (1984)). They have considered the geometry of the foulant and its interaction with the pore structure.

Parallel bundles represent the pore structure and coke deposited in wedges at the pore mouth leading to loss in surface area and catalytic activity. The geometry of these wedges was characterized by a shape factor, β, defined as follows:

$$\beta = \frac{\text{height of coke layer at the pore mouth}}{\text{depth of coke layer into the pore}}$$

Tsakalis et al. (1984) used a parallel bundle pore model in their analysis of deactivation by active site poisoning and pore plugging for catalytic coal liquefaction.

Hughes and Mann (1978) suggested that plugging was the major cause of the deactivation of a hydrodesulphurisation (HDS) catalyst. Mann et al. (1984) improved the model to include diffusion and reaction in a zeolitic catalyst where both the support and zeolite were active. Mann and Thomson (1987) extended the model to allow for different deactivation rates for the support and zeolite (Fig. 1.27). Mann et al. (1985) investigated the effect of pore structure and fouling on the selectivity in consecutive reactions. A more realistic catalyst pore structure model, the square network, which accounts for interconnectivity was then used by Sharrat (1985) and Mann et al. (1986). They adopted a method of random deposition of coke units. In this way they simulated the deactivation in a supported zeolitic catalyst.

Prasad and Valdyeswaran (1986) modelled the transient deactivation process taking into account pore size reduction due to coke deposition and the consequent changes in voidage and Knudsen diffusivity. They considered the case of a triangular reaction network taking place in an isothermal catalyst slab having uniform cylindrical Knudsen pores. It was shown that η the "instantaneous effectiveness factor" passes through a minimum value at a time that is characteristic of the system and operating conditions (Fig. 1.28). This is the time for which it is most beneficial to operate the reactor in question.

Shimura et al. (1986) in their modelling of the deactivation in hydrotreating catalyst due to coke and metal sulphides, used a parallel bundle pore structure. They divided the pore into elements and calculated the change in the radius of each element as a function of time–on–stream. They investigated the effect of pore structure on the reaction and defined optimal structures that maximise either catalyst life or initial activity. Chang and Crynes (1986) studied the relationship between pellet and pore sizes and the catalytic activity for the case of active site coverage and pore mouth reduction arising from a parallel deactivation mechanism. They concluded somewhat obviously that diffusional limitations can be reduced by increasing pore radius and

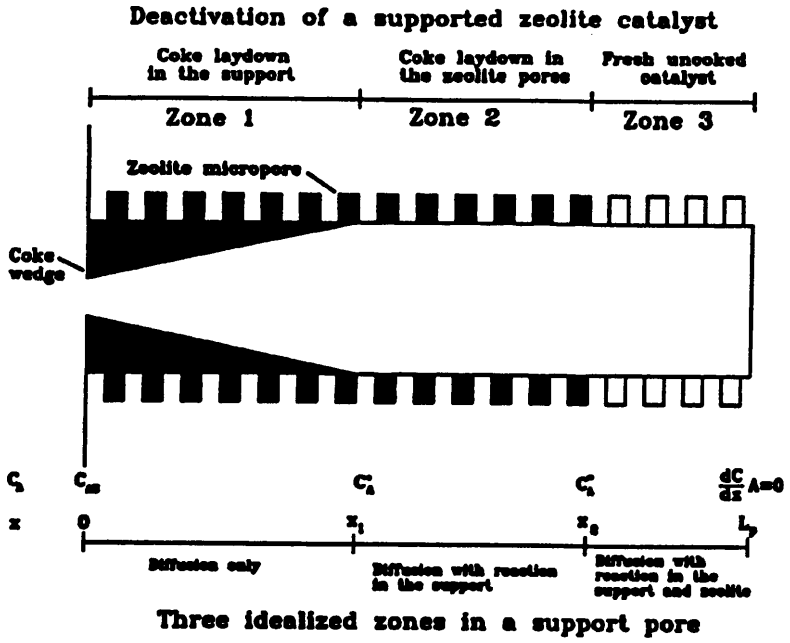

Figure 1.27 Wedge layering model (Redrawn from Mann and Thomson (1987)).

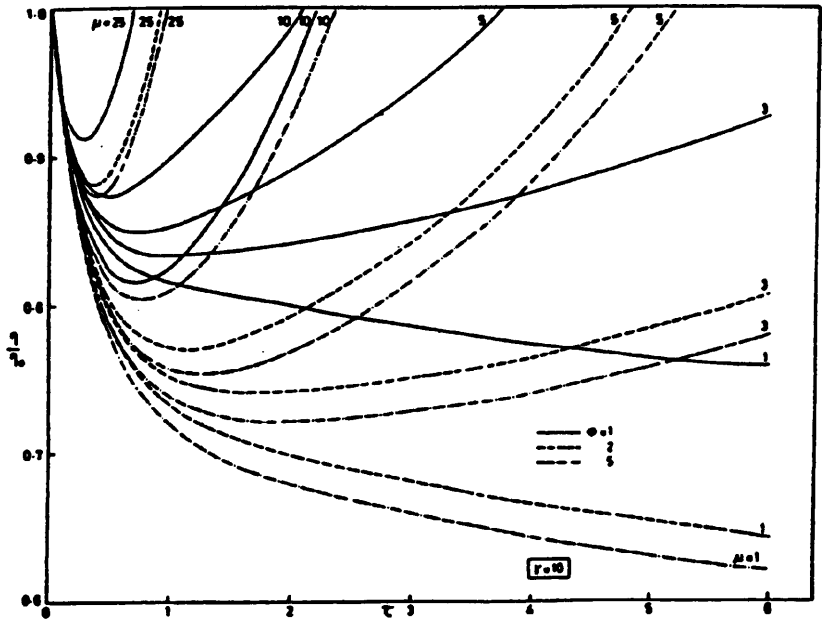

Figure 1.28 Relative effectiveness factor passing through a minimum value at a time that is characteristic of the system and operating conditions (Prasad & Valdyeswaran (1986)).

reducing pellet size.

Chang and Perlmutter (1987) have also developed a mathematical model based on the interaction between catalyst pore structure and coke distribution in the pores. The model is able to associate overall regeneration kinetics with alternative pore–distributed coke deposition patterns. They represented the catalyst support by a parallel bundle of non–intersecting pores each with circular cross section but not necessarily a cylinder. The model makes coke distribution in the pores accessible to experimental determination.

The modelling of catalyst deactivation using a pore structural approach in recent years has produced some valuable insights leading to further improvements of those models presented to explain the process of catalyst decay. These models have the advantage of easily representing blocking phenomena. They are also readily related to commonly used measures of structural changes such as porosimetry and gas–adsorption pore size measurements. One possible disadvantage of the more structural based approaches is their computer time requirements.

1.6 FLUID CATALYTIC CRACKING PROCESS:

Fluid catalytic cracking (FCC), the largest catalytic process in the world, is at the heart of a modern refinery oriented toward maximum gasoline production. The early pioneering work was carried out by Eugene Houdry (Oblad, 1983). Modern FCC was conceived at EXXON and commercially developed in about 1940 (Janig et al., 1983) using amorphous catalysts. Fluid catalysts are usually very small spherical particles ranging from 40 to 150 μm in diameter with acid sites capable of cracking large petroleum molecules to products boiling in the gasoline range (Heinemann and Somorjai, 1984). One advantage of the FCC process is the absence of diffusion limitations present in conventional gas oil cracking due to the very small size of the

catalyst particles. Since 1964 virtually all catalysts contain faujasite, a stable, large pore, Y–type zeolite dispersed in a silica/alumina matrix (Plank, 1983). Numerous designs of FCC units have appeared in the recent literature. A typical modern FCC complex is shown in Figure 1.29. One of the most important characteristics of zeolite–containing FCC catalysts is their susceptibility to loss in activity and selectivity as coke on catalyst increases (Venuto and Habib, 1979). In this regard, zeolites, in short contact time riser operation, appear to be more markedly affected by residual catalyst carbon level than conventional amorphous materials. For this reason there has been a driving force for more efficient regeneration, with levels in the range of 0.1 to 0.25wt% carbon on regenerated catalyst commonly cited as desirable (Aulund, 1976). In the case of a riser reactor the FCC catalyst deactivates through coking in just a few seconds, whereas for a fluidized bed reactor the coking process occurs over a long time. Figure 1.30 shows the reaction section of a fluidized bed cracking unit (Decroocq, 1984).

The modelling of catalyst deactivation using a pore structural approach in recent years has produced some very interesting and valuable results leading to further improvements in those models derived to tackle the complex process of catalyst decay. From this platform of knowledge it is hoped that this work and future work in this field of research will lead to the development of a more comprehensive model of catalyst deactivation and ultimately to the better a priori design of enhanced 'pore architectures' capable of inhibiting the activity decay consequences of coking and simultaneously maximising the productivity achieved over the 'life cycle' of the catalyst.

Our study of long term deactivation behaviour of FCC catalyst can provide us with useful information on how the coking process proceeds in the reactor part of the modern FCC process even though it can't inform us about the riser part. Also, it should provide important information about the structure of the catalyst and its

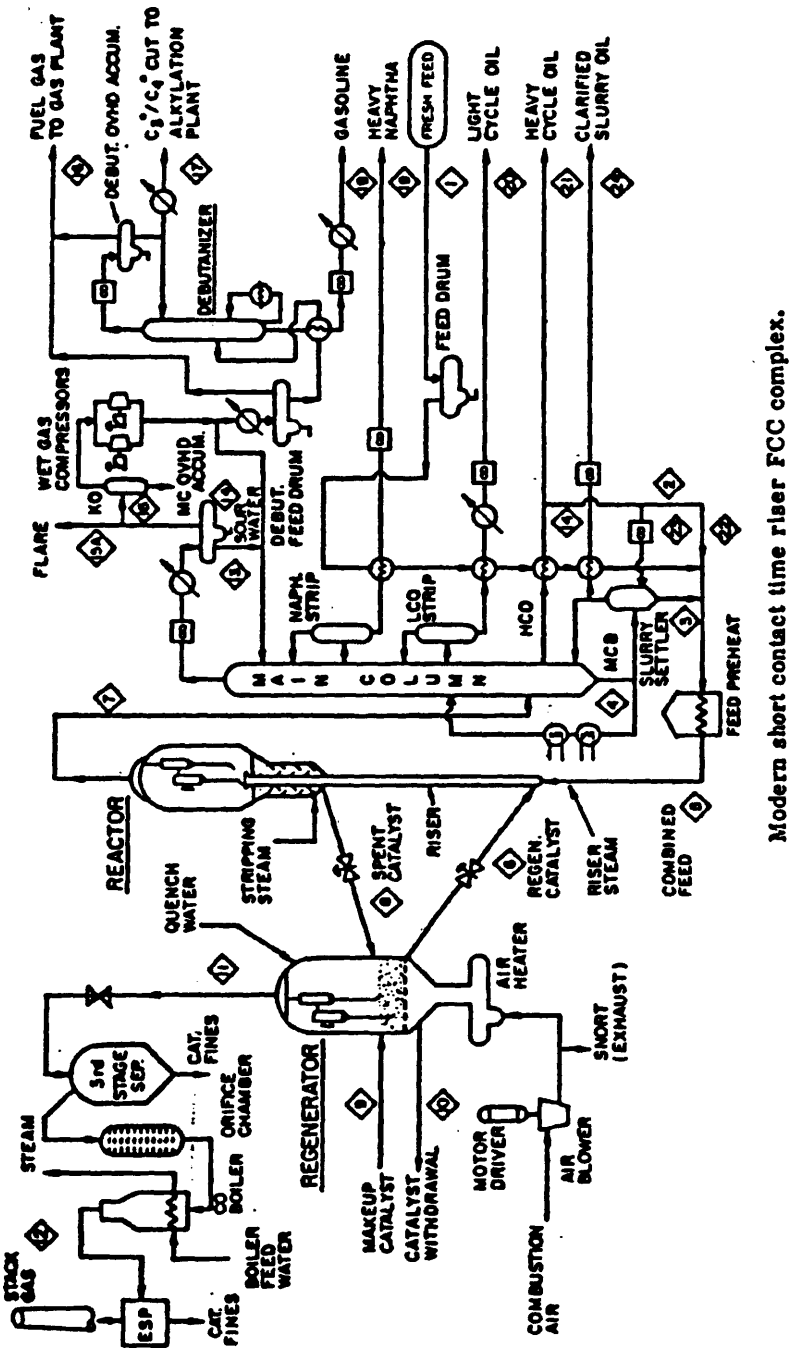

Modern short contact time riser FCC complex.

Figure 1.29 Modern short contact time riser FCC Complex (Venuto & Habib (1979)).

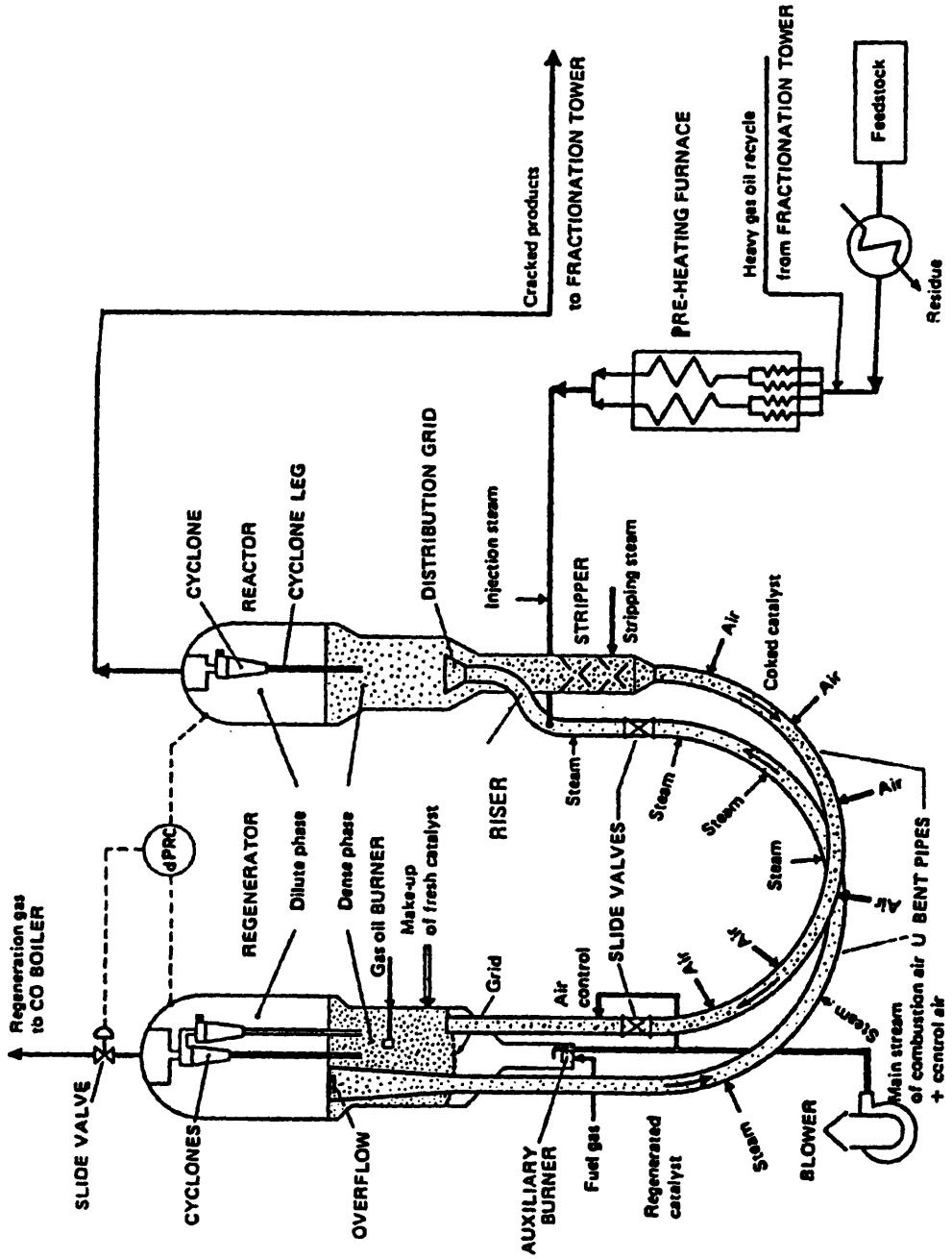

Figure 1.30 The reaction section of a fluidized bed cracking unit (Decroocq (1984)).

possible interaction with the accumulating foulant during long term deactivation by coke laydown.

CHAPTER TWO

THEORETICAL APPROACHES TO COKE LAYDOWN MODELLING

CHAPTER TWO

THEORETICAL APPROACHES TO COKE LAYDOWN MODELLING

2.1 INTRODUCTION:

This chapter deals with two possible structural models to simulate the various processes that take place in the macropores and micropores of a supported zeolitic cracking catalyst particle, namely, diffusion, reaction and deactivation caused by coke laydown.

The following two models were chosen to represent the catalyst support structure:

(1) Corrugated parallel bundle model, and

(2) Stochastic pore network model.

The zeolite contained within crystallites was assumed to be uniformly distributed along the walls of the silica alumina support pores of both the above models. Examples of each of these structural models are shown in Figure 2.1 and Figure 2.2.

Following on the work of Thomson (1986) and Sharrat (1985), the simulation of diffusion, reaction and deactivation was performed in both structures as functions of time on stream. It has been considered that the deactivation of the support and the zeolite occurs by coke laydown according to the following two mechanisms:

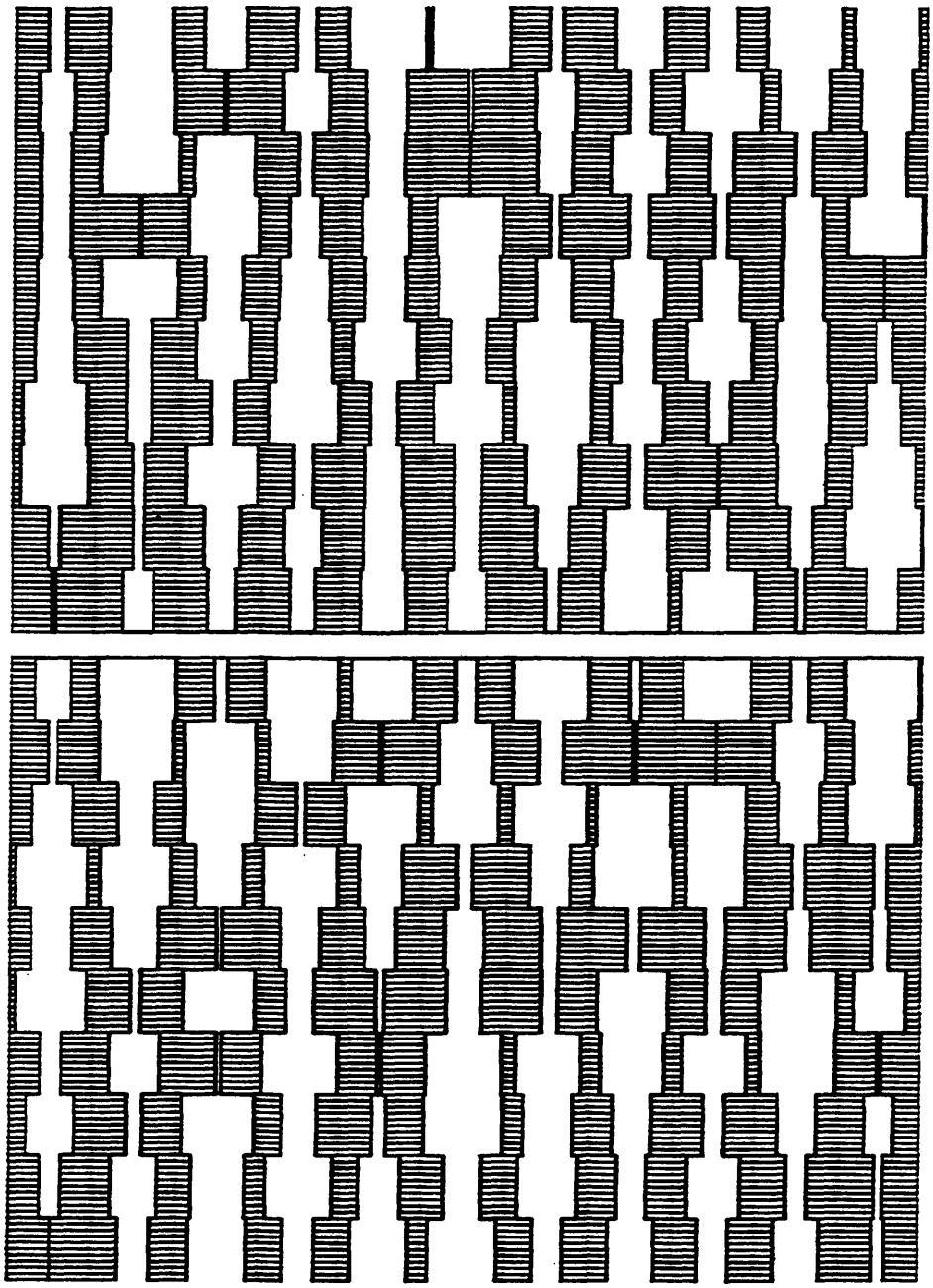

Figure 2.1 The corrugated parallel bundle model of pore structure.
(A set of 22 corrugated 10–element pores).

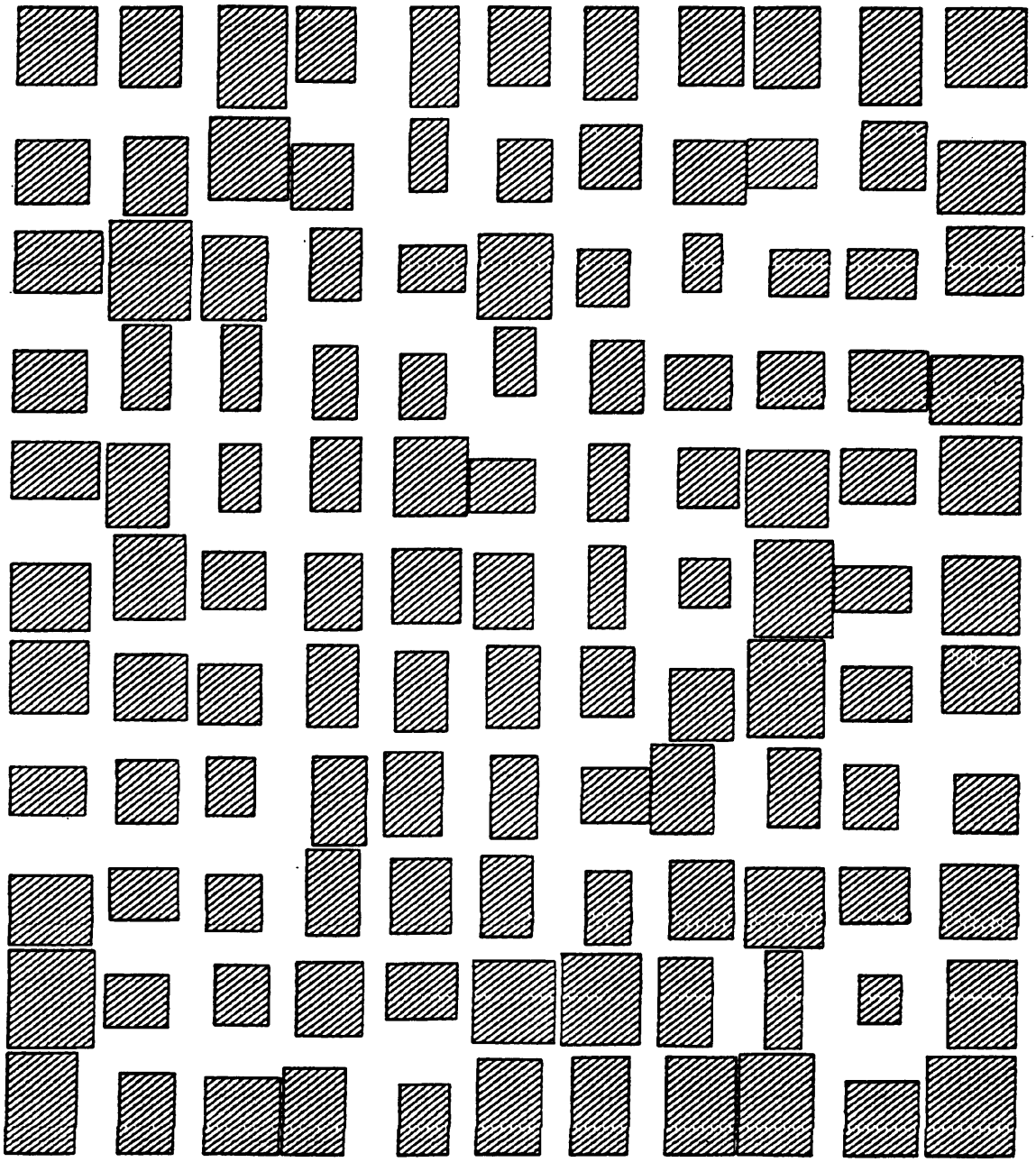

Figure 2.2 The network model of pore structure.

(Network size is 10x10).

(1) **Active site poisoning:** Deactivation occurs by loss of active sites due to coke depositing directly on the active site in the support and zeolite.

(2) **Pore plugging:** Deactivation occurs by loss of active sites due to coke deposits restricting access to what would otherwise be active sites on the support and zeolite.

The following assumptions were made in the modelling of the deactivation of the zeolitic catalyst:

(1) The species involved move by diffusion only, with no bulk flow.

(2) The species obey Dalton's law of partial pressure.

(3) The total pressure (and hence molal density) is constant throughout the pore arrangement.

(4) The reaction is first order in the reacting species and first order in active surface area.

(5) There is no change in the total number of moles on reaction.

(6) Both the support and zeolite are catalytically active, and

(7) The support and the zeolite can deactivate in different ways.

2.2 THE CORRUGATED PARALLEL BUNDLE MODEL OF PORE STRUCTURE:

2.2.1 Concentration Profile in a Corrugated Pore:

In order to evaluate the concentration profile in a pore, it is first necessary to investigate what takes place in each of the individual elements of the pore. Consider a single pore consisting of N elements in which the reaction

$$A \longrightarrow \text{Products}$$

occurs which is first order with respect to concentration of reactant and first order with respect to active surface area with equimolar, counter diffusional flow.

A mass balance for the reactant A in any pore element n, n<N, with boundary conditions as shown in Figure 2.3, can be performed and represented by the following equation:

$$\text{Inflow of A} - \text{Outflow of A} = \text{Rate of reaction of A on surface} \tag{2.1}$$

For a completely deactivated pore element equation (2.1) becomes:

$$\frac{d^2C_A}{dx^2} = 0 \tag{2.2}$$

Integrating the above equation twice using the boundary conditions, gives the concentration profile across the pore element

$$C_A(x) = C_{A,n-1} + \frac{x\ (C_{A,n} - C_{A,n-1})}{L} \tag{2.3}$$

For an active pore element of radius R_n equation (2.1) becomes:

$$\pi R_n^2 D_n \frac{d^2C_A}{dx^2} = k_s S_n C_A \tag{2.4}$$

Rearranging equation (2.4) and substituting for the reaction modulus for the pore element m_n it becomes:

$$\frac{d^2C_A}{dx^2} = m_n^2 C_A \tag{2.5}$$

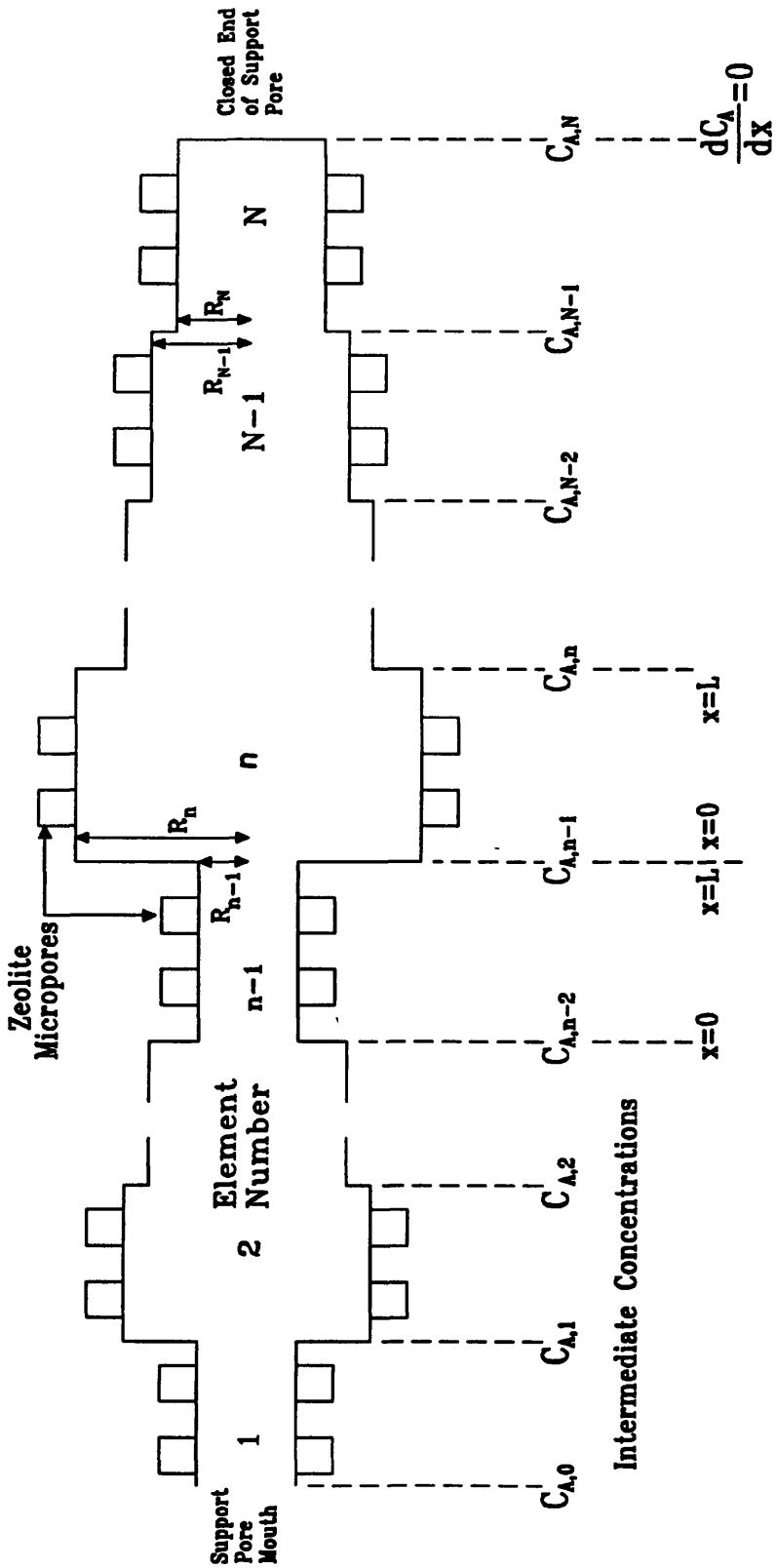

Figure 2.3: Cross section through an N element pore showing the boundary conditions and intermediate concentrations.

where the reaction modulus m_n is given by:

$$m_n^2 = \frac{k_s S_n}{\pi R_n^2 D_n} \qquad (2.6)$$

k_s and S_n are the reaction rate constant and the total active surface area of the element, respectively.

Using the following boundary conditions for any element $n \neq N$

$$C_A = C_{A,n-1} \qquad \text{at} \quad x = 0$$

$$C_A = C_{A,n} \qquad \text{at} \quad x = L$$

equation (2.4) is solved to produce the concentration profile of A throughout the pore element.

The concentration profile for A is given by:

$$C_A(x) = \frac{C_{A,n-1} \sinh(m_n (L-x)) + C_{A,n} \sinh(m_n x)}{\sinh(m_n L)} \qquad (2.7)$$

For the final closed–end element of the pore, n=N the boundary conditions are different as follows:

$$C_A = C_{A,N-1} \qquad x = 0$$

$$\frac{dC_A}{dx} = 0 \qquad x = L$$

Solving equations (2.2) and (2.4) using the above boundary conditions produces the concentration profile of A throughout the end element. For a completely deactivated pore element, equation (2.2) produces:

$$C_A(x) = C_{A,N-1} \tag{2.8}$$

For an active final closed–end element equation (2.4) produces:

$$C_A(x) = \frac{C_{A,N-1} \cosh\left(m_N(L-x)\right)}{\cosh(m_N L)} \tag{2.9}$$

To evaluate the concentration profile in the complete pore, the intermediate concentrations must be eliminated i.e. $C_{A,n}$ for n=1, N–1. A mass balance across the interface of any two adjacent pore elements n–1 and n must ensure conservation.

The flow of reactant A leaving element n–1 is:

$$\text{flow} = -D_{n-1}\, \pi R_{n-1}^2 \left.\frac{dC_A}{dx}\right|_{x=L} \tag{2.10}$$

The flow of reactant A entering the next element n is given by:

$$\text{flow} = -D_n\, \pi R_n^2 \left.\frac{dC_A}{dx}\right|_{x=0} \tag{2.11}$$

Assuming no reaction at the interface, these two flows are equal:

$$D_{n-1}\, R_{n-1}^2 \left.\frac{dC_A}{dx}\right|_{x=L} = D_n\, R_n^2 \left.\frac{dC_A}{dx}\right|_{x=0} \tag{2.12}$$

Since the catalyst particle is undergoing deactivation, then any pore element may be either active or inactive at any specific time on stream. Therefore, depending on the condition of the two adjacent pore elements n and n–1, there exist four different cases to consider when solving equation (2.12) (Table 2.1).

Table 2.1 The different cases of two adjacent pore elements.

Element number	Case number			
	1	2	3	4
(n–1)	Active	Active	Inactive	Inactive
(n)	Active	Inactive	Active	Inactive

Case number 1: Both pore elements are active:

Equation (2.7) is differentiated to get $\left.\frac{dC_A}{dx}\right|_{x=L}$ for pore element (n–1) and to get $\left.\frac{dC_A}{dx}\right|_{x=0}$ for element (n).

For the element (n–1):

$$\left.\frac{dC_A}{dx}\right|_{x=L} = \frac{d}{dx}\left[\frac{C_{A,n-2}\ \sinh(m_{n-1}(L-x)) + C_{A,n-1}\ \sinh(m_{n-1}x)}{\sinh(m_{n-1}L)}\right]_{x=L} \tag{2.13}$$

$$= \left[\frac{-\ m_{n-1}\ C_{A,n-2}\ \cosh(m_{n-1}(L-x)) + m_{n-1}C_{A,n-1}\ \cosh(m_{n-1}x)}{\sinh(m_{n-1}L)}\right]_{x=L} \tag{2.14}$$

Then:

$$\left.\frac{dC_A}{dx}\right|_{x=L} = m_{n-1}\, C_{A,n-1} \coth(m_{n-1}L) - \frac{m_{n-1}\, C_{A,n-2}}{\sinh(m_{n-1}L)} \tag{2.15}$$

For pore element (n):

$$\left.\frac{dC_A}{dx}\right|_{x=0} = \frac{d}{dx}\left[\frac{C_{A,n-1}\, \sinh(m_n(L-x)) + C_{A,n}\, \sinh(m_n x)}{\sinh(m_n L)}\right]_{x=0} \tag{2.16}$$

$$= \left[\frac{-m_n\, C_{A,n-1}\, \cosh(m_n(L-x)) + m_n\, C_{A,n}\, \cosh(m_n x)}{\sinh(m_n L)}\right]_{x=0} \tag{2.17}$$

Then:

$$\left.\frac{dC_A}{dx}\right|_{x=0} = \frac{m_n\, C_{A,n}}{\sinh(m_n L)} - m_n\, C_{A,n-1} \coth(m_n L) \tag{2.18}$$

Now, both sides of equation(2.12) can be equated using equations (2.15) and (2.18) as follows:

$$D_{n-1} R_{n-1}^2 \left[m_{n-1}\, C_{A,n-1} \coth(m_{n-1}L) - \frac{m_{n-1}\, C_{A,n-2}}{\sinh(m_{n-1}L)}\right] = D_n R_n^2 \left[\frac{m_n\, C_{A,n}}{\sinh(m_n L)} - m_n\, C_{A,n-1} \coth(m_n L)\right] \tag{2.19}$$

or:

$$C_{A,n-2}\left[\frac{D_{n-1}\, R_{n-1}^2\, m_{n-1}}{\sinh(m_{n-1}L)}\right] + C_{A,n}\left[\frac{D_n\, R_n^2\, m_n}{\sinh(m_n L)}\right] - C_{A,n-1}\left[D_{n-1} R_{n-1}^2\, m_{n-1} \coth(m_{n-1}L) + D_n R_n^2\, m_n \coth(m_n L)\right] = 0 \tag{2.20}$$

Case number 2: **Element (n–1) active and element (n) inactive:**

$$\left.\frac{dC_A}{dx}\right|_{x=L} = m_{n-1}\, C_{A,n-1} \coth(m_{n-1}L) - \frac{m_{n-1}\, C_{A,n-2}}{\sinh(m_{n-1}L)} \tag{2.21}$$

$$\left.\frac{dC_A}{dx}\right|_{x=0} = \frac{d}{dx}\left[C_{A,n-1} + \frac{x}{L}(C_{A,n} - C_{A,n-1})\right]_{x=0} = \left[\frac{C_{A,n} - C_{A,n-1}}{L}\right] \tag{2.22}$$

Since:

$$-D_{n-1}\, R_{n-1}^2 \left.\frac{dC_A}{dx}\right|_{x=L} = -D_n\, R_n^2 \left.\frac{dC_A}{dx}\right|_{x=0} \tag{2.23}$$

then:

$$-D_{n-1}\, R_{n-1}^2 \left[m_{n-1}\, C_{A,n-1} \coth(m_{n-1}L) - \frac{m_{n-1}\, C_{A,n-2}}{\sinh(m_{n-1}L)}\right] = \frac{D_n\, R_n^2}{L}(C_{A,n} - C_{A,n-1}) \tag{2.24}$$

Rearranging, we get

$$C_{A,n-2}\left[\frac{m_{n-1}\, D_{n-1}\, R_{n-1}^2}{\sinh(m_{n-1}L)}\right] + C_{A,n}\left[\frac{D_n\, R_n^2}{L}\right] - C_{A,n-1}\left[D_{n-1}\, R_{n-1}^2\, m_{n-1} \coth(m_{n-1}L) + \frac{D_n\, R_n^2}{L}\right] = 0 \tag{2.25}$$

Case number 3: **Element (n–1) inactive and element (n) active:**

$$\left.\frac{dC_A}{dx}\right|_{x=0} = \left[\frac{C_{A,n}\, m_n}{\sinh(m_n L)} - m_n\, C_{A,n-1} \coth(m_n L)\right] \tag{2.26}$$

$$\left.\frac{dC_A}{dx}\right|_{x=L} = \frac{d}{dx}\left[C_{A,n-2} + \frac{x}{L}(C_{A,n-1} - C_{A,n-2})\right]_{x=L}$$
$$= \left[\frac{C_{A,n-1} - C_{A,n-2}}{L}\right] \qquad (2.27)$$

Using equation (2.12)

$$\frac{D_{n-1}\ R_{n-1}^2}{L}(C_{A,n-1} - C_{A,n-2}) = D_n R_n^2\left[\frac{m_n\ C_{A,n}}{sinh(m_n L)}\right.$$
$$\left. - m_n C_{A,n-1}\coth(m_n L)\right] \qquad (2.28)$$

Rearranging, it becomes:

$$C_{A,n-2}\left[\frac{D_{n-1} - R_{n-1}^2}{L}\right] - C_{A,n-1}\left[\frac{D_{n-1} - R_{n-1}^2}{L} + m_n D_n R_n^2 \coth(m_n L)\right]$$
$$+ C_{A,n}\left[\frac{D_n R_n^2 m_n}{sinh(m_n L)}\right] = 0 \qquad (2.29)$$

Case number 4: **Elements (n–1) and element (n) both inactive:**

$$\left.\frac{dC_A}{dx}\right|_{x=L} = \frac{C_{A,n-1} - C_{A,n-2}}{L} \qquad (2.30)$$

$$\left.\frac{dC_A}{dx}\right|_{x=0} = \frac{C_{A,n} - C_{A,n-1}}{L} \qquad (2.31)$$

Using equation (2.12):

$$D_{n-1} R_{n-1}^2 \left[\frac{C_{A,n-1} - C_{A,n-2}}{L}\right] = D_n R_n^2 \left[\frac{C_{A,n} - C_{A,n-1}}{L}\right] \qquad (2.32)$$

Rearranging, it becomes:

$$C_{A,n-2}\left[\frac{D_{n-1}\ R_{n-1}^2}{L}\right] - C_{A,n-1}\left[\frac{D_{n-1}\ R_{n-1}^2}{L} + \frac{D_n\ R_n^2}{L}\right] + C_{A,n}\left[\frac{D_n\ R_n^2}{L}\right] = 0 \qquad (2.33)$$

The End Element of the Pore:

Conserving the mass balance across the interface between the two elements at the end of the pore, namely, N–1 and N, and assuming no reaction at the interface, as before, the flow of reactant A leaving element N–1 given by equation (2.10) is:

$$\text{Flow} = -D_{N-1}\ \pi R_{N-1}^2 \left.\frac{dC_A}{dx}\right|_{x=L}$$

The flow of reactant A entering element N given by equation (2.11) is:

$$\text{Flow} = -D_N\ \pi R_N^2 \left.\frac{dC_A}{dx}\right|_{x=0}$$

Then

$$D_{N-1}\ R_{N-1}^2 \left.\frac{dC_A}{dx}\right|_{x=L} = D_N\ R_N^2 \left.\frac{dC_A}{dx}\right|_{x=0} \qquad (2.34)$$

As in Table 2.1, the four different cases should each be considered for the end element as well.

Case number 1: Element N–1 and element N both active:

Equation (2.15) becomes:

$$\left.\frac{dC_A}{dx}\right|_{x=L} = m_{N-1}\, C_{A,N-1} \coth(m_{N-1}L) - \frac{m_{N-1}\, C_{A,N-2}}{\sinh(m_{N-1}L)} \tag{2.35}$$

From equation (2.9) for an active end element:

$$C_A(x) = \frac{C_{A,N-1} \cosh\left(m_N(L-x)\right)}{\cosh(m_N)}$$

differentiating with respect to x:

$$\left.\frac{dC_A}{dx}\right|_{x=0} = \frac{d}{dx}\left[\frac{C_{A,N-1} \cosh\left(m_N\,(L-x)\right)}{\cosh(m_N L)}\right]_{x=0} \tag{2.36}$$

$$\left.\frac{dC_A}{dx}\right|_{x=0} = \left[\frac{-\,m_N\, C_{A,N-1} \sinh(m_N(L-x))}{\cosh(m_N L)}\right]_{x=0} \tag{2.37}$$

$$= -\,m_N\, C_{A,N-1} \tanh(m_N L) \tag{2.38}$$

Using equation (2.34) and substituting equations (2.35) and (2.38):

$$D_{N-1}\, R_{N-1}^2\left[m_{N-1}\, C_{A,N-1} \coth(m_{N-1}L) - \frac{m_{N-1}\, C_{A,N-2}}{\sinh(m_{N-1}L)}\right] = D_N\, R_N^2\left[-\,m_N\, C_{A,N-1} \tanh(m_N L)\right] \tag{2.39}$$

Rearranging, it becomes:

$$C_{A,N-2}\left[\frac{D_{N-1}\, R_{N-1}^2\, m_{N-1}}{\sinh(m_N L)}\right] - C_{A,N-1}\left[D_{N-1}\, R_{N-1}^2\, m_{N-1} \coth(m_{N-1}L) + D_N\, R_N^2\, m_N \tanh(m_N L)\right] = 0 \tag{2.40}$$

Case number 2: **Element N–1 active and element N inactive:**

$$\left.\frac{dC_A}{dx}\right|_{x=L} = C_{A,N-1}\, m_{N-1} \coth(m_{N-1}L) - \frac{C_{A,N-2}\ m_{N-1}}{\sinh(m_{N-1}L)} \qquad (2.35)$$

Using equation (2.8) and differentiating:

$$\left.\frac{dC_A}{dx}\right|_{x=0} = \frac{d}{dx}\left[C_{A,N-1}\right]_{x=0}$$

Since element N is inactive for this case number 2 then:

$$\left.\frac{dC_A}{dx}\right|_{x=0} = 0$$

Substituting above equations in (2.34):

$$D_{N-1}\, R_{N-1}^2\, m_{N-1}\, C_{A,N-1} \coth(m_{N-1}L) - \frac{m_{N-1}\ C_{A,N-2}}{\sinh(m_{N-1}L)} = 0 \qquad (2.41)$$

$$C_{A,N-1} \coth(m_{N-1}L) - \frac{C_{A,N-2}}{\sinh(m_{N-1}L)} = 0 \qquad (2.42)$$

Simplifying and rearranging it becomes:

$$C_{A,N-2} - C_{A,N-1} \cosh(m_{N-1}L) = 0 \qquad (2.43)$$

Case number 3: **Element N–1 inactive and element N active:**

$$\left.\frac{dC_A}{dx}\right|_{x=L} = \frac{d}{dx}\left[C_{A,N-2} - \frac{x}{L}(C_{A,N-1} - C_{A,N-2})\right]_{x=L} = \frac{C_{A,N-1} - C_{A,N-2}}{L} \qquad (2.44)$$

$$\left.\frac{dC_A}{dx}\right|_{x=0} = -\,m_N\, C_{A,N-1}\, \tanh(m_N L) \tag{2.45}$$

using equation (2.34):

$$D_{N-1}\, R_{N-1}^2 \left[\frac{C_{A,N-1} - C_{A,N-2}}{L}\right] = D_N\, R_N^2\, [-\,m_N\, C_{A,N-1}\, \tanh(m_N L)] \tag{2.46}$$

Rearranging, it becomes

$$C_{A,N-2}\left[\frac{D_{N-1}\ R_{N-1}^2}{L}\right] - C_{A,N-1}\left[\frac{D_{N-1}\ R_{N-1}^2}{L} + m_N\, D_n\, R_n^2\, \tanh(m_N L)\right] = 0 \tag{2.47}$$

Case number 4: **Element N–1 and element N both inactive:**

$$\left.\frac{dC_A}{dx}\right|_{x=L} = \frac{C_{A,N-1} - C_{A,N-2}}{L} \tag{2.48}$$

Since element N is inactive then:

$$\left.\frac{dC_A}{dx}\right|_{x=0} = 0$$

using equation (2.34):

$$\frac{C_{A,N-1} - C_{A,N-2}}{L} = 0 \tag{2.49}$$

or

$$C_{A,N-2} - C_{A,N-1} = 0 \tag{2.50}$$

Mass conservation across every interface between two adjacent pore elements produces (N–1) equations for a pore with N elements. The matrix form of these equations becomes

$$G \cdot \underline{C} = b \tag{2.51}$$

The coefficient matrix G is tridiagonal, containing nonzero elements only on the diagonal and positions adjacent to the diagonal. Solution of equation (2.51), $\underline{C}$, provides the full set of intermediate concentrations.

The end element concentration $C_{A,N}$ is calculated from equation (2.8) or (2.9):

For an inactive end element:

$$C_{A,N} = C_{A,N-1} \tag{2.52}$$

For an active end element:

$$C_{A,N} = C_{A,N-1} \left. \frac{\cosh(m_N\ (L-x))}{\cosh(m_N L)} \right|_{x=L} \tag{2.53}$$

$$C_{A,N} = \frac{C_{A,N-1}}{\cosh(m_N L)} \tag{2.54}$$

2.2.2 Estimation of the Rate of the Reaction in a Pore:

Performing mass balances for the corrugated pore in Figure 2.3 provide:

rate of reaction of A in the pore = flow of A into the pore

(2.55)

Then:

$$\text{rate of reaction of A in the pore} = -D_1 \pi R_1^2 \left.\frac{dC_A}{dx}\right|_{x=0} \tag{2.56}$$

To calculate the rate of the reaction, two cases must be considered.

Case number 1: The first element of the pore is active:

Using equation (2.7) for the first element n=1, the concentration profile becomes:

$$C_A(x) = \frac{C_{A,0}\ \sinh(m_1(L-x)) + C_{A,1}\ \sinh(m_1 x)}{\sinh(m_1 L)} \tag{2.57}$$

$C_{A,0}$ is the bulk concentration of A at the pore mouth.

Differentiating equation (2.57) it becomes:

$$\left.\frac{dC_A}{dx}\right|_{x=0} = \frac{d}{dx}\left[\frac{C_{A,0}\ \sinh(m_1(L-x)) + C_{A,1}\ \sinh(m_1 x)}{\sinh(m_1 L)}\right]_{x=0} \tag{2.58}$$

$$\left.\frac{dC_A}{dx}\right|_{x=0} = \left[\frac{-m_1\ C_{A,0}\ \cosh(m_1(L-x)) + m_1 C_{A,1}\ \sinh(m_1 x)}{\sinh(m_1 L)}\right]_{x=0} \tag{2.59}$$

$$\left.\frac{dC_A}{dx}\right|_{x=0} = \frac{m_1\ C_{A,1}}{\sinh(m_1 L)} - m_1\ C_{A,0} \coth(m_1 L) \tag{2.60}$$

Using equation (2.56) and substituting equation (2.60) it becomes:

rate of reaction of A in the pore =

$$-D_1 \pi R_1^2 \left[\frac{m_1 C_{A,1}}{sinh(m_1 L)} - m_1 C_{A,0} \coth(m_1 L)\right] \tag{2.61}$$

Case number 2: The first element of the pore is inactive:

For a completely deactivated first element, the concentration profile is given by:

$$C_A(x) = C_{A,0} + \frac{x\ (C_{A,1} - C_{A,0})}{L} \tag{2.62}$$

$$\left.\frac{dC_A}{dx}\right|_{x=0} = \frac{C_{A,1} - C_{A,0}}{L} \tag{2.63}$$

Using equation (2.56) and substituting equation (2.63) gives finally

the rate of reaction of A in the pore =

$$-D_1 \pi R_1^2 \left[\frac{C_{A,1} - C_{A,0}}{L}\right] \tag{2.64}$$

2.2.3 Estimation of the Active Surface Area of the Support:

The active surface area of the catalyst is the sum of the active area of the support and zeolite for each of the pore elements. Since coke deposits on the wall of the catalyst, the active surface area decreases as time on stream increases. To facilitate an estimate of the amount of free active area in a support pore element, the following assumptions were made:

(1) Coke deposits randomly onto the support (Fig. 2.4).

(2) The coke units consist of discrete cubes of size d.

(3) There are N_s active sites in the element.

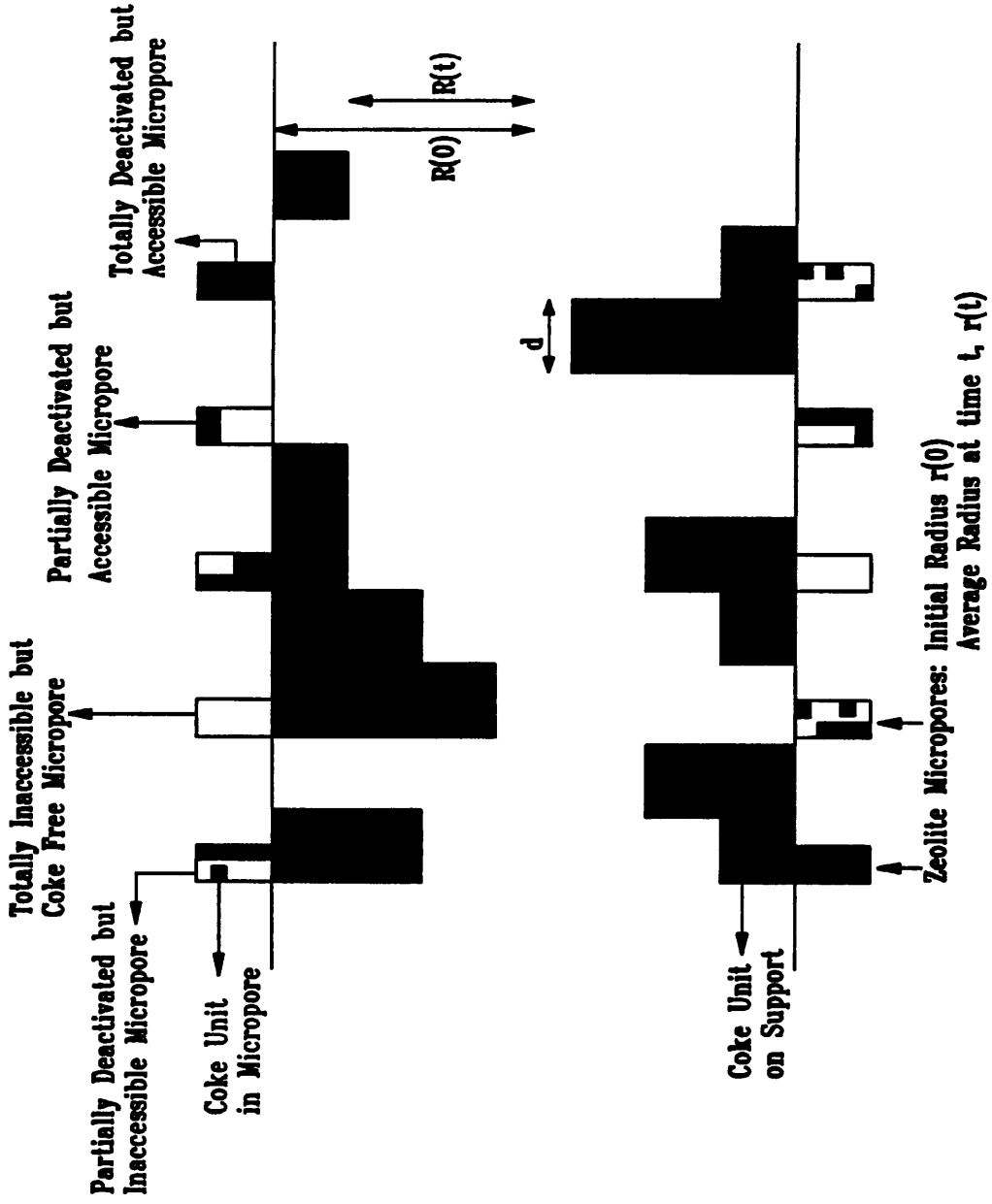

Figure 2.4: Cross section through a pore element showing coke deposition on the support and in the zeolite.

(4) A_j is the fraction of active sites covered to a depth "j" when n_c units of coke have been deposited, and

(5) Initially $A_0=1$, $A_j=0$ $j>0$

As the number of coke units deposited in the pore element 'n_c' increases, the value of A_j will decrease. Consider an increment δn_c in the amount of coke units deposited. Taking a site balance for the system will produce the corresponding changes in A_j

$$\frac{\delta A_0}{\delta n_c} = \frac{-A_0}{N_s} \tag{2.65}$$

$$\frac{\delta A_j}{\delta n_c} = \frac{A_{j-1}}{N_s} - \frac{A_j}{N_s} \qquad j>0 \tag{2.66}$$

Taking the limit

$$\frac{dA_0}{dn_c} = -\frac{A_0}{N_s} \tag{2.67}$$

$$\frac{dA_j}{dn_c} = \frac{A_{j-1}}{N_s} - \frac{A_j}{N_s} \qquad j>0 \tag{2.68}$$

$$\int_1^{A_0} \frac{1}{A_0} dA_0 = \int_0^{n_c} \frac{-1}{N_s} dn_c \tag{2.69}$$

$$A_0 = \exp(-n_c/N_s) \tag{2.70}$$

$$\frac{dA_1}{dn_c} = -\frac{A_0}{N_s} - \frac{A_1}{N_s} \tag{2.71}$$

Substituting for A_0

$$\frac{dA_1}{dn_c} = \frac{\exp(-n_c/N_s)}{N_s} - (A_1/N_s) \tag{2.72}$$

or

$$\frac{dA_1}{dn_c} + (A_1/N_s) = \frac{\exp(-n_c/N_s)}{N_s} \tag{2.73}$$

Integrating the above equation requires finding the Complementary Function and the Particular Integral and summing.

Complementary Function:

$$\frac{dA_1}{dn_c} + (A_1/N_s) = 0 \tag{2.74}$$

Let:

$$A_1 = \exp(mn_c) \tag{2.75}$$

then:

$$\frac{dA_1}{dn_c} = m \exp(mn_c) \tag{2.76}$$

and:

$$m \exp(mn_c) + \frac{\exp(mn_c)}{N_s} = 0 \tag{2.77}$$

$$m = -1/N_s \tag{2.78}$$

$$A_1 = K \exp(-n_c/N_s) \tag{2.79}$$

where K is an arbitrary constant

Particular Integral:

Let:

$$A_1 = H\, n_c \exp(-n_c/N_s) \tag{2.80}$$

then:

$$\frac{dA_1}{dn_c} = H \exp(-n_c/N_s) - \frac{H\ n_c\ \exp(-n_c/N_s)}{N_s} \tag{2.81}$$

Substituting into equation (2.73)

$$H \exp(-n_c/N_s) - \frac{H\ n_c\ \exp(-n_c/N_s)}{N_s} + \frac{H\ n_c\ \exp(-n_c/N_s)}{N_s} = \frac{\exp(-n_c/N_s)}{N_s} \tag{2.82}$$

Therefore:

$$H = 1/N_s \tag{2.83}$$

The general solution becomes:

$$A_1 = K \exp(-n_c/N_s) + \frac{n_c\ \exp(-n_c/N_s)}{N_s} \tag{2.84}$$

From assumption 5 above, $A_1 = 0$ when $n_c = 0$ implying $K = 0$, therefore:

$$A_1 = \frac{n_c\ \exp(-n_c/N_s)}{N_s} \tag{2.85}$$

Similarly:

$$\frac{dA_2}{dn_c} = \frac{A_1}{N_s} - \frac{A_2}{N_s} \tag{2.86}$$

$$\frac{dA_2}{dn_c} = \frac{n_c\ \exp(-n_c/N_s)}{N_s^2} - \frac{A_2}{N_s} \tag{2.87}$$

or:

$$\frac{dA_2}{dn_c} + \frac{A_2}{N_s} = \frac{n_c\ \exp(-n_c/N_s)}{N_s^2} \tag{2.88}$$

The Complementary Function is:

$$A_2 = K \exp(-n_c/N_s) \tag{2.89}$$

For the Particular Integral try:

$$A_2 = H\, n_c^2 \exp(-n_c/N_s) \tag{2.90}$$

Then:

$$2n_cH \exp(-n_c/N_s) - \frac{Hn_c^2 \exp(-n_c/N_s)}{N_s} + \frac{Hn_c^2 \exp(-n_c/N_s)}{N_s} = \frac{n_c \exp(-n_c/N_s)}{N_s^2} \tag{2.91}$$

$$H = \frac{1}{2\ N_s^2} \tag{2.92}$$

The general solution becomes:

$$A_2 = K \exp(-n_c/N_s) - \frac{n_c^2 \exp(-n_c/N_s)}{2\ N_s^2} \tag{2.93}$$

Eliminating K by the use of boundary conditions from assumption 5:

$$A_2 = \frac{(n_c/N_s)^2 \exp(-n_c/N_s)}{2} \tag{2.94}$$

As before for A_3:

$$\frac{dA_3}{dn_c} = \frac{A_2}{N_s} - \frac{A_3}{N_s} \tag{2.95}$$

Substituting for A_2 and rearranging:

$$\frac{dA_3}{dn_c} + A_3 = \frac{(n_c/N_s)^2 \exp(-n_c/N_s)}{2\ N_s} \tag{2.96}$$

Again, the general solution is

$$A_3 = K \exp(-n_c/N_s) \tag{2.97}$$

To find the Particular Integral let:

$$A_3 = H\, n_c^3 \exp(-n_c/N_s) \tag{2.98}$$

Then

$$3\, H\, n_c^2 \exp(-n_c/N_s) - \frac{H\ n_c^3}{N_s} \exp(-n_c/N_s) + \frac{H\ n_c^3}{N_s} \exp(-n_c/N_s) = \frac{n_c^2}{2\ N_s^3} \exp(-n_c/N_s) \tag{2.99}$$

and

$$H = \frac{1}{6\ N_s^3} \tag{2.100}$$

Eliminating the arbitrary constant K, the general solution becomes:

$$A_3 = \frac{(n_c/N_s)^3\ \exp(-n_c/N_s)}{6} \tag{2.101}$$

or

$$A_3 = \frac{(n_c/N_s)^3\ \exp(-n_c/N_s)}{3!} \tag{2.102}$$

Repeating this procedure for A_4, A_5, ...A_j it can be shown that:

$$A_j = \frac{(n_c/N_s)^j\ \exp(-n_c/N_s)}{j!} \tag{2.103}$$

This is a Poisson style distribution where (n_c/N_s) is the mean depth of coke and A_j is the fraction of surface area covered to depth j.

Let:

$$M = (n_c/N_s) \text{ mean depth of coke units} \tag{2.104}$$

then:

$$A_j = \frac{M^j \exp(-M)}{j!} \tag{2.105}$$

If assuming active site poisoning then the fraction of the surface area that is still active is that fraction on which no coke has been deposited, i.e. j=0.
Then, the free support active surface area, A_{os}, is given by

$$A_{os} = \exp(-M) \tag{2.106}$$

$$A_{os} = \exp\left[\frac{-(R(o) - R(t))}{d}\right] \tag{2.107}$$

where

R(o) :is the initial radius of the pore element,

R(t) :is the element's average radius at time t, and

d :is the size of the cubic support coke unit.

Whereas, if assuming heavy support coke laydown allowing the coke units to lay on top of each other, then the fraction of the surface area that is still active is that which is accessible even if it is covered with a thick layer of coke (Fig. 2.5). Therefore, at any time t, the fraction active support area, A_{os}, will be given as follows:

$$A_{os} = \frac{R(t)}{R(o)} \tag{2.108}$$

2.2.4 Estimation of The Active Surface Area of the Zeolite:

To overcome the difficulty of describing diffusion, reaction and coke deposition in the zeolite micropores, it will be assumed that coke deposition in the zeolite micropores can be described by a "similar" process to coking in the support which is exactly analogous but with a different coke unit size, d_z.

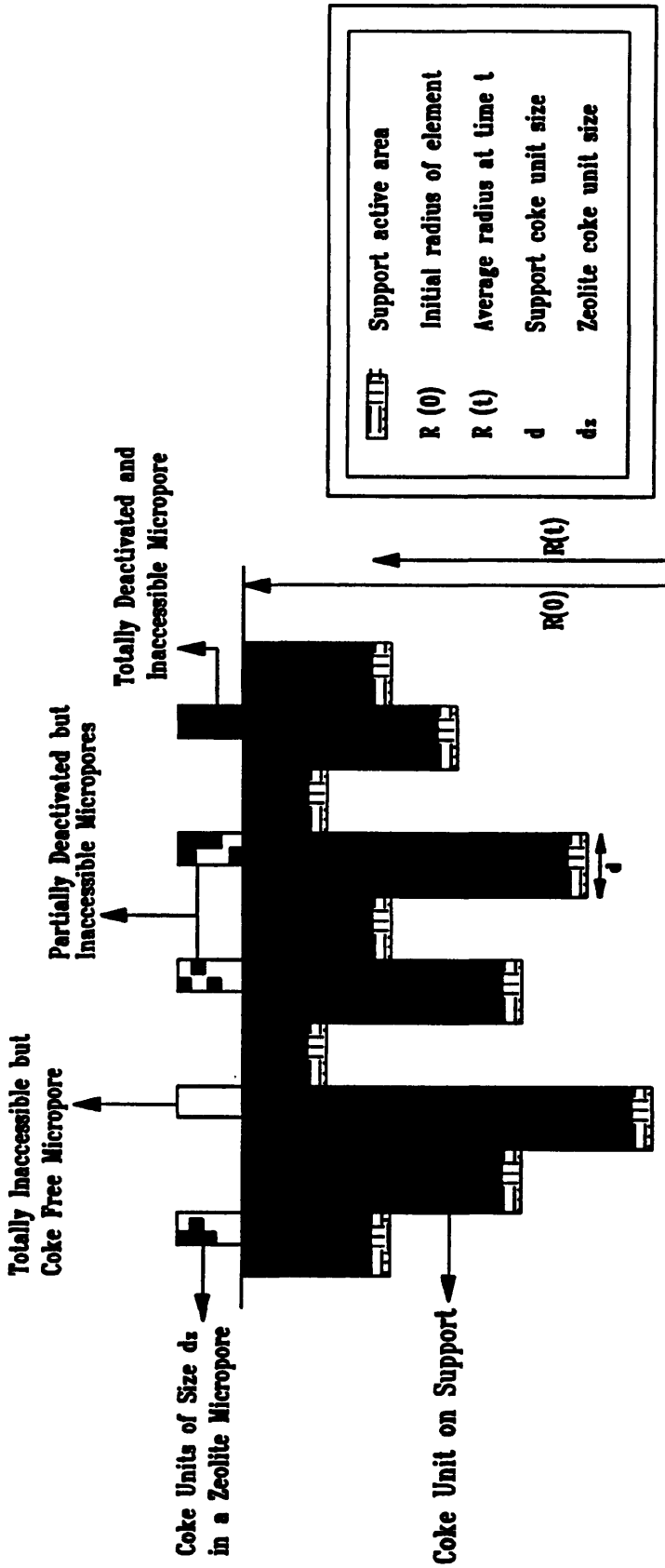

Figure 2.5: Cross section through a pore element showing the support active area for the case of heavy support coking.

Then using the "analogy" argument, the zeolite surface area will be reduced due to coke laydown by the same two mechanisms (Fig. 2.4), namely

(1) **Active Site Poisoning:** Deactivation occurs by loss of active sites due to coke depositing directly on the zeolite active site.

(2) **Pore Plugging:** Deactivation occurs by loss of zeolite active sites due to coke deposition on the support restricting access to zeolite micropores.

The fraction of zeolite surface area free from coke A_z is then similarly given by

$$A_z = \exp(-M') \tag{2.109}$$

$$A_z = \exp\left[\frac{-(R(o) - R(t))}{d_z}\right] \tag{2.110}$$

Since coke can deposit on the support and isolate potentially still active sites of the zeolite, the formula describing the free zeolite area will be changed so as to take account of that, so that

$$A_{oz} = A_z A_s \tag{2.111}$$

$$A_{oz} = \exp\left[\frac{-(R(o) - R(t))}{d_z}\right] \exp\left[\frac{-(R(o) - R(t))}{d}\right] \tag{2.112}$$

Let α be the proportion of the element's initial activity which is associated with the zeolite, then using equation (2.6) the reaction modulus, m, for the element shown in figure(2.4), becomes:

$$m^2 = \frac{k_s\ [(1-\alpha)\ 2\pi\ R(o)\ A_{os} + \alpha\ A_{oz}\ S]}{\pi\ R^2(t)\ D} \tag{2.113}$$

where

R(o) :is the initial radius of the pore element,

R(t) :is the element's average radius at time t, and

S :is the initial zeolite surface area per unit length in the element.

For a bifunctional catalyst both the support and zeolite are catalytically active, therefore, $0.0<\alpha<1.0$. If the zeolite is the only active component in the catalyst then $\alpha=1.0$, whereas, if the support is the only active component of the catalyst $\alpha=0.0$.

Assuming the zeolite is uniformly distributed throughout the support, then the amount of zeolite surface area in any pore element will be proportional to the radius of that element.

or
$$S = K\, R(o) \tag{2.114}$$

Since the total amount of zeolite surface area in the catalyst S_t is given by

$$S_t = \sum_{i=1}^{pores} \sum_{j=1}^{elements} K\, R_{ij}(o)\, L \tag{2.115}$$

Then

$$K = \frac{S_t}{\sum_{i=1}^{pores} \sum_{j=1}^{elements} R_{ij}(o)\ L} \tag{2.116}$$

Substituting equation (2.114) in equation (2.116) it gives

$$S = \left[\frac{S_t}{\sum_{i=1}^{pores} \sum_{j=1}^{elements} R_{ij}(o)\ L}\right] R(o) \tag{2.117}$$

Let:

V_g :be the specific support pore volume, and

$S_{\mu g}$:be the specific zeolite micropore surface area,

then:

$$S_t = \frac{S_{\mu g}}{V_g} \sum_{i=1}^{pores} \sum_{j=1}^{elements} \pi R_{ij}(o) L \qquad (2.118)$$

2.2.5 Rate of Coking in the Pore Element:

Assuming that the coking rate is first order with respect to support active surface area, and that both parallel and series coking mechanisms could occur simultaneously, then the rate of change of support pore radius is given by

$$\frac{dR}{dt} = -(k_{cp} C_A + k_{cs} C_p) A_{os} \qquad (2.119)$$

where

C_A :is the mean reactant concentration,

C_p :is the mean product concentration,

k_{cp} :is the lumped parallel coking rate constant, and

k_{cs} :is the lumped series coking rate constant.

2.2.6 Effectiveness Factor for a Parallel Bundle of Pores:

To measure how much the reaction rate is lowered because of the resistance to pore diffusion, define the quantity $\eta(t)$ called the "Effectiveness Factor" as follows:

$$\eta(t) = \frac{\text{Actual rate of reaction within pores at time t}}{\text{Rate of reaction if not slowed by pore diffusion}} \qquad (2.120)$$

Using equation (2.117) to calculate the zeolite area S, the rate of reaction with no

diffusional limitations is given by:

$$\text{Rate} = \sum_{i=1}^{pores} \sum_{j=1}^{elements} k_s C_{A,o} \left[(1-\alpha)\, 2\pi R_{ij}(o)\, L\, A_{os} + \alpha\, S_{ij} L\, A_{oz} \right] \tag{2.121}$$

The actual reaction rate for the parallel bundle will be the sum of the rates of reaction for each individual pore given by equation (2.64) if the first element is inactive or equation (2.61) for an active first element.

2.2.7 The Thiele Modulus for a Parallel Bundle of Pores:

The following classical relationship is used to calculate the overall observed/apparent Thiele modulus (ϕ) for the corrugated parallel bundle:

$$\eta(t) = \frac{\tanh(\phi)}{\phi} \tag{2.122}$$

2.2.8 Simulation of the Fluidised Bed Reactor:

If the behaviour of the fluidised bed reactor can be described by a C.S.T.R, or backmixed reactor, a mass balance for the reactant A over the reactor shown in Figure 2.6 gives

$$F_{A0}\, X_A = (-r_A)\, V \tag{2.123}$$

for which

$$F_{A0} = V_0\, C_{A0} \tag{2.124}$$

For first order kinetics, the reaction rate is given by:

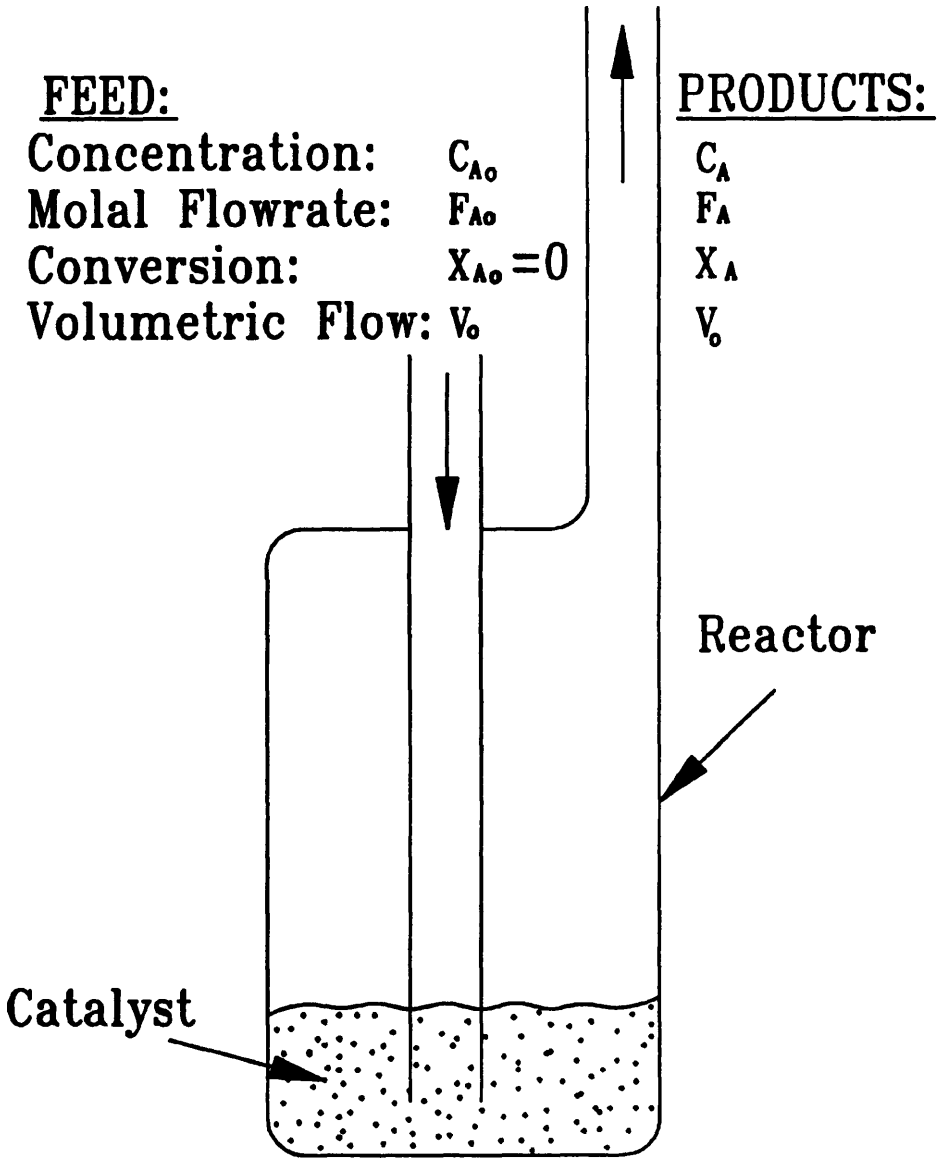

Figure 2.6: Cross section through a fluidised bed reactor.

$$-r_a = \eta(t)\, k_s\, S\, C_A \tag{2.125}$$

Combining the above equations:

$$\eta(t)\, k_s\, S\, C_A\, V = F_{A0}\, X_A \tag{2.126}$$

Since conversion X_A is given by:

$$X_A = \frac{C_{A0} - C_A}{C_{A0}} \tag{2.127}$$

$$X_A = \frac{\eta(t)\ k_s\ S\ V\ (1 - X_A)}{V_0} \tag{2.128}$$

$$X_A = \frac{\left[\dfrac{\eta(t)\ k_s\ S\ V}{V_0}\right]}{1 + \left[\dfrac{\eta(t)\ k_s\ S\ V}{V_0}\right]} \tag{2.129}$$

Since the surface area of the catalyst in the reactor (S V) is given by

$$S\,V = W_c\, S_g(t) \tag{2.130}$$

where

W_c :is the mass of the catalyst in the reactor, and

$S_g(t)$:is the specific catalyst surface area.

$$S_g(t) = \frac{V_g \sum_{i=1}^{\text{pores}} \sum_{j=1}^{\text{elements}} (1-\alpha)\ 2\pi\ R_{ij}(0)\ L\ A_{os} + \alpha\ s_{ij}\ L\ A_{oz}}{\sum_{i=1}^{\text{pores}} \sum_{j=1}^{\text{elements}} R_{ij}^2\ (0)\ L} \tag{2.131}$$

Therefore, the performance equation for the fluidised bed reactor becomes:

$$X_A = \frac{\left[\frac{\eta(t)\, k_s\, W_c\, S_c(t)}{V_0}\right]}{1+\left[\frac{\eta(t)\, k_s\, W_c\, S_c(t)}{V_0}\right]} \qquad (2.132)$$

2.2.9 Coke Content of the Corrugated Parallel Bundle of Pores:

2.2.9.1 Coke content in the support:

For cubic coke units of size d, when n_c coke units have been deposited in the support, the volume of coke V(t) in a support element at any time t is given by

$$V(t) = n_c\, d^3 \qquad (2.133)$$

where n_c is calculated from the following equation:

$$n_c = \sum_{j=1}^{\text{elements}} \frac{j\, \exp(-M) M^j}{j!}\, \frac{2\pi\, R(0)\, L}{d^2} \qquad (2.134)$$

Since:

$$\sum_{j=1}^{\text{elements}} \frac{j\, \exp(-M)\, M^j}{j!} = M \qquad (2.135)$$

Then:

$$V(t) = M\, 2\pi\, R(0)\, L\, d \qquad (2.136)$$

Then for all pores and elements in the parallel bundle:

$$V_s(t) = \sum_{i=1}^{\text{pores}} \sum_{j=1}^{\text{elements}} M_{ij}\, 2\pi\, R_{ij}(0)\, L\, d \qquad (2.137)$$

To produce the specific coke content in the support pores, $V_s(t)$ should be normalised. Then the specific coke content in the support pores is given by:

$$V_s(t) = \frac{V_s(t) \quad V_g}{\sum_{i=1}^{\text{pores}} \sum_{j=1}^{\text{element s}} \pi \; R_{ij}^2(0) \; L} \tag{2.138}$$

V_g :is the specific support pore volume.

2.2.9.2 Coke content in the zeolite:

By invoking the idea of an analogy, the volume of coke in the zeolite can be similarly calculated at any time. The zeolite active surface area in any pore element, A_z, after coke laydown in the micropores is calculated from equation (2.51), so that

$$A_z = \exp(-M') \tag{2.139}$$

where

$$M' = \frac{R(0) - R(t)}{d_z} \tag{2.140}$$

The volume of coke in the zeolite is calculated using the above equations and the following equation:

$$V(t) = M' \; SL \; d_z \tag{2.141}$$

where:

SL :is the initial zeolite surface area in the element (using equation(2.117) to calculate S).

Summing over all pores and elements, and multiplying by the normalisation factor, the specific coke on zeolite, $V_m(t)$, is then given by:

$$V_m(t) = \frac{V_g \sum_{i=1}^{\text{pores elements}} \sum_{j=1} M'_{ij} S_{ij} L \, dz}{\sum_{i=1}^{\text{pores elements}} \sum_{j=1} \pi R_{ij}^2(0) L} \qquad (2.142)$$

Then the overall catalyst specific coke content, $V_c(t)$, is given by

$$V_c(t) = V_s(t) + V_m(t) \qquad (2.143)$$

The above value is obviously equivalent to that given by an experimental coke analyser.

2.2.10 Zeolite Volume Lost During Coking:

The loss of zeolite volume during coking is caused by:

(1) Coke deposition on the zeolite surface, and,

(2) Coke deposition on the support causing blockage of access to zeolite pores.

The average coke content of the zeolite micropores in an element, f, given by:

$$f = \frac{\text{volume of coke in zeolite micropores}}{\text{volume of zeolite micropores}} \qquad (2.144)$$

Considering the relationship between volume and surface area of a cylinder, we get

$$\text{Volume of zeolite micropores} = \frac{r(0)\ SL}{2} \qquad (2.145)$$

where:

r(0) :is the initial value of the zeolite micropores, and,

S :is calculated from equation (2.117).

Using equation (2.144) and substituting for equations (2.141) and (2.145) gives

$$f = \frac{2\ M'\ d_z}{r(0)} \tag{2.146}$$

The volume of zeolite lost due only to support coking is the remaining space in the micropore, given by:

$$\text{Volume} = \frac{(1-f)\ S\ L\ r(0)}{2} \tag{2.147}$$

From equation (2.107) the free support surface area A_{os} is calculated and, therefore, the fraction of the support which is coked is given by $(1-A_{os})$. The total zeolite loss then becomes:

$$V_z(t) = \frac{(1-A_{os})(1-f)r(0)SL}{2} + M'\ S\ L\ d_z \tag{2.148}$$

For the case of no support coking: $A_{os} = 1$, then:

$$V_z(t) = M'\ S\ L\ d_z \tag{2.149}$$

If the support is totally coked: $A_{os} = 0$, then:

$$V_z(t) = \frac{r(0)\ S\ L}{2} \tag{2.150}$$

The specific zeolite volume loss $V_z(t)$ is given by:

$$V_z(t) = \frac{\sum_{i=1}^{\text{pores}} \sum_{j=1}^{\text{elements}} V_z(t)\ V_g}{\sum_{i=1}^{\text{pores}} \sum_{j=1}^{\text{elements}} \pi\ R_{ij}^2(0)\ L} \tag{2.151}$$

The above value is that loss in zeolite volume which would be detected by structural analytical methods such as low temperature gas adsorption.

The computer program (OMRANCOR) written in the FORTRAN language, solves the equations for diffusion, reaction and deactivation through a corrugated parallel bundle of pores. The listing of the program (OMRANCOR) is given in Appendix–1. Figure 2.7 shows the sequence of calculations for the solution of the diffusion, reaction and deactivation equations in a fluidised bed reactor. The program produces conversion, coke content and surface area changes in the pore assembly as a function of time on stream. It also produces values for the radii of the parallel bundle pore elements at different stages of coking. These values were used with a graphical package (GHOST80) on the university (UMIST) mainframe computer to visualise the corresponding corrugated parallel bundle of pores with coke laydown.

2.3 THE NETWORK MODEL OF PORE STRUCTURE:

The model consists of a two–dimensional square grid of cylindrical pores each of which is assigned a radius from a given pore size distribution. The assignments are made randomly. Figure 2.2 is a network of size 10x10 consisting of 220 pore elements.

2.3.1 Concentration Profile in a Pore Element of the Network:

For a single uniform cylindrical pore element, the one–dimensional steady state equation is represented by the following equation:

$$D_n \frac{d^2C_A}{dx^2} - r(C_A) = 0 \qquad (2.152)$$

For a first order reaction:

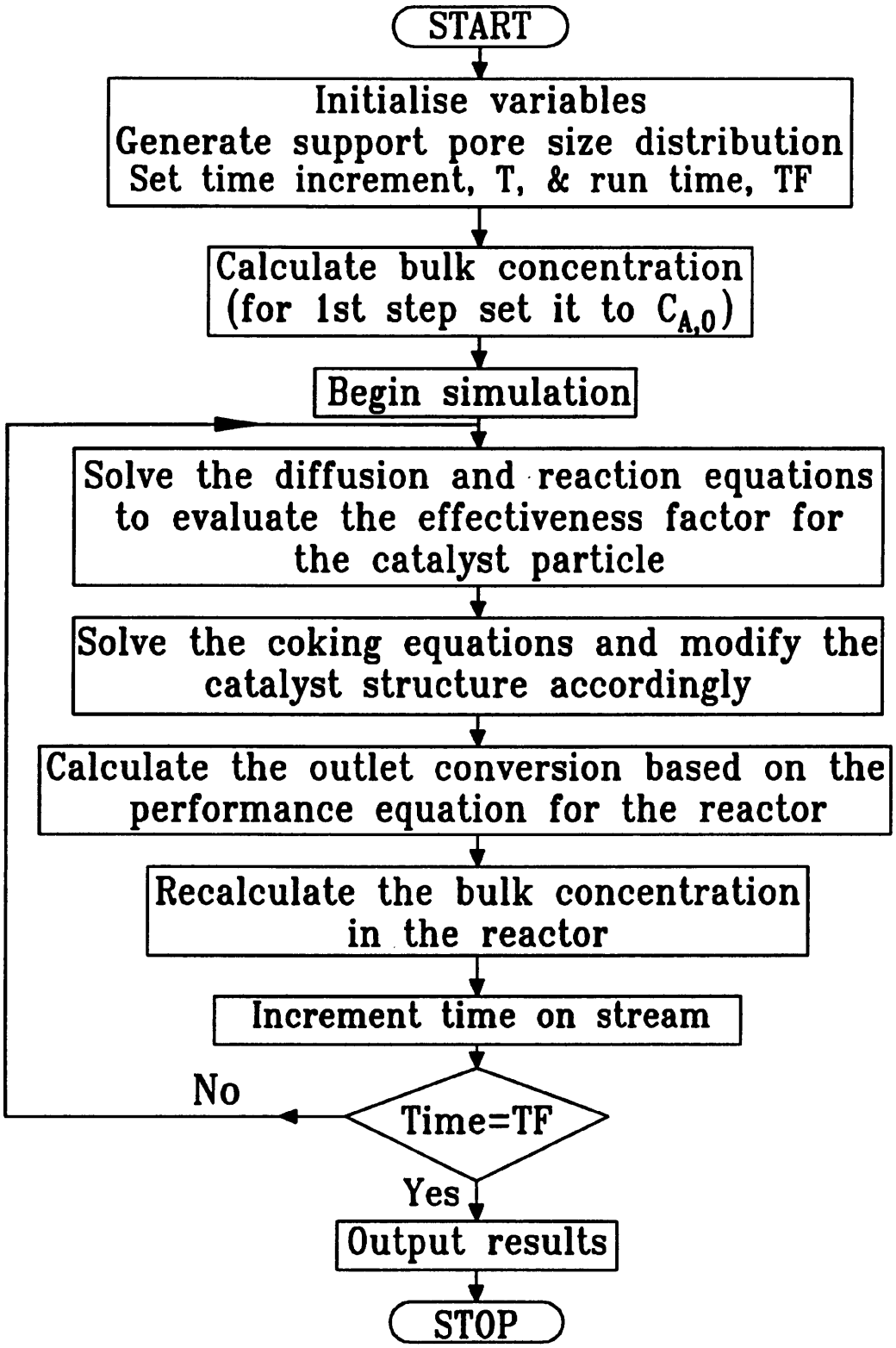

Figure 2.7: Procedure for solution of the diffusion and reaction equations in a fluidised bed reactor.

$$D_n \frac{d^2C_A}{dx^2} - k_1 C_A = 0 \tag{2.153}$$

where:

$$k_1 = \left[\frac{2ks}{r}\right].$$

The general solution is given by:

$$C_A = A \cosh\left[\frac{\phi x}{L}\right] + B \sinh\left[\frac{\phi x}{L}\right] \tag{2.154}$$

where:

$$\phi = L \left(\frac{k_1}{D_n}\right)^{\frac{1}{2}} \tag{2.155}$$

Using the boundary conditions (Fig. 2.8A) to calculate the constants:

$$C_A = C_1 \quad \text{at} \quad x = 0 \quad \text{gives} \quad A = C_1$$

$$C_A = C_2 \quad \text{at} \quad x = L \quad \text{gives} \quad B = \frac{C_2 - C_1 \cosh \phi}{\sinh \phi}$$

Then:

$$C_A = C_1 \left[\cosh\left(\frac{\phi x}{L}\right) - \sinh\left(\frac{\phi x}{L}\right) \coth \phi\right] + \frac{C_2 \sinh\left(\phi \frac{x}{L}\right)}{\sinh \phi} \tag{2.156}$$

Total flow at x=0, i.e. into pore is given by

$$\text{flow} = -\pi r^2 D_n \frac{dC_A}{dx}\Big|_{x=0}$$

or

$$\text{flow} = \pi r^2 \sqrt{k_1 D_n} \left[\frac{C_1}{\tanh \phi} - \frac{C_2}{\sinh \phi}\right] \tag{2.157}$$

2.3.2 Node Concentrations in a Pore Network:

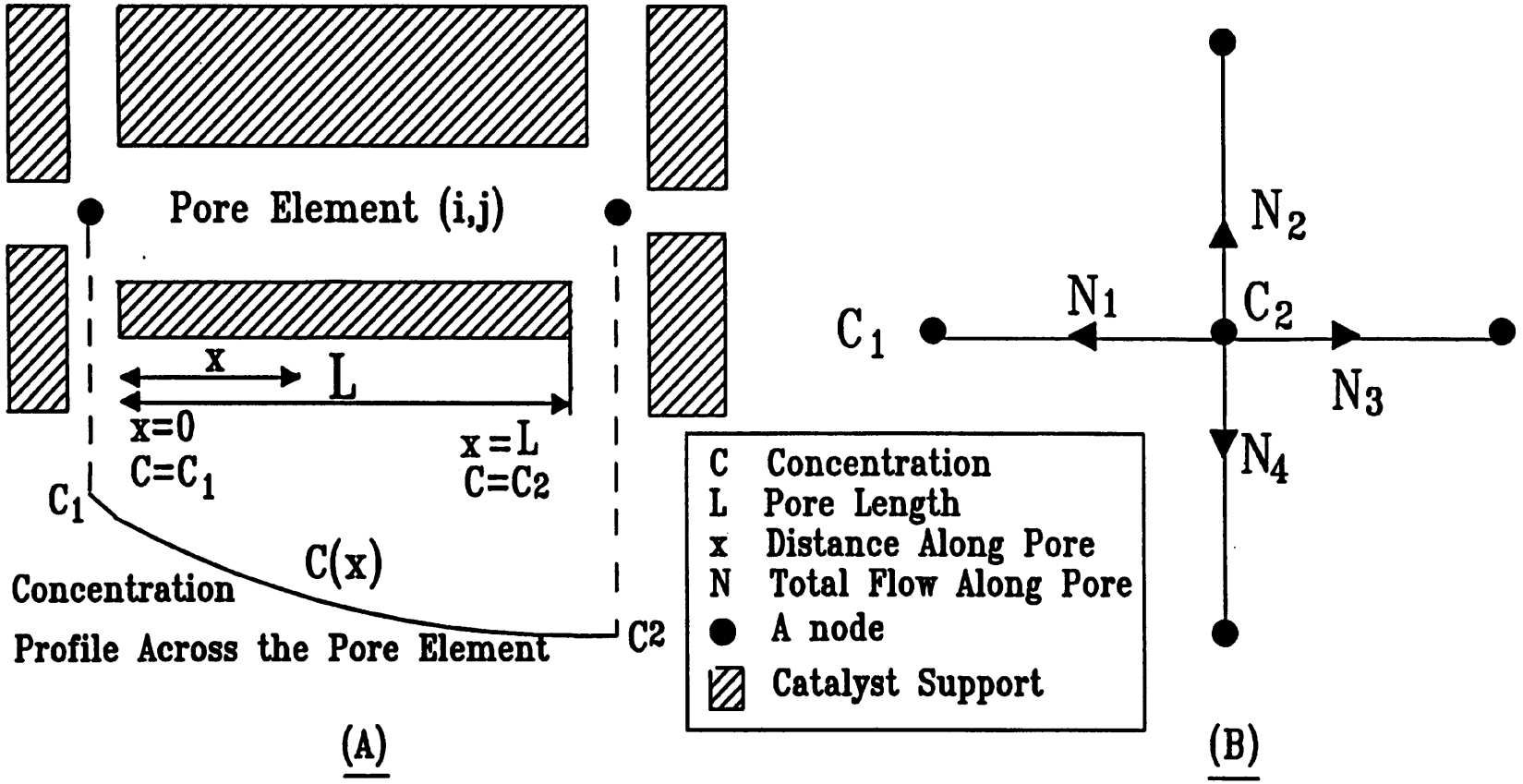

Figure 2.8 : (A) Co-ordinates and boundary conditions for a single pore element
(B) Concentrations and flows around a node in a square network.

For the pore network, of size n'xn' assuming negligible reaction at the nodes, then the sum of all in and out flows for each node is zero (Fig. 2.8B):

$$\sum_{i=1}^{m} N_i = 0 \tag{2.158}$$

where

$m = 4$ (connectivity of the node)

For diffusivity dependent on radius, it becomes

$$C_1 \sum_{i=1}^{m} \frac{r_i^2 \sqrt{D_i}}{\tanh\phi_i} - \sum_{i=1}^{m} \frac{C_{2i}\, r_i^2 \sqrt{D_i}}{\sinh\phi_i} = 0 \tag{2.159}$$

where some of the C values may be equal to the external concentration.

The above equation can be compactly written

$$C_1 \sum_{i=1}^{m} \alpha_i + \sum_{i=1}^{m} \beta_i C_{2i} = \sum_{i=1}^{m} \gamma_i \tag{2.160}$$

A network of size n'xn' nodes, gives rise to $(n')^2$ such equations which can be expressed in the matrix form:

$$\mathbf{A}.\underline{C} = \mathbf{b} \tag{2.161}$$

The solution of the above equation, $\underline{C}$, is the set of node concentrations.

Solution of the $(n')^2$ equations is simplified somewhat by the fact that the matrix **A** is sparse, that is most of the elements are zero. This facilitates rapid solution

by computer. A modified Gaussian elimination method was used instead of the more usual iterative methods. Iterative methods are unsatisfactory in this case because they often fail to converge. This arises directly from the form of the equations (Tewarkson, 1973).

2.3.3 Deactivation in a Pore Network:

Modelling the deactivation process in a pore network is similar to that in a corrugated parallel bundle of pores except for the fact that the boundary conditions for the open–ended pores of the network are different from those of the close–ended pores of the corrugated pores. When a method to determine the concentrations at the nodes of the stochastic pore network has been calculated, the same procedures followed in sections 2.2.2 to 2.2.10 are repeated. As before, it was necessary to specify those reactions which lead to coke deposition and to express their rates in an appropriate kinetic equation. The local rate of coke deposition can then be calculated for each pore element in the network using the node concentrations. The coking rate in each pore element must be linked to two other quantities; the rate of change of mean element radius and the rate of loss of local catalytic activity.

Coke deposition was assumed to be uniform within each individual pore element. The rate of coke growth in a pore element was taken to be equal to the greater of the two coking rates calculated using the concentrations at the pore ends. Changes in the network with time on stream were followed by calculation of the changes in the mean pore radii. For each pore element one equation, describing the change in the pore radii as a result of coke deposition, was required. For an n'xn' network with $2n'(n'+1)$ pore elements, the total number of equations required to describe the changes in the network is $2n'(n'+1)$. For a 10x10 network, 210 separate radius change equations would be used. These equations were integrated simultaneously using a fourth order Runge–Kutta algorithm (Appendix–2).

2.3.4 Pore Blocking in the Network:

If the pore radius in any element reaches zero, then the pore is blocked. In this case, the pore is assumed to take no further part in the system giving no conversion or mass transfer. Pore blocking can lead to isolation of regions within the network. If a single node becomes isolated, by the blocking of the four adjacent pores, then one row in the coefficient matrix A will have all terms equal to zero. The matrix has been reduced in order by one. It is necessary to take account of this when implementing the method in a computer program. It is also possible that a region becomes isolated, that is one or more pore elements and a number of nodes. In this case, the concentration calculated at any node in that region will be identically zero. This fact is potentially useful in the identification of these isolated regions, which would otherwise require a lengthy search.

The computer program (OMRAN10) written in the FORTRAN language, solves the equations for diffusion, reaction and deactivation through a stochastic pore network of size 10x10. The listing of the program (OMRAN10) is given in Appendix–3. Figure 2.7, presented earlier, shows the sequence of calculations for the diffusion, reaction and deactivation equations in a fluidised bed reactor. The program produces conversion, coke content and surface area changes in the network as a function of time on stream. It also produces values for the radii of the network pore elements at different stages of coking. These values were used with a graphical package (GSX) on an Apricot personal computer to visualise the corresponding networks showing the configuration of coke laydown amongst the pores in the network.

CHAPTER THREE

EXPLORATION OF THE THEORY USING A CORRUGATED PARALLEL BUNDLE MODEL

CHAPTER THREE

EXPLORATION OF THE THEORY USING A CORRUGATED PARALLEL BUNDLE MODEL

3.1 SIMULATION OF THE FLUIDISED BED REACTOR:

Using the equations developed in Chapter Two, theoretical simulations were carried out to assess the changes in the conversion, coke content and surface area of the catalyst as a result of changes in the deactivation mechanism, deactivation parameters or the physical properties of the catalyst particle.

In the following illustrations, the structural model used to represent the support pore structure was the corrugated parallel bundle. It was found that two thousand 10–element pores were sufficient to give a reproducible pore size distribution. These two thousand pores are referred to as a "catalyst particle". In order to simulate the fluidised bed, ten such catalyst particles with stochastically different pore size assemblies were generated. Figure 3.1 illustrates the pore number distribution, and Figure 3.2 illustrates the pore volume distribution for several such particles. Diffusion, reaction and deactivation were simulated in each particle simultaneously to produce an average activity profile for the reactor. Computer simulations of the program "OMRANCOR" (Appendix–1) were carried out for a run time of 120 minutes to explore the deactivation behaviour of the fluidised bed under different deactivation mechanisms, i.e. parallel, series and triangular deactivation. The solution was carried out using a fourth order Runge–Kutta technique (Appendix–2) with a variable time step length. A time step of one minute was used for the first 20 minutes of the simulation and this was increased to 5 minutes for the remainder of the run. The effect of changes in the different parameters (e.g. coke sizes for the support and zeolite, rate constants for the main and coking reactions and pore length) was also investigated.

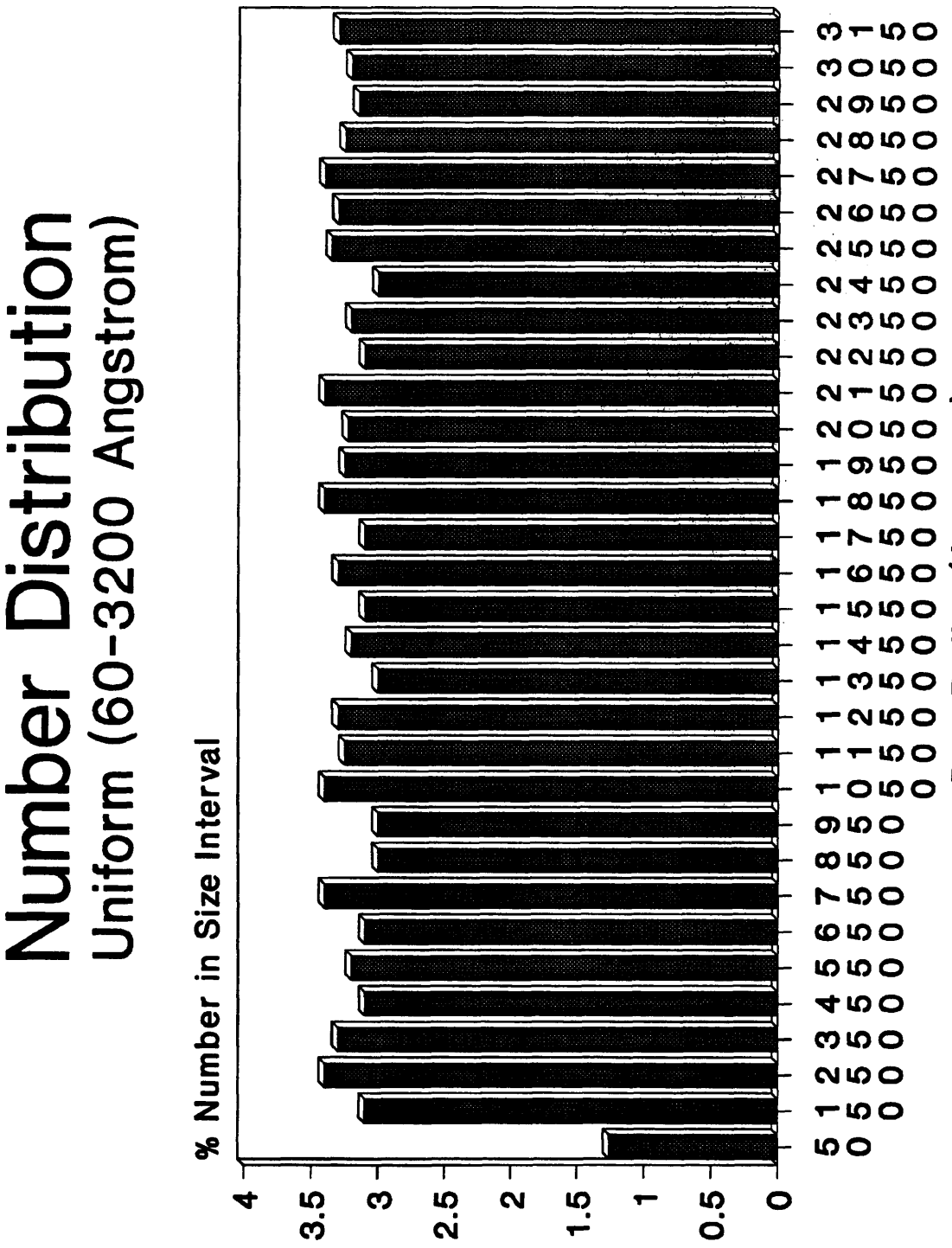

Figure 3.1 Number distribution of pore radii for the pore model.

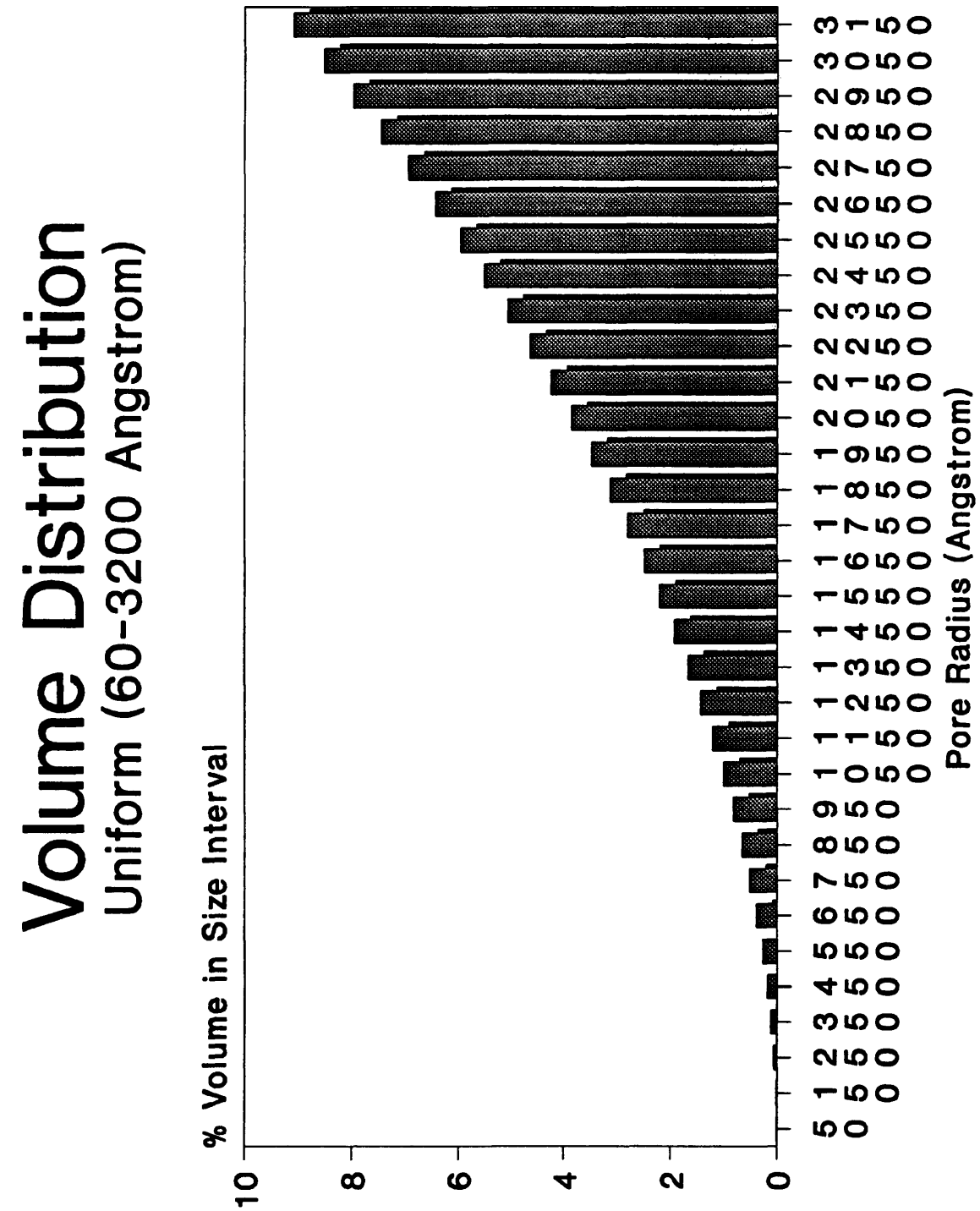

Figure 3.2 Volume distribution of pore radii for the pore model.

A variable diffusion coefficient was employed to allow for the possibility of Knudsen diffusion in the smaller support pores (Fig.3.2b). Satterfield and Sherwood (1963) provided the following equation which was used to calculate the Knudsen diffusion coefficients:

$$D = 97\ R \sqrt{\frac{T}{M}} \qquad (3.1)$$

Where

D :is diffusion coefficient in (m^2/s)

T :is the temperature at which the diffusion occurs, ^{o}K

M :is the molecular mass of the diffusing species, and

R :is the radius of the pore.

In this work, T was set to 773 ^{o}K (500 ^{o}C) which is the temperature of the experiments detailed in chapter five, and M was set to 120 (the molecular mass of cumene). Substituting into equation (3.1):

$$D = 246\ R \qquad (3.2)$$

To calculate the value of the largest pore in which Knudsen diffusion occurs, R, a value for the diffusion coefficient of 10^{-5} (m^2/s) (Thomson, 1986) was used in equation (3.2) to give:

$$R = 4.06 \times 10^{-8}\ m\ (= 406\ \text{Angstrom}) \qquad (3.3)$$

So, the diffusion coefficient inside pores greater than 406 Angstroms is $10^{-5}(m^2/s)$, whereas, diffusion coefficients for all smaller pores are proportionately smaller than $10^{-5}(m^2/s)$. For the smallest pore in the catalyst (super–D) pore size distribution with a radius of only 60 Angstroms, the diffusion coefficient was $1.48 \times 10^{-6}(m^2/s)$.

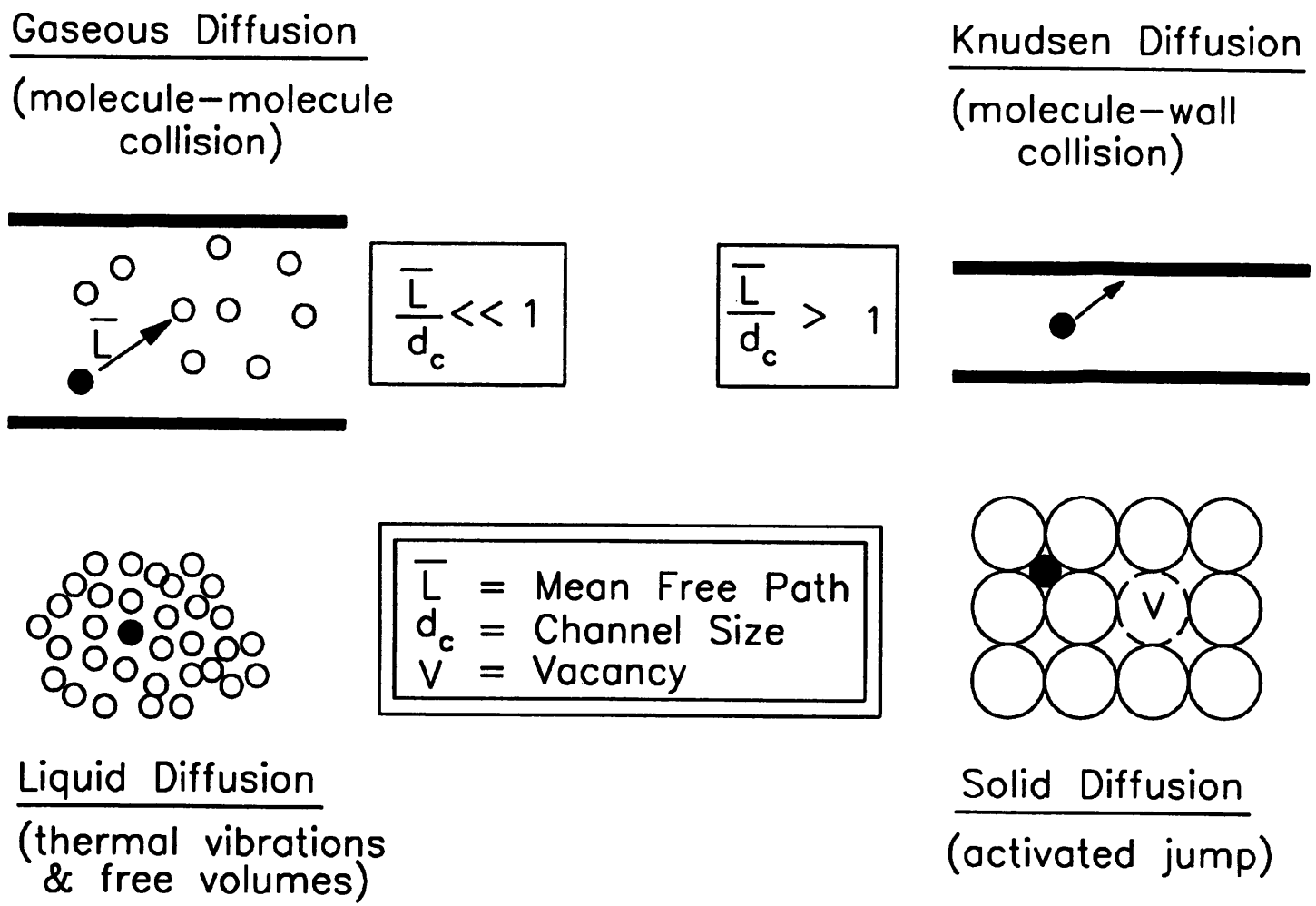

Figure 3.2b Schematic of diffusion regimes [Redrawn from Xiao & Wei(1992)].

Since these explorations will eventually be used to simulate the disproportionation of cumene over super–D catalyst, the physical properties of the catalyst such as the pore length and specific pore volume required by the program were those of the catalyst super–D. Also, following the work of Viner and Wojciechowski (1984), the coking equation (2.60) was modified to be second order in active area and first order in product and reactant concentrations, that is:

$$\frac{dR}{dt} = -(k_{cs} C_P + k_{cp} C_A) A_{os}^2 \qquad (3.4)$$

The second order term of active surface area in the above equation may arise from the fact that the actual uneven surface area of the coked catalyst is much larger than the average radius term used in equation (2.60) (Fig. 2.5). Table 3.1 provides the default values of the major parameters in the program "OMRANCOR" which were used in the simulations. These simulations should be useful when modelling the experimental deactivation behaviour.

For each of the simulations, the following figures were produced:

1) Conversion vs. time,
2) Total catalyst coke content vs. time, and,
3) Total catalyst surface area vs. time.

When necessary, figures showing changes in the effectiveness factor with time were produced wherever conditions of significant diffusional resistances prevailed.

3.2 EFFECT OF CHANGING THE COKING RATE CONSTANTS:

Investigation of the effect of changing coking rate constants for the parallel, series and triangular mechanisms of coking were carried out. Values for the coking rate constants were in the range 1.5×10^{-14} to 1.5×10^{-9} ($m^4/s/kmol$).

Table 3.1 Default values of major parameters in the program "OMRANCOR".

Parameter	Value	
Pore length	14	Microns
Zeolite coke unit size	1	Angstrom
Support coke unit size	20	Angstrom
Main reaction rate constant k_s	$6x10^{-8}$	(m/s)
Coking rate constants k_{cs} & k_{cp}	$1x10^{-10}$	$(m^4kmol^{-1}s^{-1})$
Zeolite fractional activity α	0.5	(Initially)
Catalyst:feed ratio	7.5:1	g/(g/min)
P.S.D.(Uniform Distribution)	60–3200	Angstrom

Setting the coking constants to zero represents the case of no deactivation of the catalyst which produces a flat conversion profile indicative of constant activity with zero coke content and 100% catalyst surface area active. This also, served as a simple check for the performance of the computer program used for the simulations.

3.2.1 Series Deactivation:

Setting the value of the parallel coking constant to zero, the series coking constant was increased from $1.5x10^{-14}$ to $1.5x10^{-13}$ which had little effect on the flat conversion profile indicative of negligible coking (2% drop in conversion, 0.1% coke and 10% drop in surface area(Fig. 3.3)). The relatively large drop in surface area as a result of a small amount of coke content (0.1%) is due to the high probability of the laydown of the coke units on active surface area rather than on top of each other. For a coking rate constant of $1.5x10^{-12}$, the conversion drop over the length of the simulation was 20% with 1.0% coke content and 52% drop in surface area. When the coking rate constant reaches a value of $1.5x10^{-10}$, the conversion drops to 10% over the first 15 minutes, with a final value of 3% with 4.1% coke content and 15% surface area. As the

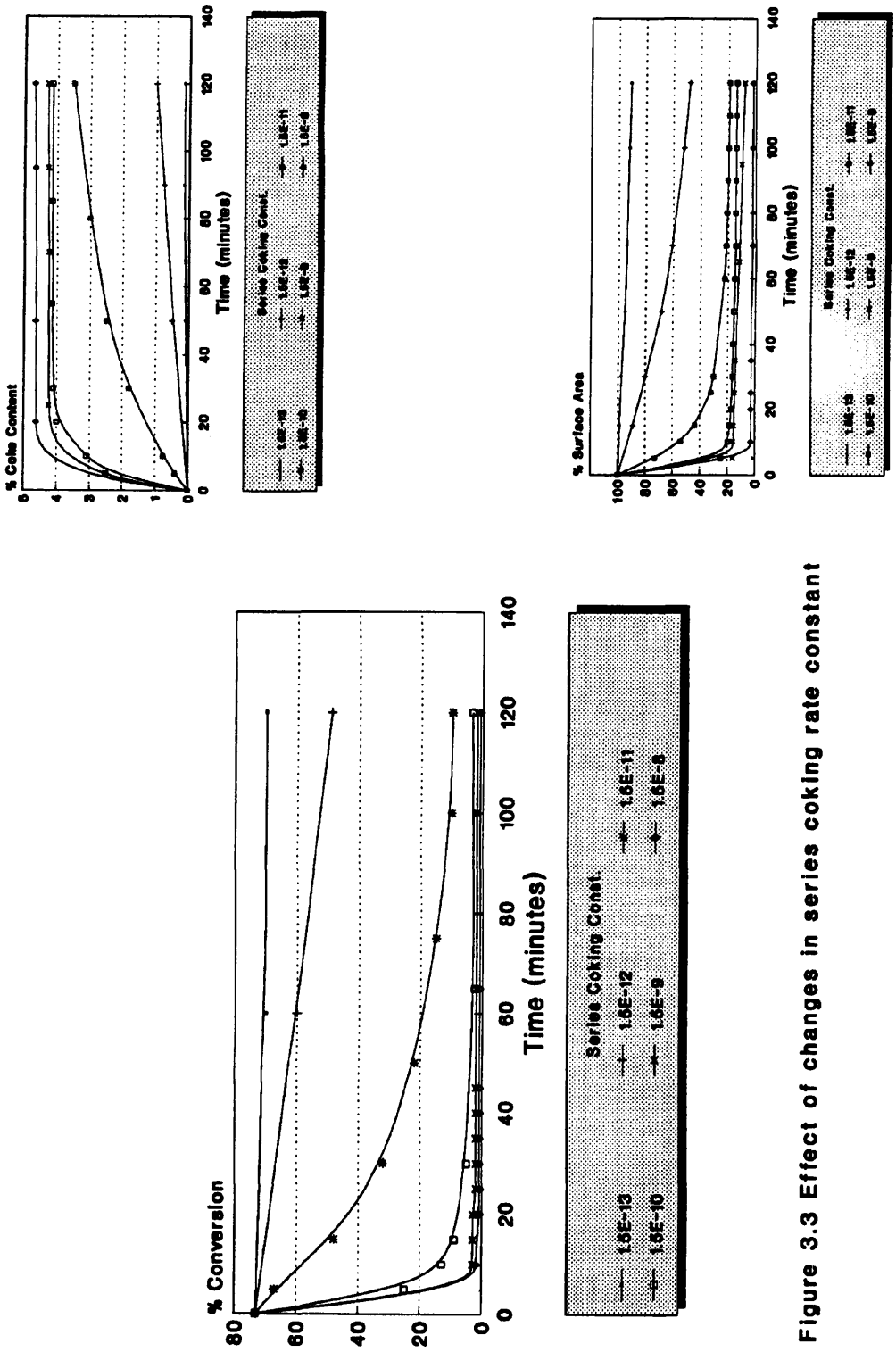

Figure 3.3 Effect of changes in series coking rate constant

coking rate constant is increased by a further order of magnitude to $1.5x10^{-9}$ the conversion dropped to 1%, coke content 4.1%, and 8% surface area all reached their final values in 2 minutes. The zeolite surface area has been fully lost during the time of the simulation for coking rate constants of $1.5x10^{-10}$ and larger.

3.2.2 Parallel Deactivation:

Setting the value of the series coking constant to zero, the parallel coking constant was increased from $1.5x10^{-14}$ to $1.5x10^{-13}$ which again had even smaller drop in conversion, 1% over the length of the simulation(Fig. 3.4), compared to series deactivation. When the parallel coking constant increased to $1.5x10^{-12}$ it produced 12% drop in conversion, 0.6% coke content and 65% surface area which again demonstrated a smaller degree of deactivation compared to the same value for series coking constant. As soon as the parallel coking constant was increased to $1.5x10^{-11}$ the conversion dropped sharply to a final value of 3% with 4.2% coke content and 13% surface area which was a greater deactivation when compared to series coking. Similar results were observed for larger coking rate constants. The zeolite surface area has been completely lost during the time of simulation for parallel coking rate constants of $1.5x10^{-11}$ and larger compared to $1.5x10^{-10}$ for series deactivation. When comparing the effect of coking rate constants, it became clear that for values less than $1.5x10^{-11}$ the series mechanism of coking was more damaging to the conversion, surface area and coke content. But for coking rate constants greater or equal to $1.5x10^{-11}$ a parallel mechanism of coking was more damaging. This result is related to the fact that the effectiveness factor values for the catalyst particles for all the simulations were found to be nearly 1.0 (i.e. diffusional resistance was negligible). This condition produces a flat concentration profile across any individual pore. Then, the coking rate in any given pore element will be proportional to the bulk concentration of the reactant (parallel coking) or the product (series coking) and the corresponding coking rate constant.

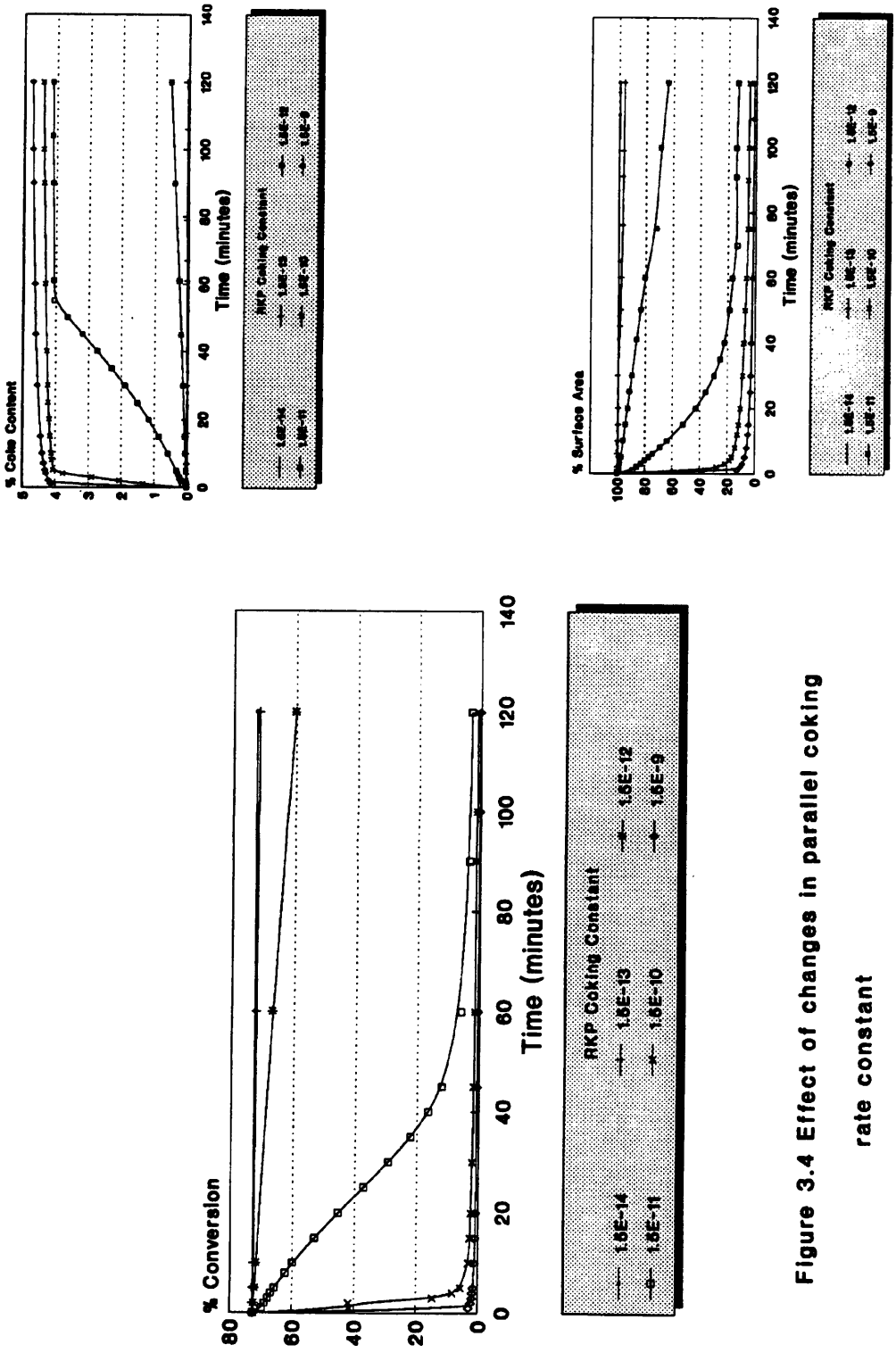

Figure 3.4 Effect of changes in parallel coking rate constant

The assumption of equimolar counter diffusion implies that the sum of the concentrations of the product and reactant is constant. Therefore, for conversions over 50% the concentration of the product is greater than the reactant, which results in the series deactivation being more pronounced. For conversions less than 50%, the concentration of the reactant is greater than the product, which results in the parallel deactivation being more significant.

3.2.3 Triangular Deactivation:

Comparing the conversion, coke content and surface area figures for the triangular coking rate constants with the series and parallel coking rate constants, it is obvious that for a given coking rate constant, the triangular deactivation is more damaging than either parallel or series deactivation alone (Fig. 3.5). For the series and parallel coking rate constants having an equal value of 1.5×10^{-12}, the triangular deactivation produced the following final values over the length of the simulation (conversion = 36%, coke content = 1.6%, surface area = 34%) compared with series alone (conversion = 50%, coke content = 1.0%, surface area = 48%) and parallel alone (conversion = 60%, coke content = 0.6%, surface area = 65%). Also, the greatest zeolite loss occurs under triangular deactivation. For a coking rate constant of 1.5×10^{-11}, total zeolite loss occurs after just 35 minutes during triangular deactivation compared with 55 minutes for parallel deactivation while under series deactivation the zeolite activity is still not completely lost at the end of the simulation time of 120 minutes.

3.3 EFFECT OF CHANGING THE COKE UNIT SIZES:

Investigation of the effect of changing the support coke size and the zeolite coke size were carried out. The simulations included the three deactivation mechanisms (parallel, series and triangular). Table 3.2 shows the coke unit sizes used in the

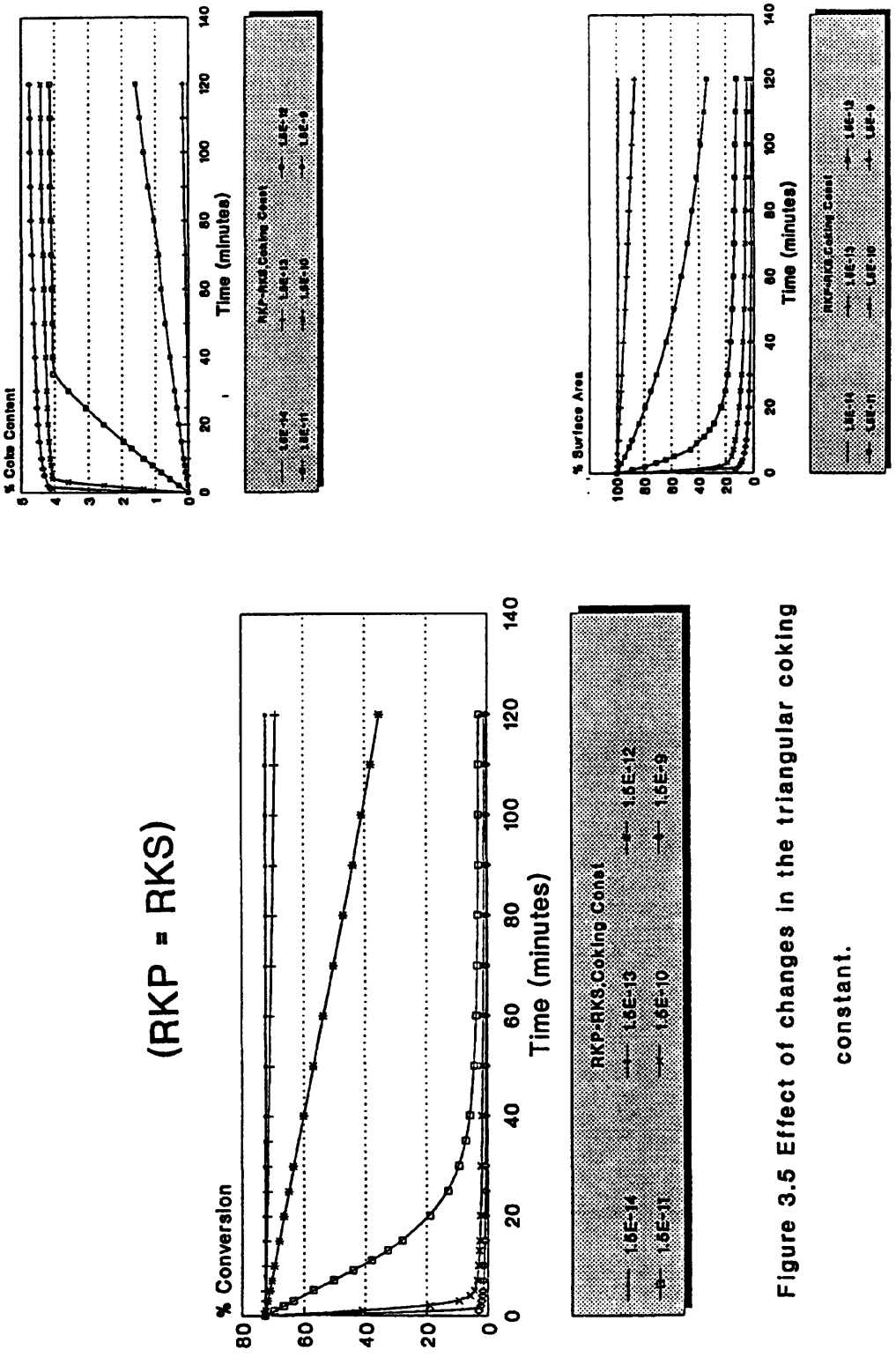

Figure 3.5 Effect of changes in the triangular coking constant.

Table 3.2 The coke unit sizes used in the investigations.

Support Coke Unit Size	Zeolite Coke Unit Size
1.0 Angstrom	0.1 Angstrom
2.0 Angstrom	0.2 Angstrom
4.0 Angstrom	0.4 Angstrom
8.0 Angstrom	0.8 Angstrom
16.0 Angstrom	1.6 Angstrom
32.0 Angstrom	3.2 Angstrom

investigations.

3.3.1 Effect of Changing Support Coke Unit Size:

The support coke unit size was changed from 1.0 Angstrom up to 32.0 Angstroms while the zeolite coke unit size was kept at 1.0 Angstrom to study the effect of only changes in the support coke unit size.

3.3.1.1 Series Deactivation:

For a support coke size of 1.0 Angstrom, the conversion dropped from an initial value of 72% to a final value of 20% under series deactivation (Fig. 3.6). When the coke size changed to larger values up to 32 Angstroms, the final conversion dropped to a value of 10%. Looking at the initial and final conversions only, one comes to the wrong conclusion that larger support coke unit sizes have a more damaging effect on the activity of the catalyst than smaller size coke units. But careful study of the conversion profiles revealed the fact that smaller support coke unit size produced a larger drop in conversion initially up to a region where conversion profiles of different

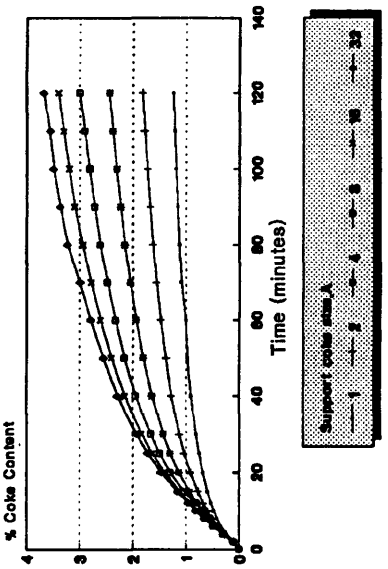

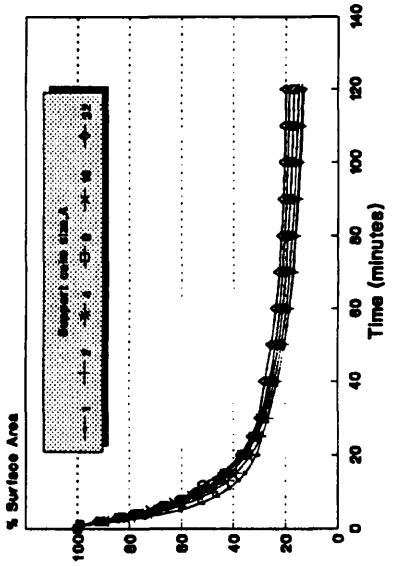

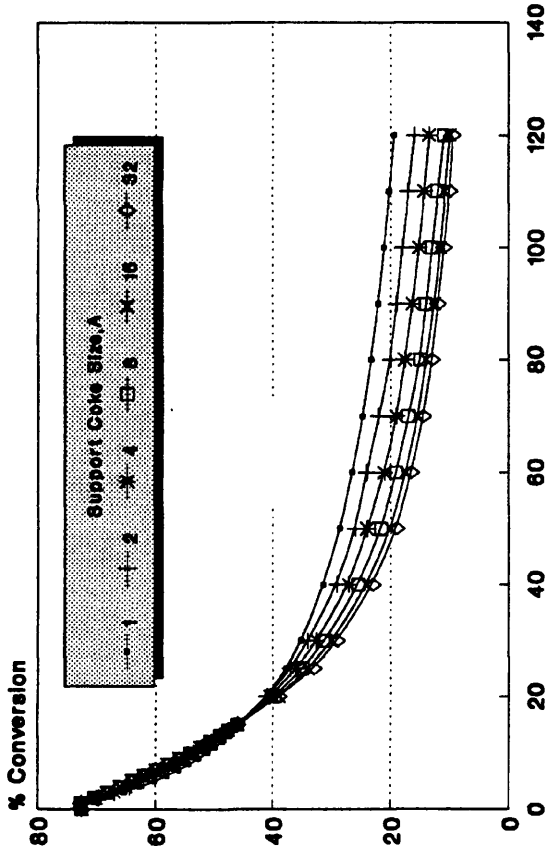

Figure 3.6 Effect of changes in the support coke unit size for series coking mechanism

support coke sizes intersect with each other (in this case at 43% after 20 minutes on stream for series deactivation). Then the conversion profiles diverge with large coke sizes producing lower conversions than the smaller coke sizes up to the end of the time of simulation (120 minutes).

3.3.1.2 Parallel Deactivation:

For the parallel mechanism of coking the same effect has been observed on the conversion profiles with an initial more damaging effect of smaller support coke unit sizes and later crossing over and then diverging with a more damaging effect of larger coke sizes (Fig. 3.7). Since the parallel deactivation is less effective at conversions greater than 50%, this shifting region is reached after a longer time on stream (25 minutes).

3.3.1.3 Triangular Deactivation:

For a triangular mechanism of coking, a similar trend is observed with a larger drop in conversion because of the combined effect of both parallel and series coking. Figure 3.8 shows that the changeover region is reached after only 15 minutes on stream.

The coke content profiles for the different deactivation mechanisms show that the support coke unit size proportions to the coke content. Under triangular deactivation, the coke content of 1.2% was achieved for a support coke size of 1.0 Angstrom after 2 hours on stream, while a coke size of 32 Angstroms, produced a coke content of 4.0% in under one hour on stream. The surface area profiles for the different deactivation mechanisms showed that the loss in surface area is inversely proportional to the support coke unit size. Under a series coking mechanism, the final surface area for 1 Angstrom coke size was 6% in comparison with 15% for 32 Angstroms support

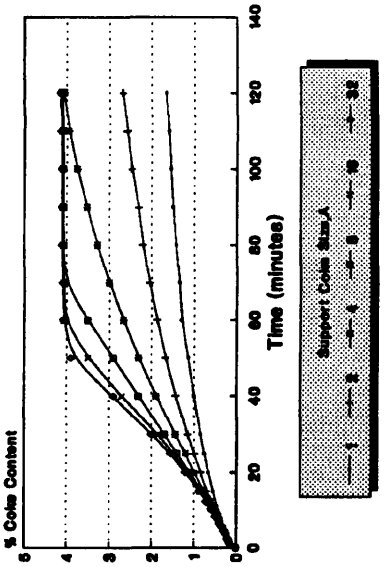

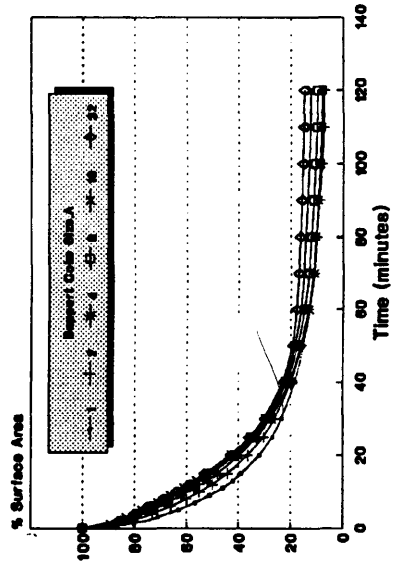

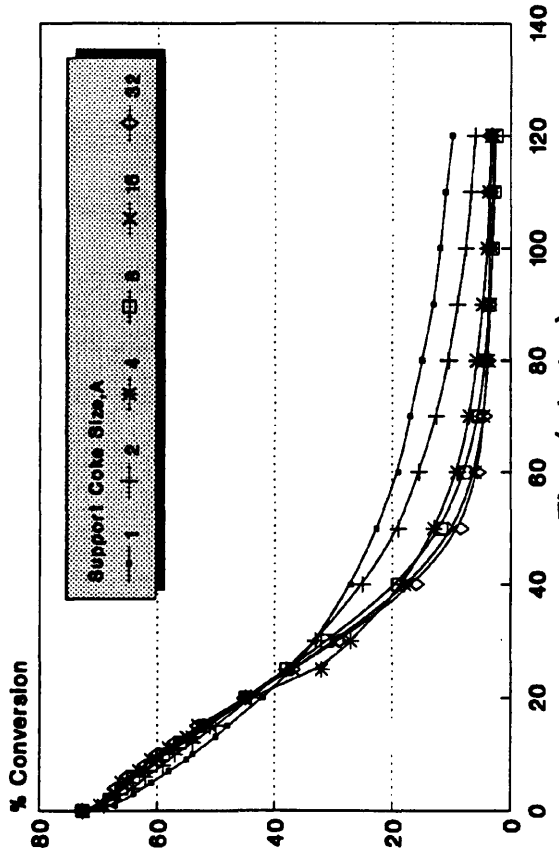

Figure 3.7 Effect of changes in support coke unit size for parallel coking mechanism

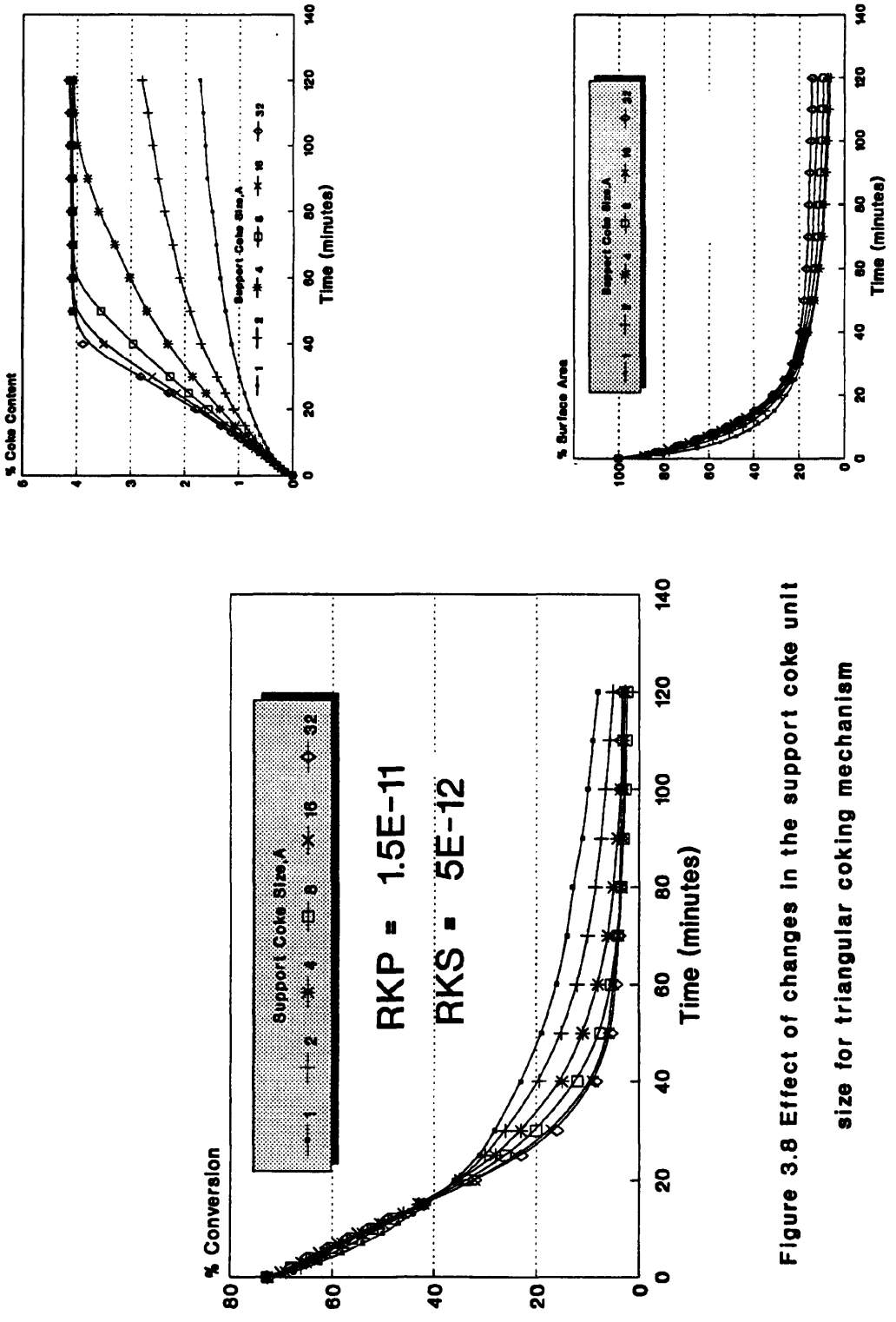

Figure 3.8 Effect of changes in the support coke unit size for triangular coking mechanism

coke unit size.

The apparent shift in the conversion profiles can be explained by the balance between the remaining active surface area and the amount of coke present in the catalyst. Initially, the smaller support coke unit sizes cause a large drop in surface area while forming a small coke content in comparison with larger coke sizes which cause a smaller drop in area but give larger coke content. When these two factors are balanced, conversion profiles intersect with each other (changeover region). After that the effect of the coke accumulation by larger size coke units becomes more detrimental to conversion than the smaller coke sizes.

3.3.2 Effect of Changing Zeolite Coke Unit Size:

The zeolite coke unit size was changed from 0.1 Angstrom up to 3.2 Angstroms while the support coke unit size was kept at 20 Angstroms to investigate the effect of only changes in zeolite coke unit size.

3.3.2.1 Series Deactivation:

For zeolite coke unit size of 0.1 Angstrom, the conversion dropped from an initial value of 72% to 10% in about 10 minutes reaching its final value of 5% after 120 minutes under the series coking mechanism (Fig. 3.9). As the zeolite coke unit size increased, the drop in conversion reduced significantly showing a strong inverse relationship between the size of the zeolite coke unit and the conversion drop. For a zeolite coke size of 3.2 Angstroms the conversion drops gradually and almost linearly over the length of the simulation (120 minutes) to a final value of 28%. Looking at the coke content profiles, we see clearly that the coke content is proportional to the zeolite coke unit size. For a zeolite coke unit size of 0.1 Angstrom, the coke content produced was 1.2% compared with a zeolite coke unit size of 3.2 Angstroms which produced

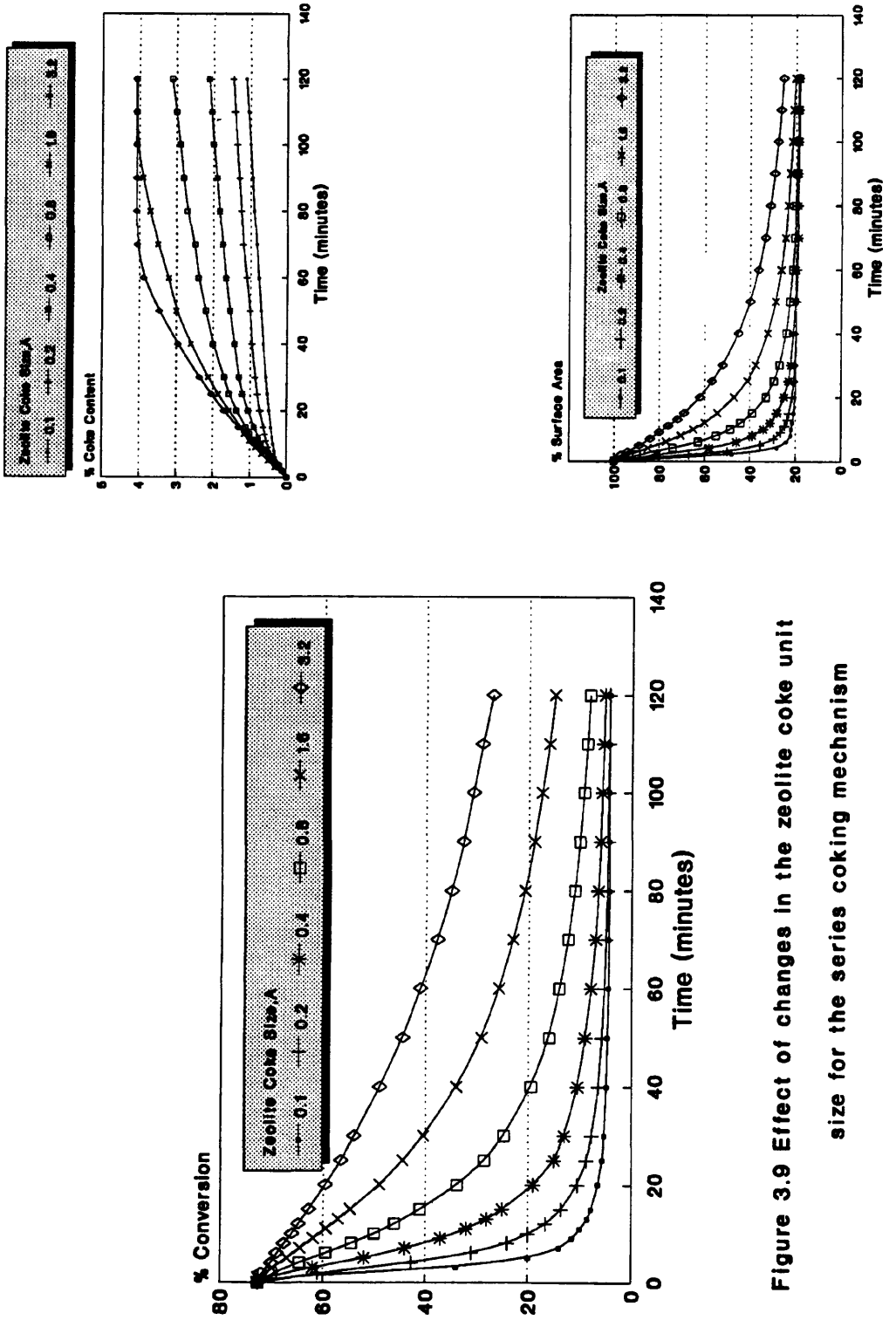

Figure 3.9 Effect of changes in the zeolite coke unit size for the series coking mechanism

4.1% coke content under series deactivation.

The shape of the surface area profiles are very much like the conversion profiles. The surface area drops very sharply with small zeolite coke unit size, with a much slower drop for larger coke sizes.

3.3.2.2 Parallel Deactivation:

For the parallel deactivation, the conversion is still inversely proportional to zeolite coke unit size. The rate of deactivation was slower than series coking at conversions higher than 50% (Fig. 3.10). As soon as conversion drops below 50% the reactant concentration becomes larger than the product concentration making the parallel deactivation more important. The final conversions are lower for parallel coking in comparison with series coking.

Surface area profiles exhibit again an inverse relationship between surface area and zeolite coke unit size.

Coke content profiles show that increasing the zeolite coke unit size produced smaller coke contents. For a coke size of 0.1 Angstrom it took 40 minutes for the coke content to reach 4% while it took 85 minutes for coke size of 3.2 Angstroms to reach same coke level. So, the zeolite coke unit size has an opposite effect on the coke content for the series and parallel deactivation mechanism.

3.3.2.3 Triangular Deactivation:

For triangular deactivation, the conversion profiles give an inverse relationship between coke size and conversion similar to other coking mechanisms with larger drops in conversion due to the combined effect of both mechanisms. Surface area profiles

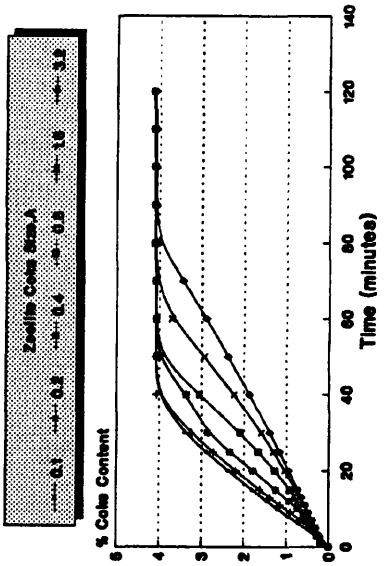

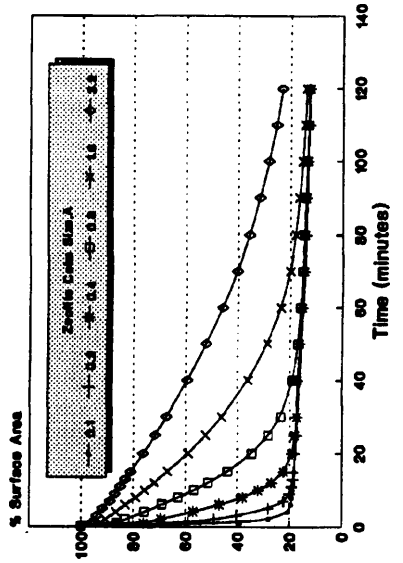

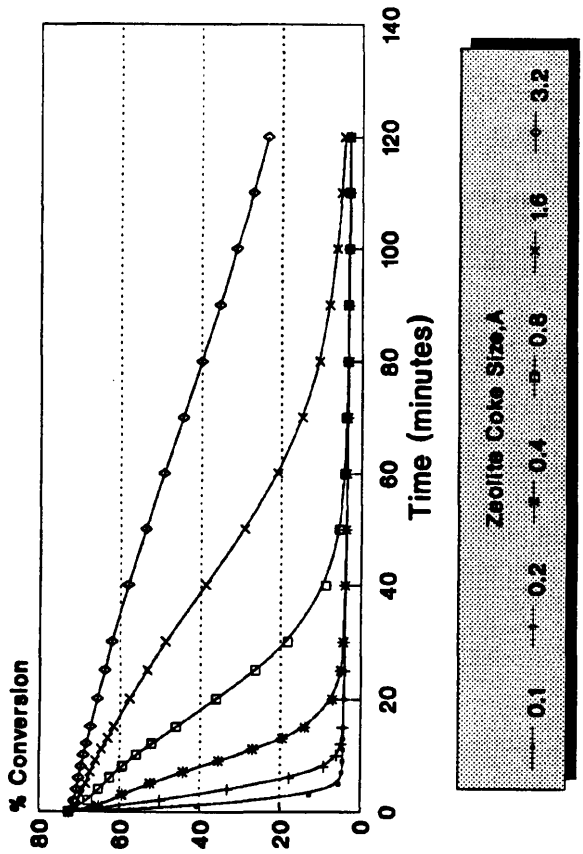

Figure 3.10 Effect of changes in the zeolite coke unit size for the parallel coking mechanism

follow conversion profiles and show the same relationship with a larger drop than other coking mechanisms (Fig. 3.11).

Coke content profiles show the competition between the two coking mechanisms which have an opposite effect on the coke content in relation to changes in zeolite coke unit size. So, in the case that the parallel rate constant is greater than the series rate constant, the coke content profiles exhibit an inverse relationship with coke size similar to parallel coking alone. While for series coking with a rate larger than the parallel coking rate, the coke profiles exhibit a directly proportional relationship between coke content and coke size, similar to series coking alone. For triangular deactivation with both parallel and series coking constants having the same value, a single unique curve for the coke content is produced regardless of the zeolite coke unit size. This is due to the assumption that the concentration of the reactant and product is always constant which produces an equal but opposite effect of the parallel and series coking on the coke content when the constants are equal.

3.4 EFFECT OF CHANGING THE PORE LENGTH:

To investigate the influence of the pore length on the conversion, coke content and surface area profiles, the pore length was multiplied by a factor of 3 starting with 14 microns and going up to 3402 microns. The investigation included the three mechanisms of coking, namely, the series, parallel and triangular deactivation. Figure 3.12 shows the conversions and effectiveness factors for the case of no deactivation.

3.4.1 Series Deactivation:

For the series deactivation, it was observed that changing the pore length from 14 microns up to 126 microns produced a negligible effect on the conversion profile (2% drop in initial conversion(Fig. 3.13)). As the pore length increased further to 378

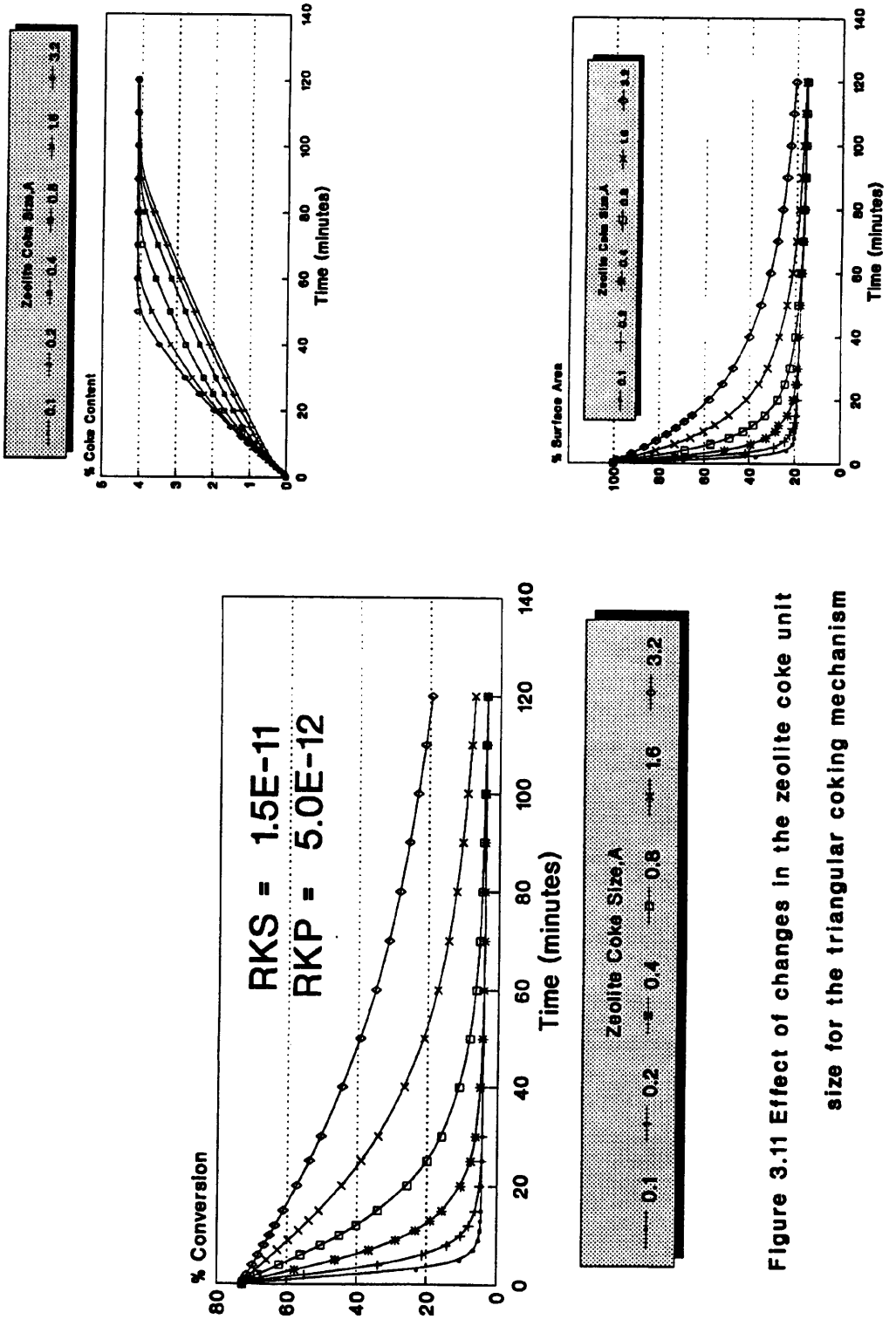

Figure 3.11 Effect of changes in the zeolite coke unit size for the triangular coking mechanism

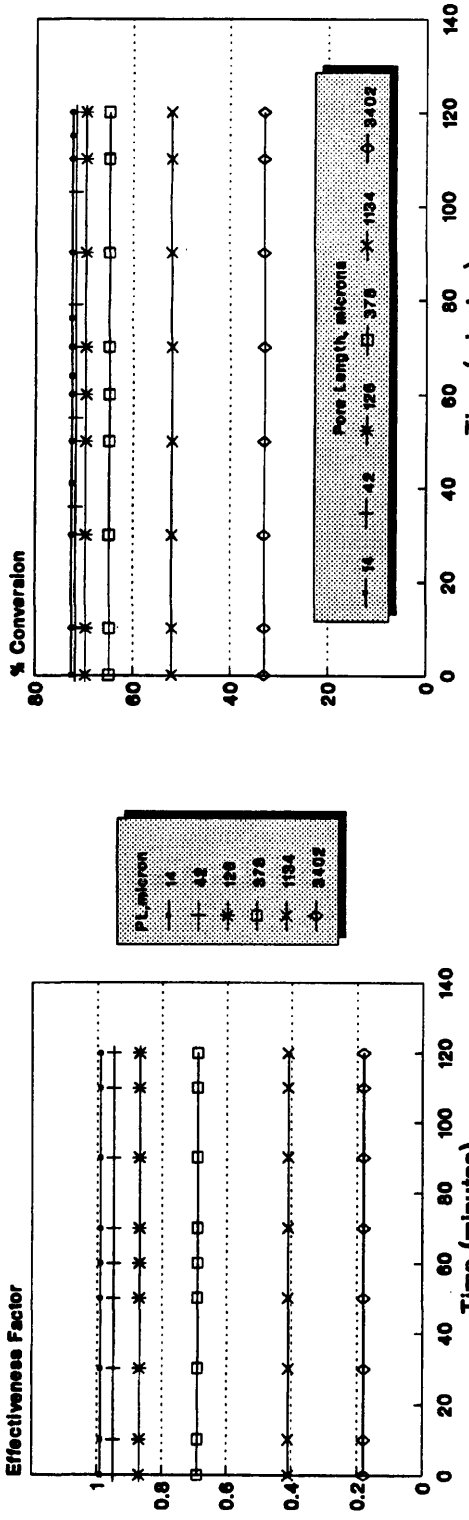

Figure 3.12 Effect of changes in the pore length on effectiveness factor and conversion for no deactivation case

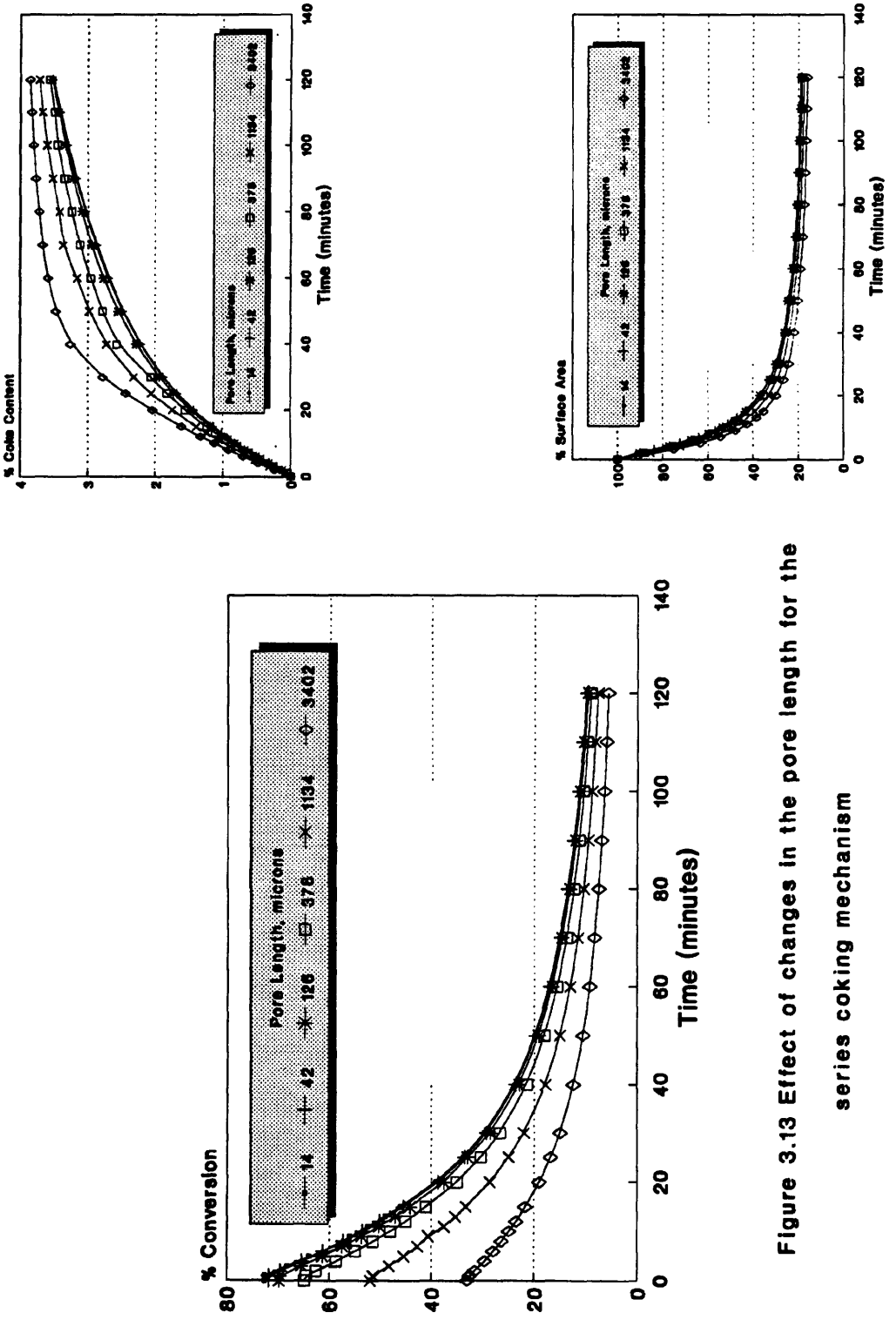

Figure 3.13 Effect of changes in the pore length for the series coking mechanism

microns the initial conversion dropped by 7%. When the pore length was at the largest value of 3402 microns the initial drop in conversion reached 40%. As the time on stream increased the conversion profiles started to converge to produce a maximum difference of 5% in the final conversions between the largest and smallest pore length. So, increasing pore length causes a reduction in the initial conversion of the catalyst and also causes a reduction of the slope of the conversion profile.

The coke content profiles show an increase in the coke content as the pore length gets larger. The coke profiles diverge up to a time on stream of 50 minutes when the largest difference in coke content is 1%, then converges to give a difference of only 0.4% at the end of the simulation (120 minutes). The surface area profiles have illustrated the fact that larger pore lengths produced a slightly larger drop in surface area compared with smaller pore lengths. The difference in surface area between the largest and smallest pore length was always less than 10%.

The change in overall effectiveness factor is reproduced in Figure 3.14 . For a short pore length of 14 microns the effectiveness factor is almost unity and remains constant to the end of the simulation. For a pore length of 126 microns the effectiveness factor starts with an initial value of 0.87, but increases with time on stream to approach unity at the end of the simulation. As the pore length increases, the effectiveness factor reduces. When pore length reaches its largest value of 3402 microns, the initial effectiveness factor is just below 0.2 and then increases with time to reach a final value of 0.82.

The above observations are consistent with the classical theory which predicts that increasing the pore length should increase the diffusional resistances in a pore and therefore decrease the effectiveness factor.

3.4.2 Parallel Deactivation:

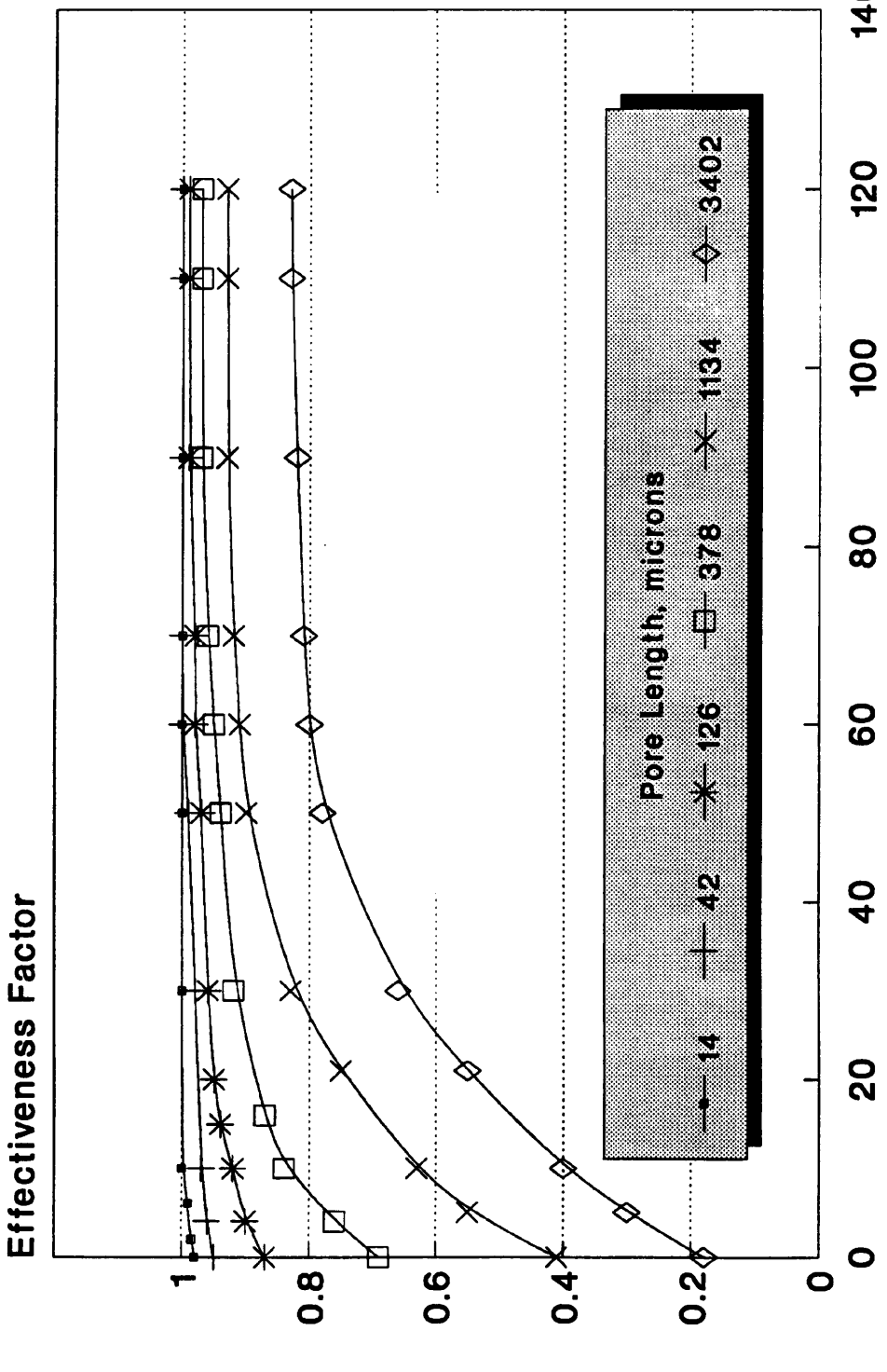

Figure 3.14 Effect of pore length on effectiveness factor for series coking mechanism.

For a parallel mechanism of coking, the effect of increasing the pore length is even more detrimental to the effectiveness factor than series deactivation. For pore lengths over 378 microns, the initial effectiveness factor is always less than 0.7 and decreases with time on stream to reach final values as low as 0.05, indicating very severe diffusional resistances across the pore length (Fig. 3.15). Conversion profiles for the parallel coking, show a decrease in conversion as the pore length increases especially for lengths over 126 microns (Fig. 3.16). Also, increasing the pore length has the effect of reducing the slope of the conversion profiles.

The coke content profiles show a decrease in the coke content as the pore length increases. The coke profiles diverge up to a time on stream of 55 minutes when the largest difference in coke content reaches 2.5% and then stays almost constant to the end of the simulation. The surface area profiles show that shorter pores produced larger surface area drops than longer pores. For a pore length of 14 microns, the area dropped to 30% of its initial value in just about 30 minutes. The same detrimental effect was observed for pore lengths up to 126 microns after which the drop in surface area started to be smaller. For the largest pore length (3402 microns), the drop in surface area was small and gradual so that after 120 minutes on stream the catalyst had approximately 50% of its surface area still active.

Classical theory predicts that increasing the pore length should increase the diffusional resistances in a pore and should result in the appearance of foulant profiles along the pore. The effect of diffusional resistances on the zeolite micropores volume loss for the largest and smallest pores (by volume) from one of the typical pore size distributions is illustrated in Figures 3.17, 3.18 and 3.19. The profiles for pore lengths of 14 microns up to 126 microns show no evidence of any foulant profile with the deactivation occurring completely uniformly throughout the largest and smallest pores (Fig. 3.17). For a pore length of 378 microns, while the coke deposition remained uniform throughout the largest pore, coke deposition was reduced in the elements that

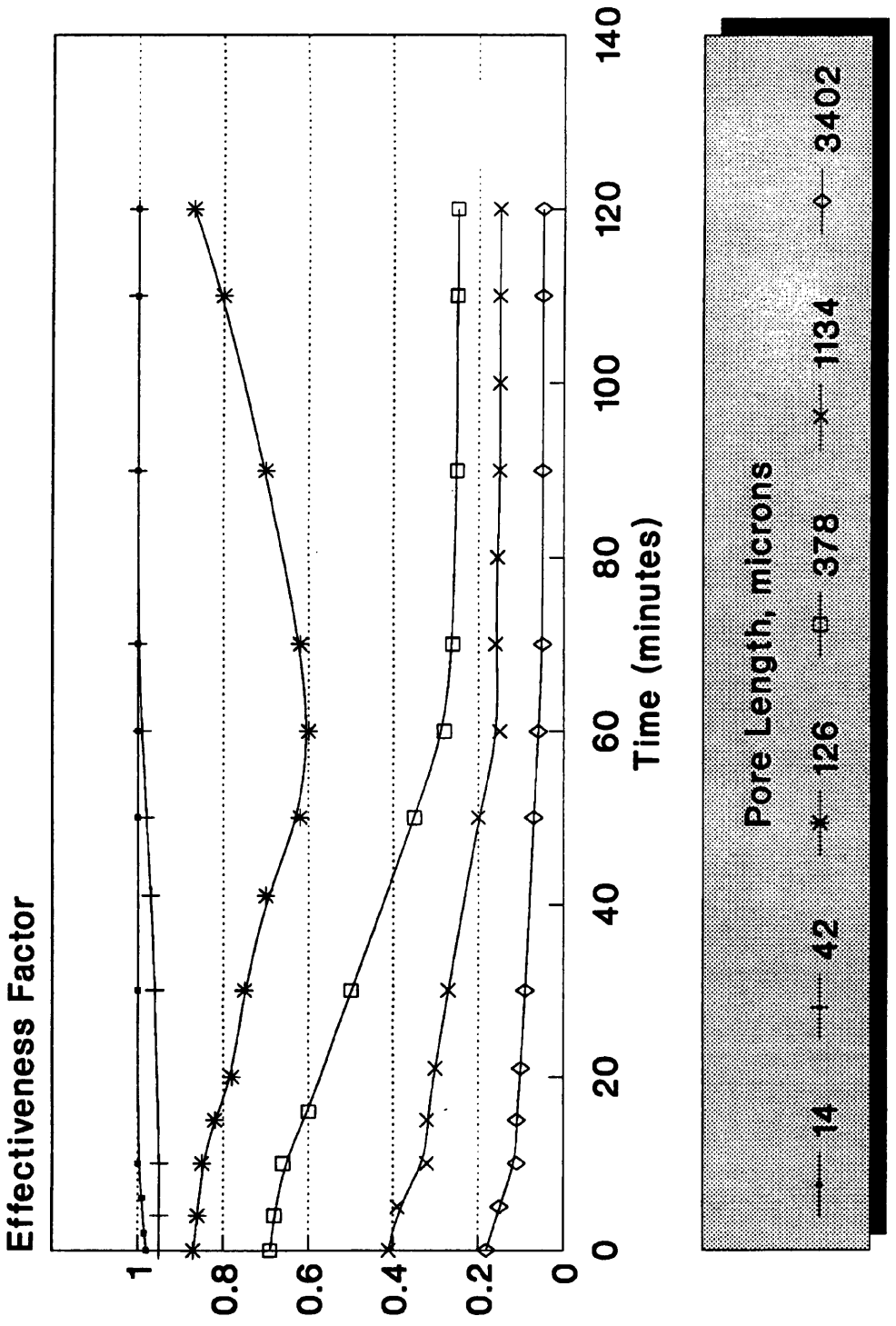

Figure 3.15 Effect of pore length on effectiveness factor for parallel coking mechanism.

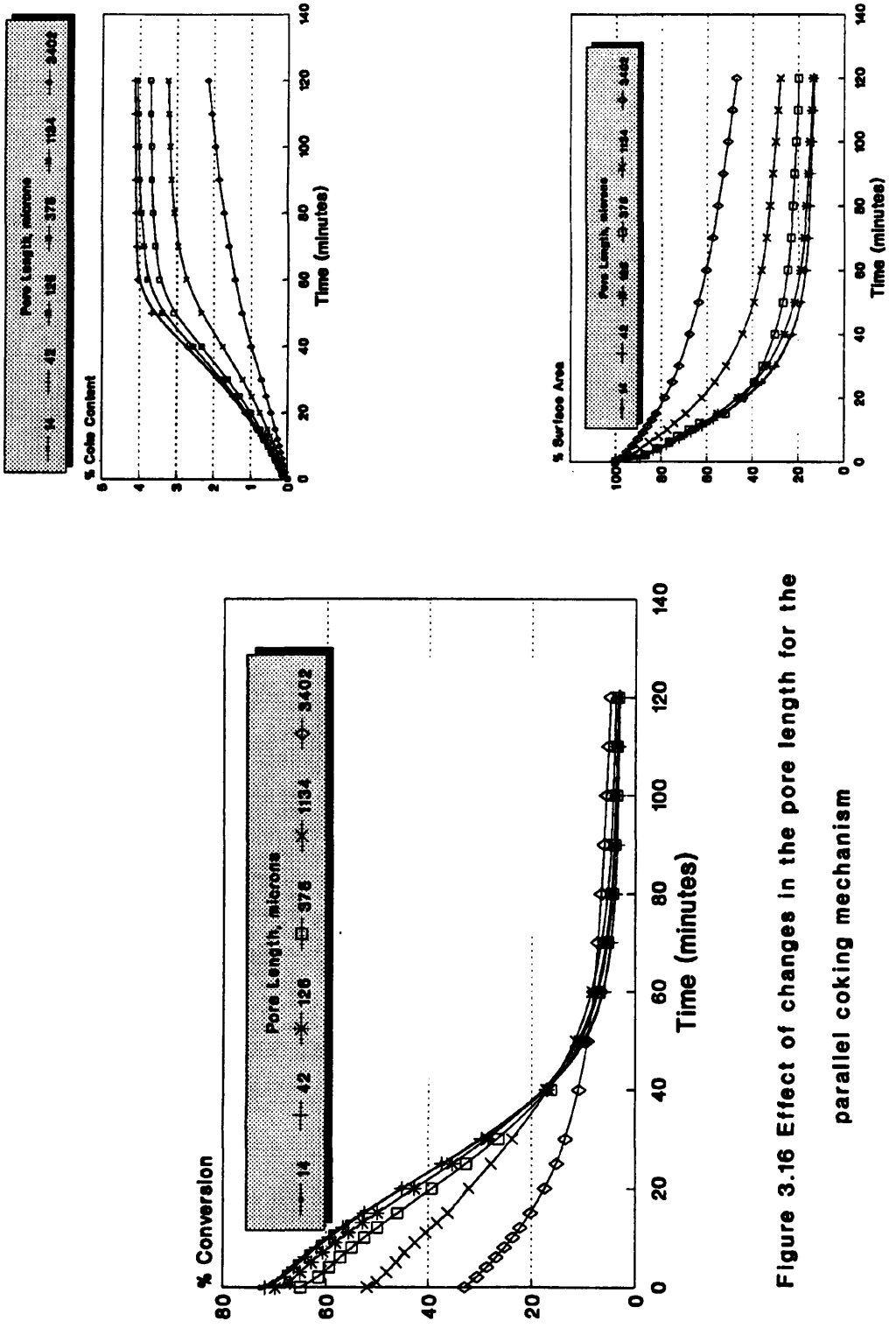

Figure 3.16 Effect of changes in the pore length for the parallel coking mechanism

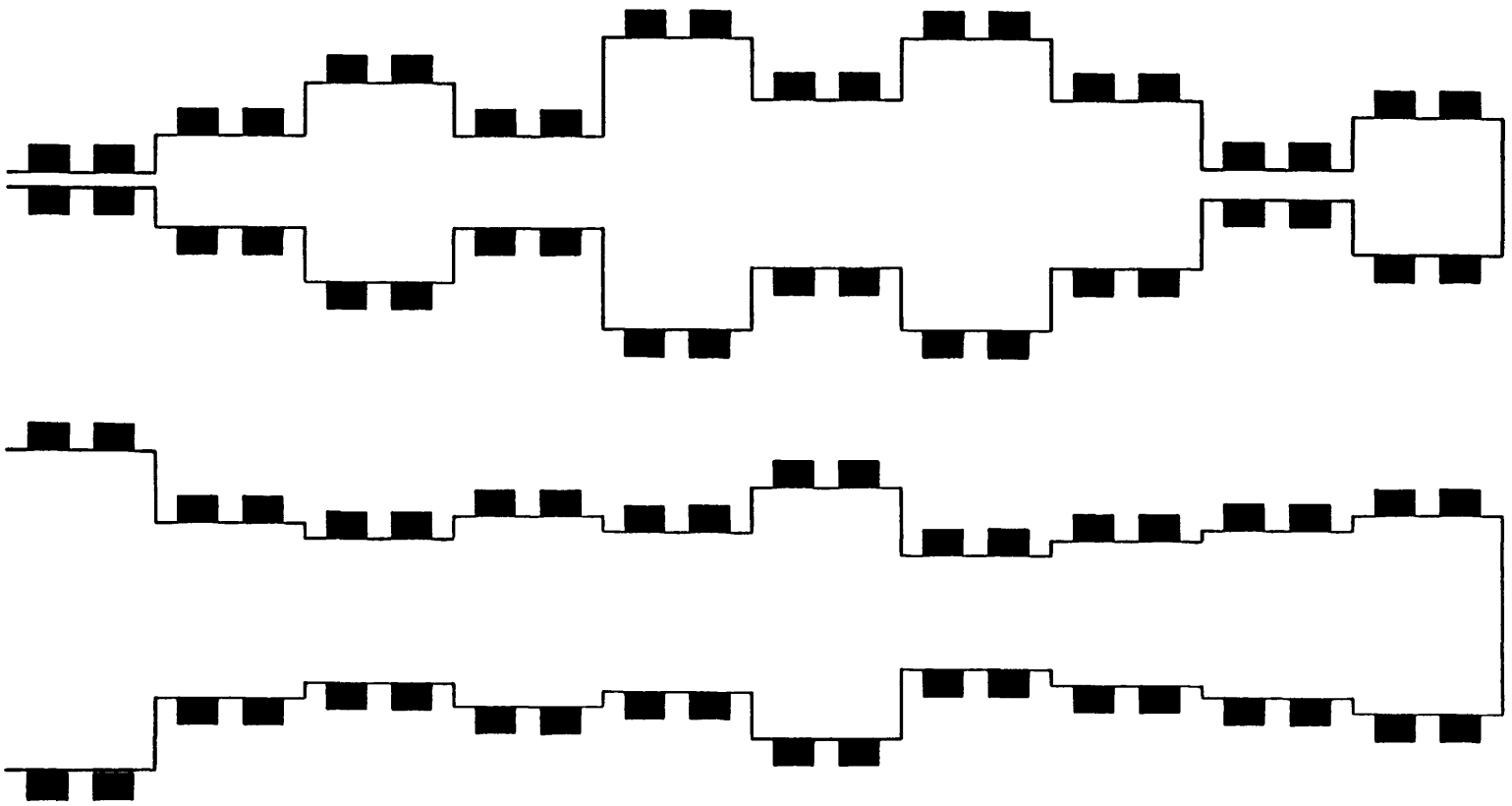

Figure 3.17:

Effect of pore length on the zeolite loss in the smallest and largest corrugated pores undergoing parallel deactivation (Pore length = 14 microns).

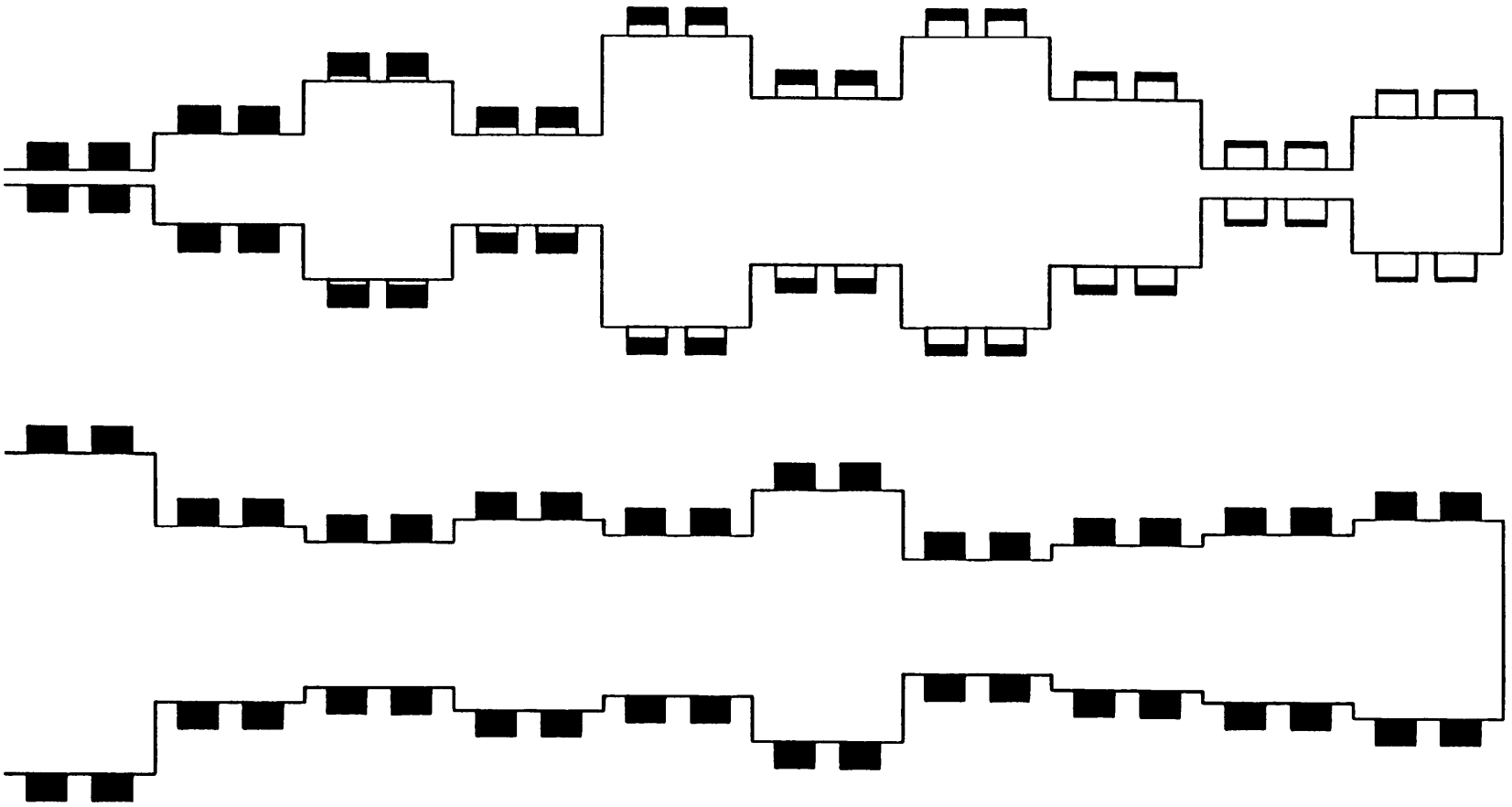

Figure 3.18:

Effect of pore length on the zeolite loss in the smallest and largest corrugated pores undergoing parallel deactivation (Pore length = 378 microns).

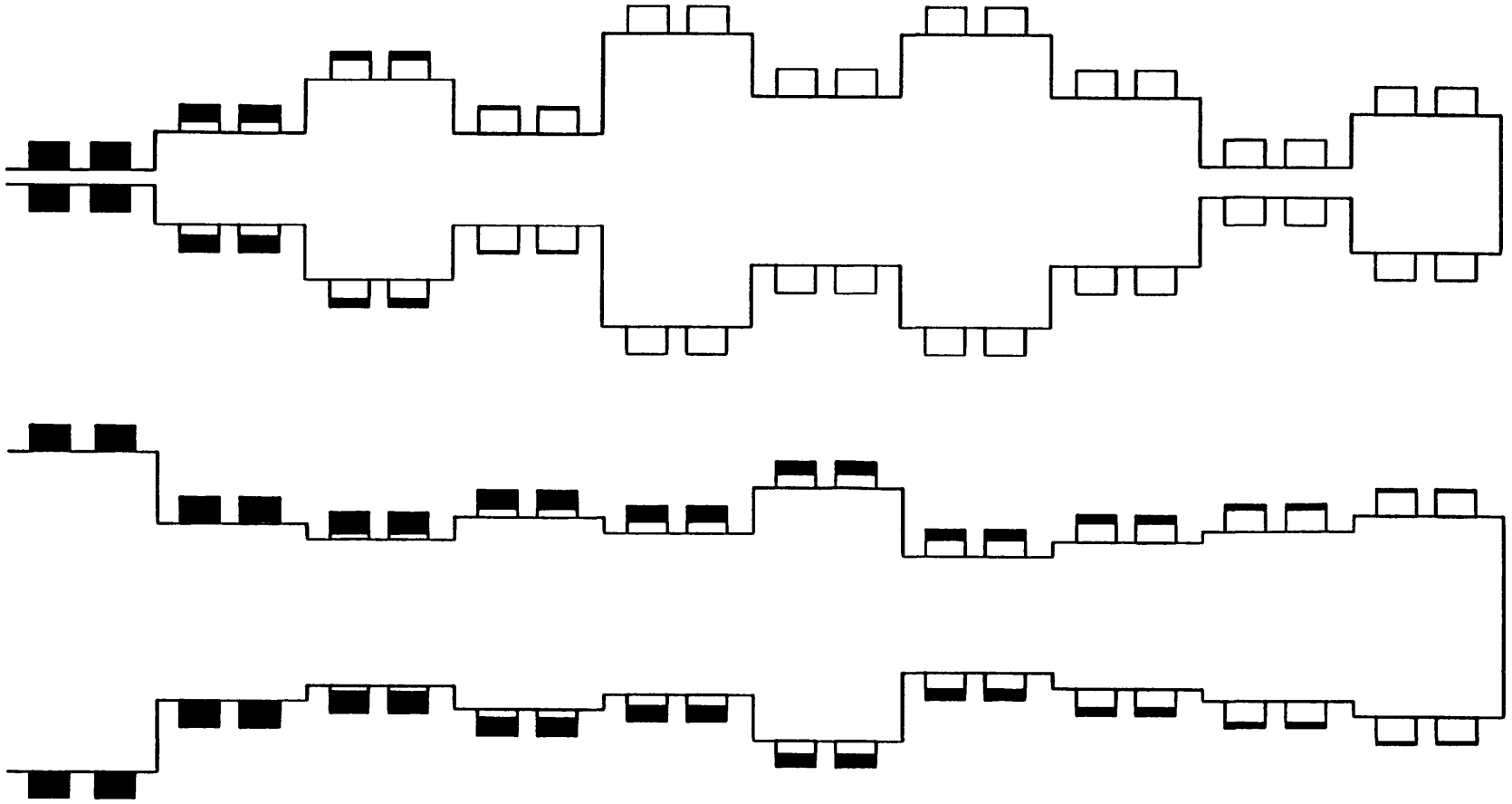

Figure 3.19:

Effect of pore length on the zeolite micropores loss in the smallest and largest corrugated pores undergoing parallel deactivation (Pore length = 1134 microns).

lie behind the smallest element in the smallest pore. This is expected, since it is in the smallest pore element where the diffusional resistances have their greatest impact (Fig. 3.18). When the pore length is increased to 1134 microns, diffusional resistances are so significant that there is a coke profile developing even in the elements of the largest pore with negligible coking in the elements that lie behind the smallest element in the smallest pore (Fig. 3.19).

3.4.3 Triangular Deactivation:

The triangular deactivation mechanism shows that increasing the pore length reduced the conversion of the catalyst to a greater extent than either parallel or series coking alone. This is again due to the combined effect of both deactivation mechanisms. Also, increasing the pore length has the effect of reducing the slope of the conversion profile (Fig. 3.20).

Coke content profiles for the triangular deactivation mechanism show the competition between the parallel and series coking which have an opposite effect in relation to changes in the pore length of the catalyst. Increasing the pore length reduces the coke content for parallel coking but increases the coke content for series coking. Then under a triangular mechanism of coking, the coke content profiles depend on the relative values of the parallel and series coking rate constants. As the coking rate constants get closer, the coke content profiles converge more and more until they merge into a single curve for all values of the pore lengths. This single unique curve is the result of the triangular deactivation mechanism with equal values for the parallel and series coking constants. The coke content is larger under triangular coking than either parallel or series coking alone.

The surface area profiles for the triangular deactivation mechanism show the competition between the parallel and series coking which have opposite effects in

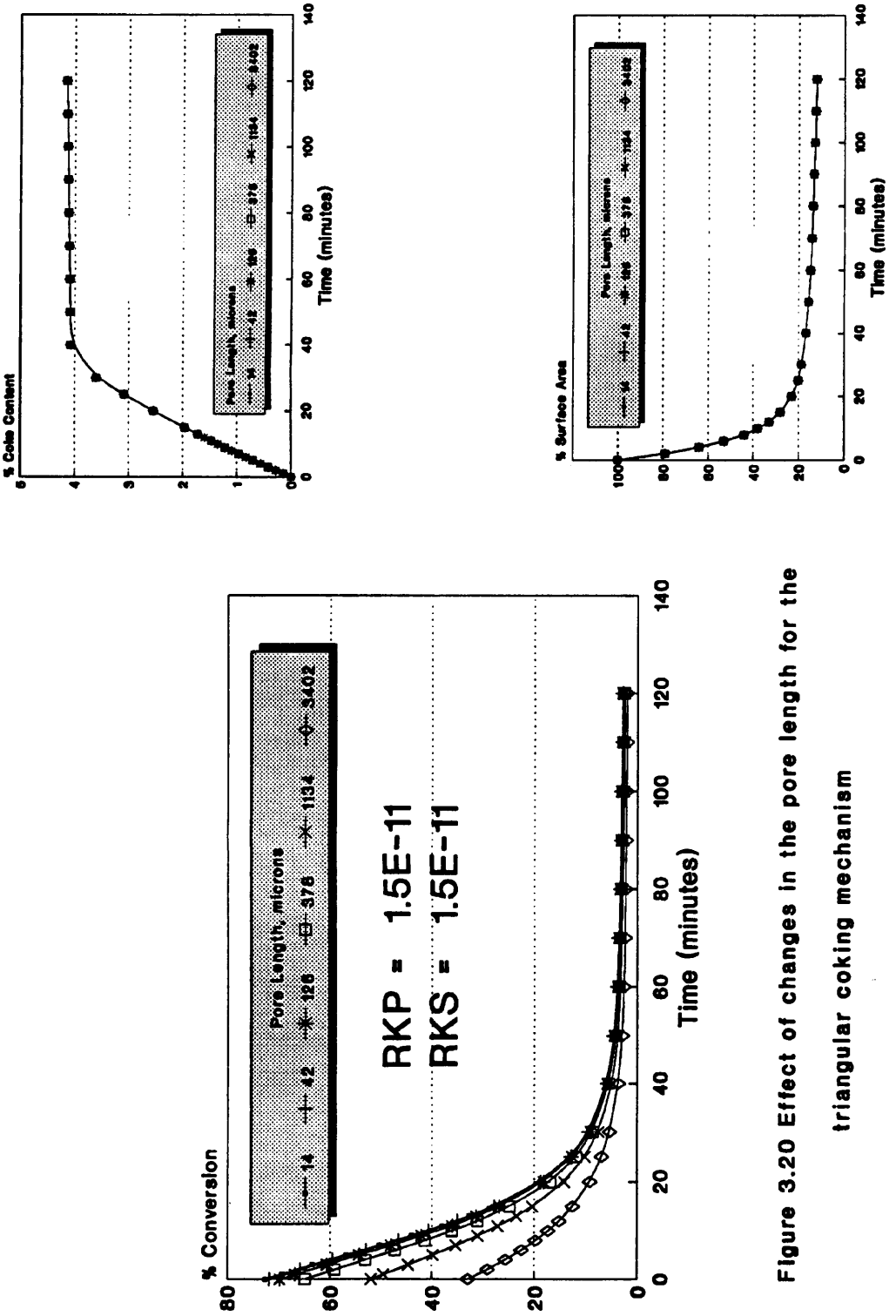

Figure 3.20 Effect of changes in the pore length for the triangular coking mechanism

relation to changes in the pore length of the catalyst. Increasing the pore length reduces the drop in surface area for parallel coking, but increases the drop in surface area for series coking.

As the parallel and series coking rate constants get closer, the surface area profiles converge more and more until they merge into a single curve for all values of the pore lengths. This single curve is the result of the triangular deactivation mechanism with equal values for the parallel and series coking constants. Again, the drop in the surface area of the catalyst is larger under triangular deactivation than under either parallel or series coking alone.

3.5 PECULIARITIES OF CONCENTRATION GRADIENTS IN INDIVIDUAL CORRUGATED PORES:

Since the rate of the main reaction on the active surface of the catalyst depends to a great extent on the ease through which the reactant particles diffuse through the pore structure of the catalyst. Also, the rate of the coking reaction, whether series, parallel or triangular mechanism, depends on the relative concentrations of the reactant and products within the pores of the catalyst particle. Therefore, an attempt is made to study the effect of pore structure on the concentration gradients within individual corrugated pores.

A set of eight 10–element pores with sizes assigned randomly from a uniform pore size distribution in the range 60–3200 Å, were chosen. The concentration gradients along these pores were calculated and investigated in detail. It was noticed that under actual experimental conditions of the cumene cracking using powder form of the zeolitic catalyst super–D, there was a negligible diffusional resistance. So, the concentration profiles across all pores were flat. But, under conditions of strong diffusional resistance (main reaction rate constant changed to 6×10^{-4} m/s) there was a

very clear change in the concentration gradient across each of the different pores. Figure 3.21 shows the concentration gradient across the eight 10–section pores. Figure 3.22 shows two of those pores with the pore radii of each element specified.

3.5.1 Comparison with Straight Parallel Bundle of Pores:

The uniform–diameter parallel bundle is the special case of the corrugated parallel bundle model with all pore sections having the same size (Fig. 3.23). It was interesting to note the great difference in the concentration gradient across a corrugated pore in comparison with its equivalent uniform–diameter pore with equal surface area. Figure 3.24 shows concentration gradients along some straight pores. Actually the drop in concentration across the straight pore was smaller than any of the other corrugated pores (Fig. 3.25). One factor is clearly the Knudsen diffusion in the pore sections with radii below 400Å which causes extra diffusional resistance and hence a drop in the concentration across that specific section whereas in the average–area straight pore only bulk diffusion takes place (always $R > 400Å$).

The more interesting observation was that a straight parallel pore with a radius equal to the smallest size in the distribution ($R = 60Å$) didn't produce the largest concentration gradient across the pore (Fig. 3.25). This observation leads to the conclusion that besides the Knudsen diffusion in the smaller pore segments, another factor should be contributing to the significant concentration drop across some pores. The next section explains this factor.

3.5.2 Effect of corrugation on the Concentration Gradient:

To clearly illustrate the effect of corrugation on the concentration gradient across a pore, a 10–section pore was chosen with all sections of radii greater than 400Å , hence, avoiding the effect of Knudsen diffusion. Comparing this pore (number two

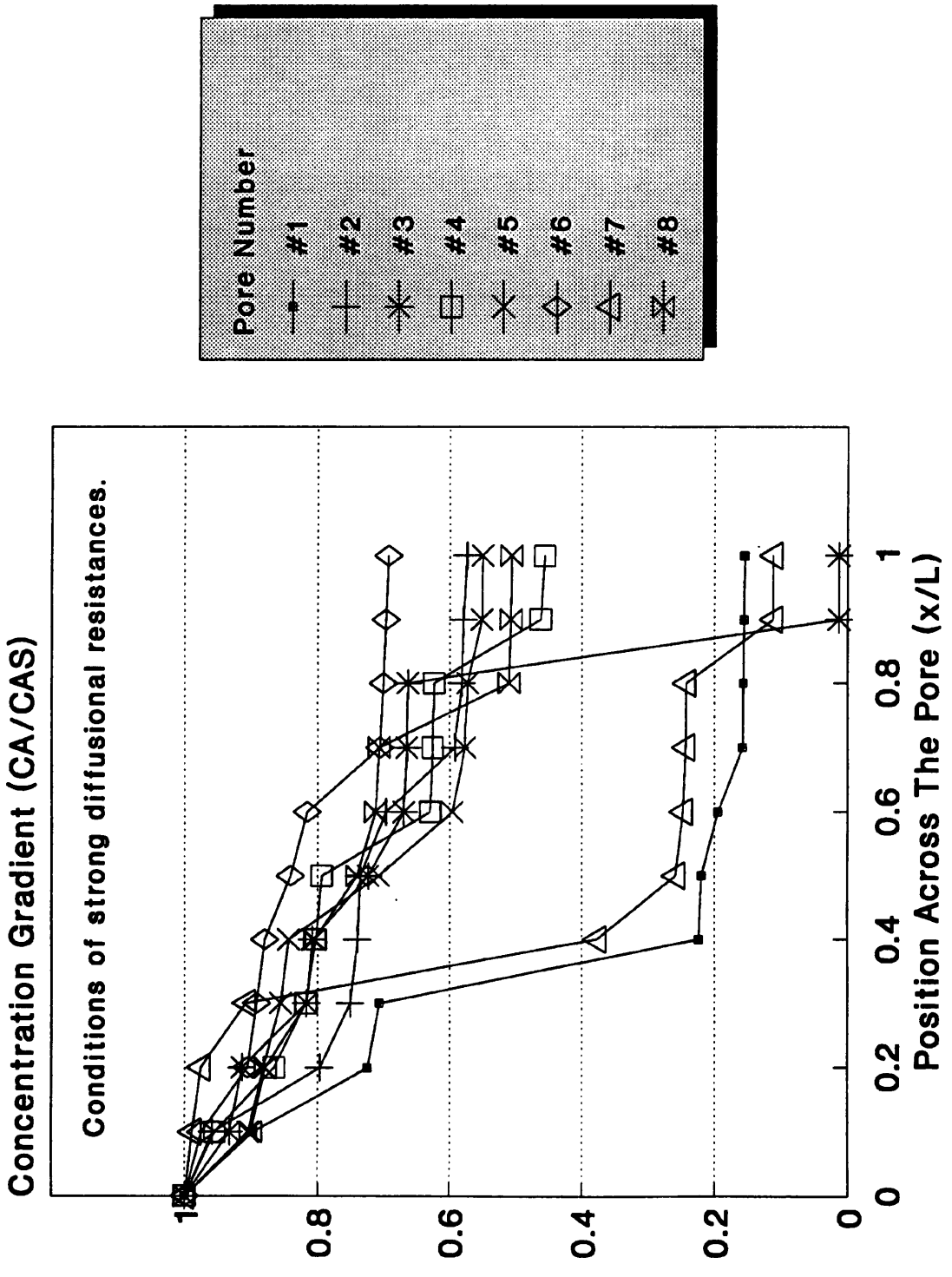

Figure 3.21 Concentration gradients across a cohort of eight 10-element corrugated pores.

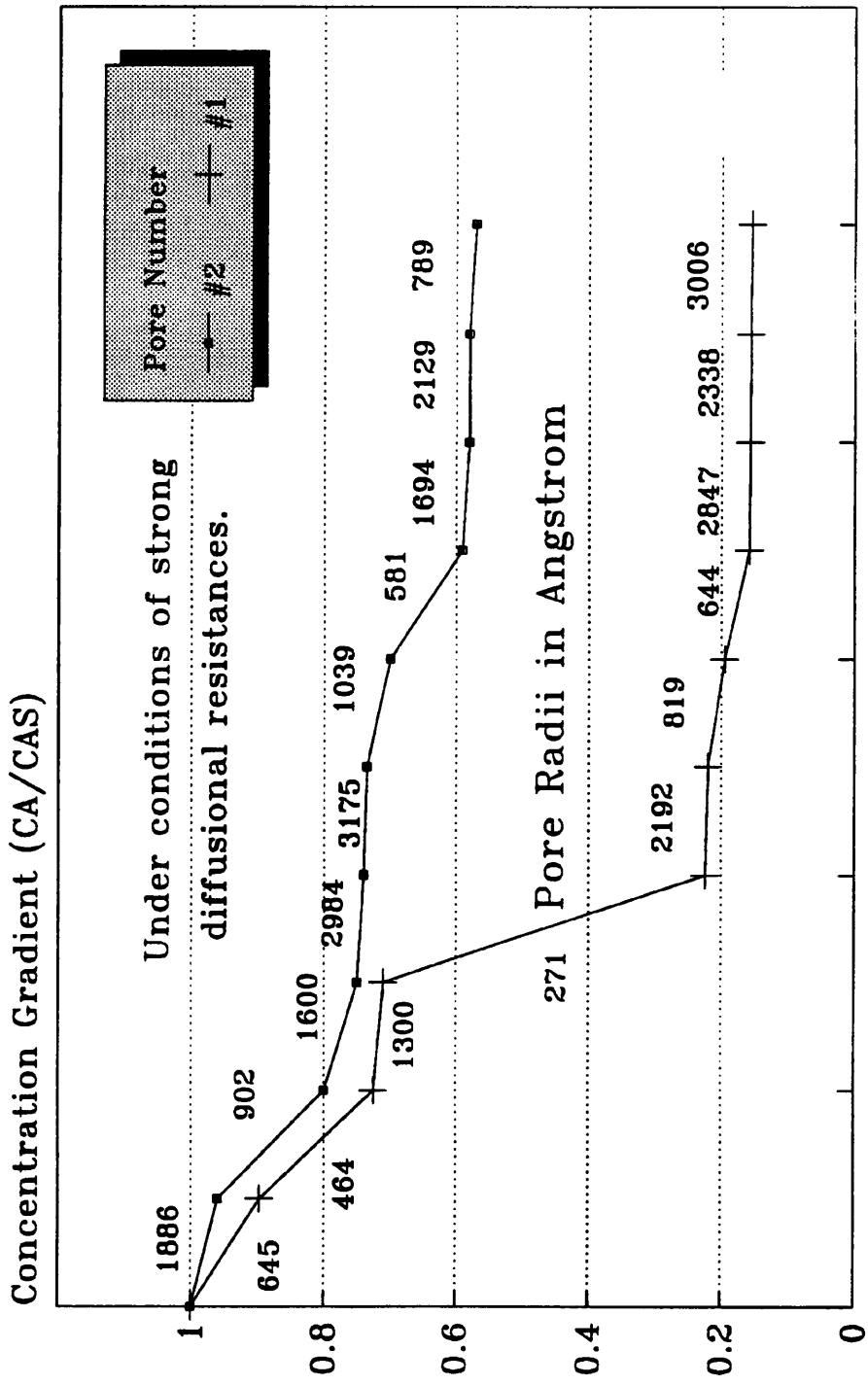

Figure 3.22 Concentration gradient across two 10-element pores.

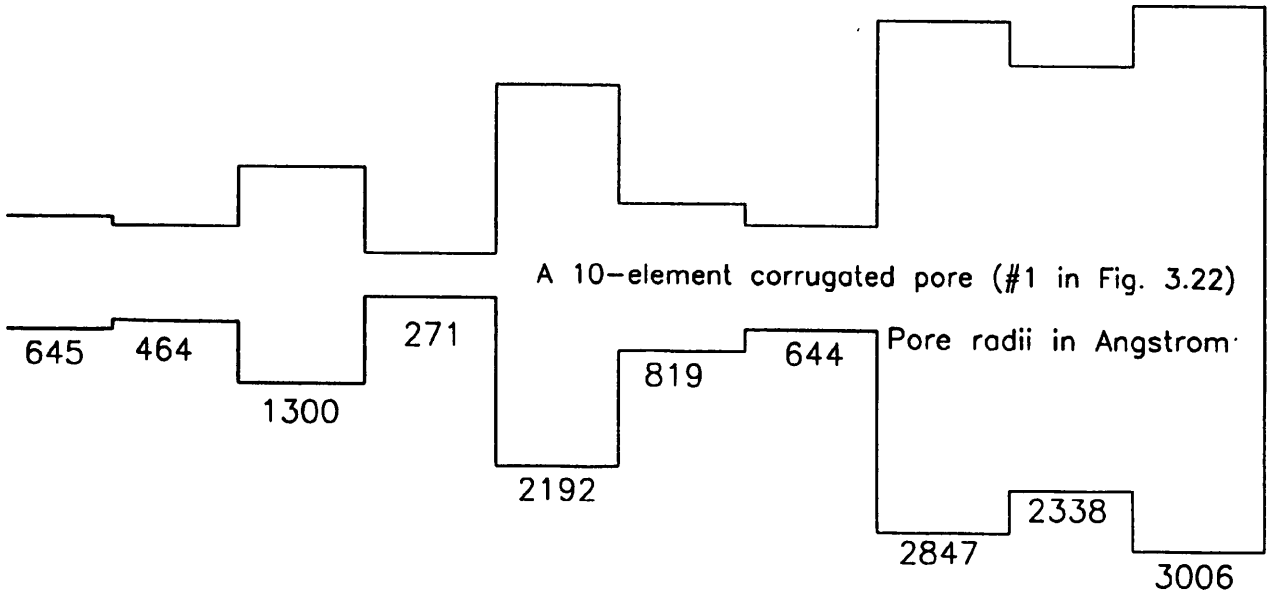

An equivalent straight cylindrical pore having same surface area
Radius = 1452 Angstrom

Figure 3.23:

A 10-element corrugated pore and its equivalent straight cylindrical pore having the same surface area.

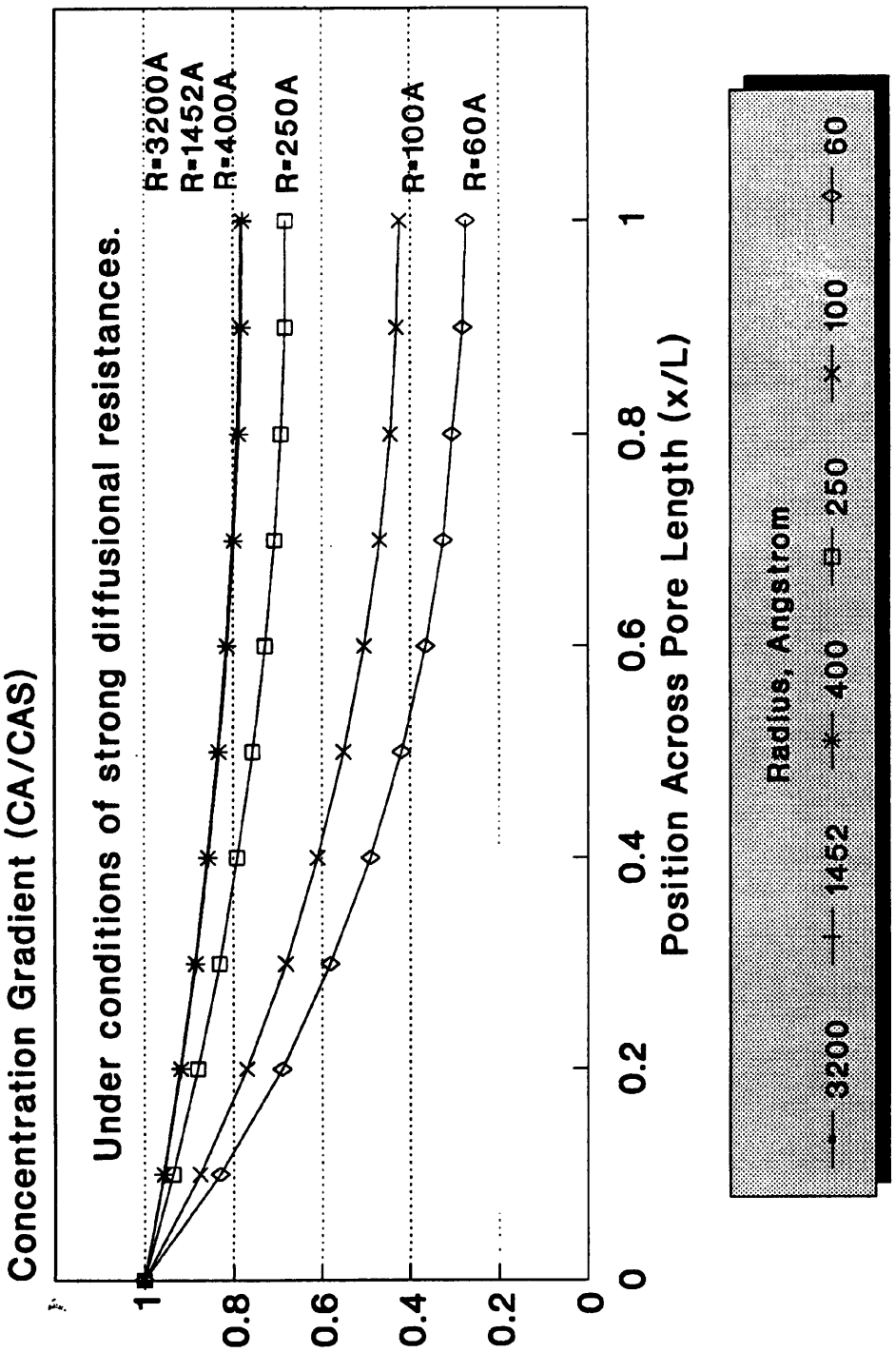

Figure 3.24 Concentration gradients across straight pores of different sizes.

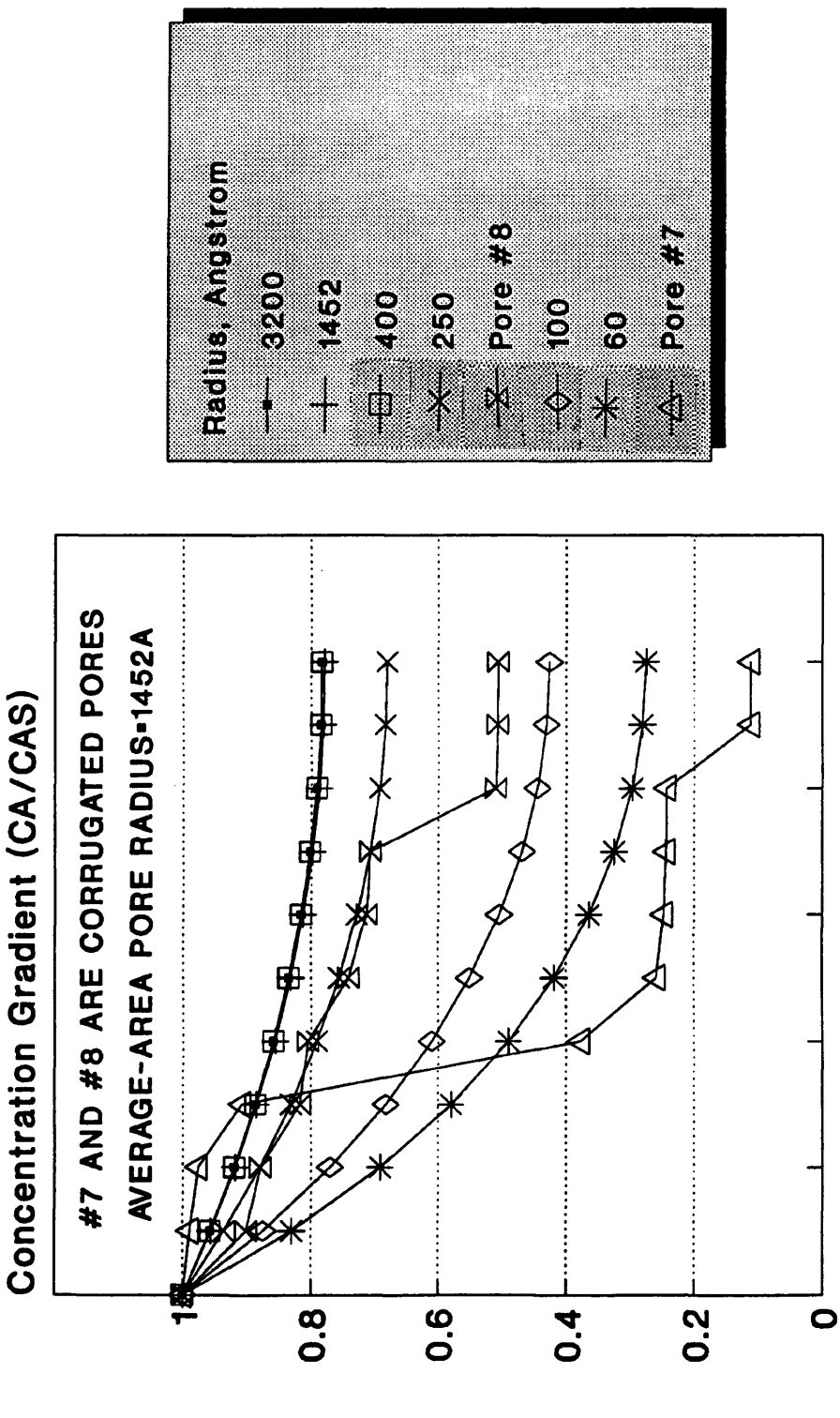

Figure 3.25 Concentration gradients for different straight and corrugated pores showing the effect of corrugation.

(Fig. 3.22)) with an equal area straight pore produced again a significant difference in the concentration gradient which clearly demonstrates the effect of corrugation. One may ask now, what happens to the concentration gradient across a corrugated pore if the location of some pore sections were changed without altering the sizes of the pore sections?

The answer is given in the next section.

3.5.3 Effect of the Location of Corrugation on the Concentration Gradient:

To illustrate the effect of the location of corrugation, a 3–section pore was chosen consisting of two 3000Å radius sections and one 60Å radius section. The location of the 60Å pore section was changed from the first to the second and to the third section and the concentration gradient calculated in each case. Figure 3.26 shows the concentration gradients across the pore length for the different combinations of sections. The largest concentration gradient occurs when the small size section is located at the first location, and the smallest occurs when it is located at the third location. For the sake of confirmation the calculations were repeated with a 10–section pore of radius 3000Å with only one section of size 60Å. The same effect was produced (Fig. 3.27).

The explanation is that the assumption that activity is proportional to wall area makes the large pores very much more active than smaller pores. If a large pore is fed by a small pore, then a large flow of reactant must pass, and there will be a correspondingly high concentration drop across the small pore. The large pores "suck" high fluxes of reactant through the small pores causing the remarkable drop in concentration.

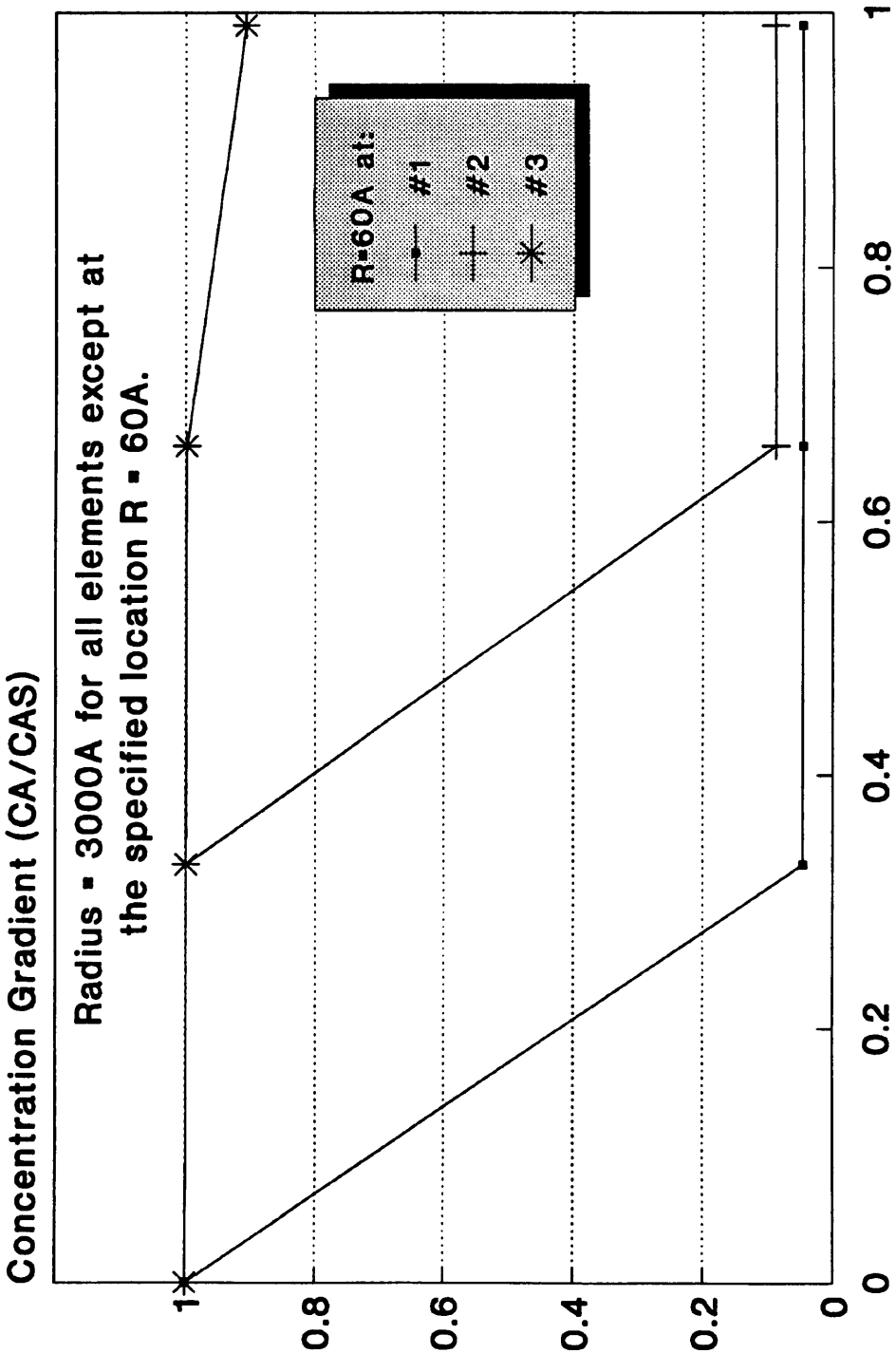

Figure 3.26 Effect of the location of corrugation in a 3-element pore.

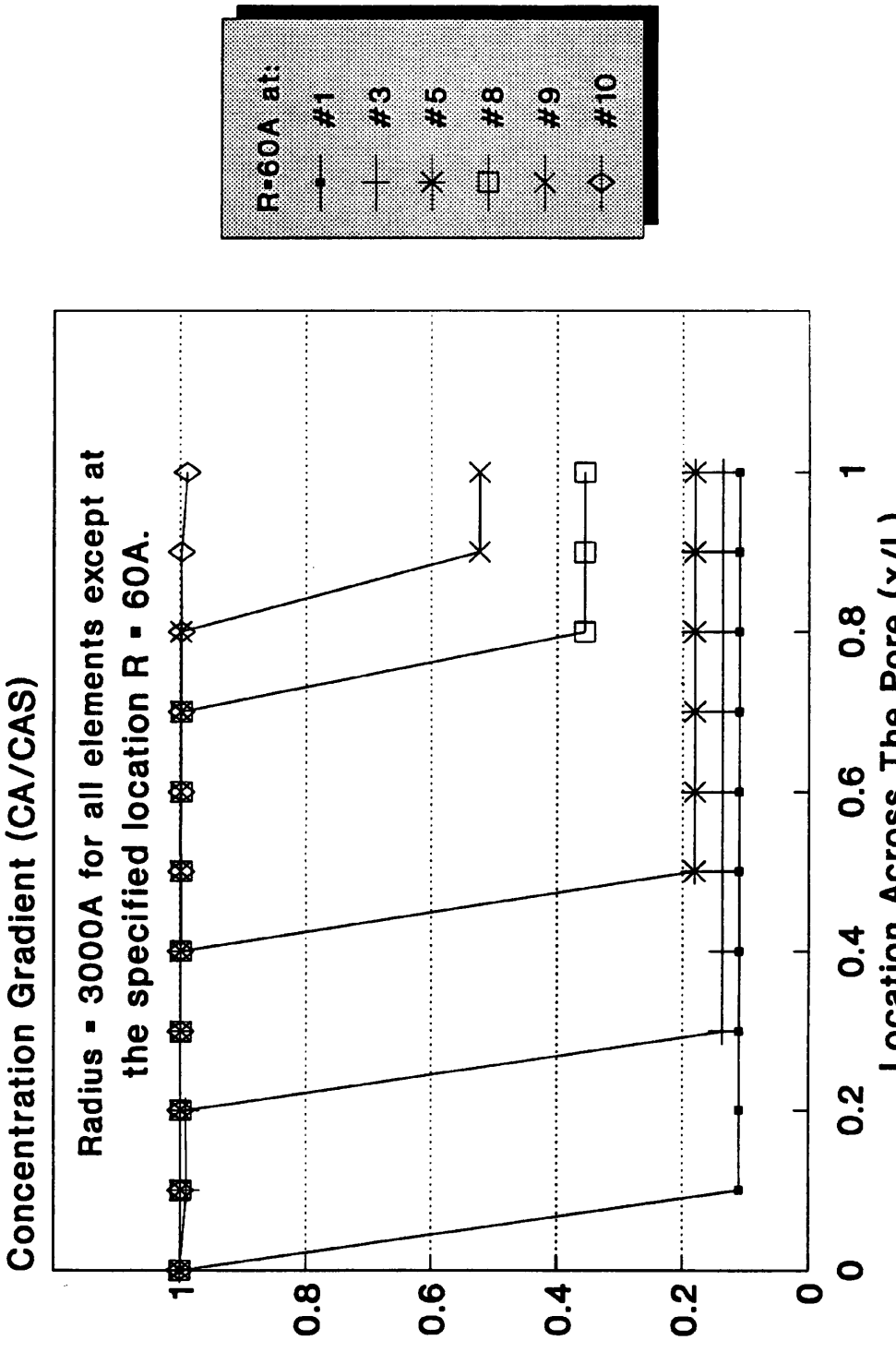

Figure 3.27 Effect of the location of corrugation in a 10-element pore.

3.5.4 Effect of Deactivation on the Concentration Gradient:

Figure 3.28 shows the concentration gradient across the 10–element(#1) corrugated pore undergoing a triangular coking mechanism at different times on stream. The deactivation parameters were same as in Table 3.1 except for the main reaction rate constant which was increased to $6x10^{-4}$ m/s. Initially, when the pore is fresh and not deactivated, the concentration level reduces to a value near zero. As time on stream increases, this concentration gradient increases to reach a final value just above 0.8 after two hours on stream.

3.6 EFFECT OF HEAVY COKE LAYDOWN IN SUPPORT PORES:

To allow heavy support coking to occur, the definition of the active surface area was changed according to Chapter Two to become that area which is accessible even if it was covered with a thick layer of coke. The structure of the catalyst particle was represented by a corrugated parallel bundle of pores. Each pore consisted of ten pore elements with uniform pore size distribution in the range from 60–3200 Å. To study the process of heavy support coking inside this corrugated parallel bundle of pores, twenty two such pores were chosen giving an assembly of 220 pore elements. These will be used later as a basis for comparison with the network pore model of size 10x10 consisting of the same total number of pore elements. Figure 3.29 shows the twenty two corrugated pore assembly under investigation, whereas, a numerical representation of the location and size of each pore element in this set is given in Figure 3.30.

Coke deposits can be potentially uniformly distributed at all times throughout the catalyst particle under one of the following conditions:

(1) If the coke particles were only weakly adsorbed onto the catalyst and were present in the feed stream in sufficiently large concentrations so that a

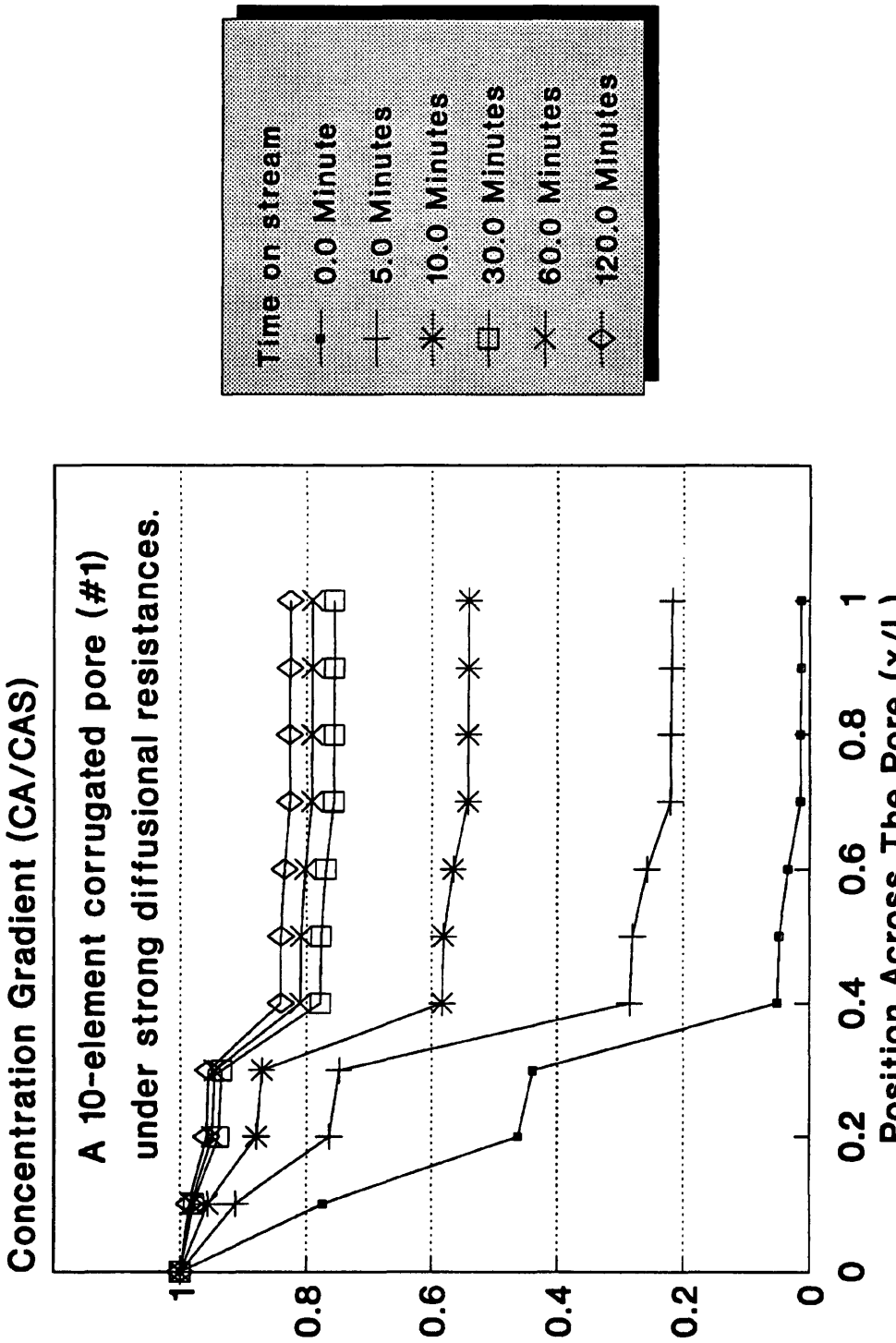

Figure 3.28 Concentration gradient as a function of time on stream.

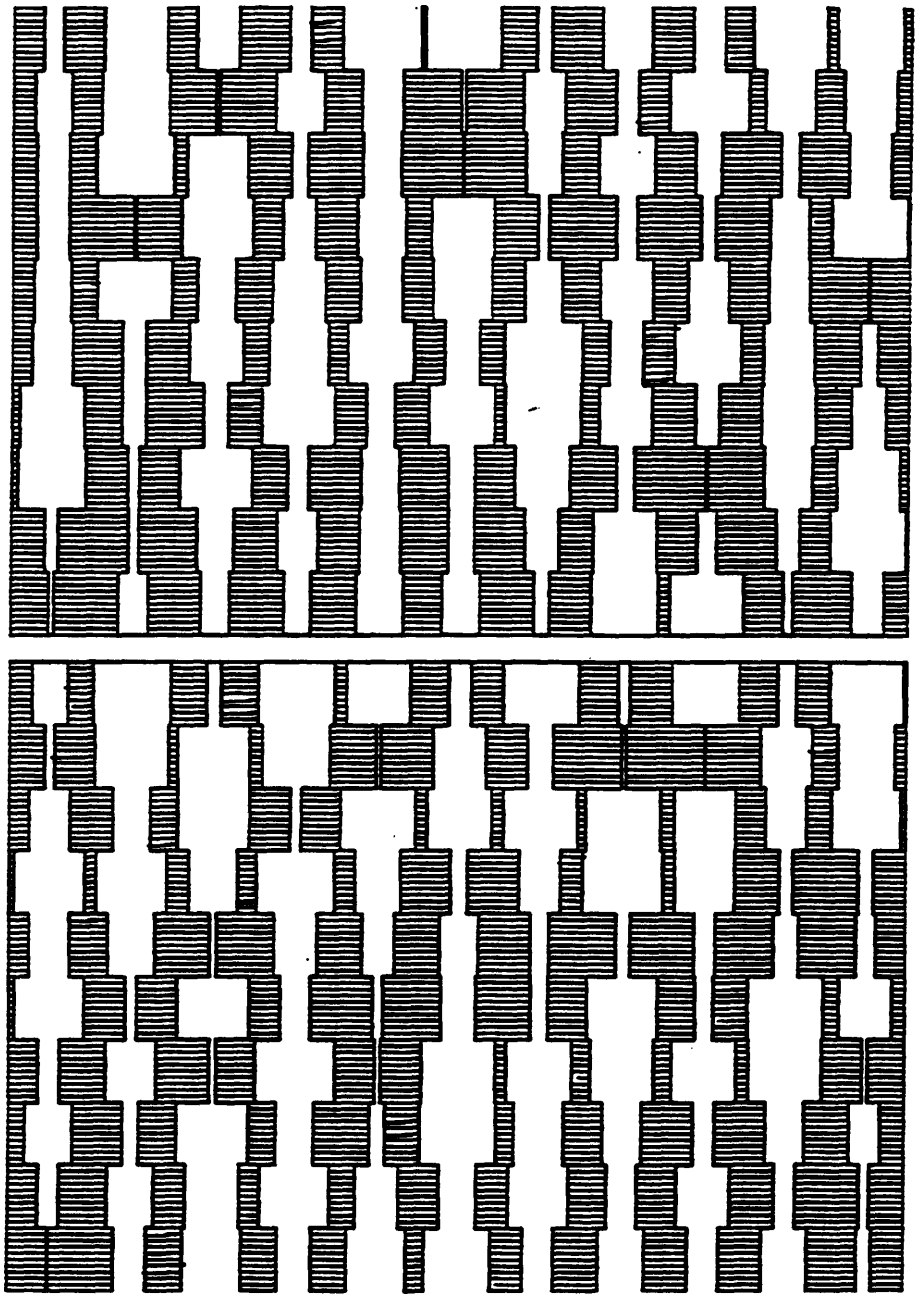

Figure 3.29 A set of 22 corrugated 10–element pores with a uniform pore size distribution in the range from 60–3200 Angstrom. (Clean, uncoked pores).

97— 885— 1923- 883— 2784- 1621- 2826- 1643- 408— 1442

1322- 1867- 665— 2029- 464— 1876- 2804- 1472- 2921- 3063

2372- 2188- 2894- 296— 2874- 299— 1964- 2874- 2877- 591

1383- 2763- 1494- 3139- 1198- 1690- 3064- 449— 2674- 3011

2399- 1746- 626— 258— 420— 1322- 1833- 2985- 218— 2551

2703- 1526- 3072- 2962- 1411- 1571- 686— 2610- 2141- 914

1245- 2402- 1966- 2606- 698— 734— 1650- 2939- 1027- 3013

1849- 1228- 1575- 2526- 2804- 578— 3174- 2954- 206— 493

1292- 2156- 895— 2597- 745— 861— 2399- 2446- 66— 2642

1885- 902— 1599- 2984- 3074- 1038- 581— 1693- 2128- 789

644— 464— 1299- 278— 2191- 819— 644— 2846- 2337- 3005

245— 562— 2742- 2606- 1666- 1524- 1335- 1352- 1511- 843

1186- 421— 466— 971— 950— 2959- 168— 3071- 2683- 2525

1165- 1480- 2897- 1004- 2166- 1553- 2844- 2443- 199— 1739

1078- 1622- 857— 2904- 2378- 2123- 1337- 675— 1967- 911

1899- 1662- 1561- 1143- 2632- 1696- 1951- 1543- 1671- 3151

1493- 1009- 1048- 2621- 1369- 2347- 2506- 65— 216— 3032

618— 1352- 2184- 3036- 3081- 1512- 465— 1473- 1682- 640

2670- 2549- 727— 2110- 1377- 2120- 853— 2249- 936— 2010

2946- 808— 133— 972— 2660- 1635- 615— 1048- 3151- 1297

416— 974— 1990- 2238- 2092- 1703- 1623- 767— 2031- 3029

1255- 3011- 2518- 1380- 674— 82— 3081- 1730- 2145- 2672

Figure 3.30 A numerical representation of the 22 corrugated pores shown in figure 3.29.

steady–state surface concentration is quickly attained.

(2) If the coke particles were formed by a reaction occurring with an effectiveness factor near unity, e.g. coke formation on cracking catalyst in powder form where pore lengths are relatively very small and effectiveness factor approaches unity.

3.6.1 Representation of the Structure of the Catalyst at Different Stages of Coke Laydown:

Assuming that the catalyst is undergoing a parallel coking mechanism, and using the same parameters as in Table 3.1, an investigation into the effect of heavy coke laydown in the support pores is attempted. The effectiveness factor is near unity indicative of negligible diffusional resistances, therefore, coke will deposit uniformly throughout the catalyst particle. Initially, uniform coking occurs within every pore element in the corrugated parallel bundle of pores. As the coke layer thickness increases, it causes the filling of the smaller pores and he eventual isolation of some of the larger partially coked pore elements. When the coke thickness reaches only 500Å, over 50 pore elements have already been isolated whereas less than half of that is the number of pores which have been filled by coke (Fig. 3.31). As the coke layer thickness increases to reach 1000Å, the number of pores fully filled with coke becomes about 50 while the number of pores isolated approaches 120 pore elements. By the time the catalyst particle is fully coked, about 70% of the total number of pores which were only partially coked, have been isolated.

Figures 3.32 to 3.37 show the corrugated parallel bundle of pores at different stages of heavy support coking up to complete deactivation. Because of pore isolation, coke tends to accumulate non–uniformly throughout the pore structure despite the potentially uniform laydown rate. Part of the interior could then naturally appear to be lightly coked with a heavier coke content (per unit weight of the catalyst) expected towards the exterior of the catalyst particle. Such a situation is often observed in coke

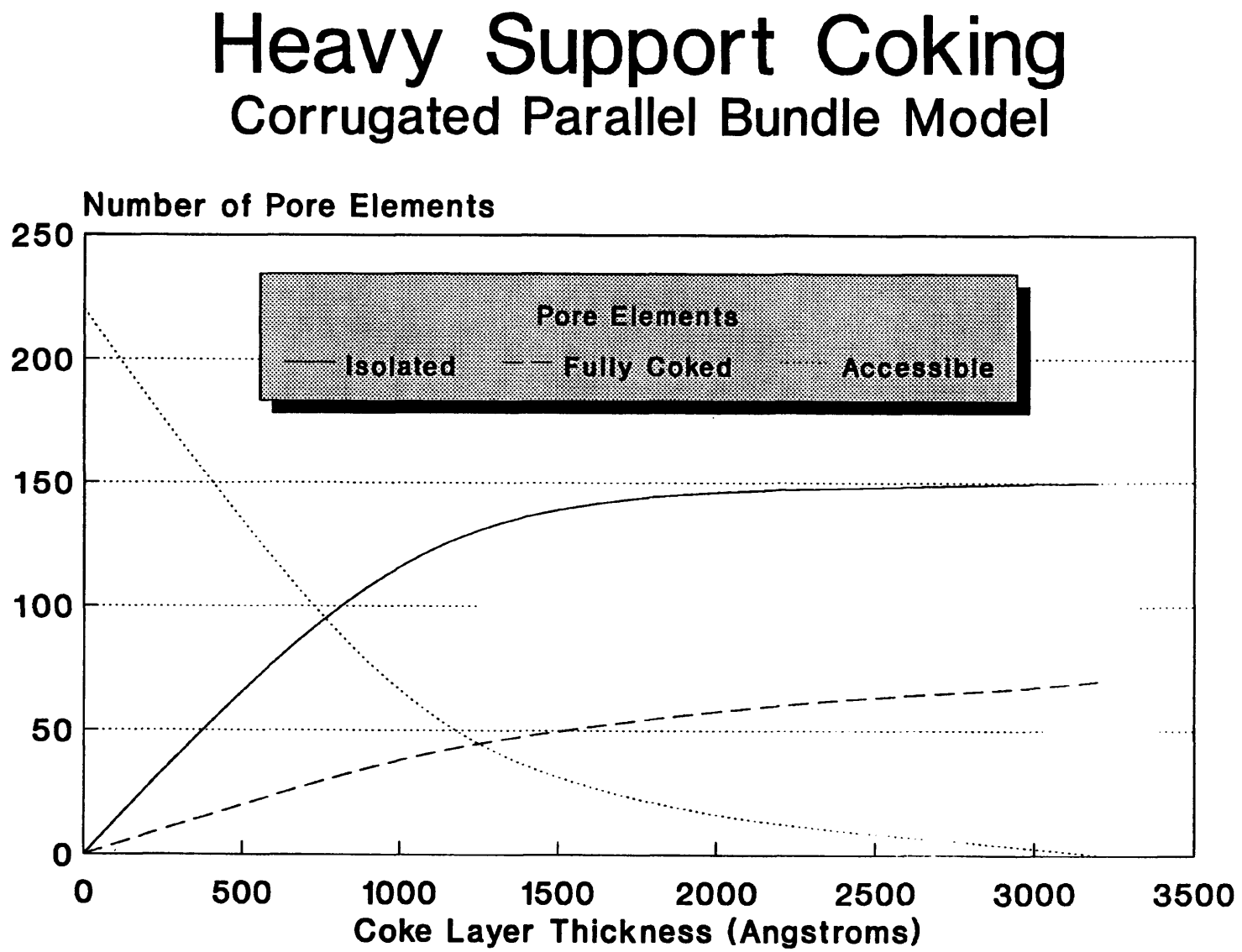

Figure 3.31 Changes in the number of accessible support pore elements for the corrugated parallel bundle model undergoing a parallel coking mechanism

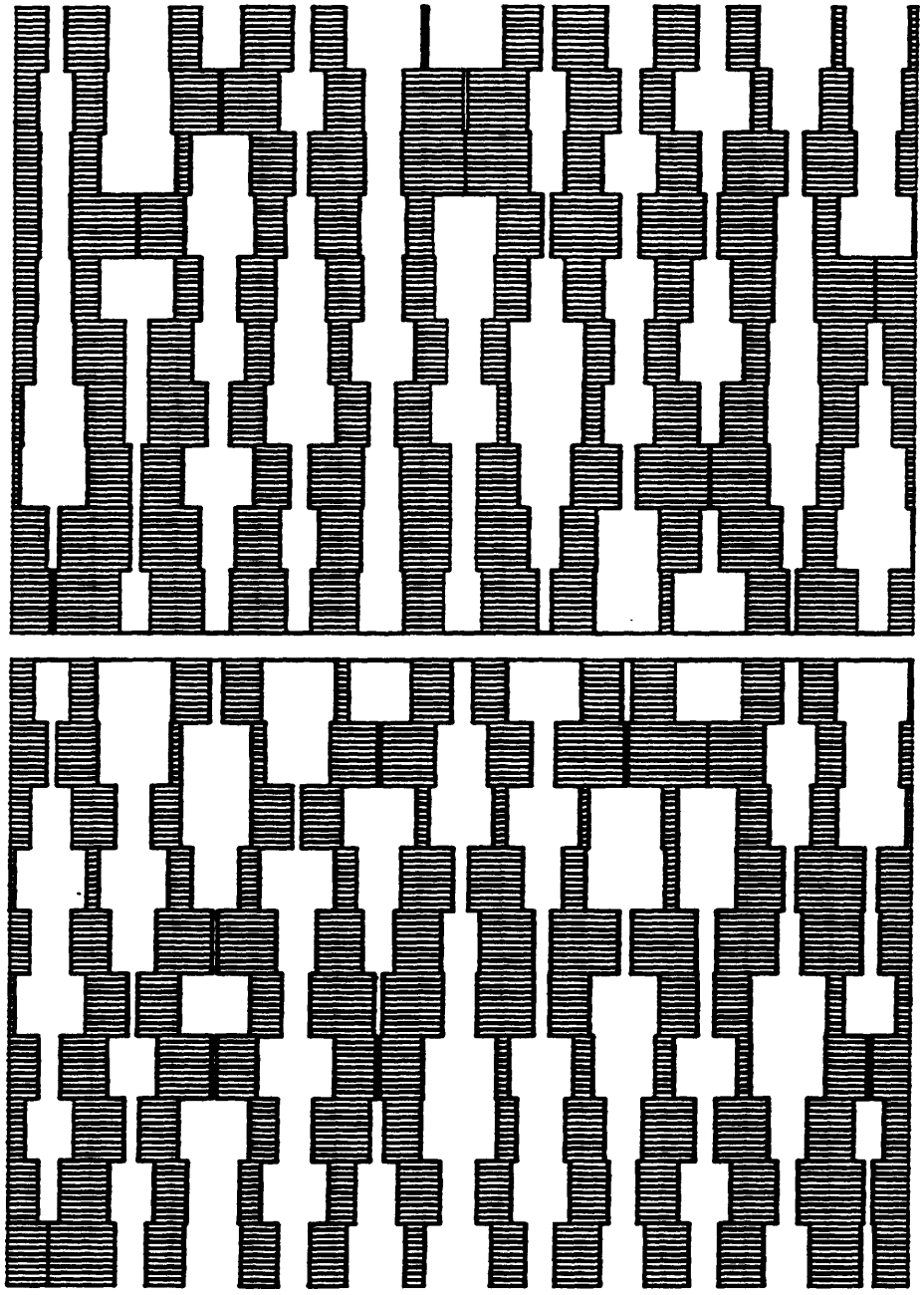

Figure 3.32 The corrugated parallel bundle of pores undergoing a parallel coking mechanism. (Coke layer thickness = 180 Angstrom).

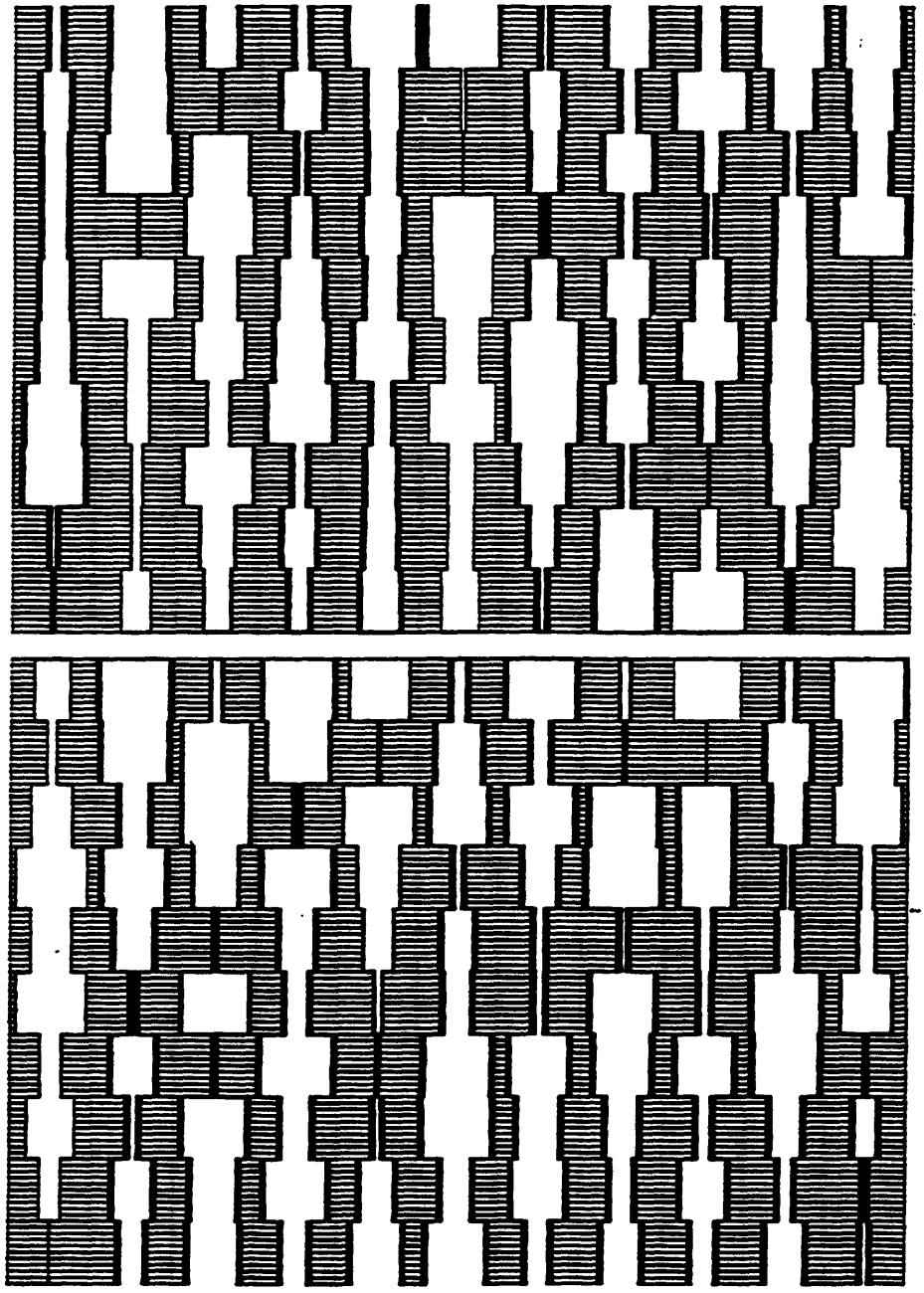

Figure 3.33 The corrugated parallel bundle of pores undergoing a parallel coking mechanism. (Coke layer thickness = 450 Angstrom).

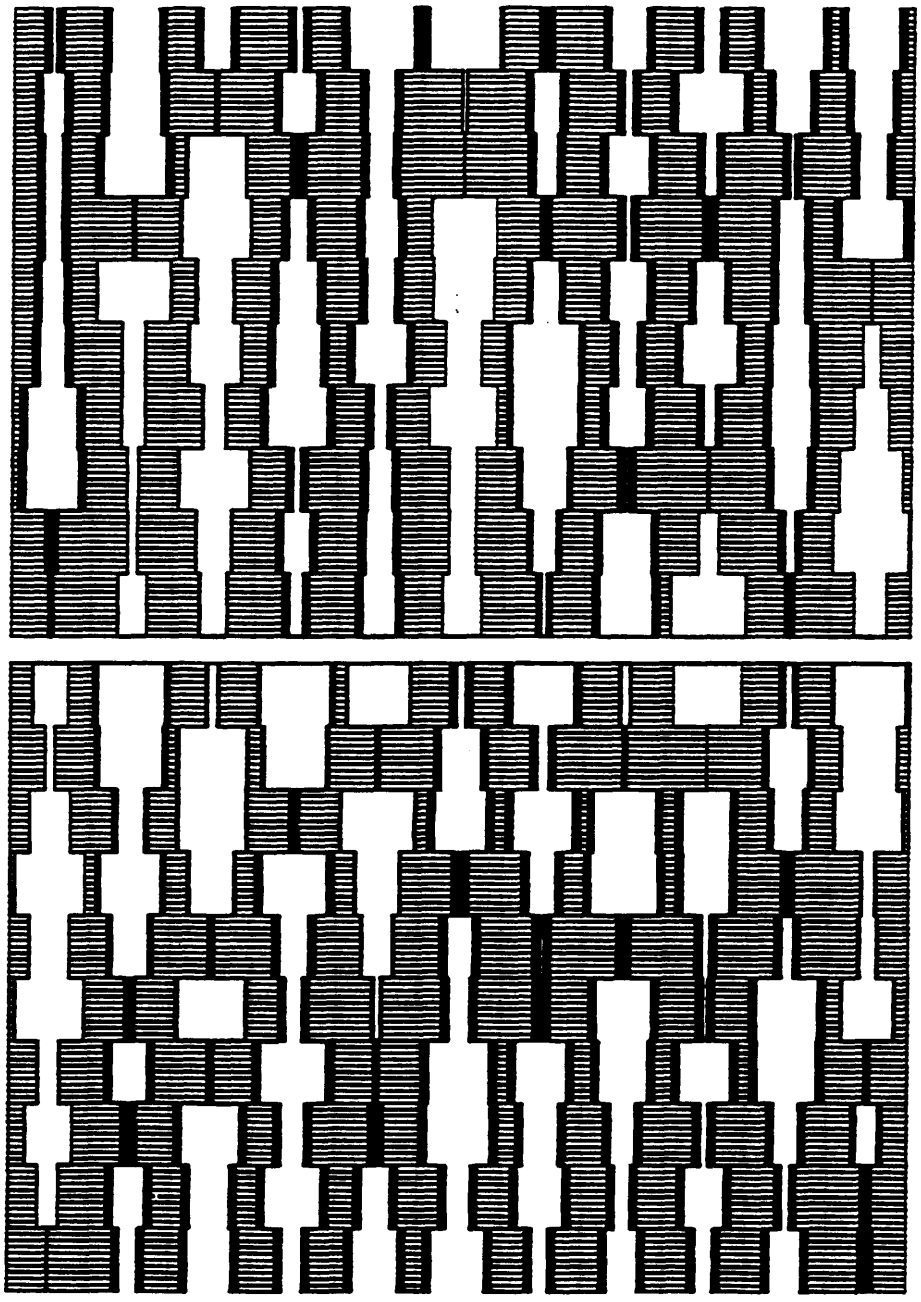

Figure 3.34 The corrugated parallel bundle of pores undergoing a parallel coking mechanism. (Coke layer thickness = 629 Angstrom).

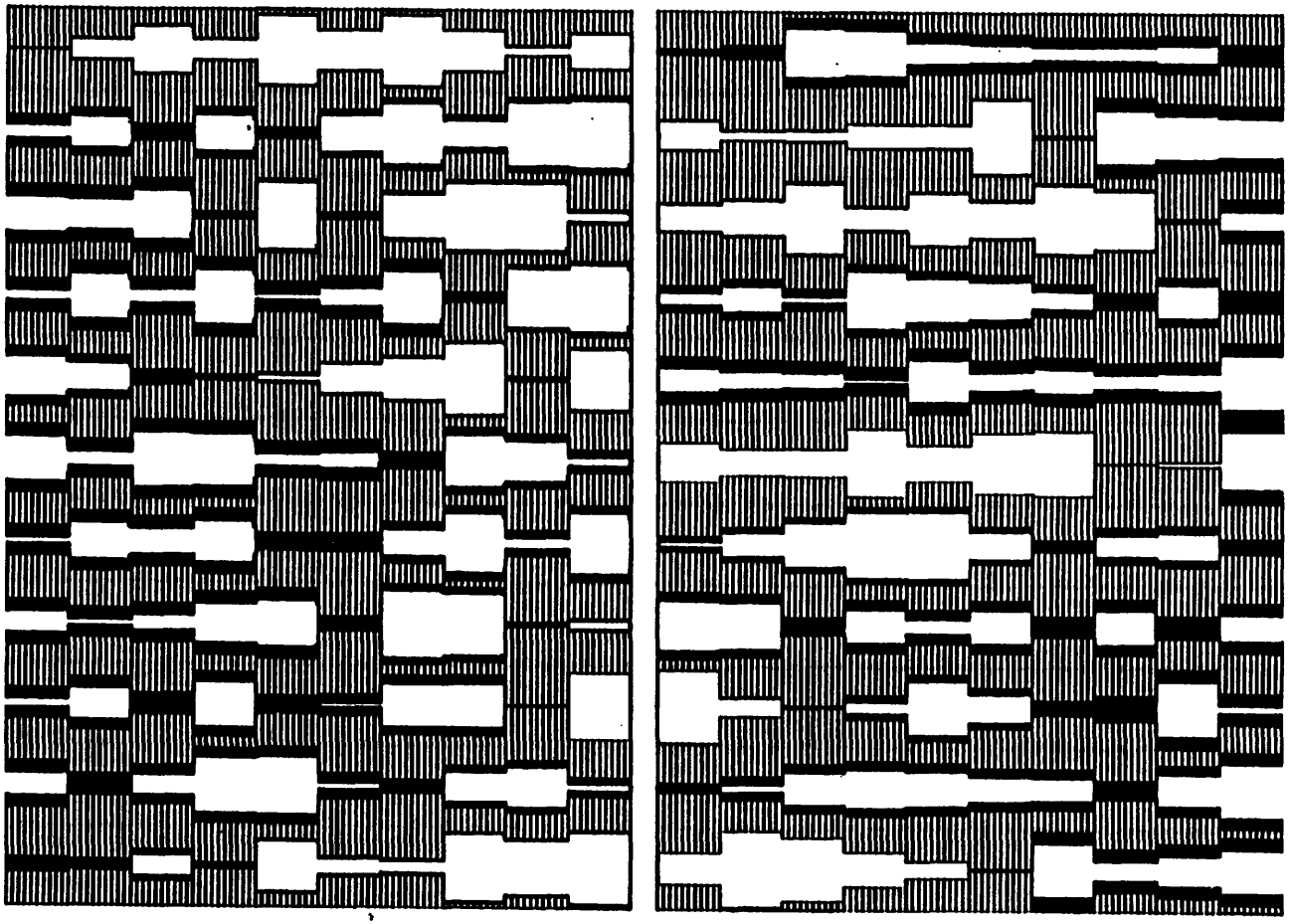

Figure 3.35 The corrugated parallel bundle of pores undergoing a parallel coking mechanism. (Coke layer thickness = 993 Angstrom).

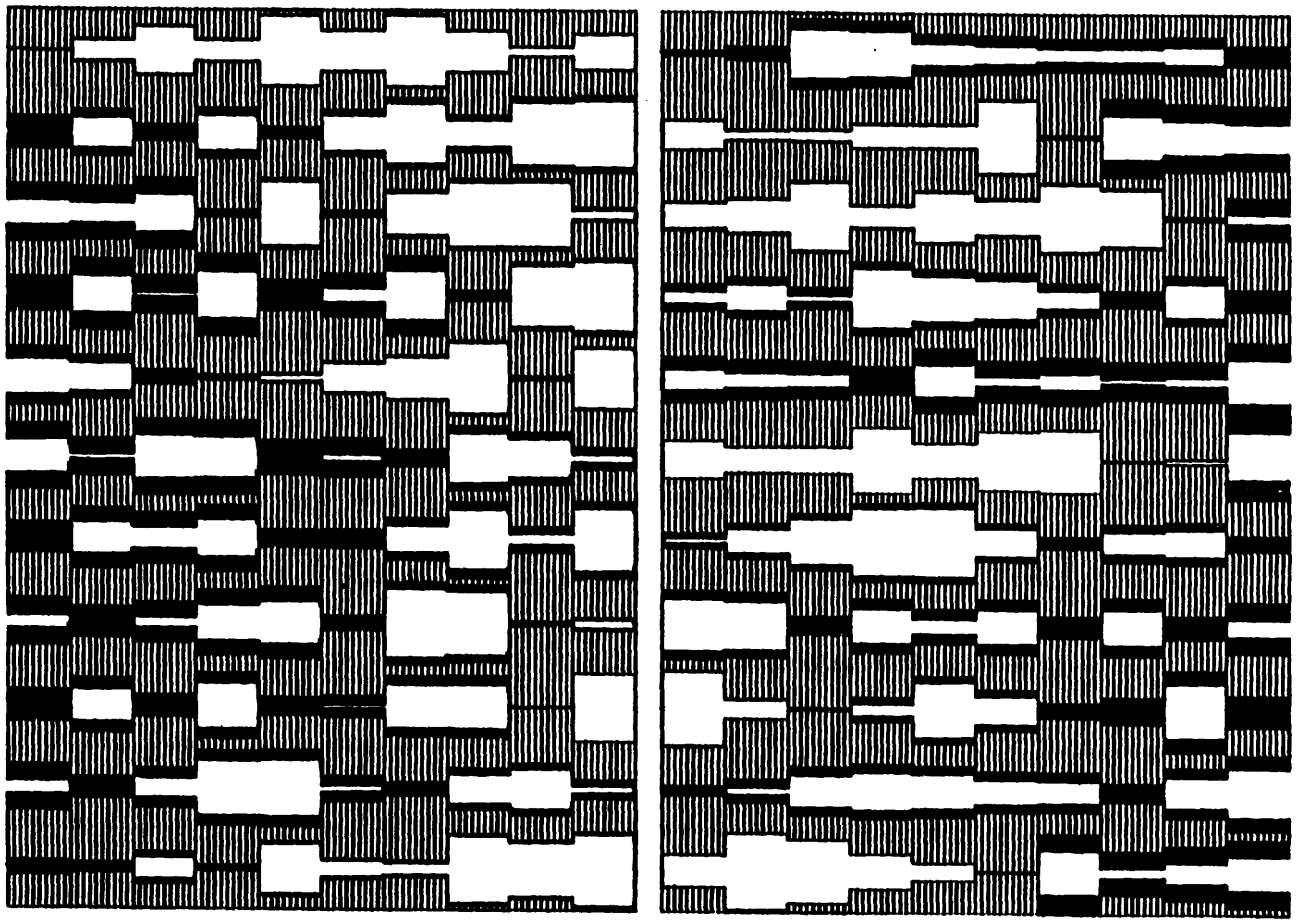

Figure 3.36 The corrugated parallel bundle of pores undergoing a parallel coking mechanism. (Coke layer thickness = 1359 Angstrom).

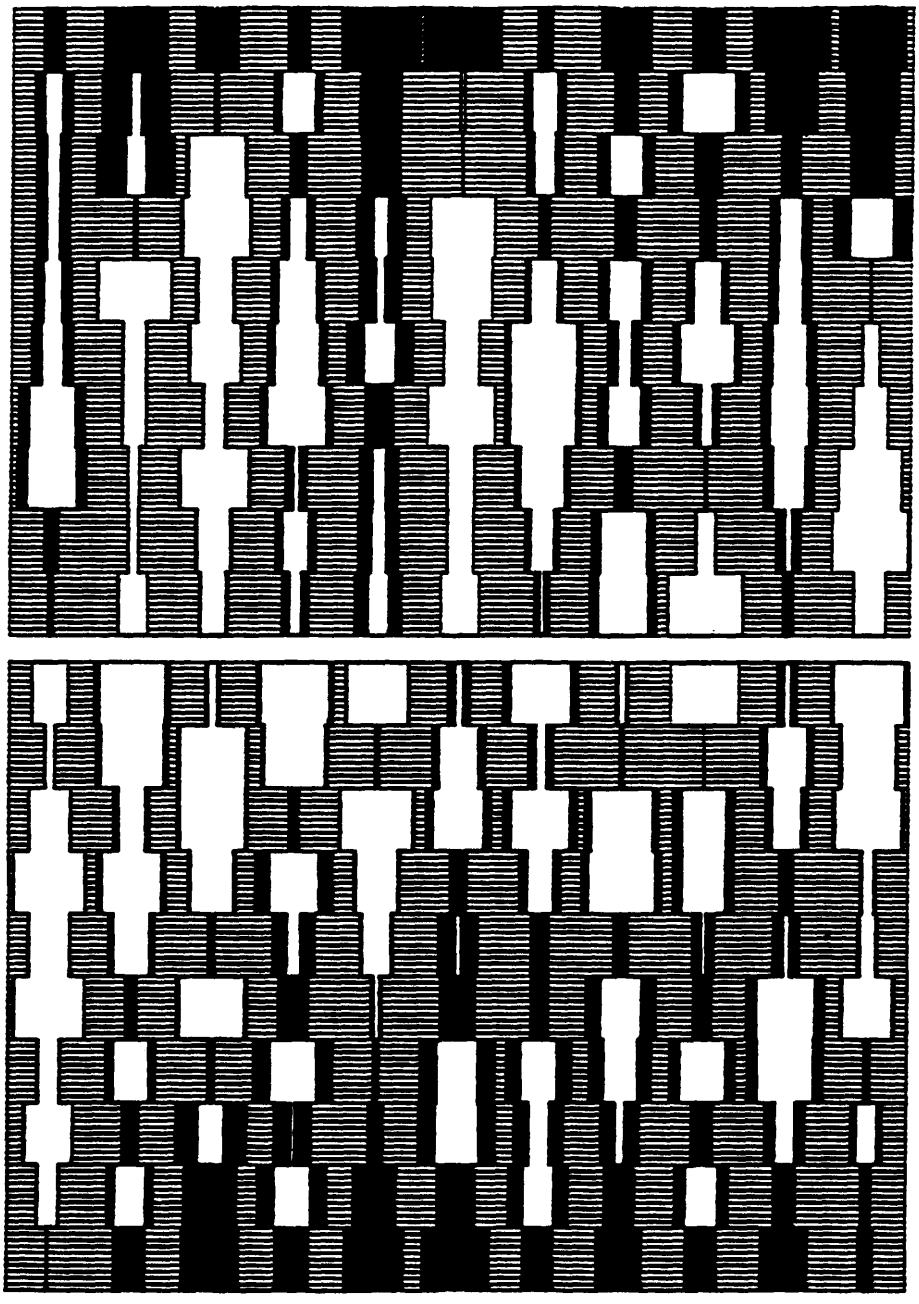

Figure 3.37 The corrugated parallel bundle of pores undergoing a parallel coking mechanism. (Coke layer thickness = 3200 Angstrom).

laydown (Butt, 1976), and it is clear that the appearance of heavy coking towards the outer pores does not necessarily mean that the coke laydown process is actually diffusion influenced.

3.6.2 Overall Coke Content of Corrugated Pores:

At the beginning of the process, the catalyst particle is clean from any coke deposits, so, all the pore elements are clean and fully accessible. As coke is produced, the process of heavy support coking takes place inside the pore structure. As the coke layer thickness increases from zero to 500Å, the coke content of the catalyst reaches approximately 4.5% (Fig. 3.38). An additional increase from 500Å to 1000Å in the coke layer thickness caused an increase of only 2% in the coke content of the catalyst.

The rate of increase in the coke content reduces drastically as the coke layer thickness gets larger and larger. Increasing the coke layer thickness from 2000Å to 3200Å had so little effect on the coke content that it increased by less than 0.5%.By the time the catalyst is fully deactivated, the coke content of it reached just over 8%.

This behaviour is due to the initial accessibility of all the pore elements to coke laydown, and as the size of the coke layer increases, the number of pore elements that are isolated (blocked) increases, therefore reducing the accessibility. Also, a given layer of coke occupies a much larger volume when the pore is empty initially, compared to the case when the pore is partially coked, because of the reduction in pore size with coking. The maximum theoretical coke content of the catalyst particle would be 16%. Figure 3.39 shows that approximately 48% of the total pore volume of the corrugated parallel bundle of pores becomes isolated during the process of heavy support coking. This corresponds to a loss of 60% of the support surface area which has become progressively inaccessible due to blockages (Fig. 3.40 and Fig. 3.41).

Heavy Support Coking
Corrugated Parallel Bundle Model

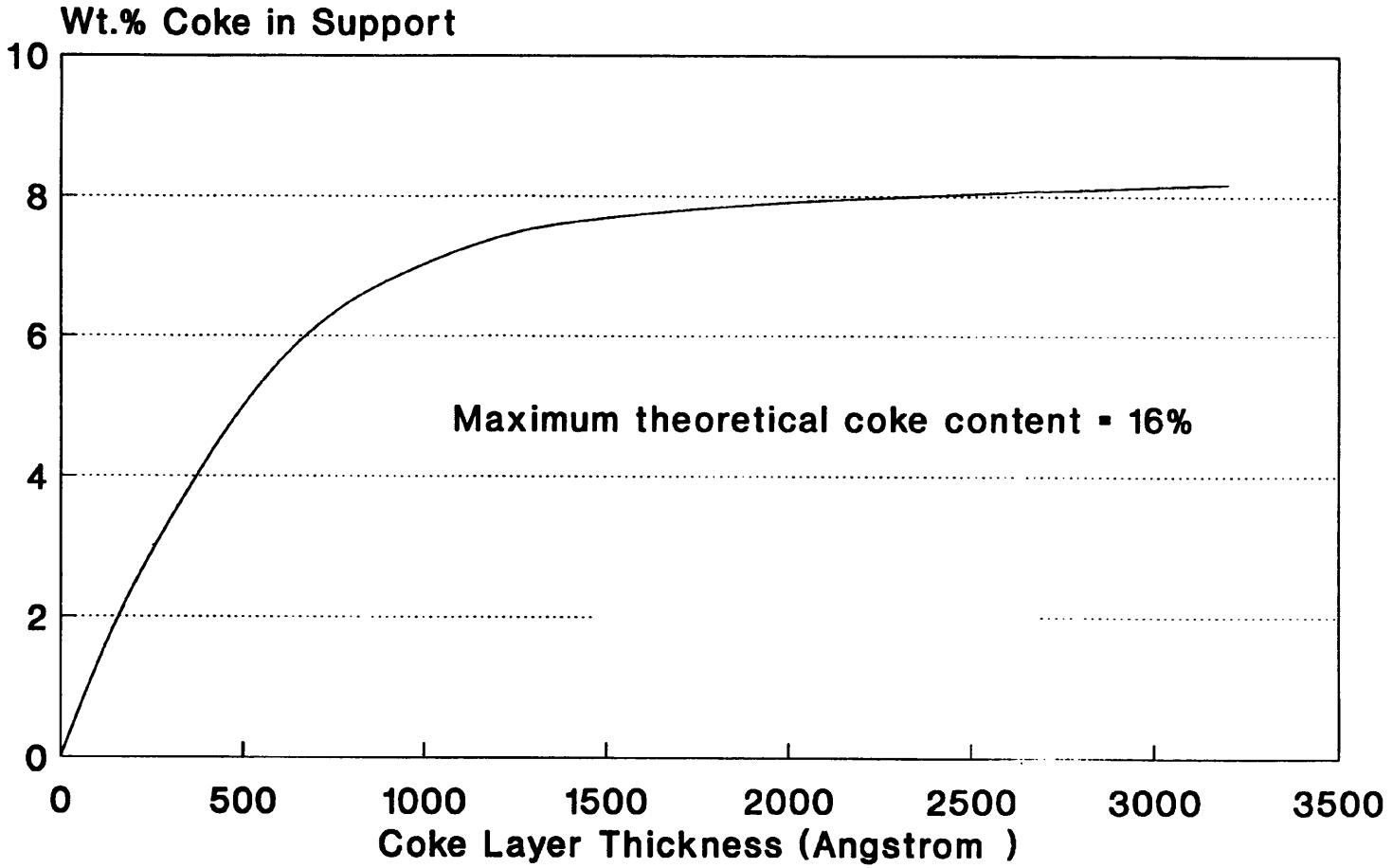

Figure 3.38 Coke content of the support for the corrugated parallel bundle pore model undergoing a parallel coking mechanism.

Heavy Support Coking
Corrugated Parallel Bundle Model

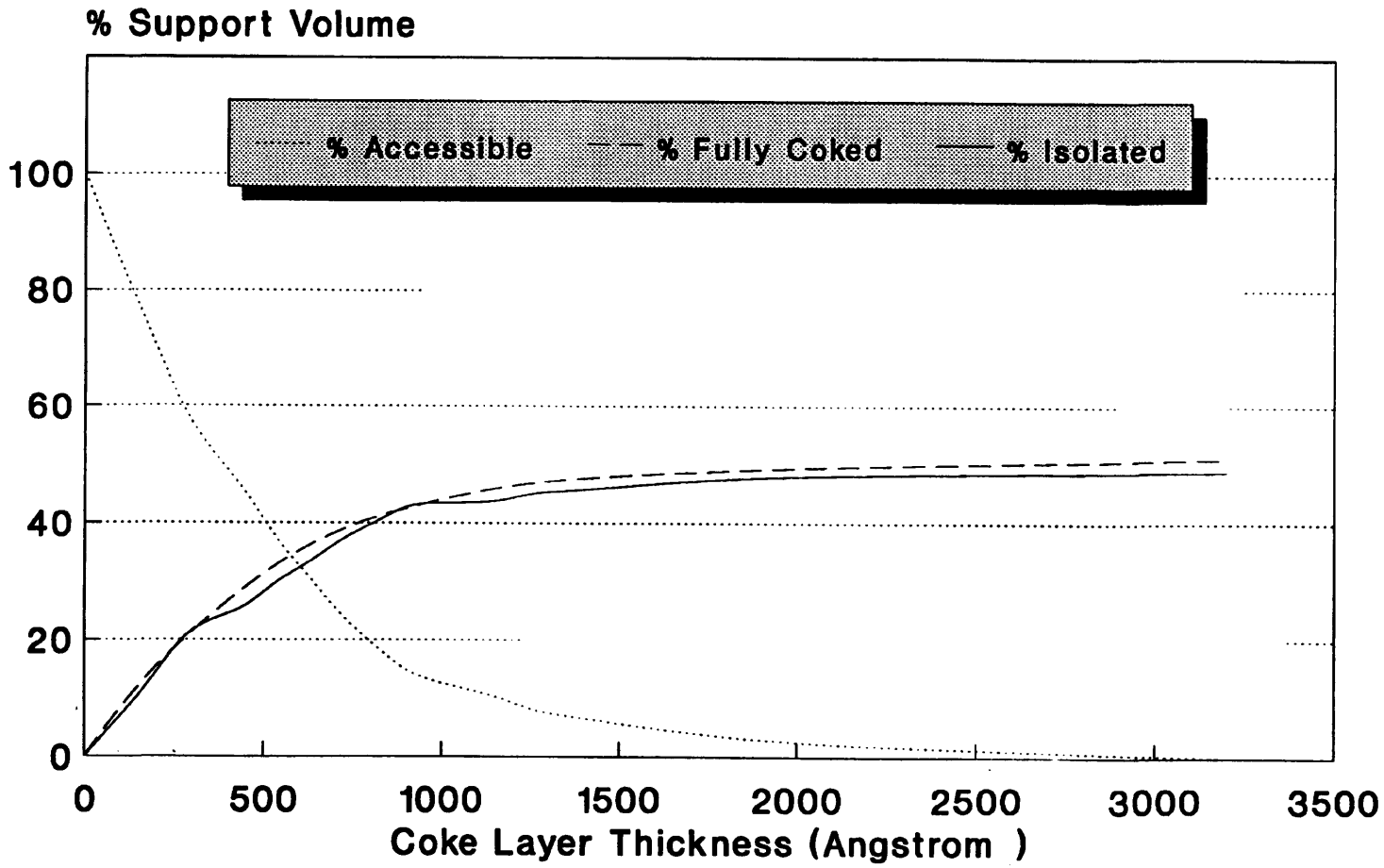

Figure 3.39 Changes in the support pore volume for the corrugated parallel bundle pore model undergoing a parallel coking mechanism.

Heavy Support Coking
Corrugated Parallel Bundle Model

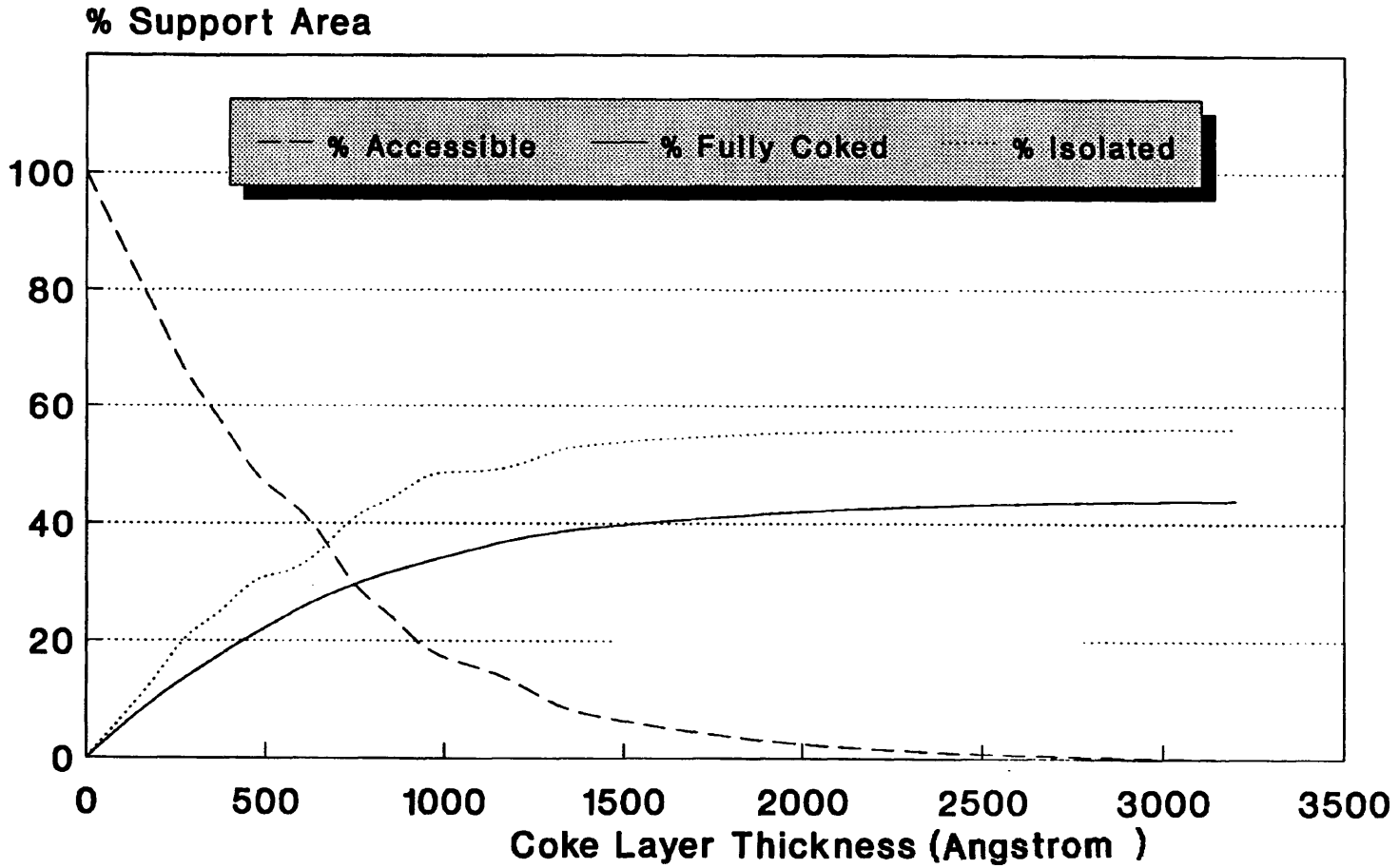

Figure 3.40 Changes in the support surface area for the corrugated parallel bundle pore model undergoing a parallel coking mechanism.

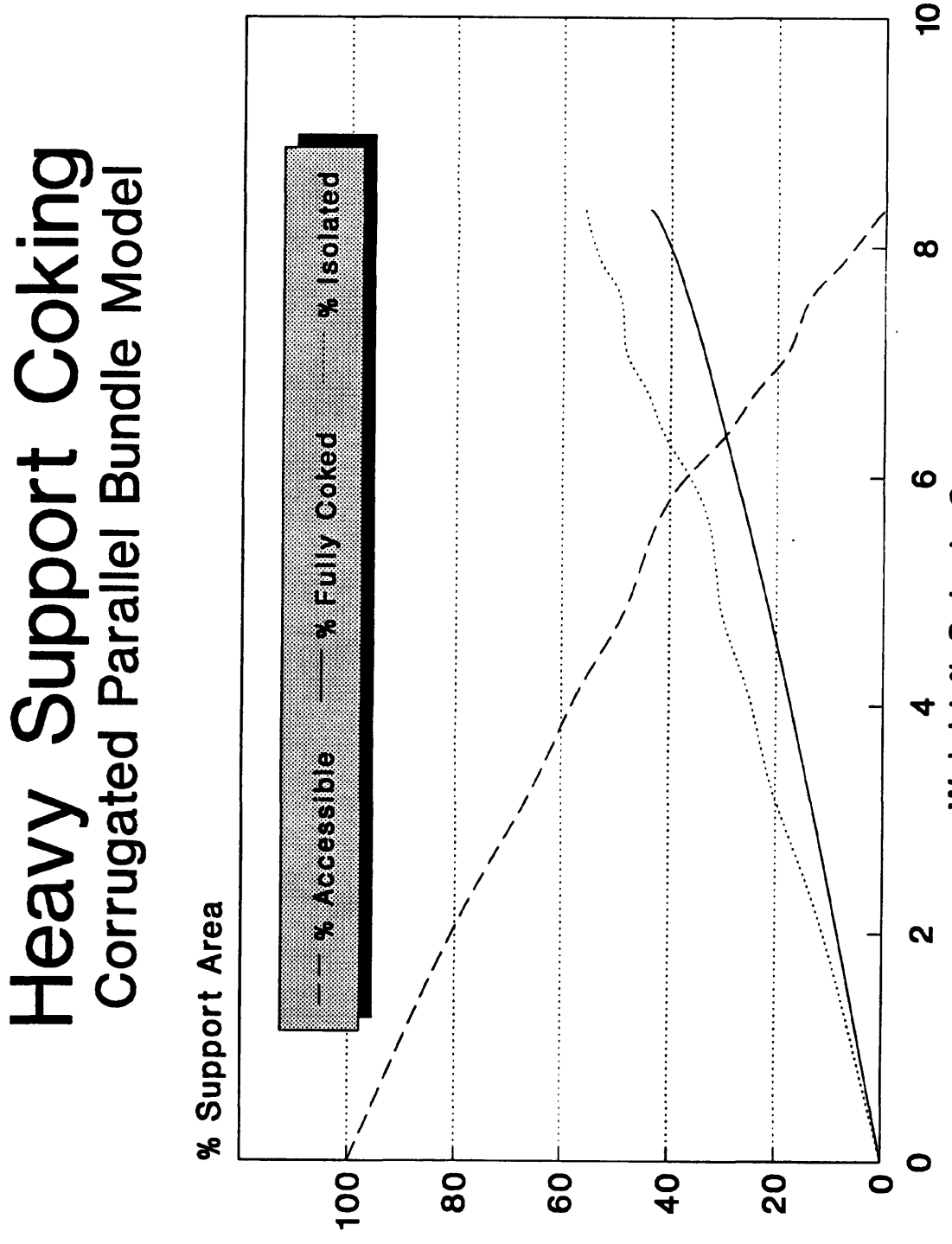

Figure 3.41 Support surface area vs. coke content for the corrugated parallel bundle pore model undergoing a parallel coking mechanism.

3.6.3 Coke Laydown without Diffusional Limitations:

Since no diffusional limitations exist, then the condition is such that the concentration of the reactant, C_A, is constant throughout the pore length. Under such conditions, the effectiveness factor approaches unity. Initially, this produces a uniform coke layer in each pore in the corrugated parallel bundle. As time on stream increases, and due to the fact that each pore is made up of different size elements, some of the internal pores become filled up with coke. Again this will produce a situation where heavier coking occurs towards the exterior of the catalyst particle compared to the lightly coked interior. Figure 3.42 shows a set of 22 corrugated 10–element pores with a bimodal pore size distribution consisting of 50% pore elements of size 60Å and 50% pore elements of size 3200Å. After complete deactivation, out of the 220 pore elements of the set, 89 large pores were isolated by the surrounding smaller pores which corresponds to a pore volume loss of more than 88% (Fig. 3.43). The maximum coke content of the catalyst represented by this set of pores is only 1.92% compared to a coke content of more than 8% for the pores with uniform pore size distribution in the range 60–3200 Å.

3.6.4 Coke Laydown with Strong Diffusional Limitations:

Under conditions of strong diffusional resistances, the effectiveness factor is far below unity and the concentration of the reactant decreases as it enters the pores. So, there exists a concentration gradient across the pore length regardless of the relative size of pore elements (corrugated, straight or single–size pores). This produces different reaction rates and therefore different product concentrations across any pore length. Since the coking reaction is a function of either product or reactant concentrations, the coke layer thickness will be different in each element across any pore length. As before, blocking phenomena will occur when some pore elements become fully coked. For the case of a parallel mechanism of coking where the coke precursor is the reactant, the

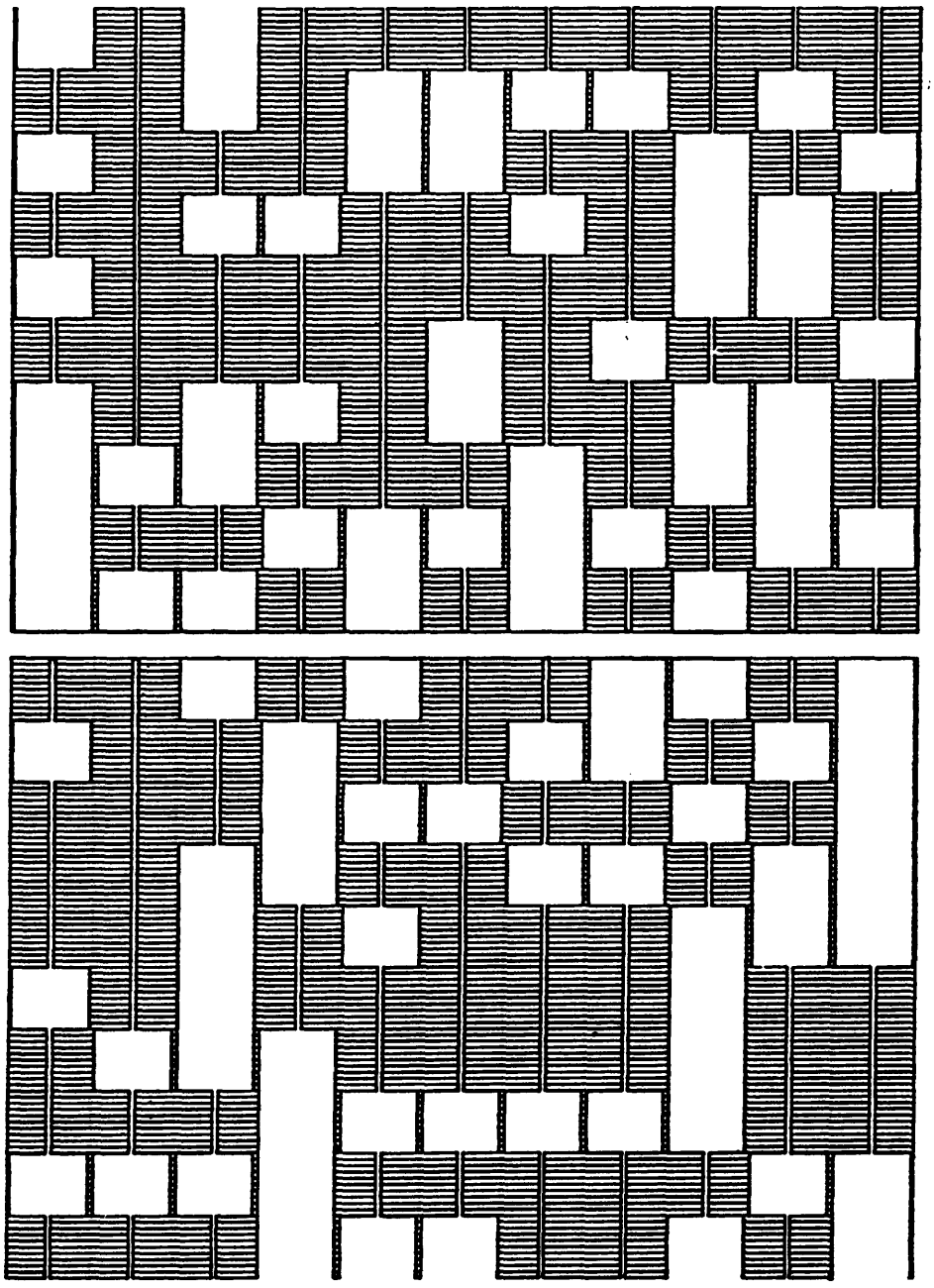

Figure 3.42 A corrugated parallel bundle pore model with a bimodal pore size distribution (clean, uncoked).

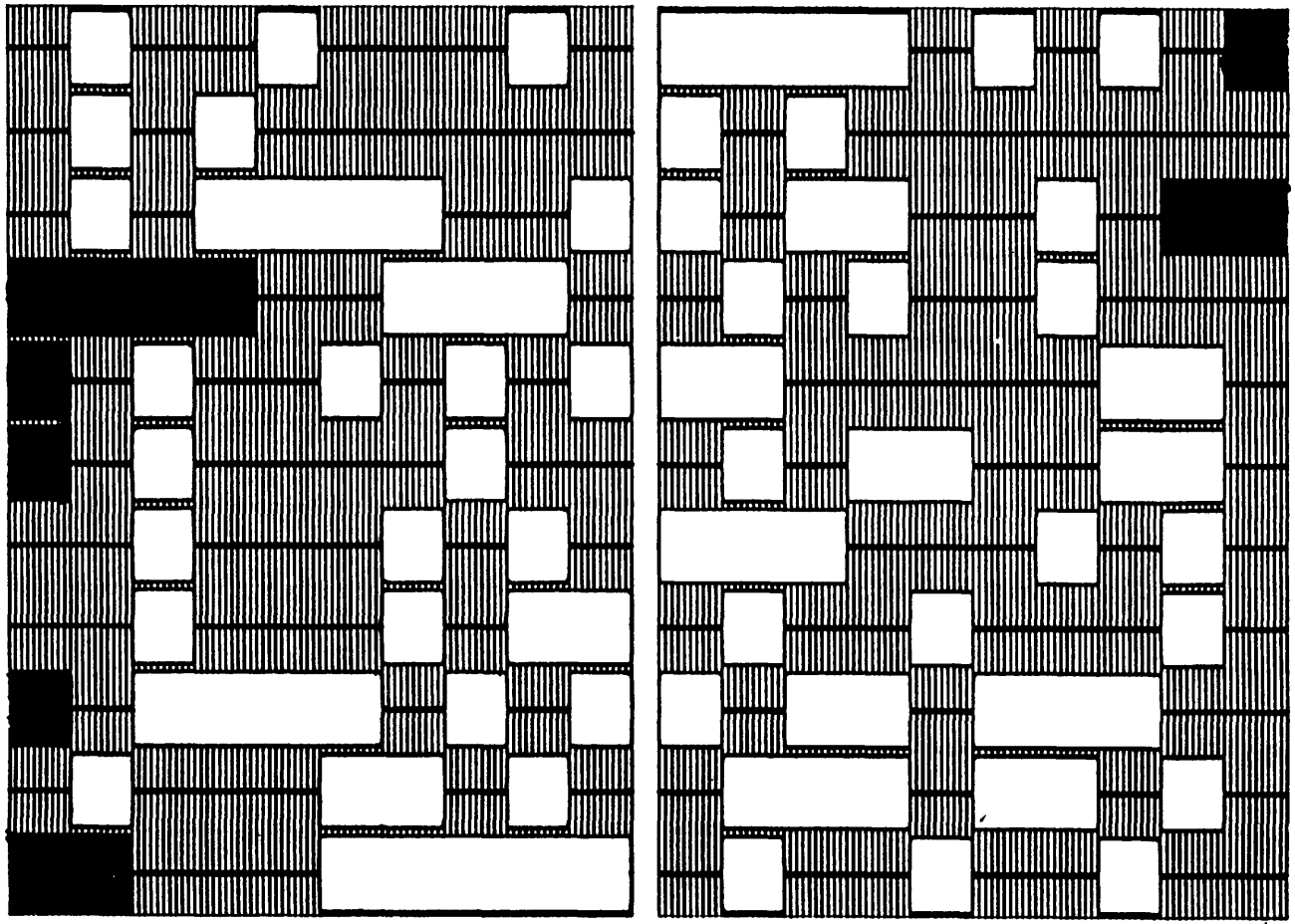

Figure 3.43 A corrugated parallel bundle pore model with a bimodal pore size distribution (after complete deactivation under conditions of negligible diffusional resistances).

coking in the outer pore elements takes place at a higher rate than the inner elements. Under conditions of very strong diffusional resistances, coke deposits almost exclusively in the external elements of pores, therefore, pore mouth blocking tends to occur.

3.6.5 Coke Laydown in the Equivalent Straight Cylindrical Model without Diffusional Limitations:

The straight cylindrical pore model consists of a parallel bundle of pores of uniform cross–section each having a radius 'R_n' assigned from the same pore size distribution 60–3200Å (Fig. 3.44). Under conditions of negligible diffusional resistances, the overall effectiveness factor of the pore model is near unity. Therefore, the coke laydown process will take place uniformly across the pores of the model, eventually, causing the complete filling of every pore in the assembly with coke (Fig. 3.45).

For the special case of the equivalent single–size average–area cylindrical pores (Fig. 3.46), where all the pores are of equal size (R=1452Å) there will be negligible concentration gradient across any of the pores. Again, this will result in a uniform coke layer thickness along all the pores, which will keep on increasing until fully coked (Fig. 3.47). Therefore, no pore blocking occurs and the total coke content of the catalyst with such pore model is equal to the theoretical maximum coke content.

3.6.6 Coke Laydown in the Equivalent Straight Cylindrical Model with Strong Diffusional Limitations:

Under conditions of strong diffusional resistances the effectiveness factor drops far below unity indicative of the presence of significant concentration gradient across the pores of the model. This will result in a larger reactant concentration at the outer section of the pores causing a larger rate of coking under a parallel mechanism. This

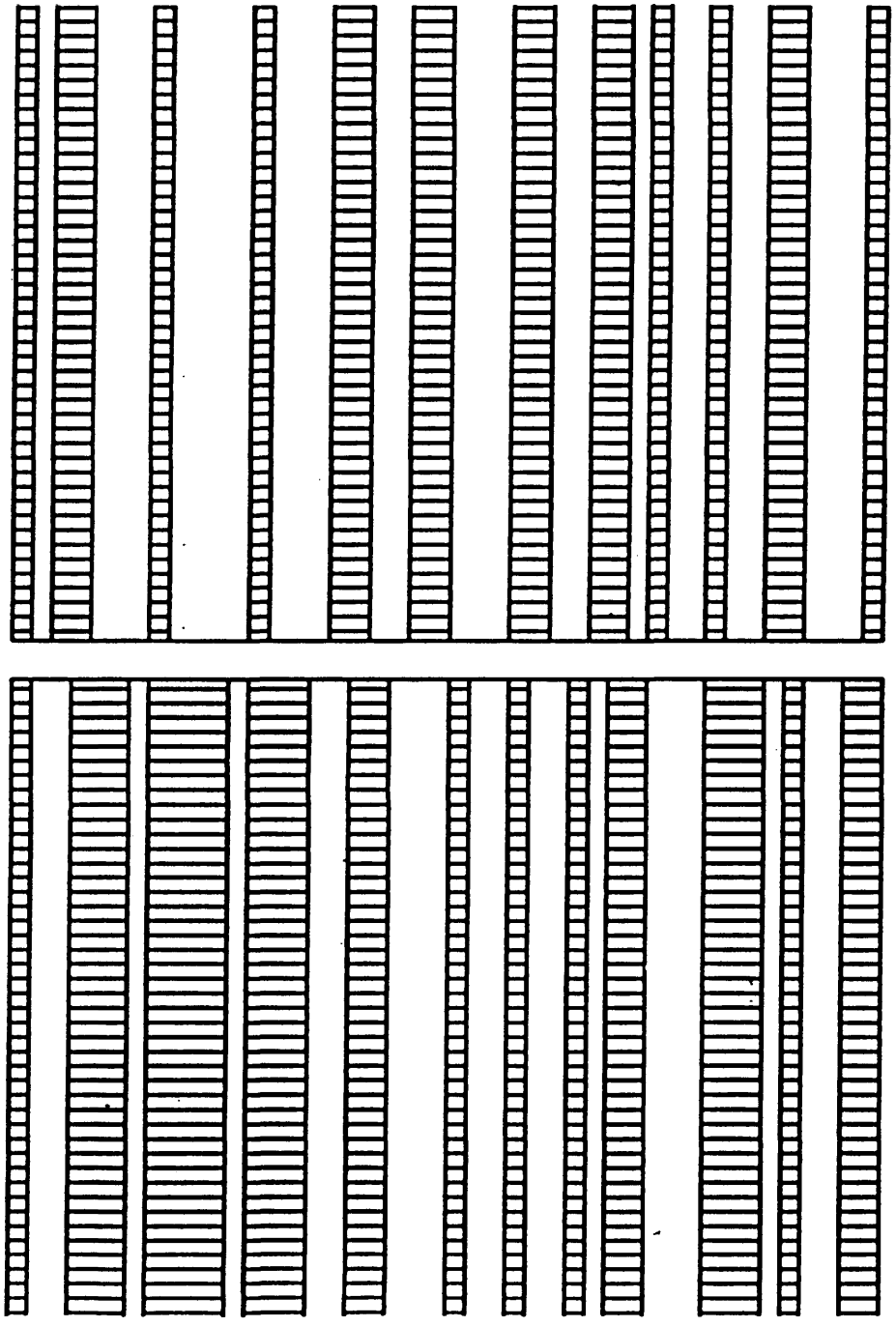

Figure 3.44 A set of 22 straight cylindrical pores with a uniform pore size distribution in the range 60–3200 Angstrom (fresh, uncoked).

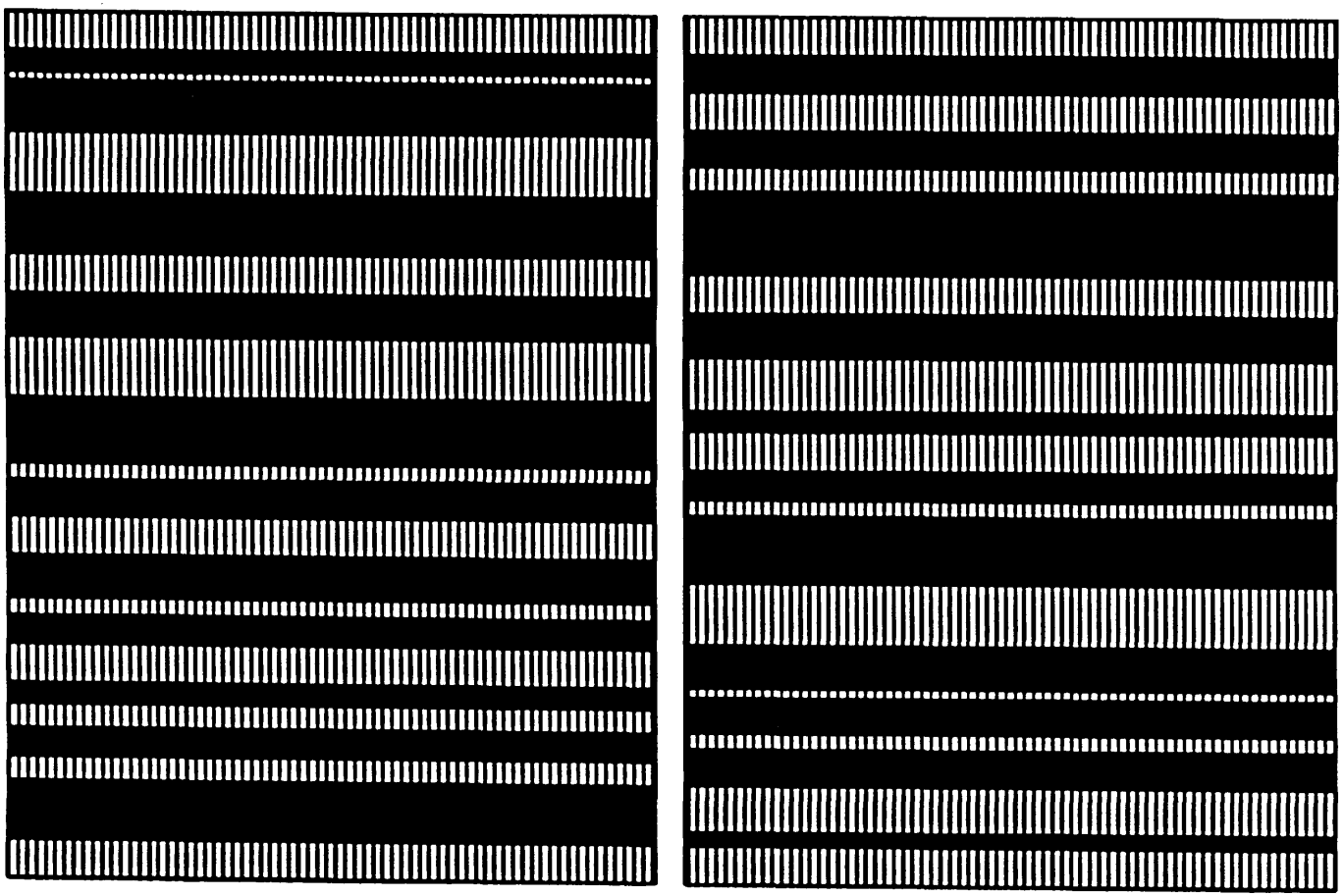

Figure 3.45 A set of 22 straight single–size average–area cylindrical pores (after complete deactivation under conditions of negligible diffusional resistances).

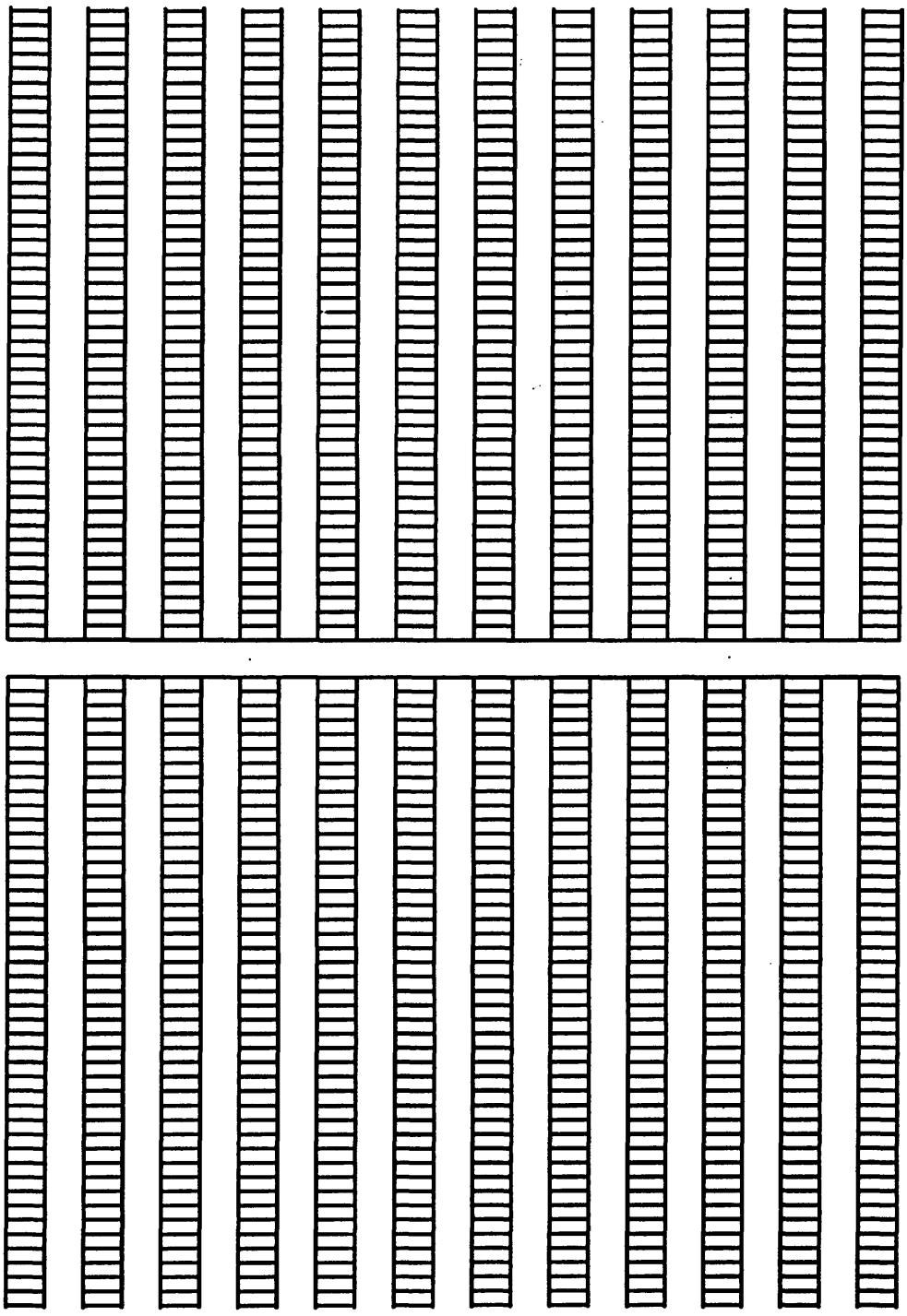

Figure 3.46 A set of 22 straight single–size average–area cylindrical pores (fresh, uncoked).

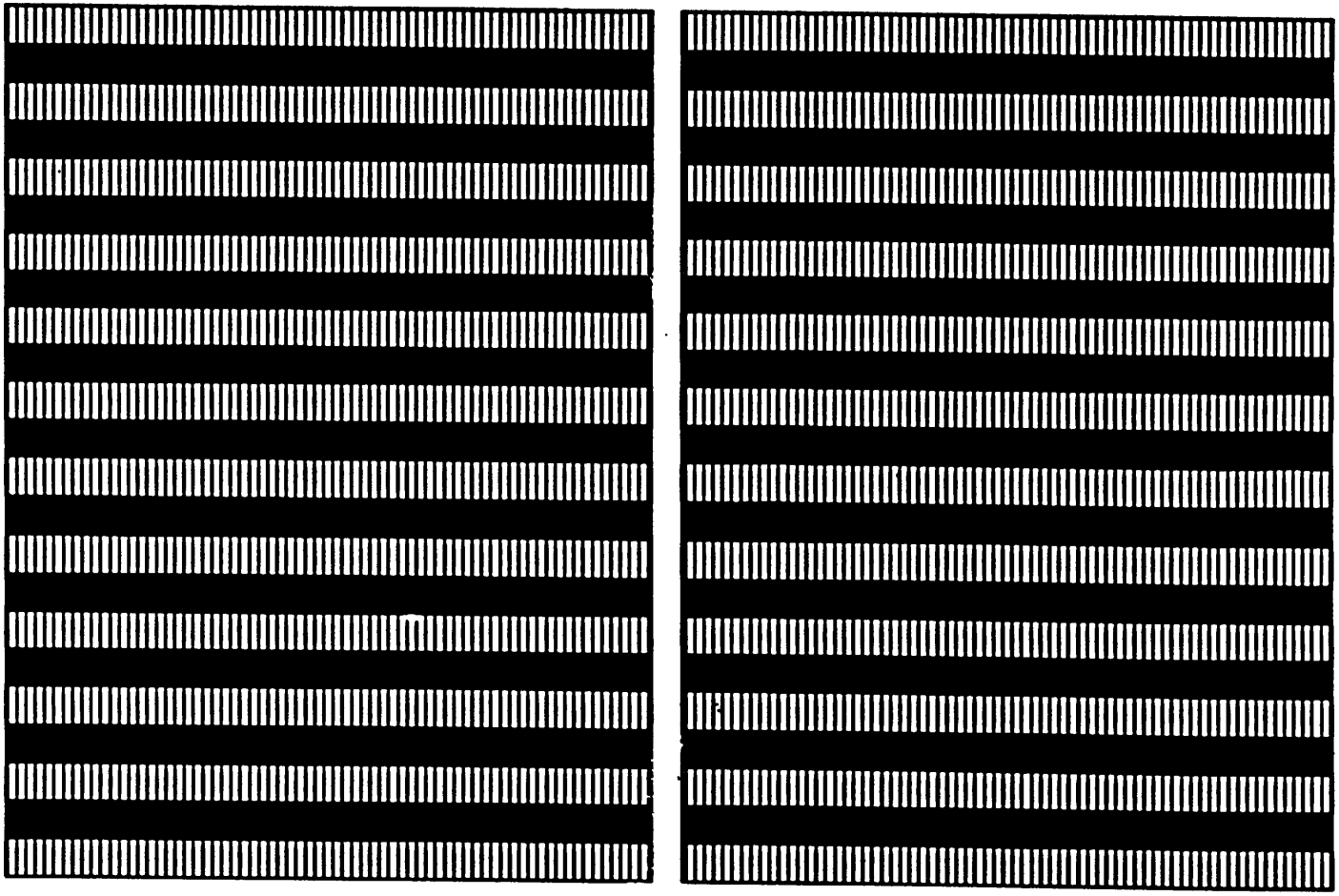

Figure 3.47 A set of 22 straight single–size average–area cylindrical pores (after complete deactivation under conditions of negligible diffusional resistances).

produces a coke layer thickness which decreases moving inside the pores causing the isolation of potentially active support surface area. With extreme conditions of diffusional resistances, pore mouth plugging will tend to occur. For the special case of single–size average–area pore model, the same blocking phenomenon will occur but with a lesser degree of pore isolation (Fig. 3.48).

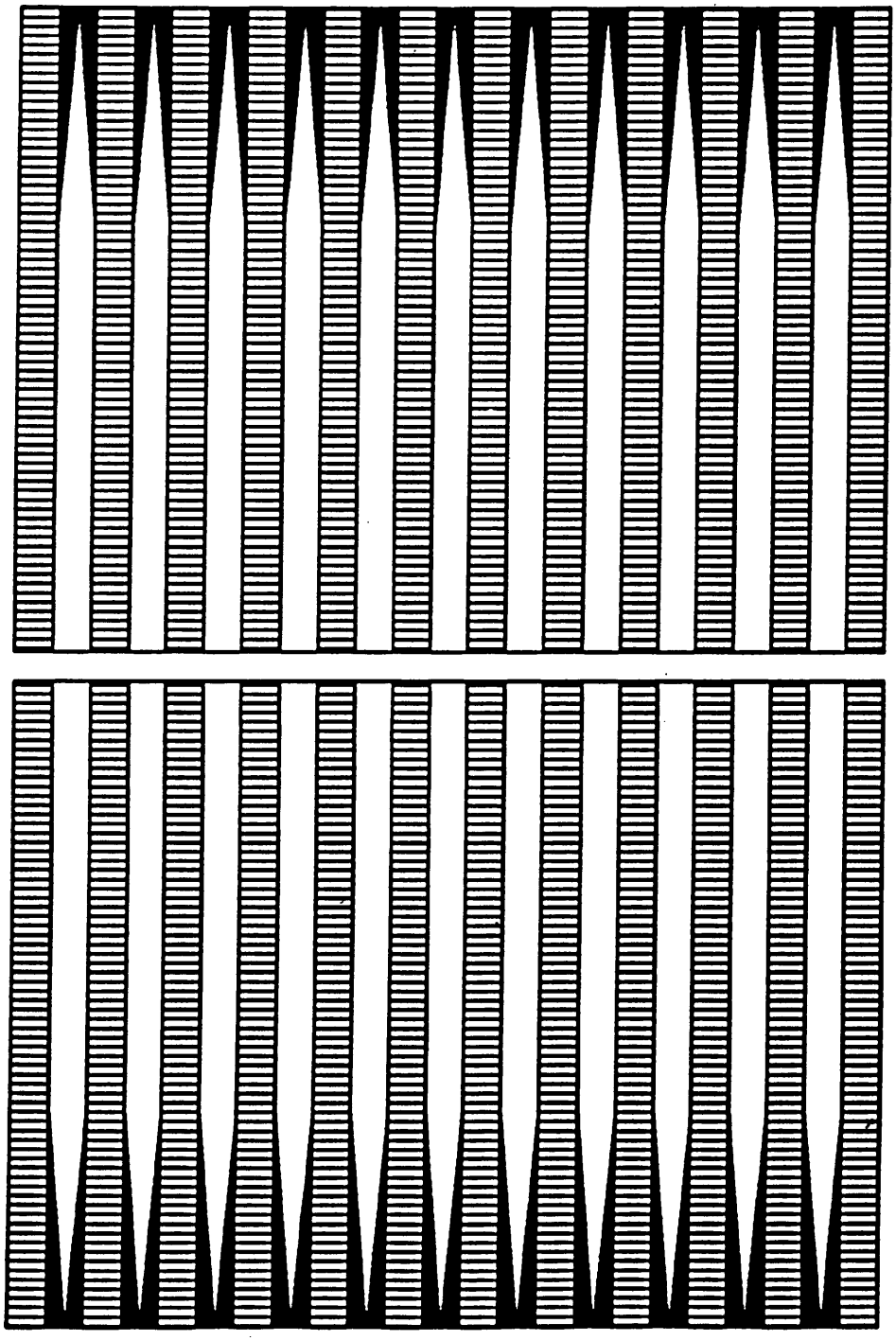

Figure 3.48 A set of 22 straight single–size average–area cylindrical pores (after complete deactivation under conditions of strong diffusional resistances).

CHAPTER FOUR

EXPLORATION OF THE THEORY USING A STOCHASTIC NETWORK PORE MODEL

CHAPTER FOUR

EXPLORATION OF THE THEORY USING A STOCHASTIC NETWORK PORE MODEL

4.1 SIMULATION OF THE FLUIDISED BED REACTOR:

In these illustrations, the structural model used to represent the support pore structure was the stochastic network. It was found that one hundred 10x10 networks were sufficient to give a reproducible pore size distribution. These one hundred networks are referred to as a "catalyst particle". In order to simulate the fluidised bed, ten such catalyst particles with equivalent but individually different sets of pore sizes were generated. Figures 4.1 and 4.2 illustrate pore number and pore volume distributions for several such particles. Diffusion, reaction and deactivation were simulated in each particle simultaneously to produce an average activity profile for the reactor. Computer simulations of the program "OMRAN10" (Appendix–3) were carried out to explore the deactivation behaviour of the fluidised bed under different deactivation mechanisms, i.e. parallel, series and triangular deactivation. The effect of changes in the fraction of the initial activity due to zeolite, the main reaction rate constant and the catalyst:feed ratio was also investigated.

Table 4.1 provides the default values of the major parameters in the program "OMRAN10" which were used in the simulations. These simulations provide a framework for modelling the experimental deactivation behaviour.

For each of the simulations, the following figures were produced:

1) Conversion vs. time,
2) Total catalyst coke content vs. time, and,
3) Total catalyst surface area vs. time.

Number Distribution
Uniform (60-3200 Angstrom)

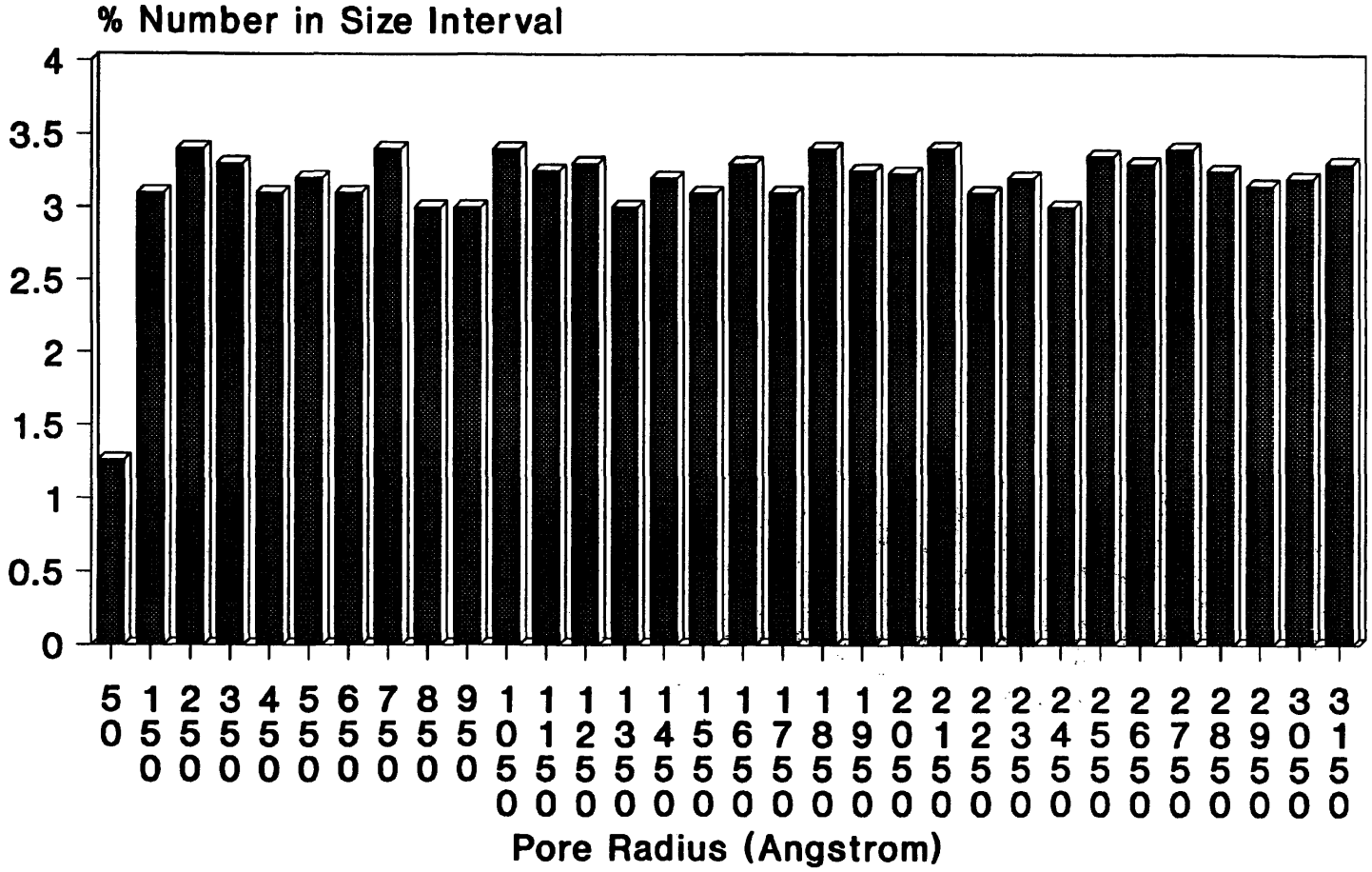

Figure 4.1 Number distribution of pore radii for the pore model.

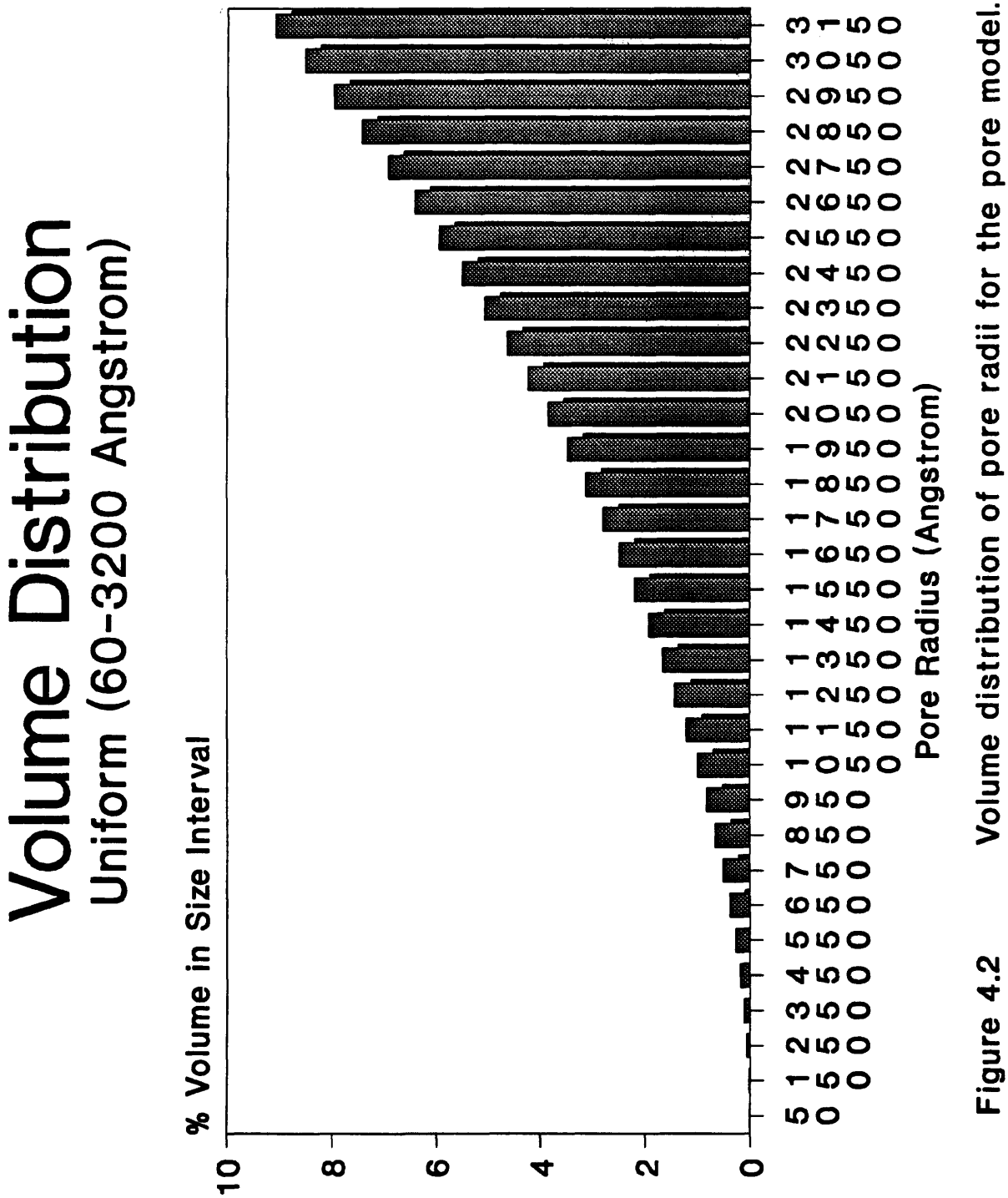

Figure 4.2 Volume distribution of pore radii for the pore model.

Table 4.1 Default values of major parameters in the program "OMRAN10".

Parameter	Value	
Network side length	14	Microns
Zeolite coke unit size	1	Angstrom
Support coke unit size	20	Angstrom
Main reaction rate constant k_s	$6x10^{-8}$	(m/s)
Coking rate constants k_{cs} & k_{cp}	$1x10^{-10}$	$(m^4kmol^{-1}s^{-1})$
Zeolite fractional activity α	0.5	(Initially)
Catalyst:feed ratio	7.5:1	g/(g/min)
P.S.D.(Uniform Distribution)	60–3200	Angstrom

When necessary, figures showing changes in the effectiveness factor with time were produced wherever conditions of significant diffusional resistances prevailed.

4.2 EFFECT OF CHANGING THE FRACTION OF INITIAL ACTIVITY DUE TO ZEOLITE α :

To investigate the influence of α on the conversion, coke content and surface area it was reduced gradually from 1.0 to 0.0. On one hand, an α value of 1.0 indicates that all the initial activity is due to the zeolite alone and the support has no catalytic activity. On the other hand, an α value of 0.0 indicates that all the initial activity is due to the support alone, and the zeolite has no catalytic activity. When the catalyst does not undergo any kind of deactivation, reducing the α value has the effect of reducing the constant conversion lines (Fig. 4.3). This is due to the fact that most of the surface area of the catalyst is in the zeolite, so the higher the fractional activity of the zeolite, the larger the conversion.

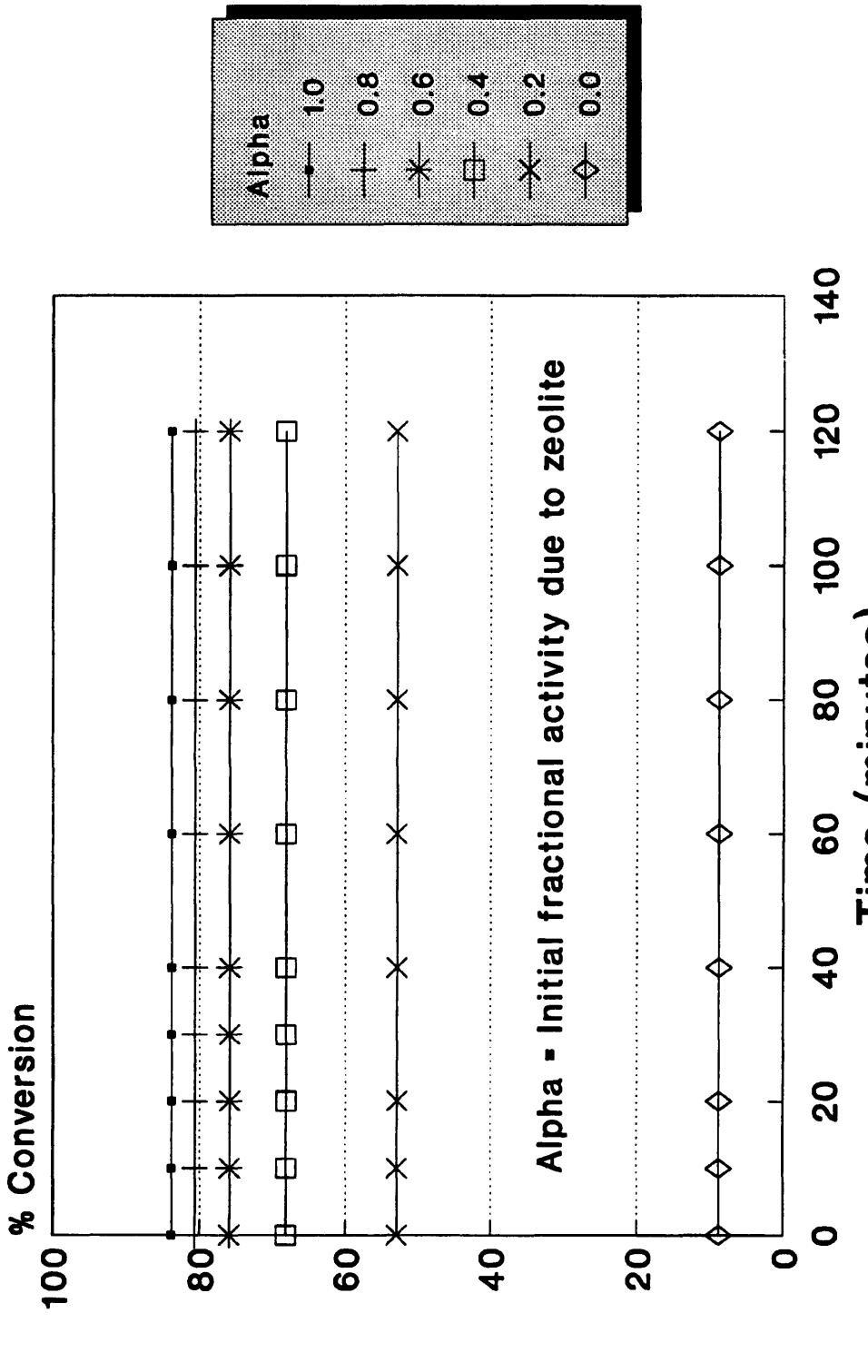

Figure 4.3 Effect of changes in the zeolite fractional activity under no coking conditions.

4.2.1 Series Deactivation:

For series deactivation, the conversion profiles show a drop in initial conversion as α is reduced (Fig. 4.4). For conversions larger than 50% the series deactivation is more effective since the product is the coke precursor, therefore, the slope of the conversion profiles reduces with time on stream. For a catalyst with 100% zeolitic activity, conversion drops from 84% to 8% over a period of two hours in comparison with a drop from 9% to 7% over the same period if all the activity was due to the support. Coke content profiles show that as the α value increases, the coke content increases. It is interesting to note that a coke content of only 1.3% corresponds to an α value of 0.0, while a slightly larger value of α such as 0.2 produces more than twice as much coke (3%). This is due to the sharp increase in conversion as α value increases from 0.0 to 0.2 which increases the concentration of the product which in turn then produces coke under the series mechanism of coking. Surface area profiles show that as the alpha value increases, the drop in surface area increases corresponding to larger coke contents. Again, the large drop in surface area as the α value increases from 0.0 to 0.2 is distinctive.

4.2.2 Parallel Deactivation:

For parallel deactivation, the conversion profiles show a drop in initial conversion as α is reduced (Fig. 4.5). The slope of the conversion profiles is initially small, but gets larger with time on stream and especially when conversion drops below 50%. This is due to the increase in the reactant concentration which is the coke precursor.

Coke content profiles show that as the α value gets larger, the coke content gets smaller. But the decrease in coke content is very gradual with no sharp changes due to the introduction of zeolite activity as was the case with series deactivation.

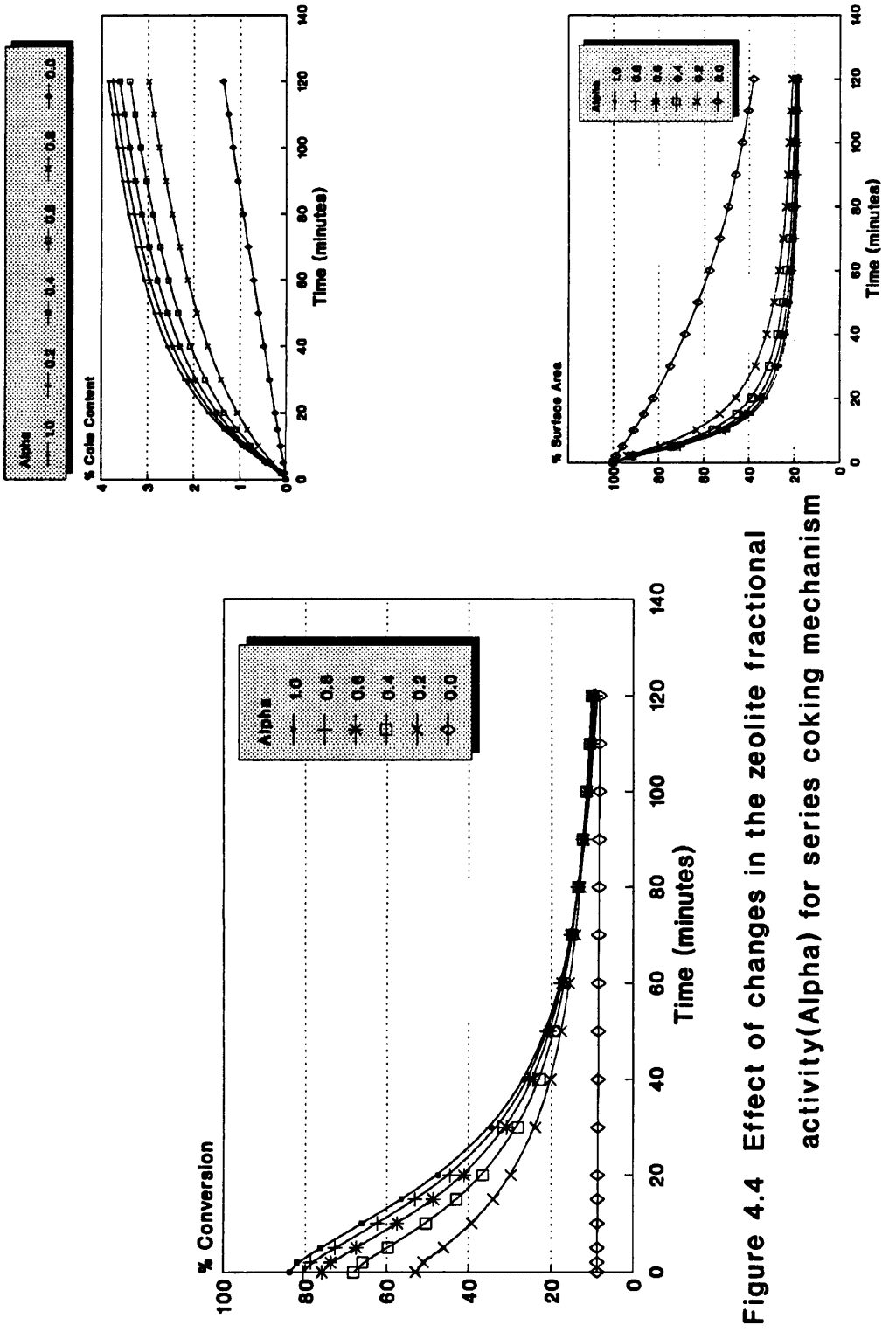

Figure 4.4 Effect of changes in the zeolite fractional activity(Alpha) for series coking mechanism

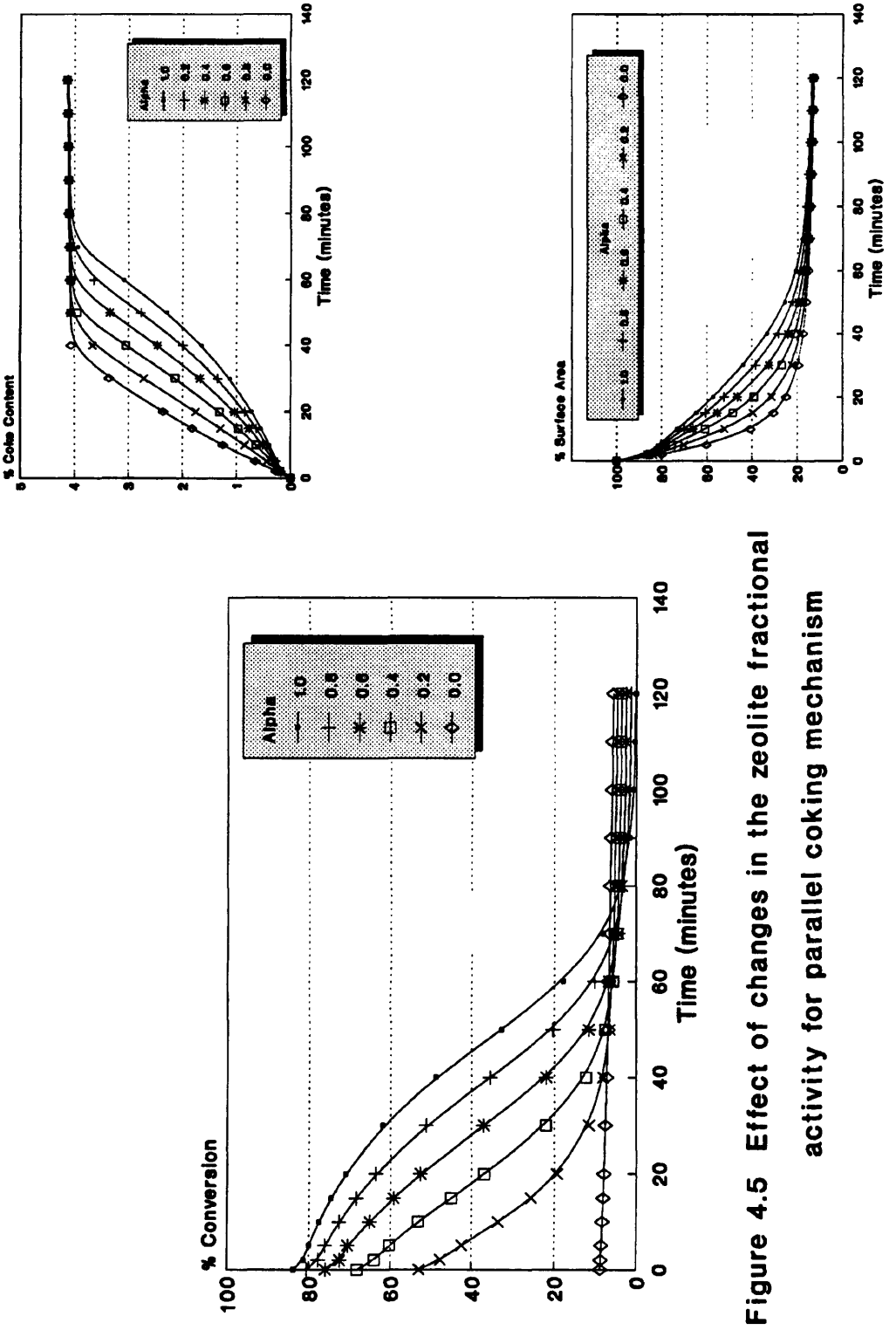

Figure 4.5 Effect of changes in the zeolite fractional activity for parallel coking mechanism

Surface area profiles, show that as the α value increases, the drop in surface area reduces due to reduction in the coke content.

4.2.3 Triangular Deactivation:

For triangular deactivation, the conversion profiles show that as α decreases, conversion decreases by a larger extent than either parallel or series deactivation alone. For the case where the parallel and series coking rate constants are equal, the conversion profiles intersect at a single point at sometime on stream (Fig. 4.6). Beyond this point the relationship between α and conversion is reversed. Now, as α gets larger the conversion gets smaller, and for an α value of 1.0 the conversion approaches 0% after one hour on stream. This is due to the fact that zeolite activity is lost much faster than the activity provided by the support.

Coke content profiles depend on the relative values of the parallel and series coking rate constants. When they are equal, a single coke profile is produced for all values of α. The surface area profiles also depend on the relative values of the series and parallel coking rate constants. For the case of equal coking constants, a single surface area profile is produced for all values of α. This is attributed to the assumption of equimolar counter diffusional flow. This results in the sum of the concentrations of the reactant and product being constant at all times. This causes the coking rate and, therefore, coke content and surface area to be independent of the conversion and α, and only dependent on the time on stream.

4.3 EFFECT OF CHANGING THE MAIN REACTION RATE CONSTANT:

To investigate the influence of changes in the reaction rate constant on conversion, coke content and surface area, it was changed gradually from $6x10^{-10}$(m/s) with conversion of only 3% up to a rate constant of $1.875x10^{-6}$(m/s)

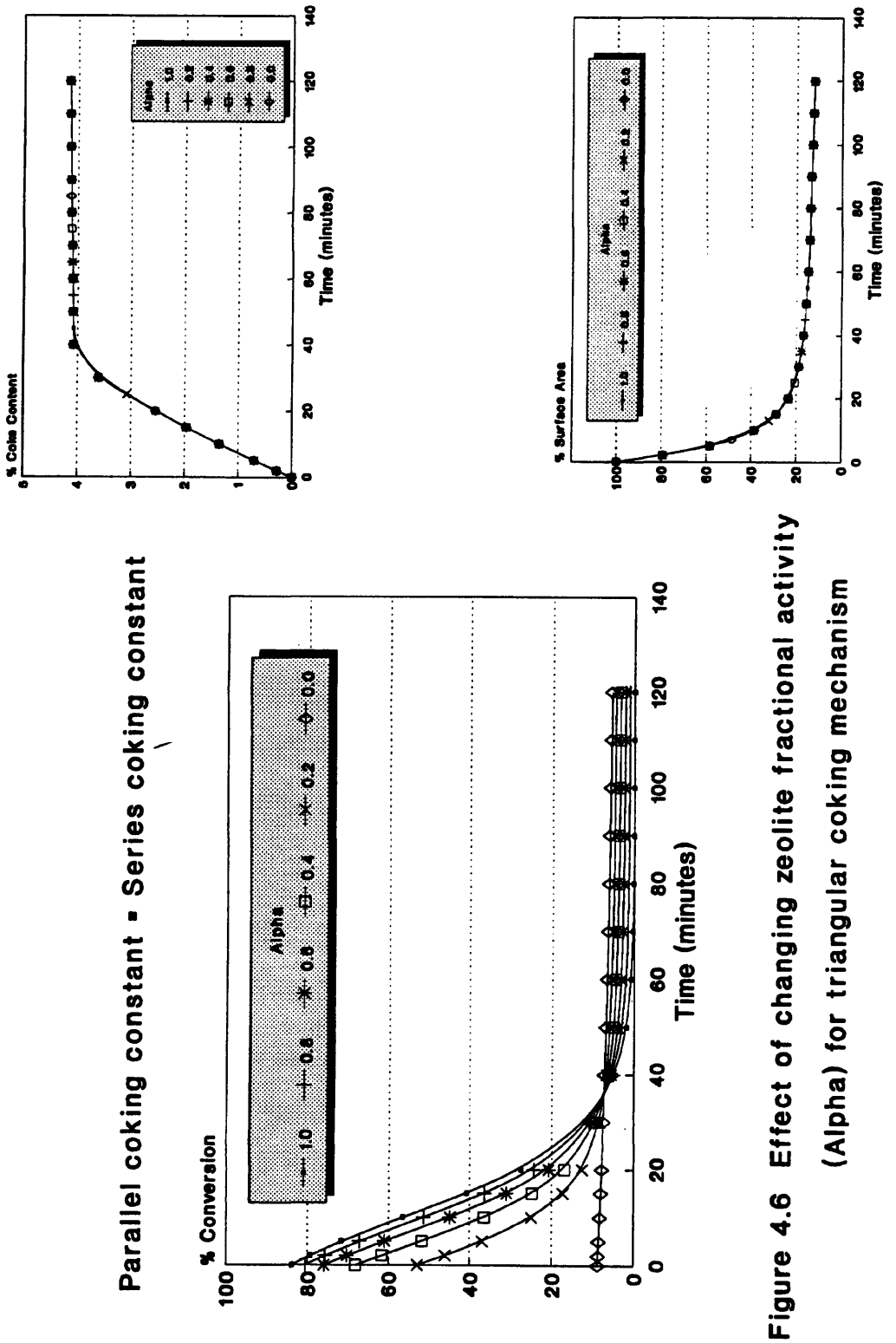

Figure 4.6 Effect of changing zeolite fractional activity (Alpha) for triangular coking mechanism

with 98% conversion (Fig. 4.7). The effectiveness values always stayed over 0.9 indicative of small diffusional resistances over the reaction rate constant range (Fig. 4.8).

4.3.1 Series Deactivation:

For series deactivation, the reaction rate constants of values up to $3x10^{-9}$ produced almost parallel straight lines similar to the no deactivation case. This is due to the very small conversions produced and therefore small product concentrations which cause negligible deactivation (Fig. 4.9). As the rate constant gets larger, the initial conversion gets larger and the drop in conversion with time on stream gets bigger. For a rate constant of $3.75x10^{-7}$, the initial conversion is 94% dropping to 40% after less than one hour on stream, while after two hours on stream it reaches a value of 22%. The coke content profiles show clearly that as the reaction rate increases, the coke content increases. While a rate constant of $6x10^{-10}$ produces less than 0.5% coke after two hours on stream, a rate constant of $1.875x10^{-6}$ produces 4% coke content in only 40 minutes on stream.

Surface area profiles show that as the reaction rate constant increases the surface area reduces. A rate constant of $6x10^{-10}$ produces a drop of 25% in surface area after two hours on stream while a rate constant of $3x10^{-9}$ produces a drop of 55% over the same time on stream. As the rate constant gets larger than $7.5x10^{-8}$, changes in the final surface area become negligible. This is due to the fact that all the zeolite surface area has been lost, and the drop in support area is very slow. Therefore, the surface area becomes insensitive to further increases in the rate constant.

4.3.2 Parallel Deactivation:

For the parallel mechanism of coking, larger rate constants produce higher

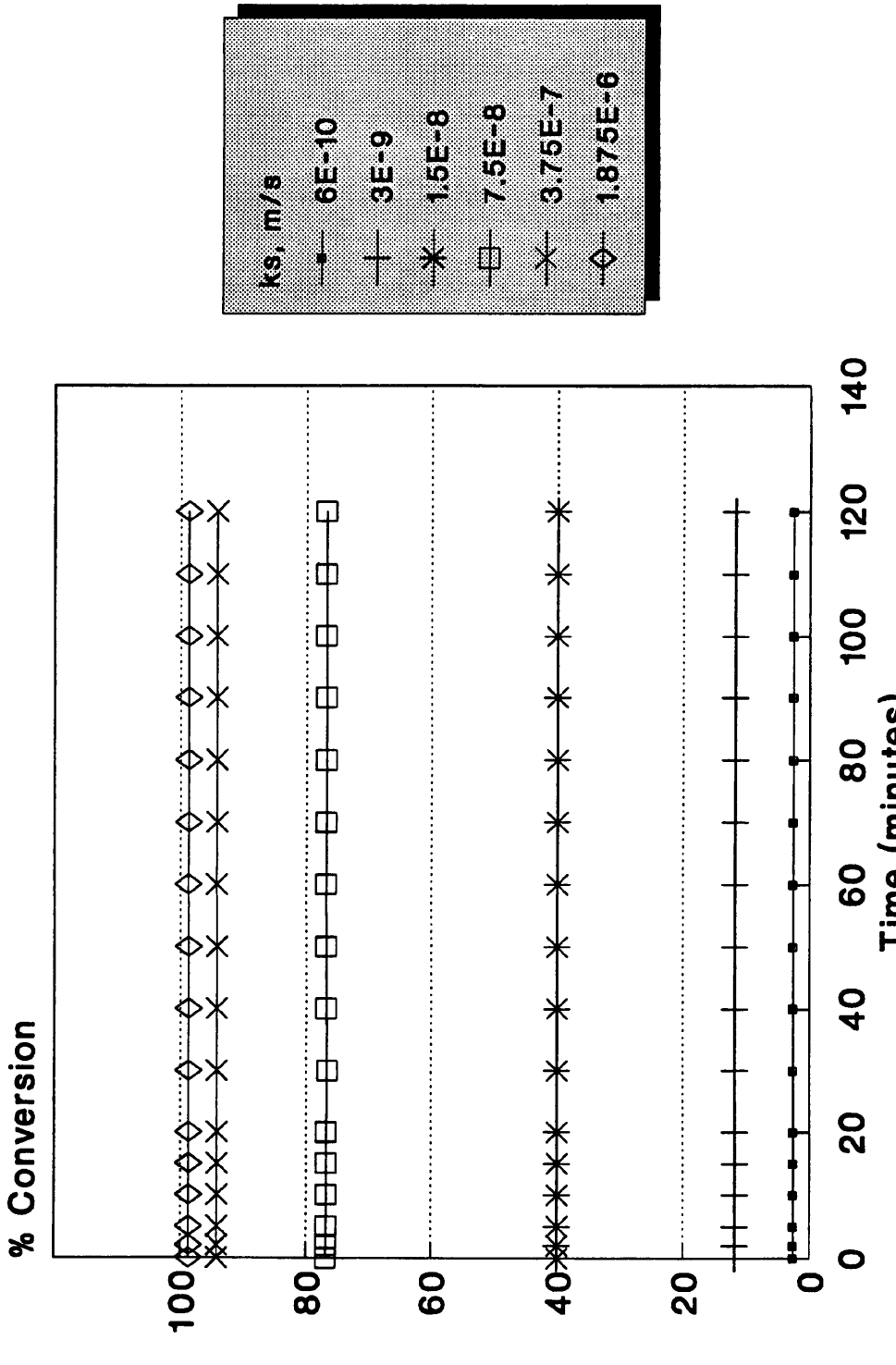

Figure 4.7 Effect of changes in the reaction rate constant on the conversion profiles under no coking conditions.

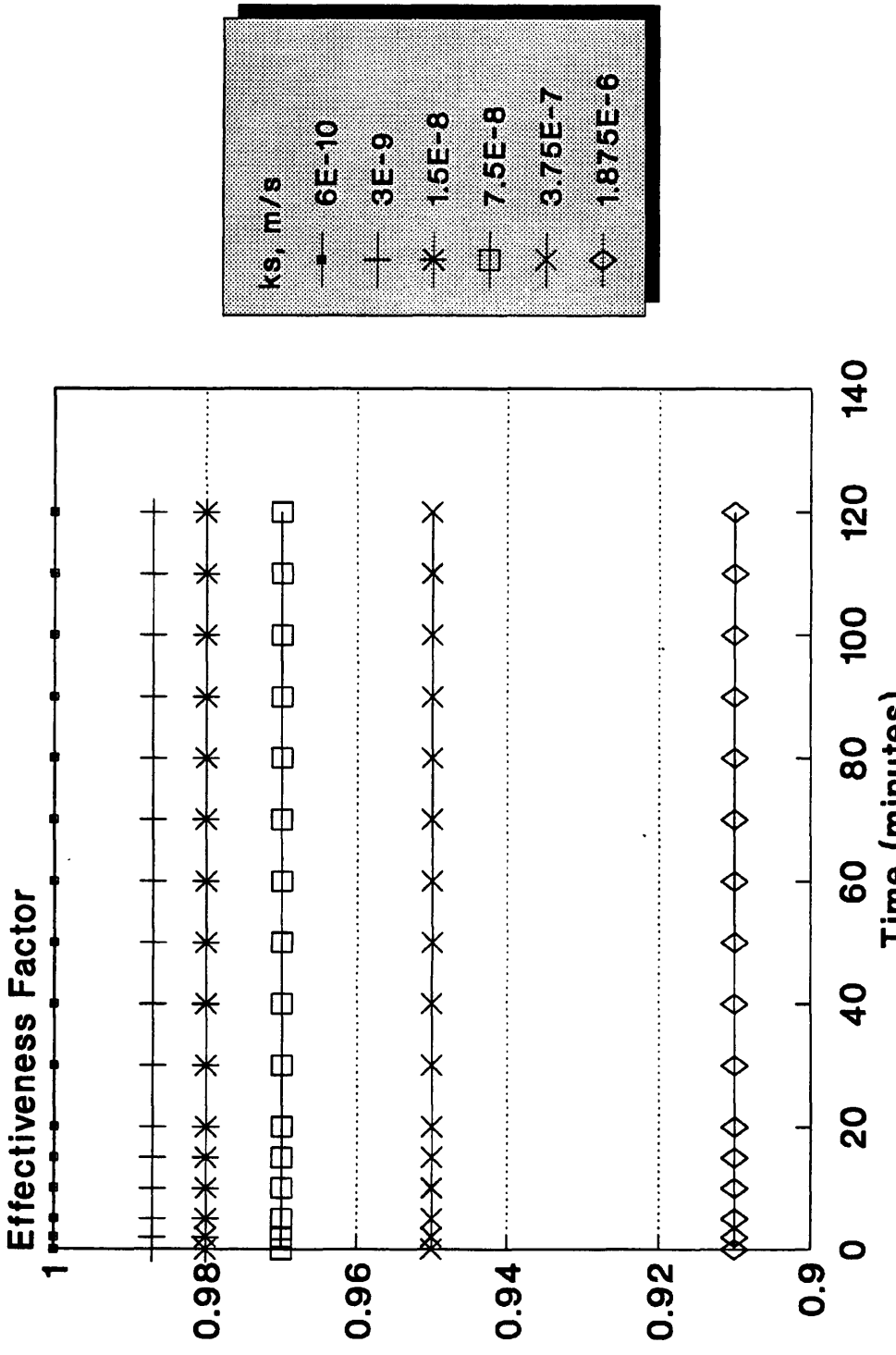

Figure 4.8 Effect of changes in the reaction rate constant on the effectiveness factor under no coking conditions.

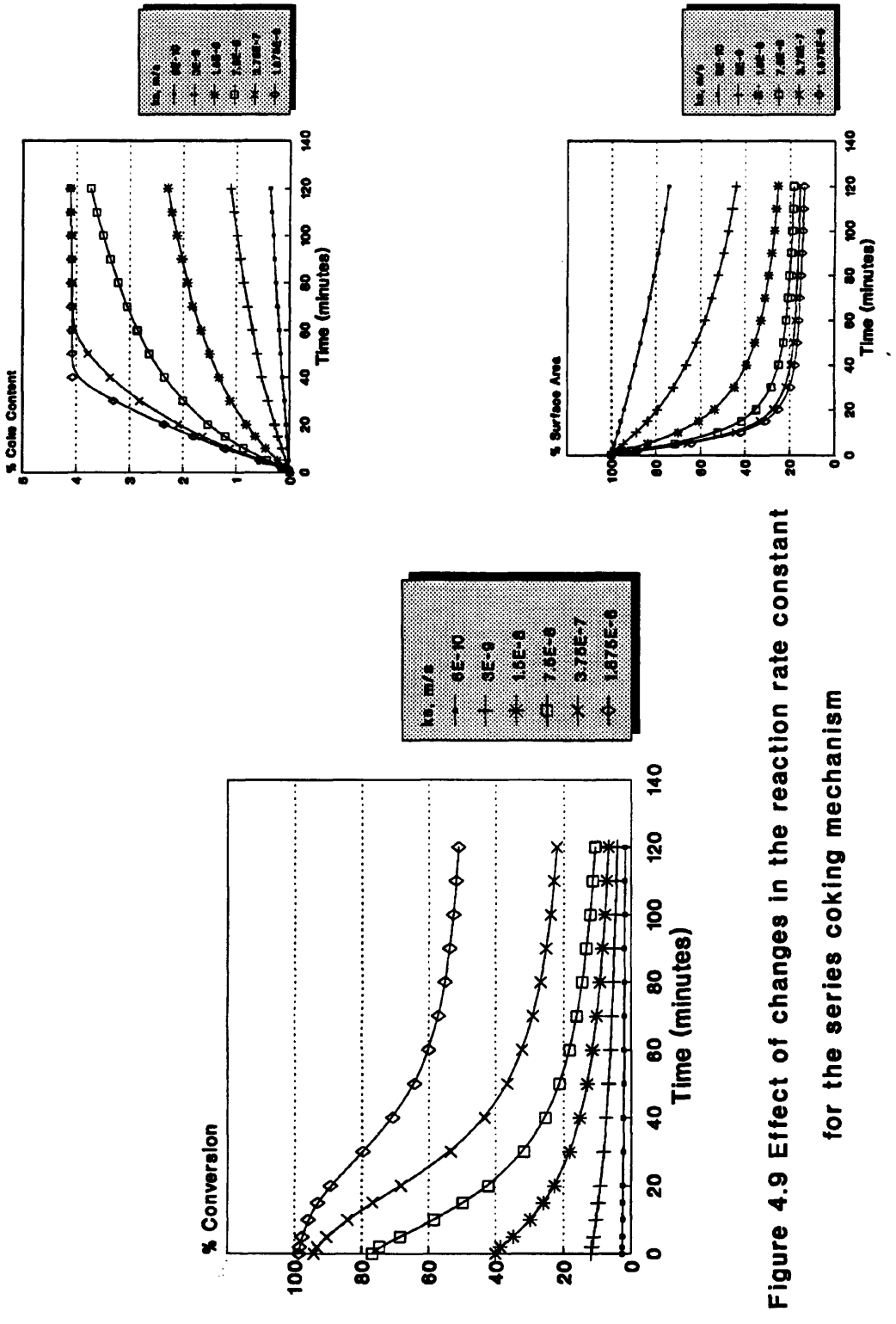

Figure 4.9 Effect of changes in the reaction rate constant for the series coking mechanism

conversions, therefore reducing the reactant concentration and hence producing negligible deactivation. For a rate constant of 1.875×10^{-6} with an initial conversion of 98%, it caused a drop of only 1% in conversion over two hours on stream (Fig. 4.10). As the rate constant gets smaller, conversion drops and coking becomes very detrimental. For a rate constant of 7.5×10^{-8} conversion drops from an initial value of 75% to a final value of 5% after two hours on stream. A further reduction in the rate constant to 1.5×10^{-8} causes the conversion to drop from 40% to 3% in only 30 minutes. Coke content profiles show that as the rate constant increases, the coke content reduces, opposite to the case of series deactivation.

For very small rate constants such as 6×10^{-10}, coke content reaches a value of approximately 4% in about 45 minutes on stream, whereas for large values such as 1.875×10^{-6} it produces less than 0.5% coke content.

Surface area profiles show that as the rate constant reduces, the drop in surface area increases, until it reaches 1.5×10^{-8} beyond which further reductions cause no significant changes in the surface area. Again, this is due to the complete deactivation of the zeolite surface area rapidly, with an accompanying very slowly deactivating support.

4.3.3 Triangular Deactivation:

Under triangular deactivation, the conversion profiles show a larger drop in conversion compared with either series or parallel coking alone (Fig. 4.11). This is due to the combined effect of both mechanisms. The behaviour of the coke content and surface area profiles follow the series or parallel profiles depending on the relative values of their coking rate constants. Under triangular deactivation we obtain a single curve for coke content profile and a single curve for the surface area profile for the special case of equal parallel and series coking rate constants. This is true provided the

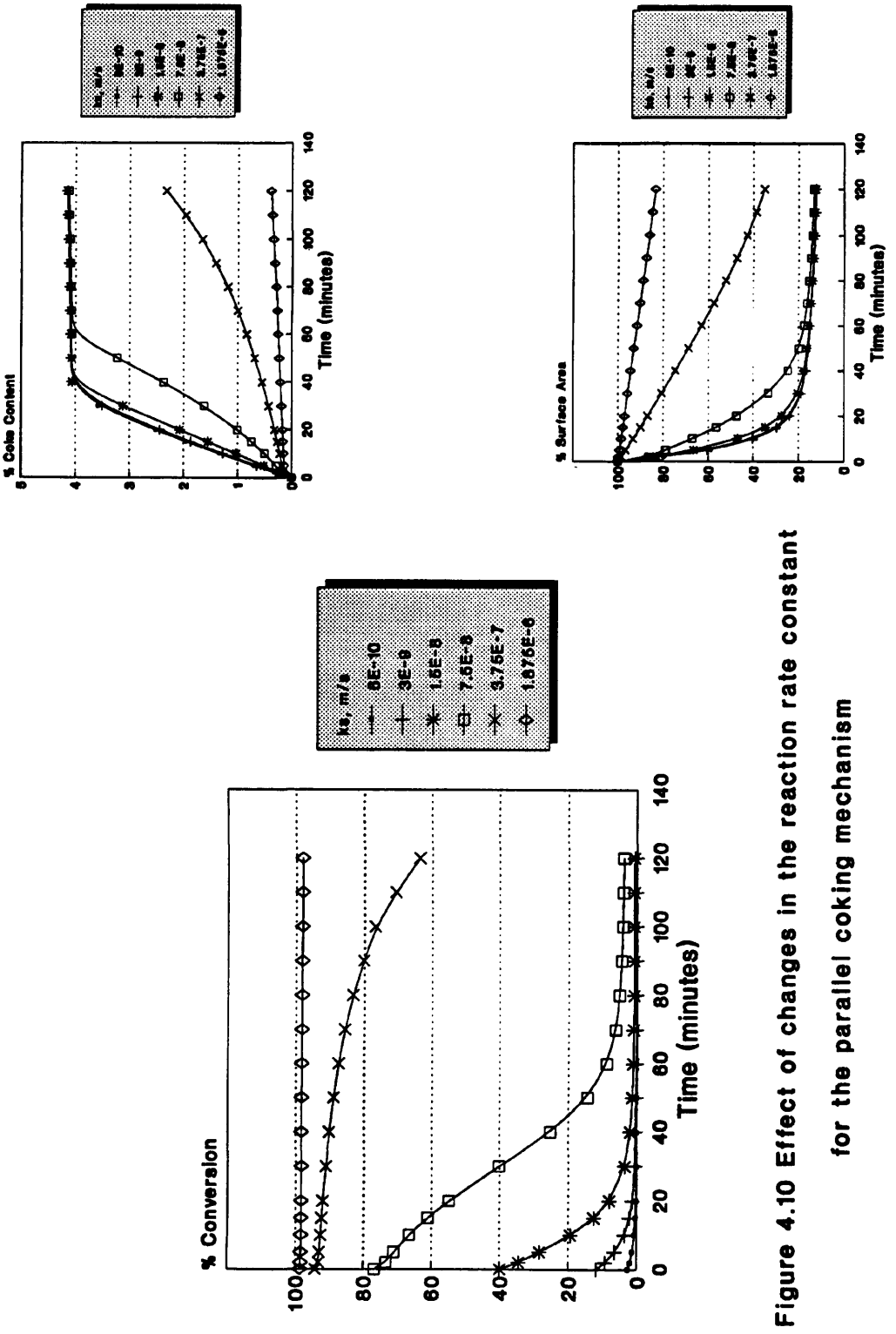

Figure 4.10 Effect of changes in the reaction rate constant for the parallel coking mechanism

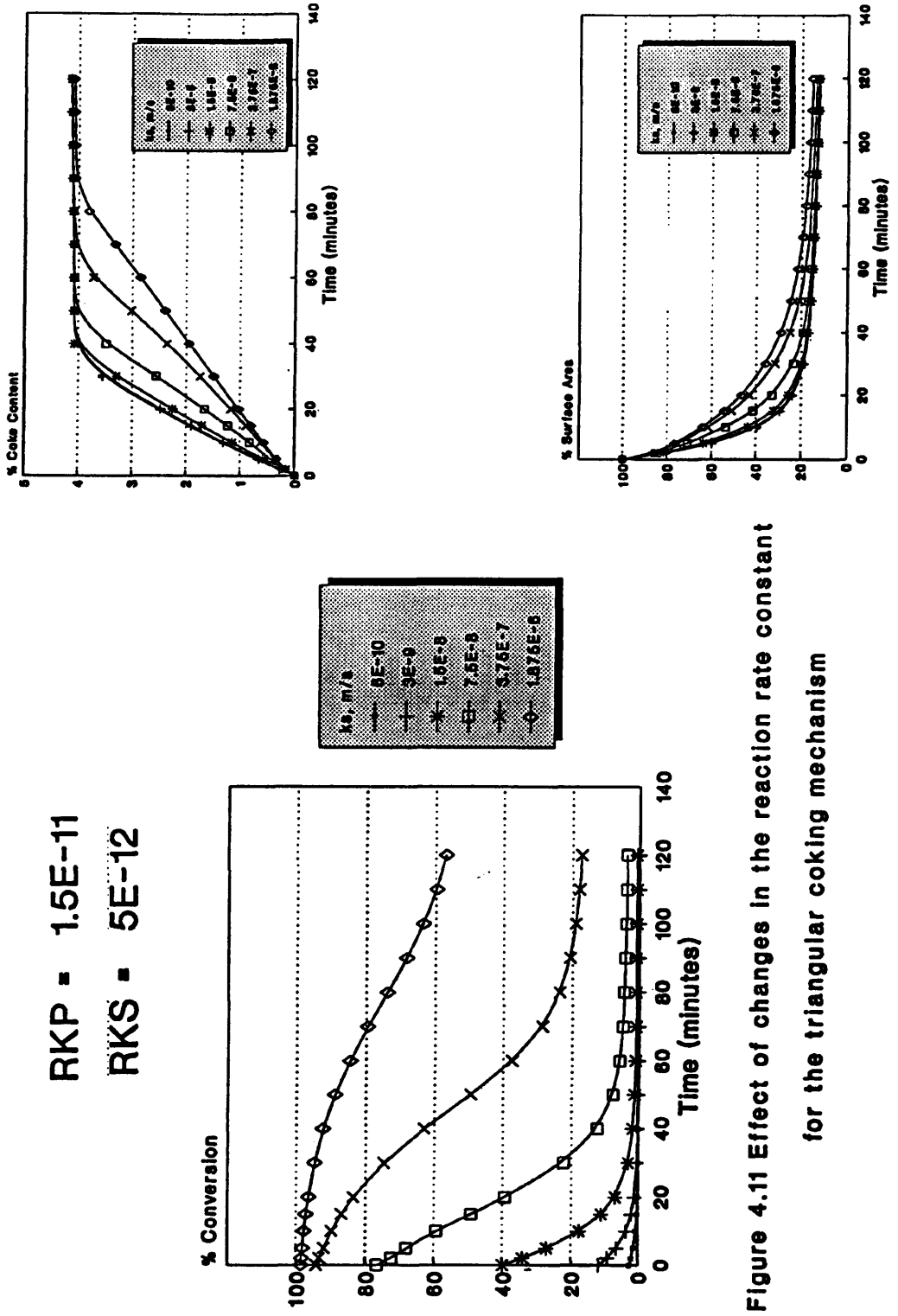

Figure 4.11 Effect of changes in the reaction rate constant for the triangular coking mechanism

assumption of equimolar counter diffusional flow holds, as explained earlier.

4.4 EFFECT OF CHANGING THE CATALYST:FEED RATIO:

To investigate the influence of changes in the catalyst:feed ratio on conversion, coke content and surface area, it was changed gradually from 1:1 g/(g/min) up to 32:1 g/(g/min). For the condition of no deactivation, increasing the catalyst:feed ratio has the effect of increasing the initial conversion (Fig. 4.12). Since there is no deactivation, the conversion profiles consist of straight parallel lines of constant conversion starting with 26% for catalyst:feed ratio of 1:1 up to 92% for 32:1.

4.4.1 Series Deactivation:

For series coking, conversion profiles show a drop in their slopes as the catalyst:feed ratio decreases, but as time on stream increases they become almost parallel (Fig. 4.13). This is due to the large deactivation taking place initially, especially for conversions over 50%, but after about 35 minutes, the conversions are well below 50% causing little coking over the remaining time period of the simulation. As an example, the difference in the initial conversions of the largest and smallest catalyst:feed ratios is almost 65% while the difference in the final conversions is less than 15%.

Coke content profiles show an increase in the coke content as the catalyst:feed ratio increases. Increasing the ratio from 1:1 to 32:1 increases the coke content from 1.8% over 2 hours on stream to over 4% in just over one hour on stream. Again, we notice a large increase in the coke content initially with a much slower increase later on stream. For a catalyst:feed ratio of 8:1, the final coke content of the catalyst reaches 3.6% after 2 hours on stream but 70% of that coke is formed in the first 50 minutes on stream. This is due to the high zeolitic activity initially, which produces

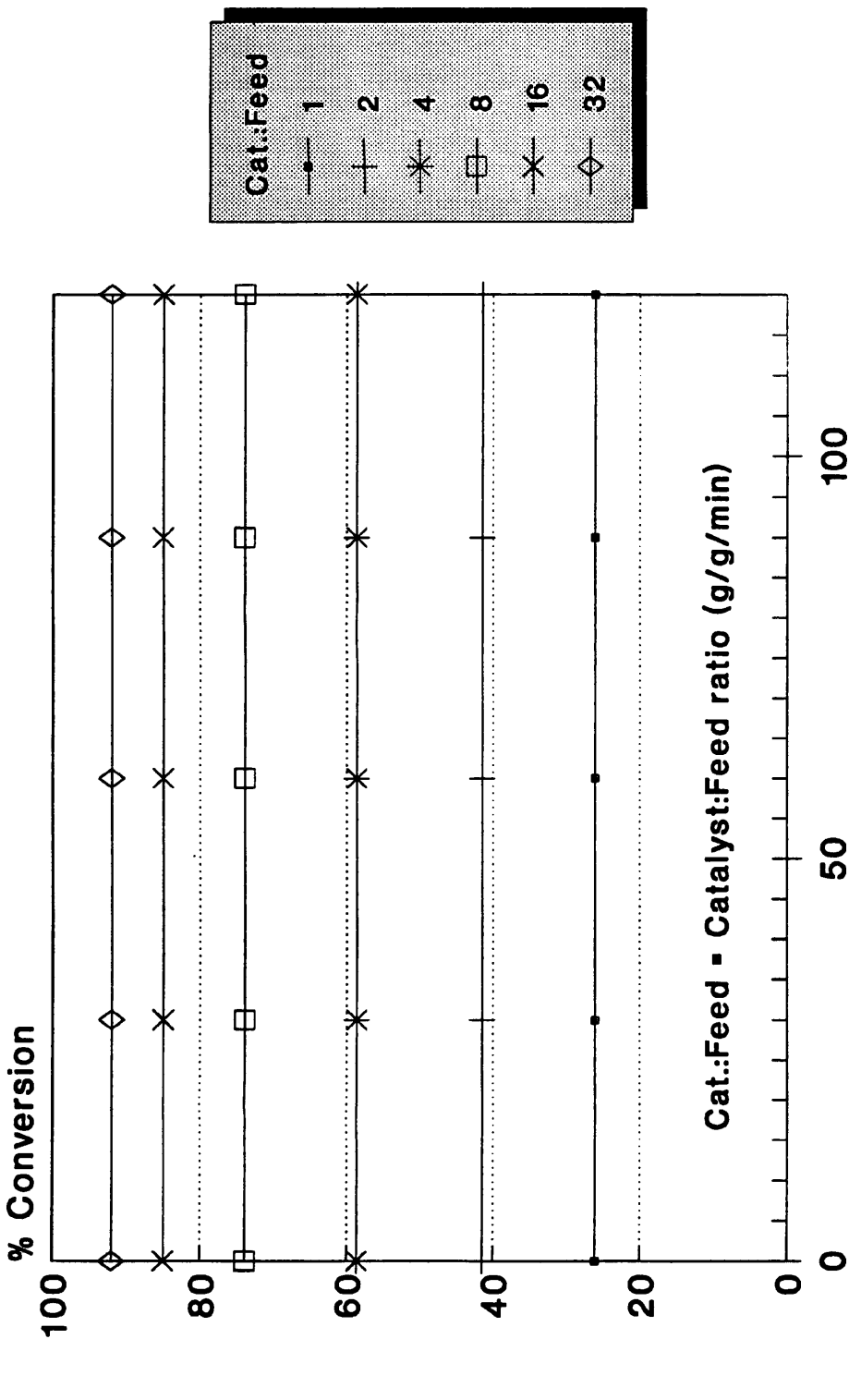

Figure 4.12 Effect of changes in the catalyst:feed ratio on the conversion profiles under no coking conditions.

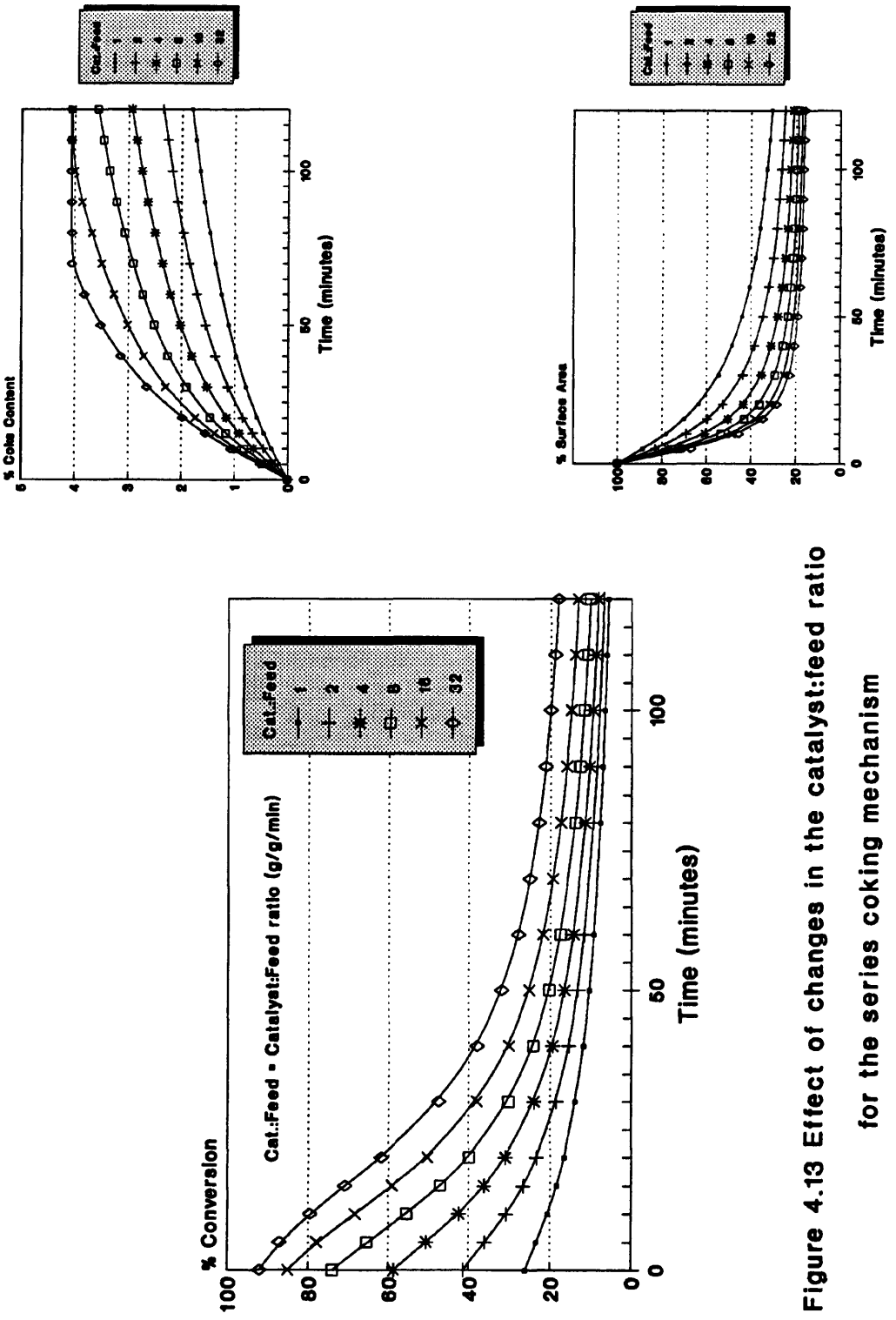

Figure 4.13 Effect of changes in the catalyst:feed ratio for the series coking mechanism

the coke precursor (the product for series deactivation), but is lost after short times on stream when slow coking is due to the low support activity.

Surface area profiles show that as the catalyst:feed ratio increases, the drop in surface area increases, too. Again, we see a very large drop in surface area initially, with a much slower drop later on stream. This is due to the fast loss of the large zeolite surface area, compared to the slow loss of the small support surface area.

4.4.2 Parallel Deactivation:

For parallel coking, the initial conversion is directly proportional to the catalyst:feed ratio. For high catalyst:feed ratios, a very small drop in conversion is observed for short times on stream (Fig. 4.14). As the conversion drops below 50%, the parallel deactivation becomes very detrimental and the conversion drops very sharply. For small catalyst:feed ratios, the initial conversion is already well below 50%, therefore, the concentration of the reactant (which is the coke precursor for parallel coking) is high. Then, the deactivation is very high at short times on stream. For example, a catalyst:feed ratio of 2:1 with an initial conversion of 41%, rapidly deactivates to give a conversion of only 10% in 15 minutes, while a catalyst:feed ratio of 32:1 with an initial conversion of 91% drops only 2% over the same time period.

Coke content profiles show that as the catalyst:feed ratio increases, the coke content reduces. Also, it shows that the rate of coking starts slow and then increases for high catalyst:feed ratios, while it starts rapidly for small ratios.

Surface area profiles show that, contrary to series coking, as the catalyst:feed ratio decreases, the surface area drop increases. The surface area loss in the first few minutes on stream is very large specially for small catalyst:feed ratios up to 8:1, but these curves converge and merge after 60 minutes on stream. This is due to the loss of

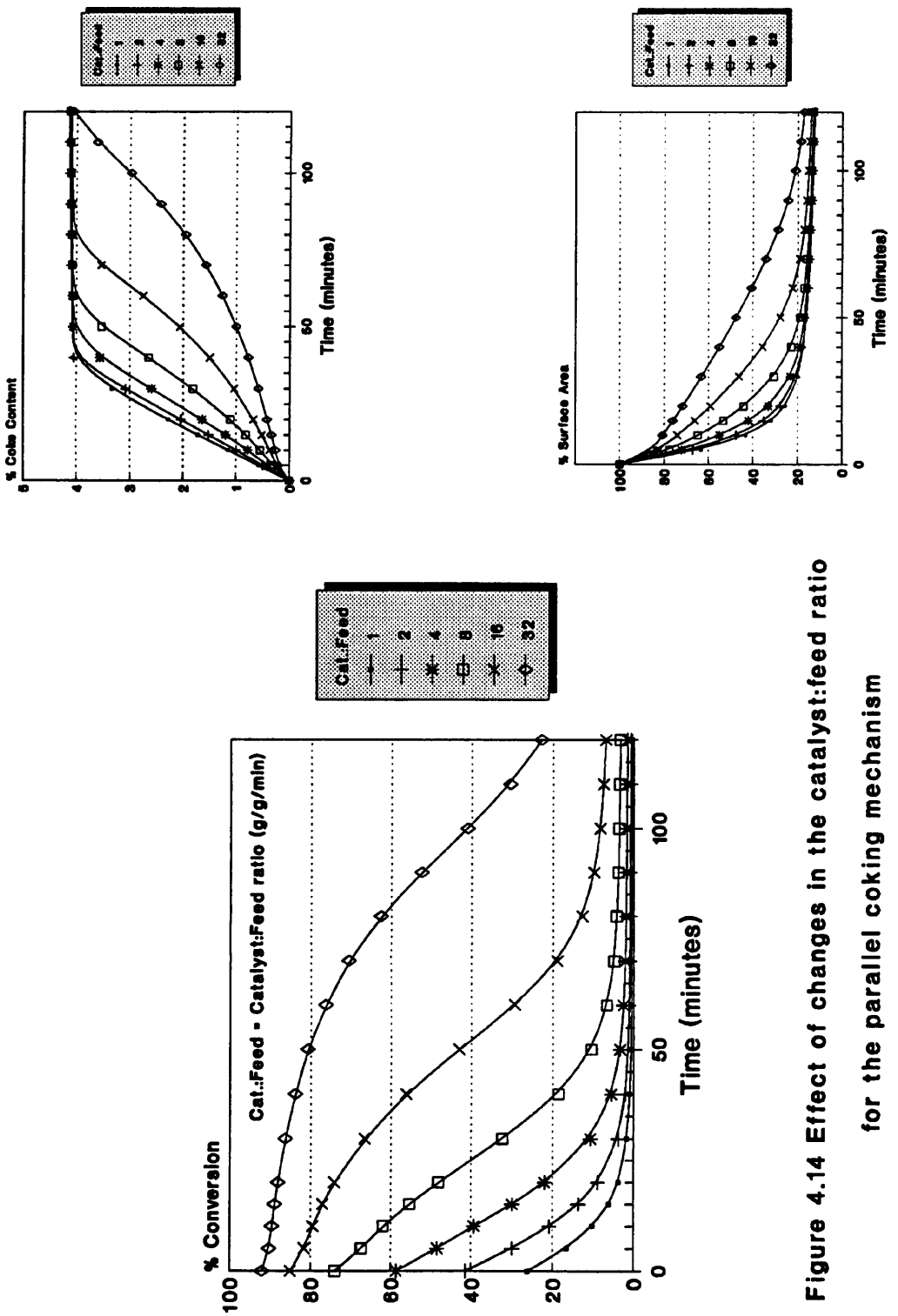

Figure 4.14 Effect of changes in the catalyst:feed ratio for the parallel coking mechanism

all zeolitic area rapidly, and the catalyst is left with the small support area which then cokes very slowly.

4.4.3 Triangular Deactivation:

Under triangular deactivation, the larger the catalyst:feed ratio the larger the conversion (Fig. 4.15). The conversion profiles show a larger drop in conversion compared with either series or parallel coking alone. This again is due to the combined effect of both mechanisms. The behaviour of the coke content and surface area profiles follow the series or parallel profiles whichever has a higher coking rate constant. For the case of equal coking constants, a single curve is obtained for the coke content and a single curve for the surface area for all values of the catalyst:feed ratios explored. The larger the coking rate constants, the larger the coke content and the smaller the surface area.

The behaviour of the coke content and surface area profiles under series deactivation in response to changes in catalyst:feed ratio is exactly opposite to those under parallel deactivation. So, with the assumption of equimolar counter diffusion, it is expected to have a single curve for each of the coke content and surface area for the case of equal parallel and series coking rate constants regardless of the catalyst:feed ratio.

4.5 EFFECT OF HEAVY COKE LAYDOWN IN SUPPORT PORES:

To allow heavy support coking to occur, the definition of the active area was changed according to Chapter Two to become that area which is accessible even if it was covered with a thick layer of coke. The structure of the catalyst particle was represented by a 10x10 network with a uniform pore size distribution in the range of 60–3200 Å (Fig. 4.16). Figure 4.17 is a numerical representation of the network under

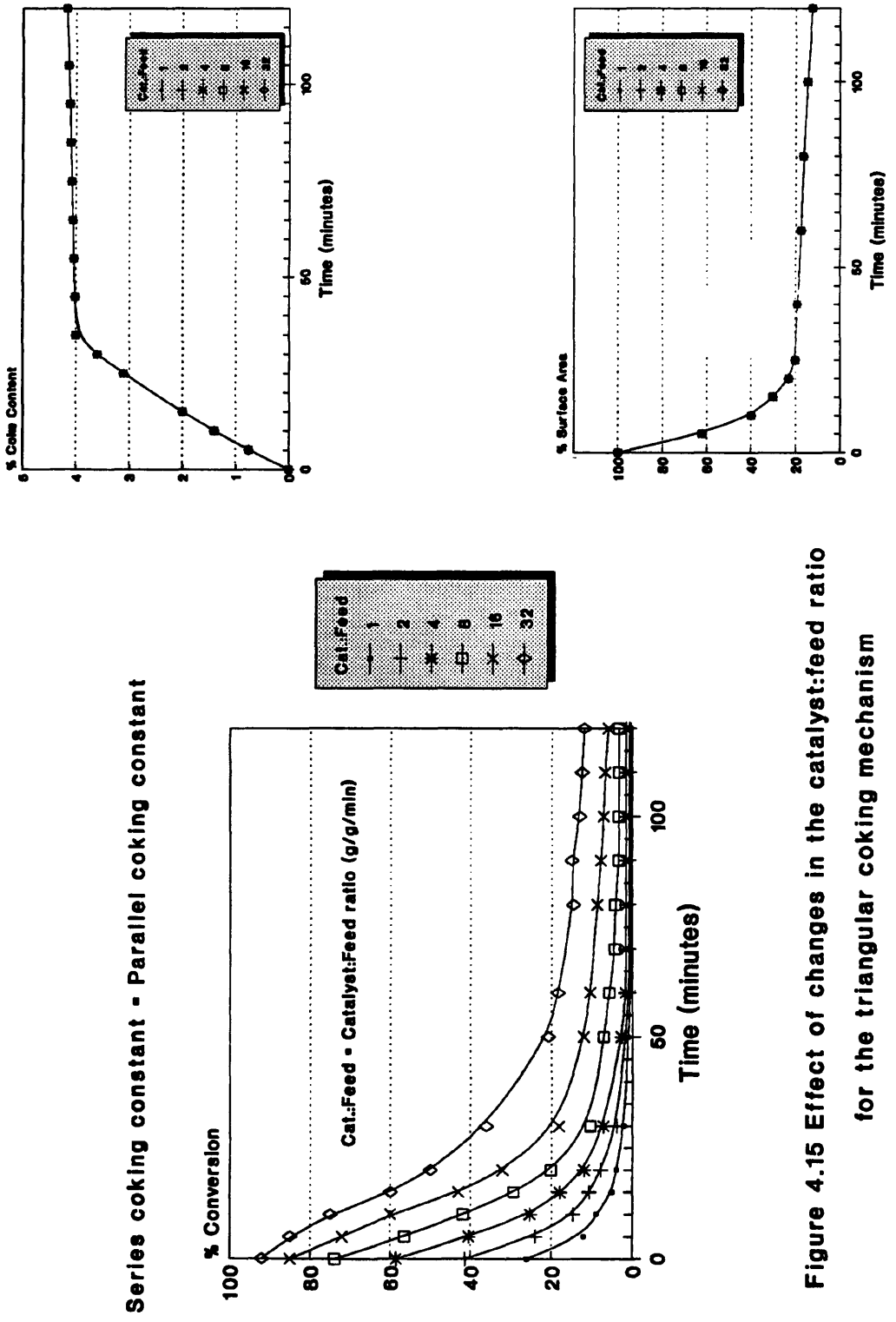

Figure 4.15 Effect of changes in the catalyst:feed ratio for the triangular coking mechanism

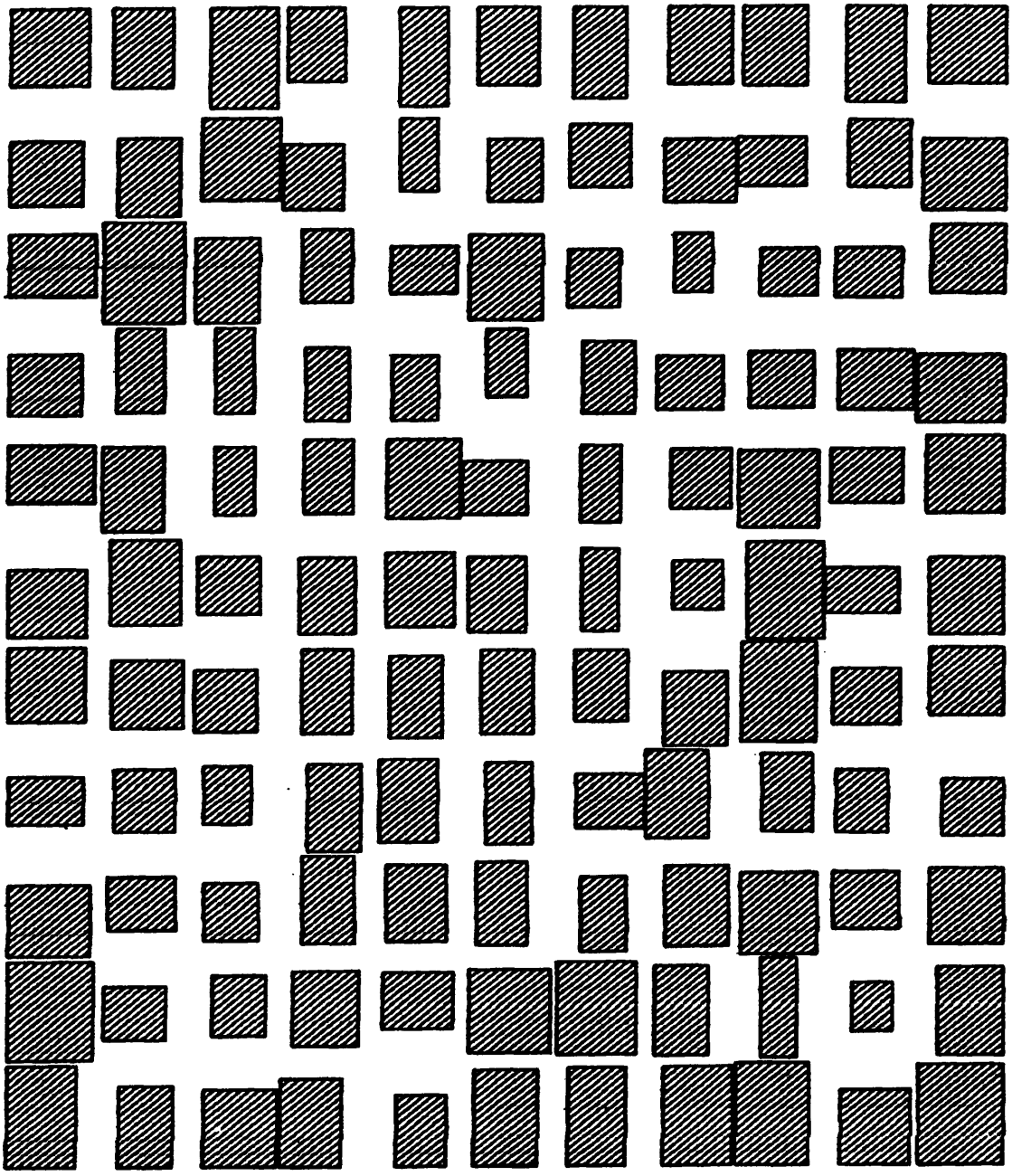

Figure 4.16 A stochastic pore network of size 10x10 with a uniform pore size distribution in the range 60–3200 Angstroms. (Fresh, uncoked network).

1292 2128 0581 3074 1599 1885 2337 0644 2191 1299

2608 + 2402 + 0493 + 2954 + 0578 + 2526 + 1228 + 2642 + 2446 + 0861 + 2597

1986 + 1245 + 0206 + 3174 + 2804 + 1575 + 1849 + 0066 + 2399 + 0745

1322 + 0258 + 1746 + 0914 + 2610 + 1571 + 2982 + 1526 + 3013 + 2939 + 0734

0420 + 0626 + 2399 + 2141 + 0686 + 1411 + 3072 + 2703 + 1027 + 1650

2874 + 0299 + 0298 + 2188 + 3011 + 0449 + 1690 + 3139 + 2763 + 2551 + 2985

1964 + 2874 + 2894 + 2372 + 2674 + 3064 + 1198 + 1494 + 1383 + 0218

1442 + 1643 + 1621 + 0883 + 0885 + 3063 + 1472 + 1876 + 2029 + 1867 + 0591

0408 + 2826 + 2784 + 1923 + 0097 + 2921 + 2804 + 0464 + 0665 + 1322

3151 + 0416 + 1990 + 2092 + 1623 + 2031 + 1255 + 2518 + 0674 + 3081 + 2145

1297 + 0974 + 2238 + 1703 + 0767 + 3029 + 3011 + 1380 + 0082 + 1730

0465 + 1682 + 2670 + 0727 + 1377 + 0853 + 0936 + 2946 + 0133 + 2660 + 0615

1473 + 0640 + 2549 + 2110 + 2120 + 2249 + 2010 + 0808 + 0972 + 1635

2632 + 1951 + 1671 + 1493 + 1048 + 1369 + 2506 + 0216 + 0618 + 2184 + 3081

1696 + 1543 + 3151 + 1009 + 2621 + 2347 + 0065 + 3032 + 1352 + 3036

2897 + 2166 + 0844 + 0199 + 1078 + 0857 + 2378 + 1337 + 1967 + 1899 + 1561

1004 + 1553 + 2443 + 1739 + 1622 + 2904 + 2123 + 0675 + 0911 + 1662

0245 + 2742 + 1666 + 0335 + 1511 + 1186 + 0477 + 0950 + 0168 + 2683 + 1165

0562 + 2608 + 1524 + 1352 + 0843 + 0421 + 0971 + 2959 + 3071 + 2525

0245 + 2190 + 2588 + 1577 + 3163 + 0779 + 0659 + 0028 + 0244 + 2862 + 0453

2394 1749 0157 3040 1499 1679 2078 0198 1784 0465

Figure 4.17 A numerical representation of the 10x10 stochastic pore network shown in figure 4.16 .

investigation, with the pore size given as numbers at the location of the pore element relative to the other pores in the network. The 10x10 network contains 220 pore elements.

Coke deposition should be uniformly distributed at all times throughout the catalyst particle under one of the following conditions:

(1) If the coke particles were only weakly adsorbed onto the catalyst and were present in the feed stream in sufficiently large concentrations so that a steady–state surface concentration is quickly attained.

(2) If the coke particles were formed by a reaction occurring with an effectiveness factor near unity, e.g. coke formation on cracking catalyst in powder form where pore lengths are relatively very small and the effectiveness factor approaches unity.

4.5.1 Representation of the Structure of the Catalyst at Different Stages of Coke Laydown:

Assuming the catalyst is undergoing a parallel coking mechanism, and using the same parameters as in Table 4.1, an investigation into the effect of heavy coke laydown in the support pores is attempted. Heavy support coking starts uniformly within the pores of the network since the effectiveness factor is near unity, indicative of negligible diffusional resistances. As the coke layer thickness increases from zero to 500Å, all the pores of sizes up to 500Å become fully coked but no sign of pore isolation is noticed. Upon increasing the coke layer thickness to 1000Å, the beginning of the process of pore isolation is clear. The pore isolation phenomenon increases as the coke thickness gets larger and larger to the extent that about twenty pore elements which were only partially coked have been isolated by a coke layer thickness of 2000Å. When the reaction continues and coke thickness on the pores reaches 3000Å, the total number of

pore segments in the network which has been isolated by smaller pores reaches about forty pores. At this stage, most of the pores inside the network are either fully coked, isolated or they are partially coked pores located at the edges of the network which can not be isolated. So, increasing the coke layer thickness to 3200Å does not further increase the amount of pore isolation. Figure 4.18 shows how the number of accessible (partially coked), fully coked and isolated pore elements changes as the coke layer thickness gets larger and larger until it reaches the maximum value of 3200Å.

Figures 4.19 to 4.23 show the network undergoing heavy support coking at different stages as the coke layer thickness gets larger and larger until it is fully deactivated at the point where all the exterior pores are filled with coke.

4.5.2 Overall Coke Content of the Network Pores:

At the beginning of the process, the network is free from any coke deposits which represents the fresh catalyst particle before it has undergone any deactivation. All pores are accessible. As coke is produced and the catalyst particle undergoes deactivation, a given layer of coke which deposits uniformly inside all pore segments of the network produces an appreciable increase in the coke content of the catalyst particle. As the process of coking continues, more and more pores are fully coked and then the isolation of pores and regions starts occurring. The same previous given layer of coke has then much less effect on the total coke content of the catalyst than at the beginning of the process. This is due to much lower accessibility of pores in the network for the further coke deposits. So, as a result fewer pore segments undergo an increase in their coke layer thickness. For example, an increase in the coke layer thickness of the network from zero to 500Å caused an increase of approximately 6% in the coke content. This is drastically larger than the 1% increase in the coke content that occurs when the coke layer thickness increases from 2000Å to 2500Å (Fig. 4.24). When the catalyst particle represented by the network of pores is fully deactivated, the

Heavy Support Coking
Network Model (10x10)

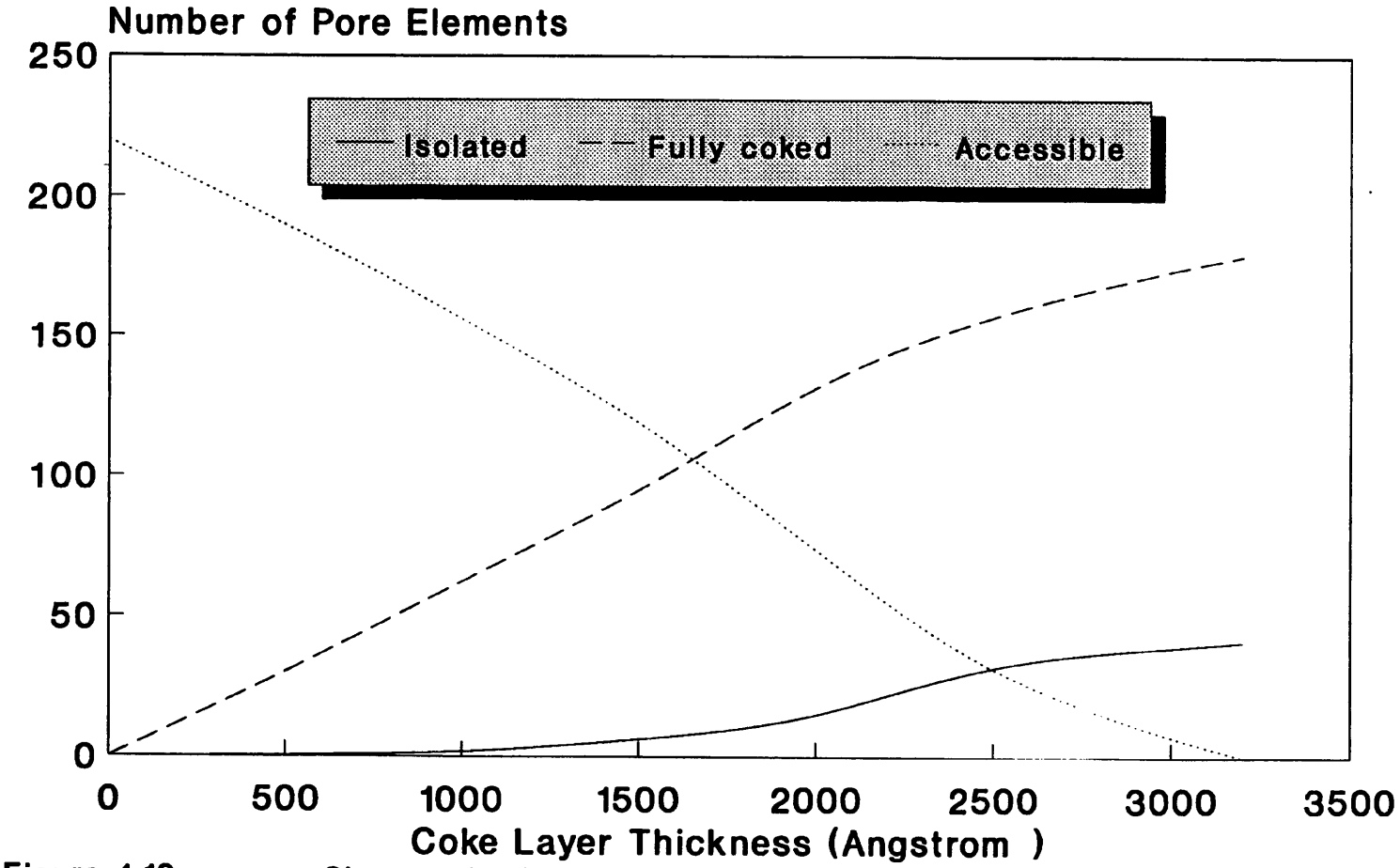

Figure 4.18 Changes in the number of accessible support pore elements for the network undergoing a parallel coking mechanism.

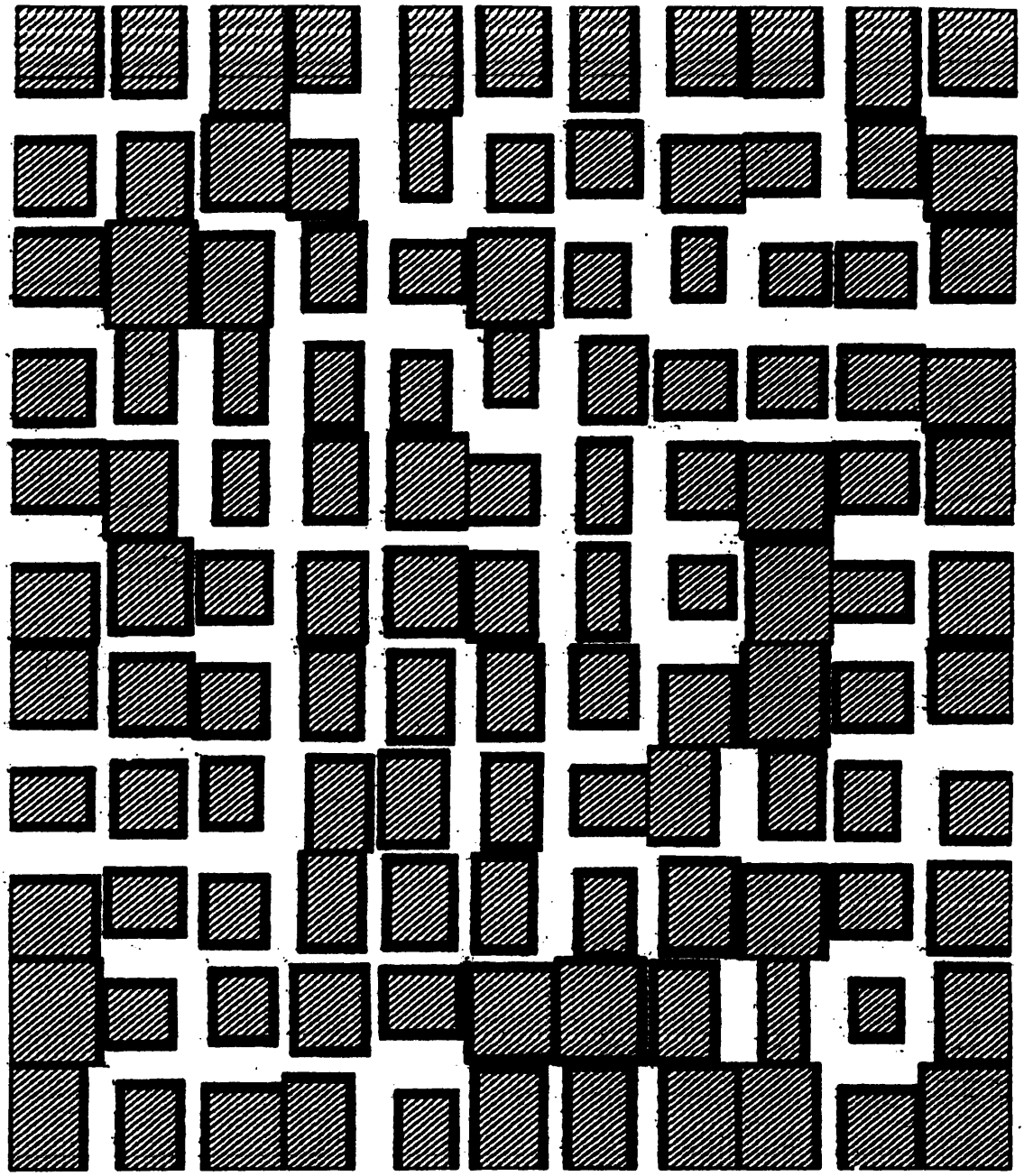

Figure 4.19 The 10x10 stochastic pore network undergoing heavy support coking. (Coke layer thickness = 712 Angstrom).

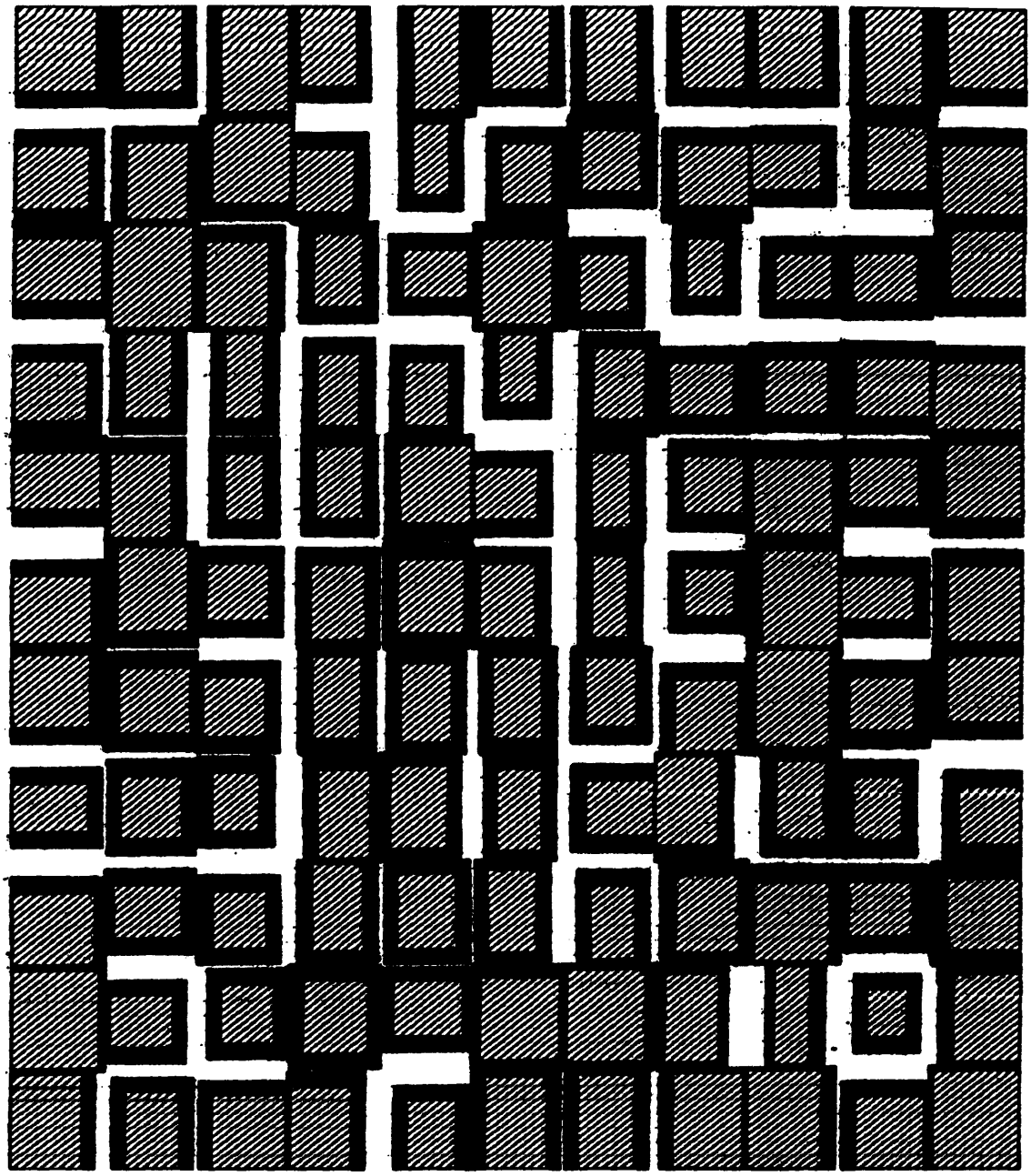

Figure 4.20 The 10x10 stochastic pore network undergoing heavy support coking. (Coke layer thickness = 1425 Angstrom).

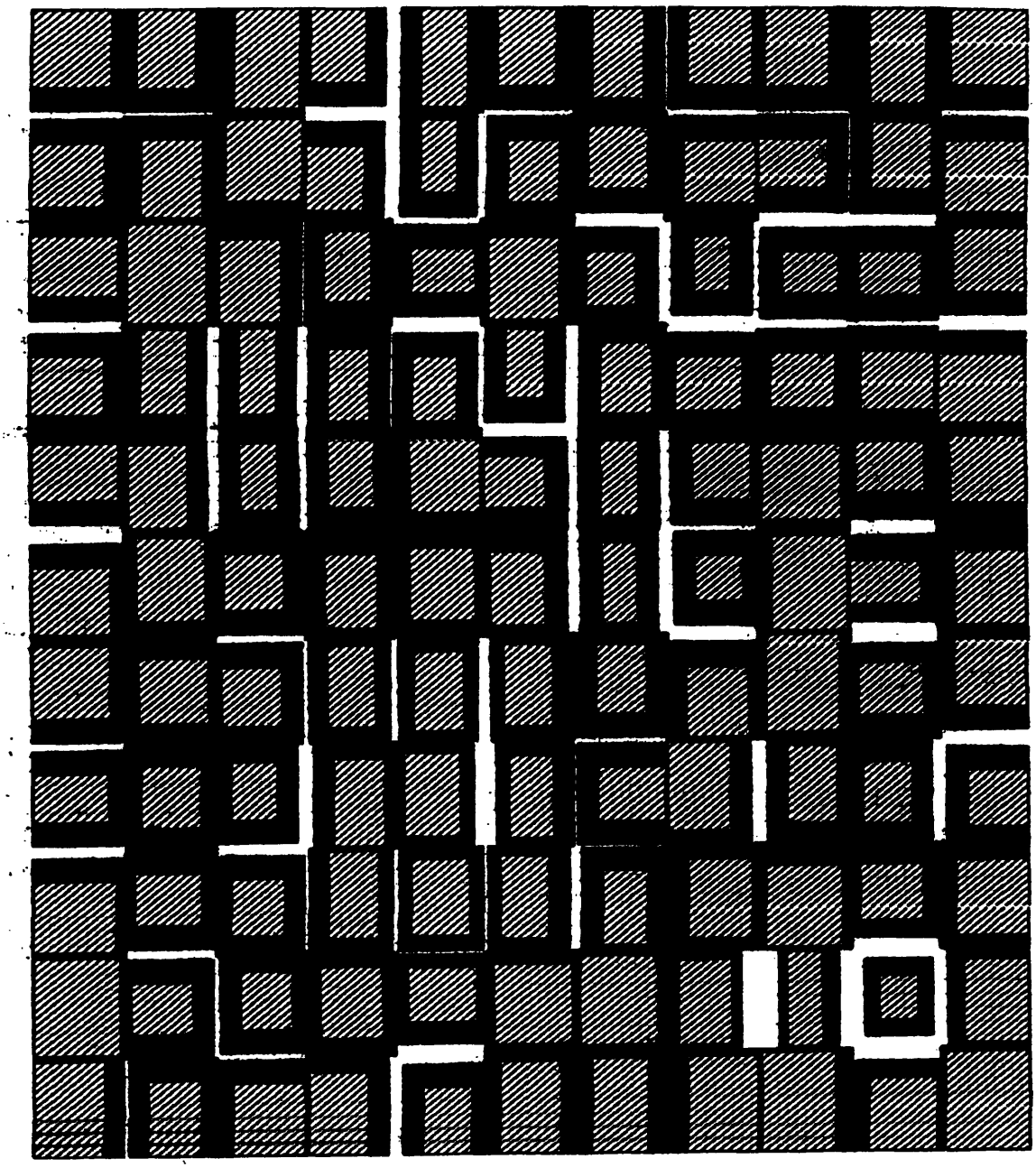

Figure 4.21 The 10x10 stochastic pore network undergoing heavy support coking. (Coke layer thickness = 2139 Angstrom).

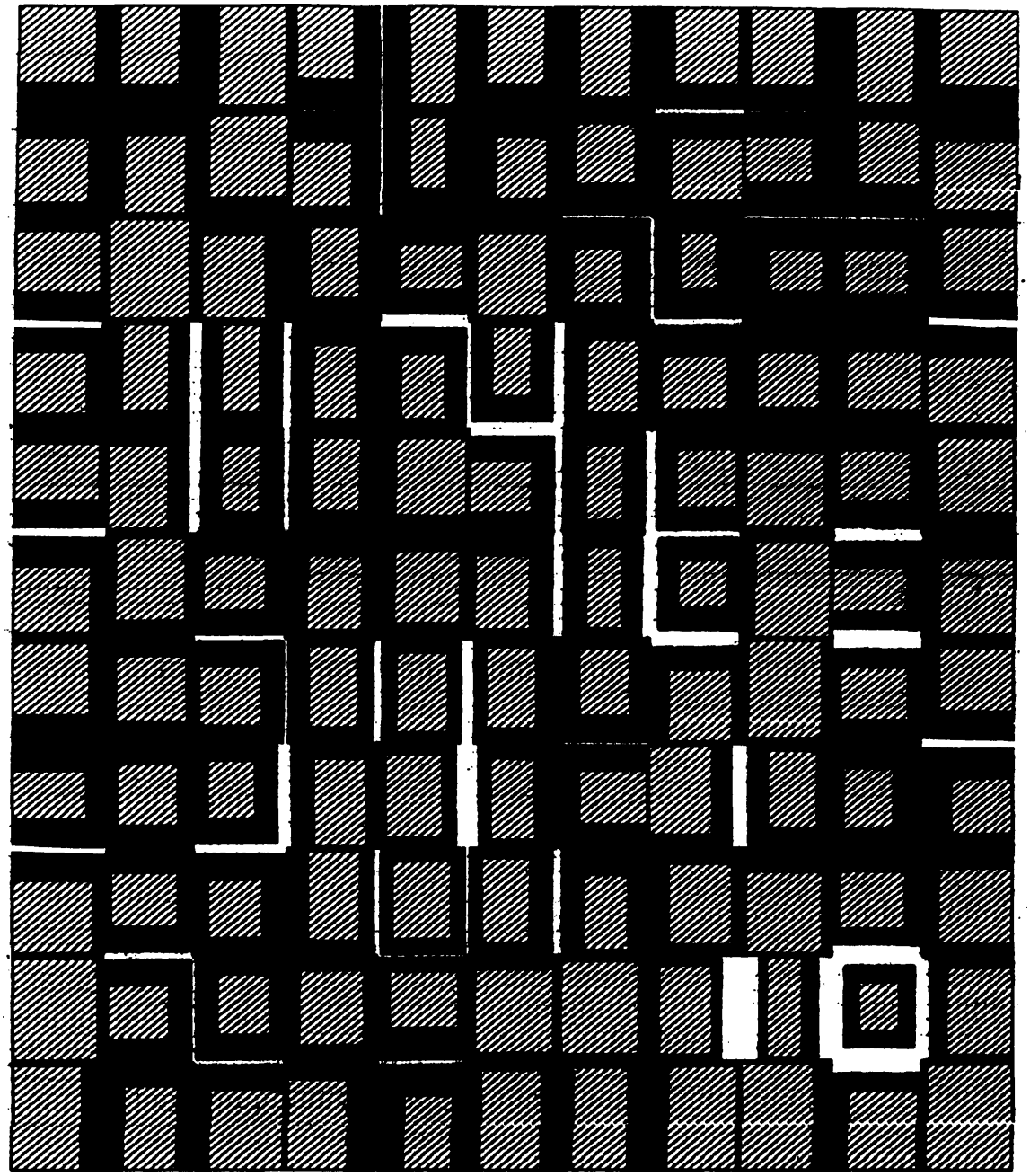

Figure 4.22 The 10x10 stochastic pore network undergoing heavy support coking. (Coke layer thickness = 2731 Angstrom).

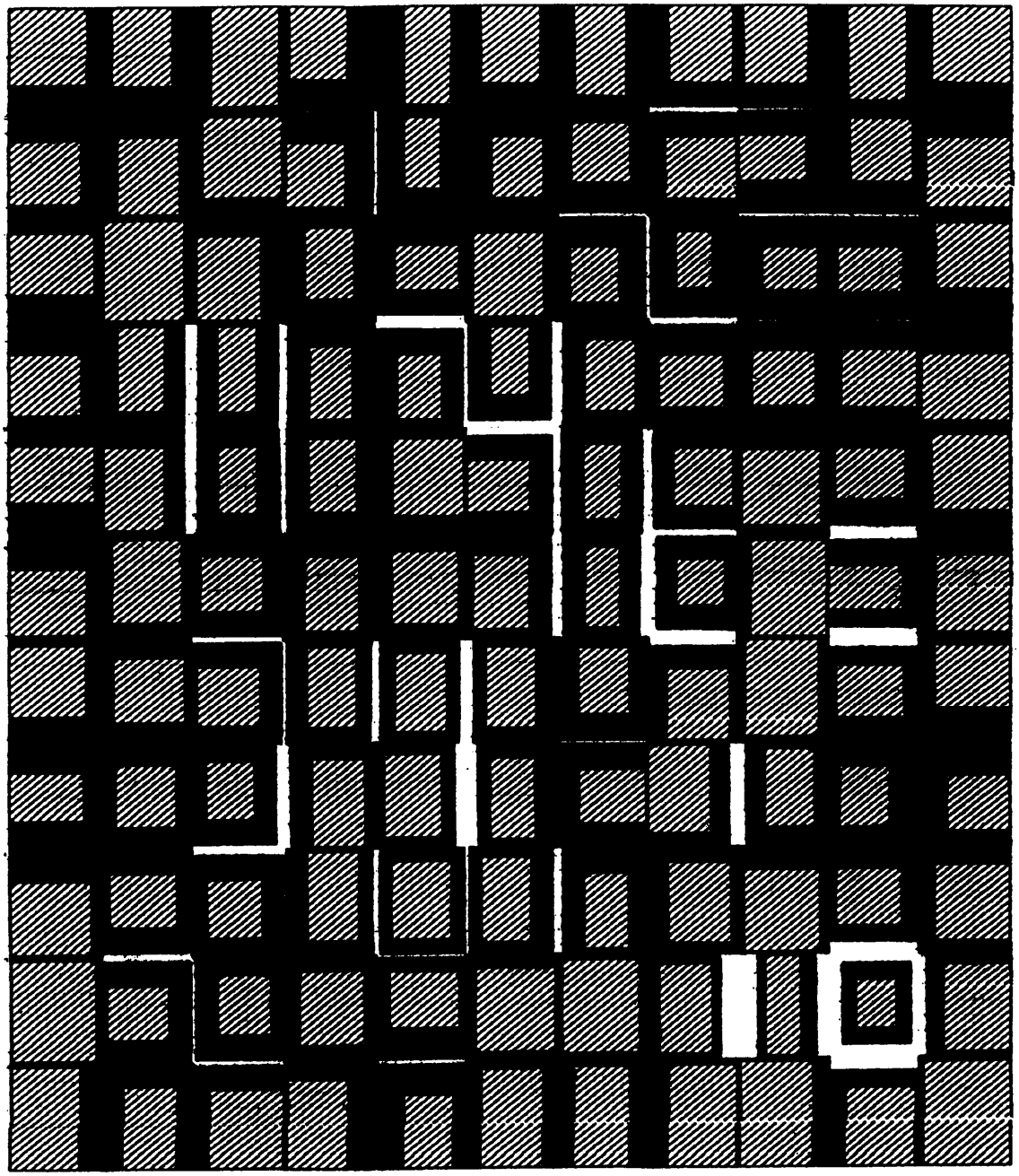

Figure 4.23 The 10x10 stochastic pore network undergoing heavy support coking. (Coke layer thickness = 3200 Angstrom).

Heavy Support Coking
Network Model (10x10)

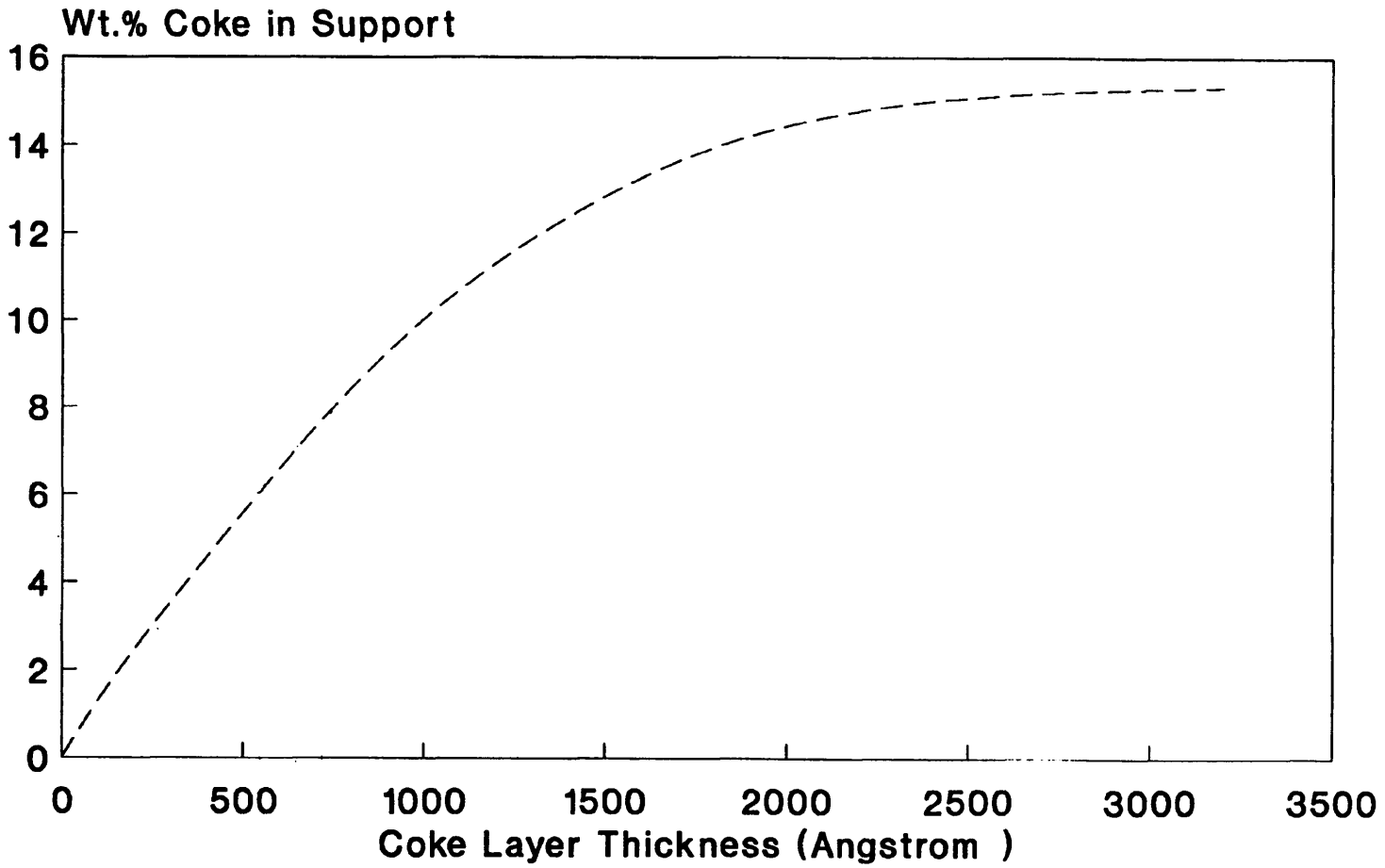

Figure 4.24 Coke content of the support for the network undergoing a parallel coking mechanism.

coke content reaches just over 15%. The maximum theoretical coke content of the catalyst particle is 16%. Thus approximately 6% of the total network volume has been isolated during the process of uniform coking (Fig. 4.25).

The changes in the support surface area accessible, coked and isolated are as the coke layer thickness gets larger and larger until the network is fully deactivated are shown in Figure 4.26. It is interesting to note that a negligible degree of pore isolation takes place inside the network until it reaches very high coke contents. Then a small increase in the coke content from about 12% to 15% causes a significant amount of pore isolation (Fig. 4.27). This is due to the relatively high degree of pore interconnectivity, which prevents the phenomenon of pore isolation until the pore elements at the edges of the network are becoming fully coked.

4.5.3 Coke Laydown without Diffusional Limitations:

When the size of the catalyst particles is very small or when the rate of the reaction is very slow, the effectiveness factor approaches unity. Under such conditions diffusional limitations become negligible, and the concentration of reactant, C_A, is constant throughout the network elements. For the parallel coking mechanism, the coke precursor is the reactant. Therefore, initially coke laydown is uniform in each element of the network. As the coke layer thickness gets larger and larger, the smaller pores become fully coked. Since the network is made up of different size elements ranging from 60 to 3200 Angstrom, the blocking phenomenon will occur once some elements with smaller sizes surrounding larger size elements are filled up with coke. Again this will produce a situation where heavier coking occurs towards the exterior of the catalyst particle compared to the lightly coked interior. In the case of a bimodal pore size distribution with very small size pores surrounding large pores, pore blocking and region isolation should become very much more significant. Figure 4.28 shows a 20x20 network with a bimodal pore size distribution consisting of 50% pores of size

Heavy Support Coking
Network Model (10x10)

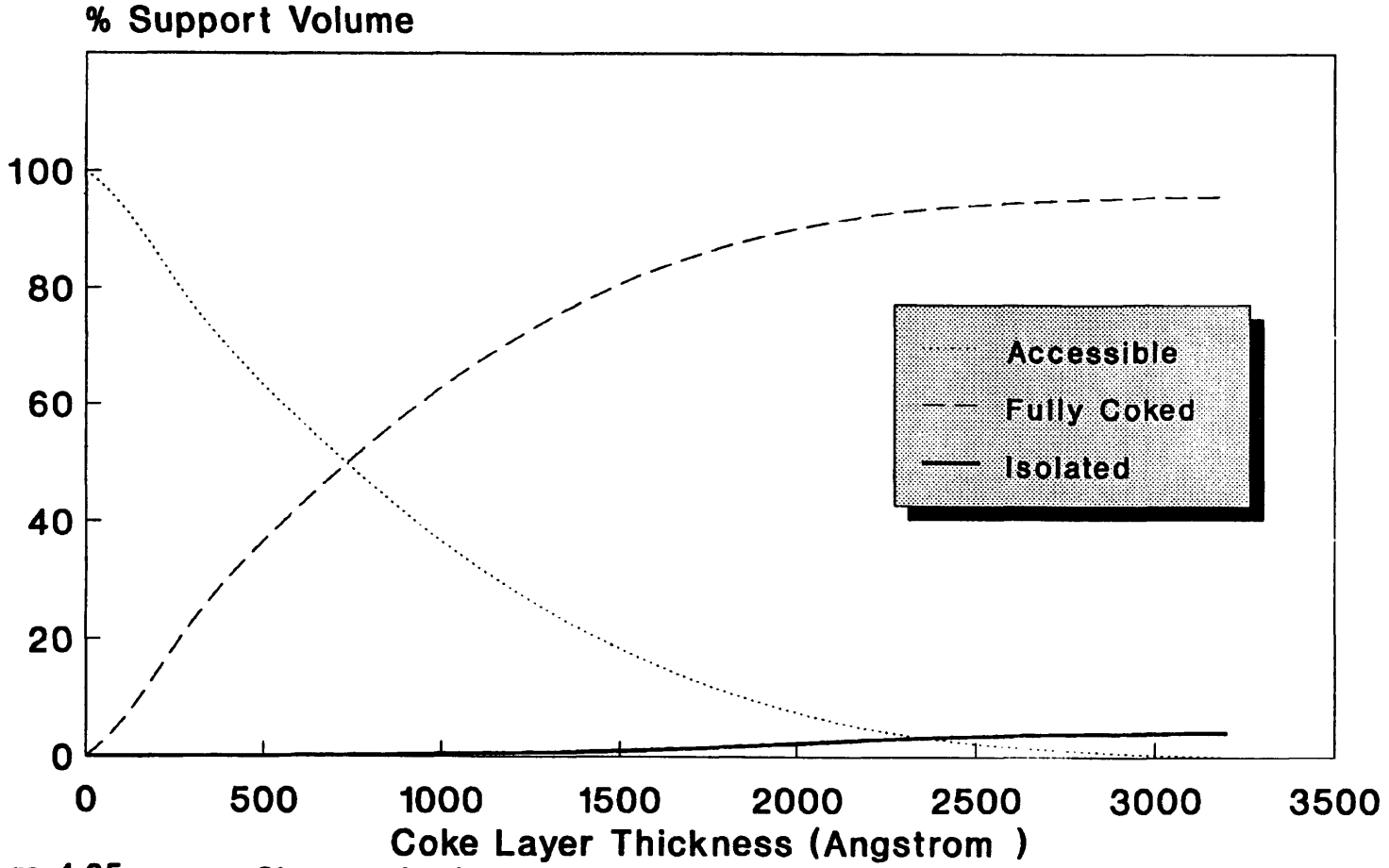

Figure 4.25 Changes in the support pore volume of the network undergoing a parallel coking mechanism.

Heavy Support Coking
Network Model (10x10)

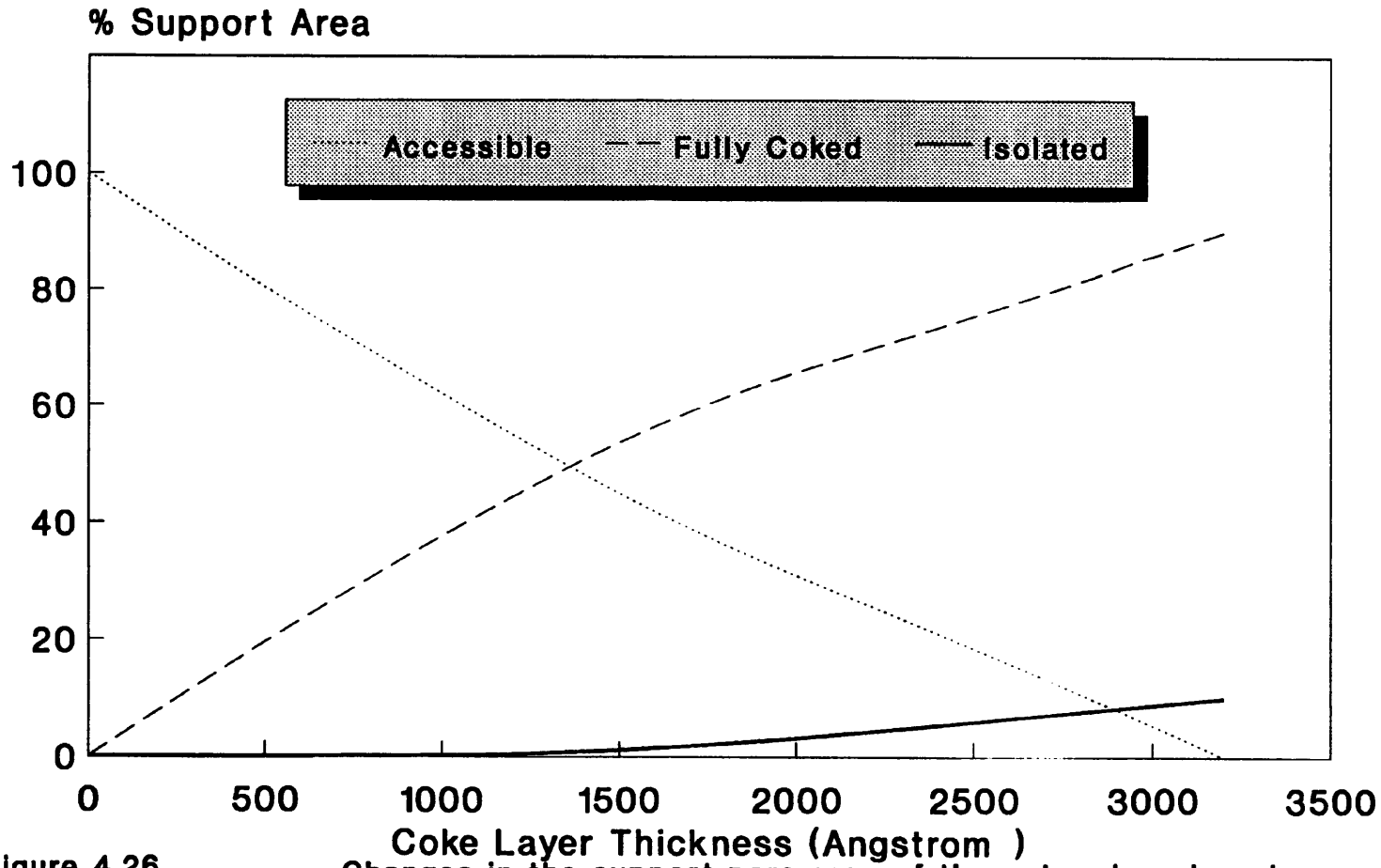

Figure 4.26 Changes in the support pore area of the network undergoing a parallel coking mechanism.

Heavy Support Coking
Network Model (10x10)

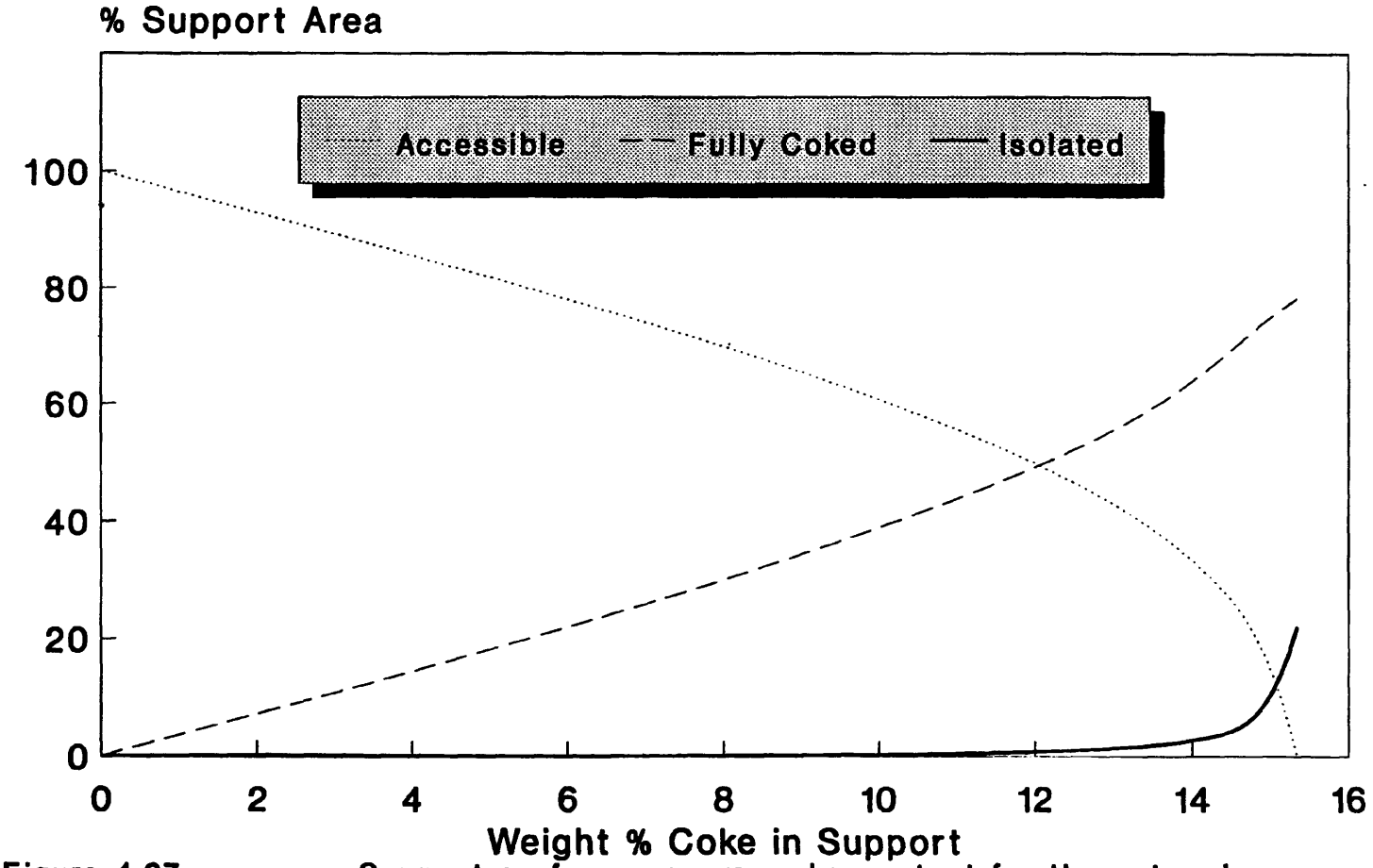

Figure 4.27 Support surface area vs. coke content for the network undergoing a parallel coking mechanism.

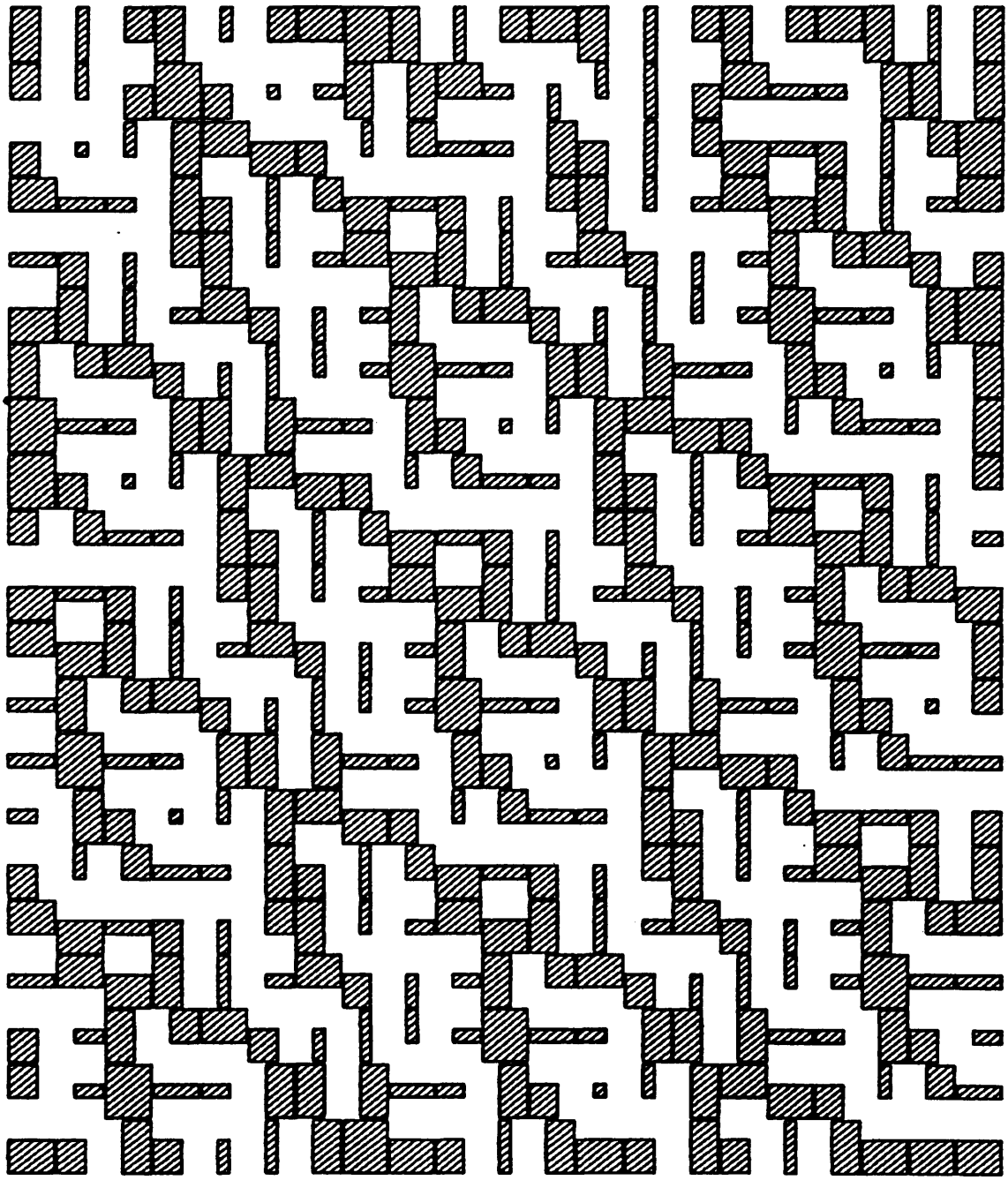

Figure 4.28 A 20x20 network with a bimodal pore size distribution.

60Å and 50% pores of size 3200Å. After complete deactivation, out of the 840 pore elements of the network, 101 pore elements of the larger size have been isolated by the smaller pore elements (Fig. 4.29). This corresponds to a loss of 23% of the network pore volume. The maximum coke content is only 12.3% compared to 15% for a similar size network with a uniform pore size distribution in the range 60–3200 Å.

4.5.4 Coke Laydown with Strong Diffusional Limitations:

When the size of the catalyst particles is very large or when the rate of the reaction is very large, the effectiveness factor falls to values far below unity indicative of strong diffusional resistances. Under such conditions, the concentration of the reactant decreases as it penetrates the network of pores. So, we have a concentration gradient across the elements of the network (Fig. 4.30). This produces different reaction rates and, therefore, different product concentrations inside any element. Since the coking reaction is a function of either product or reactant concentrations, then the coke layer thickness is different in each element in the network. Then, regardless of the coking mechanism, the blocking phenomenon will occur when some smaller size elements surrounding larger size elements are fully coked. For the case of parallel mechanism of coking where the coke precursor is the reactant, the coking in the outer pore elements takes place at a higher rate than the inner elements (Fig. 4.31). Under conditions of very strong diffusional resistances (Fig. 4.32), coke deposits almost exclusively in the external elements of the network, therefore, very significant pore mouth blocking can occur. Figure 4.33 shows a 20x20 network with a uniform pore size distribution in the range 60–3200 Å, whereas Figure 4.34 shows the same network after complete deactivation under conditions of extremely strong diffusional resistances.

4.5.5 Coke Laydown in the Network of Single–Size Average–Area Pore Elements without Diffusional Limitations:

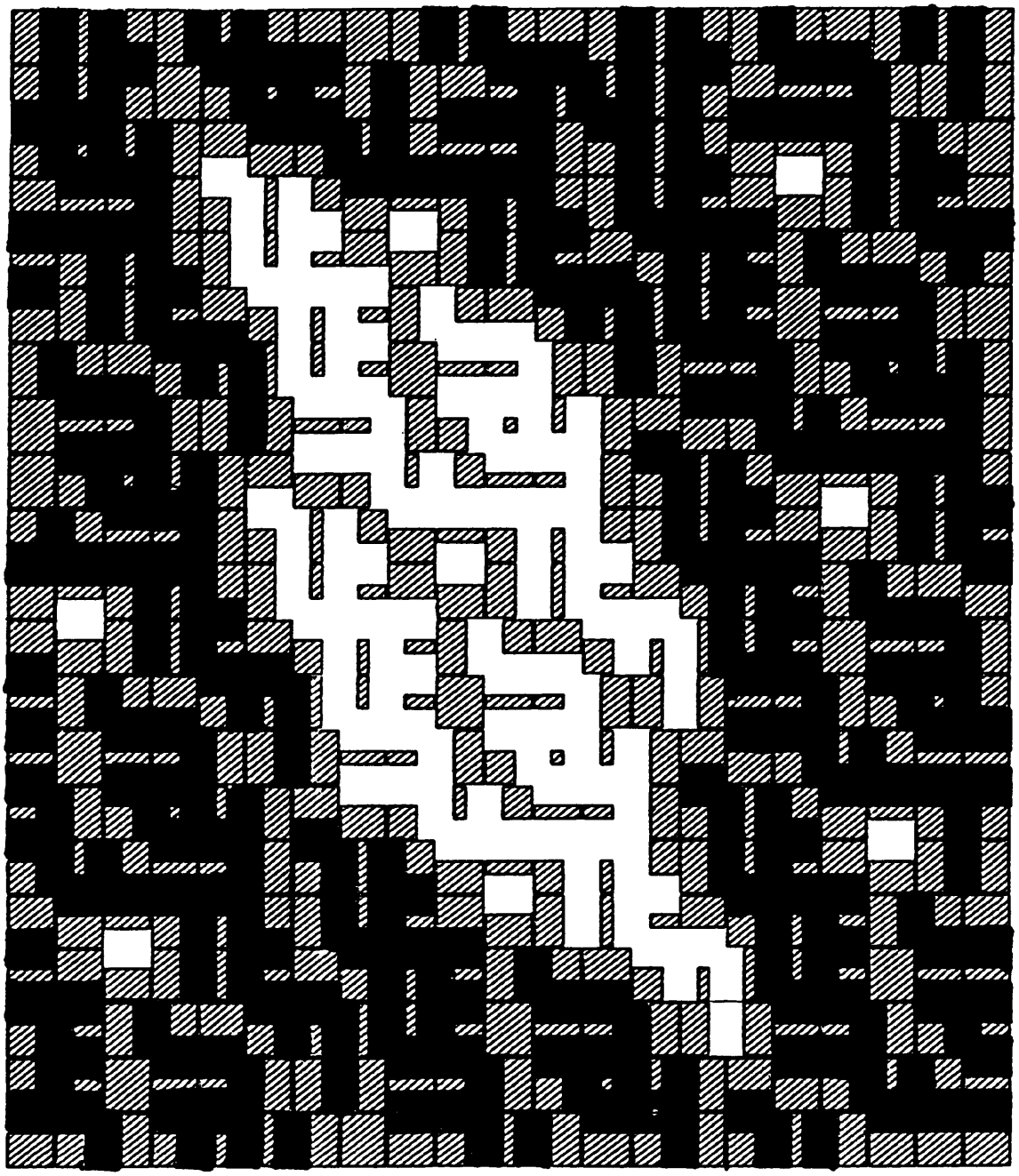

Figure 4.29 Heavy coking in the support pores of a 20x20 network with a bimodal pore size distribution showing a 23% pore volume isolation without diffusional limitations (101 pores isolated).

The outside reactant concentration = 15.00 mole/m^3

13.96	11.58	11.33	11.53	11.08	10.66	11.70	11.49	13.00	13.60
10.29	09.73	08.71	08.35	08.41	09.53	09.57	07.15	08.59	13.37
11.95	09.38	08.14	07.61	06.03	06.04	06.58	06.44	07.16	13.42
08.92	07.87	06.75	05.42	05.33	05.51	05.89	06.26	07.27	11.45
11.11	10.41	04.89	04.79	04.77	04.82	05.46	06.19	06.84	13.78
10.64	10.29	04.56	04.50	04.54	04.71	05.30	06.97	07.61	10.29
12.16	10.53	06.73	04.38	04.51	04.84	05.71	07.57	09.52	12.15
11.37	09.10	06.97	05.60	04.98	05.19	06.49	08.27	09.44	12.31
10.73	10.51	05.88	06.32	05.17	06.43	07.79	08.65	09.82	09.90
10.68	10.97	05.97	12.51	13.15	12.25	12.49	10.59	11.14	12.75

Figure 4.30 Concentration of the reactant at the nodes of the network under conditions of strong diffusional resistances.

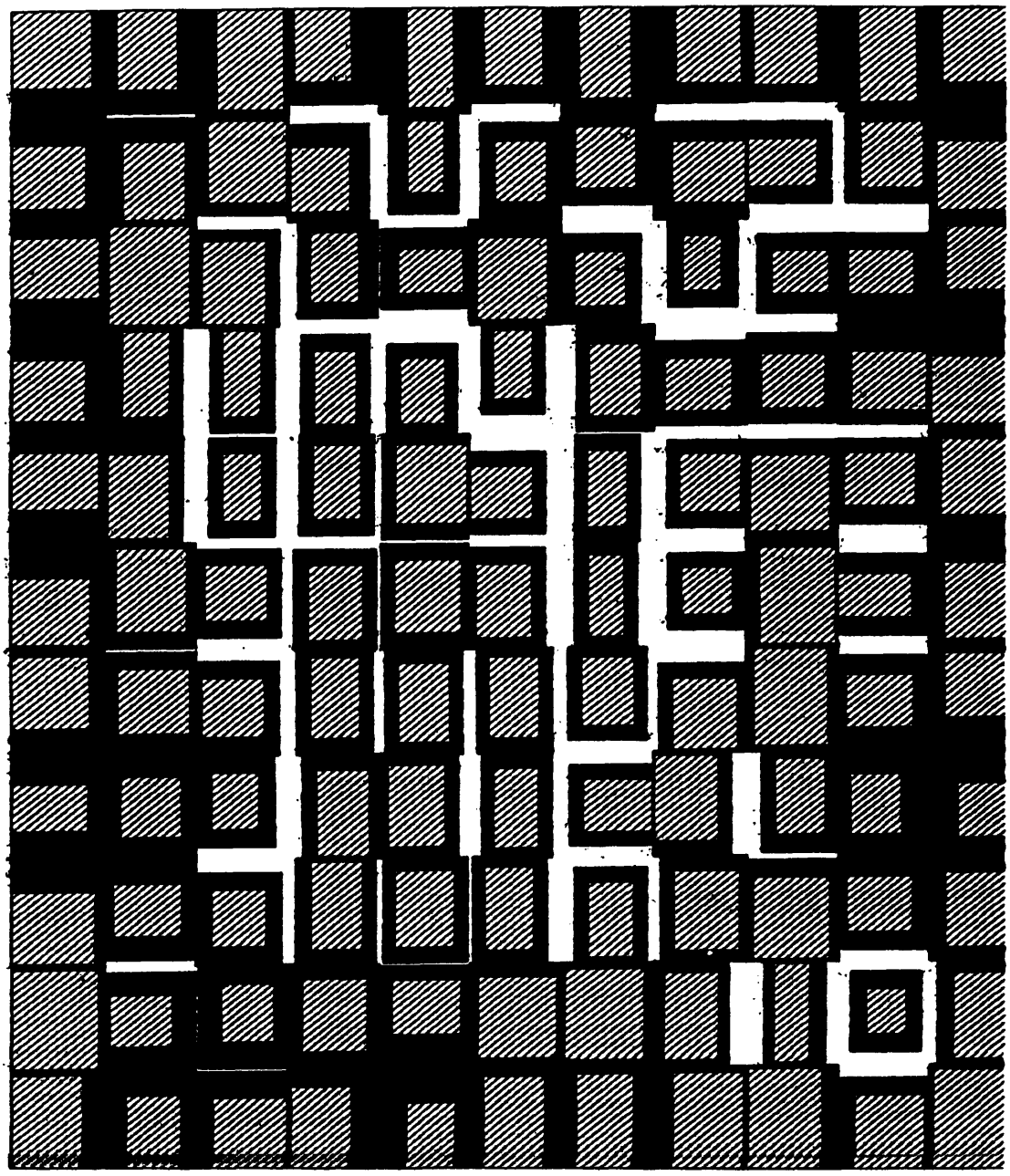

Figure 4.31 Heavy coke laydown in the support pores of a 10x10 stochastic network with strong diffusional limitations.

The outside reactant concentration = 15.00 mole/m^3

2.13	0.74	0.18	0.87	0.60	0.35	1.25	0.28	1.02	1.32
0.09	0.04	0.01	0.02	0.02	0.04	0.14	0.00	0.03	0.53
1.66	0.12	0.01	0.00	0.00	0.00	0.00	0.00	0.00	2.16
0.05	0.00	0.00	0.00	0.00	0.00	0.00	0.00	0.01	0.50
0.66	0.14	0.00	0.00	0.00	0.00	0.00	0.00	0.00	2.85
0.07	0.01	0.00	0.00	0.00	0.00	0.00	0.00	0.00	0.11
1.32	0.12	0.00	0.00	0.00	0.00	0.00	0.00	0.07	1.29
0.41	0.02	0.00	0.00	0.00	0.00	0.00	0.01	0.07	1.59
0.13	0.06	0.00	0.01	0.00	0.00	0.03	0.00	0.03	0.02
0.07	0.38	0.00	1.50	1.10	0.55	1.42	0.08	0.38	1.45

Figure 4.32 Concentration of the reactant at the nodes of the network under conditions of extremely strong diffusional resistances.

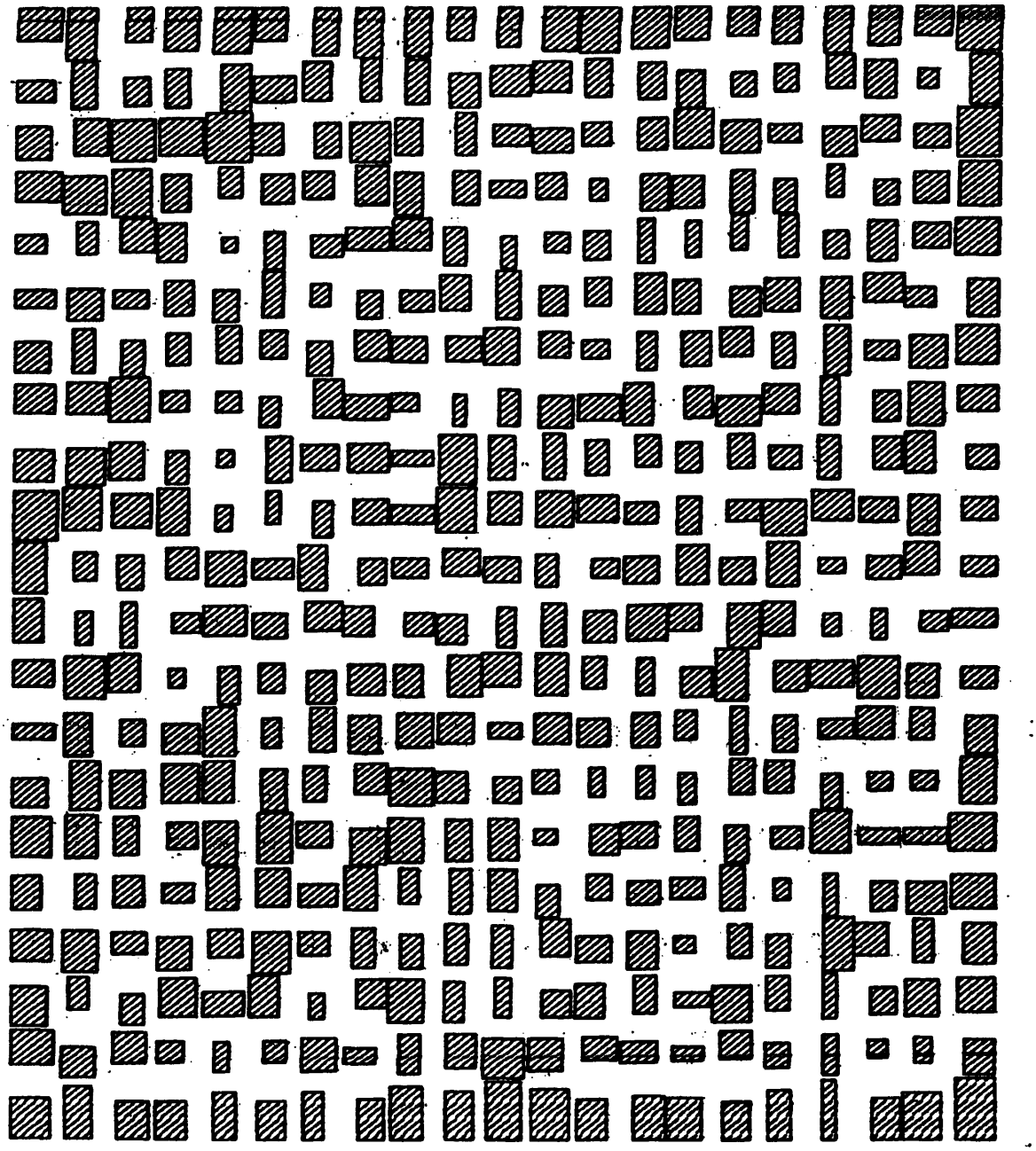

Figure 4.33 A 20x20 stochastic pore network with a uniform pore size distribution in the range 60–3200 Angstrom. (Fresh, uncoked network).

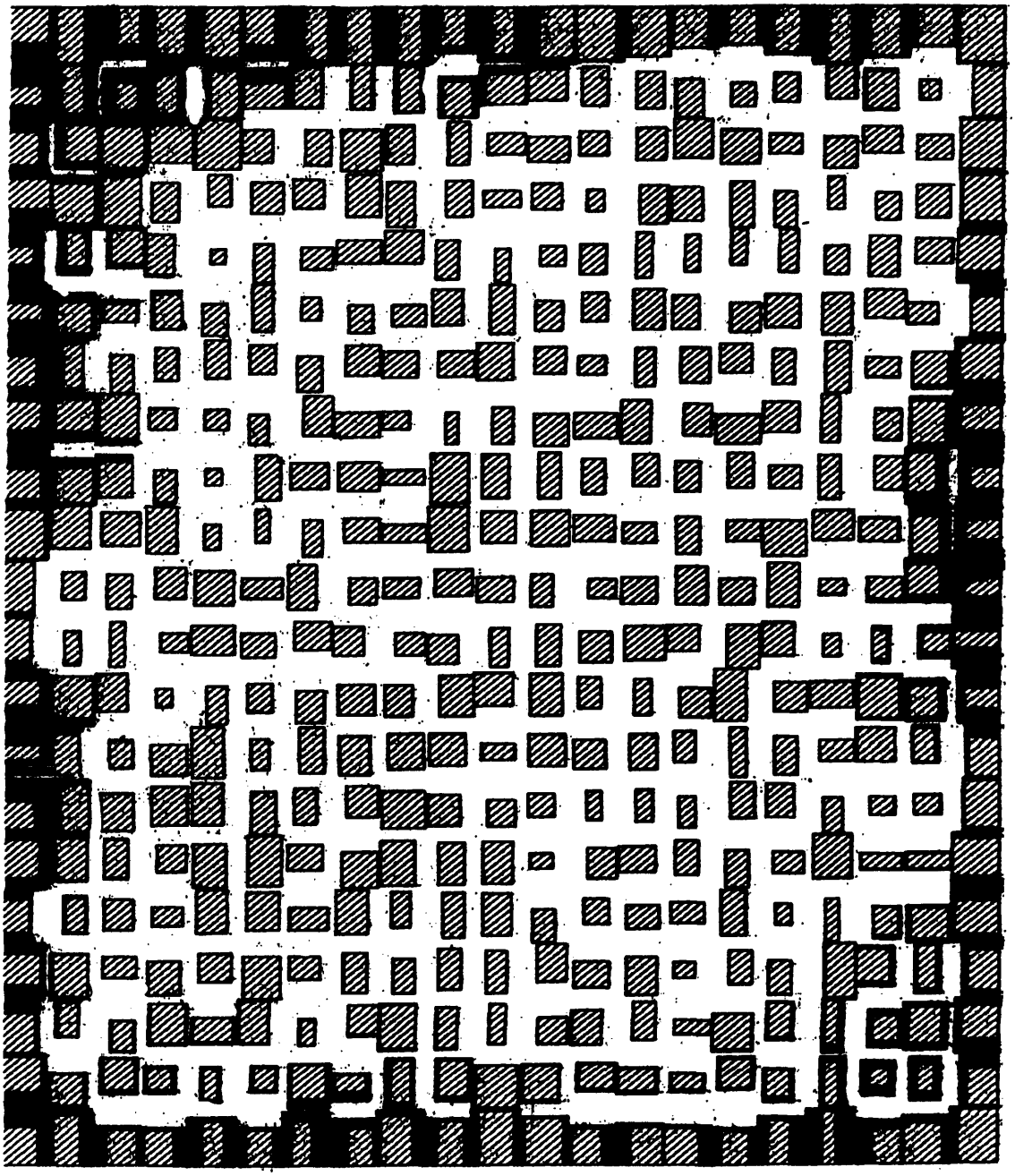

Figure 4.34 Heavy coke laydown in the support pores of a 20x20 stochastic network with extremely strong diffusional resistances.

For the special case of the network with single–size average–area pore elements, the surface area of each element is constant. Also, in the absence of diffusional resistances, at any time the concentration of reactant, C_A, is constant throughout the network elements. Therefore, the rate of reaction in each pore element is constant and the product concentration, C_P, is constant across the network. Since the coking equation is given by :

$$\frac{dR}{dt} = -(K_{C_s} C_P + K_{C_p} C_A) A_{os}^2 \qquad (3.4)$$

Therefore, regardless of the coking mechanism (parallel, series, or triangular), the rate of the coking reaction is constant throughout the network elements. Then, the coke layer thickness in all elements is constant at any given time step. The resulting network is uniformly being reduced in size due to uniform coke laydown throughout the elements. Then, no blocking phenomenon will occur. The network will keep on coking evenly until it is fully coked.

4.5.6 Coke Laydown in the Network of Single–Size Average–Area Pore Elements with Strong Diffusional Limitations:

According to the coking equation (3.4) discussed earlier, the rate of coking is first order with respect to reactant or product concentration and second order with respect to surface area. In the special case of the network of single–size average–area pore elements, the surface area of each element is constant throughout the network. Due to strong diffusional resistances the concentration of the reactant reduces moving inside the network, so that the outer elements have larger concentrations. Then, under parallel coking mechanism, the rate of coking is larger towards the exterior of the network. As soon as some smaller size elements surrounding larger size elements become fully coked, the blocking phenomenon can occur. Again, with extreme conditions of diffusional resistances pore mouth blocking can also be expected to occur.

CHAPTER FIVE

EXPERIMENTAL WORK

CHAPTER FIVE

EXPERIMENTAL WORK

5.1 INTRODUCTION:

5.1.1 Catalytic Cracking of Cumene:

Cumene (isopropyl benzene) has been used for many years in the study of the activity of numerous cracking catalysts. The catalyst under study is a supported zeolite, super–D, used commercially in fluid catalytic cracking units to crack heavy hydrocarbons into lighter products. The catalytic disproportionation of cumene to benzene and propylene was used in a laboratory scale fluidised bed reactor to study the behaviour of the catalyst under investigation. Although it first gained recognition as a single reaction scheme (Plank and Nace, 1955), with products of reaction confined to benzene and propylene, it is still representative of a typical reaction which takes place during the catalytic cracking of gas oils, namely the dealkylation of branched aromatics. Later work (Pansing and Malloy, 1965; Best and Wojciechowski, 1977) has shown that the reaction scheme representing the catalytic cracking of cumene is more complicated than was first suggested. A comprehensive list of over eighteen primary and secondary products of cumene cracking over Lanthanum Y exchanged zeolite at 430 °C have been presented by Best and Wojciechowski (1977), (Table 5.1).

Propylene was suggested to be the coke precursor (Viner and Wojciechowski, 1984) with the main reaction being first order with respect to reactant concentration accompanied by a coking reaction that is second order with respect to surface area and first order with respect to propylene concentration. Many kinetic studies of the cumene cracking reaction have described the reaction taking place at a single site via a carbonium–ion mechanism. Corrigan et al. (1953) suggested that the dealkylation of

TABLE 5.1

Major Products of Cumene Cracking
[Reproduced from Best and Wojciechowski (1977)]

Product[a]	Product Type	Yield[a]
Liquid[b]		
Benzene	Stable primary	43.2
Toluene	Secondary	0.26
Ethyl benzene	Stable primary	1.04
Styrene	Unstable impurity	0.0
(Cumene)		52.5
n–Propyl benzene	Stable primary &secondary	0.36
Ethyl toluene	Unstable primary	0.16
Cymene	Primary stable	0.16
Diethyl benzene	Unstable secondary	0.09
m–Diisopropyl benzene	Unstable primary	1.00
p–Diisopropyl benzene	Unstable primary	0.49
Gaseous[b]		
Methane	Secondary	0.10
Ethylene	Secondary	0.07
Ethane	Secondary	0.04
Propylene	Primary stable	41.4
i–Butene	Primary	0.38
Butene	Primary	0.28
n–Butane	Secondary	0.16
Butane	Secondary	0.14
Coke		
Wt % coke per g catalyst		11.9
Wt % coke per g of feed		0.39
Hydrogen/carbon mole ratio		0.382
Recovery		
Aromatic (mole %)		98.7
Side chain carbon (mole %)		100.7
Total carbon (mole %)		99.2
Total hydrogen (mole %)		99.3
Total mass (%) recovery		98.9

a Experimental data shown are for 100/140 mesh LaY at 430° C, cat/oil of 0.033 and time on stream of 85.5 sec.
b Mole %/mole of pure cumene in feed.

cumene to major products, benzene and propylene, is described by such a mechanism (Fig. 5.1).

In this present study on the fluidised bed catalytic cracking of cumene using a commercial cracking catalyst, the effect of deactivation on the overall conversion and benzene selectivity has been measured as a function of time–on–stream for different catalyst:feed ratios. Representative samples of the fresh and coked catalyst have also been studied to determine the effects of deactivation, as a result of coking, on the physical properties of the catalyst, namely the internal pore structure. A blank "dummy" experimental run was also carried out without any catalyst in the reactor, to determine if any thermal cracking of the cumene occurred under experimental conditions and also to carry out a material balance for cumene over the reactor system. The products from these experimental runs were then analysed off–line using Gas–Liquid Chromatography and from these results a measurement of the deactivation was obtained. The coke content and surface area were determined for both fresh and coked catalyst samples. This was necessary to enhance the modelling of the deactivation by a more fundamental approach.

5.1.2 Zeolites in Catalysis:

Zeolites are a class of crystalline alumino silicates. It was about the middle of the eighteenth century (1750's) when synthetic zeolites were first discovered, but only fifty years ago that industry realized their importance in the fields of ion exchange, adsorption and catalysis, especially cracking catalysts. The wide range of applications of zeolites encouraged chemists to make new forms of "synthetic zeolites" which were unknown naturally (Dwyer and Dyer, 1984). Cracking catalysts which are particularly important in hydrocarbon processing are almost all zeolitic. (Vaughan, 1979)

5.1.3 Structure of Zeolites:

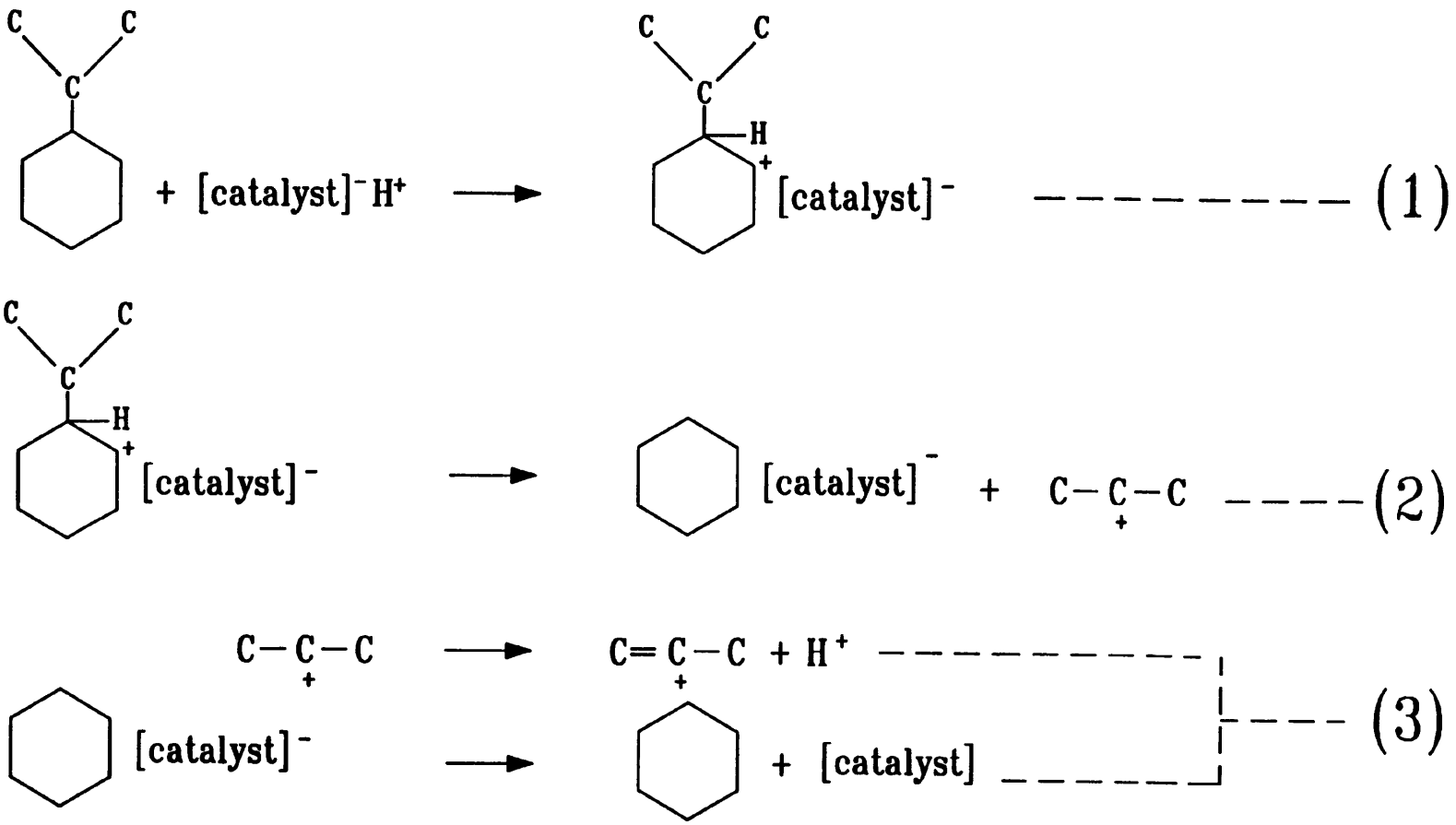

Figure 5.1: Mechanism of the dealkylation of cumene
[Reproduced from Corrigan et al. (1953)].

To enhance our understanding of the catalytic behaviour of zeolites, it is essential to study their structure. According to Dwyer and Dyer (1984) the structure of zeolites consists of the following three parts:

(1) SiO_4 and AlO_4 molecules (tetrahedra) constitute the fundamental building units of the zeolite structure (Fig. 5.2A) with each tetrahedron attached to four other molecules to form the final structure.

(2) The secondary building units are the "rings" and "boxes" which are formed by the linkage of the SiO_4 and AlO_4 tetrahedra with a variety of aperture sizes depending on the number of tetrahedra involved. (Fig. 5.2B).

(3) The final zeolite structure is the result of the different modes of assembly of the secondary building units (Fig. 5.2C).

The aluminosilica structure carries a net negative charge which is balanced by cations which are commonly rare earth metals, hydrogen or metals from the first two groups of the periodic table.

It is interesting to note that the space between the tetrahedra for channels are not uniform in cross–section, but include cavities which are often sited at the intersection with other channels. These channels are connected, according to the individual zeolite, in either one, two or three dimensions. Rees (1984) illustrated the channel sizes (in Angstrom) associated with different zeolite types in comparison with the sizes of some small molecules (Fig. 5.3).

Zeolites act as "molecular sieves" by allowing molecules with small diameters to pass through the channels and by excluding larger molecules, leading to "selectivity" based on molecular size which is a very important property of any catalyst besides its activity.

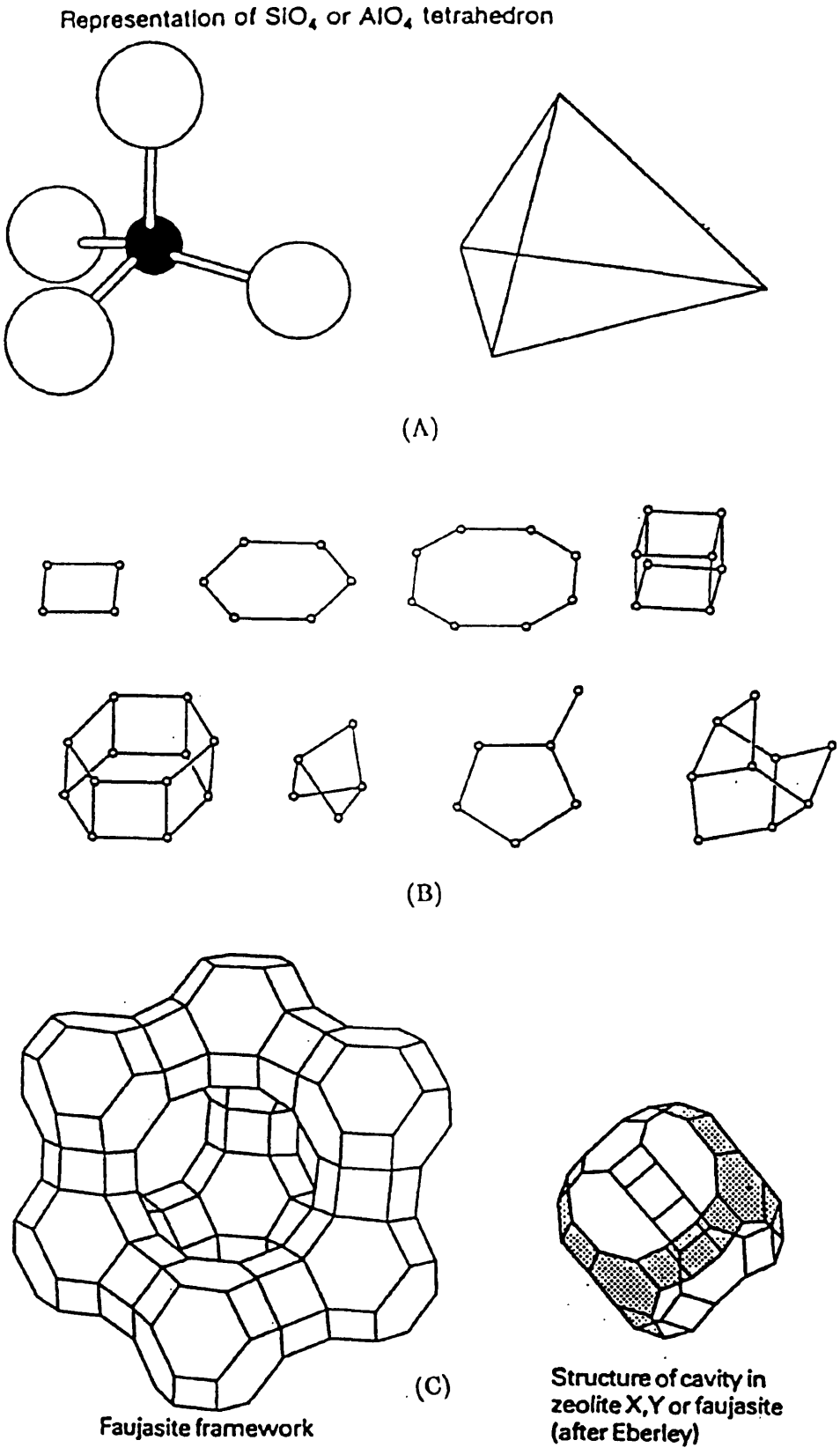

Figure 5.2 Zeolite structures (A) Fundamental building units, (B) Secondary building units and (C) Final zeolite structure (Dwyer & Dyer (1984)).

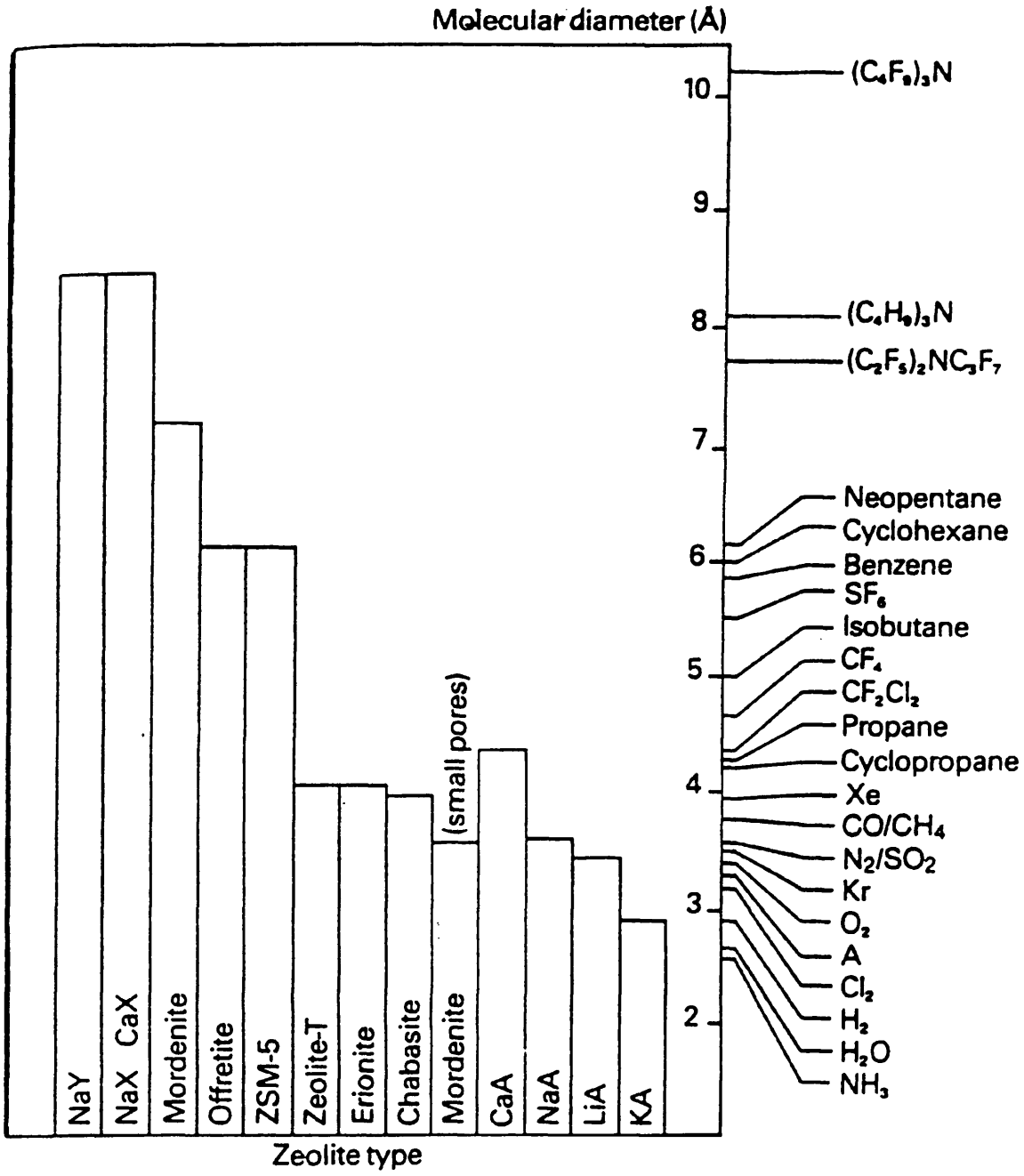

Figure 5.3 Channel sizes in zeolites (Rees (1984)).

5.1.4 Structural Design of Zeolites:

The activity and selectivity of zeolites are remarkably predicted through the control which a catalyst design has over their structure. The three crucial factors in the design of zeolites are (Vaughan, 1979):

(1) The type of the structure gives specific mesh size.

(2) The cation type used in balancing the negative charge of the aluminosilicate framework provides a greater control on the size of the mesh (fine tuning).

(3) The ratio of the Si/Al can be changed to produce the zeolite with the design structure.

5.1.5 Chemistry of Zeolite Catalysis:

The behaviour of zeolites in the catalysis of hydrocarbon reactions is complex. The catalytic activity is generally believed to be mainly associated with acidic sites (Van Hoff, 1980). Other factors controlling the activity include the Si/Al ratio, the presence of potential proton donors, the size and charge of the cations and the location of the cations in the lattice (Venuto and Landis, 1968). Zeolites generally have higher activity, selectivity and stability than catalysts such as amorphous silica–alumina. The higher activity of zeolites compared to amorphous catalysts is attributed to a higher effective concentration at the zeolite surface arising from the powerful forces associated with adsorption in zeolites. In hydrocarbon conversion, the dominant mechanism involves carbonium ion formation. Dwyer (1984) suggested that free radical routes may also be important.

5.1.6 Diffusion in Zeolites:

Diffusion through zeolites presents great difficulties. Certainly, analysis based

on diffusion in the bulk of a gas is inappropriate, since often the size of a molecule is comparable with the channel through which it moves. The Knudsen model is more realistic in this context but still assumes elastic collisions between molecules and wall. Venuto and Landis (1968) stated that species within a zeolite are subject to a variety of powerful forces, and cannot be considered to act as free molecules.

"Configurational Diffusion" was a term given by Weisz (1973) to describe the mode of diffusion found in zeolites and other media with small apertures (Fig. 5.4). He proposed that molecules have to be configured in certain limited number of ways to be able to pass through such apertures. Figure 5.5 shows the variation of measured diffusivities of n–paraffins through erionite as a function of chain length which has been presented as evidence for his argument.

5.1.7 Deactivation of Zeolites:

Zeolites, as with any other acid catalyst, deactivate through a complex mechanism of coking. Zeolite structure plays an important role in the fouling process besides the chemical aspects. Tan and Fuller (1970) reported rapid fouling of a rare–earth X–zeolite during alkylation of benzene by cyclohexene. The foulants were molecules of sizes that exceeded the channel diameter and were thus confined to cavities in the structure. Rollman and Walsh (1979) stated that the rate of coking decreases with channel diameter.

5.1.8 Models of Zeolitic Deactivation:

It is surprising to note that little original work has been attempted to apply structural information in the modelling of zeolitic deactivation. As an example, see Lin, Park and Hatcher (1983) using the approach of Froment (1980) in describing the deactivation of Lanthanum Y–zeolite in cumene cracking. The work of Theodorou and

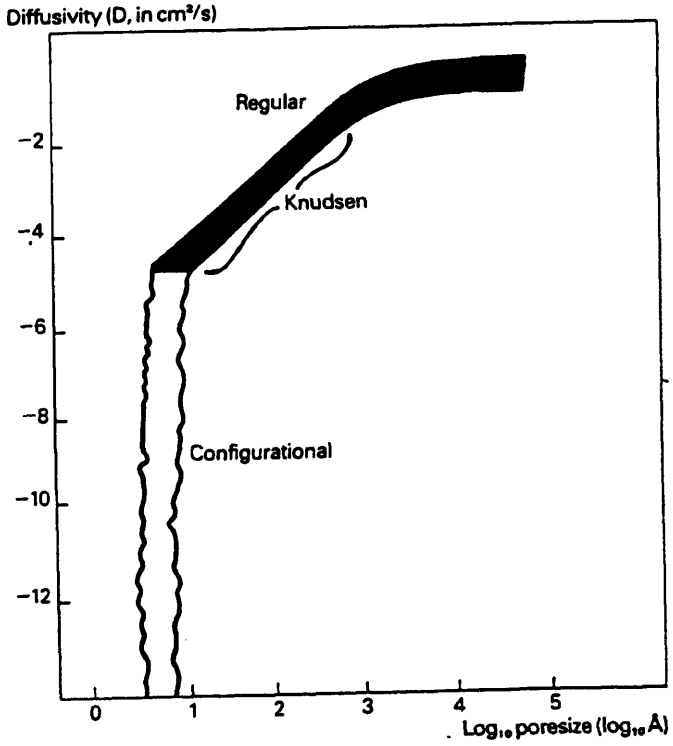

Figure 5.4 Diffusion regimes (Weisz (1973)).

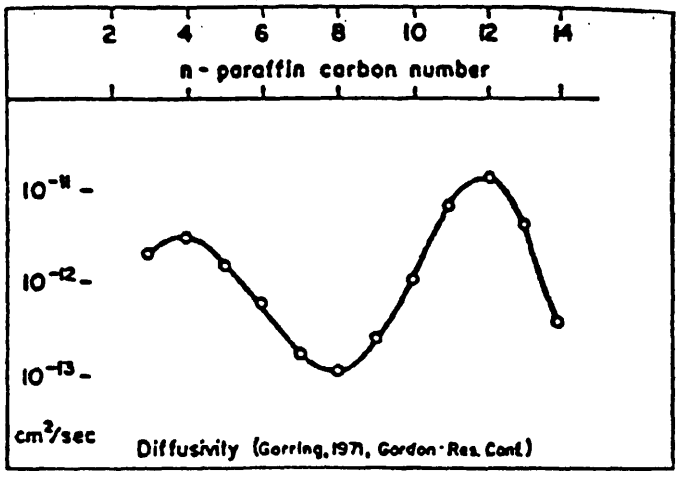

Figure 5.5 Variation of diffusion coefficient with hydrocarbon length (Weisz (1973)).

Wei (1983) in modelling the deactivation of ZSM5 zeolite using a rectangular grid was an exception. They applied the Monte–Carlo approach in predicting the properties of molecules moving by finite jumps through such a network.

5.2 LABORATORY SCALE CATALYTIC CRACKING OF CUMENE:

5.2.1 Catalyst Specification:

The catalyst used throughout the experimental work was a commercial catalyst, which is manufactured for and normally used in fluid catalytic crackers, known as super–D. It was supplied by Crosfield Chemicals Ltd., Warrington, England. The super–D in its commercial form consists of particulate spheroids with an average diameter of 81 microns and it was used in the same form for the laboratory scale catalytic cracking of cumene. Super–D particles consist of 15–18wt% ion exchanged Re sodium Y–zeolite on a support matrix of silica–alumina.

5.2.2 Catalyst Pretreatment:

Pretreatment of the catalyst powder involved heat treatment at 150 °C for 48 hours, to drive off any moisture in the fine network of pores of the catalyst particles. The catalyst was removed at the end of the period and kept in a desiccator over silica–gel until it was used in the cracking experiments.

5.2.3 Feed Specification:

The feed to the cracking experiments was cumene (isopropyl benzene), supplied by Fisons Scientific Apparatus at a purity greater than 99.5%. Cumene was chosen because it undergoes a cracking reaction which is representative of a typical reaction which takes place during catalytic cracking of gas oils, namely the dealkylation of

branched aromatics.

5.2.4 Experimental Apparatus:

The catalytic cracking of cumene was carried out in a laboratory scale fluidized bed reactor made from quartz glass at 500° C. Figure 5.6 shows a schematic diagram of the experimental apparatus. Figure 5.7 shows a photograph of the quartz glass reactor used in cumene cracking reactions. The furnace temperature was controlled by a three term Eurotherm type 810 controller to keep the reactor temperature as near constant as possible. The temperature was monitored by K type thermocouples located at different positions in the experimental apparatus. These thermocouples were interfaced with an F–1 Apricot Personal Computer via a 3–D Think Lab system which contained a 12 bit Analogue/Digital card. A digital signal was produced by the Analogue/Digital card in the range 0–4096 which approximately corresponded to 0–700° C temperature range. A platinum resistance thermometer was used for the calibration of the thermocouples.

5.2.5 Experimental Procedure:

A charge of super–D catalyst, which was pretreated in the manner described in a previous section, between 5–10 grams was placed in the bottom of the quartz glass reactor. The reactor was heated, while being purged by nitrogen, and brought gradually up to the reaction temperature over a period of one hour to avoid causing any thermal shocks or damage to the catalyst or the reactor. For the next three hours the temperature of the reactor was held as near constant as possible (to within ±5° C). During that time the feeding pump was switched on and the cumene started flowing through a three–way valve to the waste line. When the flow rate of cumene was constant (as measured by successive samples being weighed through the waste line at equal time intervals) the experiment was started. Using the three–way valve (vacuum

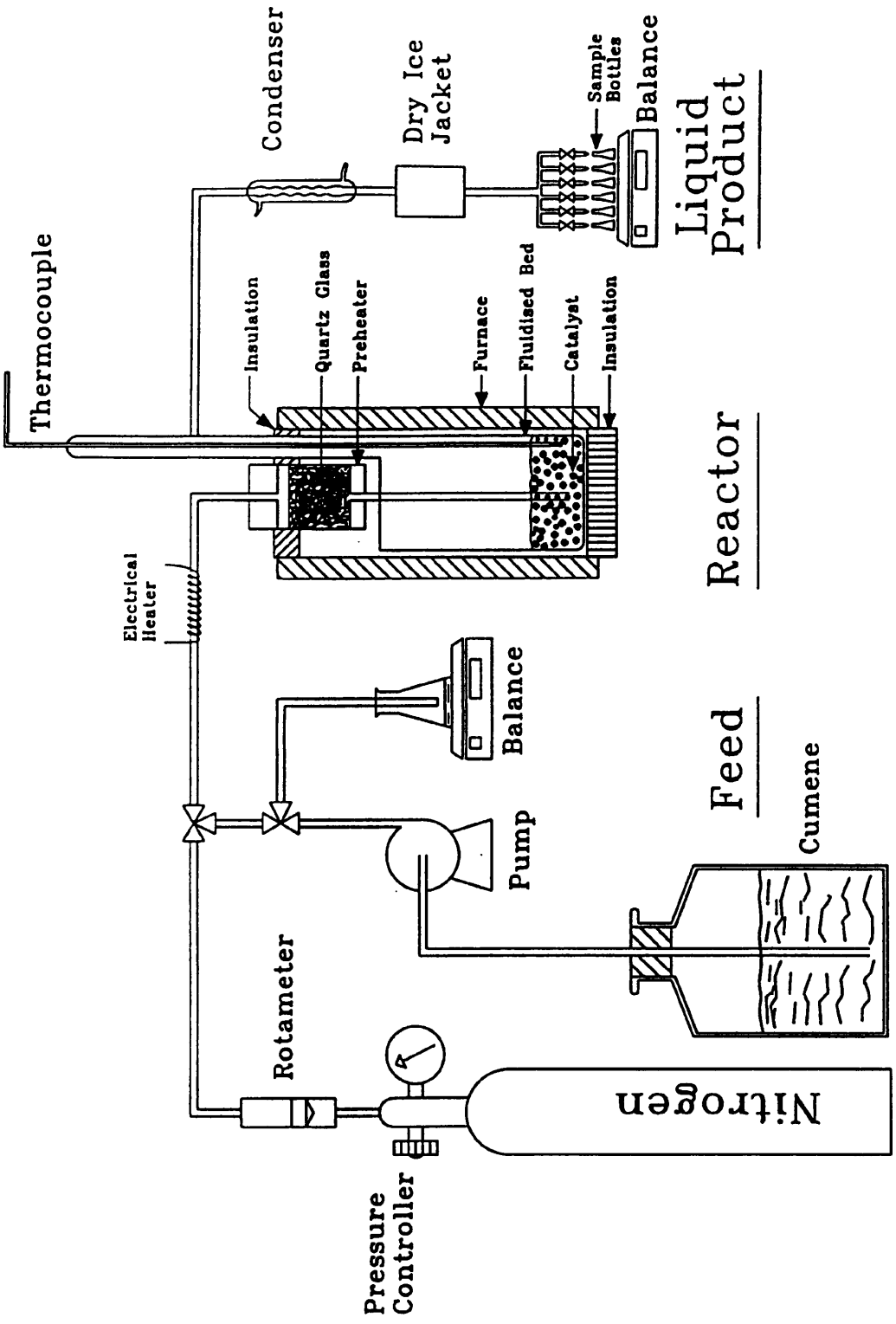

Figure 5.6: Schematic diagram of the experimental apparatus for the cracking of cumene.

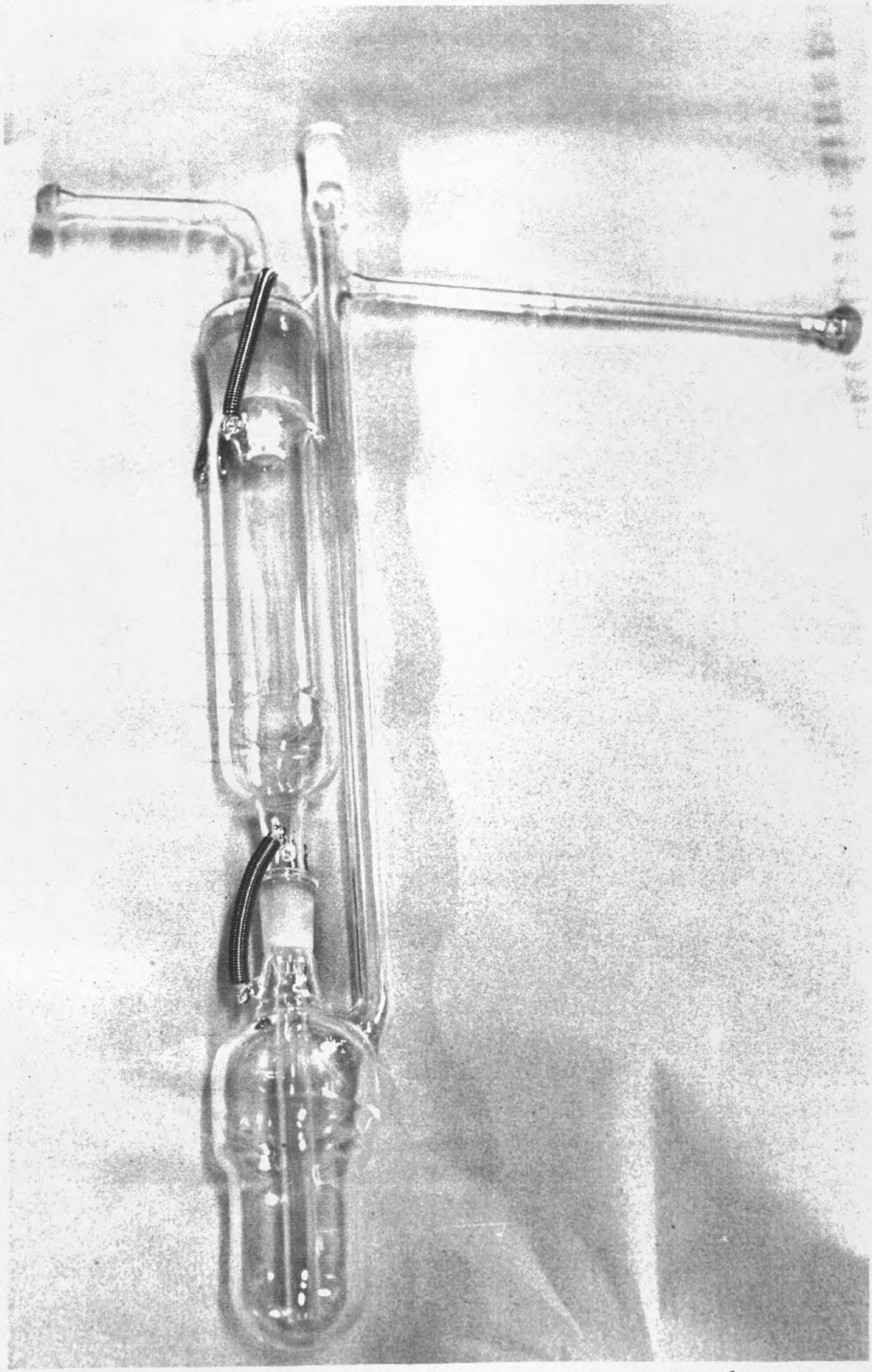

Figure 5.7 A photograph of the quartz glass reactor used in the cumene cracking reactions.

tight) the nitrogen purge was switched off and the cumene started flowing through the preheater over the quartz glass chips. The cumene was vaporized and heated to reaction temperature in the preheated section of the reactor passing over the catalyst for a fixed contact time between 1 and 120 minutes.

The products and the unconverted feed passed through a water cooled condenser and through a dry ice jacket. Liquid products of the run were collected periodically at different time intervals in sample bottles which were located on a digital balance for instantaneous reading of the product weight at any time through out the experimental run. This was recorded initially when cumene started flowing to the reactor and when each sample was collected and the weight of each sample was determined. At the end of the experimental run, cumene was switched back to the waste line for a final check of feed flow rate. A high nitrogen purge was passed through the reactor for five minutes to prevent any reactant or product species from remaining in the cracking reactor. The electric furnace was turned off and when the reactor had cooled sufficiently, the deactivated catalyst was removed from the reactor, weighed and stored in a desiccator over silica–gel until it was ready for off–line analysis. The sample bottles containing the liquid product of the catalytic cracking of cumene were tightly sealed and stored in a refrigerator to prevent evaporation of the volatile components until it was ready for its own off–line analysis. The experiment was repeated for a wide range of catalyst:feed ratios by changing the feed flow rate and changing the amount of catalyst used in the reactor.

5.2.6 A "Blank" Experimental Run:

Additional experimental runs were performed in which the cracking reactor was void of catalyst. These "blank" runs were carried out by passing cumene through the same reactor at different reaction temperatures and different feed flow rates with no catalyst present. These experiments served the following two purposes:

(1) To determine the possibility and the extent of any thermal cracking of cumene at the reaction temperatures and under experimental conditions.

(2) To perform a material balance for cumene over the reactor system.

5.3 OFF–LINE ANALYSIS:

5.3.1 Liquid Product:

The liquid products, which were collected periodically, were analysed off–line using standard chromatographic techniques (Gas–Liquid Chromatography, GLC). Figure 5.8 shows a photograph of the GLC apparatus. One and half meter glass column packed with a silicon OV17 stationary phase was found to be ideal in separating the major components of the liquid product of cumene catalytic cracking (benzene, toluene, ethyl benzene and unreacted cumene). A typical chromatogram of a known standard, using this column is shown in Figure 5.9. A Pye unicam GLC series 204 with flame ionization detectors (FID) was used in the analysis, and nitrogen was used as the carrier gas. The analysis was temperature programmed, that is the temperature in the GLC changed with time, which was essential in order to obtain a good separation between benzene (the lowest boiling product) and diethylether which was used to dilute the samples prepared for analysis.

A Trivector Trilab 2000 integrator calculated the weight percent of each component in the liquid product from the raw data produced by the GLC machine. The column was calibrated using a known standard and checked periodically with other known standards. From the GLC analysis, the % unreacted cumene in the liquid product was determined and by performing a cumene mass balance over the reactor the overall conversion at the reactor outlet was calculated. Also, by determining % benzene in the liquid product, benzene selectivity was calculated in a similar manner.

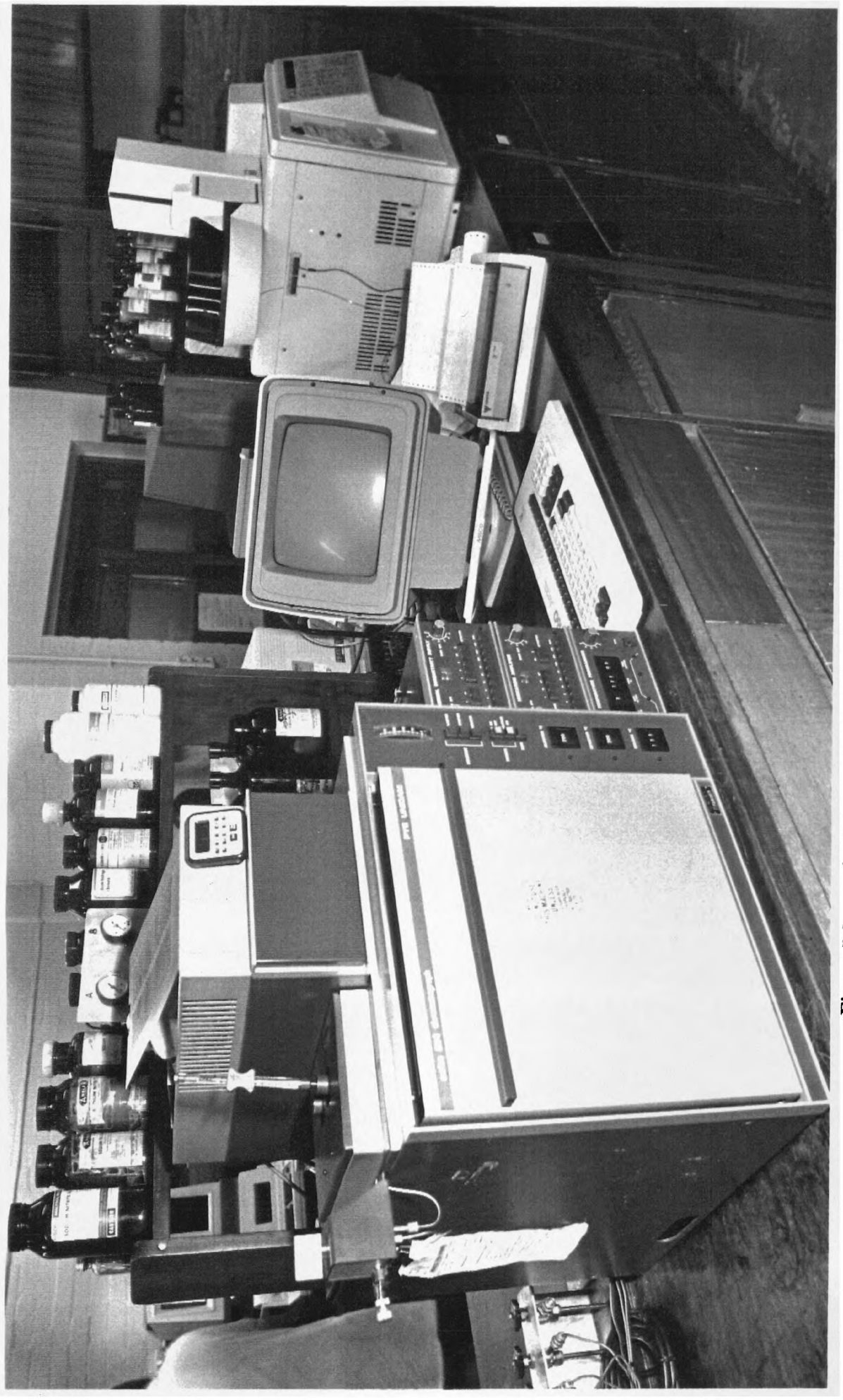

Figure 5.8 A photograph of the Gas Liquid Chromatography apparatus.

		Wt%	
(a) Standard	Cumene	52.32	
	Ethylbenzene	3.13	
	Toluene	28.16	
	Benzene	16.39	
	n-Propylbenzene	12.27	Internal Standard

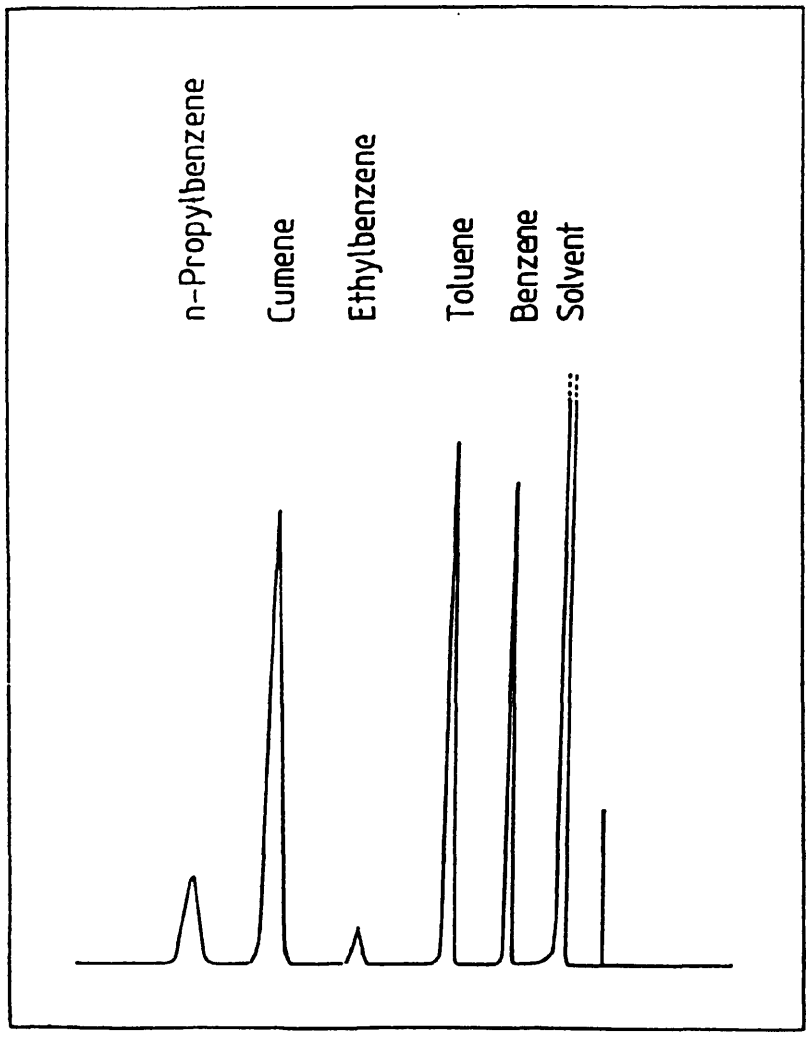

Figure 5.9 A typical chromatogram of a known standard[(a)].

5.3.1.1 Internal Standard Method of Analysis:

In practice, compounds which are chemically similar to the compound(s) of interest are chosen as internal standards. For the analysis used in this work, n–propylbenzene (supplied by Koch–Light Laboratories Ltd. as pure) was chosen as the internal standard.

Known standard solutions (on a weight basis) were made up, three for each set of analyses, which were used to calibrate the GLC for the operating conditions detailed in the previous section. The relative response factors (RRF) with respect to the internal standard for each cracked product i.e. benzene, toluene, ethyl benzene and for the unreacted cumene were calculated by a dedicated microcomputer linked to the GLC. The RRF's calculated for one standard solution were checked using the other standard solutions. The calibration was checked periodically, by injection of one of the known standards.

To ensure a linear response of the detector (FID) all of the solutions (standards and samples) were diluted approximately thirty times. As the method of analysis is based on an internal standard, dilution does not affect the results. Diethyl ether was used to dilute the samples, and as a result temperature programming was required to ensure complete separation of the solvent and benzene peaks.

This method of analysis is well known and is not described in detail here. For further information the reader is referred to a publication by Pye Unicam entitled "An Introduction to Gas Chromatography".

5.3.2 Solid Product:

The deactivated catalyst left in the reactor after each experimental run was

analysed for its coke content and surface area and was also examined under the scanning electron microscope (SEM) in comparison with fresh catalyst.

5.3.2.1 Coke Content:

The amount of carbon–on–catalyst as a result of coke deposition during the cracking of cumene, was determined using a LECO CS244 carbon/sulfur analyser. The method of analysis involved burning a known weight of coked catalyst in an induction furnace (model HF 100) and the measurement of carbon present in the product gases (CO is first converted to CO_2, and the analysis is of the total CO_2 content). A known carbon standard was used to calibrate the instrument. Fresh catalyst samples were also analysed for any residual carbon present as a result of catalyst preparation. The elemental carbon on the catalyst measured by the carbon/sulfur analyser was then multiplied by a correction factor to account for the chemical formula of the coke.

Abbot and Wojciechowski (1985) reported that coke produced from olefinic precursors has a carbon:hydrogen ratio of approximately 1:0.5. Best and Wojciechoski (1977b) have reported that during the cracking of cumene over La Y–zeolites a coke formed which had a carbon:hydrogen ratio of 1:1.25. The ratio of 1:1 was reported by Thomson (1986) after consultation with the catalyst manufacturer for the cracking of cumene over a Na Y–zeolite. The coke content was calculated in this work with the assumption that 1:1 is the molar ratio of carbon:hydrogen.

5.3.2.2 Total Surface Area:

Total surface area of a catalyst is usually determined by the Brunauer–Emmett–Teller (BET) method. The basis and background of the technique are treated in numerous articles and books (Allen, 1990; Lowell, 1979).

The structural changes in the super–D catalyst were monitored by determining the total surface area of the coked catalyst in comparison with the fresh catalyst. The determination of surface area was undertaken on a Quantasorb unit in the laboratories of Kuwait Institute For Scientific Research (KISR). The experiments were performed by the Catalyst Characterization Group of the Petroleum Technology Department. The manufacturer's instructions were closely followed and they are given in detail in Appendix–4.

5.3.2.3 Scanning Electron Microscopy (SEM):

Examination of fresh and coked catalyst was made under a scanning electron microscope. The catalyst samples were studied under different magnifications and sample photographs were taken. Figures 5.10 to 5.14 show some photographs of the fresh super–D catalyst samples which had to be platinum coated before being studied under the SEM at different magnifications. The procedures followed in the SEM sample preparation are given in Appendix–5.

5.3.2.3.1 Basic Principles of SEM:

Figure 5.15 is a diagrammatic illustration of the principle of the scanning electron microscope. A very fine probe of electrons with energies up to 40 KeV is focused at the surface of the specimen in the microscope and scanned across it in a pattern of parallel lines. One of the most important phenomena that occur at the surface under electron impact is the emission of secondary electrons with energy of a few tens of eV. Another important phenomena is the re–emission or reflection of high energy back scattered electrons from the primary beam. The intensity of emission of both secondary and back scattered electrons is very sensitive to the angle at which the electron beam strikes the surface, i.e., to the topographical features on the specimen. The magnification produced by a scanning electron microscope is defined as "the ratio

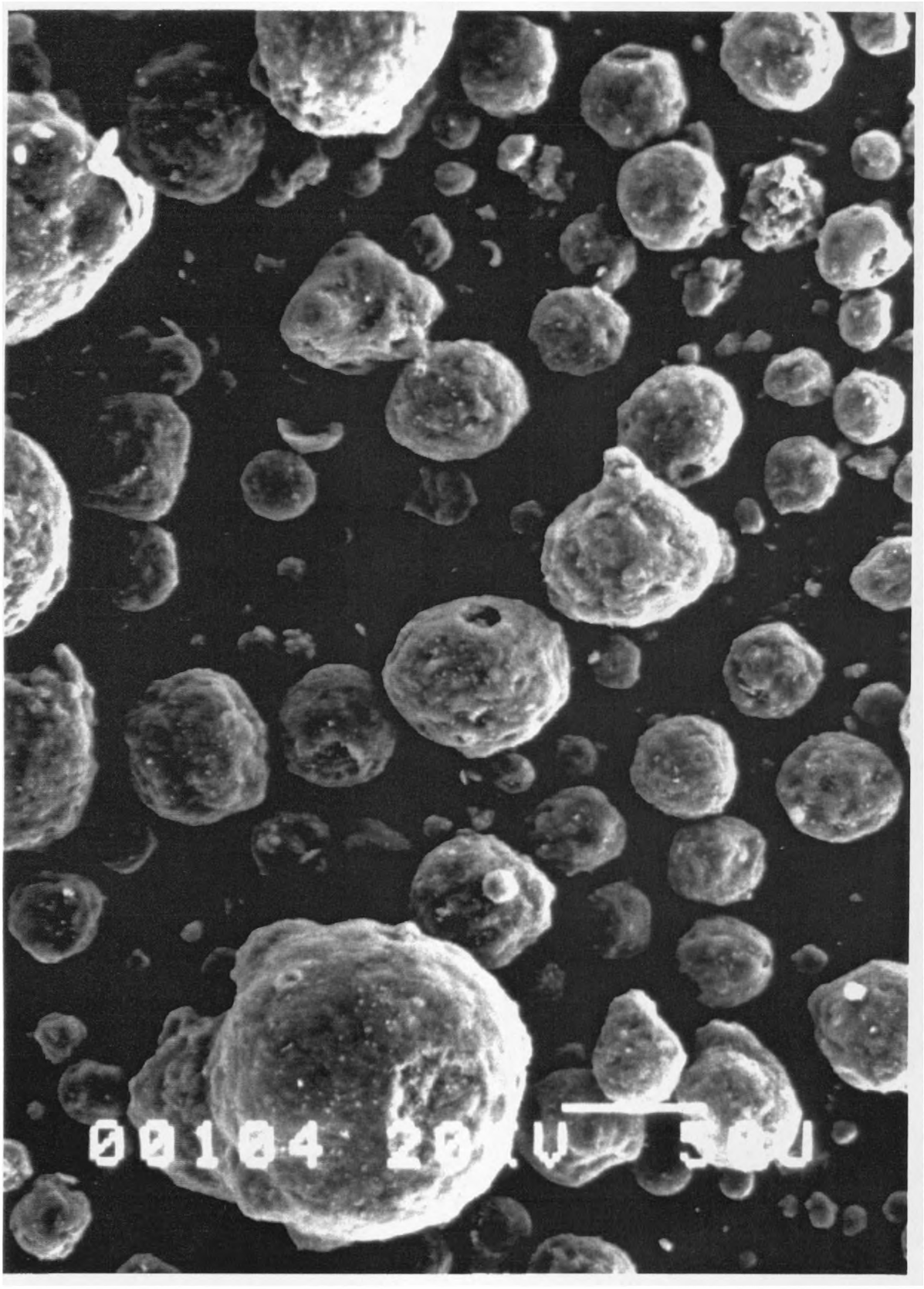

Figure 5.10 SEM photograph showing fresh super–D catalyst particles.

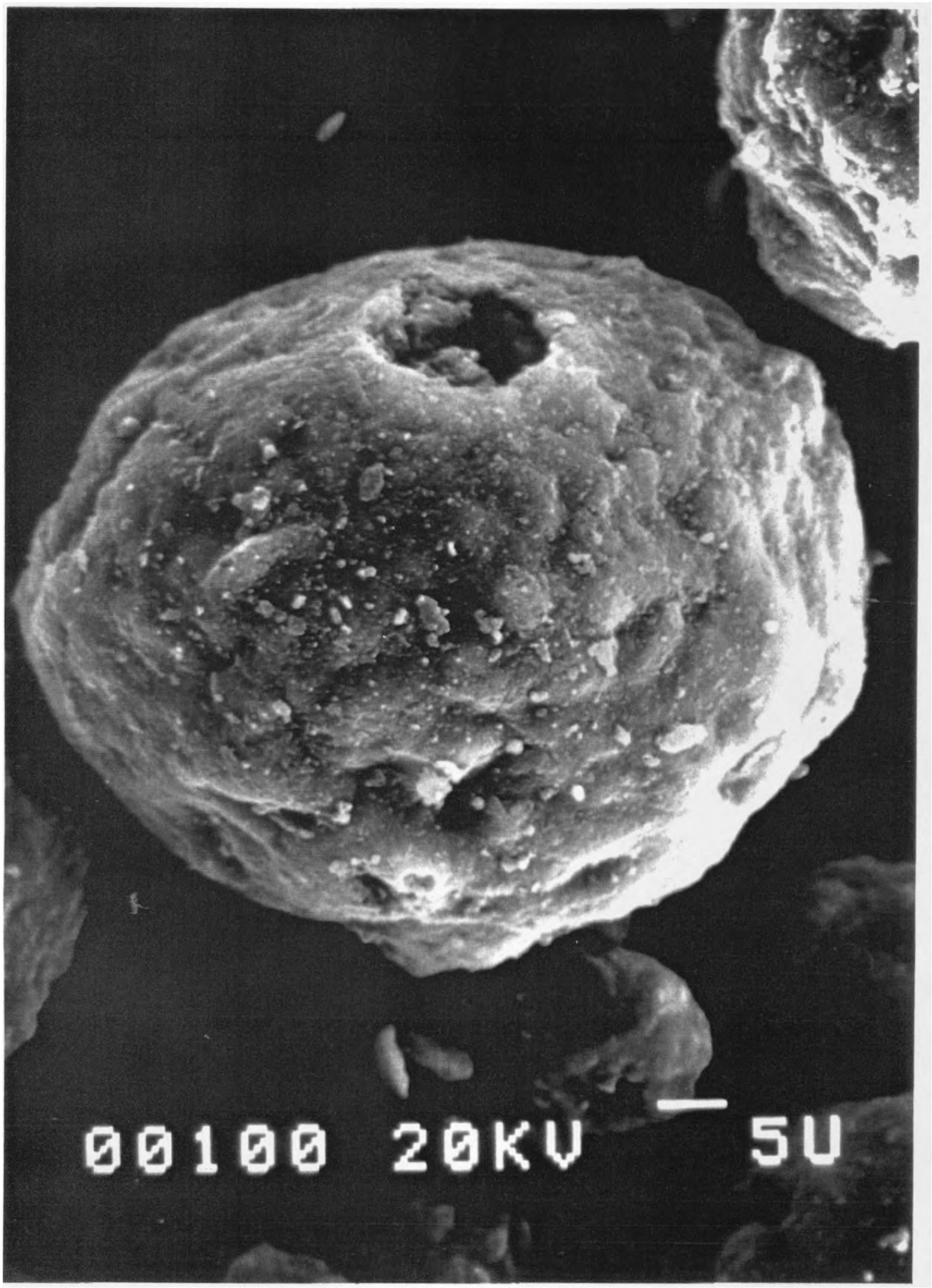

Figure 5.11 SEM photograph showing a typical fresh super–D catalyst particle.

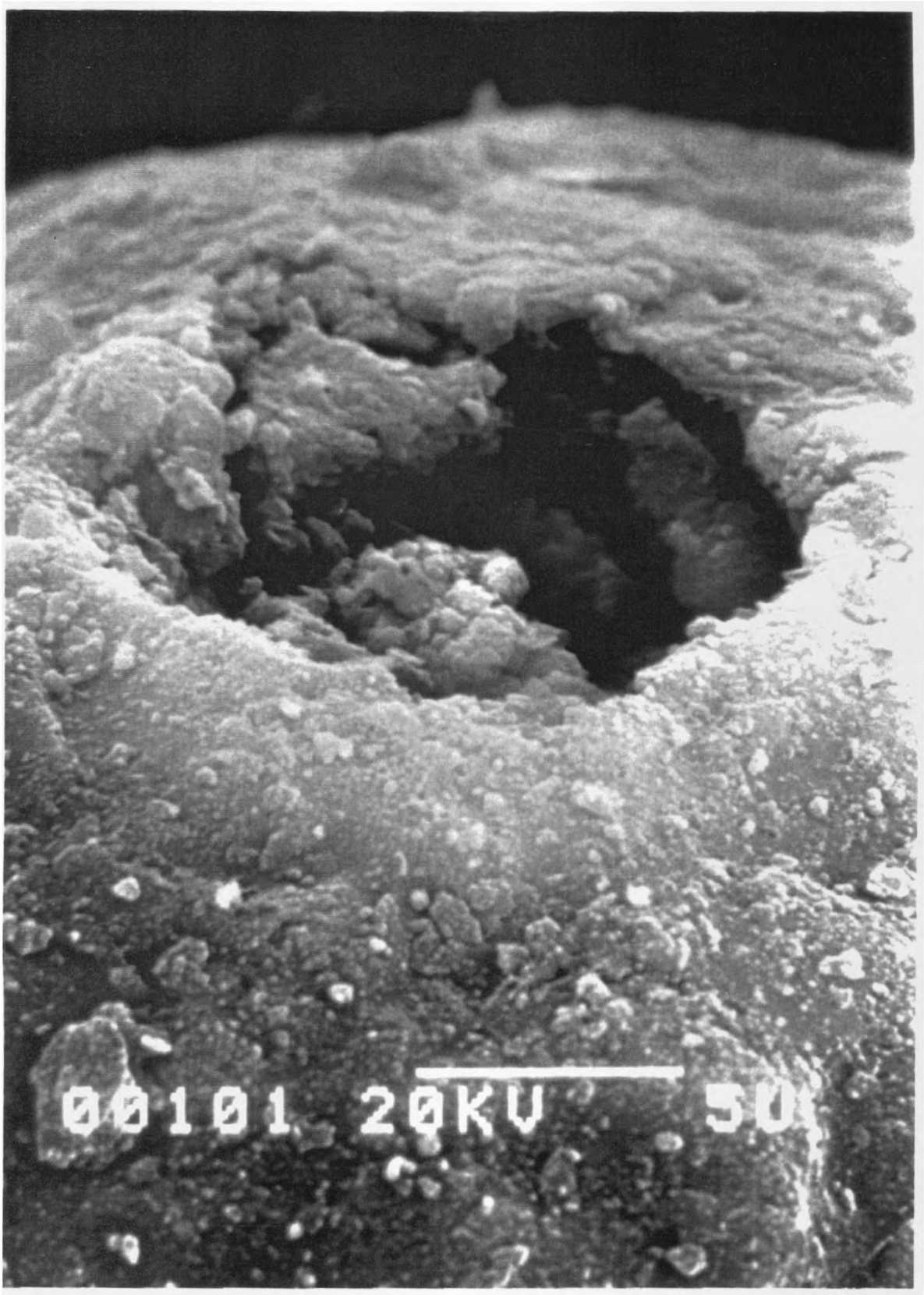

Figure 5.12 SEM photograph showing the entrance to a very large pore 'space' of a fresh super-D catalyst particle.

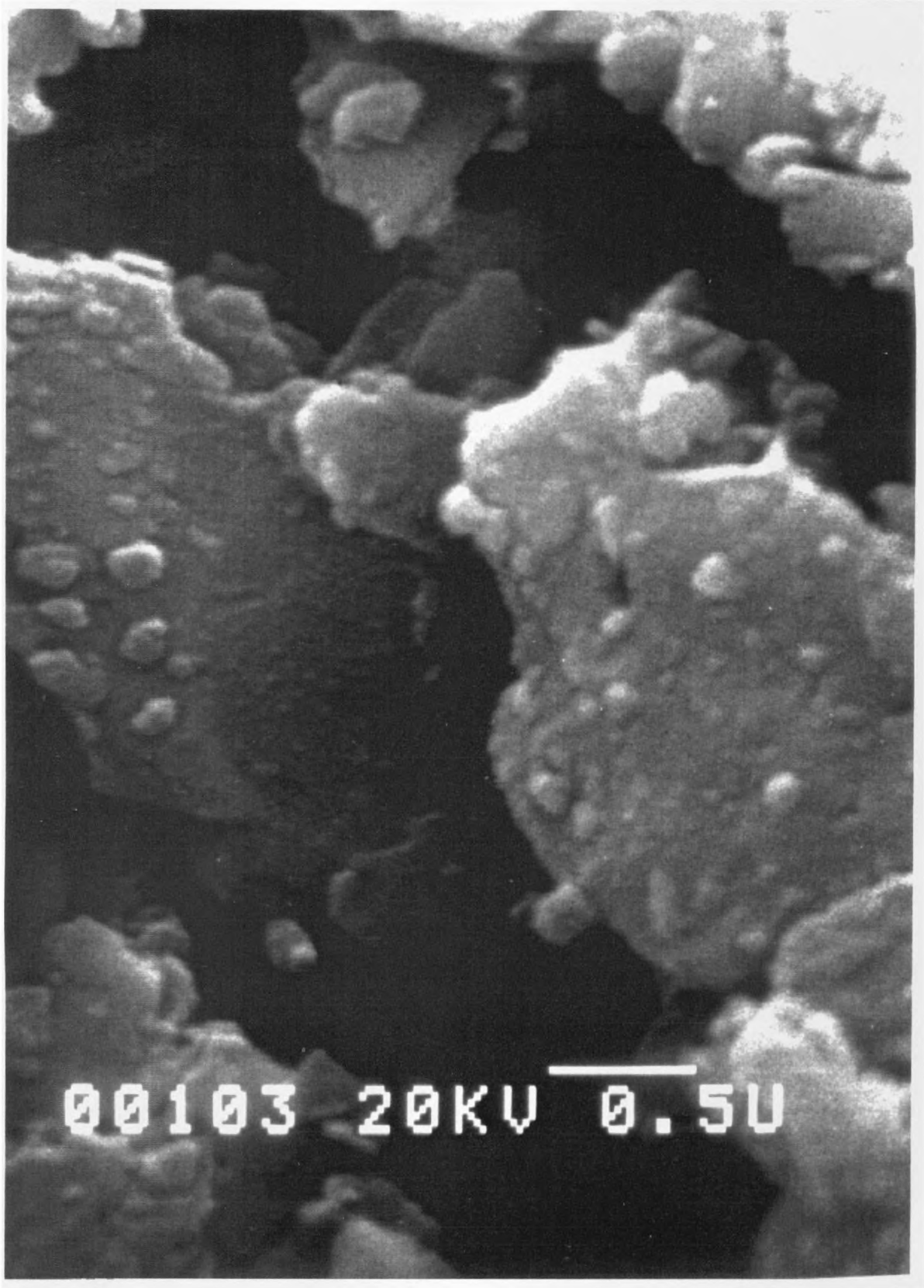

Figure 5.13 SEM photograph showing the complexity of the internal structure of a large 'space' of a fresh super–D catalyst particle.

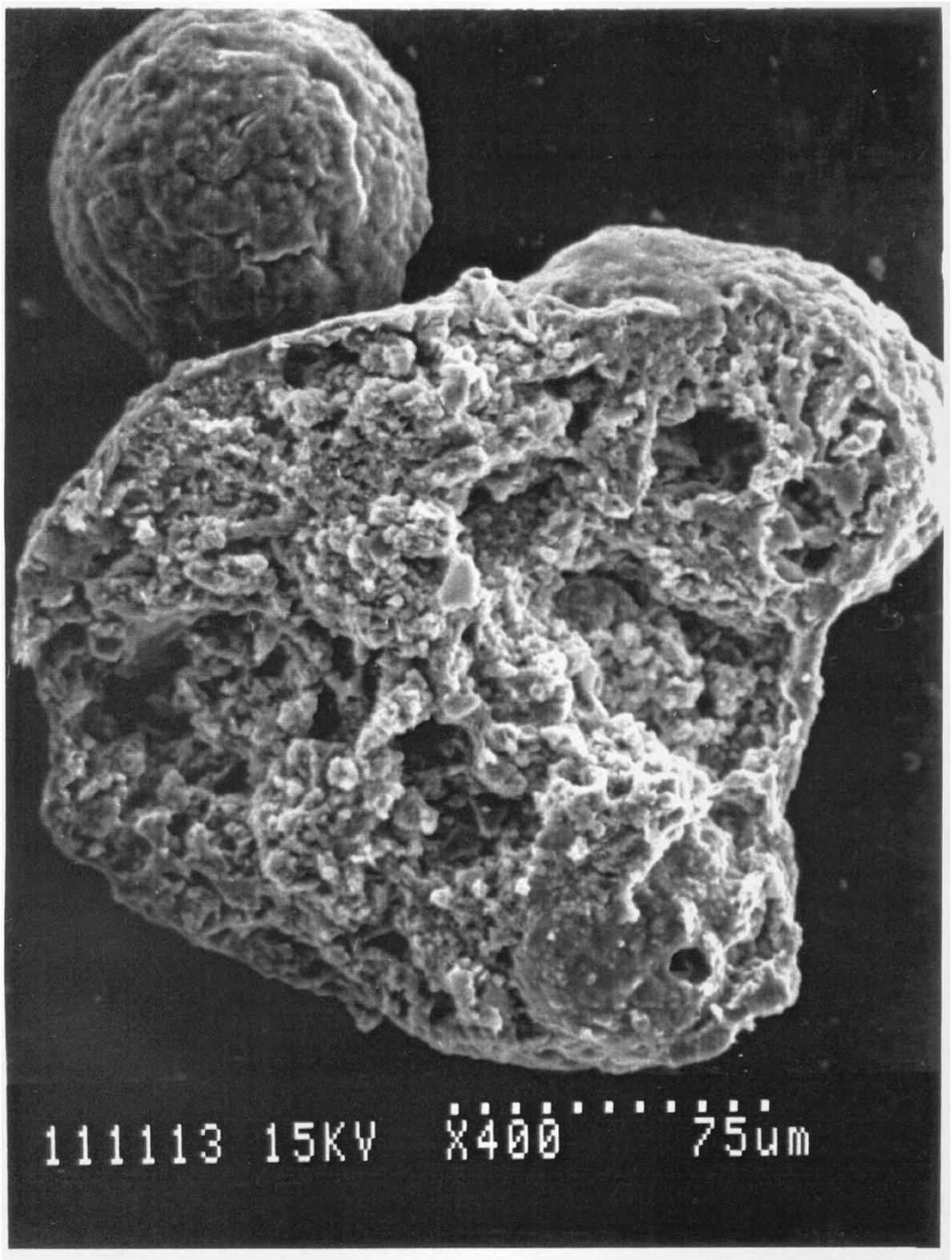

Figure 5.14 SEM photograph showing the interior of a fresh super–D catalyst particle.

The principle of the scanning electron microscope. A succession of lenses produces a finely focused electron spot on the specimen, giving rise to an electron emission signal which is collected and amplified. This amplified signal modulates the brightness of a cathode ray tube. The electron spot and the c.r.t. spot are scanned in synchronism across the specimen and the tube face respectively. A microscope results whose magnification is the ratio of scanned dimensions on specimen and c.r.t.

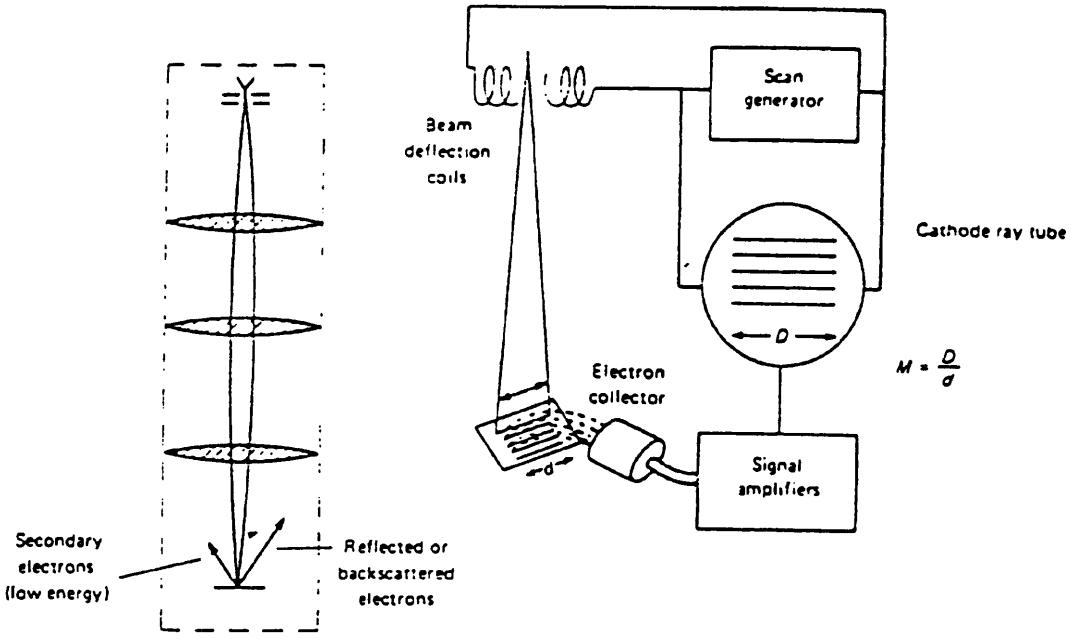

Figure 5.15 The principle of the scanning electron microscope. (Khalaf (1988)).

between the dimensions of the final image and the field scanned on the specimen". Keeping the size of the display constant, the magnification can be changed by altering the extent of scan on the specimen. In practice, the magnification switch on the SEM changes the angle through which the beam is deflected. The linear extent of the scan depends on the working distance of the specimen from the final lens.

5.4 RESULTS OF THE CUMENE CRACKING EXPERIMENTS:

5.4.1 Results of the "Blank" Run:

The results of the thermal cracking experiments revealed that up to the reaction temperature of 500 °C, no significant conversion of cumene occurred (<2%, Table 5.2). This result agrees closely with observations on work carried out using the same catalyst in a fixed bed reactor at a similar reaction temperature (Moore, 1983; Thomson, 1984) and in a fluidised bed reactor (Thomson, 1986).

Table 5.2

Thermal Cracking of Cumene at Different Reaction Temperatures:

Time on stream	% Conversion at		
(Minutes)	475 °C (A)	500 °C (B)	525 °C (C)
2 10 120	1.55 1.28 1.48	1.73 1.92 1.65	2.93 2.45 2.71
Average	1.44	1.77	2.70

(A) The liquid product consisted of ethyl benzene mainly with traces of toluene, besides the unreacted cumene.
(B) The liquid product consisted of ethyl benzene and toluene besides the unreacted cumene.
(C) The liquid product consisted of ethyl benzene, toluene besides traces of unknown peaks in the chromatogram.

N.B: Feed flow rate was fixed at 1.0 g/min for all thermal cracking runs.

The material balance for cumene over the reactor system showed interesting results. Comparison of the input (feed) flow rate of cumene to the reactor with the liquid "product" (Fig. 5.16) shows that initially these two rates were not equal (for t<10 minutes), but with increased time–on–stream the product flow rate "levelled off" at a value very close to that of the input flow rate. A material balance on the system assuming no thermal cracking losses was within 4%, which when allowing for errors in input and product flow rates measurements, demonstrated that no significant losses of cumene were incurred during the cracking reaction. A fraction of these losses could be attributed to an "initial wetting period" within the reactor, where the cumene is adsorbed onto the "dry" surfaces of the reactor components.

These results show that the overall conversion of cumene can be predicted accurately from the liquid product stream, but if it is assumed that for the whole of the time–on–stream the product flow rate is equal to the input flow rate, serious errors in the overall conversion predictions will result at short times. Thus, this result will form the basis for the calculation of the overall conversions obtained during the catalytic cracking.

5.4.2 Catalytic Cracking Results:

5.4.2.1 Cumene Conversion:

The cumene conversion (defined as the moles of cumene reacted per mole of cumene fed to the reactor at any time) was calculated for different catalyst:feed ratios and at different times on stream. The catalyst:feed ratios studied in the fluidised bed reactor ranged from 1:1 to 100:1 (g–catalyst:g–feed/min) with time–on–stream varying from 1 minute up to 120 minutes.

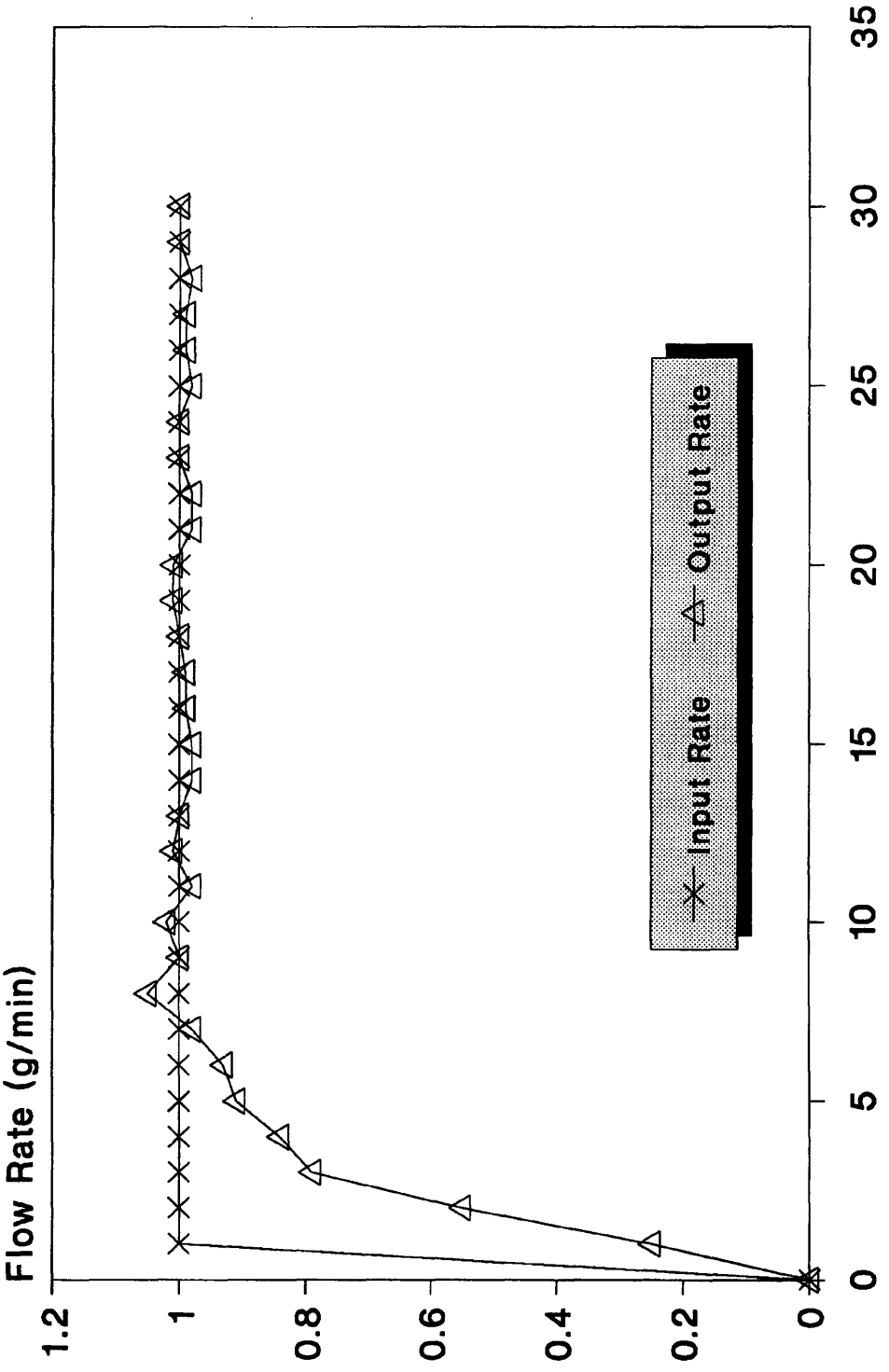

Figure 5.16 Material balance for cumene in a typical 'Blank Run'.

5.4.2.1.1 Calculation of the Differential and Integral Conversions of Cumene:

The conversion of cumene was calculated from a mass balance over the cracking reactor. The dynamic behaviour of the cracking unit was studied in the absence of any catalytic cracking (i.e. blank runs with no catalyst present) to determine the amount of liquid collected at various times–on–stream. Using data collected during the blank and cracking runs, differential conversion was calculated according to the following equation:

$$X_d(t_i) = \frac{\text{no. of cumene moles converted}}{\text{no. of cumene moles collected in blank run}} \tag{5.10}$$

$$X_d(t_i) = \frac{P_b(t_i) - [P(t_i)\ X_c(t_i)]}{P_b(t_i)} \tag{5.11}$$

where

$X_d(t_i)$: differential conversion of cumene in the time interval t_i

$P_b(t_i)$: mass of liquid product collected during the blank run in the time interval t_i,

$P(t_i)$: liquid product collected in the time interval t_i

$X_c(t_i)$: mass fraction of cumene in the liquid product collected in the time interval t_i, and

t_i :time interval between any two times t_1, t_2 within which liquid product samples collected.

The integral conversion of cumene at any time (t) is calculated according to the following equation:

$$X_i(t) = \frac{\sum_{i=1}^{n} P_b(t_i) - \sum_{i=1}^{n} [P(t_i)\ X_c(t_i)]}{\sum_{i=1}^{n} P_b(t_i)} \tag{5.12}$$

where

$X_i(t)$:integral conversion of cumene at time t

n :total number of time intervals through which n liquid product samples were collected in t time.

5.4.2.1.2 Results of the Cumene Conversion Experiments:

Figure 5.17 shows the differential conversion profiles for the different catalyst:feed ratios, namely, 1:1, 5:1, 15:1, 25:1, 50:1 and 100:1. The plots show a large drop in the conversion for the first 10 minutes on stream for all catalyst:feed ratios. The following 10 minutes show a moderate drop in the conversion followed by a very slow and gradual decline over the period from 20 to 120 minutes on the stream. For a catalyst:feed ratio of 100:1, the differential conversion of cumene drops from about 95% to 60% in the first 10 minutes compared to 17% drop over the next 10 minutes on stream with a drop of only 13% in the conversion over the remaining 100 minutes on stream. As the catalyst:feed ratio decreases, the conversion decreases accordingly. The conversion of cumene after 2 minutes on stream is 85% for a catalyst:feed ratio of 50:1, compared to 64% conversion for catalyst:feed ratio of 15:1 and to only 44% for a catalyst:feed ratio of 1:1.

5.4.2.2 Benzene Selectivity:

5.4.2.2.1 Calculation of the Differential and Integral Benzene Selectivity:

The benzene selectivity "S" was defined as the moles of benzene produced per one mole of cumene converted:

$$S = \frac{\text{no. of moles of benzene produced}}{\text{no. of moles of cumene converted}} \qquad (5.13)$$

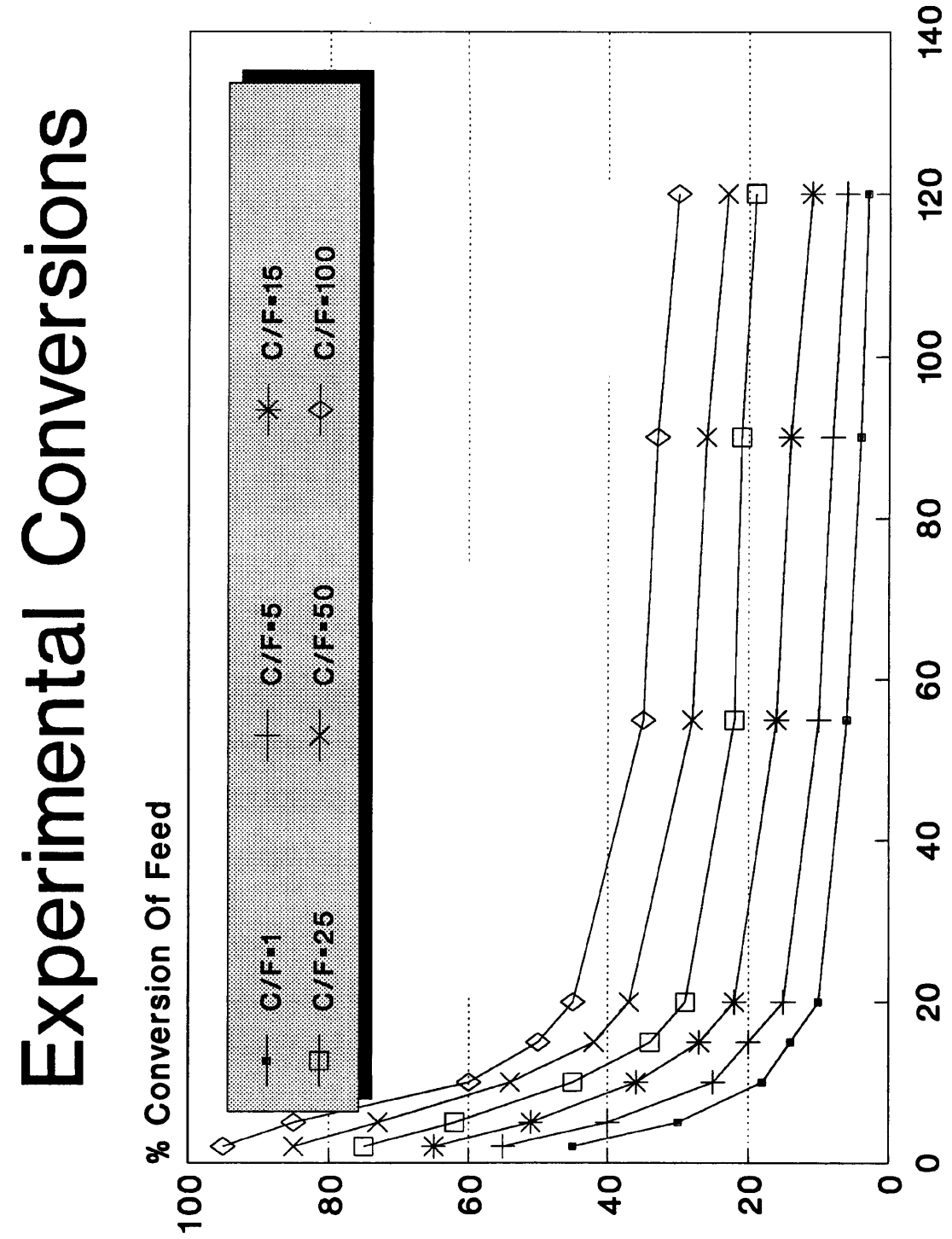

Figure 5.17 The experimental differential conversions.

The differential benzene selectivity is calculated according to the following equation:

$$S_d(t_i) = \frac{P(t_i)\ X_b(t_i)}{P_b(t_i)\ X_c(t_i)} (M_c/M_b) \qquad (5.14)$$

where

$S_d(t_i)$: the differential benzene selectivity in the time interval (t_i),

$X_b(t_i)$: mass fraction of benzene in the liquid product collected in the time interval (t_i),

M_c : the molecular weight of cumene, and

M_b : the molecular weight of benzene.

The integral benzene selectivity at any time (t) is calculated according to the following equation:

$$S_i(t) = \frac{\sum_{i=1}^{n} [P(t_i)\ \ X_b(t_i)]}{\sum_{i=1}^{n} P_b(t_i)} (M_c/M_b) \qquad (5.15)$$

where

$S_i(t)$: the integral benzene selectivity at any time (t).

5.4.2.2.2 Benzene Selectivity Results:

The selectivity of the cracking reaction to the major product benzene has been determined from the off–line analysis of the liquid product. The differential benzene selectivity (defined by the moles of benzene produced per mole of cumene reacted in the time interval) is plotted as a function of the differential conversion of cumene (Fig. 5.18).

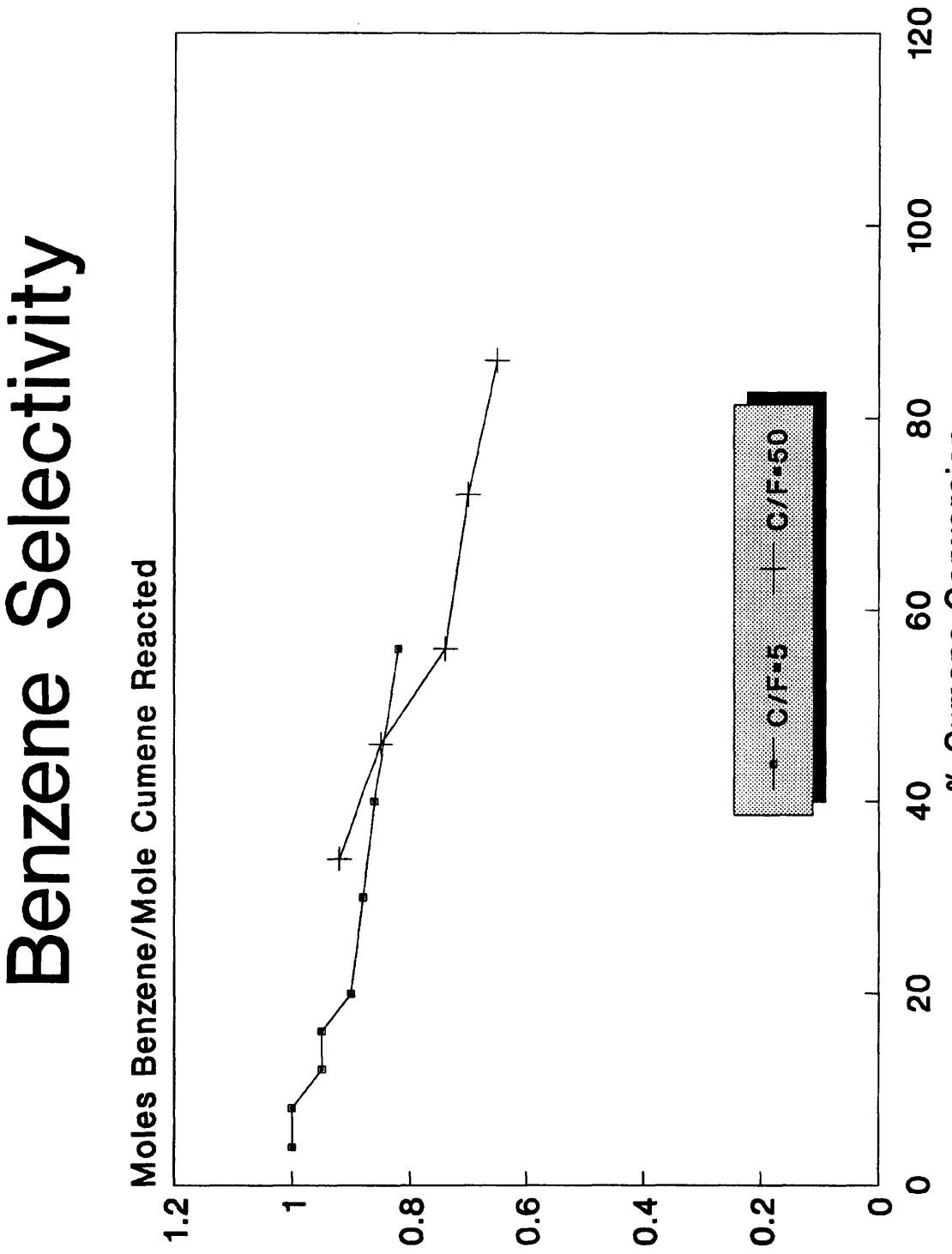

Figure 5.18 The experimental differential benzene selectivity.

It seems that at the reaction temperature of 500° C the very high activity of the catalyst initially produces low benzene selectivity. The effect of deactivation is shown to increase the benzene selectivity in comparison with that of fresh catalyst. The application of these observations can be very useful in selecting the appropriate degree of deactivation which improves the performance of the "equilibrium catalysts" to produce the product of interest. In practice, the FCC catalysts are treated to lower their initial activity in order to improve their selectivity towards the desired products.

5.4.3 Coke Content Results:

Figure 5.19 shows the % coke content of the catalyst at different times on stream for the different catalyst:feed ratios. It is clear that the coke content of the catalyst is dependent on both the time on stream and the catalyst:feed ratio. For all catalyst:feed ratios, the coke content increases with time on stream, but the rate of coking decreases as time goes on. The rate of coke deposition is very fast when conversions are high, which is typical for the series (consecutive) mechanism of coking. As the catalyst deactivates, the conversion drops and the rate of coking decreases significantly. The coke content of the catalyst increases as the catalyst:feed ratio increases. This relationship becomes stronger at longer times on stream.

5.4.4 Total Surface Area Results:

Figure 5.20 Shows the % surface area of the catalyst as it deactivates with time on stream for different catalyst:feed ratios. Similar to conversion profiles, the surface area of the catalyst drops sharply for times on stream up to 10 minutes followed by a moderate drop for times up to 20 minutes on stream. For longer times, the rate of loss of the catalyst surface area is very small. The drop in the catalyst surface area increases as the catalyst:feed ratio increases. This relationship is attributed to the larger amounts of coke deposited on the catalyst as the catalyst:feed ratio increased.

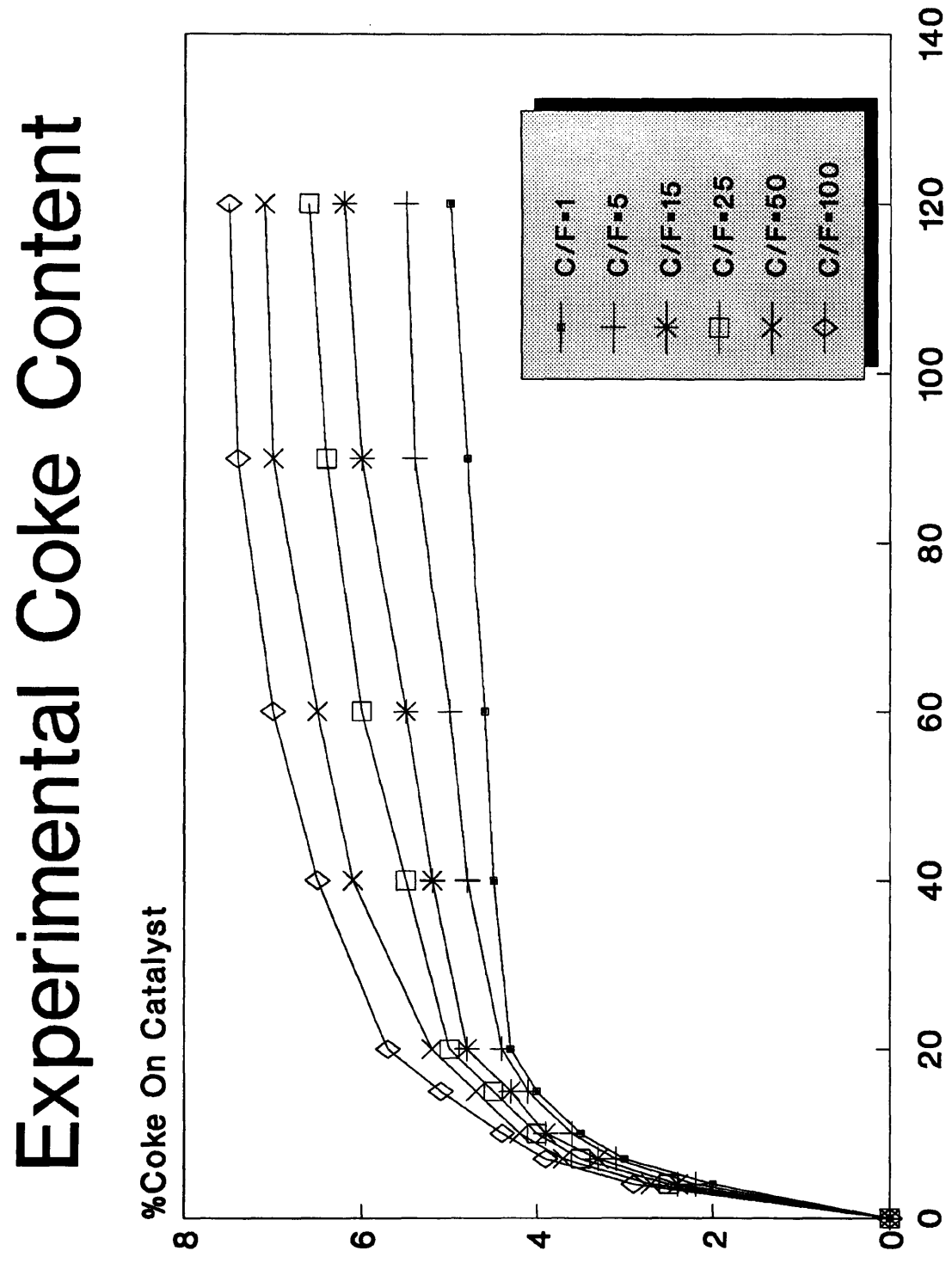

Figure 5.19 The experimental coke content profiles.

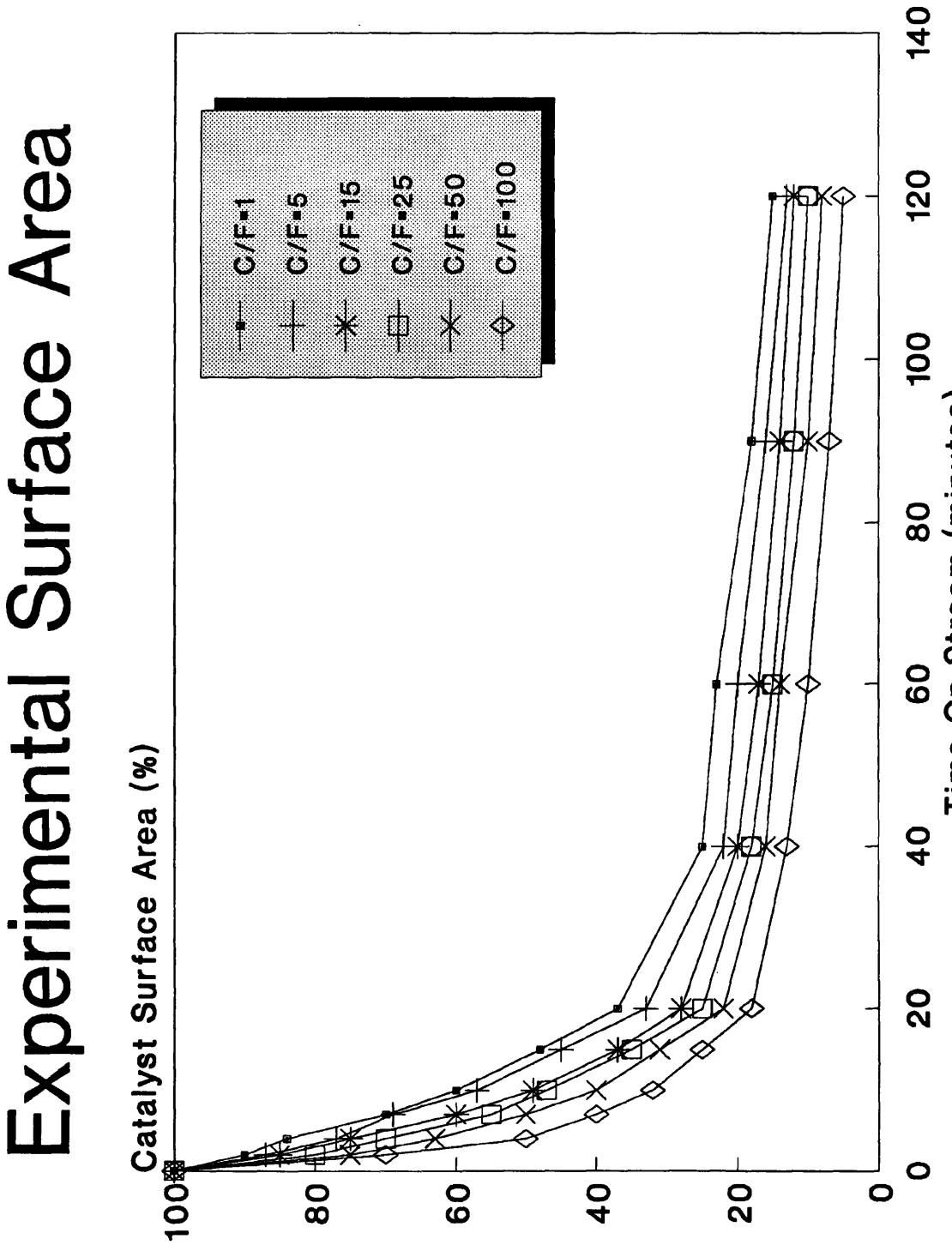

Figure 5.20 The experimental total catalyst surface area.

5.4.5 SEM Results:

SEM samples prepared for the catalyst under investigation at different stages of coking and were studied under various magnifications. Figures 5.21 to 5.27 show some photographs of the coked super–D catalyst, from cumene cracking experiments with catalyst:feed ratio of 25:1, after short and long term deactivation (10 and 120 minutes on stream). There was an apparent drop in the number of pore spaces on the surface of the coked catalyst particles in comparison with the fresh catalyst (Fig. 5.22 to Fig. 5.25). This was probably an indication of the blockage of some pores due to heavy coking. Also, the remaining pores on the surface of the coked catalyst were apparently smaller in size for the catalyst sample which has undergone longer term deactivation in comparison to the sample which has undergone short term deactivation. This may be the result of the coking of the support pores of the catalyst which occurs at longer times on stream, while the zeolite micropores are thought to be coked at short times on stream (Moore, 1983; Thomson, 1986).

A close observation revealed that the short and long term deactivation caused some catalyst particles to be less spherical than the fresh catalyst, while the long term deactivation caused some catalyst particles to become apparently agglomerated (Fig. 5.26 and Fig. 5.27).

5.5 DISCUSSION OF EXPERIMENTAL APPARATUS AND METHOD:

The cumene cracking experiments carried out in the laboratory scale fluidized bed reactor were successful to a reasonable extent in meeting the aims of the project despite a number of difficulties. The major problems encountered are listed below. These should be useful in the design of future systems for the study of this and other similar reactions. Also, the possible sources of error are discussed.

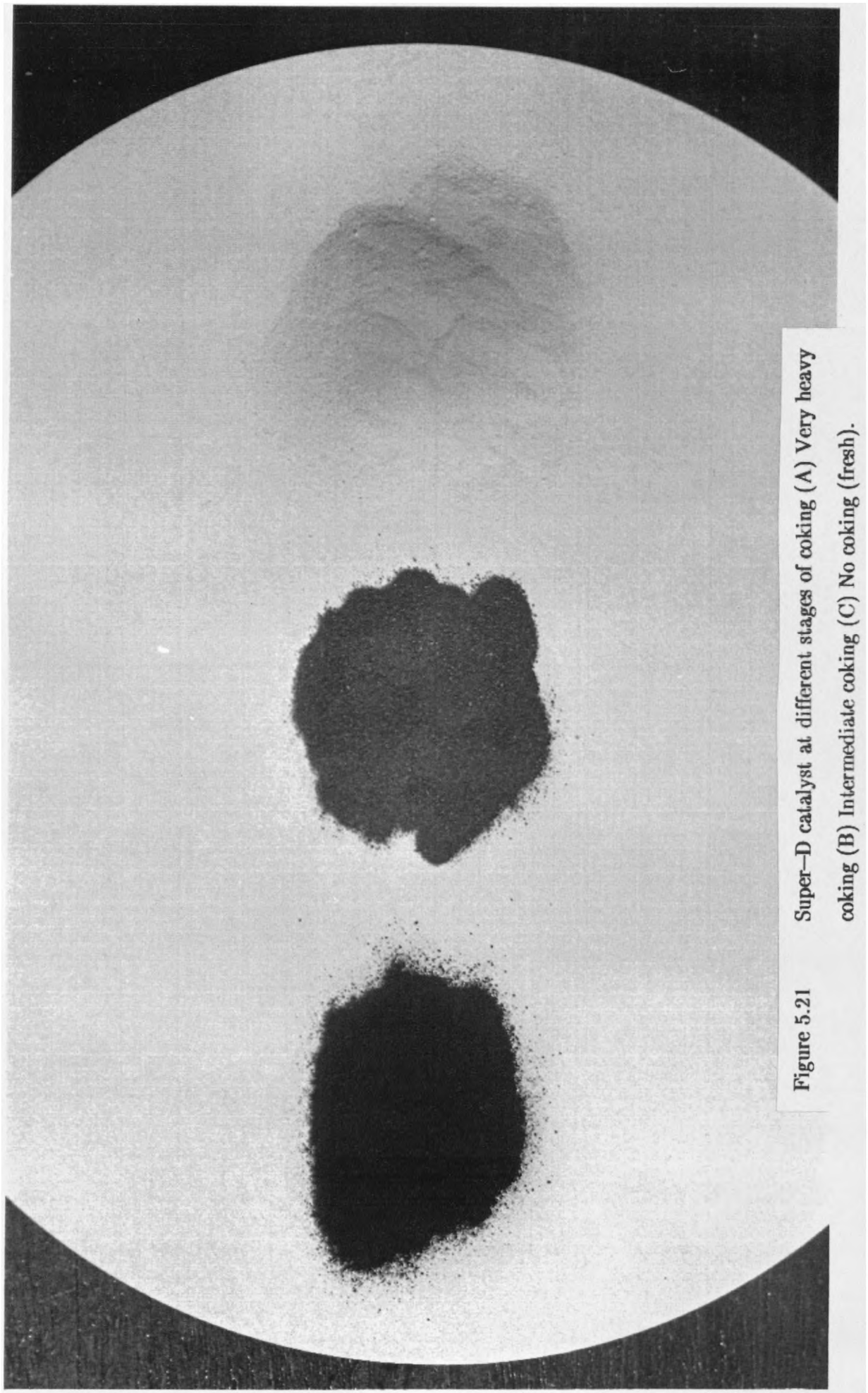

Figure 5.21 Super–D catalyst at different stages of coking (A) Very heavy coking (B) Intermediate coking (C) No coking (fresh).

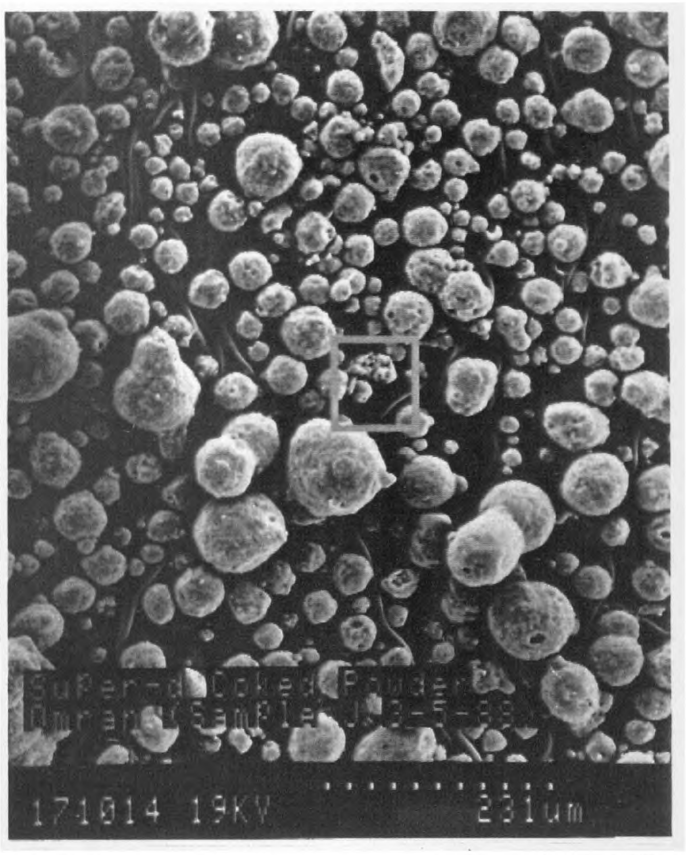

Figure 5.22 SEM photograph of coked super–D particles after 10 minutes on stream.

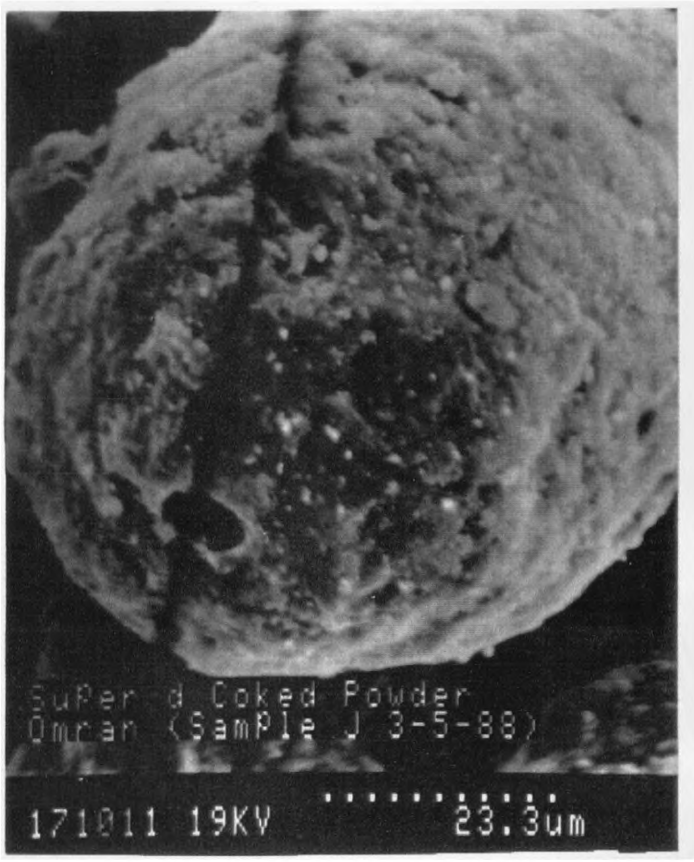

Figure 5.23 SEM photograph of a coked super–D particle after 10 minutes on stream.

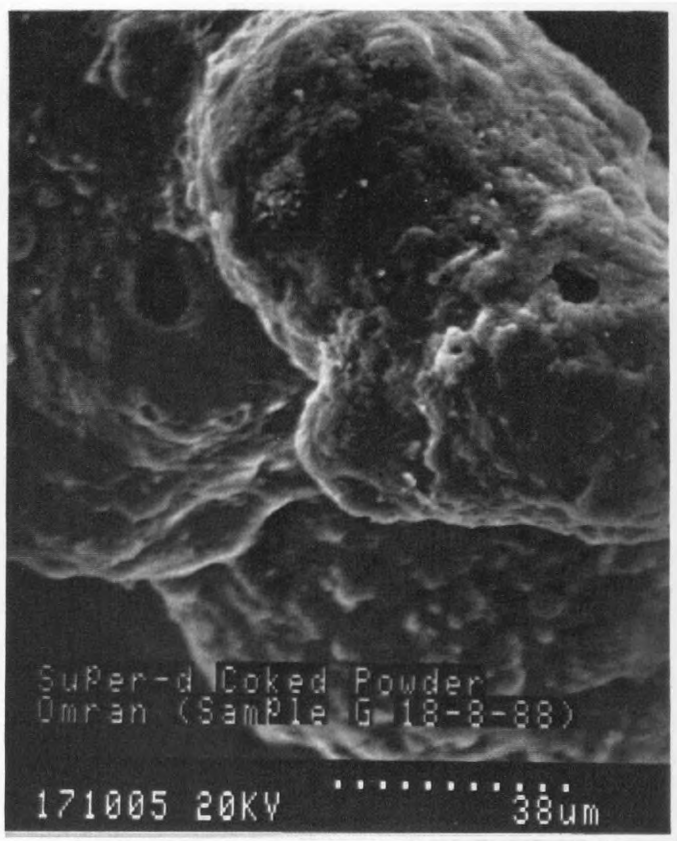

Figure 5.24 SEM photograph of coked super–D particles after 2 hours on stream.

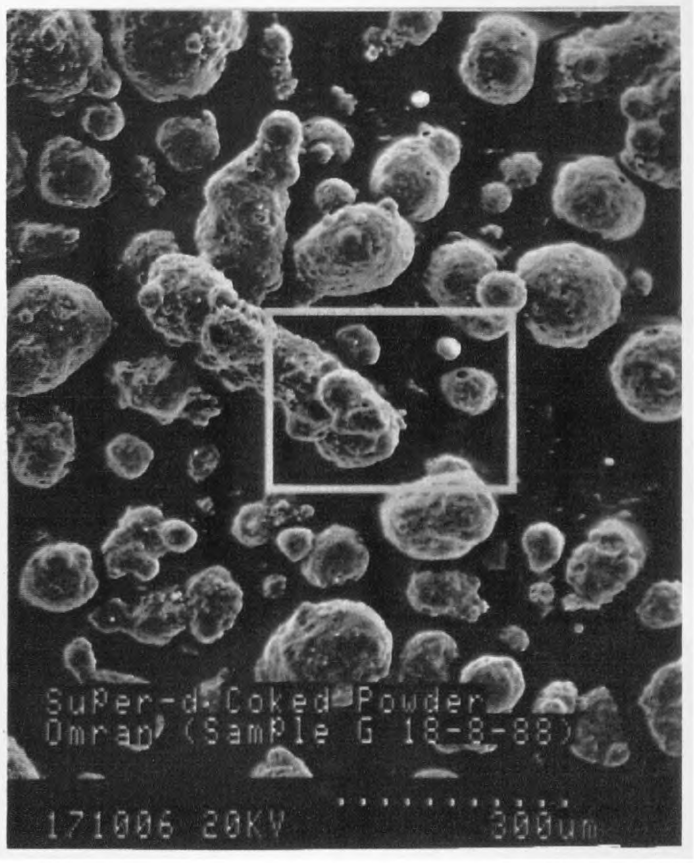

Figure 5.25 SEM photograph of coked super–D particles after 2 hours on stream.

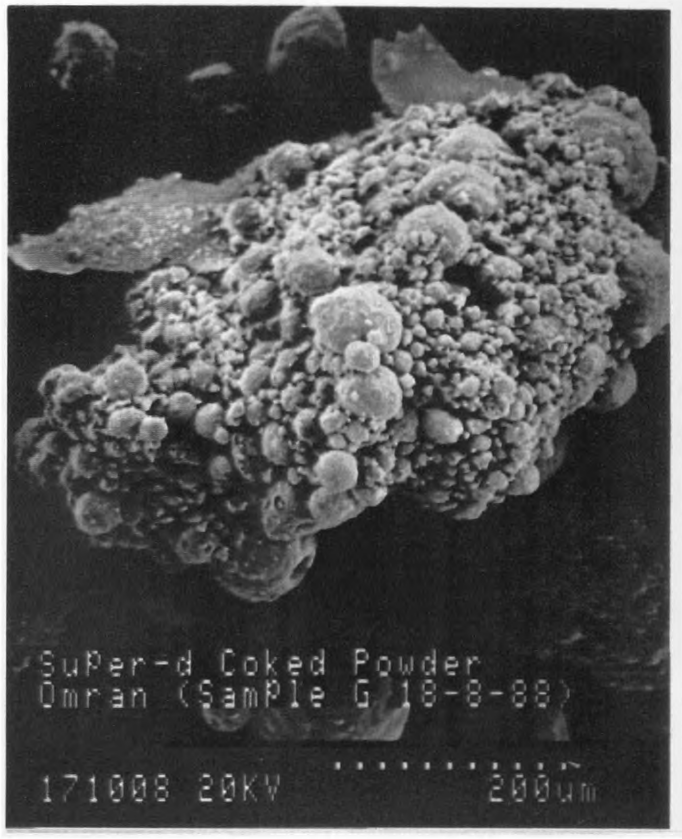

Figure 5.26 SEM photograph showing traces of catalyst particles' agglomeration after 2 hours on stream.

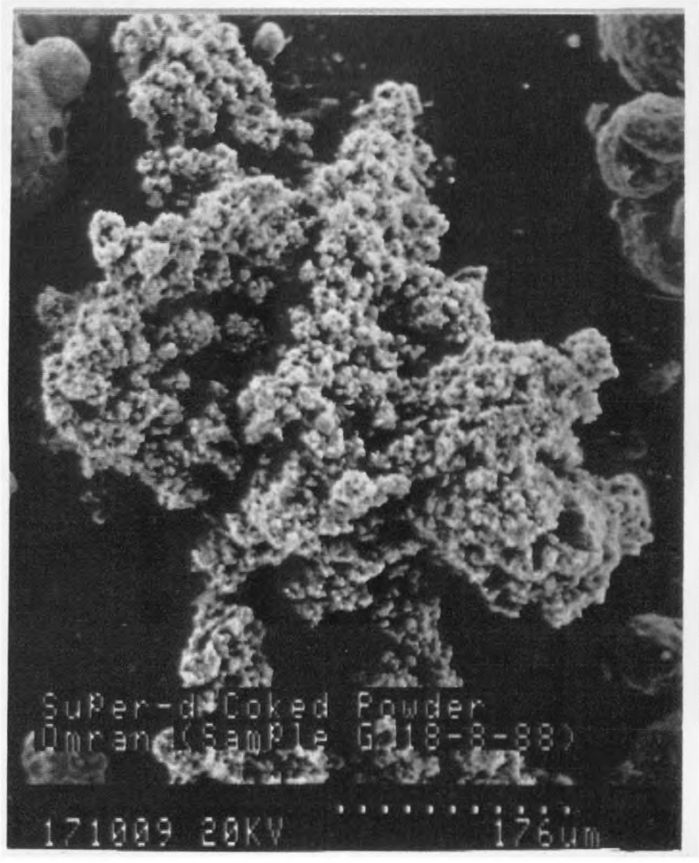

Figure 5.27 SEM photograph of coked super–D catalyst particles' agglomeration after 2 hours on stream.

5.5.1 Difficulties Encountered:

(1) The catalyst used in the experiment super–D was in the powder form consisting of very small particles of an average size of 84 microns. This caused some very fine particles to be carried over with the products during the reaction especially at higher feed rates or with the nitrogen while purging the system at the beginning and the end of the experiments.

(2) Due to the small size of the reaction zone of the reactor, only a small amount of catalyst was used (5–10 grams). Then it was possible that some of the feed might be by–passing the catalyst.

(3) Two different pumps were used in feeding the reactor with cumene. The syringe pump (The Perfuser) was very precise and gave reproducible flow rates to within 1% but because of its small capacity (50 ml) it was used for feed flow rates of less than 0.5 gm/min. A peristaltic pump had to be used for higher feed flow rates ($\geq$0.5 gm/min) which was not able to maintain steady feed rates, and variations of up to 4% from one reading to another were encountered.

5.5.2 Errors in Product Analysis:

Errors in the analysis were due to a number of sources:

(1) Difficulties in measuring the amount and composition of liquid product collected. It is probable that some of the very volatile components of the liquid product evaporated during the time it was collected to the time it was analysed. To reduce this effect, the product samples were collected in air–tight bottles and stored in a refrigerator until time of analysis.

(2) The liquid product of the cumene cracking was assumed to consist of only the four major products, regardless of the fact that over 18 primary and secondary products of cumene cracking were reported by Best and Wojciechowski (1977)

and others. It would have taken an impractically long time to identify every product component especially in the first few minutes when the catalyst is most active.

(3) Uncertainties associated with the liquid product composition measurements using chromatography. It has been estimated that the accuracy was to within ±2% by repeated measurements of the composition for the same sample.

(4) The estimated weight of coke in the product catalyst was not very accurate due to the loss of some fraction of it when filling and emptying the reactor. Also, the zeolite catalyst is a strong adsorbent which increases the possibility of gaining some weight due to substances other than coke.

5.5.3 Errors in Temperature Measurements:

Temperature measurements were, also, subject to uncertainty. Even though the Think Lab system could, in principle, measure temperatures to ±0.2°K, the measurements were likely to be less reliable due to the following reasons:

(1) The thermocouples used were of fine quality. But because of the probability of them not being rested centrally in the catalyst bed, any radial temperature gradients would then affect the measurements.

(2) Although a temperature controller (Eurotherm–810) was used to keep the reactor at constant reaction temperature, it was observed that the temperature in the reactor varied over a range of ±7°K. This was an indication of non–uniform rate of heat supply to the reactor.

CHAPTER SIX

APPLICATION OF THE THEORY

CHAPTER SIX

APPLICATION OF THE THEORY

6.1 INTRODUCTION:

Applying the theory developed in Chapter Two and using the explorations and examples of Chapter Three and Chapter Four as a general guide, an attempt to model the observed deactivation behaviour will now be presented.

6.2 REPRESENTATION OF THE CATALYST SUPPORT STRUCTURE:

The catalyst support pore structure was represented by two different pore models, namely, the corrugated parallel bundle model (Fig. 6.1) and the stochastic pore network model (Fig. 6.2).

6.2.1 Pore Size Distribution:

For both catalyst support pore structures, the catalyst had pore sizes which were assumed to be uniformly distributed in the range between 60–3200 Angstroms. The corresponding pore number and pore volume distributions for the corrugated parallel bundle model and for the network model are given in Figures 6.3 and 6.4.

The micropore volume contained within the zeolite is not included in the distribution presented here. The contribution of the zeolite to the overall pore volume of the catalyst is 0.04 cm^3g^{-1} compared to a contribution of 0.16 cm^3g^{-1} by the catalyst support, whereas, the zeolite contribution to the catalyst's total surface area is 100 m^2g^{-1}, i.e. approximately 67% of the catalyst's overall surface area is contained within the zeolite micropores (Manufacturer's figures).

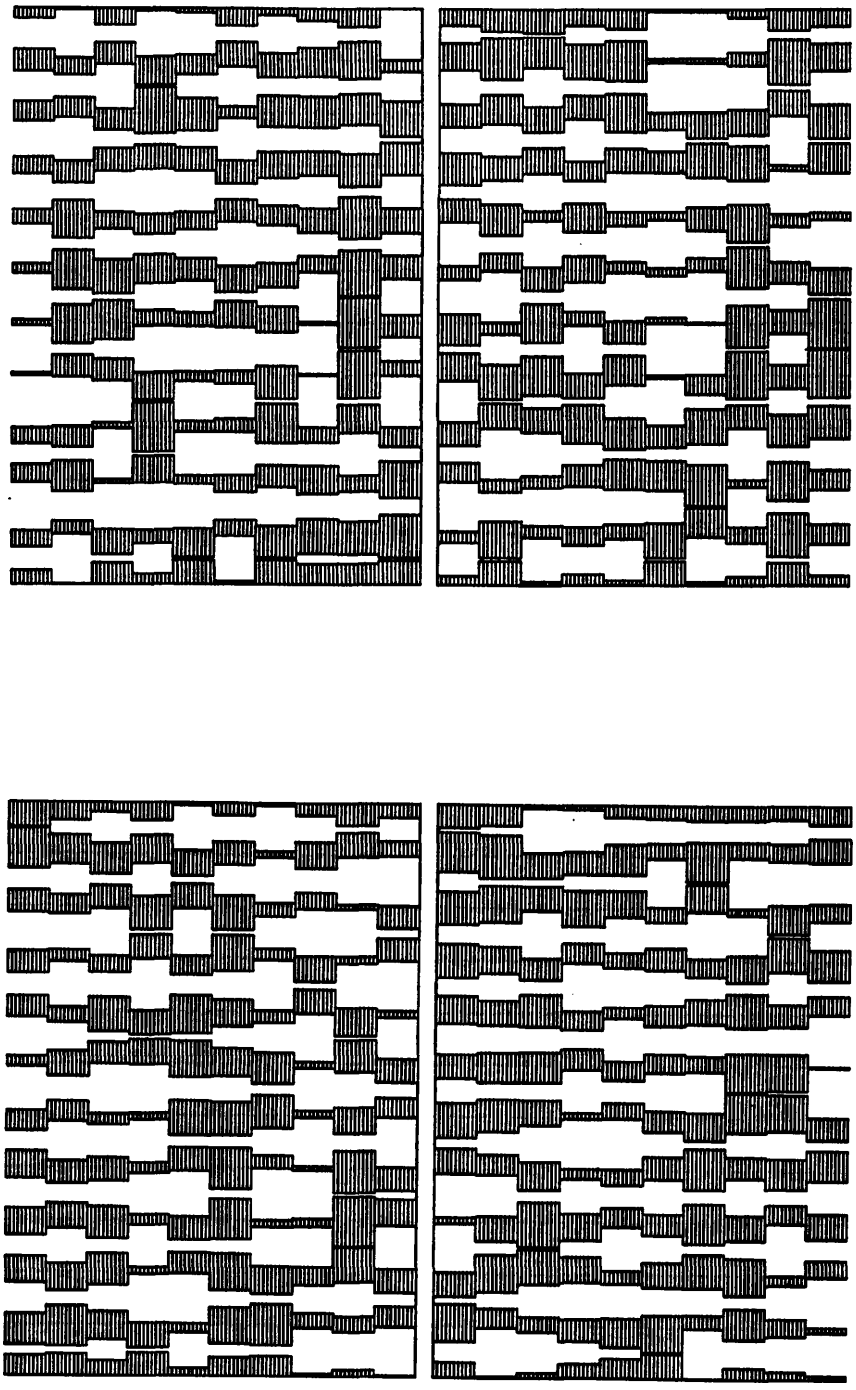

Figure 6.1 Different pore assemblies of the corrugated parallel bundle pore model with the same PSD (60–3200 Angstrom).

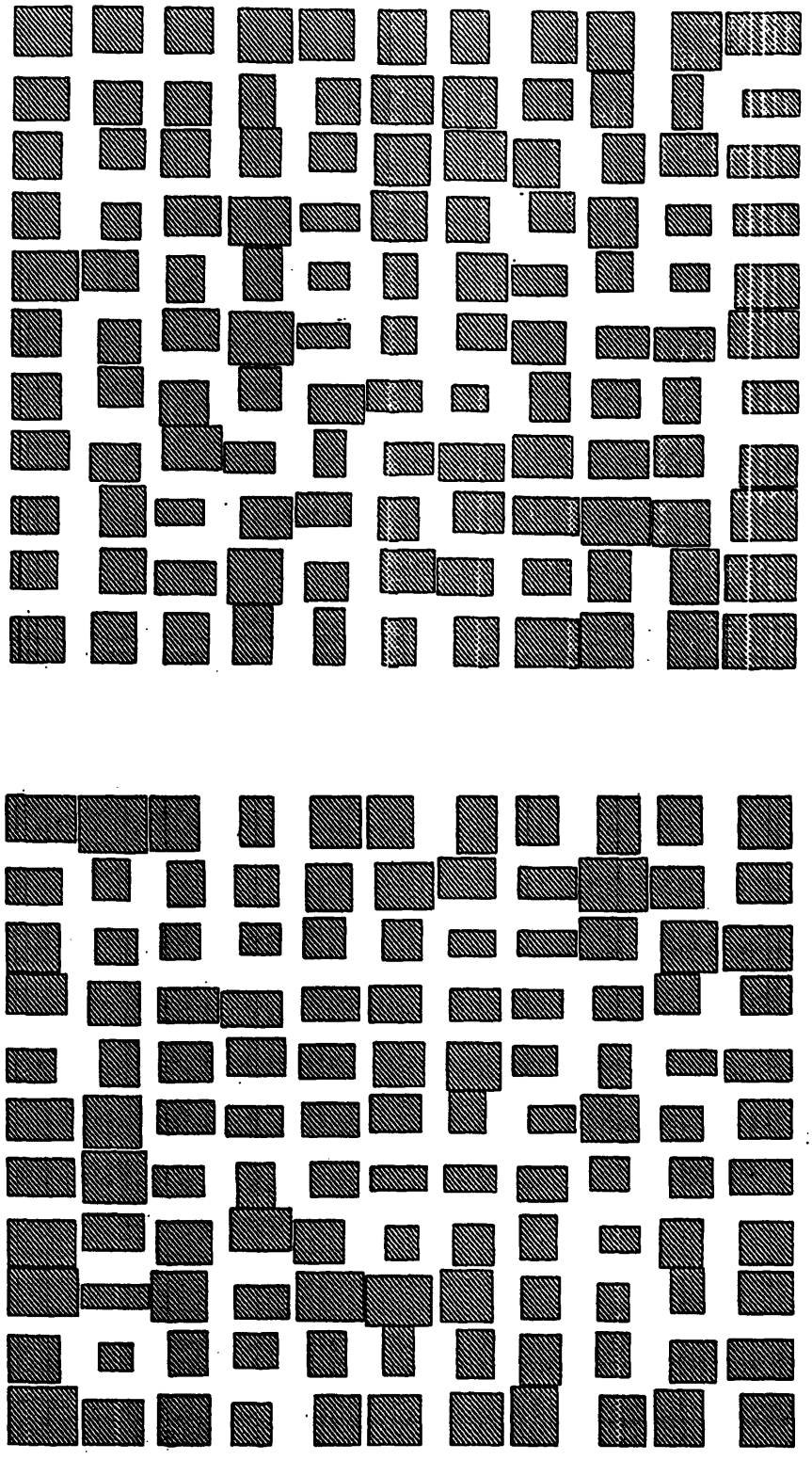

Figure 6.2 Different pore assemblies of the network model with the same pore size distribution (60–3200 Angstrom).

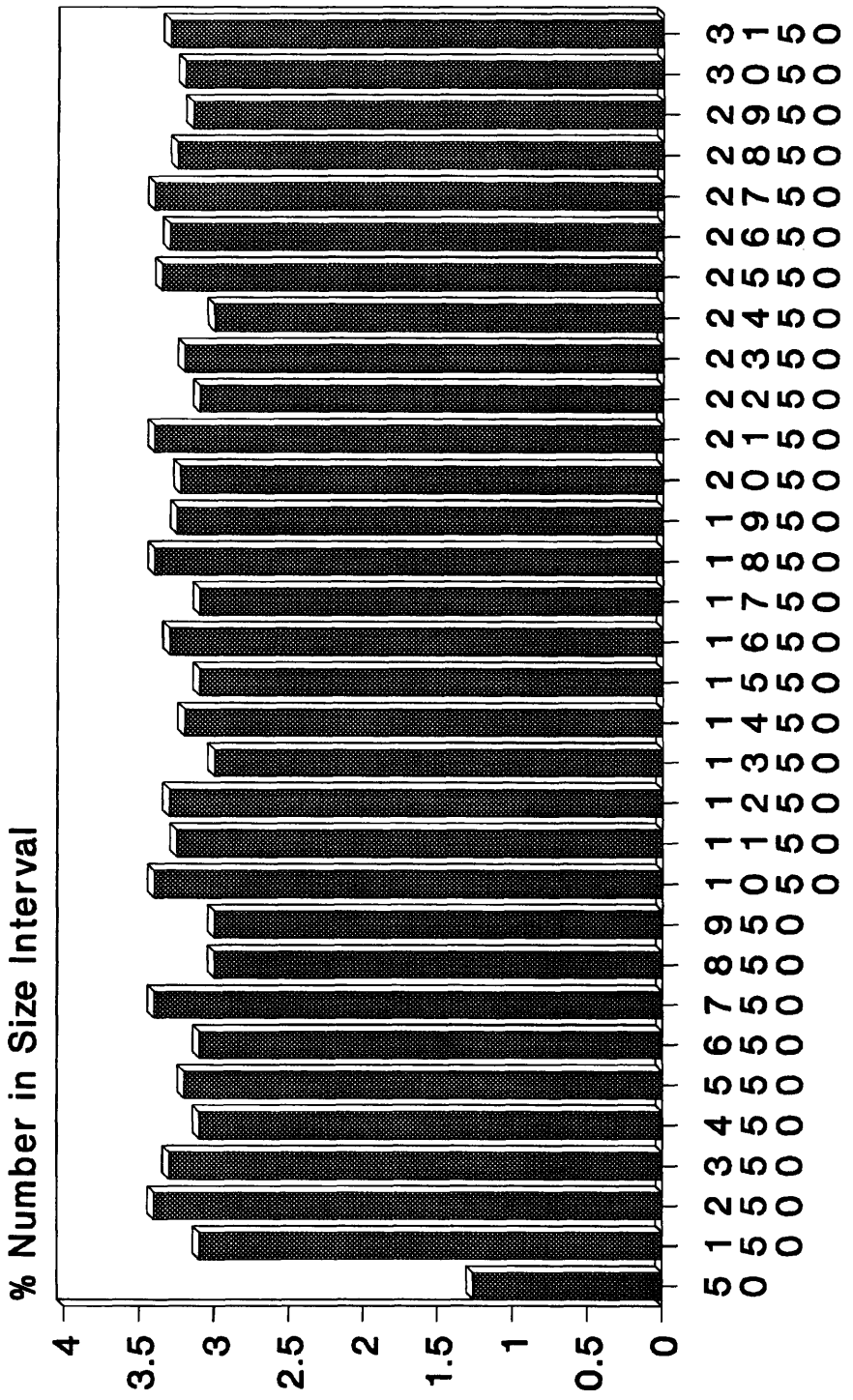

Figure 6.3 Number distribution of pore radii for both pore models.

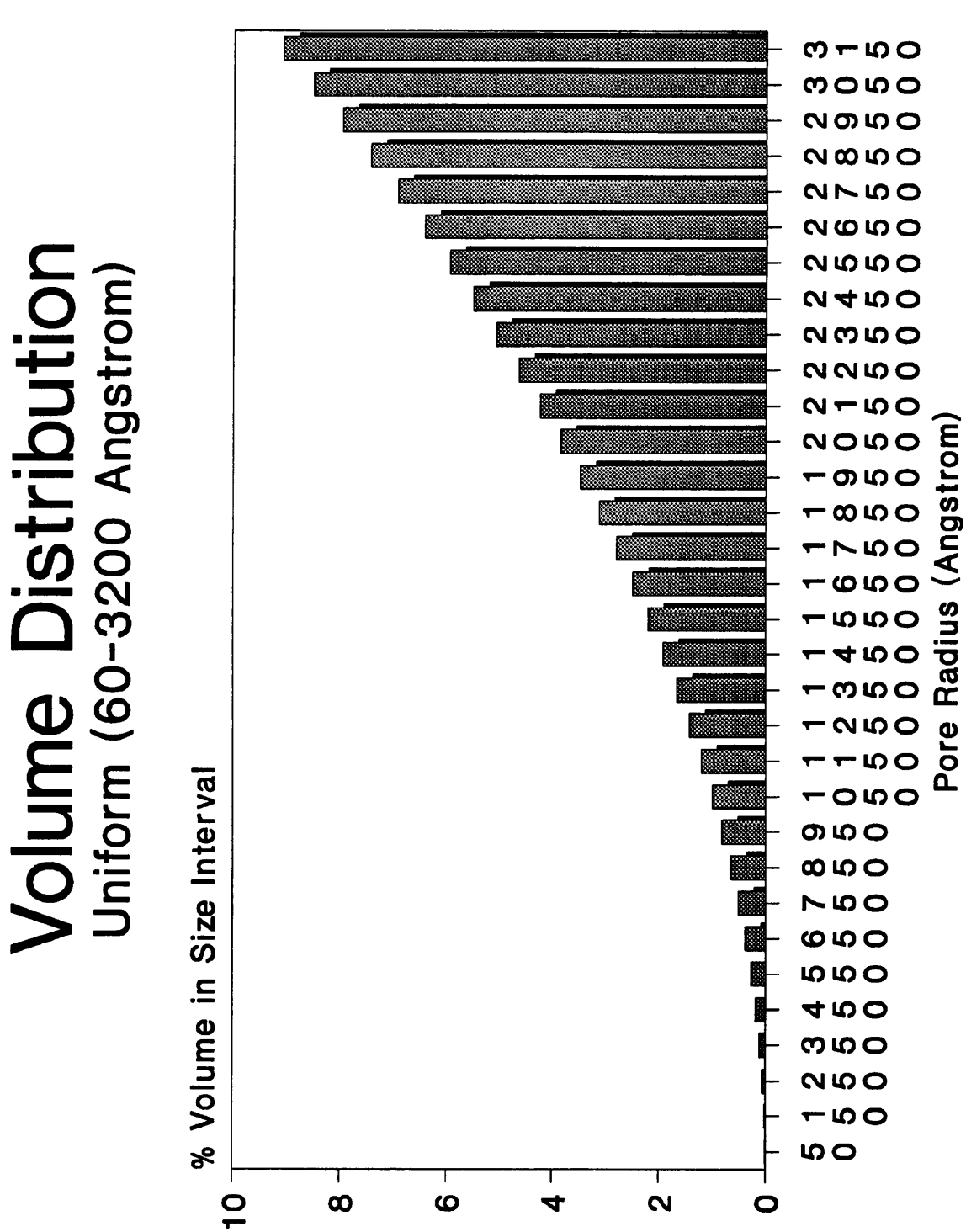

Figure 6.4 Volume distribution of pore radii for both pore models.

6.2.2 Parallel Bundle Pore Length:

For both structural models, the equivalent parallel bundle pore length (equal to the network side length), L, was calculated from the following equation (5.1) given by Levenspiel (1972):

$$L = \frac{\text{volume of the catalyst particle}}{\text{exterior surface area of the catalyst particle}} \qquad (5.1)$$

From scanning electron microscope (SEM) figures it was clear that the catalyst particles were close to spherical, so is given by:

$$L = \frac{R}{3} \qquad (5.2)$$

where R is the radius of the particle.

In order to obtain a value for R, the diameter of one hundred catalyst particles were measured from SEM images. The mean diameter found was 84 microns. Substituting back into equation (5.2) produced a value for the pore length (network side) of about 14 microns.

6.3 DETERMINING THE DEACTIVATION MECHANISM:

Deactivation in catalysts, whether by poisoning, fouling, aging or solid state transformations, can occur by one or more of the different mechanisms already explained in Chapter One, namely, series, parallel, triangular or side–by–side. In the case of the deactivation of the supported zeolitic catalyst, super–D, by coke laydown during the disproportionation of cumene in a laboratory scale fluidised bed reactor, the deactivation mechanism appears to be series. A close examination of the experimental results (Figures 5.17 to 5.20) shows clearly that at high conversion levels, the coking

rates implied by the slope of the coke content profiles, were largest, whereas at low conversion levels, the coking rates were smaller. This is characteristic of a series coking mechanism.

This agrees with the work of Viner and Wojciechowski (1984) who have shown that in the disproportionation of cumene, the deactivation of a zeolitic catalyst is a series reaction with the foulant being propylene. They further reported that decay in the system was due to propylene adsorbing on two sites and/or two propylenes dimerizing on two adjacent sites. This is also in agreement with the work of Campbell and Wojciechowski (1971) where it was shown by mass balances on reaction products that all the coke formed is due to side chain carbons from the cumene molecule, i.e. propylene. Hightower and Emmett (1965) imply the same conclusion when they report that olefins are more effective poisons than saturated molecules. A more recent work by Acharya et al. (1989) on the kinetics of cumene cracking over a silica–alumina catalyst under deactivation conditions using a thermobalance, showed that the best fit to the experimental data for coking reaction was obtained using a series type coking mechanism.

6.4 APPLICATION OF THE THEORY USING THE CORRUGATED PARALLEL BUNDLE PORE MODEL:

6.4.1 Active Site Poisoning of the Support:

Assuming poisoning of the support active sites by coke laydown, then only the original uncoked support area remains active. When the catalyst is fresh, all the accessible internal surface area of the catalyst support is active. As the coke begins to form and starts to deposit on the support walls, the original uncoked support area begins to reduce drastically causing a large drop in the activity of the catalyst. As the result of the drop in activity of the catalyst, the conversion levels drop accordingly,

and since the coking mechanism is series with the reaction product being the coke precursor, a similar drop in the rate of coking is observed.

6.4.1.1 Conversion Results:

In order to simulate the observed deactivation behaviour, an intermediate catalyst:feed ratio of 25:1 g/g/min was chosen as the starting point from which the fitted deactivation parameters will be used to simulate the other catalyst:feed ratios ranging from 1:1 to 100:1 g/g/min. Initial estimates for the various parameters of the model (k_s, k_{cs}, d, d_z and α) were provided by previous work (Mann, Sharrat and Thomson (1986), and Thomson(1986)). From the explorations and examples given in Chapters Three and Four it became clear that the model was most sensitive to changes in the product (αk_s). The effect of changes in the zeolite coke unit size, d_z, and the series coking rate constant, k_{cs}, was moderate, with the model being least sensitive to changes in the support coke unit size, d.

Extensive fitting was performed using program OMRANCOR (Appendix–1). Figure 6.5 shows the observed deactivation behaviour of the cracking reaction for the catalyst:feed ratio of 25:1 g/g/min, compared with a number of possible theoretical predictions. The best fit that could be achieved with the corrugated parallel bundle model undergoing support active site poisoning was one which produced a good estimation of the conversion for the first few minutes on stream, with the activity being under–estimated for the remaining time on stream. Table 6.1 shows the fitted values of the deactivation parameters. Figure 6.6 then shows the theoretical predictions of the conversion profiles and their experimental equivalents for all the catalyst:feed ratios. They show similar trends with conversion dropping as time on stream increases and as catalyst:feed ratio decreases. The slight initial over–estimation of the conversion predictions for the smaller catalyst:feed ratios may be due to the larger fitted α value which produces larger zeolite activity. But, as soon as the zeolite

Theoretical Conversions
The Corrugated Model

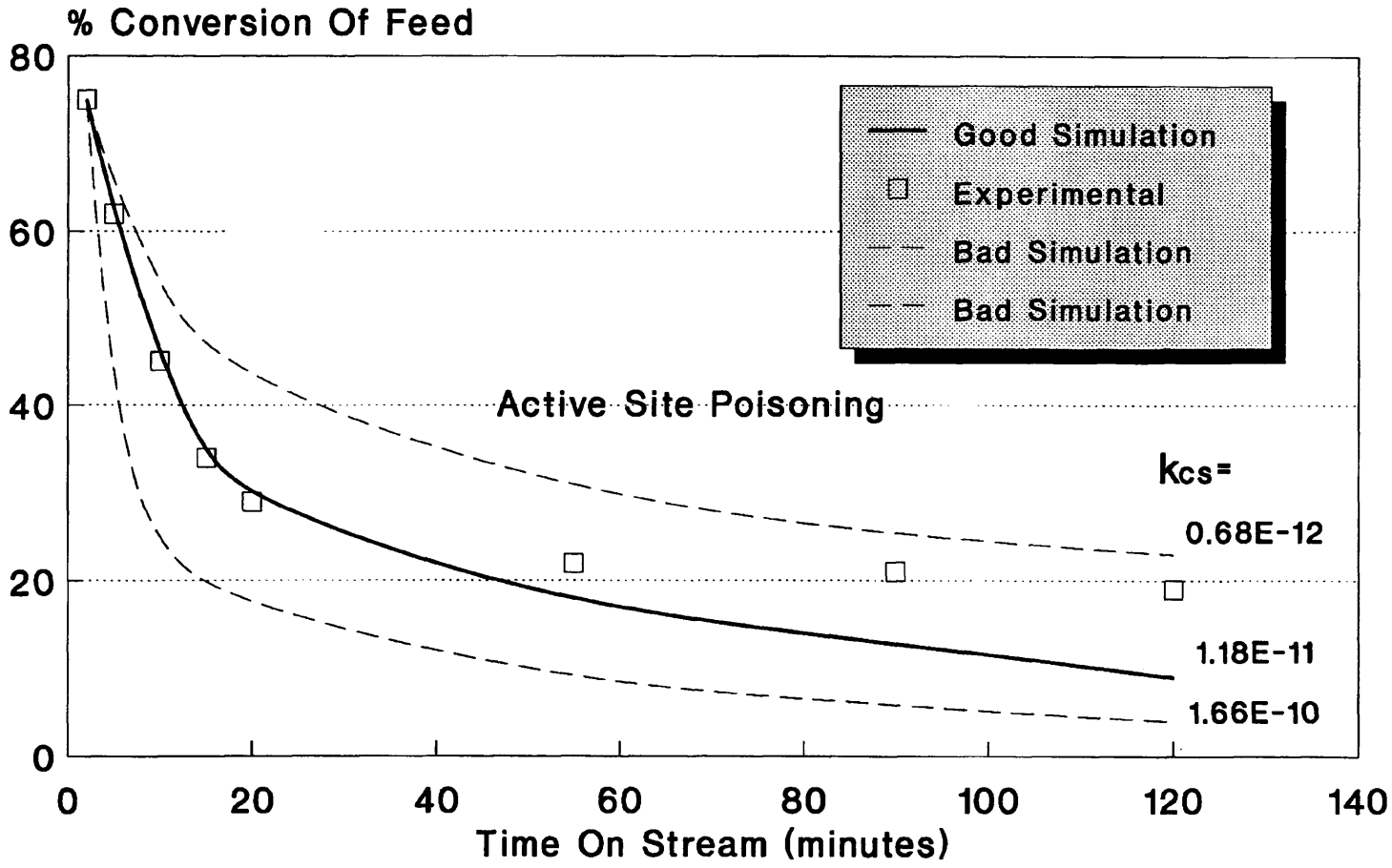

Figure 6.5 The theoretical conversion profiles for C:F=25 for the corrugated parallel bundle pore model.

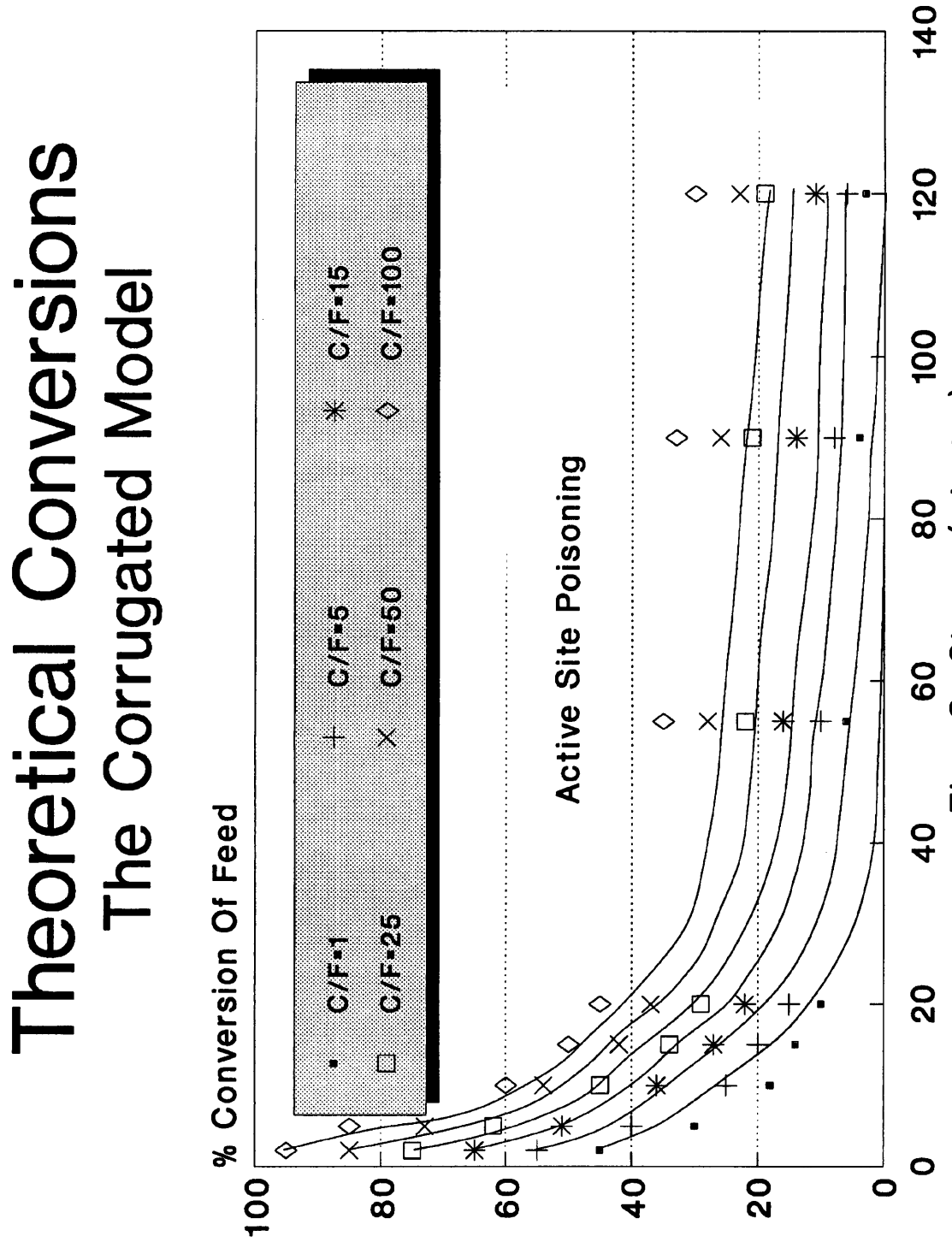

Figure 6.6 The theoretical conversion profiles for the corrugated parallel bundle pore model.

Parameter	Value	
Pore length L	14	Microns
Zeolite coke unit size d_z	1.2	Angstrom
Support coke unit size d	23	Angstrom
Main reaction rate constant k_s	$6x10^{-8}$	(m/s)
Zeolite fractional activity α	0.86	(Initially)
Series coking rate constant k_{cs}	$1.18x10^{-11}$	$m^4kmol^{-1}s^{-1}$
P.S.D.(Uniform Distribution)	60–3200	Angstrom

Table 6.1 Fitted values of the deactivation parameters for the corrugated parallel bundle pore model undergoing active site poisoning.

is lost because of coke laydown inside the micropores or due to blockage caused by coking on the support restricting access to any still active zeolite area, the predicted conversions subsequently become lower than the experimental conversions. The reason for this is the lower activity attributed to the support and the support poisoning causing a drastic reduction in the available active surface area for both the main reaction and the coking reaction.

6.4.1.2 Coke Content of the Catalyst:

Figure 6.7 shows the predicted coke content profiles and their experimental equivalents. They show similar trends with the coking rate decreasing as the time on stream increases. Also, they both show that the coke content of the catalyst increases as the catalyst:feed ratio is increased. However, the theoretical coke content profiles produce a significant under–estimation for all times on stream with much lower final values of coke content for all catalyst:feed ratios. For the catalyst:feed ratio of 100:1

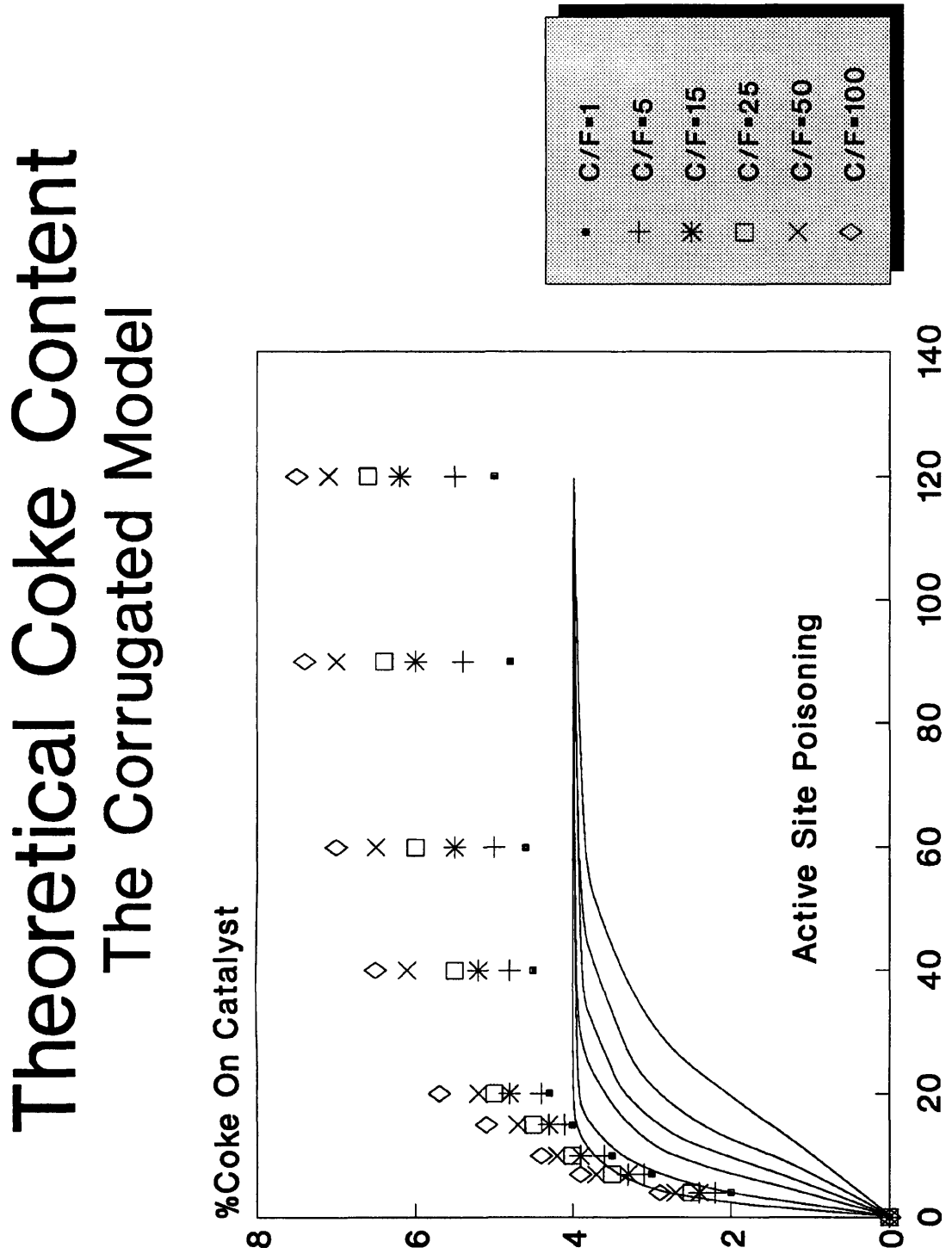

Figure 6.7 The theoretical coke content profiles for the corrugated parallel bundle pore model.

g/g/min the predicted coke content was about 4%, compared to an experimental coke content of nearly 8%.

6.4.1.3 Surface Area of the Catalyst:

Figure 6.8 shows the predicted total catalyst surface area and the experimental results. They show similar trends with the surface area reducing as the time on stream increases. Also, they both show that as the catalyst:feed ratio increases, the total catalyst surface area reduces. Although the theoretical profiles produce a reasonable estimate of the total area for the first few minutes on stream, they diverge from experimental results for longer times on stream producing an over–estimation of the area for all catalyst:feed ratios.

6.4.2 Heavy Support Coking:

From the explorations and examples of Chapter Three and Chapter Four, it became clear that the maximum coke content of the catalyst, assuming the poisoning of the active sites, was just about 4%. Most of the coke was deposited inside the zeolite micropores with a thin layer of coke on the support pores. The experimental coke content results show that coke levels were twice as high as those predicted with the poisoning type of coking, approaching 8%. This clearly shows that the support stays active even when the original surface area is completely covered with a thick layer of coke. Therefore, the definition of the support active area was modified to allow for heavy support coking with the coke units assumed to lay on top of each other. The new definition of the active support area becomes that accessible area even if it is covered with a thick layer of coke as shown in Figure 2.5 in Chapter Two. This allowed for heavy support coking while remaining partially active. Then the catalyst becomes completely deactivated only when the support pores become totally inaccessible due to coking or isolation by blockage.

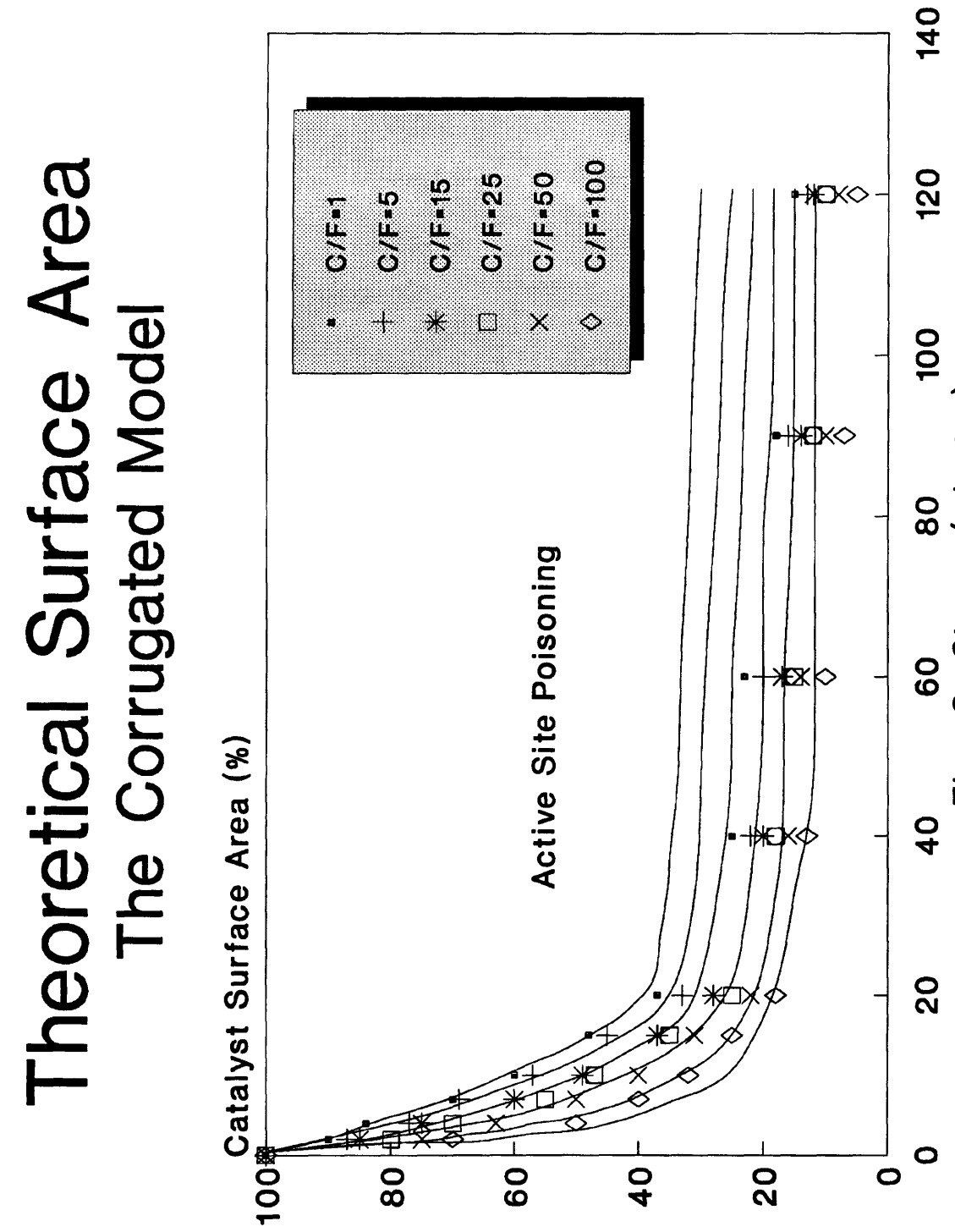

Figure 6.8 The theoretical total catalyst surface area for the corrugated parallel bundle pore model.

6.4.2.1 Conversion Results:

Figure 6.9 shows the observed deactivation behaviour of the cracking reaction for the catalyst:feed ratio of 25:1 g/g/min compared with a number of theoretical predictions. The best fit that could be achieved with the corrugated parallel bundle pore model undergoing heavy support coking was one which produced an excellent estimation of the conversion for almost the first 60 minutes on stream with a slight under–estimation for the remaining time on stream. Table 6.2 shows the fitted values of the deactivation parameters. Figure 6.10 shows the theoretical predictions of the conversion profiles for all the catalyst:feed ratios. It is clear that the degree of correlation between the experimental and theoretical results is best at low catalyst:feed ratios and reduces as this ratio is increased. Again, the final under–estimation of the conversion is due to a larger fitted α value which produces a larger initial zeolitic activity. As the zeolite micropores are lost as a result of coking and blocking, the theoretical conversions become lower than the experimental conversions, which is due to lower activity attributed to the support and due to pore blockage caused by heavy support coking.

Parameter	Value	
Pore length L	14	Microns
Zeolite coke unit size d_z	1.13	Angstrom
Support coke unit size d	23	Angstrom
Main reaction rate constant k_s	$6x10^{-8}$	(m/s)
Zeolite fractional activity α	0.86	(Initially)
Series coking rate constant k_{cs}	$1.32x10^{-11}$	$m^4kmol^{-1}s^{-1}$
P.S.D.(Uniform Distribution)	60–3200	Angstrom

Table 6.2 Fitted values of the deactivation parameters for the corrugated parallel bundle pore model undergoing heavy support coking.

Theoretical Conversions
The Corrugated Model

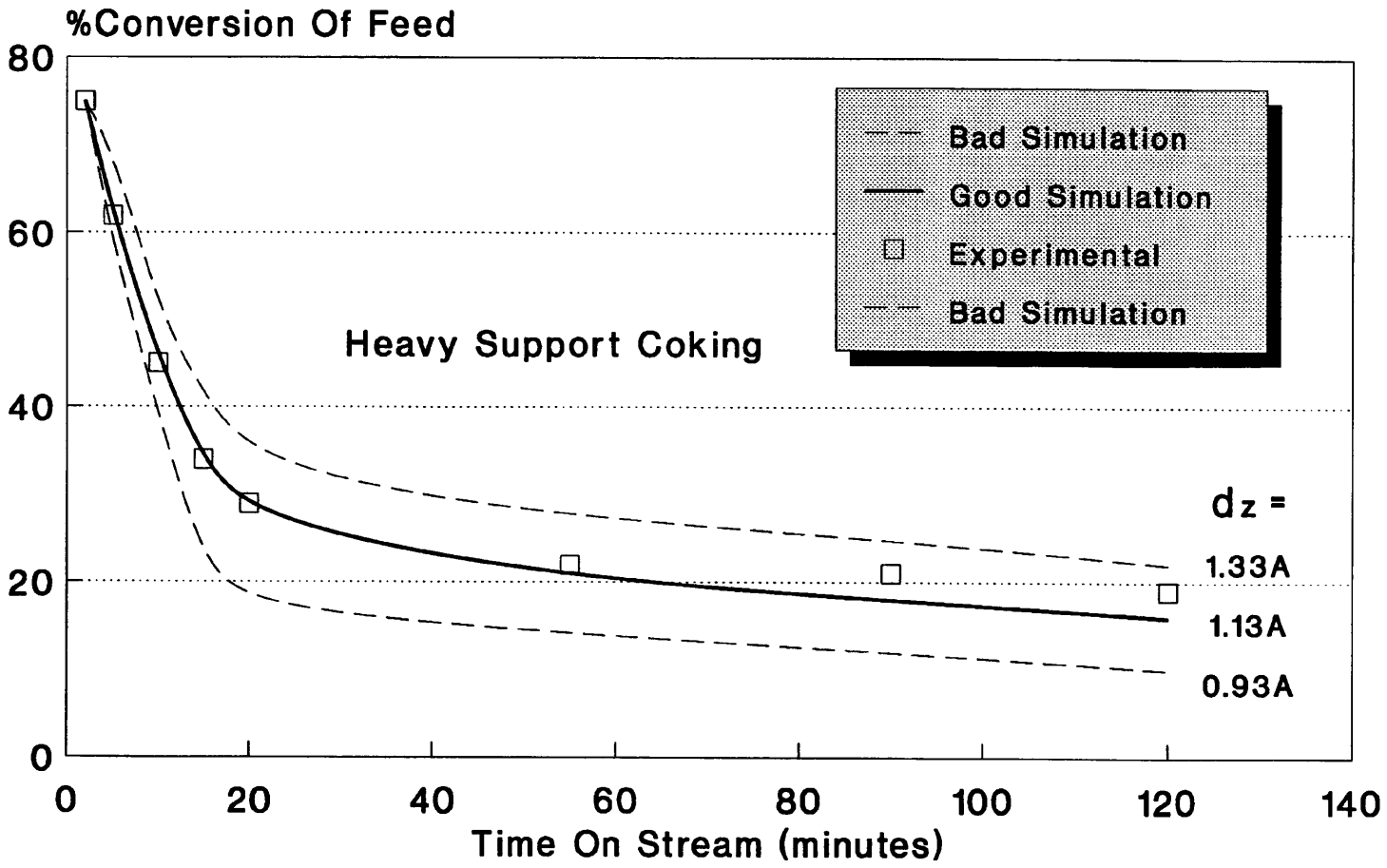

Figure 6.9 The theoretical conversion profiles for C:F=25 for the corrugated parallel bundle pore model.

Theoretical Conversions
The Corrugated Model

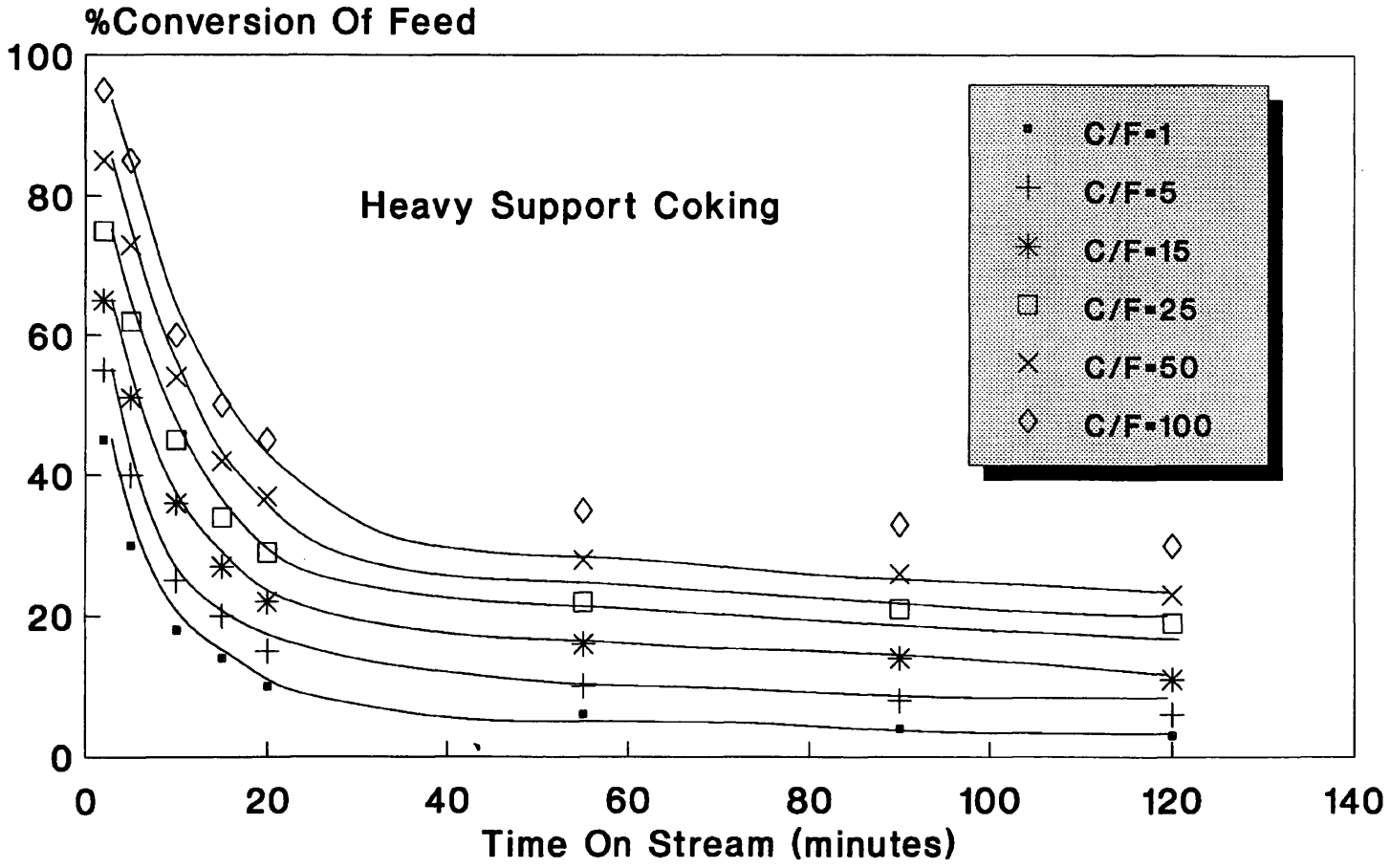

Figure 6.10 The theoretical conversion profiles for the corrugated parallel bundle pore model.

6.4.2.2 Coke Content of the Catalyst:

Figure 6.11 shows the predicted coke content profiles and their experimental equivalents. They show similar trends with the coking rate decreasing as the time on stream increases. Also, they both show that the coke content of the catalyst increases as the catalyst:feed ratio is increased. The theoretical coke content profiles show a significant under–estimation compared to the experimental values for all times on stream producing lower final coke contents. This discrepancy was due to the pore blockage phenomena that started to occur in the corrugated parallel bundle once some smaller external support pore elements were fully coked causing the isolation of some larger internal pore elements reducing the available volume for more coke to be accommodated. This was also partially due to the lower activity associated with the support compared with the zeolite indicated by the α value.

6.4.2.3 Surface Area of the Catalyst:

Figure 6.12 shows the predicted total catalyst surface area and the experimental results. They show similar trends with the surface area reducing as the time on stream increases. Also, they both show that as the catalyst:feed ratio increases, the total catalyst surface area reduces. However, the theoretical profiles produce a slight under–estimation of the total surface area for all times on stream and for all catalyst:feed ratios. As explained earlier, this was mainly due to support pore blockage causing a reduction in the accessible surface area.

6.5 APPLICATION OF THE THEORY USING THE STOCHASTIC NETWORK PORE MODEL:

6.5.1 Active Site Poisoning of the Support:

Theoretical Coke Content
The Corrugated Model

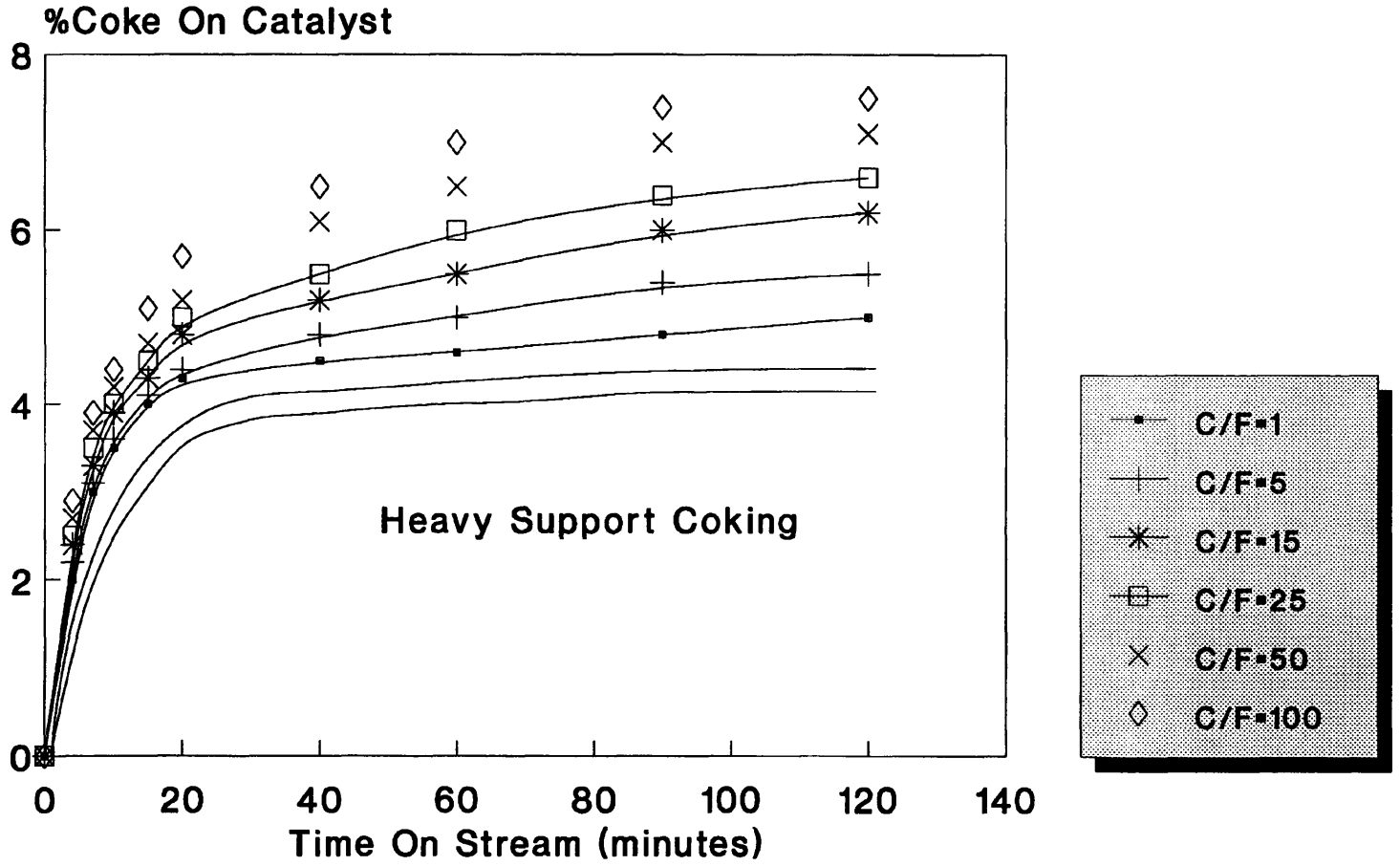

Figure 6.11 The theoretical coke content profiles for the corrugated parallel bundle pore model.

Theoretical Surface Area
The Corrugated Model

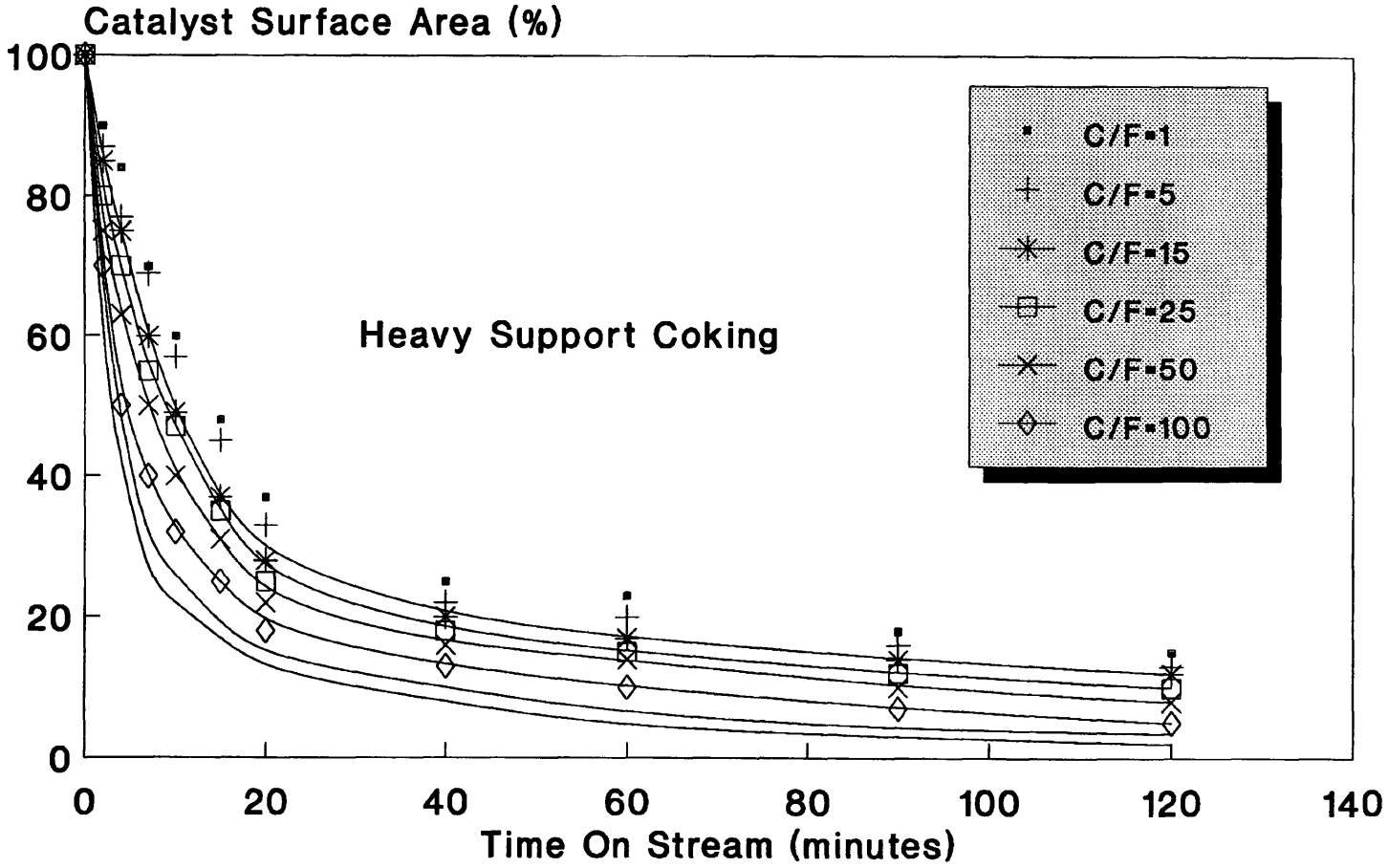

Figure 6.12 The theoretical total catalyst surface area for the corrugated parallel bundle pore model.

For both support pore models the effectiveness factor varied between 0.99 and 1.0 and the apparent overall Thiele modulus for the catalyst was approximately 0.13. This implied that the reaction was in the regime of negligible diffusional resistances and that the concentration profile along the pores should be negligible. Also, since the levels of coke content deposited on the support pores under the active site poisoning mechanism were very small, preventing pore blockage to any significant degree, it was reasonable to expect that network pore model would produce similar simulations to those produced with the corrugated parallel bundle pore model. Therefore, it can be expected that it will similarly fail to predict the levels of coke produced during the experiments.

6.5.2 Heavy Support Coking:

6.5.2.1 Conversion Results:

In order to simulate the observed deactivation behaviour, an intermediate catalyst:feed ratio of 25:1 g/g/min was again chosen as the starting point from which the fitted deactivation parameters will be used to simulate the other catalyst:feed ratios ranging from 1:1 to 100:1 g/g/min. Initial estimates for the various parameters of the model (k_s, k_{cs}, d, d_z and α) were provided by previous work (Mann, Sharrat and Thomson (1986), and Thomson(1986)).

Figure 6.13 shows the observed deactivation behaviour of the cracking reaction for the catalyst:feed ratio of 25:1 g/g/min compared with a number of theoretical predictions. The best fit that could be achieved with the network pore model undergoing heavy support coking was one which produced a close correlation between the experiment and the theory for this middle range catalyst:feed ratio. Table 6.3 shows the fitted values of the deactivation parameters. The same parameters were used to see how well they simulated the other experimental runs with different catalyst:feed

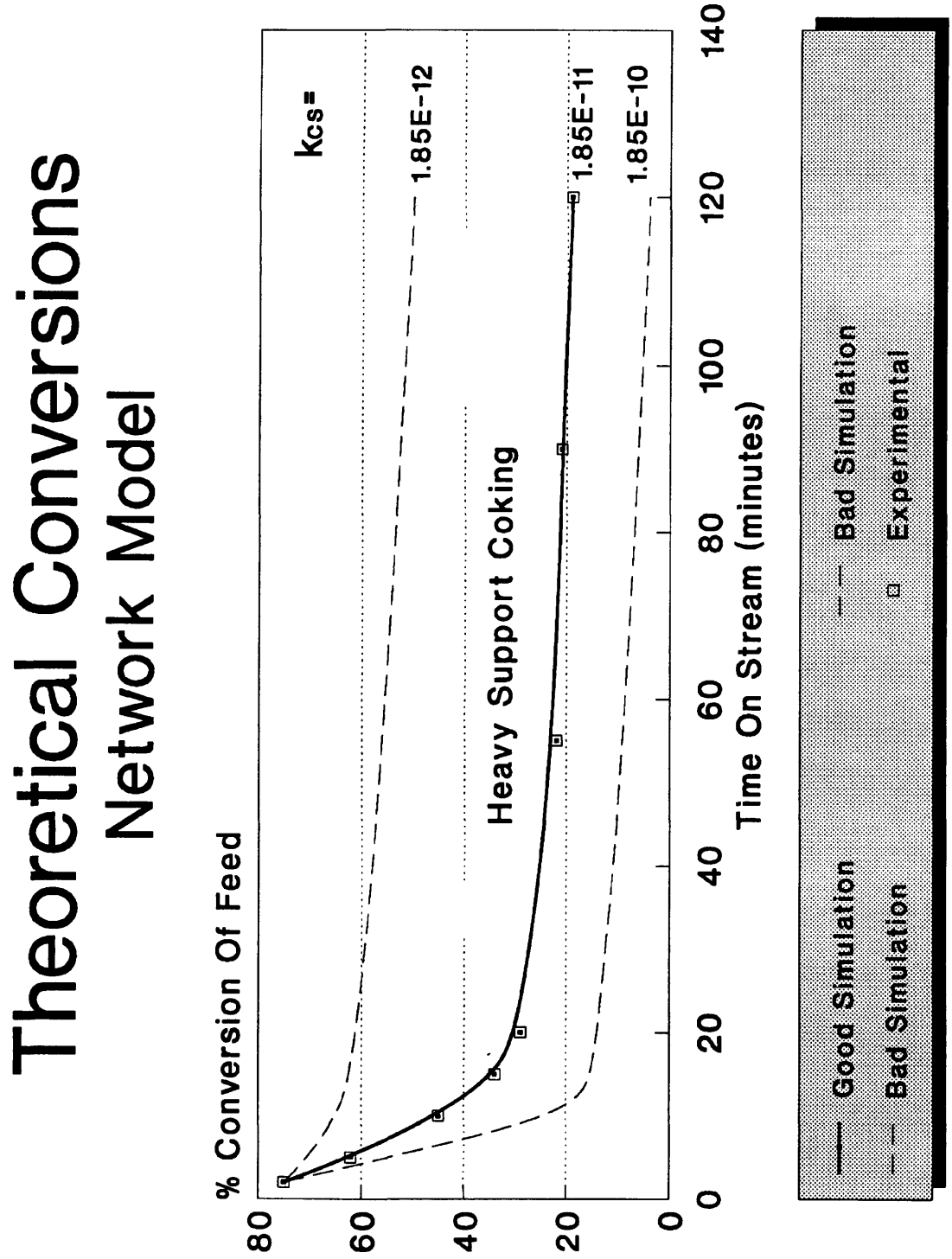

Figure 6.13 The theoretical conversion profile for C:F=25 for the network pore model.

Parameter	Value	
Pore length L	14	Microns
Zeolite coke unit size d_z	0.91	Angstrom
Support coke unit size d	21	Angstrom
Main reaction rate constant k_s	$6x10^{-8}$	(m/s)
Zeolite fractional activity α	0.79	(Initially)
Series coking rate constant k_{cs}	$1.85x10^{-11}$	$m^4kmol^{-1}s^{-1}$
P.S.D.(Uniform Distribution)	60–3200	Angstrom

Table 6.3 Fitted values of the deactivation parameters for the stochastic network pore model undergoing heavy support coking.

ratios. Figure 6.14 shows these theoretical predictions of the conversion profiles for all the experimental catalyst:feed ratios. It is clear that the network theory is successful in reproducing the observed activity over the whole length of time and for the entire range of catalyst:feed ratio to within 4%. Having obtained a fit for the activity behaviour, checks were carried out on the predicted coke content and total surface area of the catalyst to test the all round validity of the proposed model of deactivation.

6.5.2.2 Coke Content of the Catalyst:

Figure 6.15 shows the predicted coke content profiles and their experimental equivalents. They show similar trends with the coking rate decreasing as the time on stream increases. Also, they both show that the coke content of the catalyst increases as the catalyst:feed ratio is increased. Actually, the theoretical coke content profiles produced a high degree of correlation with the experimental values for the whole time on stream and for the entire catalyst:feed ratios.

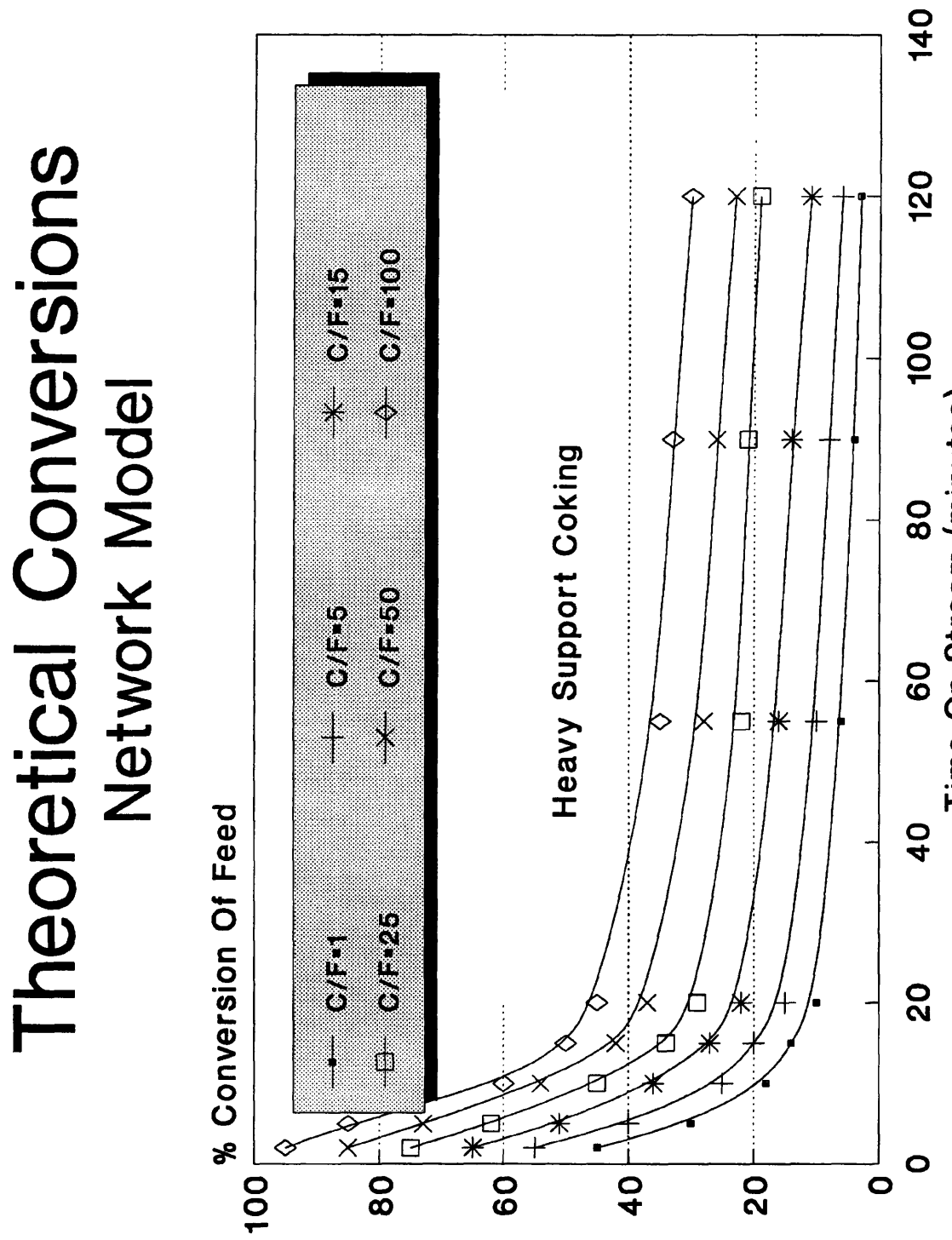

Figure 6.14 The theoretical conversion profiles for the network pore model.

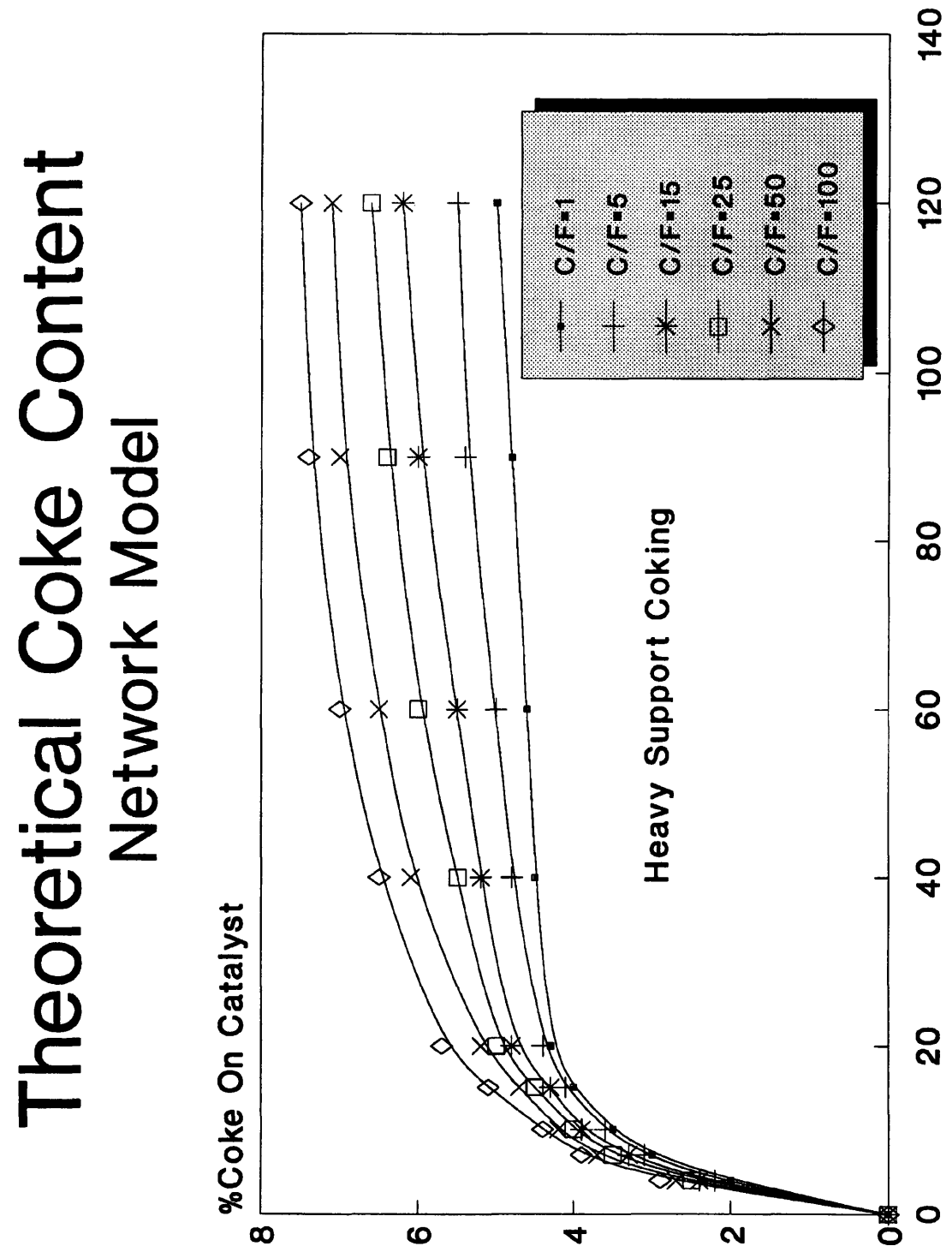

Figure 6.15 The theoretical coke content profiles for the network pore model.

6.5.2.3 Surface Area of the Catalyst:

Figure 6.16 shows the predicted total catalyst surface area and the experimental results. They show similar trends with the surface area reducing as the time on stream increases. Also, they both show that as the catalyst:feed ratio increases, the total catalyst surface area reduces. The theoretical profiles produce a reasonable fit for the total surface for the whole length of time and for the entire set of catalyst:feed ratios.

6.6 DISCUSSION:

It has been shown that the deactivation of the supported zeolitic catalyst super–D can be simulated by either active site poisoning or heavy support coking mechanism. Therefore, it was not possible to differentiate between the two possible coking mechanisms by only studying the experimentally obtained conversion/time on stream data. By extending the deactivation model to predict the amount of coke accumulated with time and the associated change in the accessible surface area of the catalyst, it became possible to compare their performances. The significant under–estimation of the coke content and the over–estimation of the surface area by the active site poisoning mechanism dismissed it as a possible coking mechanism, and confirmed the likelihood of a heavy support coking mechanism.

Because of the difference in the two support pore structures, there will be for any given set of fitting parameters, a difference in the reaction rates producing a difference in the conversions achieved. In this case, the network model out performed the corrugated model and as a consequence the coking rate constant had to be raised from 1.32×10^{-11} to 1.85×10^{-11} ($m^4/kmol/s$) to reduce the activity to a level that resembles the activity profiles measured from the experiments. Also, the initial

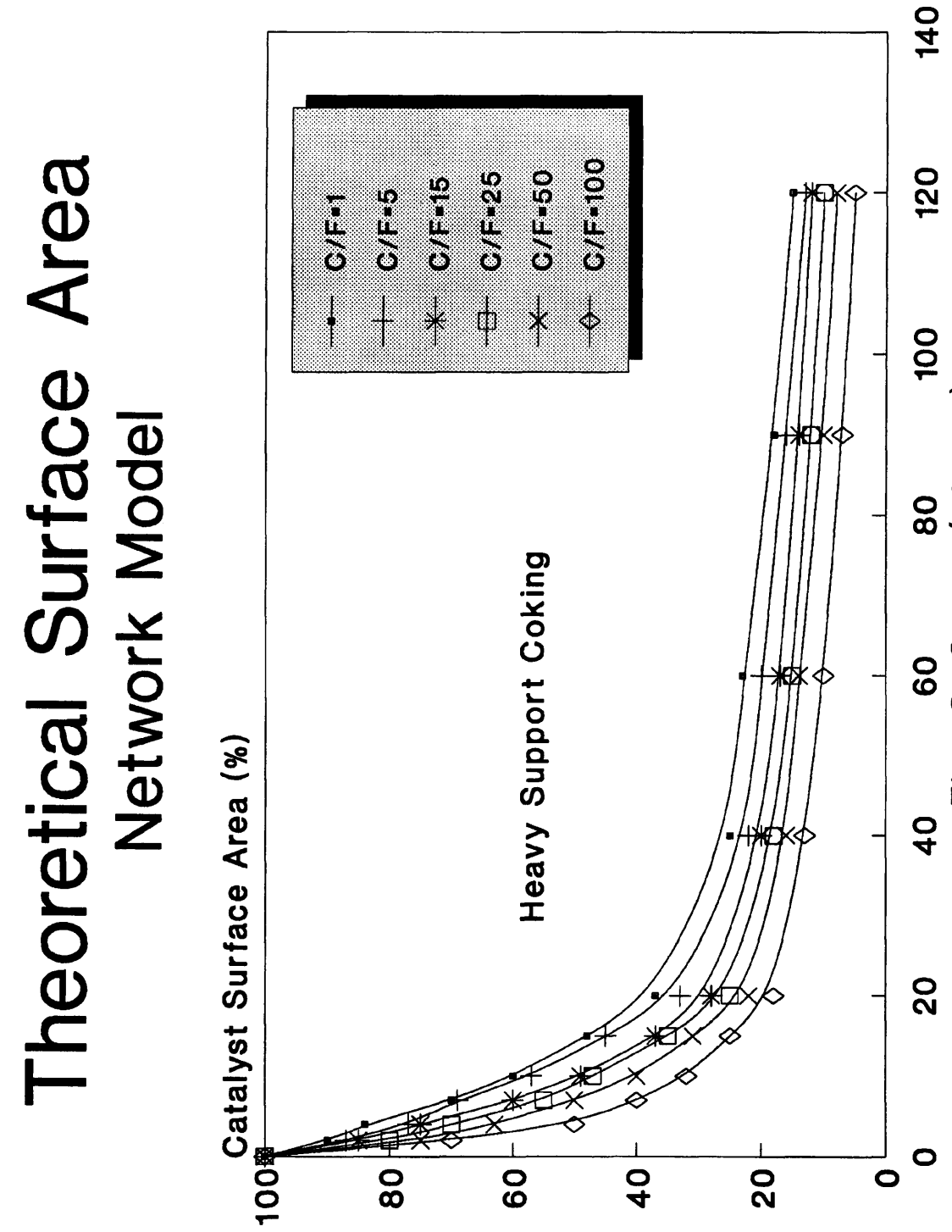

Figure 6.16 The theoretical total catalyst surface area for the network model.

conversion of the network model had to be reduced by lowering the fitted initial fractional activity due to zeolite, α, from 0.86 for the corrugated model to 0.79 for the network model.

Both pore models predict two distinct deactivation zones, the first being a very rapid decline in the activity followed by a much slower rate of deactivation. For the corrugated pore model, Figure 6.17 shows that the zeolite surface area available is reduced very sharply and is completely wiped out when the catalyst fractional coke content reached a value just over 0.2 while the overall surface area disappeared at a value of 0.67 indicative of complete deactivation. For the network pore model, Figure 6.18 shows a similar prediction of rapid zeolite loss with complete deactivation occurring when the catalyst fractional coke content reached nearly 0.94. Therefore, the performance of both models for the first deactivation zone representing the coking of the zeolite micropores was good. As soon as the support macropores started coking heavily, the theoretical predictions of the corrugated model started to diverge from the experimental results producing under–estimations in conversion, coke content and surface area, while the network model reproduced the observed deactivation and closely simulated the coke content and associated surface area profiles for the entire duration of the experiments. The discrepancy between the theory and experiment in the case of the corrugated pore model could be attributed to the over–estimation in the degree of pore blockage causing a large reduction in the predicted coke contents compared to the network model (Fig. 6.19). Figure 6.20 shows the number of support pore elements isolated and Figure 6.21 shows the corresponding support pore volume isolated for both models clearly showing the effect of pore interconnectivity in the network model in keeping the degree of pore isolation very small compared to the corrugated model. Figures 6.22 to 6.25 show visualisations of the coking process within the corrugated and the network pore models until they become completely deactivated.

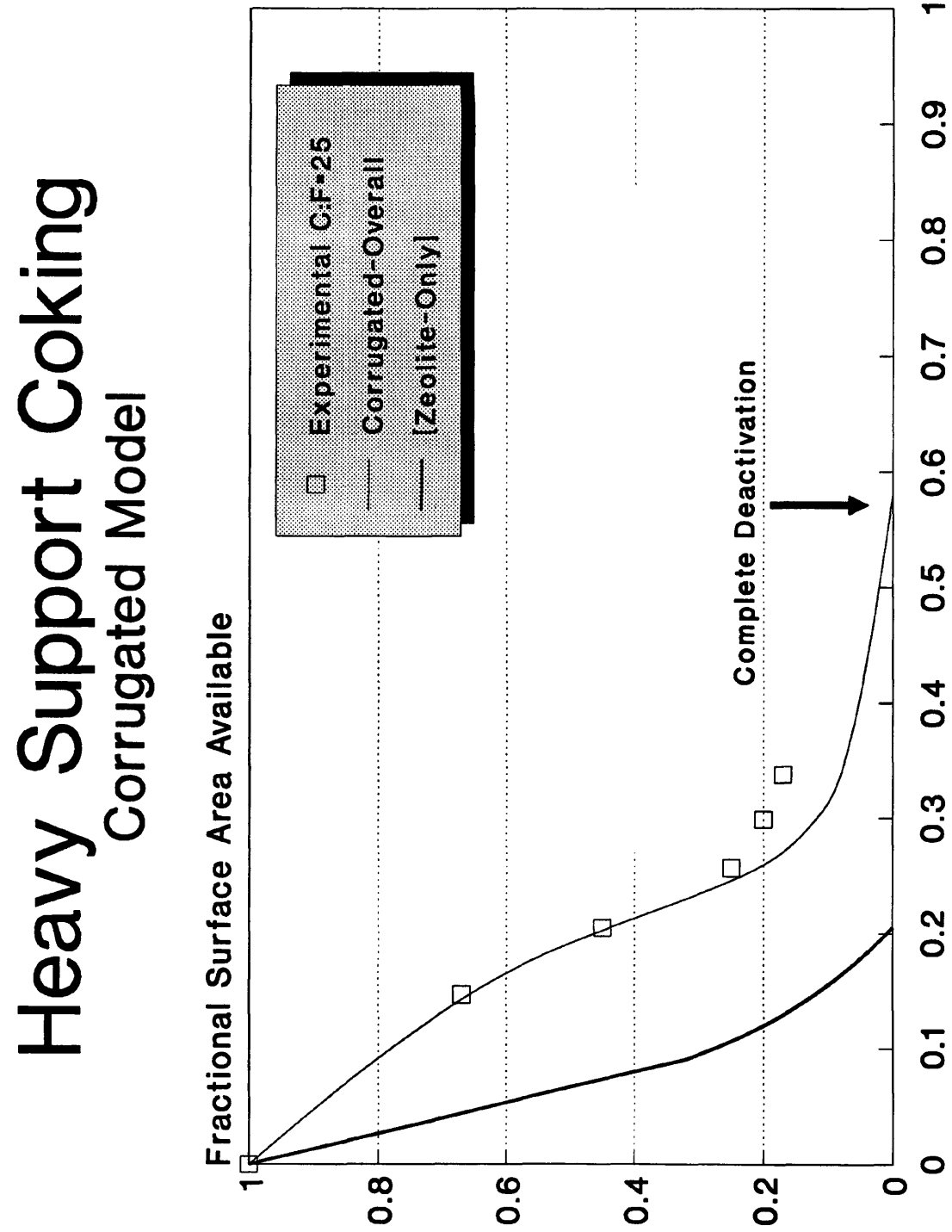

Figure 6.17 Theoretical surface area vs. coke content for the corrugated model at C:F=25.

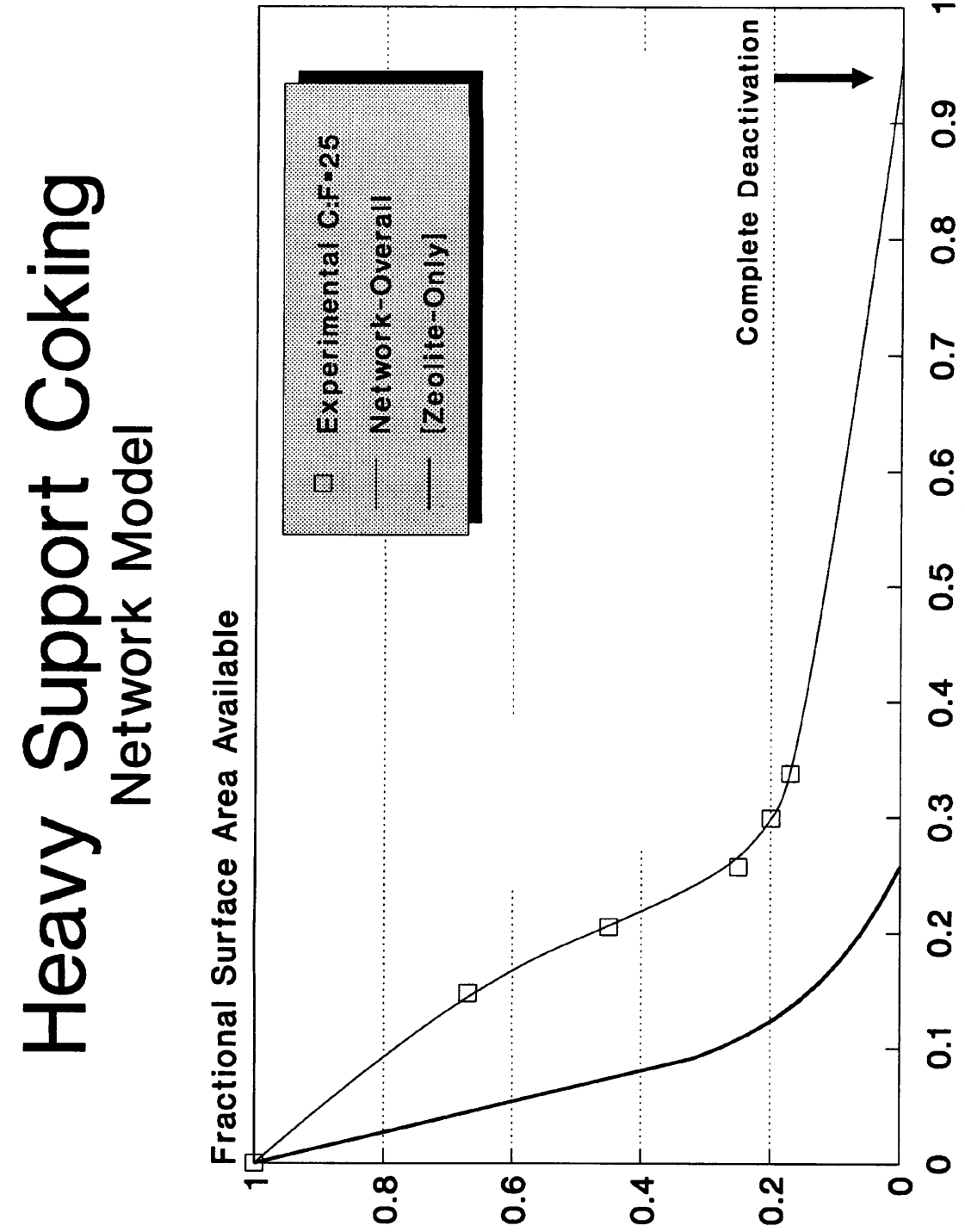

Figure 6.18 Theoretical surface area vs. coke content for the network model at C:F=25.

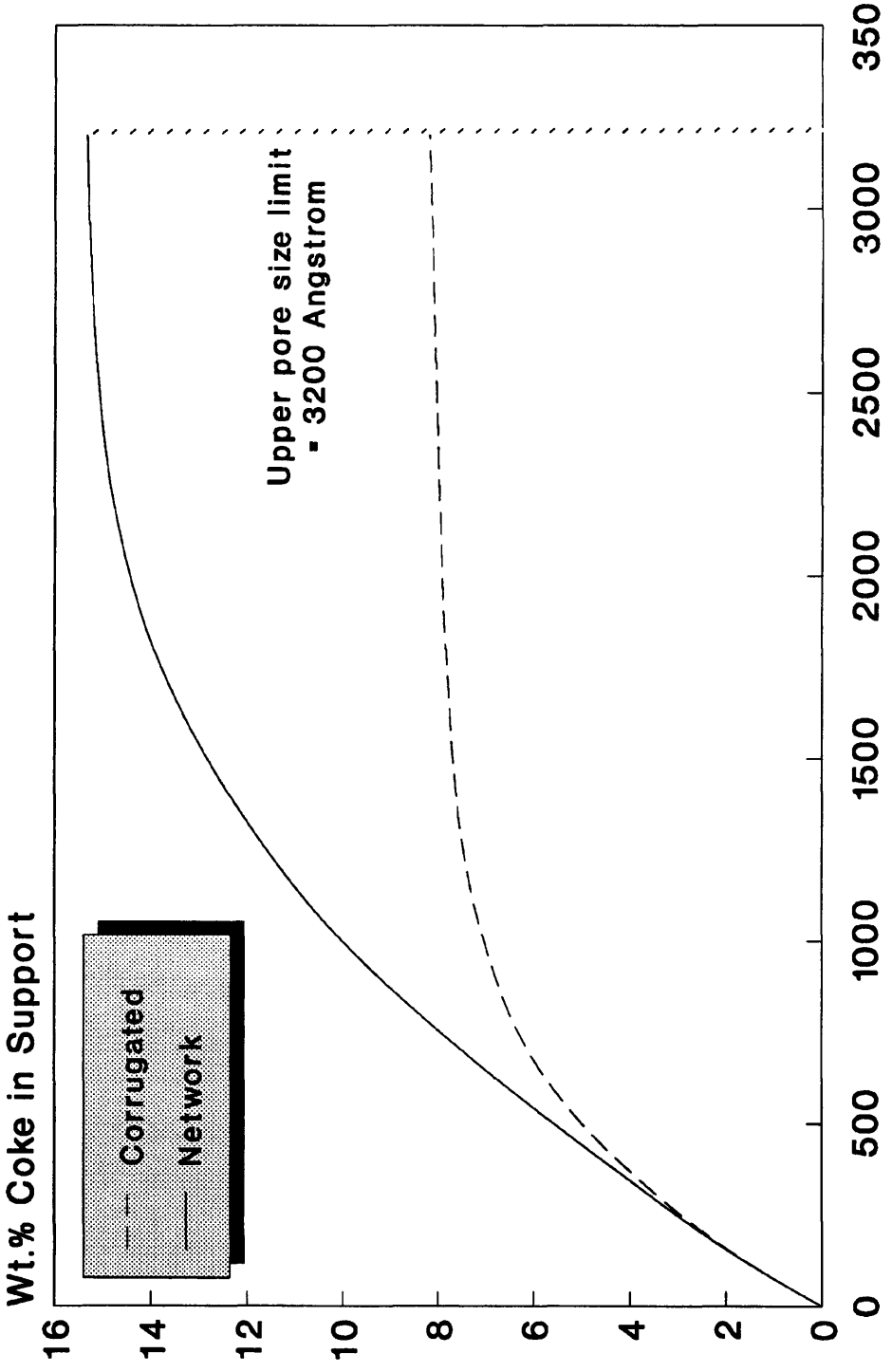

Figure 6.19 Coke content in the support of both models as the coke layer thickness increases.

Heavy Support Coking

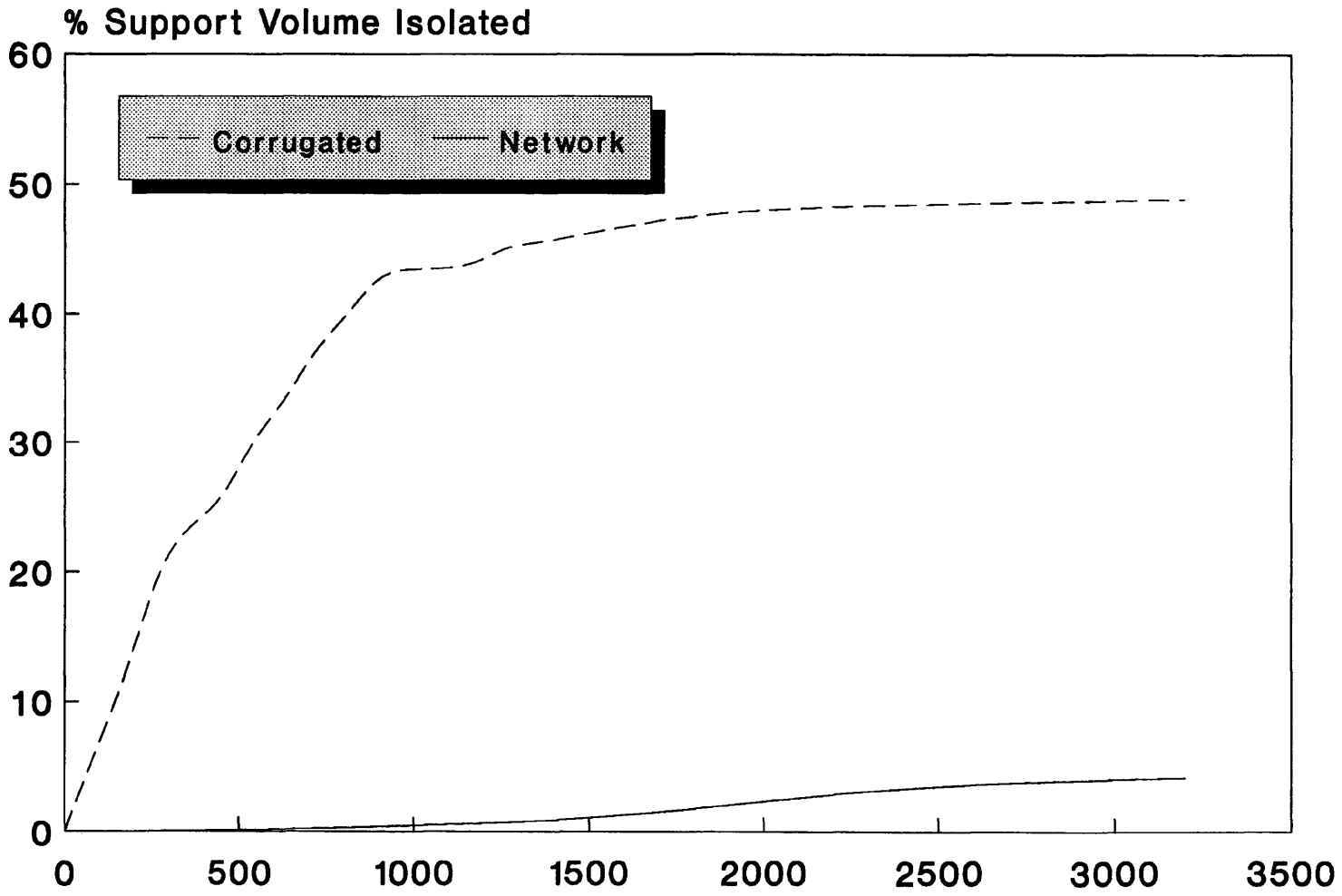

Figure 6.20 Changes in the support pore volume for both models as the coke layer thickness increases.

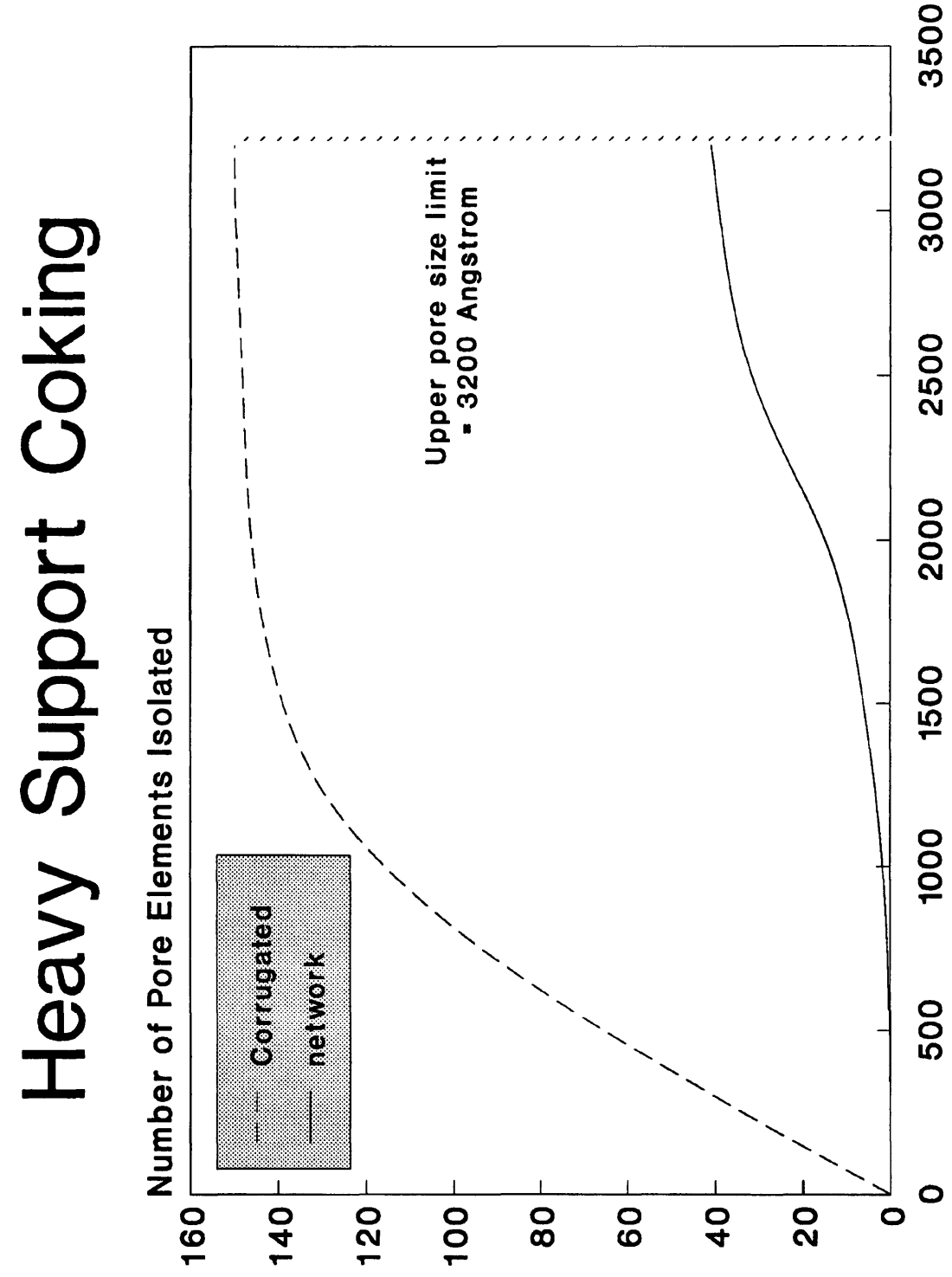

Figure 6.21 Changes in the number of isolated support pore elements for both models.

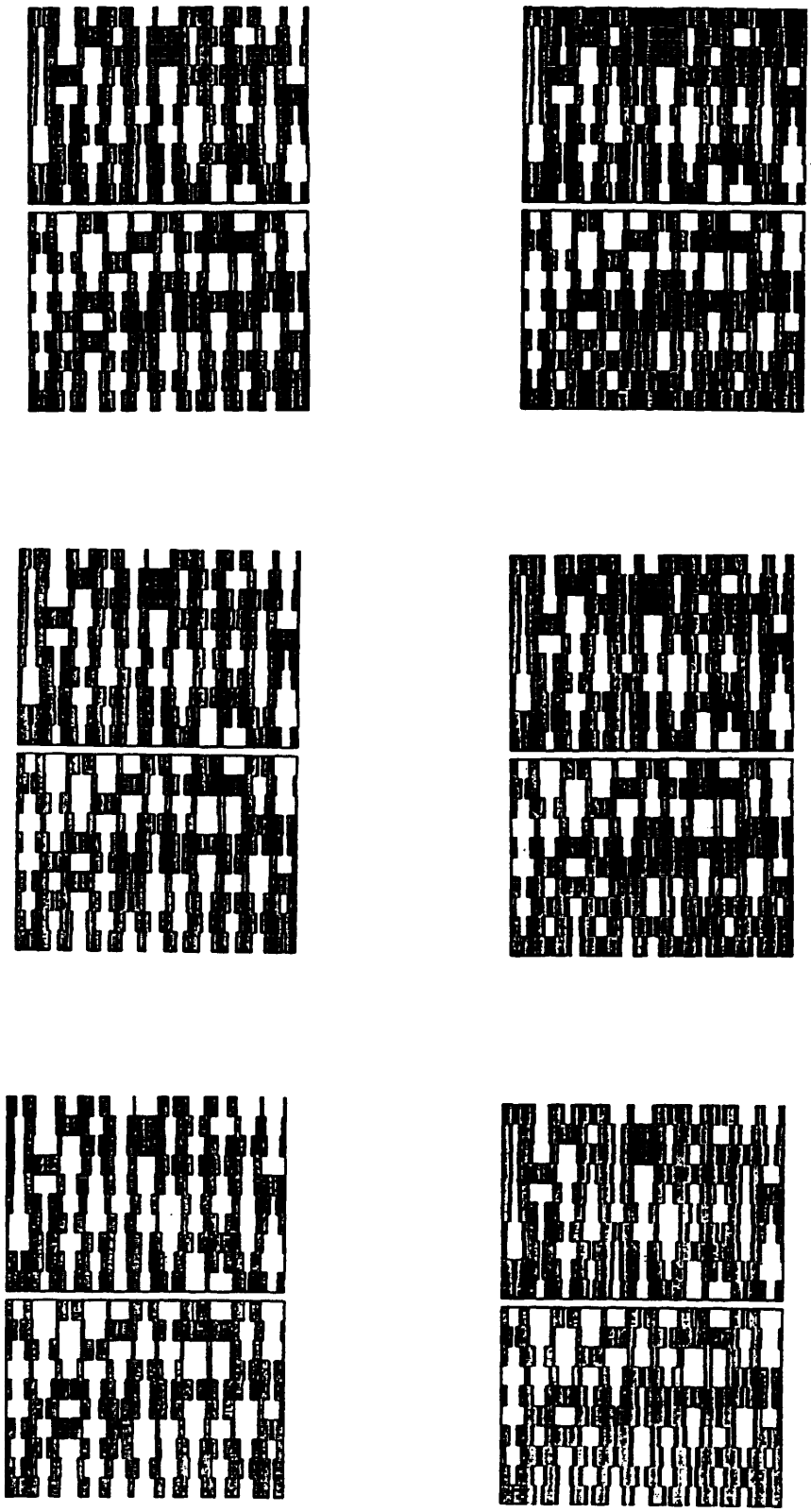

Figure 6.22 The corrugated parallel bundle at different stages of coking.

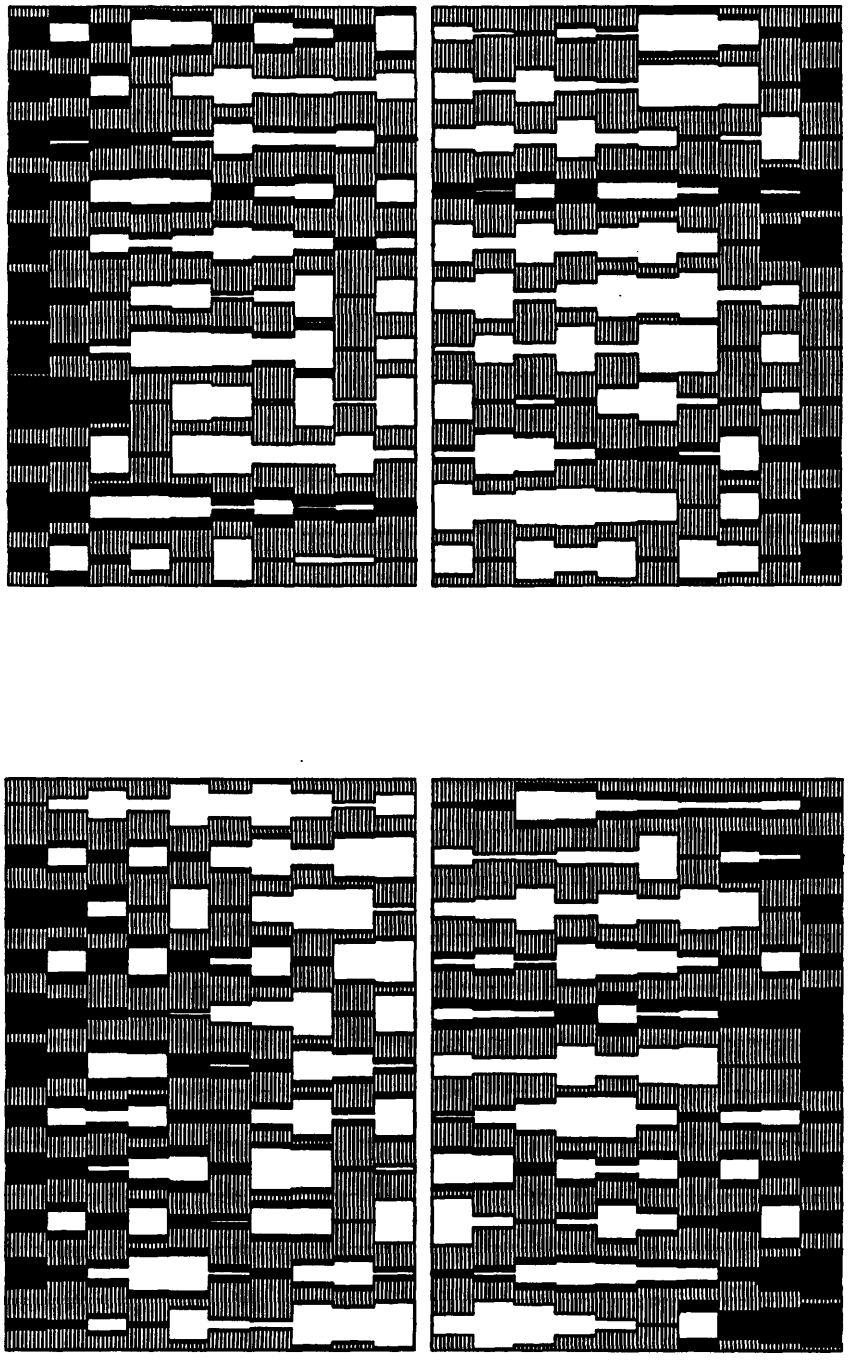

Figure 6.23 Different sets of the corrugated parallel bundle after complete deactivation.

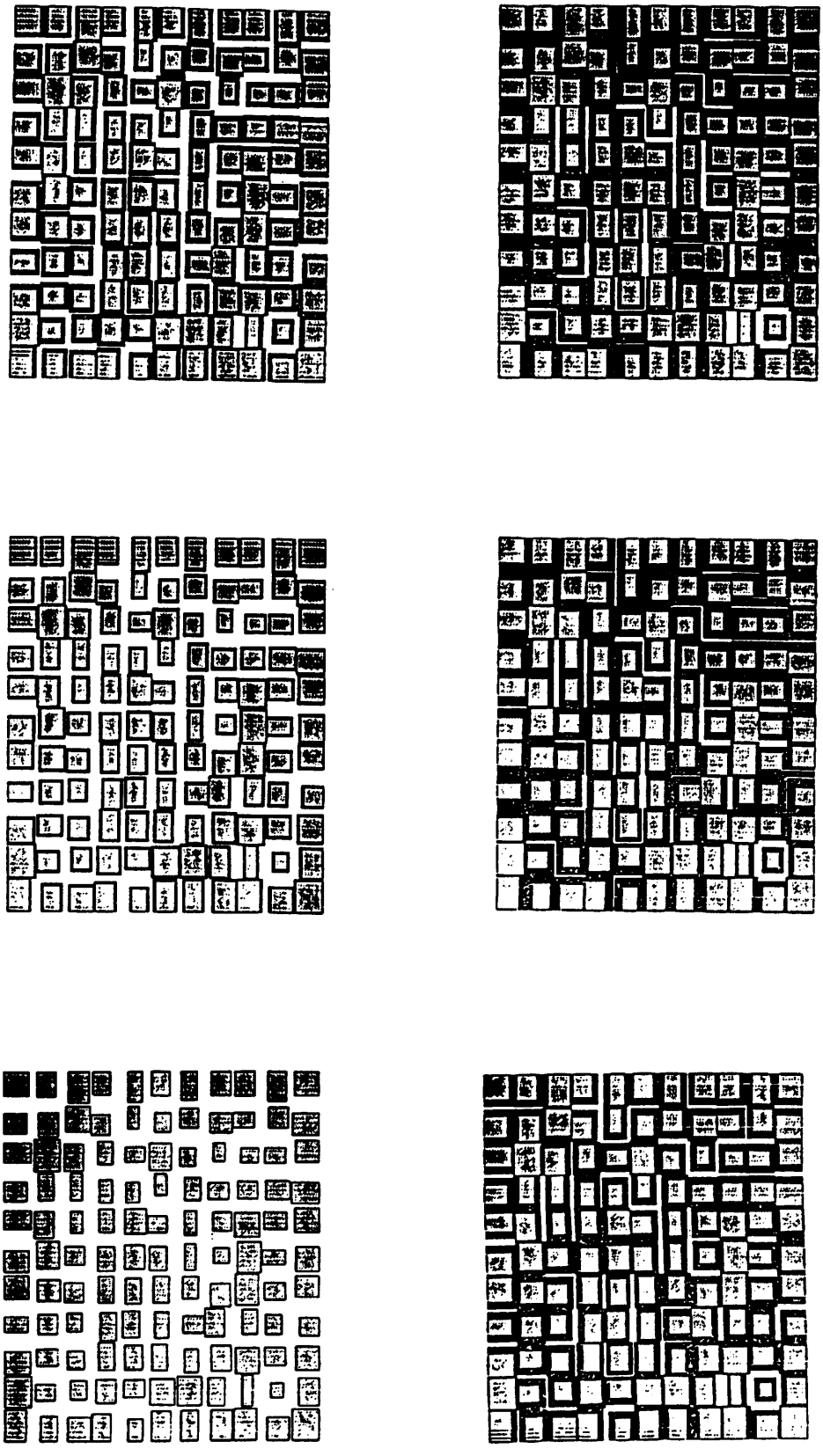

Figure 6.24 The network pore model at different stages of coking.

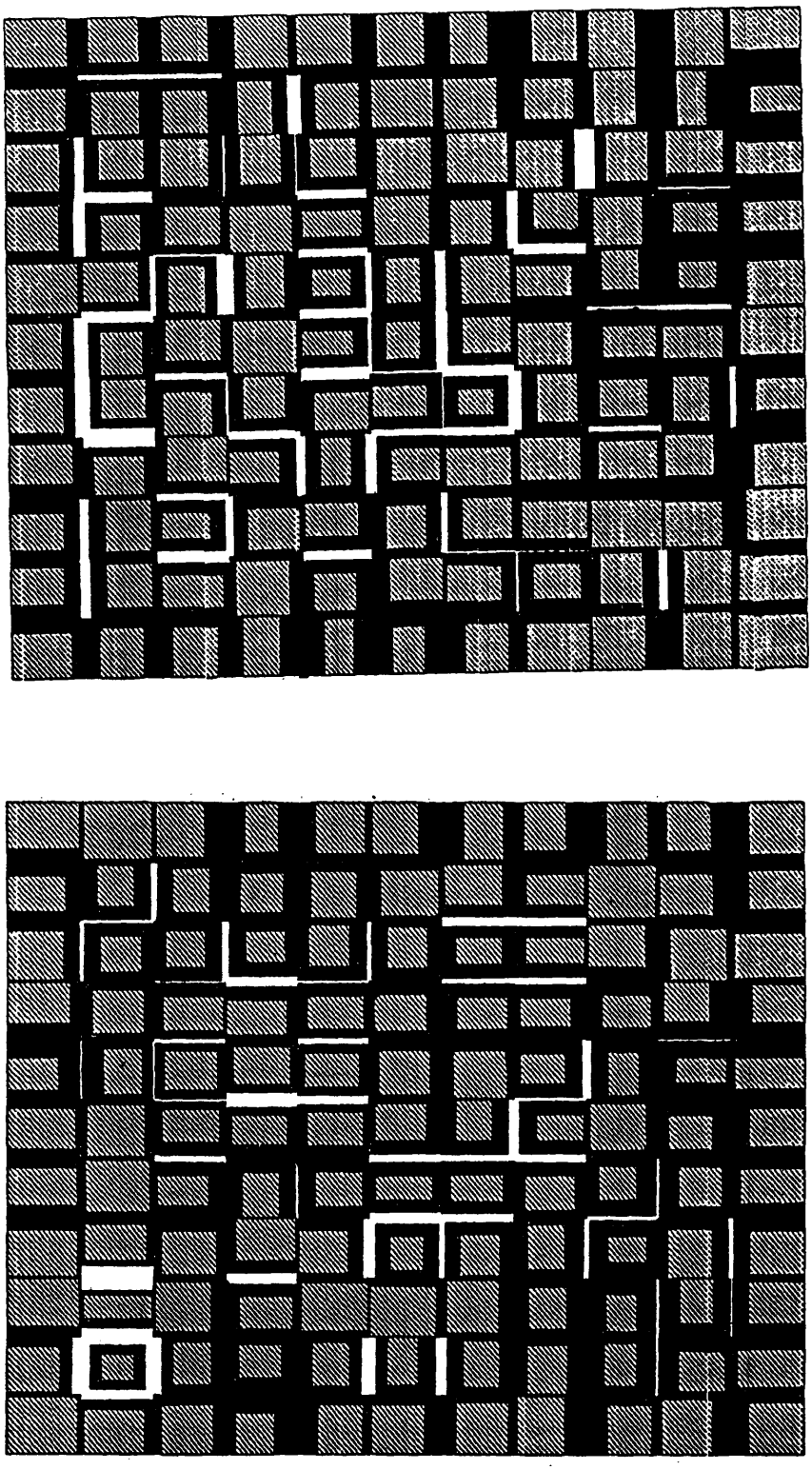

Figure 6.25 Different sets of the network pore model after complete deactivation.

Under the experimental conditions, the effectiveness factor was near unity indicative of negligible diffusional resistances. The performance of the special case of straight parallel bundle pore model was compared with that of the general corrugated and the network pore models. It was interesting to note the close performance to the network model in predicting the changes in the surface area of the catalyst as the coke content increased except for the fact that it could not predict the pore blockage phenomena which accounted for about 6% of the total catalyst area (Fig. 6.26). If the conditions were changed so that diffusional resistances became very significant, e.g. by changing the catalyst particle size to be pellets rather than powder form, the effectiveness factor drops to values far from unity and pore blockage takes place in all pore models including the parallel bundle. Under these conditions, the performance of the parallel bundle diverges from that of the network model predicting much larger coke levels while the corrugated model significantly under–estimated the coke contents (Fig. 6.27).

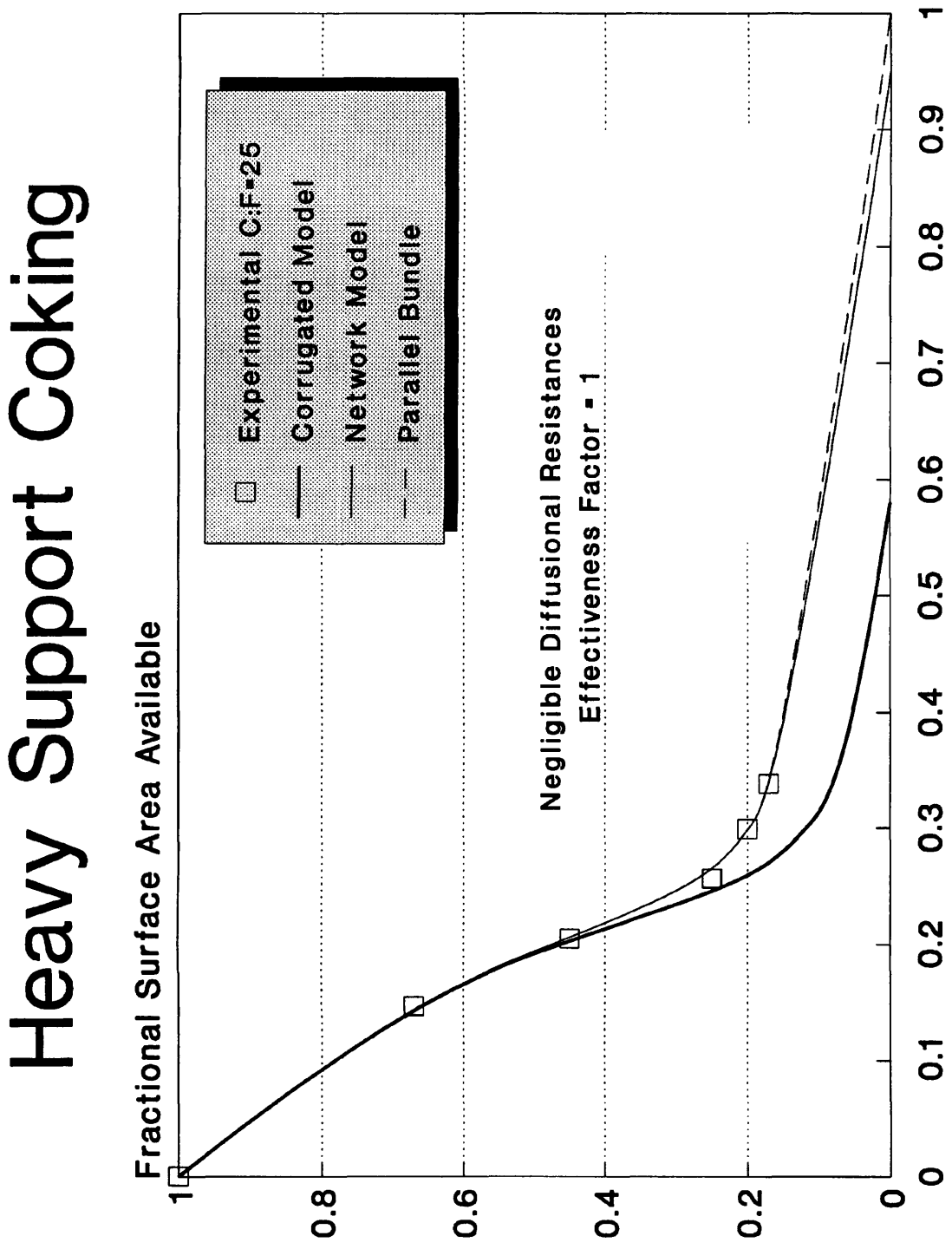

Figure 6.26 Theoretical surface area vs coke content for both models at C:F=25.

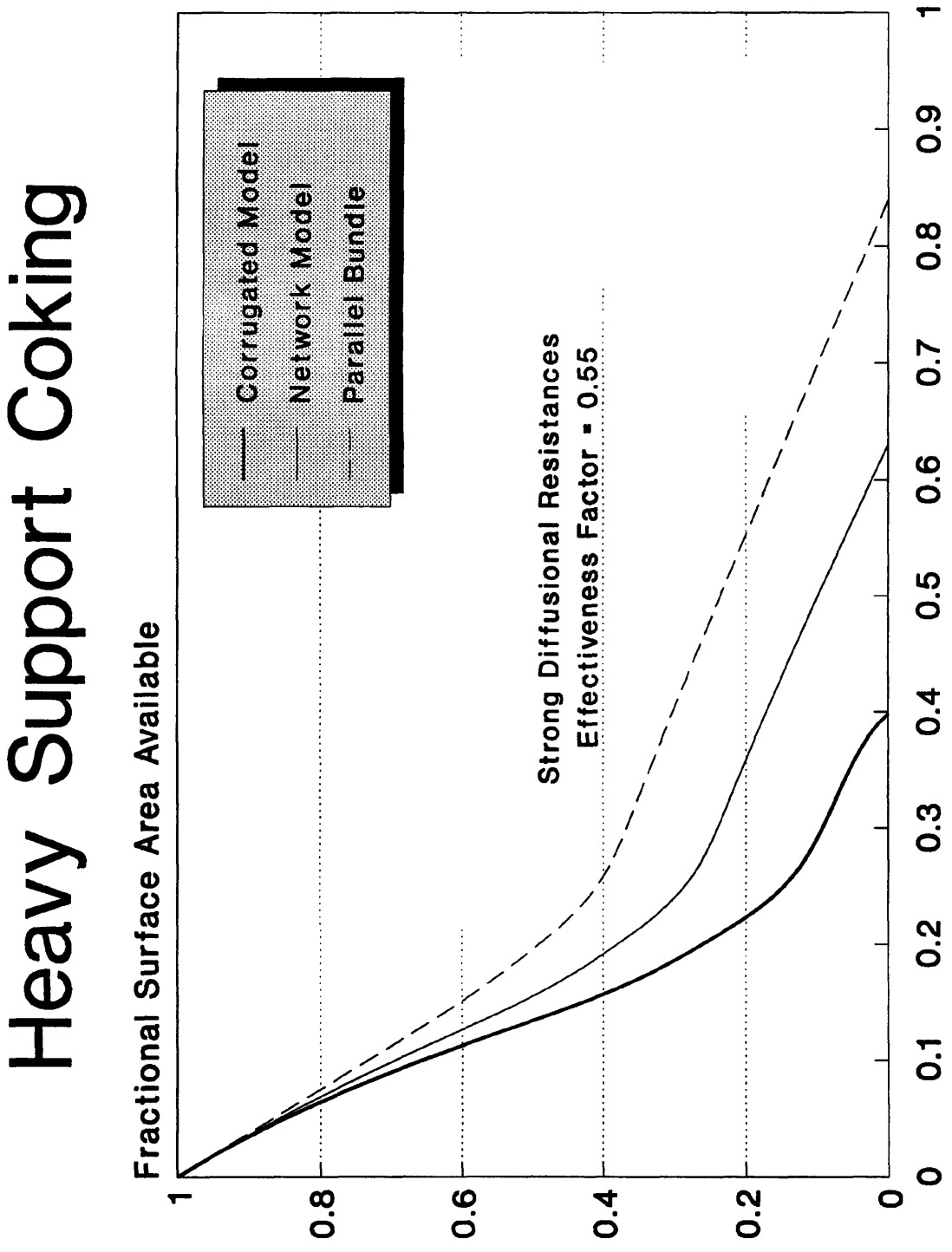

Figure 6.27 Theoretical surface area vs coke content for both models under strong diffusional resistances.

CHAPTER SEVEN

CONCLUSIONS AND SUGGESTIONS FOR FURTHER WORK

CHAPTER SEVEN

CONCLUSIONS AND SUGGESTIONS FOR FURTHER WORK

7.1 CONCLUSIONS:

This work has been concerned with both the practical and the theoretical aspects of the deactivation of a commercial supported zeolitic catalyst by coking. Deactivation studies have been carried out in a fluidised bed reactor using cumene as a feedstock at a reaction temperature of 500° C and run times up to two hours. The catalyst:feed ratio was varied from 1:1 g/g/min to 100:1 g/g/min. A blank experimental run with no catalyst in the reactor showed that at the reaction temperature, there was negligible thermal cracking.

The results of these experiments have shown a definite correlation between activity and the catalyst:feed ratio. For all the catalyst:feed ratios, there has been a very rapid initial deactivation of the catalyst followed by a less marked activity loss. The experimental coke content profiles show an initial rapid rate of coking of the catalyst followed by a much slower rate of coking. The experimental surface area results showed a large drop in the total catalyst surface area at the initial period followed by a much slower drop for the remaining time on stream. These results have shown that the rapid activity loss , coke build–up and surface area reduction were due to zeolite coking, with the slower rate of deactivation being due to the support coking.

A reaction kinetic and coke laydown model has been proposed to account for the catalyst deactivation by coke deposition. Coke is assumed to deposit randomly on the support and in the zeolite micropores allowing for deactivation by both active site coverage and pore blockage. The support pore structure was represented by two different models:

(1) The corrugated parallel bundle pore model.

(2) The stochastic network pore model.

Computer simulations of diffusion, reaction and coke laydown have been carried out in both of these model structures to study the influence of the various parameters on the deactivation. In these simulations, three different deactivation types were investigated, namely, the series, parallel and the triangular. Using the information gathered from these simulations as a guide, an attempt was made to see if the model could successfully describe the observed deactivation behaviour of the commercial catalyst super–D.

It was found that the timewise deactivation could be equally well represented by either a support active site poisoning coking mechanism or a heavy support coking mechanism, though from investigations of the coke accumulation within the catalyst, the latter appeared to be more representative of the total deactivation behaviour. The best fit to the experimental results for the coking reaction was obtained using a series type coking mechanism.

From the two pore structural models under consideration, the network model provided the better overall fit. However the corrugated parallel bundle model could not accurately reproduce either the coke content or the surface area profiles. On the other hand not only did the network pore model reproduce the observed deactivation, but it also closely simulated the coke content and associated surface area profiles for the entire 2 hour duration of the catalytic cracking runs and over a hundredfold range of catalyst:feed ratios that were used in the experiments.

7.2 SUGGESTIONS FOR FURTHER WORK:

7.2.1 Experimental Developments:

The results of this work have shown that the initial rapid deactivation of the cracking catalyst appears to be representative of the zeolite micropores coking and blockage. Further studies in this field of research should attempt to investigate the deactivation behaviour of the catalyst at much shorter times on stream and to move towards a more industrially related operation such as a riser–cracker type reactor. The riser cracker unit operates by mixing vapourised oil feed and catalyst at the bottom of the reactor. The feed and catalyst then rise up the reactor driven by the velocity of the vapour where reaction occurs. A typical residence time is of the order of few seconds. Although the vapour velocity tends to drive the individual catalyst particles up the reactor, the effect of gravity and inertia is such as to drag the particles downwards, with the result that the solid velocity is less than that of the vapour. The difference is known as the slip velocity and equations exist that can describe this. A slip velocity of zero implies plug flow up the reactor. The major change that would have to be made to the computer program is changing the performance equation to that of the riser cracker unit. That is, cocurrent flow of catalyst and feed, including this slip velocity.

Similarly, it ought to be possible to adapt the system of equations to model the behaviour in the regenerator. Here coke is burned off the catalyst and the equations that describe the rate of reaction could be modified to be a function of coke content of the pore element rather than a function of the pore active area as they are at present.

The selectivity of a catalyst plays an important role in any reaction involving heterogeneous catalysts, and in this work it was observed how the benzene selectivity was affected by the extent of the deactivation of the cracking catalyst. The extension of the coking models presented in this work to investigate the effects of coke deposition

on the catalyst's selectivity should prove invaluable and ultimately lead to the specification of improved pore architectures of cracking catalysts, which are more selective in the face of coke laydown while retaining high activity.

At the moment no attempts at product gas measurement and analysis have been made. Attempts at on line gas–liquid chromatography and/or mass spectrometry could provide the means for producing a total mass balance and/or carbon balance for the system.

The validity of the model could be tested by using a reaction whose kinetics are well known. If several samples of a catalyst could be produced whose chemical composition was the same but which differed in their pore structure, ie producing pellets of catalysts at differing die pressures, then the differences in the catalysts' activity and selectivity could be attributed only to the support pore structure of the catalysts. This factor which is incorporated into the present model, should thus be able to predict the changes in activity and selectivity performance.

New attempts should also be made into finding out where in the catalyst coke actually deposits as this would produce direct information as to the coke laydown geometry and to the extent of any associated diffusional limitations that might exist. At the moment S.E.M. techniques have been used in an attempt to do this but these results have presently proven inconclusive, but could be reinforced by both image analysis and the Nuclear Magnetic Resonance (N.M.R.) techniques.

7.2.1 Theoretical Developments:

Whilst the stochastic network pore model does represent a step closer to reality than the classical straight and corrugated parallel bundle pore models, there is still a large gap between this and the actual catalyst structure. The pore network model, as

presented could and should be modified and improved in a number of ways amongst these are:

(1) The model is two dimensional while catalyst particles are three dimensional. Unless the three dimensional nature of the pore structure can be incorporated it is likely that problems will be encountered in, for example, the estimation of blocked volumes. In practice problems would arise through an increase in the amount of computation required.

(2) The square network is too restrictive a framework for realistic representation of a complex pore structure. The introduction of other parameters such as variable pore length will increase flexibility. This could give rise to other problems. In particular it is probable that the available experimental data would be insufficient to determine the values of such parameters.

(3) The next logical step would be to combine the two models presented in this work to produce a network of pores where each pore segment is made up of a corrugated pore.

(4) The ideal straight cylindrical smooth pore segments used in the stochastic pore networks might be replaced by unsymmetrical irregular pores of variable shapes. Fractal pores such as the ones generated by Mann and Wasilewski (1990) might also be used.

(5) The topology of a stochastic pore network could be altered by changing the pore connectivity by setting some pore radii (chosen randomly) to zero. The maximum pore connectivity would not exceed the original unaltered network connectivity.

The equations derived in Chapter Two were only set up as a platform for further work and are therefore understandably crude and have great scope for improvement. The model assumes equimolar counter–diffusional flow to be occurring in the pores. From the stoichiometry of the cumene cracking equation, this is clearly

not the case. Attempts should be made to incorporate this although solution of diffusion–reaction equations in this case appears to be along way off.

The proposed method of coke deposition in the zeolite micropores is pure conjecture and this needs to be tightened up by linking further developments in the method of coke deposition with structural experiments such as N.M.R. and S.E.M..

NOMENCLATURE

NOMENCLATURE

A_j	Fraction of support surface area covered to a depth j in coke
A_{os}	Fraction of support free surface area in a pore element
A_{oz}	Fraction of zeolite free surface area in a pore element based on coke deposition in the zeolite and support
A_z	Fraction of zeolite free surface area in a pore element based on coke deposition in the zeolite
$C_A(x)$	Concentration profile along a pore element ($kmol/m^3$)
$C_{A,n}$	Intermediate concentration between pore elements n–1 and n ($kmol/m^3$)
C_{A0}	Bulk concentration ($kmol/m^3$)
$C_{A,0}$	concentration in the pore element at x=0 ($kmol/m^3$)
C_p	Mean product concentration in a pore element ($kmol/m^3$)
d	Size of coke unit in a support pore element (m)
D_n	Diffusion coefficient in a pore element n (m^2/s)
d_z	Size of coke unit in zeolite micropores (m)
F_{A0}	Flow rate of A into the reactor (kmol/s)
F_A	Flow rate of A out of the reactor (kmol/s)
f	Average coke content of the zeolite micropores in a pore element
G	Coefficient matrix
K	Proportionality constant
k_{cp}	Parallel coking rate constant ($m^4/s/kmol$)
k_{cs}	Series coking rate constant ($m^4/s/kmol$)
k_s	Surface rate constant for main reaction (m/s)
L	Length of a pore element (m)
M	Mean depth of coke units in a support pore element
M'	Mean depth of coke units in the zeolite micropores in a pore element
m_n	Reaction modulus for pore element n (m^{-1})

N	Number of elements in a pore
N_s	Number of active sites in a pore element
n	A pore element
n'	Matrix order and n'xn' network size
n_c	Number of coke units in a pore element
$R(0)$	Initial radius of pore element (m)
$R(t)$	Average radius of pore element after time t (m)
R_n	Radius of pore element n (m)
$(-r_A)$	Rate of reaction of A ($kmol/m^3/s$)
$r(0)$	Initial radius of the zeolite micropores (m)
$r(t)$	Radius of the zeolite micropores after time t (m)
S_n	Total active surface area in pore element n (m^2)
$S_g(t)$	Specific catalyst surface area after time t (m^2/g)
S_g	Specific zeolite surface area (m^2/g)
t	Time (s)
V	Volume of catalyst in reactor (m^3)
$V_c(t)$	Specific coke content of the catalyst (m^3/g)
V_g	Specific support volume (m^3/g)
$V_m(t)$	Specific coke content of the zeolite micropores (m^3/g)
$v_m(t)$	Volume of coke in the zeolite micropores (m^3)
v_o	Volumetric flowrate of A (m^3/s)
$V_s(t)$	Specific coke content of the support pores (m^3/g)
$v_s(t)$	Volume of coke in a pore element (m^3)
$V_z(t)$	Specific volume of zeolite lost (m^3/g)
$v_z(t)$	Volume of zeolite lost in a pore element (m^3)
W_c	Mass of catalyst in reactor (g)
x	Length along a pore element (m)
X_A	Conversion
α	Fraction of initial activity associated with the zeolite

$\eta(t)$	Effectiveness factor for the catalyst as a whole
ϕ	Observed/apparent Thiele modulus for the catalyst

Subscripts:

i	Pore number
j	Element number

REFERENCES

REFERENCES

Abbasi M., Evans J. & Abramson I.; (1983) AIChE J., **29**, 617.

Abbot J. & Wojciechowski B.; (1985), Canad. J. Chem. Eng., **63**, 278.

Abbot J. & Wojciechowski B.; (1988), Canad. J. Chem. Eng., **66**, 817.

Absil R., Batt J. & Dranogg J.; (1984), J. Catal., **85**, 415.

Acharya D.R., Hughes R. & Li K.; (1989), Appl. Catal., **52**, 115.

Adkins B., Milburn D. & Davis B.; (1988), Ind. Eng. Chem., Prod. Res. Dev., **27**(5), 796.

Agrawal R. & Wei J.; (1984), Ind. Eng. Chem., Process Des. Dev., **22**, 56.

Allen T.; (1990), "Particle Size Measurement", 4th. Edn., Chapman & Hall, p540.

Androutsopoulos G. & Mann R.; (1979), Chem. Eng. Sci., **34**, 1203.

Androutsopoulos G.; (1976), Ph. D. Thesis, University of Manchester.

Angelli M., Gonzalcz M. & Ponzi E.; (1982), Chem. Eng. J., **25**, 175.

Anthony R. & Liu R.; (1981), AIChE J. **27**, 1024.

Apesteguia C., Brema G., Garetto T., Borgna A. & Parera J.; (1983), Proceedings, 10th Interamerican Congress of Chemical Engineering, Santiago de Chile, Chile, Vol.1, p106.

Aulund L.; (1976), Oil Gas J., **74**(48), 60.

Baiker A., Monti D. & Fan S.; (1984), J. Catal., **88**, 81.

Bartholomew C.; (1982), Catal. Rev.–Sci. Eng., **24**(1), 67.

Bartholomew C.; (1984), Chem. Eng., **91**(23), 98.

Beekman J. & Froment G.; (1980), Chem. Eng. Sci., **35**, 805.

Beekman J. & Froment G.; (1982), Ind. Eng. Chem., Fundam., **21**, 243.

Beekman J.; (1990), Chem. Eng. Sci., **45**, 2603.

Best D.A. & Wojciechowski B.W.; (1977), J. Catal., **47**, 343.

Best D.A. & Wojciechowski B.W.; (1977), J. Catal., **47**, 11.

Beuther H. & Schmid B.; (1963), Proceedings 6th World Petroleum Congress Sec. III, Frankfurt, Main Paper 20.

Beyne A.O.E. & Froment G.F.; (1990), Chem. Eng. Sci., **45**, 2089.

Bharati S. & Bhatia S.; (1987), Ind. Eng. Chem., Prod. Res. Dev., **26**(9), 854.

Biswas J, Bickle G., Gary P. & Do D.; (1987), Paper in "Studies in Surface Science and Catalysis: Catalyst Deactivation", Vol.**34**, Elsevier, Amsterdam, p553.

Blanding F.; (1953), Ind. Eng. Chem., **45**, 1186.

Bond G.; (1962), "Catalysis by Metals", Academic Press, New York.

Butt J.B.; (1976), J. Catal., **41**, 190.

Cadet V., Raatz F., Lynch J & Marcilly C.; (1991), Appl. Catal., **68** (1–2), 263.

Cambell D. & Wojciechowski B.; (1971), J. Catal, **23**, 307.

Carberry J.; (1976), "Chemical and Catalytic Reaction Engineering", McGraw–Hill, New York, p399.

Carberry J.; (1987), Quad. Ing. Chem. Ital., **23**(9–10), 3.

Castiglioni B.; (1983), Hydrocarbon Process., **32**, 35.

Chang H. & Crynes B.; (1986), AIChE J., **32**, 224.

Chang Y. & Perlmutter D.; (1987), AIChE J., **33**(6), 940.

Chatzis I. & Dullien F.; (1977), J. Pet. Tech., **15**, 97.

Chen O.T. & Riwker R.G.; (1979), Chem. Eng. Sci., **34**, 51.

Conner W. & Lane A.; (1984), J. Catal., **89**, 217.

Corella J. & Asua J.; (1980), Chem. Eng. Sci., **35**, 1447.

Corella J., Asua J. & Bilbao J.; (1981), Canad. J. Chem. Eng., **59**, 647.

Corella J. & Asua J.; (1982a), Ind. Eng. Chem. Process Des. Dev., **21**, 55.

Corella J. & Asua J.; (1982b), Ind. Eng. Chem. Process Des. Dev., **21**, 551.

Corella J., Asua J. & Aznar M.; (1984), An. Quim., **80**, 715.

Corella J. & Menendes M.; (1986), Chem. Eng. Sci., **41**, 1817.

Corella J., Adanez J. & Monzon A.; (1988), Ind. Eng. Chem., Prod. Res. Dev., **27**, 375.

Corella J. & Monzon A.; (1988), Ind. Eng. Chem., Prod. Res. Dev., **27**, 369.

Corrigan T.E., Garrer H.F., Rase H.F. & Kirk R.S.; (1953), Chem. Eng. Prog., **49**, 603.

Coughlin R., Hasan A. & Kawakami K.; (1984), J. Catal., **88**, 163.

Decroocq D.; (1984), "Catalytic Cracking of Heavy Petroleum Fractions", Technip, Paris, p83.

Delmon B., & Grange P.; (1980), a paper in "Studies in Surface Science and Catalysis: Catalyst Deactivation", Vol.**6**, Elsevier, Amsterdam, p545.

Dodd G. & Kiel O.; (1959), J. Phys. Chem., **63**, 1646.

Dullien F.A.; (1975), AIChE J., **21**, 299.

Dumez F. & Froment G.; (1976), Ind. Eng. Chem., Process Des. Dev., **15**, 291.

Duncan T., Winslow P. & Bell A.; (1985), J. Catal, **93**, 1.

Dwyer J. & Dyer A.; (1984), Chemistry and Industry, **7**, 237.

Dwyer J.; (1984), Chemistry and Industry, **7**, 258.

Eberly P., Kimberlin C. (Jr), Miller W. & Drushel H.; (1966), Ind. Eng. Chem., Process Des. Dev., **5**, 193.

Eendy T. & Pratt K.; (1982), Chem. Eng. Sci., **37**, 37.

El–Kady F. & Mann R.; (1981), J. Catal., **69**, 147.

El–Kady F. & Mann R.; (1982), App. Catal., **3**, 211.

El–Kady F. & Mann R.; (1982), App. Catal., **3**, 234.

El–Nashaie S., Al–Ubaid A. & Soliman M.; (1988), Paper in "Studies in Surface Science and Catalysis: Catalyst Deactivation", Vol .**36**, Elsevier, Amsterdam, p89.

Everrett D.; (1988), Paper in "Studies in Surface Science and Catalysis: Catalyst Deactivation", Vol. **39**, Elsevier, Amsterdam, p1.

Evans R. III, Watson G. & Mason E.; (1961), J. Chem Phys., **25**, 2076.

Fatt I.; (1956), Petr. Trans. AIME **207**, 144.

Foster R. & Butt J.; (1966), AIChE J., **12**, 180.

Frevel L. & Kressley L.; (1963), J. Anal. Chem., **35**, 1492.

Froment G. & Bischoff K.; (1961), Chem. Eng. Sci., **16**, 189.

Froment G. & Bischoff K.; (1962), Chem. Eng. Sci., **17**, 105.

Froment G.; (1980), Paper in "Studies in Surface Science and Catalysis: Catalyst Deactivation", Vol. **6**, Elsevier, Amsterdam, p1.

Gavalas G., Phichitkul & Voecks G.; (1984), J. Catal., **88**, 65.

Ghabaee K.; (1986), Ph.D Thesis, University of Manchester.

Golshan H.; (1979), Ph.D Thesis, University of Manchester.

Hashimoto K., Masuda T. & Isobe K.; (1988), J. Chem. Eng. Jap., **21**(3), 249.

Hatcher W.J. (Jr); (1985), Ind. Eng. Chem., Prod. Res. Dev., **24**, 10.

Hayes R., Thomas W. & Hayes K.; (1985), J. Catal., **92**, 312.

Heaton C.A.; (1991), "An Introduction to Industrial Chemistry", 2nd Edition, Blackie & Son Ltd., p73.

Hegedus L. & McCabe R.; (1980), Paper in "Studies in Surface Science and Catalysis: Catalyst Deactivation", Vol.6, Elsevier, Amsterdam, p471.

Heinemann H. & Somorjai G.; (1984), "Catalysis and Surface Science", Marcel Dekker Inc., New York & Basel, p223.

Hightower J. & Emmett P.; (1965), J. Am. Chem. Soc., **87**, 939.

Holloway P. & Kramer D.; (1977), Report SAND, 1389.

Horng D. & Liapis A.I.; (1987), Chem. Eng. Res. Des., **65**, 123.

Hughes C. & Mann R.; (1978), ACS. Symp. Series, **65**, 201.

Hughes R.; (1984), "Deactivation of Catalysts", Academic Press, London.

Ilavsky J., Burianek J., Brunovska A. & Markos J.; (1986), Zb. Pr. Chemickotechnol. Fak. SVST, Volume date 1979–1981, p219.

Jacob S., Gross B., Voltz S. & Weekman V.; (1976), AIChE J., **22**, 701.

Janig C., Martin H. & Cambell D.; (1983), "Heterogeneous Catalysis" (Davis B. & Hettinger W., eds.), ACS Symposium Ser., 222.

Jodra L., Aragon J. & Palancar M.; (1981), Afinidad, **38**, 14.

John T. & Wojciechowski B.; (1975), J. Catal., **37**, 240.

Johnson M. & Stewart W.; (1965), J. Catal., **61**, 155.

Kelly R., Candela G., Madey T., Newburg D. & Schehl R.; (1983), J. Catal., **80**, 235.

Khalaf K.; (1988), Ph.D. Thesis, University of Manchester.

Khang S. & Levenspiel O.; (1973), Ind. Eng. Chem., Fundam., **12**, 185.

Klavetter E.A., Liapis A.I., Crosser O.K. & Litchfield R.J.; (1982), Chem. Eng. Sci., **37**, 997.

Klavetter E.A., Liapis A.I., Crosser O.K. & Litchfield R.J.; (1984), Chem. Eng. Commun., **28**, 369.

Klavetter E.A., Liapid A.I., Crosser O.K. & Litchfield R.J.; (1984), Chem. Eng. Commun., **31**, 237.

Kovach S., Castle L., Bennet J. & Schrodt J.; (1978), Ind. Eng. Chem., Prod. Res. Dev., **17**, 62.

Kruyer S.; (1958), Trans. Faraday Soc., **54**, 1758.

Ksenzhek O.S.; (1963), Russ. J. Phys, Chem., **37**, 691.

Kwon B. & Pickett G.; (1975), SPLULA 16th Annual Logging Symposium.

Lapidus G., Lane A., Ng K. & Conner, W. (1985), Chem. Eng. Commun., **38**, 33.

Larocca Miguel, Farag Hang, Ng Siauw & De Lasa Hugo; (1990), Ind. Eng. Chem., Prod. Res. Dev., **29**(11), 2181.

Lee J. & Luss D.; (1969), Ind. Eng. Chem., Fundam., **8**, 596.

Levenspiel O.; (1972b), "Chemical Reaction Engineering", 2nd Edn., John Wiley & Sons Inc.

Levy L. & De Groot P.; (1982), J. Catal, **76**, 385.

Liapis A.T. & Litchfield R.J.; (1979), Chem. Eng. Sci., **34**, 975.

Lin C., Park S. & Hatcher W.J.; (1983), Ind. Eng. Chem., Process Des. Dev., **22**, 609.

Lin C. & Slattery J.; (1982), AIChE J., **28**, 311.

Lin C. & Hatcher W.J.; (1982), ACS, **196**, 249.

Lowell S.; (1979), "Introduction to Powder Surface Area", John Wiley & Sons, New York, p16.

MacIver D., Tobin H. & Barth R.; (1963), J. Catal., **2**, 485.

Mandelbrot B., (1977), "The Fractal Geometry of Nature", Freeman W.H. (Ed.).

Mann R., El–Kady F. & Moore I.; (1984), Proc. ISCRE8 (I. Chem. E. Symposium Series 87).

Mann R., El–Kady F. & Marzin R.; (1985), Chem. Eng. Sci., **40**, 249.

Mann R., Sharrat P. & Thomson G.; (1986), Chem. Eng. Sci., **41**, 708.

Mann R., Sharrat P. & Thomson G.; (1986), Chem. Eng. Sci., **41**, 711.

Mann R. & Thomson G.; (1987), Chem. Eng. Sci., **42**, 555.

Mann R. & Sharrat P.; (1988), Chem. Eng. Sci., **43**, 1875.

Mann R. & Wasilewski M.C.; (1990), Trans. I. Chem. Eng., **68**(A), March.

Markami Y., Kobayashi T., Hattori T. & Masuda M.; (1968), I & EC Fund., **7**, 599.

Markos J. & Brunovska A.; (1988), Collect. Czech. Chem. Commun., **53**(1), 45.

Masai M., Shiraishi E., Yoshimura T., Nishiyama S. & Suruya T.; (1984), Proceedings, 9th Iberoamerican Symposium on Catalysis, Lisbon, Portugal, Vol. 1, p561.

Mason E., Malinauskas A. & Evan R.B.III; (1967), J. Chem. Phys., **46**, 3199.

Mason E. & Malinauskas A.; (1983), "Gas Transport in Porous Media– The Dusty Gas Model", Elsevier, New York, USA.

Mayer R. & Stowe R.; (1966), Phys. Chem., **70**, 3867.

McClung Ronald G.; (1990), Oil Gas J., **88**(41), 98.

Mills G., Boedeker E. & Oblad A.; (1950), I. Amer. Chem. Soc., **72**, 1554.

Mirodatos C., Paraliand H. & Primet M.; (1984), Proceedings, 9th Iberoamerican Symposium on Catalysis, Lisbon, Portugal, Vol. 1, p571.

Monhanty K., Ottino J. & Davis H.; (1982), Chem. Eng. Sci., **37**, 905.

Moore I.; (1983), Ph.D. Thesis, University of Manchester.

Murphy J.R.; (1970), Oil Gas J., **68**(47), 72.

Nace D., Voltz S. & Weekman V.; (1971), Ind. Eng. Chem., Process Des. Dev., **10**, 530.

Nam I. & Kittrell J.; (1984), Ind. Eng. Chem., Process Des. Dev., **23**, 237.

Namba S., Nakanishi S. & Yashima T.; (1984), J. Catal., **88**, 505.

Newson E.; (1975), Ind. Eng. Chem., Process Des. Dev., **14**, 27.

Nicholson D. & Petropoulos J.; (1968), Brit. J. App. Phys., **1**, 1379.

Nicholson D. & Petropoulos J.; (1971), J. Phys. D. App. Phys.; **4**, 181.

Noda H., Tone S. & Otaoke T.; (1974), J. Chem. Eng. Japan, **7**, 110.

Oblad A.; (1983), "Heterogeneous Catalysis" (Davis B. & Hettinger W., eds.), ACS Symposium Ser., 222.

Ochoa J., Stroeve P. & Whitaker S.; (1986), Chem. Eng. Sci., **41**, 2999.

Oxenreiter M., Frye C., Hoekstra G. & Stroke J.; (1972), Paper Presented at the Japanese Pet. Inst. Nov.30.

Ozawa Y.& Bischeff K.; (1968), Ind. Eng. Chem., Process Des. Dev., **7**, 67.

Pacheco M. & Petersen E.; (1984), J. Catal., **86**, 75.

Pacheco M. & Petersen E.; (1984), J. Calal., **88**, 400.

Paloumbis S. & Petersen E.; (1982), ACS Symp. Series, **196**, 489.

Pansing W.F. & Malloy J.B.; (1965), Ind. Eng. Chem., Process Des. Dev. **4**, 181.

Pearce R. & Patterson W.R.; (1981), eds., "Catalysts and Chemical Processes", Glasgow, Blackie & Son Ltd., p30.

Petersen E.; (1958), AIChE J., **4**, 343.

Plank C. & Nace D.M.; (1955), Ind. Eng. Chem., **47**, 2347.

Plank C.; (1983), "Heterogeneous Catalysis" (Davis B. & Hettinger W., eds.), ACS Symposium Ser., 222.

Polinski L., Stiegel G. & Saroff L.; (1981), Ind. Eng. Chem., Process Des. Dev., **20**, 470.

Pozzi A. & Rase H.; (1958), Ind. Eng. Chem., **50**, 1075.

Prasad K. & Valdyeswaran R.; (1986), Ind. Eng. Chem., Fundam., **25**, 184.

Qamar I. & Goodwin J.; (1983), Eighth North American Meeting of the Catalysis Soc., May 1–4, Philadelphia, Paper C–22.

Rautiainen E.P.H. & Wei J.; (1990), Chem. Eng. Commun., **98**, 113.

Rees L.V.C.; (1984), Chemistry and Industry, **7**, 252.

Reyes B. & Jensen K.;(1985), Chem. Eng. Sci., **40**, 1723.

Reyes Sebastian C. & Scriven L.E.; (1991), Ind. Eng. Chem., Prod. Res. Dev., **30**(1), 71.

Rollman L.D. & Walsh D.E.; (1979), J. Catal., **56**, 139.

Rostrup–Nielsen J.R.; (1974), J. Catal., **33**, 184.

Ruderhausen C. & Watson C.; (1954), Chem. Eng. Sci., **3**, 110.

Ryan D., Carbonell R. & Whitaker S.; (1980), Chem. Eng. Sci., **35**, 10.

Ryan D., Carbonell R. & Whitaker S.; (1981), AIChE Symposium Series, **77**, 46.

Satterfield C.N. & Sherwood T.K.; (1963), "The Role of Diffusion in Catalysis", Addison Wesley Publishing Company, Reading Ma, p16.

Sharrat P.; (1985), M.Sc. Thesis, University of Manchester.

Shimura M., Shinto Y. & Takeuchi C.; (1986), Ind. Eng. Chem., Fundam., **25**, 330.

Simon R. & Kelsat F.; (1971), Soc. Pet. Eng. J., **99**, 212.

Smith D.M.; (1986), AIChE J., **32**, 239.

Smith D.M.; (1986), AIChE J., **32**, 329.

Smith D.M.; (1986), AIChE J., **32**, 1039.

Soong Y., Krishna K. & Biloen P.; (1986), J. Catal., **97**, 330.

Stainslaus A. & Absi Halabi M.; (1984), "Catalyst Characterization Handbook", K.I.S.R., Kuwait, p27.

Stiegel G., Tischer R., Cillo D. & Karain N.; (1985), Ind. Eng. Chem., Prod. Res. Dev., **24**, 206.

Stohl F. & Stephens H.; (1987), Ind. Eng. Chem., Prod. Res. Dev., **26**(12), 2466.

Tan L. M. & Bennett C. O.; (1985), J. Catal., **96**, 408.

Tan C. H. & Fuller O. M.; (1970), Canad. J. Chem. Eng., **48**, 174.

Ternan M. & Packwood R.; (1986), NATO ASI Series, Ser. E. **110** (Chem. React. Des. Technol.), p63.

Tewarkson R.P.; (1973), "Sparse Matrices", Academic Press, New York, p2.

Theodorou D. & Wei J.; (1983), J. Catal., **83**, 205.

Thiele E.; (1939), Ind. Eng. Chem., **31**, 916.

Thomson G.; (1984), M.Sc. Thesis, University of Manchester.

Thomson G.; (1986), Ph.D. Thesis, University of Manchester.

Trimm D.L.; (1985), "Catalyst Characterisation, Evaluation and Deactivation", Lecture Notes, K.I.S.R. Kuwait Feb 2–6, p85.

Tsakalis K., Tsotsis T. & Stiegel G.; (1984), J. Catal., **88**, 188.

Van Hoff J.H.C.; (1980), "Chemisty and Chemical Engineering of Catalytic Cracking", Eds. Prins & Schmitt., p161.

Vaughan D.E.W.; (1979), The Chem. Soc. (London) Special Publication, **33**, p294.

Venuto P.B. & Habib E.T; (1979), Catal. Revs. Sci. Eng., **18**, 1.

Venuto P.B. & Habib E.T.; (1979), "Fluid Catalytic Cracking with Zeolite Catalysts", Marcel Dekker Inc., p134.

Venuto P.B. & Landis P.S.; (1968), Ind. Eng. Chem., Fundam., **7**, 274.

Viner M. & Wojciechowski B.; (1982), Canad. J. Chem. Eng., **60**, 127.

Viner M. & Wojciechowski B.; (1984), Canad. J. Chem. Eng., **62**, 870.

Voorhies A. (Jr); (1945), Ind. Eng. Chem., **37**, 318.

Wakao N., Kimura H. & Shibata M.; (1969), J. Chem. Eng. Japan, **2**, 51.

Wakao N., & Smith J.; (1962), Chem. Eng Sci., **17**, 825.

Wakao N. & Narusa Y.; (1974), Chem. Eng. Sci., **29**, 1304.

Walker P.M.; (1991), "Chambers Science and Technology Dictionary", W & R Chambers Limited.

Wall G. & Brown R.; (1981), J. Colloid. Interface Sci., **82**, 141.

Wardlaw N.C.; (1980), APE, 8843.

Wardlaw N.C. & Mckeller M.; (1981), Powder Tech., **29**, 127.

Wardlaw N.C.; (1982), J. Canad. Pet. Tech., May–June, 21.

Wasilewski M.; (1986), M.Sc. Dissertation, University of Manchester.

Weekman V. & Nace D.; (1970), AIChE J., **16**, 379.

Weisz P.B.; (1969), Oil Gas J., **67**(45), 82.

Weisz P.B.; (1973), Chem. Technol., **3**, 498.

Wheeler A.; (1951), Adv. Catal., **3**, 250.

Whitaker S.; (1967), AIChE J., **13**, 420.

Whitaker S.; (1986), Chem. Eng. Sci., **41**, 3015.

Xiao J. & Wei J.; (1992), Chem.Eng. Sci., **47**, 1123.

APPENDICES

APPENDIX–1

```
      PROGRAM LAY10
C----------C *** THIS PROGRAM SOLVES THE EQUATIONS FOR DIFFUSION AND RE action c
C*** THROUGH A SQUARE GRID WITH PORES OF CONSTANT LENGTH BUT HAVING
C * **
CDIFFERENT RADII. THE REACTIONS A -> B -> COKE AND B > COKE
C *** IN SE ries are
CMODELLED ASSUMING THAT THE A > B STEP IS
C *** FIRST ORDER IN A AND FI rst order
CIN PORE WALL AREA. THE STEP
C *** B> COKE IS ASSUMED TO BE FIRST ORDER  In b,
CAND SECOND ORDER
C *** IN FREE PORE WALL AREA (CF. VINER & W'SKI).
C  *** the
CPORE SIZES, AND THUS THE CONCENTRATION PROFILES ARE
C *** MODIFIED BY  the
CLAYDOWN OF THIS COKE. THE LAYDOWN RATE
C *** EQUATION IS PROGRESSED BY  a fourth
CORDER RUNGE-KUTTA METHOD.
C ***                C IS A MATRIX OF
CCONCENTRATIONS
C ***                RADIUS,RADO AND RAD1 STORE THE PO re radii
C***                RATCO IS THE LOCAL RATE OF COKING
C -------------- -------
C----------------------------------------
      REAL*8 G05CAF,DUMMY
      INTEGER ZELVO,ZERO(100)
      COMMON RADO,RAD1 /A/ DCO,PL,RKP,RKS,COKAM,RATCO,C,CB,RATE
     +,NN,VFREE,AREAS,AREAZ
      COMMON /C/ COUT,COUTR
      DIMENSION C(0:11,0:11),CB(0:11,0:11),RADO(0:10,0:10,2)
     +,NN(0:11,0:11)
      DIMENSION RADIUS(0:10,0:10,2),RATCO(0:10,0:10,2,4)
     +,RAD1(0:10,0:10,2)
      PARAMETER (PI=3.141592)
C *** RESULTS FROM UP TO 40 TIME STEPS
CC    DIMENSION RESU(41,30),CONVER(41)
      DIMENSION RESU(200,30),CONVER(41)
      OPEN (30)
      REWIND 30
C     OPEN (10,FILE='LAY10')
      OPEN (10)
      REWIND 10
C     OPEN (2,FILE='ISOTHERM')
      OPEN (20)
C     OPEN (2)
      REWIND 20
      OPEN (99)
      REWIND 99
C     OPEN (10,FILE='LST:')
C ---------------------------------------------------------------
C *** ENTER PARAMETERS DESCRIBING THE SYSTEM
C ---------------------------------------------------------------
CCCCCCCCC  DATA USED   CCCCCCCCCCCCCCCCCCCCCCCCCCCCCCC
      READ(30,*) PL,DCO,RK,COUT,CONIN,TSTEP,NLT
     +          ,RKP,RKS,SCOK
      NTR=1
      NLAY=1
CCCCCCCCCCCCCCCCCCCCCCCCCCCCCCCCCCCCCCCCCCCCCCCCCCCCCCCCCCCCCCCCCCCCC
      WRITE(*,*) PL,DCO,RK,COUT,CONIN,TSTEP,NLT,NTR
     +          ,RKP,RKS,SCOK,NLAY
CCCCCCCCC  OMRAN ADDED DATA
      WRITE(10,*) PL,DCO,RK
      WRITE(10,*) COUT,CONIN,TSTEP
      WRITE(10,*) NLT,NTR,RKP
```

```
      WRITE(10,*) RKS,SCOK,NLAY
CC    WRITE(10,*) PROZ,DECRAT
      WRITE(10,*) '********** END OF DATA ********** '
CCCCCCCCC  OMRAN ADDED ABOVE DATA
CCCCCCCCCCCCCCCCCCCCCCCCCCCCCCCCCCCCCCCCCCCCCCCCCCCCCC
      WRITE (10,*) 'PORE LENGTH IN MICRO-METRES             ',PL
      WRITE (10,*) 'DIFF,N COEFF,T IN UNITS OF 10^-6 M^2/S  ',DCO
      WRITE (10,*) 'RATE CONSTANT, 10^-9 M/3                ',RK
      WRITE (10,*) 'PARALLEL COKING RATE CONST              ',RKP
      WRITE (10,*) 'SERIES COKING RATE CONST                ',RKS
CCCCCCC
CCCCCCC   PAGE 2  CCCCCCCCCCCCCCCCCCCCCCCCCCCCCCCCCCCCCCCCCCCCCCCC
CCCCCCC
      WRITE (10,*) 'OUTSIDE CONCENTRATION, IN MOL/M^3       ',COUT
      WRITE (10,*) 'INITIAL CONVERSION                      ',CONIN
      WRITE (10,*) 'COKE SIZE, ANGSTROM                     ',SCOK
      WRITE (10,*) 'NUMBER OF AXIAL DIVISIONS               ',NLAY
CC    WRITE (10,*) 'PROPORTION OFACTIVITY WHICH IS ZEOLITE  ',PROZ
CC    WRITE (10,*) 'RATIO OF DECAY CONSTANTS ZEOLITE/SUPPORT  ',DECRAT
CCCCCCCCCCCCCCCCCCCCCCCCCCCCCCCCCCCCCCCCCCCCCCCCCCCCCCCCCCCCCCCCCCC
CCCCCCCCCCCCCCCCCC B
CC    READ(30,*)  PROZ,DECRAT
CCCCCCCCCCCCCCCCCC
C     PRINT *,'ENTER PORE LENGTH IN MICRO-METRES '
C     READ *,PL
C     PRINT *,'ENTER DIFFUSION COEFFICIENT IN UNITS OF 10^-6 M^2/S '
C     READ *,DCO
C     PRINT *,'ENTER RATE CONSTANT, IN UNITS OF 10^-9 M/S '
C     READ *,RK
C     PRINT *,'ENTER TOTAL OUTSIDE CONCENTRATION, IN MOL/M^3 '
C     READ *,COUT
C     PRINT *,'ENTER INITIAL CONVERSION, DECIMAL 0-1 '
C     READ *,CONIN
C     PRINT *,'ENTER TIME STEP FOR COKING, SECONDS ,'
C     READ *,TSTEP
C     PRINT *,'ENTER NO. OF STEPS PER TRIAL '
C     READ *,NLT
C     PRINT *,'ENTER NUMBER OF TRIALS '
C     READ *,NTR
C *** THE COKING RATE CONSTANTS IMPLICITLY INCLUDE THE COKE DENSITY
C     PRINT *,'ENTER PARALLEL COKING RATE CONST (*10^-10)'
C     READ *,RKP
C     PRINT *,'ENTER SERIES COKING RATE CONST (*10^-10)'
C     READ *,RKS
C     PRINT *,'ENTER MEAN COKE SIZE, ANGSTROM '
C     READ *,SCOK
C     PRINT *,'ENTER NO OF AXIAL LAYERS '
C     READ *,NLAY
CCCCCCCCCCCCC  OMRAN PUT FOLLOWING FROM SUBROUTINE EFFIC
C     PRINT *,'INPUT PROPORTION OF ACTIVITY WHICH IS ZEOLITE '
C     READ *,PROZ
C     PRINT *,'INPUT RATIO OF DECAY CONSTANTS ZEOL/SUPPORT'
C     READ *,DECRAT
C     WRITE(*,*) 'PROZ=',PROZ,'DECRAT=',DECRAT
      SCOK=SCOK*1E-10
      RKS=-RKS*1E-10
      PL=PL*1.E-6
      RKP=-RKP*1E-10
      RK=RK*1E-9
      DCO=DCO*1.E-6
CCCCCCCCCCOMRAN ADDED
      DO 789 IJK=1,1
CC    PRINT*,'IJK=',IJK
      IF(IJK.EQ.1) GOTO 333
```

```
CC    PROZ=PROZ-0.2
CC    WRITE(10,*)'PROZ     = ',PROZ
CC    SCOK=SCOK*2
CC    WRITE(10,*)'SCOK     = ',SCOK
CC    PL  =PL*5
CC    WRITE(10,*)'PL       = ',PL
CC    RK  =RK*10
CC    WRITE(10,*)'RK       = ',RK
CC    RKS =RKS*05
CC    WRITE(10,*)'RKS      = ',RKS
CC    CONIN =CONIN-0.05
CC    WRITE(10,*)'CONIN (INITIAL CONV.     = ',CONIN
CCCCCCCCCC
CCCCCCCCCC
 333  DO 12 I=1,41
 12   CONVER(I)=0
C *** NLAY IS THE NUMBER OF AXIAL LAYERS
      DO 1111 LAYER=1,NLAY
C *** CLEAR THE MATRIX WHICH STORES THE RESULTS - RESU
      DO 13 I=1,41
      DO 13 J=1,30
 13   RESU(I,J)=0
      NLOOP2=0
C *** NTR IS THE NUMBER OF TRIALS PER LAYER
      DO 9999 NTRIAL=1,NTR
C -------------------------------------------------------------
C *** INITIALISE THE RANDOM NUMBER GENERATOR (MISSES THE FIRST
C *** N NUMBERS FROM THE SEQUENCE).
C -------------------------------------------------------------
CCCCCC OMRAN ADDED FOR CHECK
C     WRITE(*,*)'OK 1'
CCCCCC   OMRAN CANCELLED THE NEXT TWO LINES  CCCCCCCCCCC
C     DO 50 I=1,220
C 50  CALL RAND (R)
CCCCCCCCCCCCCCCCCCCCCCCCCCCCCCCCCCCCCCCCCCCCCCCCCCCCCCCCCC
C *** T=TIME,VNET=NETWORK VOLUME,ZEVIN=ZEOLITE VOLUME. INITIAL
C *** ZEOLITE VOLUME IS ASSUMED PROPORTIONAL TO WALL AREA.
      T=0
      VNET=0
      ZEVIN=0
      DO 52 I=1,100
      ZERO(I)=0
 52   CONTINUE
C -------------------------------------------------------------
C *** NOW SET UP THE PARAMETER MATRICES, USING . NDOM VALUES OF
C *** RADIUS CALLED FROM RCALC.GRIDPRIN PRINTS OUT THE GRID.
C *** THE POROSIMETRY DATA WAS FITTED TO A 10*10  PORE
C *** SIZE DISTRIBUTION,DESCRIBED HERE BY DIVISION INTO
C *** SEVEN REGIONS OF UNIFORM PROBABILITY DISTRIBUTION.
C -------------------------------------------------------------
       WRITE(10,*) 'SOME RADII IN ANGSTROM ARE AS FOLLOWS '
      DO 100 I=0,10
CC           PRINT*,'I=',I
          DO 100 J=0,10
CC           PRINT*,'J=',J
             DO 100 K=1,2
CC           PRINT*,'K=',K
C              CALL RAND (RND)
CCCCCCCCC   OMRAN ADDED THIS RANDOM NUMBER GENEREATOR
               RND=G05CAF(DUMMY)
CCC            WRITE(*,*) RND
CCCCCCCCCCCCC
               IF(RND.LT.0.504) THEN
               R=30+20*RND/0.504
```

```
                GOTO 85
                ENDIF
                IF (RND.LT.0.550) THEN
                R=50+50*(RND-0.504)/0.046
                GOTO 85
                ENDIF
                IF (RND.LT.0.623) THEN
                R=100+100*(RND-0.550)/0.073
                GOTO 85
                ENDIF
                IF(RND.LT.0.742) THEN
                R=200+300*(RND-0.623)/0.119
CCCCCCC
CCCCCCC   PAGE  3   CCCCCCCCCCCCCCCCCCCCCCCCCCCCCCCCCCCCCCCCCCCCCCCC
CCCCCCC
                GOTO 85
                ENDIF
                IF(RND.LT.0.843) THEN
                R=500+500*(RND-0.742)/0.101
                GOTO 85
                ENDIF
                R=1000+1000*(RND-0.843)/0.157
 85             CONTINUE
CCCCCCCC OMRAN ADDED THE FOLLOWING
      R=60+RND*3140
CC    R=1600
CCC   R=60+RND*3140
CC    R=05+RND*2000
CCCCCCCCCCCCCCCCCCCCCCCC
      IF(I.EQ.0)THEN
      WRITE(10,*)R
CC    WRITE(*,*)R
      ENDIF
CCCCCCCCCCCCCCCCCCCCCC
CC    R=1600
CC    IF(RND.LT.0.500) THEN
CC    R=60
CC    ELSE
CC    R=3200
CC    ENDIF
CC    R=60+RND*100000
CCCCCCCCCCC
CCCCCC OMRAN ADDED FOR CHECK
C     WRITE(*,*)'OK 2'
C     WRITE(*,*) R
                R=R*1.0E-10
                RAD0(I,J,K)=R
                RAD1(I,J,K)=R
                VNET=VNET+R*R
                ZEVIN=ZEVIN+R
 100            RADIUS(I,J,K)=R
      WRITE(10,*)'**************************************************'
CCCCCC  OMRAN ADDED THE FOLLOWING
CCC   RADIUS(I,J,K)=RADIUS(I,J,K)*1.E+10
CCC   WRITE(10,*)( RADIUS(I,1,1),I=1,10)
CCC   RADIUS(I,J,K)=RADIUS(I,J,K)*1.E-10
CCCCCCCCCCCCCCCCCCCCCCCCCCCCCCCCCCCCCC
      DO 101 I=0,10
      RADIUS(0,I,2)=0
      RAD0(0,I,2)=0
      VNET=VNET-RAD1(0,I,2)*RAD1(0,I,2)
      ZEVIN=ZEVIN-RAD1(0,I,2)
      RAD1(0,I,2)=0
      RADIUS(I,0,1)=0
```

```
      RADO(I,0,1)=0
      VNET=VNET-RAD1(I,0,1)*RAD1(I,0,1)
      ZEVIN=ZEVIN-RAD1(I,0,1)
 101  RAD1(I,0,1)=0
      VNET=VNET*PI*PL
C *** RADCON WRITES THE PORE RADII TO DISC
      CALL RADCON(RADIUS)
C *** SET INITIAL STEP LENGTH TO 1 TIMESTEP PER STEP
      NSTP=1
      NLOOP1=0
      DO 2000 NLOOP=1,NLT
C *** ZERO(1) IS USED AS A FLAG TO INDICATE AN INDEFINITE RESULT
C *** FROM THE MATRIX INVERSION SUBROUTINE
      IF (ZERO(1).EQ.2) THEN
      GOTO 2000
      ENDIF
C ---------------------------------------------------------------
C *** GENERATE COKING RATES FOR R-K ALGORITHM. THE RATES ARE STORED
C *** IN RATCO. AFTER THE FIRST CALL OF CRATE THE CONCENTRATION
C *** PROFILE, WHICH CORRESPONDS TO THE RADII AT TIME T, IS PRINTED
C *** USING GRIDPRIN. THE CORRESPONDING PRODUCTIVITIES AND COKE
C *** CONTENTS ARE ALSO PRINTED.
C ---------------------------------------------------------------
      IF (NLOOP.GT.15) THEN
C *** AFTER FIFTH STEP MULTIPLY STEP LENGTH BY 5
      NSTP=5
CC    IF (NLOOP.GT.18) THEN
CC    NSTP=15
CC    NSTP=1
      IF (5*(NLOOP/5).NE.NLOOP) THEN
      GOTO 2000
      ENDIF
      NLOOP1=NLOOP1+1
      ELSE
      NLOOP1=NLOOP
      ENDIF
CCCCCC OMRAN ADDED FOR CHECK
C     WRITE(*,*)'OK 3'
C *** SET BOUNDARY CONDITIONS FOR THE GRID IN TERMS OF THE
C *** CONVERSION IN THE PREVIOUS AXIAL LAYER
      COUTR=COUT*(1-CONVER(NLOOP1))
      DO 51 I=0,11
      C(I,0)=COUTR
      C(I,11)=COUTR
CCCCCCC
CCCCCCC   PAGE 4   CCCCCCCCCCCCCCCCCCCCCCCCCCCCCCCCCCCCCCCCCCCCCC
CCCCCCC
      C(0,I)=COUTR
 51   C(11,I)=COUTR
C *** CRATE SOLVES THE DIFFUSION/REACTION EQUATIONS.
CCC   CALL CRATE (SCOK,1,RK,ZERO,ZEV,AREAS,AREAZ)
      CALL CRATE(SCOK,1,RK,ZERO,ZEV,AREAS,AREAZ)
CCCCCC OMRAN ADDED FOR CHECK
C     WRITE(*,*)'OK 4','ZERO(1)=',ZERO(1)
C     WRITE(*,*)'OK CRATE 1 '
      IF (ZERO(1).EQ.2) THEN
CCCCCC OMRAN ADDED FOR CHECK
C     WRITE(*,*)'OK 5'
      GOTO 2000
      ENDIF
C *** STORE RATES, COKE VOL, ZEOLITE VOL ETC. IN RESU.
      IF (NLOOP.EQ.1) RATMAX=RATE
      RESU(NLOOP1,5)=RESU(NLOOP1,5)+RATE
      RATE=RATE*100/RATMAX
```

```
      RESU(NLOOP1,17)=RESU(NLOOP1,17)+COKAM*100/VNET
      RESU(NLOOP1,18)=RESU(NLOOP1,18)+VFREE*100/VNET
      RESU(NLOOP1,20)=RESU(NLOOP1,20)+ZEV*100/ZEVIN
      COKAM=COKAM*1E15
      RESU(NLOOP1,2)=T
      RESU(NLOOP1,3)=RESU(NLOOP1,3)+COKAM
      RESU(NLOOP1,4)=RESU(NLOOP1,4)+RATE
      RESU(NLOOP1,1)=RESU(NLOOP1,1)+1
      DO 680 NC=0,10
CCCCCCC
      RESU(NLOOP1,NC+6)=RESU(NLOOP1,NC+6)+1.0E10*(RADO(5,NC,2)
     +-RAD1(5,NC,2))
CCCCCCCC
 680  CONTINUE
C *** INCREMENT TIME COUNTER
      T=T+TSTEP*NSTP
C *** GENERATE NEW RADII TO FEED TO CRATE. SEARCH GRID TO FIND PORES
C *** WHICH HAVE SHRUNK TO <20 ANGSTROM IN RADIUS AND SET THESE TO ZERO.
C *** RECOR THE POSITION OF THE NODES JOINED BY BLOCKED PORES BY
C *** INCREMENTING NN
      DO 700 I=0,10
         DO 700 J=0,10
            DO 700 K=1,2
CCCCCCCCCCCCCCCCCCCCCCCCCC
CCCCCCCCC OMRAN ADDED THE FOLLOWING
CCCCCC OMRAN ADDED RATCO(0,0,1,1)....(0,0,2,2)
CC    RATCO(0,J,K,1)=0.0
CC    RATCO(I,0,K,1)=0.0
CC    RATCO(0,J,K,2)=0.0
CC    RATCO(I,0,K,2)=0.0
CC    RATCO(0,J,K,3)=0.0
CC    RATCO(I,0,K,3)=0.0
CC    RATCO(0,J,K,4)=0.0
CC    RATCO(I,0,K,4)=0.0
CCCCCCCCC OMRAN ADDED THE ABOVE
            RAD1(I,J,K)=RADIUS(I,J,K)+TSTEP*NSTP*RATCO(I,J,K,1)/2
            IF (RAD1(I,J,K).LT.5.0E-10) THEN
            NN(I,J)=NN(I,J)+1
            NN(I+2-K,J+K-1)=NN(I+2-K,J+K-1)+1
            RAD1(I,J,K)=0
            ENDIF
 700  CONTINUE
CCCCCC    OMRAN ADDED
CCC      WRITE(10,*) ' AREAS =',AREAS,'AREAZ=',AREAZ
CCC      WRITE(*,*) ' AREAS =',AREAS,'AREAZ=',AREAZ
CCCCCCCCCCC
CCCC     WRITE(10,5678) ' AREAS =',AREAS,'AREAZ=',AREAZ
         WRITE(10,*) ' AREAS =',AREAS,'AREAZ=',AREAZ
         WRITE(77,5678)   AREAS,AREAZ
CCCCCC OMRAN ADDED  CCCCCCCCCCCCCCCCCCCCCC
          AREASSS=AREAS*0.2
          AREAZZZ=AREAZ*0.8
          AREATOT=AREASSS+AREAZZZ
          WRITE(99,5577)   AREASSS,AREAZZZ,AREATOT
CCCCCCCCCCCCC
CC       WRITE(99,5678)   AREAS,AREAZ
 5678 FORMAT (1H ,F7.3,'  ',F7.3)
CC       WRITE(10,*) ' AREAS =',AREAS,'AREAZ=',AREAZ
CC       WRITE(77,*)  AREAS,AREAZ
CC       WRITE(99,*)   AREAS,AREAZ
CC      CALL CRATE (SCOK,2,RK,ZERO,ZEV)
      CALL CRATE(SCOK,2,RK,ZERO,ZEV,AREAS,AREAZ)
      AZ=AZ+1
CCCCCC OMRAN ADDED FOR CHECK
```

```
C     WRITE(*,*)'OK 5','ZERO(1)=',ZERO(1)
C     WRITE(*,*)'OK CRATE 2 '
      IF (ZERO(1).EQ.2) THEN
      GOTO 2000

      ENDIF
      DO 710 I=0,10
          DO 710 J=0,10
              DO 710 K=1,2
              RAD1(I,J,K)=RADIUS(I,J,K)+TSTEP*NSTP*RATCO(I,J,K,2)/2
              IF (RAD1(I,J,K).LT.5.0E-10) THEN
              NN(I,J)=NN(I,J)+1
              NN(I+2-K,J+K-1)=NN(I+2-K,J+K-1)+1
              RAD1(I,J,K)=0
              ENDIF
 710   CONTINUE
CC    CALL CRATE (SCOK,3,RK,ZERO,ZEV)
      CALL CRATE(SCOK,3,RK,ZERO,ZEV,AREAS,AREAZ)
      AZ=AZ+1
CCCCCC OMRAN ADDED FOR CHECK
C     WRITE(*,*)'OK 6','ZERO(1)=',ZERO(1)
C     WRITE(*,*)'OK CRATE 3 '
      IF (ZERO(1).EQ.2) THEN
      GOTO 2000
      ENDIF
      DO 720 I=0,10
          DO 720 J=0,10
              DO 720 K=1,2
              RAD1(I,J,K)=RADIUS(I,J,K)+TSTEP*NSTP*RATCO(I,J,K,3)
CCCCCCC
CCCCCCC   PAGE 5  CCCCCCCCCCCCCCCCCCCCCCCCCCCCCCCCCCCCCCCCCCCCCCCC
CCCCCCC
              IF (RAD1(I,J,K).LT.5.0E-10) THEN
              NN(I,J)=NN(I,J)+1
              NN(I+2-K,J+K-1)=NN(I+2-K,J+K-1)+1
              RAD1(I,J,K)=0
              ENDIF
 720   CONTINUE
CC    CALL CRATE(SCOK,4,RK,ZERO,ZEV)
      CALL CRATE(SCOK,4,RK,ZERO,ZEV,AREAS,AREAZ)
      AZ=AZ+1
CCCCCC OMRAN ADDED FOR CHECK
C     WRITE(*,*)'OK 7','ZERO(1)=',ZERO(1)
C     WRITE(*,*)'OK CRATE 4 '
      IF (ZERO(1).EQ.2) THEN
      GOTO 2000
      ENDIF
      DO 730 I=0,10
          DO 730 J=0,10
              DO 730 K=1,2
C -------------------------------------------------------------
C *** MAKE R-K STEP
C -------------------------------------------------------------
      RADIUS(I,J,K)=RADIUS(I,J,K)+TSTEP*NSTP*(RATCO(I,J,K,1)
     ++2*RATCO(I,J,K,2)+2
     +*RATCO(I,J,K,3)+RATCO(I,J,K,4))/6
       IF (RADIUS(I,J,K).LT.5.0E-10) THEN
       RADIUS(I,J,K)=0
       NN(I,J)=NN(I,J)+1
       NN(I+2-K,J+K-1)=NN(I+2-K,J+K-1)+1
       ENDIF
 730  RAD1(I,J,K)=RADIUS(I,J,K)
CCCCCCCCC
CCC       WRITE(10,*) ' AREAS =',AREAS,'AREAZ=',AREAZ
```

```
CCCCCCCCCCC
 2000 CONTINUE
C *** NLOOP2 STORES THE NUMBER OF THE LAST FILLED ROW OF RESU
C *** FINAL CALL TO CRATE TO FIND FINAL RATES, VOLUMES ETC.
      IF (ZERO(1).EQ.2) THEN
      NLOOP2=MAXO(NLOOP2,NLOOP1-1)
      GOTO 9000
      ENDIF
CCC   CALL CRATE (SCOK,1,RK,ZERO,ZEV)
      CALL CRATE (SCOK,1,RK,ZERO,ZEV,AREAS,AREAZ)
CCC      WRITE(10,5566) ' AREAS =',AREAS,'AREAZ=',AREAZ
         WRITE(10,*) ' AREAS =',AREAS,'AREAZ=',AREAZ
         WRITE(77,5566)   AREAS,AREAZ
CCCCCCC OMRAN ADDED  CCCCCCCCCCCCCCCCCCCCCCCC
          AREASSS=AREAS*0.2
          AREAZZZ=AREAZ*0.8
          AREATOT=AREASSS+AREAZZZ
          WRITE(99,5577)   AREASSS,AREAZZZ,AREATOT
 5577 FORMAT (1H ,F7.3,'  ',F7.3,'  ',F7.3)
CCCCCCCCCCCCC
CCC      WRITE(99,5566)   AREAS,AREAZ
 5566 FORMAT (1H ,F7.3,'  ',F7.3)
      IF (ZERO(1).EQ.2) THEN
      NLOOP2=MAXO(NLOOP2,NLOOP1)
      ELSE
      RESU(NLOOP1+1,17)=RESU(NLOOP1+1,17)+COKAM*100/VNET
      RESU(NLOOP1+1,18)=RESU(NLOOP1+1,18)+VFREE*100/VNET
      RESU(NLOOP1+1,20)=RESU(NLOOP1+1,20)+ZEV*100/ZEVIN
      COKAM=COKAM*1E15
      RESU(NLOOP1+1,2)=T
      RESU(NLOOP1+1,5)=RESU(NLOOP1+1,5)+RATE
      RESU(NLOOP1+1,3)=RESU(NLOOP1+1,3)+COKAM
      RESU(NLOOP1+1,1)=RESU(NLOOP1+1,1)+1
      DO 1680 NC=0,10
      RESU(NLOOP1+1,NC+6)=RESU(NLOOP1+1,NC+6)+1.0E10*(RAD0(5,NC,2)
     +-RAD1(5,NC,2)
     +)
 1680 CONTINUE
      RATE=RATE*100/RATMAX
      RESU(NLOOP1+1,4)=RESU(NLOOP1+1,4)+RATE
      NLOOP2=NLOOP1+1
      ENDIF
 9000 ZELVO=NINT(ZEV*1000)
CCC   WRITE(20,*)ZELVO
C *** WRITE FINAL COKED RADII TO DISC
      CALL RADCON(RADIUS)
 9999 CONTINUE
C *** PRINT RESULTS
      WRITE (10,4499) LAYER
C     WRITE (10,*) LAYER
C4499 FORMAT (1H ,/1H ,'AXIAL SEGMENT NUMBER',I3)
 4499 FORMAT (1H ,/1H ,'AXIAL SEGMENT NUMBER',I3,///)
CCCCCC    OMRAN ADDED
CC       WRITE(10,*) ' AREAS =',AREAS,'AREAZ=',AREAZ
CC       WRITE(*,*) ' AREAS =',AREAS,'AREAZ=',AREAZ
CCCCCCCCCCCC
      WRITE (10,4501)
CCCCCCC
CCCCCCC   PAGE  6   CCCCCCCCCCCCCCCCCCCCCCCCCCCCCCCCCCCCCCCCCCCCCCCCCCC
CCCCCCC
C     WRITE (10,*)
C4501 FORMAT (1H ,'TIME/S  COKE VOL./10^-15M^3 ACTIVITY/% RATE/MOL/S')
 4501 FORMAT (1H ,'TIME/S  COKE VOL./10^-15M^3 ACTIVITY/% RATE/MOL/S',/)
      DO 4500 IO=1,NLOOP2
```

```
      DO 4505 I1=3,18
CCCCCCC CMRAN
C     WRITE(*,*) 'RESU(I0,1) = ',RESU(I0,1)
C     WRITE(*,*) 'RESU(I0,I1) = ',RESU(I0,1)
CCCCCCCCCCCC
CC    PRINT*,'I0=  ',I0 ,'I1  =',I1
CC    PRINT*,'RESU(I0,1)=',RESU(I0,1)
CC    PRINT*,'RESU(I0,I1)=',RESU(I0,I1)
CCCCCCCCC
CCCCCCCCC
      RESU(I0,I1)=RESU(I0,I1)/RESU(I0,1)
CCCCCCC OMRAN
CC    WRITE(*,*) 'RESU(I0,1) = ',RESU(I0,1)
CC    WRITE(*,*) 'RESU(I0,I1) = ',RESU(I0,1)
CCCCCCCCCCCC
 4505 CONTINUE
      RESU(I0,19)=100-RESU(I0,18)-RESU(I0,17)
      RESU(I0,20)=RESU(I0,20)/RESU(I0,1)
 4500 CONTINUE
      DO 4600 I0=1,NLOOP2
CCCC  WRITE(*,*) CONVER(I0),CONIN,RESU(I0,4),NLAY,FLOAT(NLAY)
      CONVER(I0)=CONVER(I0)+CONIN*RESU(I0,4)/(100*FLOAT(NLAY))
      WRITE (10,4601) (RESU(I0,I1),I1=2,5)
      WRITE (77,7777) (RESU(I0,I1),I1=2,5)
 7777 FORMAT (1H ,F6.0,' ',E11.4,'         ',F7.2,'    ',E11.4)
C     WRITE (10,*) (RESU(I0,I1),I1=2,5)
 4600 CONTINUE
 4601 FORMAT (1H ,F6.0,' ',E11.4,'         ',F7.2,'    ',E11.4)
      WRITE (10,4502)
 4502 FORMAT (//,1H ,'TIME/S  %VOL COKED   %VOL FREE %VOL BLOCKED  %ZEO
     +LITE VOL CONVERSION',/)
C    + % VOL BLOCKED % ZEOLITE VOL
C    +  CONVERSION')
      DO 4550 I0=1,NLOOP2
      WRITE (10,4551) RESU(I0,2),(RESU(I0,I1),I1=17,20),CONVER(I0)
CCCCCCCCC
CCCCCCCCC
      WRITE (77,7788)   (RESU(I0,I1),I1=17,20),CONVER(I0),RESU(I0,2)
 7788  FORMAT (1H ,  F7.2,'      ',F7.2,
     +'    ',F7.2,'      ',F7.2,'      ',F7.3 ,
     +'   ',F6.0)
C     WRITE (10,*) RESU(I0,2),(RESU(I0,I1),I1=17,20),CONVER(I0)
CCCCCCCCCCC   OMRAN ADDED
        RESU(I0,21)=RESU(I0,17)*0.16
        RESU(I0,22)=(100.0-RESU(I0,20))*0.04
        RESU(I0,23)=RESU(I0,21)+RESU(I0,22)
        RESU(I0,24)=CONVER(I0)*100.0
        WRITE (99,4551) RESU(I0,2),(RESU(I0,I1),I1=21,24),CONVER(I0)
CCC
CCC
CCCCCCCCCCCCCCCCCCCCCCCCCCCCCCCCCCCCCCCCCCCCCCCCCCCCCCCCCCCCCCCC
 4550 CONTINUE
 4551  FORMAT (1H ,F6.0,'    ',F7.2,'      ',F7.2,
     +'    ',F7.2,'       ',F7.2,
     +'   ',F7.3)
       WRITE (10,4701)
 4701 FORMAT            (//,1H ,' TIME /S     COKE DEPTH PROFILE ACROSS
     + PELLET / ANGSTROM',/)
      DO 4800 I0=1,NLOOP2
CC    PRINT*,'NLOOP2=',NLOOP2
      WRITE (10,4801) RESU(I0,2),(RESU(I0,I1),I1=6,16)
CCC   WRITE (10,4801) RESU(I0,2),(RESU(I0,I1),I1=6,16)
C     WRITE (10,*) RESU(I0,2),(RESU(I0,I1),I1=6,16)
 4800 CONTINUE
```

```
CCCCC     OMRAN CHANGED FORMAT
C4801 FORMAT (1H ,F5.0,11F6.0)
 4801 FORMAT (1H ,F7.0,11F5.0)
C4801 FORMAT (1H ,F7.0,10F5.0,/,1H ,11F5.0)
 1111 CONTINUE
C -------------------------------------------------------------
C *** NOW CLOSE FILES AND END
C -------------------------------------------------------------
CCCCCC  VALUES OF DATA AT END 'OMRAN ADDED'
      WRITE(10,*) PL,DCO,RK
      WRITE(10,*) COUT,CONIN,TSTEP
      WRITE(10,*) NLT,NTR,RKP
      WRITE(10,*) RKS,SCOK,NLAY
      WRITE(99,*) PL,DCO,RK
      WRITE(99,*) COUT,CONIN,TSTEP
      WRITE(99,*) NLT,NTR,RKP
      WRITE(99,*) RKS,SCOK,NLAY
CCCC  WRITE(10,*) PROZ,DECRAT
      WRITE(10,*) '**********  END OF DATA  ********** '
 789  CONTINUE
      CLOSE(20)
      CLOSE (10)
      STOP
      END
C -------------------------------------------------------------
C ***
C ***                SUBROUTINES.
C ***
C -------------------------------------------------------------
C -------------------------------------------------------------
C *** CRATE FINDS THE MAXIMUM RATE OF COKING IN EACH PORE.
C *** IF ISTEP IS 1 THE COKE CONTENT AND PRODUCTIVITY ARE ALSO
C *** CALCULATED.
C -------------------------------------------------------------
CC    SUBROUTINE CRATE (SCOK,ISTEP,RK,ZERO,ZEV)
      SUBROUTINE CRATE (SCOK,ISTEP,RK,ZERO,ZEV,AREAS,AREAZ)
      COMMON RADO,RAD1 /A/ DCO,PL,RKP,RKS,COKAM,RATCO,C,CB,RATE,NN,VFREE
      COMMON /B/ BM /C/ COUT,COUTR
      DIMENSION COEF1(0:10,0:10,2),COEF2(0:10,0:10,2),RADO(0:10,0:10,2)
      DIMENSION ETA(0:10,0:10,2),C(0:11,0:11)
      DIMENSION RAD1(0:10,0:10,2),RATCO(0:10,0:10,2,4),CB(0:11,0:11)
      DIMENSION NN(0:11,0:11)
      DIMENSION BM(23,100)
      INTEGER ZERO(100)
      PARAMETER (PI=3.141592)
C -------------------------------------------------------------
C *** INITIALISE THE DIFFUSION/REACTION PARAMETERS
C -------------------------------------------------------------
      ZEV=0
C *** EFFIC RETURNS THE LOCAL EFFICIENCY OF EACH PORE AS A FUNCTION
C *** OF THE LEVEL OF COKING
CCCCCCC
CCCCCCC   PAGE  7   CCCCCCCCCCCCCCCCCCCCCCCCCCCCCCCCCCCCCCCCCCCCCCCC
CCCCCCC
CCCCCC OMRAN ADDED FOR CHECK
C     WRITE(*,*)'OK CRATE SUBROUTINE 2 '
      CALL EFFIC (ETA,SCOK,ZEV,AREAS,AREAZ)
CC    CALL EFFIC (ETA,SCOK,ZEV)
      DO 100 I=0,10
          DO 100 J=0,10
              DO 100 K=1,2
              IF (RAD1(I,J,K).GT.5.0E-10) THEN
              THIEL=SQRT(2*RK*ETA(I,J,K)/(RAD1(I,J,K)*DCO))
              PIRT=THIEL*DCO*RAD1(I,J,K)*RAD1(I,J,K)
```

```
            THIEL=THIEL*PL
C *** THIEL IS THE THIELE MODULUS
            COEF2(I,J,K)=PIRT/SINH(THIEL)
            COEF1(I,J,K)=PIRT/TANH(THIEL)
            ELSE
            COEF1(I,J,K)=0
            COEF2(I,J,K)=0
            ENDIF
 100   CONTINUE
C ---------------------------------------------------------------
C *** SET UP THE MAIN MATRIX. THIS STORES THE DIFFUSION/REACTION
C *** EQUATIONS IN COMPACT FORMAT.
C ---------------------------------------------------------------
CCCCCC OMRAN ADDED FOR CHECK
C     WRITE(*,*)'OK CRATE SUBROUTINE 3 '
      CALL MATSET(COEF1,COEF2,ETA,RK)
      DO 110 I=1,10
         DO 110 J=1,10
CCCCCCCCCCCCCCCCCCCCCCCCCCCCCCCCCCCCCCCCCCCC
CC  THIS LINE OMRAN PUT IT
CCC   NN(I,J)=3
CCCCCCCCCCCCCCCCCCCCCCCCCCCCCCCCCCCCCCCCCCCC
C *** IF NN=4 FOR A NODE THEN IT IS COMPLETELY BLOCKED. THIS
C *** INFORMATION IS STORED IN ZERO TO ALLOW THE EQUATION SOLVING
C *** ROUTINE TO IGNORE THE CORRESPONDING ROW IN THE MATRIX.
CCCCCC OMRAN ADDED FOR CHECK
C     WRITE(*,*)'OK CRATE SUBROUTINE 5 '
         IF (NN(I,J).EQ.4) THEN
         ZERO(10*I+J-10)=1
         ENDIF
 110   CONTINUE
C ---------------------------------------------------------------
C *** SOLVE THE EQUATIONS
C ---------------------------------------------------------------
CCCCCC OMRAN ADDED FOR CHECK
C     WRITE(*,*)'OK CRATE SUBROUTINE 6 '
      CALL MATSOLVE(ZERO)
CCCCCC OMRAN ADDED FOR CHECK
C     WRITE(*,*)'OK CRATE SUBROUTINE 7 '
CCCCC OMRAN ADDED THIS LINE
C     WRITE(*,*)'ZERO(1)=',ZERO(1)
CCCCCCCCCCCCCCCCCCCCCCCCCCC
      IF (ZERO(1).EQ.2) THEN
C     WRITE(*,*)'OK CRATE SUBROUTINE 8 '
      RETURN
      ENDIF
      DO 50 I=1,100
 50    ZERO(I)=0
CCCCCCCCCCCCCCCC
C     WRITE(*,*)'ZERO(1)=',ZERO(1)
C     WRITE(*,*)'ZERO(9)=',ZERO(9)
C *** PLACE THE CONCENTRATION PROFILE IN C(I,J)
      DO 400 I=1,10
      DO 400 J=1,10
      C(I,J)=BM(22,10*I+J-10)
C     WRITE(*,*)'OK CRATE SUBROUTINE 9A'
C *** DETECT BLOCKED REGIONS BY SEARCHING FOR NODES WHERE C IS VERY
C *** SMALL. (IF A REGION IS BLOCKED C=0 AT ALL NODES)
      IF (C(I,J).LT.1.0E-6) THEN
C     WRITE(*,*)'OK CRATE SUBROUTINE 9B'
      ZERO(10*I+J-10)=1
      CB(I,J)=0
      ELSE
C     WRITE(*,*)'OK CRATE SUBROUTINE 9C'
```

```
C *** CB+C=COUT ALLOWS CALCULATION OF CB
      CB(I,J)=COUT-C(I,J)
      ENDIF
 400   CONTINUE
C     WRITE(*,*)'OK CRATE SUBROUTINE 10'
C *** RESET NN FOR THE NEXT STEP
      DO 500 I=0,11
      DO 500 J=0,11
 500   NN(I,J)=0
C     WRITE(*,*)'OK CRATE SUBROUTINE 11'
C ---------------------------------------------------------------
C *** NOW FIND NETT ACTIVITY FOR THE CATALYST AND THE AMOUNT
CCCCCCC
CCCCCCC   PAGE  8   CCCCCCCCCCCCCCCCCCCCCCCCCCCCCCCCCCCCCCCCCCCCCCCCCC
CCCCCCC
C *** OF COKE PRESENT.
C *** HAVING FOUND SOLN. FOR CONC. FIND THE LOCAL COKING RATES
C ---------------------------------------------------------------
CCCCC OMRAN CHANGED I=0 TO I=1,10
      DO 1000 I=0,10
CCC   DO 1000 I=1,10
C     WRITE(*,*)'OK CRATE SUBROUTINE 12A'
CCCCC OMRAN CHANGED J=0 TO J=1,10
          DO 1000 J=0,10
CCC       DO 1000 J=1,10
CCCCCCC  OMRAN SET CB(0,0)=0.0
CC    CB(0,0)=0.0
CC    CB(0,J)=0.0
CC    CB(I,0)=0.0
CC    CB(I,11)=0.0
CC    CB(11,J)=0.0
CC    C(0,0)=COUT
CC    C(I,0)=COUT
CC    C(0,J)=COUT
CC    C(11,J)=COUT
CC    C(I,11)=COUT
CCCCCCCC  OMRAN ADDED ALL ABOVE LINES
C     WRITE(*,*)'OK CRATE SUBROUTINE 12B'
C     WRITE(*,*)'1000 I= ',I,'1000 J= ',J
C     WRITE(10,*) I,  J  ,   ISTEP
C     WRITE(10,*) AMAX1(C(I,J),C(I+1,J))
C     WRITE(10,*) 'CB(I,J)=',CB(I,J),   ETA
C     WRITE(10,*) 'CB=',CB,'ETA=',ETA
C     WRITE(10,*) AMAX1(C(I,J),C(I+1,J)) ,C(I,J),C(I+1,J)
C     WRITE(*,*) 'I=',I,'J=', J,'ISTEP=',ISTEP
C     WRITE(*,*) 'AMAX1(C(I,J),C(I+1,J))=',AMAX1(C(I,J),C(I+1,J))
C     WRITE(*,*) 'RKP=',RKP,'CB=',CB,'ETA=',ETA(I,J,1)
      RATCO(I,J,1,ISTEP)=(RKP*AMAX1(C(I,J),C(I+1,J))+RKS*AM
     +AX1(CB(I,J),CB(I+1,J)))*(ETA(I,J,1)*ETA(I,J,1))
CCC  +AX1(CB(I,J),CB(I+1,J)))
C     WRITE(*,*)'OK CRATE SUBROUTINE 13A'
      RATCO(I,J,2,ISTEP)=(RKP*AMAX1(C(I,J),C(I,J+1))+RKS*AM
     +AX1(CB(I,J),CB(I,J+1)))*(ETA(I,J,2)*ETA(I,J,2))
CCC  +AX1(CB(I,J),CB(I,J+1)))
C     WRITE(*,*)'OK CRATE SUBROUTINE 13B'
C     WRITE(*,*) 'RKS=',RKS,'C=',C,'ETA=',ETA(I,J,1)
 1000 CONTINUE
C     WRITE(*,*)'OK CRATE SUBROUTINE 14'
C *** IF THIS IS THE FIRST CALL OF A R/K STEP THEN FIND THE COKE
C *** VOL,REACTION RATE AND NFREE VOL
      IF (ISTEP.EQ.1) THEN
      RATE=0
      COKAM=0
      VFREE=0
```

```
      DO 3000 I=0,10
         K=2
         IF (I.EQ.0) GOTO 2200
         DO 2100 J=0,10
      RATE=RATE+(C(I,J)+C(I,J+1))*(COEF1(I,J,K)-COEF2(I,J,K))
     +*ETA(I,J,K)
      IF ((C(I,J).GT.1.0E-6).AND.(C(I,J+1).GT.1.0E-6)) THEN
           VFREE=VFREE+RAD1(I,J,2)*RAD1(I,J,2)
           ENDIF
 2100 COKAM=COKAM+(RAD1(I,J,K)+RAD0(I,J,K))*(RAD0(I,J,K)-RAD1(I,J,K))
 2200     K=1
          DO 2300 J=1,10
      RATE=RATE+(C(I,J)+C(I+1,J))*(COEF1(I,J,K)-COEF2(I,J,K))
     +*ETA(I,J,K)
           IF ((C(I,J).GT.1.0E-6).AND.(C(I+1,J).GT.1.0E-6)) THEN
           VFREE=VFREE+RAD1(I,J,1)*RAD1(I,J,1)
           ENDIF
 2300 COKAM=COKAM+(RAD1(I,J,K)+RAD0(I,J,K))*(RAD0(I,J,K)-RAD1(I,J,K))
 3000  CONTINUE
C     WRITE(*,*)'OK CRATE SUBROUTINE 15'
      RATE=RATE*RK
      COKAM=COKAM*PI*PL
      VFREE=VFREE*PI*PL
      ENDIF
      RETURN
      END
C -----------------------------------------------------------------
C *** MATSET INITIALISES THE MATRIX BM.
C -----------------------------------------------------------------
      SUBROUTINE MATSET(COEF1,COEF2,ETA,RK)
      COMMON /B/ BM /C/ COUT,COUTR
      DIMENSION BM(23,100)
      DIMENSION COEF1(0:10,0:10,2),COEF2(0:10,0:10,2)
      DIMENSION ETA(0:10,0:10,2)
C *** SET ALL ELMENTS TO ZERO
      DO 110 I=1,22
      DO 110 J=1,100
 110   BM(I,J)=0
C *** ELEMENTS IN BODY OF GRID
      DO 120 I=2,9
      DO 120 J=2,9
          INDEX=10*I+J-10
      BM(11,INDEX)=COEF1(I-1,J,1)+COEF1(I,J,1)+COEF1(I,J-1,2)+COEF1(I
     +,J,2)
          BM(10,INDEX)=-COEF2(I,J-1,2)
          BM(12,INDEX)=-COEF2(I,J,2)
          BM(1,INDEX)=-COEF2(I-1,J,1)
CCCCCCC
CCCCCCC   PAGE 9   CCCCCCCCCCCCCCCCCCCCCCCCCCCCCCCCCCCCCCCCCCCCCCCC
CCCCCCC
          BM(21,INDEX)=-COEF2(I,J,1)
         BM(22,INDEX)=0
 120  CONTINUE
C *** LEFT AND RIGHT EDGES
      DO 130 I=2,9
      J=1
      INDEX=10*I-9
      BM(11,INDEX)=COEF1(I-1,J,1)+COEF1(I,J,1)+COEF1(I,J-1,2)+COEF1(I
     +,J,2)
          BM(12,INDEX)=-COEF2(I,J,2)
          BM(1,INDEX)=-COEF2(I-1,J,1)
          BM(21,INDEX)=-COEF2(I,J,1)
         BM(22,INDEX)=COEF2(I,J-1,2)*COUTR
      J=10
```

```
      INDEX=10*I
      BM(11,INDEX)=COEF1(I-1,J,1)+COEF1(I,J,1)+COEF1(I,J-1,2)+COEF1(I
     +,J,2)
          BM(10,INDEX)=-COEF2(I,J-1,2)
          BM(1,INDEX)=-COEF2(I-1,J,1)
          BM(21,INDEX)=-COEF2(I,J,1)
         BM(22,INDEX)=COEF2(I,J,2)*COUTR
 130   CONTINUE
C *** TOP AND BOTTOM EDGES
      DO 140 J=2,9
      I=1
      INDEX=J
      BM(11,INDEX)=COEF1(I-1,J,1)+COEF1(I,J,1)+COEF1(I,J-1,2)+COEF1(I
     +,J,2)
          BM(10,INDEX)=-COEF2(I,J-1,2)
          BM(12,INDEX)=-COEF2(I,J,2)
          BM(21,INDEX)=-COEF2(I,J,1)
         BM(22,INDEX)=COEF2(I-1,J,1)*COUTR
      INDEX=90+J
      I=10
      BM(11,INDEX)=COEF1(I-1,J,1)+COEF1(I,J,1)+COEF1(I,J-1,2)+COEF1(I
     +,J,2)
          BM(10,INDEX)=-COEF2(I,J-1,2)
          BM(12,INDEX)=-COEF2(I,J,2)
          BM(1,INDEX)=-COEF2(I-1,J,1)
         BM(22,INDEX)=COEF2(I,J,1)*COUTR
 140   CONTINUE
C *** CORNERS
          BM(11,1)=COEF1(0,1,1)+COEF1(1,1,1)+COEF1(1,0,2)+COEF1(1,1,2)
          BM(12,1)=-COEF2(1,1,2)
          BM(21,1)=-COEF2(1,1,1)
          BM(22,1)=COUTR*(COEF2(1,0,2)+COEF2(0,1,1))
      BM(11,10)=COEF1(0,10,1)+COEF1(1,10,1)+COEF1(1,10,2)
     ++COEF1(1,9,2)
          BM(10,10)=-COEF2(1,9,2)
          BM(21,10)=-COEF2(1,10,1)
         BM(22,10)=COUTR*(COEF2(1,10,2)+COEF2(0,10,1))
      BM(11,91)=COEF1(9,1,1)+COEF1(10,1,1)+COEF1(10,0,2)
     ++COEF1(10,1,2)
          BM(12,91)=-COEF2(10,1,2)
          BM(1,91)=-COEF2(9,1,1)
         BM(22,91)=COUTR*(COEF2(10,0,2)+COEF2(10,1,1))
      BM(11,100)=COEF1(9,10,1)+COEF1(10,10,1)+COEF1(10,9,2)
     ++COEF1(10,10,2)
          BM(10,100)=-COEF2(10,9,2)
          BM(1,100)=-COEF2(9,10,1)
         BM(22,100)=COUTR*(COEF2(10,10,2)+COEF2(10,10,1))
      RETURN
CCCCCCC
CCCCCCC   PAGE 10   CCCCCCCCCCCCCCCCCCCCCCCCCCCCCCCCCCCCCCCCCCCCCCC
CCCCCCC
      END
C ---------------------------------------------------------------
C *** MATSOLVE SOLVES THE EQUATIONS HELD BY BM
C ---------------------------------------------------------------
      SUBROUTINE MATSOLVE(ZERO)
      COMMON /B/ BM
      DIMENSION BM(23,100)
      INTEGER ZERO(100)
C *** SCALE THE ROWS
      DO 100 I=1,100
      IF (ZERO(I).EQ.0) THEN
      BM(1,I)=BM(1,I)/BM(11,I)
      BM(10,I)=BM(10,I)/BM(11,I)
```

```
      BM(12,I)=BM(12,I)/BM(11,I)
      BM(21,I)=BM(21,I)/BM(11,I)
      BM(22,I)=BM(22,I)/BM(11,I)
      BM(11,I)=1
      ENDIF
C *** REJECT SMALL ELEMENTS
      IF (ABS(BM(1,I)).LT.1.0E-4) THEN
      BM(1,I)=0
      ENDIF
      IF (ABS(BM(10,I)).LT.1.0E-4) THEN
      BM(10,I)=0
      ENDIF
      IF (ABS(BM(12,I)).LT.1.0E-4) THEN
      BM(12,I)=0
      ENDIF
      IF (ABS(BM(21,I)).LT.1.0E-4) THEN
      BM(21,I)=0
      ENDIF
      IF (ABS(BM(22,I)).LT.1.0E-4) THEN
      BM(22,I)=0
      ENDIF
  100  CONTINUE
      DO 200 I=1,99
       IF (ZERO(I).EQ.1) THEN
       GOTO 200
       ENDIF
       JMAX=MIN0(I+10,100)-I
          DO 200 J=1,JMAX
          RATIO=BM(11-J,I+J)
          IF (RATIO.EQ.0) THEN
          GOTO 200
          ELSE
          RATIO=RATIO/BM(11,I)
             DO 180 K=12,21
             BM(K-J,I+J)=BM(K-J,I+J)-RATIO*BM(K,I)
  180       CONTINUE
             BM(22,I+J)=BM(22,I+J)-RATIO*BM(22,I)
          ENDIF
  200  CONTINUE
      DO 300 I=100,1,-1
      IF (ZERO(I).EQ.1) THEN
      GOTO 300
      ENDIF
      S=0
      JMAX=MIN0(100-I,10)
          DO 280 J=1,JMAX
          S=S+BM(J+11,I)*BM(22,I+J)
  280      CONTINUE
      IF (BM(11,I).EQ.0) THEN
      PRINT *, 'INDEFINITE RESULT IN MATSOLVE'
CCCCCCC
CCCCCCC   PAGE 11   CCCCCCCCCCCCCCCCCCCCCCCCCCCCCCCCCCCCCCCCCCCCCCCCCCC
CCCCCCC
CCCC OMRAN CHANGED THE FOLLOWING ACCORDING TO THESIS PAGE 154
CC    ZERO(I)=2
CC    RETURN
      BM(22,I)=0
CC
CC
C
C
CCCCCCC ONE LINE DELETED AND TWO LINES ADDED
      ELSE
      BM(22,I)=(BM(22,I)-S)/BM(11,I)
```

```
      ENDIF
  300  CONTINUE
      RETURN
      END
C -----------------------------------------------------------------
C *** RADCON WRITES THE RADII TO DISC IN AN INTEGER FORM
C -----------------------------------------------------------------
      SUBROUTINE RADCON(RADIUS)
      REAL RADIUS(0:10,0:10,2),RAD(21,11)
      INTEGER RADINT(21,11)
      DO 1025 I=1,21
         IF( I/2*2.EQ.I) THEN
           DO 1022 J=1,11
           RAD(I,J)=RADIUS(I/2,J-1,2)*1.0E10
           RADINT(I,J)=NINT(RAD(I,J))
CCCCCCCCCCCCCCCCC  OMRAN ADDED
CC         RADINT(I,J)=RADINT(I,J)-000
CC         IF(RADINT(I,J).LE.0.0) RADINT(I,J)=0.0
CCCCCCCCCCCCCCCCCCCCC
 1022       CONTINUE
           WRITE(20,*) (RADINT(I,J),J=1,11)
         ELSE
           DO 1023 J=1,10
           RAD(I,J)=RADIUS(I/2,J,1)*1.0E10
           RADINT(I,J)=NINT(RAD(I,J))
CCCCCCCCCCCCCC  OMRAN ADDED
CC         RADINT(I,J)=RADINT(I,J)-000
CC         IF(RADINT(I,J).LE.0.0) RADINT(I,J)=0.0
CCCCCCCCCCCCCCCCCC
 1023       CONTINUE
           WRITE(20,*) (RADINT(I,J),J=1,10)
         ENDIF
 1025  CONTINUE
      RETURN
      END
CCCCCCC
CCCCCCC   PAGE 12   CCCCCCCCCCCCCCCCCCCCCCCCCCCCCCCCCCCCCCCCCCCCCCCCCC
CCCCCCC
      SUBROUTINE EFFIC (ETA,SCOK,ZEV,AREAS,AREAZ)
CC    SUBROUTINE EFFIC (ETA,SCOK,ZEV)
      COMMON RAD0,RAD1
      DIMENSION RAD1(0:10,0:10,2),RAD0(0:10,0:10,2),ETA(0:10,0:10,2)
CCCC  THIS LINE ADDED OMRAN
CCCCCC OMRAN ADDED FOR CHECK
C     WRITE(*,*)'OK EFFIC SUBROUTINE 8 '
CCCC  NNN=1.0
      AAZZ=0
      IF (NNN.NE.1) THEN
      PRINT *,'INPUT PROPORTION OF ACTIVITY WHICH IS ZEOLITE '
      READ(30,*) PROZ
CC    READ *,PROZ
      PRINT *,'INPUT RATIO OF DECAY CONSTANTS ZEOL/SUPPORT'
      READ(30,*) DECRAT
CC    READ *,DECRAT
      WRITE(10,*) 'PROPORTION OF ACTIVITY WHICH IS ZEOLITE= ',PROZ
      WRITE(10,*) 'RATIO OF DECAY CONSTANTS ZEOLITE/SUPPORT = ',DECRAT
      NNN=1
      ENDIF
      ZEV=0
CCCCC OMRAN ADDED CCCCCCCCCCCCCCCCCCCCCCCCCCCCCCCCCC
       FRES=0
       FRESZ=0
       AREAS=0
       AREAZ=0
```

```
CCCCCCCCCCCCCCCCCCCCCCCCCCCCCCCCCCCCCCCCCCCCCCCCCCCC
      DO 100 I=0,10
                DO 100 J=0,10
                      DO 100 K=1,2
CCCCCCCCCCCCCCCCCCCCCCCCCCCCCCCCCCCCCCCCCCCCCCCCCCCCCCCCCCCCCCC
CCC   IF RAD1 DROPS BELOW ZERO THEN SET THE RAD1 ZERO
CCC   AND PORE EFFECIENCY TO ZERO
CCCCCCCCCCCCCCCCCCCCCCCCCCCCCCCCCCCCCCCCCCCCCCCCCCCCCCCCCCCCCCCC
      IF (RAD1(I,J,K).LE.0) THEN
      ETA(I,J,K)=0
      RAD1(I,J,K)=0
      ELSE
CCCCCCCCCC  OMRAN ADDED TWO LINES
CC    PROZ=.3
CC    DECRAT=06
CCCCCCCCCCCCCCCCCCCCCCCC
CCCCCCC
CC    PRINT *,'SCOK=',SCOK,'DECRAT=',DECRAT,'PROZ=',PROZ,'ZEV=',ZEV
CCCCCCC
      FRES=EXP((RAD1(I,J,K)-RAD0(I,J,K))/SCOK)
CCC   FRES=RAD1(I,J,K)/RAD0(I,J,K)
CCCCCCC
CC    PRINT *,'FRES=',FRES
CCCCCCC
      FRESZ=FRES*EXP(DECRAT*(RAD1(I,J,K)-RAD0(I,J,K))/SCOK)
CCCCCCC   OMRAN ADDED
CC    PRINT *,'FRES=',FRES
CC    PRINT *,'FRESZ=',FRESZ
CCCCCCC
CC    PRINT *,'RAD1(I,J,K)',RAD1(I,J,K)
CC    PRINT *,'RAD0(I,J,K)',RAD0(I,J,K)
CCCCCCC
      ETA(I,J,K)=((1-PROZ)*FRES+PROZ*FRESZ)*RAD0(I,J,K)/RAD1(I,J,K)
CCCCCCC
CC    PRINT *,'ETA(I,J,K)=',ETA(I,J,K)
CCCCCCC
      ZEV=ZEV+FRESZ*RAD0(I,J,K)
CCCCCC  OMRAN ADDED
      AREAS=AREAS+FRES
      AREAZ=AREAZ+FRESZ
CCCCCCCCCCCCCCCCCCCCCCCCC
      ENDIF
 100  CONTINUE
CCCCCCCC   OMRAN ADDED
      AREAS=AREAS/224.
      AREAZ=AREAZ/224.
CCCCC   TO GET % AREA ACTIVE INSTEAD OF FRACTION
      AREAS=AREAS*100.
      AREAZ=AREAZ*100.
CCCCCCCCCCCCCCCCCCCCCCCCCCCCCCCCCCCCCCCCCCCCCCCCCCCC
C     AAZZ=AAZZ+1
CC       WRITE(*,*) ' AAZZ=     ',AAZZ
CC       IF(AAZZ.NE.1.)THEN
CC       ENDIF
CCCCC    WRITE(*,*) ' AREAS =',AREAS,'AREAZ=',AREAZ
CCCCC    WRITE(*,*)  AREAS,AREAZ,ZEV
CCCCCCCCC
      RETURN
      END
      SUBROUTINE RAND(R)
C     R=0.01
      RND=0.90
      RETURN
C     STOP
```

END

APPENDIX–2

APPENDIX–2

The Fourth Order Runge–Kutta Algorithm:

The current pore radii are most conveniently represented by a vector $\underline{r}$ whose elements are the individual radii. Suppose that the radii at time t_0 are represented by $\underline{r}$. To find the radii at time t_0+t_s , where t_s is the time step length, the fourth order Runge–Kutta algorithm was implemented as follows:

Let $\underline{r}'(\underline{r})$ be the vector whose elements are the rates of change of radius of the individual pores calculated when the radii are $\underline{r}$. Four separate values of the rate vector must be calculated:

$$\underline{r}_1' = \underline{r}'(\underline{r})$$

$$\underline{r}_2' = \underline{r}'(\underline{r} + (1/2)\, t_s\, \underline{r}_1')$$

$$\underline{r}_3' = \underline{r}'(\underline{r} + (1/2)\, t_s\, \underline{r}_2')$$

$$\underline{r}_4' = \underline{r}'(\underline{r} + t_s\, \underline{r}_3')$$

From these, the radii at t_0+t_s are given by:

$$\underline{r}(t_0+t_s) = (1/6)\, t_s\, (\underline{r}_1' + 2\, \underline{r}_2' + 2\, \underline{r}_3' + \underline{r}_4') + \underline{r}$$

APPENDIX–3

```
C  USER SUPPLIED VARIABLE                VARIABLE NAME IN PROGRAM
C  ------------------------              ------------------------
C  NUMBER OF PORES                        NPORES
C  NUMBER OF ELEMENTS                     ELEM
C  PORE SIZE DISTRIBUTION                 RADO(NPORES,ELEM)
C  CATALYST PHYSICAL PROPERTIES :
C  ------------------------------
C       SPECIFIC PORE VOLUME              VPORE
C       SPECIFIC ZEOLITE SURFACE AREA     AREAZ
C       PARALLEL BUNDLE PORE LENGTH       PL
C       CATALYST MASS                     CMASS
C       FEED FLOW RATE                    FLOW
C  DEACTIVATION PARAMETERS:
C  ------------------------
C       FRACTION OF INITIAL ACTIVITY      ALPHA
C       DUE TO ZEOLITE
C       SERIES COKING RATE CONSTANT       RKS
C       PARALLEL COKING RATE CONSTANT     RKP
C       SUPPORT COKE UNIT SIZE            SCOK
C       ZEOLITE COKE UNIT SIZE            SCOKZ
C       INITIAL BULK CONCENTRATION        COUT
C       NUMBER OF R-K STEPS               NLT
C       INITIAL R-K STEP SIZE             NSTEP
C-------------------------------------------------------------
C              PAGE -1- DEACT
C-------------------------------------------------------------
      PROGRAM PHDMAK
      REAL*8 GOSCAF,DUMMY
      REAL   RADI(10,22),RADO(10,22),RADIUS(10,22),KS,RATCO(
     +10,22,4),CORR(10,22)
      REAL   RESULT(0:50,20),SURF,TVOL,FRESUP(10,22),
     +FREZEO(10,22),NSTEP
      INTEGER NPORES,ELEM,N(22)
      COMMON /DATA1/RADI
      COMMON /DATA10/ CONST
      COMMON /DATA9/ RADO
      COMMON /DATA4/ N
      COMMON /DATA5 / RATCO,RATE
      COMMON /MEGA/ PL,COUT,RKP,RKS
      COMMON /DATA7/ FRESUP,FREZEO
      OPEN(19,FILE='FILE19')
      REWIND 19
      OPEN(8,FILE='FILE5')
      REWIND 8
      OPEN(88)
      REWIND 88
      OPEN(10,FILE='FILE10')
      REWIND 10
      OPEN(3,FILE='PORE')
      REWIND 3
      OPEN(9,FILE='FILE9')
      REWIND 9
CC    OPEN(99,FILE='FILE99')
      OPEN(99)
      REWIND 99
      OPEN(66)
      REWIND 66
CCCCCCCCCCCCCCC SIMULATION OF PROGRAM CCCCCCCCCCCCC
C     DO 417 IJK=1,10
C     IF (IJK.EQ.1) THEN
C        GO TO 777
C     ELSEIF (IJK.NE.1) THEN
C        KS=KS*10.00
C     ELSEIF (IJK.EQ.3) THEN
C        ALPHA=.0001
C        KS=KS*1.05953
```

```
C     ELSEIF (IJK.EQ.4) THEN
C        PL=10000
C     ELSEIF (IJK.EQ.5) THEN
C        PL=0.014
C        SCOK=SCOK*1.05
C     ELSEIF (IJK.EQ.6) THEN
C        SCOK=0.020
C     ELSEIF (IJK.EQ.7) THEN
C        SCOK=2000
C        SCOKZ=SCOKZ*1.05
C     ELSEIF (IJK.EQ.8) THEN
C        SCOKZ=1000
C     ELSEIF (IJK.EQ.9) THEN
C         SCOKZ=.001
C         ALPHA=ALPHA*1.05
C     ELSEIF (IJK.EQ.10) THEN
C        RKP=-5E-20
C777  ENDIF
CCCCCCCCCCCCCCCCCCCCCCCCCCCCCCCCCCCCCCCCCCCCCCC
C*************************************************************
C                 ENTER PARAMETERS                            *
C*************************************************************
C     WRITE(*,*) 'ENTER PORE LENGTH IN MICRONS'
      READ(19,*) PL
C     WRITE(*,*) 'ENTER DIFFUSION COEFFICIENT (10.E-6 M**2/S)'
      READ(19,*) D
C     WRITE(*,*) ' ENTER RATE CONSTANT (10.E-9 M/S)'
      READ(19,*) KS
C     WRITE(*,*) 'ENTER TOTAL OUTSIDE CONCENTRATION (KMOL/M**3)'
      READ(19,*) COUT
C     WRITE(*,*) 'ENTER COKING STEP IN SECONDS'
      READ(19,*) TSTEP
C     WRITE(*,*) 'ENTER NUMBER OF STEPS PER SIMULATION'
      READ(19,*) NLT
C     WRITE(*,*) 'ENTER PARALLEL AND SERIES COKING CONSTANTS (*10.E
C    +-10)'
      READ(19,*) RKP,RKS
C     WRITE(*,*) 'ENTER MEAN COKE SIZES FOR ZEOLITE $ SUPPORT (ANG)
C    +'
      READ(19,*) SCOKZ,SCOK
C     WRITE(*,*) 'ENTER NUMBER  OF PORES AND NUMBER OF PORE ELEMENT
C    +S'
      READ(19,*) NPORES,ELEM
C     WRITE(*,*) 'ENTER FRACTION OF INITIAL ACTIVITY DUE TO ZEOLITE
C    +'
      READ(19,*) ALPHA
C     WRITE(*,*) 'INPUT CAT MASS (GM) AND SUPPORT PORE VOLUME ,CM**
C    +3/GM'
C     WRITE(*,*) 'AND FEED FLOWRATE ,M**3/S'
CCCCC  1   (GRAM/MINUTE) =0.858E-5 M**3/SEC
CCCCC  0.5 (GRAM/MINUTE) =0.429E-5 M**3/SEC
      READ(19,*) CMASS,VPORE,FLOW
      WRITE(9,*) '************ START DATA ****************************'
      WRITE(9,*) 'PL    =',PL,'D     =',D
      WRITE(9,*) 'KS    =',KS,'COUT  =',COUT
      WRITE(9,*) 'TSTEP =',TSTEP,'NLT   =',NLT
      WRITE(9,*) 'RKP   =',RKP,'RKS   =',RKS
      WRITE(9,*) 'SCOKZ =',SCOKZ,'SCOK  =',SCOK
      WRITE(9,*) 'NPORES=',NPORES,'                ELEM  =',ELEM
      WRITE(9,*) 'ALPHA =',ALPHA,'CMASS =',CMASS
      WRITE(9,*) 'VPORE =',VPORE,'FLOW  =',FLOW
      WRITE(9,*) '************** END OF DATA ***************************'
      WRITE(9,*) '************ START DATA ****************************'
      WRITE(66,*) 'PL    =',PL,'D     =',D
      WRITE(66,*) 'KS    =',KS,'COUT  =',COUT
      WRITE(66,*) 'TSTEP =',TSTEP,'NLT   =',NLT
```

```
      WRITE(66,*) 'AKP   =',AKP,'AKS   =',AKS
      WRITE(66,*) 'SCOKZ =',SCOKZ,'SCOK  =',SCOK
      WRITE(66,*) 'NPORES=',NPORES,'          ELEM  =',ELEM
      WRITE(66,*) 'ALPHA =',ALPHA,'CMASS =',CMASS
      WRITE(66,*) 'VPORE =',VPORE,'FLOW  =',FLOW
      WRITE(66,*) '************** END OF DATA *************************'
C*************** INITIALIZE THE PORE RADII AND OTHER VARIABLES ******
      CONVER=0
C     DO 27 J=1,NPORES
C  27 READ (3,*) (RADO(I,J),I=1,ELEM)
      WRITE(10,101)
  101 FORMAT(1H ,'RANDOM VALUES ASSIGNED FOR RADII OF ELEMENTS IN THE RA
     +NGE 60-3200 A .')
CCCCCCCC PORE SIZE DISTRIBUTION CCCCCCCCCCCCCCCCCCC
      RMIN=60
      RMAX=3200
C     RMIN=60
C     RMAX=3200
      WRITE(9,*) 'RMIN = ',RMIN,  'RMAX  = ', RMAX
CCCCC   THE FOLLOWING TO MISS SOME RANDOM NUMBERS  CCCCCCCCCCCCCCCC
      DO 279 JKI=1,500
      RANGE=RMAX-RMIN
      NUM=(G05CAF(DUMMY)*RANGE)+RMIN
  279 CONTINUE
CCCCCCCCCCCCCCCCCCCCCCCCCCCCCCCCCCCCCCCCCCCCCCCCCCCCCCCC
      DO 100 J=1,NPORES
      WRITE(10,102)  J
  102 FORMAT(1H ,'PORE NUMBER  = ',I5 / '----------------------',// )
      DO 200 I=1,ELEM
      RANGE=RMAX-RMIN
      NUM=(G05CAF(DUMMY)*RANGE)+RMIN
CC    NUM=(G05CAF(DUMMY)*3200)+60
CCC   NUM=1
CC    NUM=(G05CAF(DUMMY)*3141)+60
C     WRITE(*,*) DUMMY,G05CAF(DUMMY),NUM
C     WRITE(10,101)
C     NUM=(G05CAF(DUMMY)*999)+60
C     NUM=600
CC    NUM=1600
CCCCCC TO MAKE BIMODAL DISTRIBUTION ADDED BELOW
CCC   IF(DUMMY.LE.0.5) THEN
CC    IF(NUM.LE.1600) THEN
CC    NUM=3000
CC    ELSE
CC    NUM=200
CC    ENDIF
CCCCCC TO MAKE BIMODAL DISTRIBUTION  ADDED ABOVE
CCC   IF(NUM.LE.1600) THEN
      RADO(I,J)=NUM
CCC   OMRAN SET RADO(1,1)=RMAX  FOR CONVENIENCE
      RADO(1,1)=RMAX
CC    RADO(2,1)=RMIN
CCCC   OMRAN ADDED ABOVE
CC    CORR(I,J)=RADO(I,J)*1.0E-10
      WRITE(10,103)  I,J,RADO(I,J)
CCC   WRITE(8,*) RADO(I,J)
  103 FORMAT(5X,'RADO(',I2,',',I5,')=',F8.2)
C*****************************************************************
CCCCCCCC  TEST OF PROGRAM ,SET RADIUS OF 1000A TO ALL ELEMENTS
C     RADO(I,J)=1452.
C     PRINT*,'RADIUS=',RADO(I,J)
C     WRITE(*,*) 'RADIUS=  ',RADO(I,J)
      IF (J.GT.3) THEN
         GO TO 200
      ELSE
      WRITE(9,*)            RADO(I,J)
```

```
C*****************************************************************
      ENDIF
 200  CONTINUE
C     WRITE(9,*)  ( RADO(I,J) I=1,ELEM)
C     WRITE(*,*)  ( RADO(I,J) I=1,ELEM)
C123  FORMAT(5X,10F8.2)
C     WRITE(9,*)             RADO(I,J)
C     WRITE(*,*)             RADO(I,J)
C     WRITE(9,*)             RADO(I,J)
 100  CONTINUE
      DO 208 J=1,NPORES
      WRITE(10,107)     (RADO(I,J),I=1,ELEM)
 107  FORMAT(F6.1,2X,F6.1,2X,F6.1,2X,F6.1,2X,F6.1,
     +       2X,F6.1,2X,F6.1,2X,F6.1,2X,F6.1,2X,F6.1,/)
 208   CONTINUE
      WRITE(9,*) 'RMIN = ',RMIN,  'RMAX  = ', RMAX
      TVOL=0
      SURF=0
      DO 1 J=1,NPORES
        N(J)=ELEM
C     PRINT*,'ELEM',ELEM,'N(J)',N
        DO 1 I=1,ELEM
           RADO(I,J)=RADO(I,J)*1.0E-10
           TVOL=TVOL+RADO(I,J)**2
           SURF=SURF+RADO(I,J)
    1 CONTINUE
      TOTAL=ELEM*NPORES
C*********************************************************
C                    RESULTS TABLE                      *
C*********************************************************
C
CTHE VARIOUS BITS OF DATA ARE STORED IN THE MATRIX 'RESULTS 'AND ARE AS
C     FOLLOWS:
C
C*********************************************************
C                 PAGE -2- DEACTIVATE                   *
C*********************************************************
C.............COUNTER
C RESULT(I,1).....TIME ON STREAM
C RESULT(I,2).....ACTIVITY OF THE MODEL
C RESULT(I,3).....% VOL OF COKE IN SUPPORT
C RESULT(I,4).....% OF SUPPORT AREA THAT IS ACTIVE
C RESULT(I,5).....% VOL OF COKE IN THE ZEOLITE
C RESULT(I,6).....% VOL OF ZEOLITE LOST DUE TO COKING AND BLOCKAGE
C RESULT(I,7).....% OF ZEOLITE AREA THAT IS ACTIVE
C RESULT(I,8).....% OF PORE ELEMENTS THAT ARE BLOCKED
C RESULT(I,9).....% ACTIVE SUPPORT LOST DUE TO BLOCKING
C RESULT(I,10)....% ACTIVE ZEOLITE LOST DUE TO BLOCKING
C RESULT(I,13)....% WT COKE IN SUPPORT (WT.% PER GRAM OF CATALYST)
C RESULT(I,15)....% WT COKE IN ZEOLITE (WT.% PER GRAM OF CATALYST)
C RESULT(I,16)....% WT COKE IN CATALYST (TOTAL WT% PER GRAM CATALYST)
C
C    VOLUME PERCENTAGES ARE PERCENTAGES OF SUPPORT VOLUME
C
C*************************************************************
C                 SET INITIAL OUTSIDE CONCENTRATIONS
C*****************************************************************
      VPORE=VPORE*1.0E-06
      COUT=COUT*1.0E-03
      CO=COUT*(1-CONVER)
      NSTEP=1
      D=D*1.0E-06
      T=0
      PL=PL*1.0E-06/ELEM
      KS=KS*1.0E-09
C     RKP=-RKP
```

```
C     RKS=-RKS
      SCOK=SCOK*1.0E-10
      SCOKZ=SCOKZ*1.0E-10
      AREAZ=100.0*3.1416*TVOL*PL/VPORE
      CONST=AREAZ/(SURF*PL)
C     READ(19,*) PL,SCOK,SCOKZ
CCC*************************************************************
CCCCCCC AN EXTRA 10.0 IN THE ORIGINAL PROGRAM INSTEAD OF 1.0
CCCC  PL=PL*10.E-06/ELEM
C     PL=PL*1.0E-06/ELEM
CCC*************************************************************
C     SCOK=SCOK*1.0E-10
C     SCOKZ=SCOKZ*1.0E-10
CCC   DO 417 IJK=1,06
CCCCCCCCCCCCCCCCCCCCCCCCCCCCCCCCCCCCCCC
C     READ(19,*) RKP,RKS
CCC    FOR SIMULATIONS CHANGING DEACTIVATION PARAMETERS
CCC
      DO 417 IJK=1,6
CCC
      IF (IJK.EQ.1) THEN
         GO TO 777
      ELSE
C     ELSEIF (IJK.EQ.2) THEN
C     PL=50*1E-6
C     ELSEIF (IJK.EQ.3) THEN
C
CCC   FLOW=FLOW*2.0
C
C     PL=100*1E-6
CC    PL=PL*3
C     KS=KS*05.
      RKS=RKS*10.0
CC    RKP=RKP*10.0
CCCCC
CC    CMASS=CMASS*2.0
CCCCCC
CC    ALPHA=ALPHA+0.20
CC    ALPHA=ALPHA+0.199
C     SCOK=SCOK-10.*1.0E-10
CC    SCOKZ=SCOKZ*2.0
CC    SCOKZ=SCOKZ/3.0
CC    SCOK=SCOK*2.0
C     ELSEIF (IJK.LE.10) THEN
C     GO TO 777
C     ELSE
C     FLOW=FLOW*2.0
C     WRITE(9,*) '************* START DATA ******************************'
C     WRITE(9,*) 'PL    =',PL,'D     =',D
C     WRITE(9,*) 'KS    =',KS,'COUT  =',COUT
C     WRITE(9,*) 'TSTEP =',TSTEP,'NLT   =',NLT
C     WRITE(9,*) 'RKP   =',RKP,'RKS   =',RKS
C     WRITE(9,*) 'SCOKZ =',SCOKZ,'SCOK  =',SCOK
C     WRITE(9,*) 'NPORES=',NPORES,'              ELEM  =',ELEM
C     WRITE(9,*) 'ALPHA =',ALPHA,'CMASS =',CMASS
C     WRITE(9,*) 'VPORE =',VPORE,'FLOW  =',FLOW
C     WRITE(9,*) '************** END OF DATA ****************************'
 777  ENDIF
C*************** INITIALIZE THE PORE RADII AND OTHER VARIABLES ******
C       RKS=RKS*1.05
C     ELSEIF (IJK.EQ.2) THEN
C       RKS=RKS/1.05*0.95
C     ELSEIF (IJK.EQ.3) THEN
C       RKS=RKS/0.95
C       KS=KS*1.05953
C     ELSEIF (IJK.EQ.4) THEN
```

```
C       KS=KS/1.05*0.95
C     ELSEIF (IJK.EQ.5) THEN
C       KS=KS/0.95
C       SCOK=SCOK*1.05
C     ELSEIF (IJK.EQ.6) THEN
C       SCOK=SCOK/1.05*0.95
C     ELSEIF (IJK.EQ.7) THEN
C       SCOK=SCOK/0.95
C       SCOKZ=SCOKZ*1.05
C     ELSEIF (IJK.EQ.8) THEN
C       SCOKZ=SCOKZ/1.05*0.95
C     ELSEIF (IJK.EQ.9) THEN
C        SCOKZ=SCOKZ/0.95
C        ALPHA=ALPHA*1.05
C     ELSEIF (IJK.EQ.10) THEN
C        ALPHA=ALPHA/1.05*0.95
      DO 471 J=1,NPORES
          N(J)=ELEM
               DO 471 I=1,ELEM
               RADI(I,J)=RADO(I,J)
              CORR(I,J)=RADO(I,J)
  471      RADIUS(I,J)=RADO(I,J)
          CO=COUT
          T=0
C*********************************************************
C                    PAGE - 3 -  DEACT            *
C*********************************************************
C         READ(19,*) RKP,RKS
CCCCCC    FLOW=FLOW/2.0
CCCCCC  THE ABOVE LINE WAS PRESENT IN ORIGINAL PROGRAM
          DO 15 I=0,50
             DO 15 J=1,10
   15 RESULT(I,J)=0
          RESULT(0,2)=100
          RESULT(0,4)=100
          RESULT(0,7)=100
CCCCCC OMRAN ADDED
          RESULT(0,14)=20
          RESULT(0,17)=80
CCCCCC OMRAN ADDED ABOVE
          WRITE(9,2321) IJK
 2321 FORMAT(//,1H1,'RESULTS FOR FLUIDIZED BED SIMULATION ',I2//)
          WRITE(9,*) 'RKS =',RKS,' RKP= ',RKP
          WRITE(9,*) 'ALPHA= ',ALPHA,'KS= ',KS
          WRITE(9,*) 'SCOK= ',SCOK,' SCOKZ= ',SCOKZ
          WRITE(*,*) 'SCOK= ',SCOK,' SCOKZ= ',SCOKZ
          WRITE(*,*) 'KS= ',KS,'ALPHA= ',ALPHA
          WRITE(*,*) 'RKS =',RKS,' RKP= ',RKP
          WRITE(*,*) '-------------------------------------------------'
C************** OUTPUT INITIAL CONDITIONS TO DATA FILES ***************
          WRITE(9,*) 'PORE SECTION LENGTH IN METERS(PL/ELEM)',PL
          WRITE(9,*) 'DIFFUSION COEFFICIENT (M**2/S) ',D
          WRITE(9,*) 'RATE CONSTANT (M/S) ',KS
          WRITE(9,*) 'TOTAL OUTSIDE CONCENTRATION (KMOL/M**3) ',COUT
          WRITE(9,*) 'PARALLEL AND SERIES COKING CONSTANTS ',RKP,RKS
          WRITE(9,*) 'MEAN COKE SIZES FOR ZEOLITE & SUPPORT ',SCOKZ,SCO
     +K
          WRITE(9,*) 'NUMBER OF PORES AND PORE ELEMENTS ',NPORES,ELEM
          WRITE(9,*) 'FRACTION OF INITIAL ACTIVITY DUE TO ZEOLITE ',ALP
     +HA
          WRITE(9,*) '-------------------------------------------------'
CCCCCCCCCCCCCC
C     WRITE(*,*) 'TIME  ACTIV   %VOL %SUPT    %VOL   %VOL %ZEOL  %PORE
C    +%SUP %ZEO EFF. THIEL'
C     WRITE(*,*) 'SEC   %CONV   COKE AREA     COKE   ZEOL AREA   ELEM
C    +LOST LOST FACT MODLS '
```

```
C     WRITE(*,*) '            SUPT ACTIV    ZEOL   LOST ACTIV  BLOC
C    +BLOC  BLOC'
C     WRITE(*,*) '-------------------------------------------------
C    +----------------------------'
CCCCCCCCCCCCCCCC
      WRITE(9,*) 'TIME  ACTIV   %VOL %SUPT    %VOL   %VOL %ZEOL  %POR %S
     +UP %ZEO EFF.  THIEL'
      WRITE(9,*) 'SEC   %CONV   COKE AREA    COKE   ZEOL AREA   ELEM LO
     +ST LOST FACT  MODLS '
      WRITE(9,*) '            SUPT ACTIV    ZEOL   LOST ACTIV  BLOC BL
     +OC BLOC'
      WRITE(9,*) '-------------------------------------------------
     +-------------------'
CCCCCCCCCCCCCC                          CCCCCCCCCCCCCCCCCCCCCCCCCC
C************** BEGIN TIMEWISE SIMULATION *************************
CCCCCCCCCCCCCC                          CCCCCCCCCCCCCCCCCCCCCCCCCC
          ZYX=0.0
         WRITE(66,*)'VOLUMES ARE % VOLUMES OF SUPPORT ALONE'
         WRITE(66,*)'%WT COKE IS ASSUMING ALL COKE IN SUPPORT ALONE'
         WRITE(66,*)'THICKNESS IS COKE LAYER THICKNESS FOR EVEN COKING'
         WRITE(66,*)'*************************************************'
         WRITE(66,*)'                                                  '
         WRITE(66,*)'THICKNESS ,%WTCOK ,%VOLFREE, %VOLCOKED, %VOLBLOCK,
     + %AREA FREE,%AREA COKED, %AREA BLOK'
          DO 2 NLOOP=1,NLT
CC        IF (NLOOP.LE.15) THEN
          IF (NLOOP.LE.15) THEN
            NSTEP=1.0
          ELSE
              NSTEP=5.0
          ENDIF
C*************** CHANGE OF STEP LENGTH ******************************
          T=T+TSTEP*NSTEP
          CALL COKRAT(1,KS,CO,SCOKZ,SCOK,NPORES,ALPHA)
C         WRITE(*,*) 'IT RETURNS FROM COKRAT ONCE'
          IF(NLOOP.EQ.1) THEN
          RATMAX=RATE
          DRATE=0
          DO 37 J=1,NPORES
             DO 37 I=1,N(J)
CCC          DRATE=DRATE+(1-ALPHA)*2*3.1416*RADO(I,J)*PL
CCC          DRATE=DRATE+ALPHA*CONST*RADO(I,J)*PL
             DRATE=DRATE+(1-ALPHA)*2*3.1416*RADO(I,J)*PL*FRESUP(I,J)
             DRATE=DRATE+ALPHA*CONST*RADO(I,J)*PL*FREZEO(I,J)
   37  CONTINUE
          SPAREA=DRATE*VPORE/(TVOL*3.1416*PL)
          DRATE=DRATE*KS*CO
          EFF=RATMAX/DRATE
          THIELE=20
C
C         THIELE=0.00460
C
          DO 34 I=1,1000
          TTT=TANH(THIELE)/EFF
          VARY=(THIELE-TTT)/(THIELE+TTT)/2
          IF(ABS(VARY).LE.0.001) GOTO 33
C         IF(ABS(VARY).LE.1E-05) GOTO 33
          THIELE=TTT
   34  CONTINUE
          THIELE=999
C
C         THIELE=0.00485
C
CCCC   THE FOLLOWING LINE NOT IN PROGRAM OF THOMSON
C         THIELE=TTT
CCCCC
```

```
   33  IF(ABS(VARY).LT.0.001) THEN
C  33  IF(ABS(VARY).LT.1E-05) THEN
          THIELE=(TTT+THIELE)/2
C
C         THIELE=0.00485
C
          ENDIF
           GROUP=EFF*KS*CMASS*SPAREA/FLOW
CCCCCCC
CCCCC          GROUP=EFF*KS*CATFEED*SPAREA
CCCCCC
          CONVER=GROUP/(1+GROUP)
          RESULT(0,2)=CONVER*100
          RESULT(0,12)=CONVER*100
CCCCCCCCCCC
CC        WRITE(*,*) EFF,KS,CMASS,SPAREA,FLOW,GROUP,CONVER
CCCCCCCCCCC
C         WRITE(*,*) T,TSTEP,NSTEP,THIELE,EFF,GROUP,CONVER
CCCCCCCC
C         WRITE(9,*) '  TIME ,MIN   %COKVOL SUP  %COKVOL Z  %ZAREA ACT
C    +  %SUPAREA PLUG '
C         WRITE(*,*) (RESULT(0,I),I=1,10),EFF,THIELE
CCCCCC CHANGE TIME TO MINUTES
CC        RESULT(0,1)=RESULT(0,1)/60.
CCCCC    CONCENTRATION AT INTERFACES INSIDE PORES
CCCC    RESULT(0,14)=AFRE*0.20
        RESULT(0,14)=RESULT(0,4)*0.20
        RESULT(0,17)=RESULT(0,7)*0.80
        RESULT(0,18)=RESULT(0,14)+RESULT(0,17)
          WRITE(9,909) (RESULT(0,I),I=1,10),EFF,THIELE
CCCC      WRITE(*,909) (RESULT(0,I),I=1,10),EFF,THIELE
CCCCCCC   WRITE(*,909) (RESULT(0,I),I=11,20),EFF,THIELE
          WRITE(99,999) (RESULT(0,I),I=11,18),EFF,THIELE
          ENDIF
          DO 3 J=1,NPORES
               DO 3 I=1,N(J)
C     WRITE(*,*) J,I,NPORES,N(J),RADIUS(I,J),TSTEP,NSTEP,RATCO(I,J,1)
    3  RADI(I,J)=RADIUS(I,J) +TSTEP*NSTEP*RATCO(I,J,1)/2
C     WRITE(*,*) 'IS EVERYTHING OK'
C*****************************************************
C                      PAGE -4- DEACT                *
C*****************************************************
C
C*****************************************************
C   CHECK FOR BLOCKED PORES                          *
C*****************************************************
C
          DO 11 J=1,NPORES
               MMM=N(J)
               DO 11 I=MMM,1,-1
                    IF(RADI(I,J).LE.1.0E-10) THEN
CCCCCCCCCC          IF(RADI(I,J).LE.999.0E-10) THEN
                      N(J)=I-1
                      RADIUS(I,J)=0
                      RADI(I,J)=0
                    ENDIF
   11  CONTINUE
          CALL COKRAT(2,KS,CO,SCOKZ,SCOK,NPORES,ALPHA)
C         WRITE (*,*) 'IT RETURNS FROM COKRAT TWICE'
          DO 4 J=1,NPORES
             DO 4 I=1,N(J)
    4   RADI(I,J)=RADIUS(I,J) + TSTEP*NSTEP*RATCO(I,J,2)/2
          DO 21 J=1,NPORES
               MMM=N(J)
               DO 21 I=MMM,1,-1
                    IF(RADI(I,J).LE.1.0E-10) THEN
```

```
                    N(J)=I-1
                    RADIUS(I,J)=0
                    RADI(I,J)=0
                  ENDIF
   21  CONTINUE
       CALL COKRAT(3,KS,CO,SCOKZ,SCOK,NPORES,ALPHA)
C      WRITE(*,*) 'IT RETURNS COKRAT THREE TIMES'
       DO 5 J=1,NPORES
          DO 5 I=1,N(J)
CCCCC  WRITE(*,*) RADIUS(I,J),RADI(I,J)
    5  RADI(I,J)=RADIUS(I,J) + TSTEP*NSTEP*RATCO(I,J,3)
       DO 31 J=1,NPORES
          MMM=N(J)
          DO 31 I=MMM,1,-1
CCCC            IF(RADI(I,J).LE.9.0E-10) THEN
                IF(RADI(I,J).LE.1.0E-10) THEN
                  N(J)=I-1
                  RADIUS(I,J)=0
                  RADI(I,J)=0
       ENDIF
   31  CONTINUE
       CALL COKRAT(4,KS,CO,SCOKZ,SCOK,NPORES,ALPHA)
C      WRITE (*,*) 'IT RETURNS FROM COKRAT FOUR TIMES'
C*******************************************************
C      MAKE RUNGE KUTTA STEP                          *
C*******************************************************
       AFRE=0.0
       ACOK=0.0
       ABLK=0.0
       AFB=0.0
       VVV=0.0
       VFR=0.0
       VCOK=0.0
       VBL=0.0
       CCC=0.0
          DO 67 J=1,NPORES
             DO 6 I=1,N(J)
          RKSTEP=(RATCO(I,J,1)+2*RATCO(I,J,2)+2*RATCO(I,J,3)+RATCO(I,
     +J,4))
          RKSTEP=RKSTEP/6.0*NSTEP*TSTEP
CCCC   OMRAN ADDED BELOW  ,ASSUMING THICKNESS OF COKE LAYER IS CONSTANT
CCCC   THROUGH THE PORE SEGMENTS AND IT EQUALS THAT OF RADIUS(1,1)
CCCC   OMRAN SET RADIUS(1,1)=3200A FOR CONVENIENCE
       IF(I.EQ.1.AND.J.EQ.1) THEN
       ZYX=ZYX-RKSTEP
       THICK=ZYX*1.0E10
       ENDIF
CCCC   OMRAN ADDED ABOVE TO CALCULATE COKE THICKNESS
CCC       CCC=CCC+(-RKSTEP)**2.0
CCC       WRITE(*,*) RADIUS(I,J),RKSTEP
CCC       WRITE(9,*) RADIUS(I,J),RKSTEP,CORR(I,J)
          RADIUS(I,J)=RADIUS(I,J)+RKSTEP
C*******OMRAN ADDED ABOVE TO PRODUCE RADII FOR DRAWING 22 PORES
       CORR(I,J)=CORR(I,J)+RKSTEP
CCC    CORR(I,J)=RADIUS(I,J)
CC     IF(CORR(I,J).LE.9.0E-10) CORR(I,J)=0.0
       IF(CORR(I,J).LE.1.0E-10) CORR(I,J)=0.0
CC        WRITE(9,*) RADIUS(I,J),RKSTEP,CORR(I,J)
CC        WRITE(*,*) RADIUS(I,J),RKSTEP,CORR(I,J)
C*******OMRAN ADDED TO PRODUCE RADII FOR DRAWING CORRUGATED PORES
        AFRE=AFRE+RADIUS(I,J)
        VFR=VFR+RADIUS(I,J)**2.0
CCC    VVV=VVV+CORR(I,J)**2.0
CC        WRITE(9,*)      RKSTEP
CC     IF(N(J).LE.9) CORR(N(J)+1,J)=0.0
CC     WRITE(9,*)'RKSTEP=',RKSTEP
```

```
    6  RADI(I,J)=RADIUS(I,J)
       IF(N(J).LE.9) CORR(N(J)+1,J)=0.0
 67    CONTINUE
CCC    WRITE(9,*) NPORES,ELEM,N(1)
CCCC  OMRAN ADDED BELOW
CC     ZYX=ZYX-RKSTEP
CC     THICK=ZYX*1.0E10
       DO 345 J=1,NPORES
        DO 345 I=1,ELEM
CCC        WRITE(9,*) RADIUS(I,J),CORR(I,J)
       VVV=VVV+CORR(I,J)**2.0
       AFB=CORR(I,J)+AFB
  345  CONTINUE
CCCC  OMRAN ADDED ABOVE
       VVV=(VVV/T[illegible])*100.
       AFB=(AFB/S[illegible] *100.
       VFR=(VFR/T[illegible] *100.
       AFRE=(AFRE/S[illegible])*100.
       VBL=VVV-VFR
       ABLK=AFB-AFRE
       VCOK=100.-VFR-VBL
       ACOK=100.-AFRE-ABLK
       WTCOK=VCOK*0.16
CCCC   VVV IS % VOLUME OF SUPPORT FREE+BLOCKED
CCCC   VCOK IS % VOLUME OF SUPPORT FREE+BLOCKED
CCCC   VFR IS % VOLUME OF SUPPORT FREE
CCCC   VBL IS % VOLUME OF SUPPORT BLOCKED
CCCC   AFRE IS % AREA OF SUPPORT FREE
CCCC   ACOK IS % AREA OF SUPPORT COKED
CCCC   ABLK IS % AREA OF SUPPORT BLOCKED
CCC    WTCOK IS % WT COKE IN SUPPORT ASSUMING SP VOL=0.16 CC/GM
CC     WRITE(*,*)'THICK=',THICK
CC     WRITE(*,*) ' VFR=',VFR,'VBL=',VBL,'VCOK=',VCOK
CC     WRITE(9,*)'THICK=',THICK ,'%WT COKE IN SUPP',WTCOK
CC     WRITE(9,*)  'VFR=',VFR,'VBL=',VBL,'VCOK=',VCOK
CC     WRITE(9,*)  'VFR=',VFR,'VBL=',VBL,'VCOK=',VCOK
CC     WRITE(9,917)THICK,WTCOK,VFR,VCOK,VBL
       WRITE(66,917)THICK,WTCOK,VFR,VCOK,VBL,AFRE,ACOK,ABLK
  917     FORMAT(1X,08(F7.2,3X),/)
C 917     FORMAT(F5.0,1X,06(F6.2,1X),1(F5.1,1X),1F5.3,1X,F6.2)
CC         WRITE(9,*) RADIUS(I,J)
CCC        WRITE(*,*) RADIUS(I,J)
C*******OMRAN ADDED TO PRODUCE RADII FOR DRAWING CORRUGATED PORES
CC     IF(NLOOP.EQ.NLT) THEN
CC      ENDIF
C*******OMRAN ADDED ABOVE TO PRODUCE RADII FOR DRAWING 22 PORES
           DO 41 J=1,NPORES
C     PRINT*,'NPORES',NPORES,'N(J)',N
                MMM=N(J)
                DO 41 I=MMM,1,-1
CCC
CC               IF(CORR(I,J).LE.1.0E-00) CORR(I,J)=0.0
CCC  OMRAN ADDED TO CAUSE BLOCKING FOR R=20 ANG
                      IF(RADI(I,J).LE.20.0E-10) THEN
CCCCCCCCCCCC          IF(RADI(I,J).LE.5.0E-10) THEN
                        N(J)=I-1
                        RADIUS(I,J)=0
                        RADI(I,J)=0
CCCC          CORR(I,J)=0.0
                      ENDIF
CC     WRITE(8,*) RADI(I,J)
   41  CONTINUE
CC     KJI=N(J)
CC     DO 234 J=1,NPORES
CC         DO 234 I=1,KJI
CC     IF(NLOOP.EQ.1) KJI=ELEM
```

```
CC          CORR(I,J)=CORR(I,J)+RKSTEP
CC          IF(CORR(I,J).LE.1.0E-10) CORR(I,J)=0.0
C 234   CONTINUE
CCCC
CCC   TO STORE PORE RADII IN FILE FOR DRAWING
       DO 246 J=1,NPORES
           DO 246 I=1,ELEM
           CORR(I,J)=CORR(I,J)*1.0E+10
CC         WRITE(88,*)  CORR(I,J)
CC         WRITE(88,468)  CORR(I,J)
  468      FORMAT(1X,F6.1)
           CORR(I,J)=CORR(I,J)*1.0E-10
CCC        WRITE(8,*) (CORR(I,J),I=1,ELEM)
  246   CONTINUE
CCCCCCCCCCCCCCCCCCCCCCCCCCCCCCCCCCCCCCCCCCCCCCCCCCCCCCCCCCCCCCCCCCC
           CALL COKRAT(1,KS,CO,SCOKZ,SCOK,NPORES,ALPHA)
           CONVER =RATE/RATMAX
           ACTIV =RATE/RATMAX*100
C*********************************************************
C     OUTPUT RESULTS TO RESULTS MATRIX                   *
C*********************************************************
           DIFRAT=0
           THIELE=20
C     PRINT*,'NPORES',NPORES,'N(J)',N
           DO 28 J=1,NPORES
              DO 28 I=1,N(J)
C     PRINT*,'RADO(I,J)=',RADO(I,J)
C     PRINT*,'DIFRAT=',DIFRAT
C     PRINT*,'FRESUP(I,J)=',FRESUP(I,J)
C     PRINT*,'FREZEO(I,J)=',FREZEO(I,J)
       DIFRAT=DIFRAT + (1-ALPHA)*2*3.1416*RADO(I,J)*PL*FRESUP(I,J)
CC    PRINT*,'DIFRAT2=',DIFRAT
CCC OMRAN ADDED
      IF(DIFRAT.LE.1.E-30) THEN
      DDD=DIFRAT
      ELSE
CC    PRINT*,'DIFRAT222=',DIFRAT,'RATE=',RATE
C     PRINT*,'DIFRAT',DIFRAT
C*********************************************************
C              PAGE -5- DEACT                            *
C*********************************************************
           DIFRAT=DIFRAT+ALPHA*CONST*RADO(I,J)*PL*FREZEO(I,J)
      ENDIF
CC    PRINT*,'DIFRAT3=',DIFRAT,'DDD=',DDD
CC    PRINT*,'DIFRAT333=',DIFRAT,'RATE=',RATE
   28  CONTINUE
           SPAREA=DIFRAT*VPORE/(TVOL*3.1416*PL)
CC    PRINT*,'SPAREA',SPAREA
           DIFRAT=DIFRAT*CO*KS
CC    PRINT*,'DIFRAT4=',DIFRAT
CC    PRINT*,'DIFRAT=',DIFRAT,'CO=',CO,'KS=',KS,'RATE=',RATE
           EFF=RATE/DIFRAT
CC    PRINT*,'DIFRAT5=',DIFRAT ,'EFF=',EFF
CCC  OMRAN ADDED  BELOW
CCCC     PRINT*,'EFF',EFF
           IF(EFF.GT.1.0) EFF=1.0
CCC        IF(EFF.LT.0.0010) EFF=1.0
CCC  OMRAN ADDED  ABOVE
CC     PRINT*,'THIELE=',THIELE,'EFF=',EFF,'TTT=',TTT,'VARY=',VARY
           DO 29 I=1,1000
           TTT=TANH(THIELE)/EFF
           VARY=(THIELE-TTT)/(THIELE+TTT)/2
           IF(ABS(VARY).LE.0.001) GOTO 30
           THIELE=TTT
   29  CONTINUE
CC    PRINT*,'THIELE2=',THIELE,'EFF2=',EFF,'TTT2=',TTT,'VARY2=',VARY
```

```
          THIELE=999
   30   IF(ABS(VARY).LT.0.001) THEN
          THIELE=(TTT+THIELE)/2
          ENDIF
          GROUP=EFF*KS*CMASS*SPAREA/FLOW
          CONVER=GROUP/(1+GROUP)
          CO=COUT*(1-CONVER)
          RESULT(NLOOP,1)=T
          RESULT(NLOOP,2)=CONVER*100
          VOL=0.0
          AA=0
          AB=0
          AC=0
          AD=0
          AE=0
          AF=0
          AG=0
          DO 22 J=1,NPORES
            DO 22 I=1,ELEM
CC     PRINT*, FRESUP(I,J),FREZEO(I,J)
CCCC   OMRAN ADDED BELOW
         IF(FREZEO(I,J).LE.1.0E-5) THEN
           FACTOR= 0.0
           ELSE
               FACTOR=-LOG(FREZEO(I,J)/FRESUP(I,J))
           ENDIF
CCCCC OMRAN ADDED ABOVE
CCC             FACTOR=-LOG(FREZEO(I,J)/FRESUP(I,J))
            POISS=4.0E-10/SCOKZ
CCC    PRINT*, FRESUP(I,J),FREZEO(I,J),FACTOR,POISS
             IF(FACTOR.LE.POISS)THEN
              AF=AF+FACTOR*(CONST*RADO(I,J)*PL)*SCOKZ
C*********************************************************
C    NUMBER OF COKE UNITS *VOLUME OF ONE COKE ELEMENT   *
C*********************************************************
           COK=FACTOR*SCOKZ/4.0E-10
           AG=AG+(1-FRESUP(I,J))*(1-COK)*4.0E-10*(CONST*RADO(I,J)*PL)
C*********************************************************
C  ZEOLITE 'SPACE' LOST DUE TO SUPPORT COVERAGE         *
C*********************************************************
C
          AG=AG+FACTOR*(CONST*RADO(I,J)*PL)*SCOKZ
C
C*********************************************************
C  ADD ON THE COKE CONTENT IN THE ZEOLITE TO CALCULATE  *
C  THE TOTAL LOSS IN VOLUME                             *
C*********************************************************
          ELSE
            AF=AF+(CONST*RADO(I,J)*PL*4.0E-10)
            AG=AG+(CONST*RADO(I,J)*PL*4.0E-10)
C*********************************************************
C         ZEOLITE TOTALLY FULL                          *
C*********************************************************
          ENDIF
   22    VOL=VOL+2.0*RADO(I,J)*SCOK*(-LOG(FRESUP(I,J)))
          RESULT(NLOOP,5)=AF/(TVOL*PL*3.1416)*100
CCCCCCCCOMRAN ADDED TO AVOID SOME DIFFICULTIES IN RESULT(NLOOP,5)
           NNLL=NLOOP-1
           IF(RESULT(NLOOP,5).LT.RESULT(NNLL,5)) THEN
           RESULT(NLOOP,5)=RESULT(NNLL,5)
           ENDIF
CCCCC  OMRAN ADDED ABOVE
CCCCC PRINT*, AF,TVOL,PL,RESULT(NLOOP,5)
CCCC
          RESULT(NLOOP,6)=AG/(TVOL*PL*3.1416)*100
           IF(RESULT(NLOOP,6).LT.RESULT(NNLL,6)) THEN
```

```
          RESULT(NLOOP,6)=RESULT(NNLL,6)
          ENDIF
          RESULT(NLOOP,3)=VOL/TVOL*100
          DO 23 J=1,NPORES
             DO 23 I=1,N(J)
                AA=AA+FRESUP(I,J)*RADO(I,J)
  23           AB=AB+FREZEO(I,J)*RADO(I,J)
          RESULT(NLOOP,4)=AA/SURF*100
          RESULT(NLOOP,7)=AB/SURF*100
          DO 24 J=1,NPORES
             DO 24 I=N(J)+1,ELEM
C*************************************************************
C             PAGE -6- DEACT                                  *
C*************************************************************
             AC=AC+1
             AD=AD+FRESUP(I,J)*RADO(I,J)
  24     AE=AE+FREZEO(I,J)*RADO(I,J)
          RESULT(NLOOP,8)=AC/TOTAL*100
          RESULT(NLOOP,9)=AD/SURF*100
          RESULT(NLOOP,10)=AE/SURF*100
CCCCCCCCCCC    OMRAN ADDED   CCCCC
CCCCCC   ASSUME SUPPORT VOLUME=0.16 CM**3/GM
CCCCCC   ASSUME ZEOLITE VOLUME=0.04 CM**3/GM
CCCCCC   ASSUME CATALYST VOLUME=0.20 CM**3/GM
CCCCCC   ASSUME COKE DENSITY=1.0 GM/CM**3
CCCCCC   ASSUME ZEOLITE AREA= 100 M**2/GM
CCCCCC   ASSUME SUPPORT AREA= 25  M**2/GM
CCCCCC
       RESULT(NLOOP,11)=RESULT(NLOOP,1)
       RESULT(NLOOP,12)=RESULT(NLOOP,2)
CCC    RESULT(NLOOP,13)=RESULT(NLOOP,3)*0.16
       RESULT(NLOOP,13)=WTCOK
       RESULT(NLOOP,15)=RESULT(NLOOP,5)*0.04*5.0
       RESULT(NLOOP,16)=RESULT(NLOOP,13)+RESULT(NLOOP,15)
CCCC   RESULT(NLOOP,14)=RESULT(NLOOP,4)*0.20
       RESULT(NLOOP,14)=AFRE*0.20
       RESULT(NLOOP,17)=RESULT(NLOOP,7)*0.80
       RESULT(NLOOP,18)=RESULT(NLOOP,14)+RESULT(NLOOP,17)
CCCC
CCCC
CCCCCCCCCCCCCCCCC  OMRAN ADDED ABOVE
C         WRITE(9,*) ' TIME&CONV'
CCCCCCC
CCCCCCCCC  WRITE(*,909) (RESULT(NLOOP,JJJ),JJJ=11,20),EFF,THIELE
           WRITE(99,999) (RESULT(NLOOP,JJJ),JJJ=11,18),EFF,THIELE
CCCCCCCC
CCCC   PRINT*,'EFF=',EFF,'THIELE=',THIELE
           WRITE(9,909) (RESULT(NLOOP,JJJ),JJJ=1,10),EFF,THIELE
C 909    FORMAT(1H ,06(F10.5),/,1H ,6(F10.5),/)
C 909    FORMAT(1H ,F5.0,2X,11(F6.2,2X))
C 909    FORMAT(F5.0,1X,06(F6.2,1X),4(F4.1,1X),F6.2)
  909    FORMAT(F5.0,1X,06(F6.2,1X),3(F4.0,1X),F5.3,1X,F6.2)
C 909    FORMAT(F5.0,1X,06(F6.2,1X),3(F4.1,1X),F5.3,1X,F6.2)
  999    FORMAT(F5.0,1X,06(F6.2,1X),1(F5.1,1X),1F5.3,1X,F6.2)
CC909    FORMAT(F5.0,1X,06(F6.2,1X),3(F4.1,1X),F5.1,1X,F6.2)
CC999    FORMAT(F5.0,1X,06(F6.2,1X),2(F5.1,1X),1X,F6.2)
CCCCCCCCCC   INTERMEDIATE CONCENTRATIONS  CCCCCCCCCCCCCCCCCCCCCC
C          WRITE(*,*)  (A(J,4,1),J=0,10),COUT,CO
C          WRITE(9,*)  (A(J,4,1),J=0,10),COUT,CO
CCCCCCCCCCCCCCCCCCCCCCCCCCCCCCCCCCCCCCCCCCCCCCCCCCCCCCCCCCCCCCCCC
    2      CONTINUE
C*************************************************************
C             OUTPUT RESULTS TO SCREEN                        *
C*************************************************************
CC     DO 25 I=0,NLT
CC 25  WRITE(8,*) (RESULT(I,J),J=1,9)
```

```
          WRITE(10,*) RESULT(NLT,6)
          DO 112 J=1,NPORES
             DO 112 I=1,N(J)
  112    RADIUS(I,J)=NINT(RADIUS(I,J)*1.0E10)
C 113    WRITE(*,*) I,J
CCCCCCCCCC
CCCCCCCCC
C        WRITE(10,*)  (A(J,4,1),J=0,10),COUT,CO
          DO 113 J=1,NPORES
          DO 113 I=1,ELEM
CCC      WRITE(8,*)  RADIUS(I,J)
         WRITE(10,*) RADIUS(I,J)
 113   CONTINUE
CCCCCCCCCCCCCCCC
C          DO 113 J=1,NPORES
C        WRITE(8,*) (RADIUS(I,J),I=1,ELEM)
C 113    WRITE(10,*) (RADIUS(I,J),I=1,ELEM)
  417 CONTINUE
C 417 CONTINUE
C       WRITE(*,*) D
          STOP
          END
C*******************************************************
C              SUBROUTINES                          *
C*******************************************************
C
C*******************************************************
C     COKDAT ACTS AS ADRIVER SUBROUTINE             *
C*******************************************************
          SUBROUTINE COKRAT(ISTEP,KS,CO,SCOKZ,SCOK,NPORES,ALPHA)
          REAL  A(0:10,4,2000),RADI(10,22),M(10,22),KS,L
          REAL  B(0:10,22),D(10,22),RADO(10,22)
          REAL  RATCO (10,22,4),THETA(10,22),FRESUP(10,22),FREZ
     +EO(10,22)
          INTEGER N(22)
          COMMON /DATA7/ FRESUP ,FREZEO
          COMMON /DATA4/ N
          COMMON /DATA1/ RADI
          COMMON /DATA8/ M
          COMMON /DATA5/ RATCO,RATE
          COMMON /DATA2/ A
          COMMON /DATA3/ THETA
          COMMON /MEGA/ PL,COUT,RKP,RKS
          COMMON /DATA6/D
          COMMON /DATA9/ RADO
          PI=3.1416
          L=PL
          CALL AREA(NPORES,ALPHA,SCOK,SCOKZ,KS)
          CALL COEFST(NPORES,CO,L)
          CALL TRIDG(NPORES)
C****** SET CONC OF A AT EACH END OF THE PORE & CALC CONC OF B AT EACH
C    +NODE
          DO 2 J=1,NPORES
             A(0,4,J)=CO
             IF(N(J).EQ.0) GOTO 2
C****** NO REACTION  ************************************
             IF(M(N(J),J).EQ.0) THEN
C****** DIFFUSION IN END PORE SEGMENT ******************
             A(N(J),4,J) =A(N(J)-1,4,J)
             ELSE
C****** REACTION IN END PORE SEGMENT *******************
             A(N(J),4,J)=A(N(J)-1,4,J) / COSH(M(N(J),J)*L)
             ENDIF
    2  CONTINUE
C
C         WRITE(*,*) A(0,4,1),A(1,4,1),A(2,4,1),A(9,4,1),A(10,4,1)
```

```
C
          DO 13 J=1,NPORES
             DO 13 I=0,N(J)
   13        B(I,J)= COUT-A(I,4,J)
C*********************************************************
C              PAGE -7- DEACT                            *
C*********************************************************
          IF(ISTEP.EQ.1) THEN
C*****CALC MAIN RATE
          RATE=0
          DO 3 J=1,NPORES
             IF(N(J).EQ.0) GOTO 3
C******** NO REACTION IN PORE
          IF(M(1,J).GT.0.0) THEN
C*********REACTION IN FIRST PORE ELEMENT
      RATE=RATE+D(1,J)*RADI(1,J)**2*(M(1,J)*A(1,4,J)/SINH(M(1,J)
     +*L)-M(1,J)*A(0,4,J)/TANH(M(1,J)*L))
          ELSE
C*****DIFFUSION IN FIRST PORE ELEMENT
             RATE=RATE+(A(1,4,J)-A(0,4,J))/L*D(1,J)*RADI(1,J)**2
          ENDIF
    3   CONTINUE
          RATE=-RATE*PI
          ENDIF
C***** CAL COKING RATES BASED ON 1ST ORDER IN CONC ,2ND ORDER IN AREA
          DO 4 J=1,NPORES
             DO 4 I=1,N(J)
          AMEAN=(A(I-1,4,J)+A(I,4,J))/2.0
          BMEAN=(B(I-1,J)+B(I,J))/2.0
CCC       WRITE(*,*)              FRESUP(I,J)
          RATCO(I,J,ISTEP)=AMEAN*(FRESUP(I,J))**2*RKP
          RATCO(I,J,ISTEP)=BMEAN*(FRESUP(I,J))**2*RKS+
     +   RATCO(I,J,ISTEP)
CC        RATCO(I,J,ISTEP)=AMEAN*(FRESUP(I,J))**2*RKP
CC        RATCO(I,J,ISTEP)=BMEAN*(FRESUP(I,J))**2*RKS+
CC   +   RATCO(I,J,ISTEP)
    4  CONTINUE
          RETURN
          END
C*************************************************
          SUBROUTINE TRIDG(NPORES)
C***THIS ROUTINE SOLVES THE TRIDIAGONAL MATRIX TO FIND THE CONCENTRATION
          REAL  A(0:10,4,2000)
          INTEGER N(22)
          COMMON /DATA4 /N
          COMMON /DATA2/A
          DO 1  J=1,NPORES
             IF(N(J).LE.1) GOTO 1
             DO 2 I=2,N(J)-1
             A(I,2,J)=A(I,2,J)-A(I,1,J)/A(I-1,2,J)*A(I-1,3,J)
    2      A(I,4,J)=A(I,4,J)-A(I,1,J)/A(I-1,2,J)*A(I-1,4,J)
          NM1=(N(J)-1)-1
          A(N(J)-1,4,J)=A(N(J)-1,4,J)/A(N(J)-1,2,J)
          DO 3 I=1,NM1
             M=(N(J)-1)-I
    3       A(M,4,J)=(A(M,4,J)-A(M,3,J)*A(M+1,4,J))/A(M,2,J)
    1   CONTINUE
          RETURN
          END
C*****COEFST SETS THE COEFFICIENTS FOR TRIGD
          SUBROUTINE COEFST (NPORES,CO,L)
          REAL  A(0:10,4,2000),RADI(10,22),L,M(10,22),D(10,22)
          INTEGER N(22)
          COMMON /DATA6 / D
          COMMON /DATA4 / N
          COMMON /DATA1 / RADI
```

```
      COMMON /DATA8 / M
      COMMON /DATA2 / A
      DO 2 J=1,NPORES
        IF(N(J).LE.1) GOTO 2
        DO 1 I=1,N(J)-2
C****************************************************
C           PAGE -8- DEACT                         *
C****************************************************
C     FOUR ALTERNATIVES FOR OPEN TO OPEN PORES
C          1) REACTION - REACTION
C          2) REACTION - DIFFUSION
C          3) DIFFUSION - REACTION
C           4) DIFFUSION - DIFFUSION
C     THESE FOUR ARE DEALT WITH BELOW
C****************************************************
        IF(M(I,J).GT.0.0.AND.M(I+1,J).GT.0.0) THEN
C
C     REAC/REAC
C
        A(I,1,J)=M(I,J)*D(I,J)*RADI(I,J)**2/SINH(M(I,J)*L)
        A(I,2,J)=-M(I,J)*D(I,J)*RADI(I,J)**2/TANH(M(I,J)*L)
        A(I,2,J)=A(I,2,J)-M(I+1,J)*D(I+1,J)*RADI(I+1,J)**2/TANH(M(I+1
     + ,J)*L)
        A(I,3,J)=M(I+1,J)*D(I+1,J)*RADI(I+1,J)**2/SINH(M(I+1,J)*L)
        A(I,4,J)=0
CCCCCCCCCCCC
CCCCCCCCCCCCC
C         WRITE(*,*)  (A(J,4,1),J=0,10),COUT,CO
C         WRITE(10,*)  (A(J,4,1),J=0,10),COUT,CO
CCCCCCCCC
CCCCCCCCC
C         WRITE(*,*) A(I,1,J),A(I,2,J),A(I,3,J)
C****************************************************
        ELSEIF(M(I,J).GT.0.0.AND.M(I+1,J).EQ.0.0) THEN
C
C     REAC/DIFF
C
        A(I,1,J)=M(I,J)*D(I,J)*RADI(I,J)**2/SINH(M(I,J)*L)
        A(I,2,J)=-M(I,J)*D(I,J)*RADI(I,J)**2/TANH(M(I,J)*L)
        A(I,2,J)=A(I,2,J)-D(I+1,J)*RADI(I+1,J)**2/L
        A(I,3,J)=D(I+1,J)*RADI(I+1,J)**2/L
        A(I,4,J)=0
C****************************************************
        ELSEIF(M(I,J).EQ.0.0.AND.M(I+1,J).GT.0.0) THEN
C
C     DIFF/REAC
C
        A(I,1,J)= D(I,J)*RADI(I,J)**2/L
        A(I,2,J)= -D(I,J)*RADI(I,J)**2/L
        A(I,2,J)=A(I,2,J)-M(I+1,J)*D(I+1,J)*RADI(I+1,J)**2/TANH(M(I+1
     +,J)*L)
        A(I,3,J)=M(I+1,J)*D(I+1,J)*RADI(I+1,J)**2/SINH(M(I+1,J)*L)
        A(I,4,J)=0
C****************************************************
        ELSEIF(M(I,J).EQ.0.0.AND.M(I+1,J).EQ.0.0) THEN
C
C     DIFF/DIFF
C
        A(I,1,J)=D(I,J)*RADI(I,J)**2/L
        A(I,2,J)=-D(I,J)*RADI(I,J)**2/L -D(I+1,J)*RADI(I+1,J)**2/L
        A(I,3,J)=D(I+1,J)*RADI(I+1,J)**2/L
        A(I,4,J)=0
        ENDIF
    1   CONTINUE
        A(1,4,J)=-A(1,1,J)*CO
C****************************************************
```

```
C     FOUR ALTERNATIVES FOR OPEN TO CLOSED PORES
C          1) REACTION - REACTION
C          2) REACTION - DIFFUSION
C          3) DIFFUSION - REACTION
C          4) DIFFUSION - DIFFUSION
C     THESE FOUR ARE DEALT WITH BELOW
C*************************************************************
          IF (M(N(J)-1,J).GT.0.0.AND.M(N(J),J).GT.0.0) THEN
C
C     REAC/REAC
C
          A(N(J)-1,1,J)=M(N(J)-1,J)*D(N(J)-1,J)*RADI(N(J)-1,J)**2/SINH(
     +M(N(J)-1,J)*L)
       A(N(J)-1,2,J)=-M(N(J)-1,J)*D(N(J)-1,J)*RADI(N(J)-1,J)**2/TANH(M(
C*************************************************************
C           PAGE -9- DEACT                                  *
C*************************************************************
     +N(J)-1,J)*L)
      A(N(J)-1,2,J)=A(N(J)-1,2,J) - M(N(J),J)*D(N(J),J)*RADI(N(J),J)**
     +2*TANH(M(N(J),J)*L)
          A(N(J)-1,4,J)=0
C*************************************************************
          ELSEIF (M(N(J)-1,J).GT.0.0.AND.M(N(J),J).EQ.0.0) THEN
C
C     REAC/DIFF
C
      A(N(J)-1,1,J)=M(N(J)-1,J)*D(N(J)-1,J)*RADI(N(J)-1,J)**2/SINH
     +(M(N(J)-1,J)*L)
      A(N(J)-1,2,J)=-M(N(J)-1,J)*D(N(J)-1,J)*RADI(N(J)-1,J)**2/TANH
     +(M(N(J)-1,J)*L)
          A(N(J)-1,4,J)=0
C*************************************************************
          ELSEIF (M(N(J)-1,J).EQ.0.0.AND.M(N(J),J).GT.0.0) THEN
C
C     DIFF/REACT
C
          A(N(J)-1,1,J)=D(N(J)-1,J)*RADI(N(J)-1,J)**2/L
          A(N(J)-1,2,J)=-M(N(J),J)*D(N(J),J)*RADI(N(J),J)**2*TANH(M(N(J
     +),J)*L)
          A(N(J)-1,2,J)=A(N(J)-1,2,J)-D(N(J)-1,J)*RADI(N(J)-1,J)**2/L
          A(N(J)-1,4,J)=0
C*************************************************************
          ELSEIF (M(N(J)-1,J).EQ.0.0.AND.M(N(J),J).EQ.0.0) THEN
C
C     DIFF/DIFF
C
          A(N(J)-1,1,J)=1
          A(N(J)-1,2,J)=-1
          A(N(J)-1,4,J)=0
          ENDIF
   2  CONTINUE
          RETURN
          END
C**********THIS ROUTINE ESTABLISHES THE VALUES OF M
          SUBROUTINE AREA (NPORES,ALPHA,SCOK,SCOKZ,KS)
          REAL  RADO(10,22),RADI(10,22),THETA(10,22),FRESUP(10,
     +22)
          REAL  FREZEO(10,22),M(10,22),KS,D(10,22)
          INTEGER N(22)
          COMMON /DATA6 / D
          COMMON /DATA10/ CONST
          COMMON /DATA7 / FRESUP,FREZEO
          COMMON /DATA3 / THETA
          COMMON /DATA4 / N
          COMMON /DATA1 / RADI
          COMMON /DATA8 / M
```

```
      COMMON /DATA9 / RADO
      DO 2 J=1,NPORES
         DO 2 I=1,N(J)
            IF(RADI(I,J).LE.400.0E-10) THEN
              D(I,J)=246.19*RADI(I,J)
            ELSE
              D(I,J)=1.0E-5
            ENDIF
2  CONTINUE
       DO 1 J=1,NPORES
          DO 1 I=1,N(J)
          ZAREA=CONST*RADO(I,J)
          FRESUP(I,J)=RADI(I,J)/RADO(I,J)
CC      WRITE(*,*)       RADI(I,J),RADO(I,J) ,SCOKZ, FRESUP(I,J)
        IF(((RADI(I,J)-RADO(I,J))/SCOKZ).LE.-100.) THEN
         FREZEO(I,J)=0.0
         ELSE
          FREZEO(I,J)=EXP((RADI(I,J)-RADO(I,J))/SCOKZ)*FRESUP(I,J)
         ENDIF
CC      WRITE(*,*)  FREZEO(I,J)
CCCCC       FRESUP(I,J)=EXP((RADI(I,J)-RADO(I,J))/SCOK)
CC          IF((RADI(I,J)-RADO(I,J))/SCOKZ.GE.-1.0E-10)  THEN
CC          FREZEO(I,J)=EXP((RADI(I,J)-RADO(I,J))/SCOKZ)*FRESUP(I,J)
CC          ELSE
CC          FREZEO(I,J)=0.0
CC          ENDIF
            THETA(I,J)=(1-ALPHA)*2*3.1416*RADO(I,J)*FRESUP(I,J)
            THETA(I,J)=THETA(I,J)+ALPHA*FREZEO(I,J)*ZAREA
CCCCC     WRITE(*,*)  THETA(I,J),KS,RADI(I,J),D(I,J)
          M(I,J)=SQRT(THETA(I,J)*KS/(RADI(I,J)**2*3.1416*D(I,J)))
1   CONTINUE
      RETURN
      END
```

APPENDIX–3

Microfiche listing of the program OMRAN10 which solves the equations for diffusion, reaction and deactivation in the stochastic network pore model.

APPENDIX–4

APPENDIX–4

Experimental Procedure for Surface Area Measurement

The manufacturer's instructions for using the Quantasorb Unit were as follows:

(1) Take a catalyst sample (0.1 g) in the sample tube. Fix it in the sample holder in the Adsorption Unit (in the pretreatment position). Put the heating mantle around the sample tube and clamp it. Pass nitrogen (20 cm^3/min) through the sample tube.

(2) Switch on Quantasorb Unit and flow controller.

(3) Put liquid nitrogen in the Dewar flask around the trap in the right hand side of the unit. Adjust the temperature control–knob until the temperature reaches 400° C. Keep it under these conditions (temperature 400° C, nitrogen flow rate 20 cm^3/min) for 90 minutes and switch on the recorder.

(4) Allow for the sample tube to cool to room temperature. Transfer it to the adsorption position (at the front panel of the unit) and pass nitrogen through the sample by opening the valve at the top of the Quantasorb Unit. Set the attenuation at 32 (Quantasorb) and bridge current at 150 mA. Set the recorder span at 5 and chart speed at 0.5 cm/min. Put the by–pass valve to the by–pass position. Open the helium cylinder and helium valve in the Quantasorb. Adjust the helium flow control valve in the flow controller to get flow rate of 18 cm^3/min. Adjust the nitrogen flow control valve until the flow rate of N_2 is 2 cm^3/min. Open the by–pass valve (at the top) to the sample position and allow the gas mixture (10% N_2 in He) to pass through the sample. Wait for 30 minutes till a steady base line is observed in the recorder. Zero the integrator reading in the counter. Put the polarity switch in the adsorption position (up). Immerse the sample tube in liquid nitrogen.

A peak will appear in the recorder due to adsorption. The adsorption is complete when the recorder pen has returned to the base line, and the reading becomes constant. Note down the integrator reading. Zero the integration counts and change the polarity switch to the desorption position (down). Bring the base line to the original position. Remove the liquid nitrogen flask from the sample.

(5) Desorption of nitrogen takes place and a peak appears in the recorder. When the recorder pen returns to the base line and the integrator reading becomes a constant, note down the reading.

(6) Withdraw 2.5 cm^3 of N_2 in a gas syringe from the OUT position in the Quantasorb and inject it into the carrier stream in the IN position. Watch the calibration peak and note down the calibration counts when the reading becomes constant.

(7) Turn the valve at the top of the unit to the by–pass position.

(8) Make another mixture containing 12.5% N_2 in helium. (Increase the nitrogen flow rate to 2.5 cm^3/min and decrease helium flow rate to 17.5 cc/min)

(9) Repeat steps 4 to 8.

(10) Make another mixture containing 15% N_2 in helium, (nitrogen flow rate 3 cm^3/min and helium flow rate 17 cm^3/min).

(11) Repeat steps 4 to 8.

(12) Shut down the unit as follows:

Switch off the recorder

Switch off the Quantasorb unit

Close the N_2 and the cylinders

Close the N_2 and helium valves in the Quantasorb Unit.

(13) Determine the weight of the catalyst in the sample tube.

Surface Area Calculation

Total surface area of a catalyst is usually determined by the Brunauer–Emmett–Teller (BET) method. The basis and background of the technique are treated in numerous articles and books(Allen, 1990; Lowell, 1979).

The usual form of the BET equation that describes the adsorption as a gas upon a solid surface is:

$$\frac{P/P_o}{V(1-P/P_o)} = \frac{1}{V_m C} + \left(\frac{C-1}{V_m C}\right)\left(\frac{P}{P_o}\right)$$

where

V is the volume of gas adsorbed at pressure P,

P_o is the saturation pressure (the vapour pressure of liquefied gas at the adsorbing temperature),

V_m is the volume of gas required to form an adsorbed monomolecular layer, and,

C is a constant related to the energy of adsorption.

When experimental data are plotted as $(P/P_o)/[V\{1-(P/P_o)\}]$ the ordinate against (P/P_o) as the abscissa, a straight line results for P/P_o values between 0.05 and 0.35. Intercept and slope are $(1/V_m C)$ and $(C-1)\ V_m C$ respectively.

$$\text{slope} + \text{intercept} = \frac{C-1}{V_m C} + \frac{1}{V_m C} = \frac{1}{V_m}$$

The monolayer volume is thus expressed as the reciprocal of slope plus intercept. The total number of gas molecules (N_m) is the monolayer volume (in cc/stp) is given by:

$$N_m = \frac{V_m}{22400} \times \text{Avogadro's number}$$

Total surface area, S, is given by:

$$S = (N_m)\,(S')$$

where

S' is the area covered by one adsorbed molecule

Since area covered by one adsorbed nitrogen molecule is given by:

$$S' = 16.2\ \mathring{A}^2$$

or

$$S' = 16.2 \times 10^{-20}\ m^2$$

Substituting back into previous equations, the total surface area, S, is calculated as follows

$$S = \frac{V_m}{22400} \times 6.023 \times 10^{23} \times 16.2 \times 10^{-20}\ m^2$$

or

$$S = 4.35 \times V_m\ m^2$$

Quantasorb Adsorption Unit for Surface Area Measurement

APPENDIX–5

APPENDIX–5

SEM Sample Preparation

Platinum Coating:

(1) Connect pump power supply plug to coater unit and connect the correct vac line to the pump.

(2) Ensure Argon cylinder is on and that the vent and leak valves are closed.

(3) Place sample in holder and adjust platinum source to correct height above sample (~ 2cm)

(4) Set selector switch to pump

(5) Allow vac to reach .08 mbar then leak in Argon for a couple of seconds so that vac drops to .02 mbar, close the leak valve – repeat this step then allow vac to drop to ~.03 mbar.

(6) Set voltage at about 1.4 KV and set selector on "SET HT". Leak in Argon until a deflection of 16 – 18 mA is seen on the dial then set selector switch to "Control".

(7) Set timer switch for desired duration and press start button. The unit will now coat for set time (try 2 minutes at first).

(8) When coating is over set selector switch to 'off' and open vent valve until pressures stabilize. Close vent and leak valves and switch off Argon cylinder. Then remove sample.

Carbon Coating: **(essential if EDX analysis is required):**

(1) Connect the vac. pump power supply plug to left socket on coater unit and connect the coater unit vac. line to the pump.

(2) Replace the carbon fibre filament between the electrodes trimming off any excess. (use the screwdriver as the unit will be hot if it has just been used).

(3) Place sample in the holder (if the sample is deep then lower the sample holder accordingly). Close lid and place electrode unit in position.

(4) Close the vent and switch on the pump at the front of the coater unit.

(5) When a vac of .08 mbar is reached switch the selector switch to continuous and select about 30% on the voltage control. Allow the fibre to glow bright orange for 30 seconds to drive off any moisture then switch selector to 'off' position.

(6) Allow the vac to drop to .03 mbar, place selector switch in pulse position and set voltage switch on 65%. Pulse power through the fibre for one–second bursts until the fibre burns out (one–second bursts with 6–second gaps).

(7) Set selector switch in 'off' position, and voltage control to 0%. Switch off pump and open vent. When the pressure has stabilized the sample may be removed.

APPENDIX–6

APPENDIX–6

Detailed Specification of Experimental Apparatus

(1) Glassware:

Cracking Reactor:

material of construction:	Quartz glass (96% silica)
dimensions:	see Fig. 5.7

Inlet Section:

material of construction:	Pyrex Glass (Borosilicate)
dimensions:	see Fig. 5.7

Outlet Section:

material of construction:	Quartz glass (96% silica)
dimensions:	see Fig. 5.7

Product Condenser (Liebig):

material of construction:	Pyrex (Borosilicate)
dimensions:	100 cm^2 surface area
	300 mm overall length

(2) Electrical Equipement:

Feed Pump:

(for flowrate $\geq$ 0.5 gm/minute)

Watson–Marlowe peristaltic pump (502S) with pumphead module (501R)

silica tubing feed line– 1.66 mm bore.

(for flowrate < 0.5 gm/minute)

The Perfuser syringe pump, with a capacity of 50 ml.

(3) Tube Furnace:

Dimensions:	150 mm inside diameter
	450 mm length
Power Rating:	750 Watt

(4) Chemicals:

Cumene:

Supplier:	Fison Scientific Apparatus Ltd.
Purity:	99.5% minimum (GLC Assay)
Boiling point:	148–153° C
Specific Gravity:	0.862–0.865

Nitrogen:

Supplier:	BOC Ltd.
Details:	Oxygen free

(5) Temperature Control and Recording:

Control: Three term Eurotherm type 810 controller

Thermocouples: K–type thermocouples

Calibration of Thermocouples: Carried out using a platinum resistance thermometer.

(6) Temperature Recording:

The thermocouple interfaced with an apricot computer via 3D think lab system containing a 12 bit analogue/digital card. The A/D card produced a digital signal in the range 0–4096 which corresponded approximately to the temperature range 0–700° C.

Operating Conditions For GLC Analysis

Equipment Description:

Pye Unicam GCD chromatograph Series 204 linked to a Hewlett Packard 18652 A/D converter. Electronic integration by a Hewlett Packard integrator.

Conditions:

Column	1.5mx4mm i.d. glass packed with 5% Bentone 34, 5% SP 1200 on 80–100 mesh Chromo–sorb W.
Column Temperature	Programmed: 80° C for 2 minutes then at 16° C/min to 110° C.
Carrier Gas and Flow	Nitrogen at 45 ml/min
Detector	Flame Ionization Detector (FID)
Detector Temperature	200° C
Attenuation	$64x10^2$
Injection Type	Syringe–on–column
Injection Temperature	200° C
Sample	0.5 μl of cracked products
Chart Speed	0.5 cm/min.

The LECO CS244 Analyser

The illustration below shows a simplified line diagram explaining the operation of the LECO CS244 Carbon/Sulphur analyser. The catalyst is

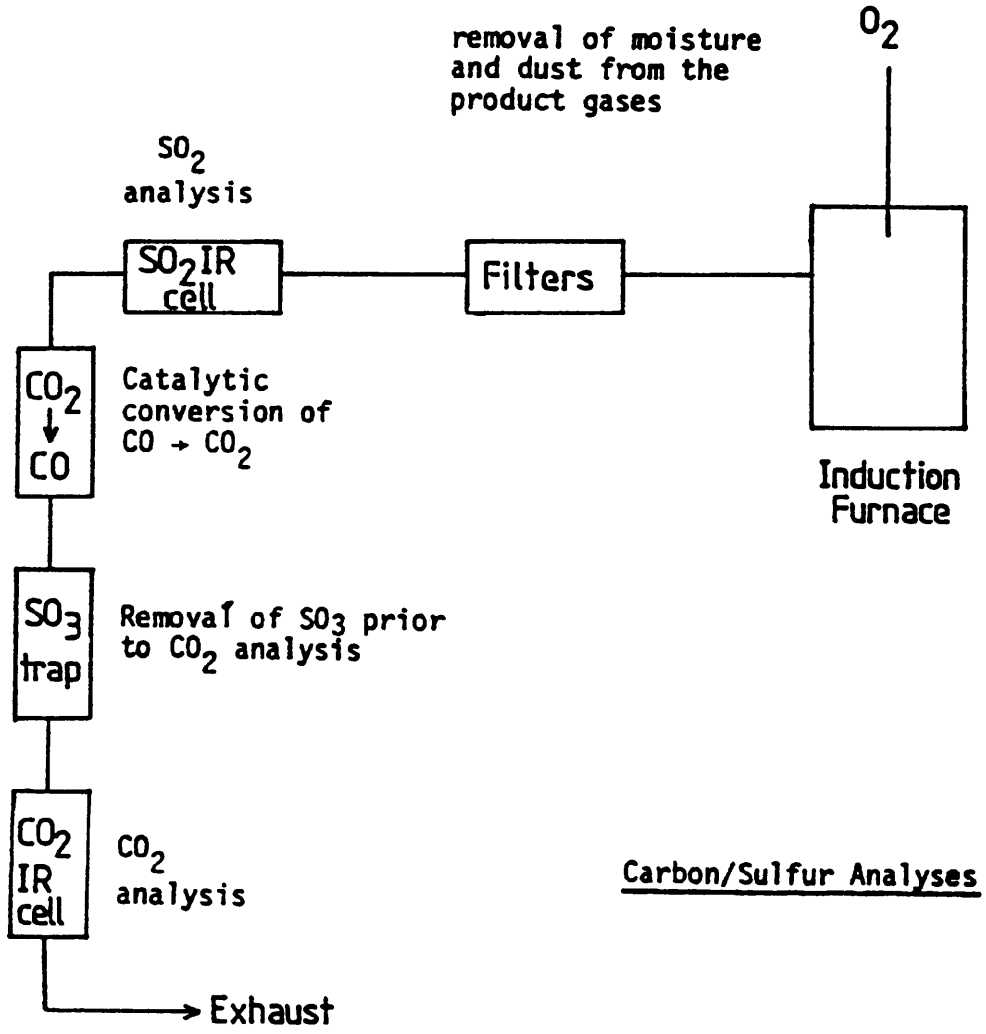

automatically weighed and an equal amount of Iron chip combustion accelerator added to the sample. The sample and accelerator are then placed in the induction furnace where they are burned in the presence of oxygen. The product gases are then analysed by Infra Red Spectroscopy (IR).